Deep Excavation

Theory and Practice

Chang-Yu Ou

Deep Excavation

Theory and Practice

BALKEMA - Proceedings and Monographs
in Engineering, Water and Earth Sciences

Deep Excavation

Theory and Practice

Chang-Yu Ou

Department of Construction Engineering,
National Taiwan University of Science and Technology,
Taipei, Taiwan

Taylor & Francis
Taylor & Francis Group
LONDON / LEIDEN / NEW YORK / PHILADELPHIA / SINGAPORE

Typeset in Times New Roman by
Newgen Imaging Systems (P) Ltd, Chennai, India
Printed and bound in Great Britain by
Antony Rowe Ltd, Chippenham, Wiltshire

Published by: Taylor & Francis/Balkema
P.O. Box 447, 2300 AK Leiden, The Netherlands
e-mail: Pub.NL@tandf.co.uk
www.balkema.nl, www.tandf.co.uk, www.crcpress.com

British Library Cataloguing in Publication Data
A catalogue record for this book is available from the British Library

Library of Congress Cataloging in Publication Data
Ou, Chang-Yu, 1954–
Deep excavation/Chang-Yu Ou.
p. cm.
1. Excavation. I. Title.

TA730.O92 2006
622′.2–dc22 2006003498

ISBN10: 0–415–40330–8 (hbk) ISBN13: 978–0–415–40330–6 (hbk)
ISBN10: 0–203–96834–4 (ebk) ISBN13: 978–0–203–96834–5 (ebk)

Cover picture: Courtesy of C.H. Cheng

Contents

Preface

Excavation is an important segment of foundation engineering. For example, in the construction of the foundations or basements of high rise buildings, underground oil tanks, subways or mass rapid transit systems, etc. Though books on general foundation engineering introduce the basic analysis and design of excavations, they are usually too simple to cope with analysis and design in practice. With economic development and urbanization, excavation goes deeper and is larger in scale, sometimes it is carried out in difficult soils. These conditions require advanced analysis and design methods and construction technologies.

The author has focused on studies of soil behavior and excavation problems since beginning to teach in a university and has published many journal and conference papers concerning the subjects. At the same time, working with industrial builders, the author has also taken part in many large-scale excavation projects and accumulated experience in analysis and design. Supported by study results and analysis experience, the author has opened a course on deep excavation at the university. Based on interaction between research results, analysis experience, and teaching experience, this book is meant for both teachers and engineers engaged in advanced analysis and design.

Aimed at both theoretical explication and practical application, the book covers a large scope. From basic to advanced, the book tries to attain theoretical rigorousness and consistency. Each chapter is followed by problems and solutions so that the book can be readily taught at senior undergraduate and graduate levels. On the other hand, this book also tries to cope with design practice. Because it cites the best methods currently used in engineering circles, this book can be readily used for analysis and design in actual excavations. In addition, a free computer program, VEX, developed by the author for excavation analysis is provided along with the book to readers. Not only does the program help readers to understand excavation behavior, it also can be used as a design tool for excavations.

The book is divided into 12 chapters, and the contents are summarized as follows:

Chapter 1 introduces the flow of analysis and design of excavations. Chapter 2 introduces the basic properties of soils and the representative values for various urban soils around the world. The chapter also explains the principles of drained and undrained strengths of soils and the test methods to obtain them. Chapter 3 introduces commonly used excavation methods and retaining-strut systems. The excavation of the Taipei National Enterprise Center (TNEC), referred to many times as an example in the book, is also introduced in this chapter. Chapter 4 introduces the concept of lateral earth pressure and its application to excavation.

Chapter 5 introduces the ultimate analysis, the uplift analysis, and sand boiling analysis for excavations. Also, reasonable factors of safety for these analyses are discussed in this

chapter. Chapter 6 introduces the hand calculation for the estimation of excavation-induced deformation, ground settlement, and the stress of the strut-retaining wall. The method, which is based on hand calculation, is called the simplified method in the book. Chapter 7 introduces deformation and ground settlement analysis by using the beam on elastic foundation method. Chapter 8 introduces deformation and ground settlement analysis by using the finite element method.

Chapter 9 introduces methods of dewatering, well theories, and the design of excavation dewatering. Chapter 10 introduces the design of structural components in braced excavations and anchored excavations. These components include the retaining wall, the strut, the wale, the center post, and the anchor. Chapter 11 introduces building protection during excavation, including the determination of allowable settlement, commonly used building protection methods, and auxiliary methods. Chapter 12 introduces the principles of monitoring instruments, items of instruments, determination of alert and action values, and the application of feedback analysis.

Finally, I have to acknowledge the very considerable contribution of my former doctoral students, Prof. P. G. Hsieh, who often discussed excavation theories with me, and Y. G. Tang, who helped in the development of the computer program, VEX, and both are very important for the production of this book.

A free computer program, VEX, regarding excavation analysis and design can be downloaded from the website (http://web.ntust.edu.tw/~ou/). The powerpoint file and details of the solution procedures of the problem set for each chapter are available for potential instructors. The interested instructors are encouraged to make a request to me.

Chang-Yu Ou
ou@mail.ntust.edu.tw

Chapter 1

Introduction to the analysis and design of excavations

When Terzaghi (1943) was first considering the stability of excavations, he defined those whose excavation depths were smaller than their widths as shallow excavations while those with depths larger than their widths were deep excavations. Years later, Terzaghi and Peck (1967), and others, including Peck *et al.* (1977), revised that excavations whose depths were less than 6 m could be defined as shallow excavations and those deeper than that as deep excavations, considering that use of sheetpiles or soldier piles grows uneconomical once the excavation depth goes beyond 6 m. Generally speaking, the analysis methods for shallow excavations are comparatively simple. In fact, more and more excavation projects are located in populous urban areas. To avoid damage to adjacent properties caused by excavation, diaphragm walls are commonly used as retaining walls. What's more, computer programming has done most of the job of analysis and design, which applies to all depths, following the same theories. Therefore, it is not meaningful to distinguish between deep and shallow excavations any more.

Analysis of deep excavations is usually required before going into design. Deep excavation analysis is a typical soil–structure interaction problem. Soil is a nonlinear, inelastic, and anisotropic material. Its behavior is normally affected by water contents. Some types of soils have the characteristics of consolidation and creep. Theoretically, analysis of deep excavation involves simulations of elastoplastic behavior of soil, interface behavior between soil and retaining walls, and the excavation process. Some simulation theories are not fully developed, and some are too complicated to be used in practice. Thus, to analyze exclusively according to contemporary theories is not practical at the present stage. To sum up, a reasonable excavation analysis, at the present stage, should make use of conventional soil mechanics and simple structural mechanics, along with appropriate modifications according to field observation. Concerning excavation analyses, please see Chapters 5–8 for detailed discussion.

A complete deep excavation design includes a retaining system, a strutting system, a dewatering system, excavation procedure, a monitoring system, building protection, etc. Figure 1.1 illustrates the general course of deep excavation design, which can be paraphrased as follows:

1.1 Geological investigation and soil tests

Deep excavation projects include the construction of building basements, subway stations, and so on, whose depths may range from several meters to 30 or 40 m. The process of an excavation may encounter different kinds of soils underneath the same excavation site—from soft clay to hard rocks. The closer the construction site to a hillside, the more complicated

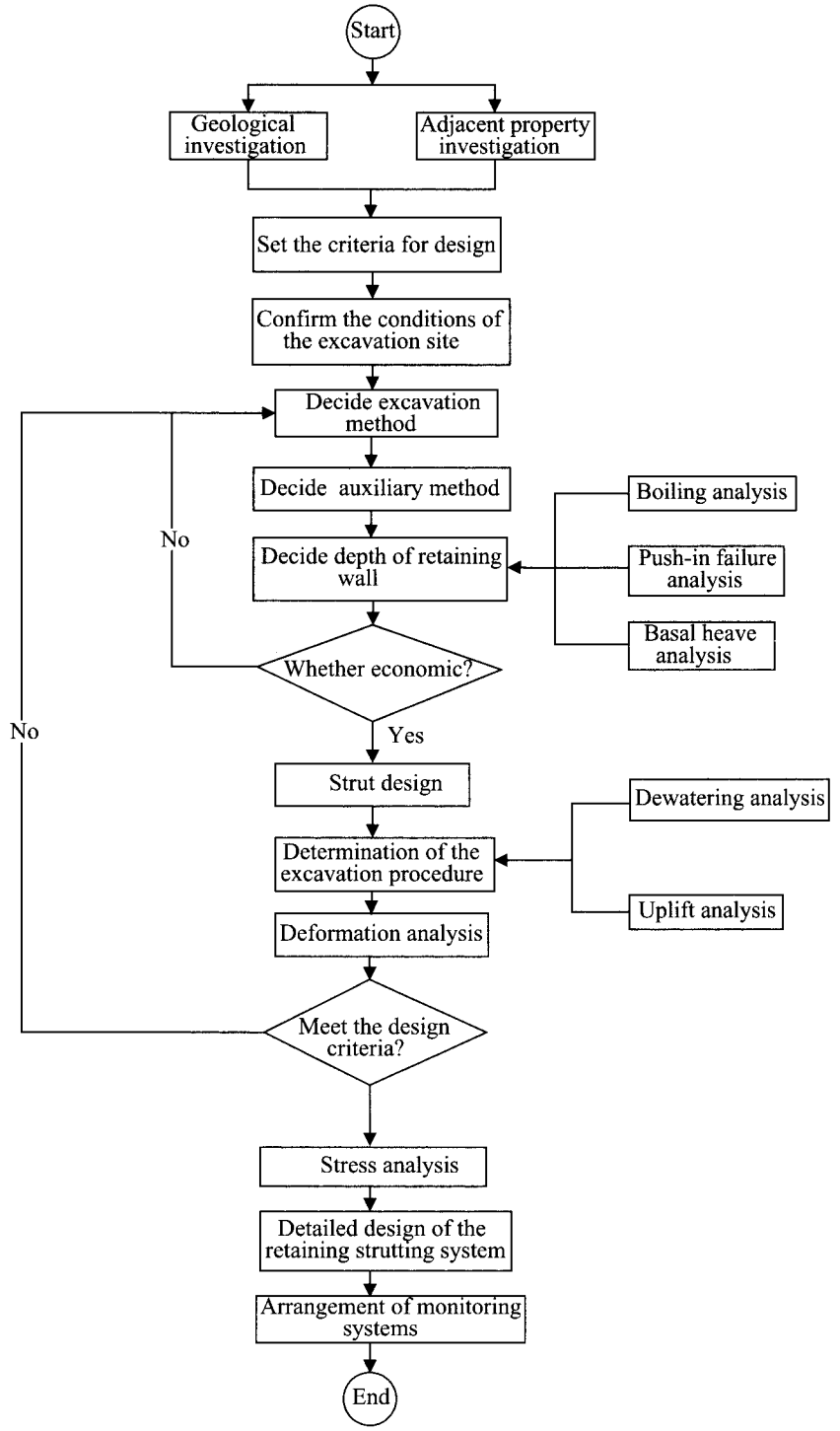

Figure 1.1 Flow chart for analysis and design of an excavation.

the geological condition. The geological condition determines the type and construction of retaining walls and greatly influences the excavation behavior as well. In addition to the geological condition, the distribution of groundwater also contributes to the excavation behavior. For example, it may fall below the hydrostatic water pressure in an urban area because of the long-term overuse of groundwater. On hillsides, there might exist an artesian aquifer, which has a rather high pressure. In seaside areas, seawater may permeate into the soils and tides will make the water level fluctuate daily. To sum up, the geological investigation of an excavation project aims at the soil conditions underneath the construction site and the distribution of groundwater.

There are many soil tests for deep excavations. These include tests of basic soil behavior, such as unit weight, specific weight, water content, Atterberg limit, etc., and tests of mechanical behavior, such as consolidation and strength, etc. According to the information from the soil tests, engineers can judge whether the soil is a drained or an undrained material. Since the strength differs significantly between drained and undrained materials, the choice of analysis methods and retaining walls varies accordingly. The more precise the results of soil tests, the more reasonable are the analysis results and the more economical are the retaining and excavation systems. However, the merits of soil tests can not be seen directly and therefore are often neglected.

1.2 Conditions of the adjacent properties

From the perspective of mechanics, deep excavation necessarily gives rise to movement of the soils near the excavation site. However, if the movement or settlement is too large, it will damage neighboring buildings or public facilities. Some buildings or facilities are especially sensitive to settlement, a little of which may bring about cracks in beams or columns, while others can stand more settlement. The allowable settlement of a building or a facility is highly correlated to its foundation type, construction material, structural type, and age. Therefore, investigation of the condition of adjacent properties and public facilities before designing an excavation project is required to determine the allowable settlement, which in turn determines the type of retaining and strutting systems and the selection of auxiliary methods.

1.3 Confirmation of the conditions of an excavation site

According to the shape, area, and elevation of the excavation site, along with geological conditions, the distribution of groundwater, and conditions of neighboring properties, we can decide on a provisional retaining method and an excavation method. Therefore, it is necessary to have a thorough understanding of the conditions of the excavation site.

1.4 Designing criteria

Whether an excavation is successful is significant to the lives and properties of many people. Thus, an appropriate design criterion must be selected before design.

A deep excavation design criterion should include, at least, the method of stability analysis, the methods of simplified and advanced deformation and stress analyses, a dewatering scheme, the design of structural components, property protection, etc. This book explores theories, as well as their application to deep excavation, from both the theoretical and practical

perspectives. Getting familiar with the contents, should not only help the reader to understand excavation behavior and design and analyses, but also help develop a suitable excavation design criterion.

1.5 Collecting case histories of the nearby excavations

The first job of excavation design is to decide the type of retaining wall and the excavation method. Though we can choose the most reasonable methods based on geotechnical theories, geological conditions, and neighboring property conditions, an excavation analysis does not always predict the excavation behavior exactly because geological investigation may not cover all kinds of soils to be encountered during excavation and because the simulation of the excavation process may not be complete. A case history of nearby excavation, equivalent to a full-scale excavation experiment, helps design the excavation project no matter if it was successful or not in the end.

1.6 Auxiliary methods

A deep excavation may have difficulty meeting design criteria, due to poor geological conditions or deteriorated adjacent buildings. Even if it reaches the criterion, it may be very expensive. Auxiliary methods can help solve the dilemma. These include soil improvement methods, counterfort methods, cross wall methods, micropiles and underpinning methods, etc. Please see Chapter 11 for the design of auxiliary methods.

1.7 Excavation analyses

Excavation analyses consist of stability analyses, deformation analyses, and stress analyses. Stability analyses, including ultimate failure analyses, sand boiling analyses, and uplift analyses, aim at avoiding failure or collapse. Ultimate failure analyses and sand boiling analyses can determine how deeply the retaining wall should penetrate into the soil. Uplift analyses can decide on dewatering schemes at different stages. As to stability analyses of excavation, please see Chapter 5. For dewatering analyses, see Chapter 9.

Deformation analyses are done to find the lateral deformation of retaining walls, the heave of the excavation bottom, and the settlement of the soil outside the excavation zone. The lateral deformation and the settlement of the soils not only affect the safety of the retaining wall but also affect the adjacent properties. As to the heave of the excavation bottom, it is correlated to the capacity of the strutting system.

Stress analyses involve those of strut load and of bending moment and shear of retaining walls. The data on the strut load is necessary for the detailed design of struts or anchors, while that of the bending moment and the shear is relevant to the choice of the appropriate type and dimension of retaining walls, and sometimes to the design of reinforcements. Concerning methods of stress and deformation analyses of excavations, please refer to Chapters 6–8.

1.8 Layout of the strutting system

A strutting system comprises either horizontal struts or anchors, which contribute to the resistance to the lateral earth pressure generated by excavation. Stability analyses determine

the penetration depth of a retaining wall. Once stability analysis is finished, the tentative locations and vertical distances of the struts can be determined. The procedure of installation and of the later removal of the struts for the construction of floor slabs basically determines the locations and vertical distances of the struts. Deformation and stress being analyzed, the type and size of the struts are accordingly decided. Concerning the detailed design of strutting systems, please see Chapter 10.

1.9 Monitoring system

In spite of thorough geological investigations, soil tests, rigorous analyses and design, excavation theories, based on many hypotheses, can hardly cope with the many uncertainties of geological conditions. Therefore, excavation has to be carried out along with monitoring instruments, which tell, immediately, changes of stress and displacement generated by excavation. The engineers in charge can thereby check the safety of excavation at any time. For large scale excavations, the geological uncertainty increases and a monitoring system is urgently required. Concerning the items and design of monitoring systems for deep excavation, please see Chapter 12.

1.10 Protection of neighboring properties

Due to the unbalanced earth pressures on the two sides of a retaining wall, excavation produces displacement of retaining walls and settlement of the ground. The buildings and public facilities within the range of the settlement may have differential settlement. When settlement goes beyond the allowable amount, the nearby buildings or public facilities may develop cracks or be damaged. The damages may turn out to be structural or non-structural. However, hardly any proprietors will accept them, either way. To avoid such damages, prediction of the settlement is necessary to decide whether and how to take protecting measures. There are many ways to protect neighboring properties. Some of them can be deduced from theoretical analyses. Others rely on engineering experience and empirical data. Chapter 11 introduces various measures to protect adjacent properties and related analyses.

Chapter 2

Basic properties and mechanical characteristics of soils

2.1 Introduction

This chapter will introduce the basic properties and the strength characteristics of soils. Though basic soil properties can be distinguished into many items, we will concentrate on those that are directly relevant to deep excavations. Some representative values of the basic properties of urban soils in the world are collected as references for beginners to have an idea about the characteristics of urban soils and for engineers to help design excavation projects. To save space, this chapter will not go into the defining of soil properties, which can be found in detail in introductory books on soil mechanics and foundation engineering. There are some soil properties easily neglected, however, and the chapter will digress slightly to talk about them in brief.

Effective stress is one of the most important principles in soil mechanics. Though the stress can be distinguished into effective stress and total stress, only the former influences the characteristics of consolidation and strength of soils. The total stress does not. Thus, this chapter uses considerable space to explicate the drained and undrained strengths of soils on the basis of the principle of effective stress. Many concepts about soil strength to be introduced in this chapter, though not included in the general textbooks on soil mechanics, have been applied in engineering practice for years. Readers are advised to study the part introducing the relations between effective stress and drained and undrained strength.

2.2 Basic properties

This section will investigate the soil properties related to analyses and designs of deep excavations, such as the specific gravity, the unit weight, the water content, the Atterberg limits, the permeability, the compression index, and the swelling index. To help comprehend the engineering properties of soils and to offer as primary information for analyses and design of deep excavations, this section introduces the range of soil properties in some urban areas in the world, such as San Francisco bay mud (Bonaparte and Mitchell, 1979), Boston blue clay (Lambe and Whitman, 1969; Ladd and Foote, 1974; Pestana, 2001), Chicago silty clay (Finno *et al.*, 2002a,b), London clay (Ng, 1992; Simpson, 1992; Dawson *et al.*, 1996; Higgin *et al.*, 1996), Mexico City clay (Lo, 1962; Mesri *et al.*, 1975; Diaz-Rodriguez *et al.*, 1992), Bangkok clay (Moh *et al.*, 1969; Bergado *et al.*, 1991), Singapore marine clay (Lee *et al.*, 1998; Chu *et al.*, 2002; Tan *et al.*, 2002), Shanghai clay (Ou, 2001), and Taipei silty clay and sand (Wu, 1987; Moh *et al.*, 1989). Comparing the basic properties of soils with these various urban areas, one can develop a further understanding of the engineering characteristics of soils.

2.2.1 Specific gravity

Except for some types such as peat and highly organic soil, the specific gravities (G_s) of soils do not vary significantly. Table 2.1 lists the magnitudes of the specific gravities of some general types of soils. Table 2.2 gives those of some well-known urban soils. Since specific gravities do not range widely, using the data from Table 2.1 or 2.2 is acceptable when the test results are not available before designing.

2.2.2 Unit weight and water content

The unit weight and the water content of soils correlate with their degrees of denseness, degrees of saturation, mineral compositions, and overburden depth. The degrees of denseness of sandy soils have something to do with their grain sizes and gradations; those of clayey soils, however, are affected by their over-consolidation ratios (OCR).

Table 2.3 illustrates the saturated unit weights and the water contents for some urban soils. Theoretically, the mineral compositions and degrees of denseness in the same urban areas do not vary significantly. Therefore, when the soils over an area are near 100% saturation, their saturated unit weights and the water contents should be very similar. Nevertheless, the deeper the overburden layer, the larger the unit weight, and the smaller the water content. Near ground clays are often over-consolidated because of desiccation and the fluctuation of groundwater. Under the same conditions, the unit weights of over-consolidated soils are larger than those of normally consolidated soils while their water contents are smaller. Though Table 2.3 does

Table 2.1 Specific gravities of some soils

Soil type	G_s
Gravel	2.65–2.68
Sand	2.65–2.68
Clay	2.62–2.68
Clay (inorganic)	2.68–2.75
Clay (organic)	2.58–2.75
Peat	1.30–1.90

Table 2.2 Typical values of specific gravity for some urban soils

Soil type	G_s
San Francisco bay mud (CH)	2.69–2.73
Boston blue clay (CL)	2.76–2.79
Chicago silty clay (CL)	2.63–2.76
London clay (CH)	2.72–2.76
Mexico City clay (MH)	2.35–2.65
Bangkok clay (CH)	2.59–2.74
Singapore marine clay (CH)	2.62–2.78
Shanghai clay (CL)	2.72–2.74
Taipei silty clay (CL)	2.69–2.71
Taipei silty sand	2.64–2.73

Table 2.3 Typical values of saturated unit weight and saturated water content for some urban soils

Soil type	*w (%)*	γ_{sat}(kN/m^3)
San Francisco bay mud (CH)	88–96	14.4–14.8
Boston blue clay (CL)	34–38	18.2–18.7
Chicago silty clay (CL)	21–33	18.1–19.0
London clay (CH)	23–27	19.9–20.3
Mexico City clay (MH)	439–574	11.0–14.4
Bangkok clay (CH)	66–92	14.4–15.9
Singapore marine clay (CH)	66–92	15.5–16.5
Shanghai clay (CL)	28–42	17.2–18.6
Taipei silty clay (CL)	18–42	17.7–19.3
Taipei silty sand	14–36	18.2–20.0

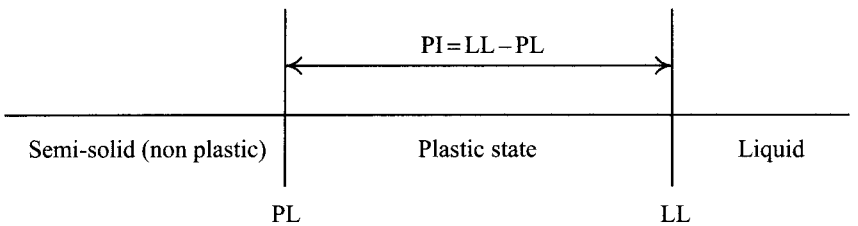

Figure 2.1 Definition of Atterberg limits.

not handle factors such as overburden depth, it is still useful to understand the possible range of the unit weights and water contents, as these are also important references for preliminary design.

According to the phase relationship of soils, the porosity of soils can be calculated from their water content and the specific gravity.

2.2.3 *Atterberg limit*

The commonly used Atterberg limits include the liquid limit (LL) and the plastic limit (PL), whose definitions can be illustrated by Figure 2.1. As it illustrates, the plastic index PI = LL − PL. The physical meaning of the plastic index refers to the corresponding range of water content within the range of the soil plasticity (though LL, PL, and PI refer to the water contents or their range in some specific states, their expressions do not contain a percentage). A high plastic index implies that the plasticity of soil can be maintained when substantial water is added to the soil in the initial plastic state (w_n = PL%). On the other hand, a low plastic index indicates that the plasticity is susceptible to changes of the water content. To sum up, PI is often used to represent the plastic properties of soils.

Besides, the LL value is related to the capability of clay minerals to absorb water, which is in turn related to the degree of plasticity of soils. Therefore, LL and PI are often used as indices to categorize the soil as well.

Table 2.4 Atterberg limits for some soils

Soil type	LL	PL	PI
Kaolinite	35–100	25–35	—
Illite	50–100	30–60	—
Montmorillonite	100–800	50–100	—
San Francisco bay mud (CH)	85–88	35–44	43–54
Boston blue clay (CL)	40–49	20–25	18–23
Chicago silty clay (CL)	30–42	17–22	14–20
London clay (CH)	70–80	24–29	47–70
Mexico City clay (MH)	425–550	57–150	300–493
Bangkok clay (CH)	76–102	29–47	23–27
Singapore marine clay (CH)	75–100	22–30	52–62
Shanghai clay (CL)	28–42	17–24	10–19
Taipei silty clay (CL)	25–40	17–24	8–16

In general, the higher the degree of plasticity, the higher its toughness, undrained shear strength, dry strength, and compressibility; on the other hand, the lower is its permeability. Therefore, the strength of clayey soils and the empirical formulae of engineering properties are correlated to PI or LL or both.

Table 2.4 lists the values of LL, PL, and PI of some urban soils. For the convenience of comparison, the LL and PL values of typical clay minerals such as Kaolinite, Illite, and Montmorillonite are also included.

The liquid limit, the plastic limit, and the water content can be used to predict the degree of consolidation of soils. This is because the density of an overconsolidated soil is usually higher in the natural state than shown during the Atterberg limit test (remolded state). Thus, considering that the porosity or natural water content of the saturated overconsolidated soil is smaller than that in the normally consolidated state, we can conclude reasonably:

w_n is about LL%	The soil is normally consolidated.
w_n is smaller than PL%	The soil is highly overconsolidated.
w_n is between LL% and PL%	The soil is overconsolidated.
w_n is larger than LL%	The soil is unstable.

When the natural water content (w_n) is larger than LL%, it follows that the undrained shear strength is low and the soil is susceptible to collapse or to becoming mobile once it is disturbed. The reason why the soil can remain solid and stable is the vertical overburden stress or the intergranular cementation. The above explanation can be summed up by the following expression of the liquid index (LI):

$$\mathrm{LI} = \frac{w_n - \mathrm{PL}}{\mathrm{LL} - \mathrm{PL}} \tag{2.1}$$

Combining the equation with the above discussion, we can conclude that: when LI $\approx$ 1.0, it is normally consolidated soils; when LI $<$ 1.0, overconsolidated soils; when LI $>$ 1.0, soft or sensitive soils.

2.2.4 Permeability

According to Darcy's law (1856), the velocity of flows of water in soils can be expressed by the following equation:

$$v = ki \tag{2.2}$$

where

v = discharge velocity
k = coefficient of permeability
i = hydraulic gradient (dimensionless).

It can be seen from the above equation that the velocity of the flow of water in soil grows with the increase of the coefficient of permeability. The coefficient of permeability indicates the capability of water to flow in soil, and is one of the basic properties of soils. It can be obtained from laboratory tests or in situ pumping tests. Laboratory permeability tests include the constant head, the falling head, and the triaxial permeability tests. On the other hand, it can also be obtained from empirical formulae. The equation suggested by Hazen (1892) is often used, as follows

$$k = (100 \sim 150)D_{10}^2 \tag{2.3}$$

where k = coefficient of permeability (cm/s), D_{10} = effective diameter (mm).

Table 2.5 gives the possible range of the coefficients of permeability and could be useful for reference when designing an excavation. Table 2.6 offers some typical coefficients of permeability for some urban soils.

Generally speaking, the coefficient of permeability is not necessarily required in deep excavation analysis and design. An advanced analysis of deep excavation sometimes has to consider the dissipation of porewater pressure or consolidation and therefore has to take advantage of coefficient of permeability.

2.3 Consolidation

The compression index (C_c) of clayey soils is the slope of the straight-line segment on the $e - \log p$ curve, which is produced in the primary consolidation stage of the consolidation

Table 2.5 Coefficients of permeability of some soils

Soil type	*k* (cm/sec)
Clean gravel	$>10^{-1}$
Coarse to fine soil	10^{-1}–10^{-3}
Fine sand, silty sand	10^{-3}–10^{-5}
Silt, silty clay	10^{-4}–10^{-6}
Clay	$<10^{-7}$

Table 2.6 Typical values of permeability for some urban soils

Soil type	*k* (cm/sec)
San Francisco bay mud (CH)	$(2.0–100) \times 10^{-9}$
Boston blue clay (CL)	$(1.0–100) \times 10^{-9}$
Chicago silty clay (CL)	$<10^{-7}$
London clay (CH)	$(0.5–100) \times 10^{-8}$
Mexico City clay (MH)	$(1.0–100.0) \times 10^{-9}$
Bangkok clay (CH)	$(4.0–60) \times 10^{-7}$
Singapore marine clay (CH)	$(1.0–7.0) \times 10^{-9}$
Shanghai clay (CL)	—
Taipei silty clay (CL)	$(0.5–2.0) \times 10^{-7}$
Taipei silty sand	$(0.5–6.0) \times 10^{-4}$

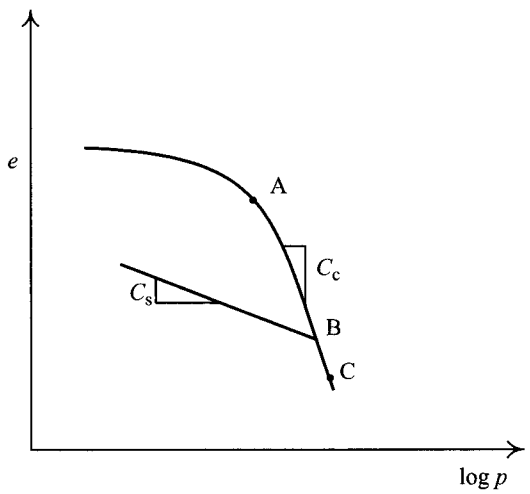

Figure 2.2 Definitions of the compression index and the swelling index.

test. As shown in Figure 2.2, C_c can be represented by the following formula:

$$C_c = \frac{e_1 - e_2}{\log p_2 - \log p_1} \tag{2.4}$$

where e = porosity, p = consolidation pressure.

C_c should be obtained through the one-dimensional consolidation test or the triaxial consolidation test. Table 2.7 lists the typical values of C_c for some urban soils.

Many investigators have established the relationships between basic soil properties and C_c through regression analyses, as Table 2.8 illustrates. To select the most suitable empirical formula for local types of soils, a further laboratory test is necessary.

Table 2.7 Compression indices of some urban soils

Soil type	C_c
Normally consolidated, medium sensitive	0.2–0.5
Peat	10.0–15.0
Organic clay	>4.0
San Francisco bay mud (CH)	0.8–1.8
Boston blue clay (CL)	0.3–0.4
London clay (CH)	0.23
Chicago silty clay (CL)	0.18–0.25
Mexico City clay (MH)	7–10
Bangkok clay (CH)	0.5–1.52
Singapore marine clay (CH)	0.77–0.97
Shanghai clay (CL)	0.25–0.35
Taipei silty clay (CL)	0.33–0.50

Table 2.8 Some empirical equations for C_c (after Rendon-Herrero, 1980)

Equation	*Regions of applicability*
$C_c = 0.009\ (LL - 10)$[1]	Normally consolidated clays
$C_c = 0.007\ (LL - 7)$[2]	Remolded clays
$C_c = 0.156e_0 + 0.0107$	All clays
$C_c = 1.15(e_0 - 0.35)$	All clays
$C_c = 0.30(e_0 - 0.27)$	Inorganic cohesive soil; silt, silty clay
$C_c = 0.75(e_0 - 0.50)$	Soils with low plasticity
$C_c = 0.01w_n$	Chicago clays
$C_c = 0.208e_0 + 0.0083$	Chicago clays
$C_c = 0.0115w_n$	Organic soils, peats, organic silt and clay
$C_c = 0.0046(LL - 9)$	Brazilian clays
$C_c = 1.21 + 1.055(e_0 - 1.87)$	Motley clays from Sao Paulo city
$C_c = 0.015(w_n - 8)$ or $C_c = 0.54(e_0 - 0.23)$[3]	Taipei silty clay

Notes
1 Terzaghi and Peck (1967)
2 Skempton (1944)
3 Moh *et al.* (1989)

As Figure 2.2 shows: the swelling index is the slope of the unloading curve, which can be calculated by the following equation:

$$C_s = \frac{e_3 - e_4}{\log p_4 - \log p_3} \tag{2.5}$$

The value of the swelling index can also be obtained through laboratory tests. However, if test data is not available, the C_s/C_c ratio can be assumed to be between 0.05 and 0.1. Table 2.9 provides some typical C_s/C_c values for some urban soils for analysis and design references.

Generally speaking, deep excavation analyses and design do not often use C_c and C_s. However, some deformation moduli used in the numerical analysis can be derived from these values (please see Chapters 7 and 8).

Table 2.9 Typical values of compression index and swelling index for some urban soils

Soil type	C_s/C_c
San Francisco bay mud (CH)	0.08–0.15
Boston blue clay (CL)	0.24–0.33
London clay (CH)	0.046
Chicago silty clay (CL)	0.12–0.17
Mexico City clay (MH)	0.04–0.05
Bangkok clay (CH)	0.13–0.22
Singapore marine clay (CH)	0.16–0.21
Shanghai clay (CL)	0.08–0.21
Taipei silty clay (CL)	0.15–0.32

2.4 Concept of effective stresses

The principle of effective stress is one of the most important theories in soil mechanics since soil behaviors are highly related to it. In this book, drained/undrained shear strength, lateral earth pressure, and soil deformation are all explained in terms of effective stress. Considering its importance, this section will expound its basic concept though it is normally introduced in textbooks on soil mechanics.

As Figure 2.3a shows, the total stress (σ), which acts at a point O in soil, can be represented by the following equation:

$$\sigma = \gamma H_1 + H_2 \gamma_{sat} \tag{2.6}$$

where γ = unit weight of soil above the groundwater table, γ_{sat} = saturated unit weight of soil.

The above mentioned total stress can also be called the body stress, which is produced by the gravitational force acting on the mass. Thus, total stress acting at any point in soil is the sum of the weights of all the materials (including solids and water) above the point. As Figure 2.3a shows, considering the wavy plane AB passing through the contact points between particles, part of the total stress acts on porewater while the rest acts on solid particles, according to the principle of force equilibrium. Suppose the total area of the contact points is A' and the area of the section of soil is A (Figure 2.3b), the area occupied by the porewater would then be $A - A'$. Thus, the force acting on porewater would be

$$F_w = (A - A')u \tag{2.7}$$

where u = porewater pressure.

Suppose $F_1, F_2, \ldots$ are the intergranular contact forces (see Figure 2.3c), the resultant of the vertical components of the intergranular contact forces on the wavy plane AB is

$$F_s = \sum (F_{1,v} + F_{2,v} + \cdots) \tag{2.8}$$

where $F_{1,v}, F_{2,v}, \ldots$ are the vertical components of $F_1, F_2, \ldots$. Thus,

$$\sigma A = F_w + F_s \tag{2.9}$$

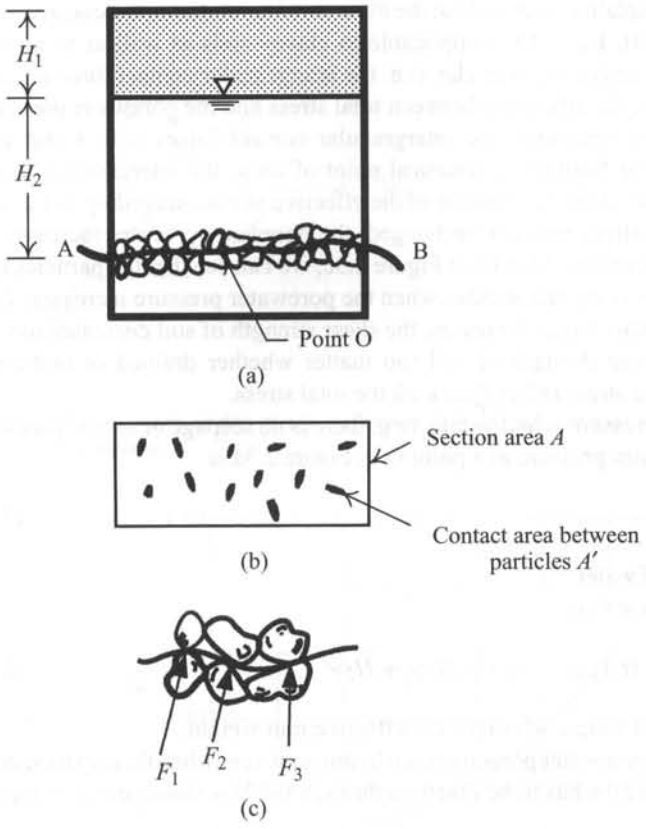

Figure 2.3 Definitions of the effective stress: (a) soil profile, (b) section view of the wavy plane AB, (c) contact stress between soil particles.

then,

$$\sigma = \left(1 - \frac{A'}{A}\right)u + \frac{F_s}{A} = (1-a)u + \sigma' \tag{2.10}$$

where $a = A'/A$, $\sigma' = F_s/A$. Since $a \approx 0$, the above equation can be rewritten as follows:

$$\sigma = \sigma' + u \tag{2.11}$$

where σ' is called the effective stress.

Known from the above derivation, the effective stress represents, in theory, the average intergranular contact stress on a unit cross-sectional area, which consists of solid areas and pore areas. However, the effective stress is not the true intergranular stress. The reason is that the intergranular contact area (A_1') is usually so small ($A_1' \rightarrow 0$) that the true intergranular contact stress ($F_{1,v}/A_1'$) becomes enormous. Eq. 2.10 represents the principle of effective stress first proposed by Terzaghi (1925, 1936). It was originally meant to apply to granular soils (ex. sands). Clayey soils do not necessarily contact intergranularly since their clayey

minerals are tightly enveloped by absorbed water. Therefore, the principle of effective stress for granular soils can not explain clayey soils at the theoretical level. Nevertheless, according to Skempton's study (1960), Eq. 2.10 is applicable to clayey soils as well as to granular soils. It follows that the effective stress in clay (i.e. the intergranular contact force on a unit cross-sectional area) equals the difference between total stress and the porewater pressure.

Since the effective stress represents the intergranular contact forces over a unit gross cross-sectional area, judging from the mechanical point of view, the intergranular friction (i.e. shear strength) increases with the increase of the effective stress. According to Eq. 2.11, on condition that the total stress remains unchanged, the porewater pressure increases and then the effective stress decreases. Also from Figure 2.3c, we can see that the particles have a tendency to be pushed away by one another when the porewater pressure increases. Thus, when the intergranular contact stress decreases, the shear strength of soil decreases too.

The conclusion is that the strength of soil (no matter whether drained or undrained) correlates with the effective stress rather than with the total stress.

Suppose the porewater pressure is hydrostatic (e.g. there is no seepage or excess porewater pressure, etc.). The porewater pressure at a point O in Figure 2.3a is

$$u = H_2\gamma_w \tag{2.12}$$

where γ_w = unit weight of water.

Then the effective stress at O is

$$\sigma' = \sigma - u = H_1\gamma + H_2(\gamma_{sat} - \gamma_w) = H_1\gamma + H_2\gamma' \tag{2.13}$$

where γ' = submerged unit weight of soil or the effective unit weight.

On the other hand, if the porewater pressure is not hydrostatic (i.e. when there exits seepage or excess porewater pressure), u has to be obtained through field measurement or computed in other ways.

2.5 Parameters of porewater pressure

Under undrained conditions, changes of stresses on soil will lead to changes of the porewater pressure inside. As Figure 2.4a shows, supposing the stresses on soil in the three directions separately, σ_1, σ_2, and σ_3, are in equilibrium and their increases are equal to $\Delta\sigma_3$, the increase of the porewater pressure inside would be

$$\Delta u = B\Delta\sigma_c \tag{2.14}$$

where B = porewater pressure parameter.

When a soil mass is 100% saturated, which means the stress increases and all act on porewater, $B = 1.0$. Thus, B is closely relevant to the degree of saturation. Figure 2.5 shows the relations between B and the degree of saturation.

As Figure 2.4b illustrates, if the stress increases ($\Delta\sigma_1$), comes exclusively in a principal direction, the porewater pressure induced by $\Delta\sigma_1$ would be

$$\Delta u = AB\Delta\sigma_1 \tag{2.15}$$

where A is also a porewater pressure parameter.

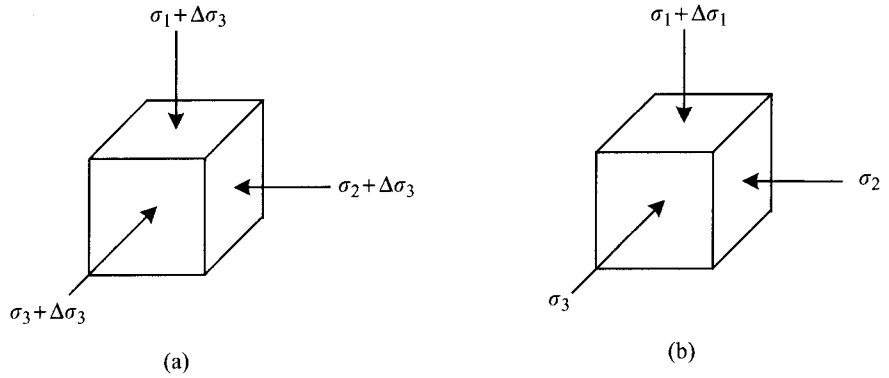

Figure 2.4 Soil element under stress increment: (a) isotropic stress increment, (b) uniaxial stress increment.

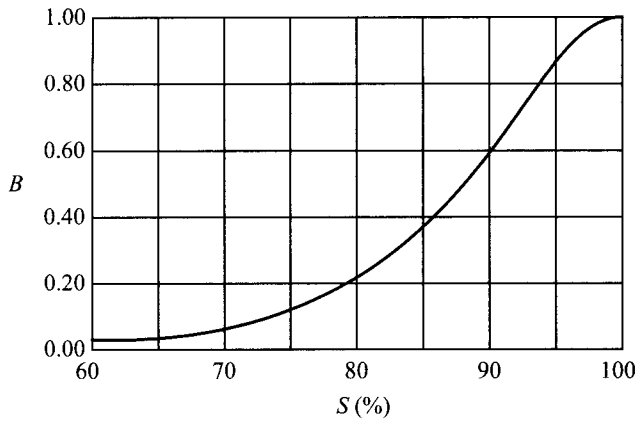

Figure 2.5 Relation between porewater pressure parameter *B* and degree of saturation *S*.

The porewater pressure parameters A and B were first proposed by Skempton (1954), and are also called Skempton's porewater pressure parameters.

The parameter A is related to the type of soil and changes with the shear strain in soil. The parameter A at failures is usually denoted by A_f, which decreases with the increase of the overconsolidation ratio. Figure 2.6 shows the relations between A_f and OCR for typical soil. The values can be used to evaluate the strength behavior at failures. According to the principle of effective stress, the porewater pressure at failure will affect the effective stress and the failure strength of soils accordingly.

Assuming the stress increases on a soil mass in the three separate directions $\Delta\sigma_1$, $\Delta\sigma_2$, and $\Delta\sigma_3$ (similar to the triaxial test), the stress increase can be divided into isotropic stress increases and unaxial stress increases, as Figure 2.7 illustrates. According to Eqs 2.14 and 2.15, the increase of porewater pressure under undrained conditions would be

$$\Delta u = B\Delta\sigma_3 + AB(\Delta\sigma_1 - \Delta\sigma_3) = B[\Delta\sigma_3 + A(\Delta\sigma_1 - \Delta\sigma_3)] \tag{2.16}$$

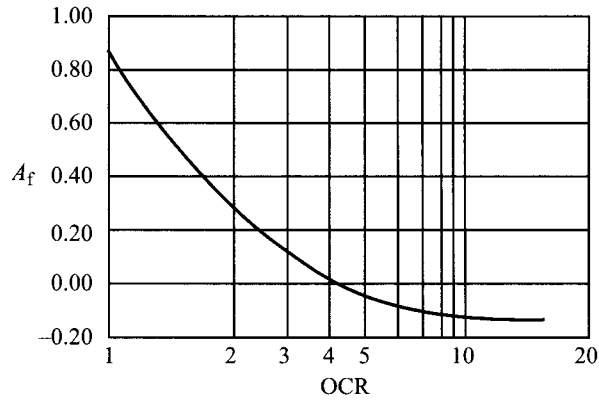

Figure 2.6 Relation between porewater pressure parameter A_f and OCR.

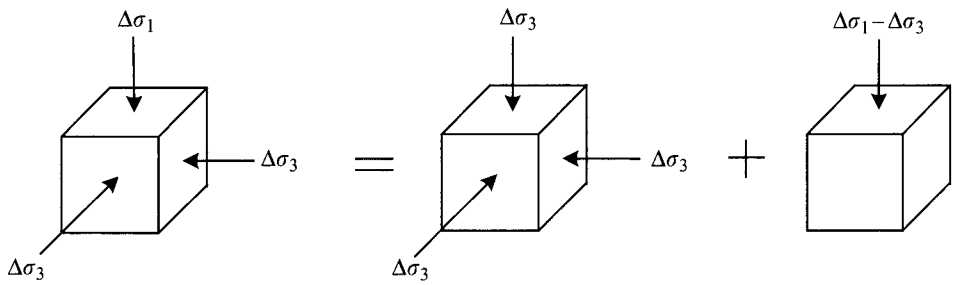

Figure 2.7 Stress increment of a soil element divided into isotropic stress increment and uniaxial stress increment.

2.6 Failure of soils

2.6.1 Mohr-Coulomb failure theory

Mohr (1900) predicts that, when the major (σ_1) and the minor (σ_3) principal stresses acting on a point in a material have a specific functional relation, the material will fail. The relation can be expressed as

$$(\sigma_1 - \sigma_3) = f(\sigma_1 + \sigma_3) \tag{2.17}$$

where f indicates the specific function, which varies with the types of material. Figure 2.8a shows a Mohr's circle depicted according to Eq. 2.17. Different combinations of σ_1 and σ_3 that engender failure will form different Mohr's circles, from which a Mohr failure envelope can be obtained, as shown in Figure 2.8b. The function which represents the Mohr failure envelope is f in Eq. 2.17, indicating that a specific function at failure exists between σ_1 and σ_3.

Coulomb (1776) suggests that the shear strength of soils can be represented as follows:

$$\tau_f = c + \sigma \tan\phi \tag{2.18}$$

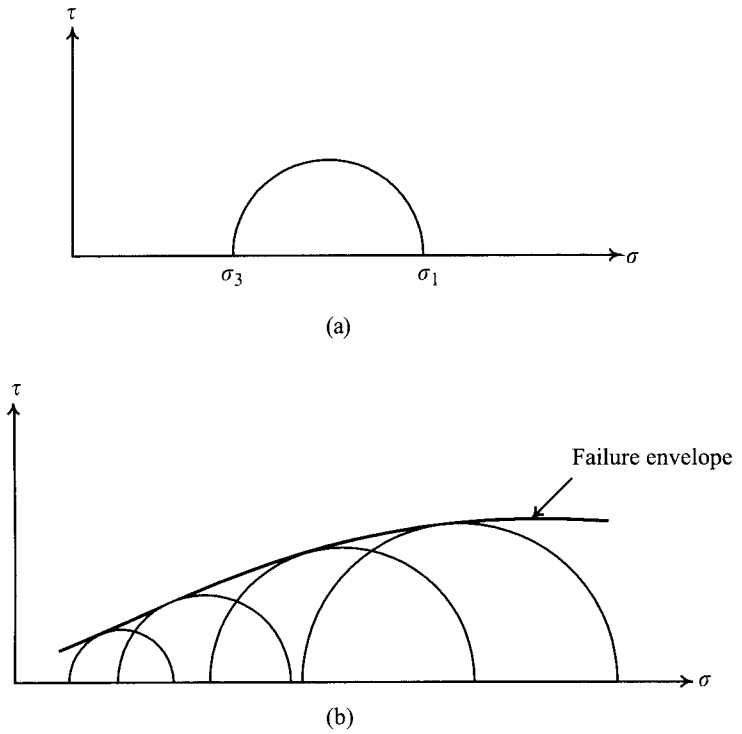

Figure 2.8 Mohr's theory: (a) Mohr's circle, (b) envelope of Mohr's circles.

where τ_f is the shear strength of soil, σ is the normal stress on the failure surface, c represents the cohesion, and ϕ the angle of internal friction. The cohesion and internal friction are also called the strength parameters of soil.

Though stress can be distinguished into total stress and effective stress, only the latter is relevant to engineering behavior (such as strength and deformation, etc.), as explained by the principle of effective stress. Thus, Eq. 2.18 should be rewritten into the following:

$$\tau_f = c' + \sigma' \tan \phi' \tag{2.19}$$

where c' and ϕ' denote the effective cohesion and the effective angle of internal friction. σ' represents the effective normal stress on the failure surface.

In soil mechanics, it is assumed that the Mohr failure envelope, as illustrated in Figure 2.8b, can be represented by the Coulomb equation, that is, Eq. 2.19. As Figure 2.9 shows, with the above assumption, according to the theory of Mohr's circles, the angle (α_f) between the failure surface and the direction of the major principal stress is

$$\alpha_f = 45° + \frac{\phi'}{2} \tag{2.20}$$

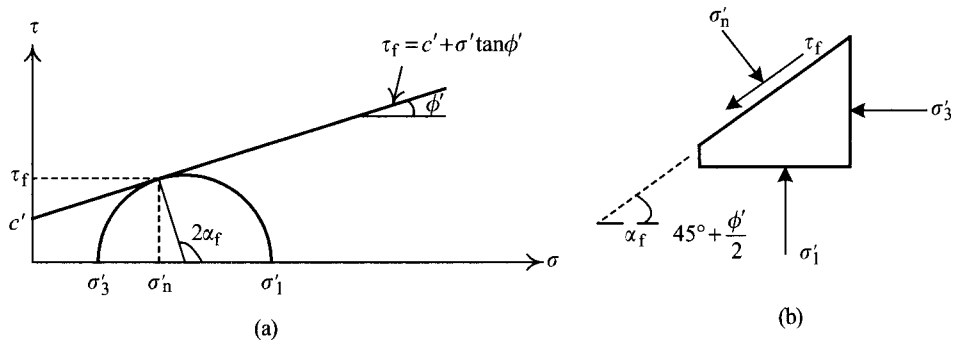

Figure 2.9 Failure angle determined by Mohr's circle: (a) Mohr's circle and its envelope, (b) stress on the failure surface.

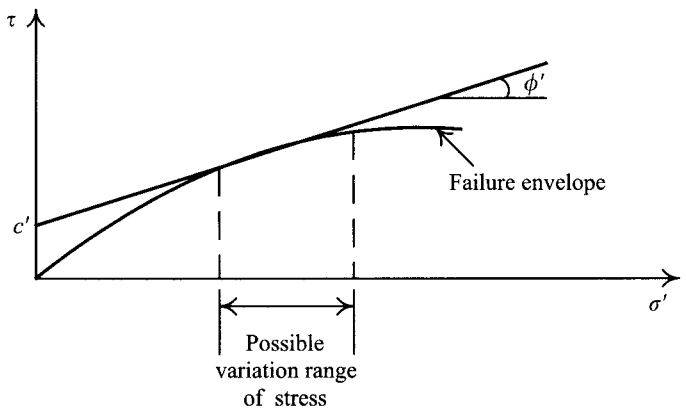

Figure 2.10 Apparent cohesion and apparent friction angle for cohesionless soils.

It should be noted that the above ϕ' is the effective friction angle because soil failure is related to the effective stress and has nothing to do with the total stress according to the principle of effective stress.

In addition to the Mohr-Coulomb failure criterion, some other commonly used criteria are von Mises, Tresca, and Drucker-Prager criteria, etc. However, many studies (e.g. Lade and Duncan, 1973) have shown that the Mohr-Coulomb failure criterion is a reliable criterion to predict soil failures. Thus, the book will adopt it as the failure criterion for soils.

For cohesive soils, the Mohr failure envelope is almost a straight line and thus one can directly derive c' and ϕ' from the Mohr-Coulomb failure criterion. On the other hand, the Mohr failure envelope for cohesionless soils is usually a curve and one has to derive the curve from regression using the Coulomb equation within the range of stress interesting to us. As shown in Figure 2.10, the thus acquired c' and ϕ' are not the true c' and ϕ' of the soil. They simply represent the parameters proper for the segment within a range of stress which is of interest to us and are designated separately as the apparent cohesion (c') and the apparent friction angle (ϕ').

Actually, there is no cohesion between particles for cohesionless soils. When calculating the lateral earth pressure using the apparent cohesion and the apparent friction angle, we may have a negative value, which means that the soil is able to bear tensile forces, that is impossible. Therefore, Duncan *et al.* (1980) proposed that Mohr failure envelopes indiscriminately pass through the origin (which means $c' = 0$) for cohesionless soils. Thus, when the principal stresses of a failure circle are σ_1' and σ_3', the corresponding effective friction angle can be derived from the following equation:

$$\phi' = \sin^{-1}\left(\frac{\sigma_1' - \sigma_3'}{\sigma_1' + \sigma_3'}\right) \tag{2.21}$$

Obviously, the effective friction angle for cohesionless soils decreases with the increase of the confining pressure. Duncan *et al.*, also found that the value of ϕ' has a linear relationship with the logarithm value of the confining pressure, as shown in Figure 2.11 and is also expressed by the following equation:

$$\phi' = \phi_0' - \Delta\phi' \log_{10}\left(\frac{\sigma_3'}{P_a}\right) \tag{2.22}$$

where

P_a = the atmospheric pressure, $P_a = 10.33\ \text{t/m}^2 = 101.34\ \text{kN/m}^2$,
ϕ_0' = effective angle of internal friction when $\sigma_3' = P_a$,
$\Delta\phi'$ = slope of the curve in Figure 2.11, whose value is the decrease of ϕ' when σ_3' increases 10 times.

2.6.2 Some commonly used laboratory shear strength tests

There are many laboratory tests to obtain the shear strength of soils. Among them, the most commonly used are the triaxial test, the direct shear test, and the direct simple shear test. This section will introduce the methods and characteristics of these three tests.

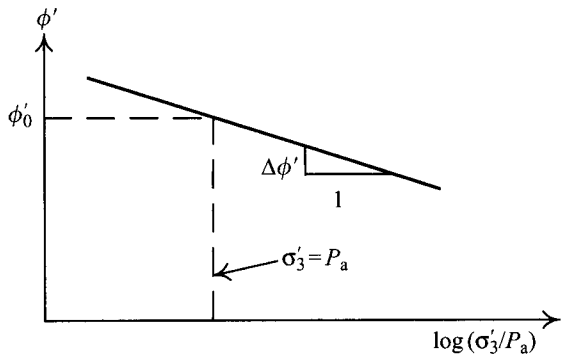

Figure 2.11 Relation between internal fiction angle and confining pressure for the cohesionless soil.

2.6.2.1 *Triaxial test*

Figure 2.12 illustrates the configuration of a triaxial apparatus. As is shown, the cylindrical soil specimen is enveloped by a rubber membrane to control the drainage conditions. The upper cap and the pedestal of the specimen are connected to the tubes **ab** and **cd** in order to measure the volume change of the specimen during the drained test. They can also be used to measure the porewater pressure during the undrained test. The triaxial test is carried out in two stages. At the first stage, add cell pressure onto the specimen. At the second stage, add axial pressure, under which shear stress will begin to act in the specimen, until the specimen fails. By controlling the cell pressure and the axial pressure, the stress conditions can be made $\sigma_2 = \sigma_3 = \sigma_c$ or $\sigma_1 = \sigma_2 = \sigma_c$ and thus many types of stress path tests can be carried out (see Section 2.6.3).

There are at least three types of triaxial tests, depending on the drainage conditions: the consolidated drained (CD) test, the consolidated undrained (CU) test, and the unconsolidated undrained (UU) test. The load and drainage conditions of the CD, CU, and UU tests are shown in Figure 2.13. The above CD and CU tests usually go through a consolidation stage under isotropic compression, that is, the consolidating stresses in each direction at the first stage are made equal (i.e. $\sigma_1 = \sigma_2 = \sigma_3$). Thus, the CD and CU tests are also designated as CID and CIU tests. Besides, to simulate the K_0 consolidation condition of the in situ soil before shearing, we sometimes have specimens consolidated under the K_0 condition and then carry out the shear test. Thus, the CD and CU tests are also called CK_0D and CK_0U tests. Concerning the characteristics and applications of the CD (CK_0D) and CU (CK_0U) tests, please refer to Sections 2.7 and 2.8.

Theoretically, the triaxial test is applicable to any kind of soil. However, a tube sample has to be trimmed before putting it to the triaxial test. With no cohesion, however, trimming is impossible for sand. Therefore, triaxial tests are not suitable for the strength testing of sand unless a special testing method is adopted. In addition, the traditional triaxial cell is too small for gravelly soil and a larger-size triaxial cell is usually adopted.

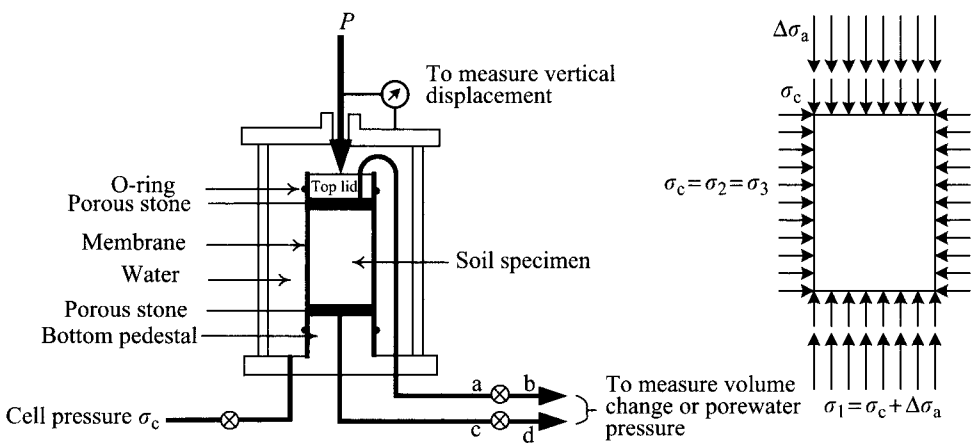

Figure 2.12 Triaxial test apparatus.

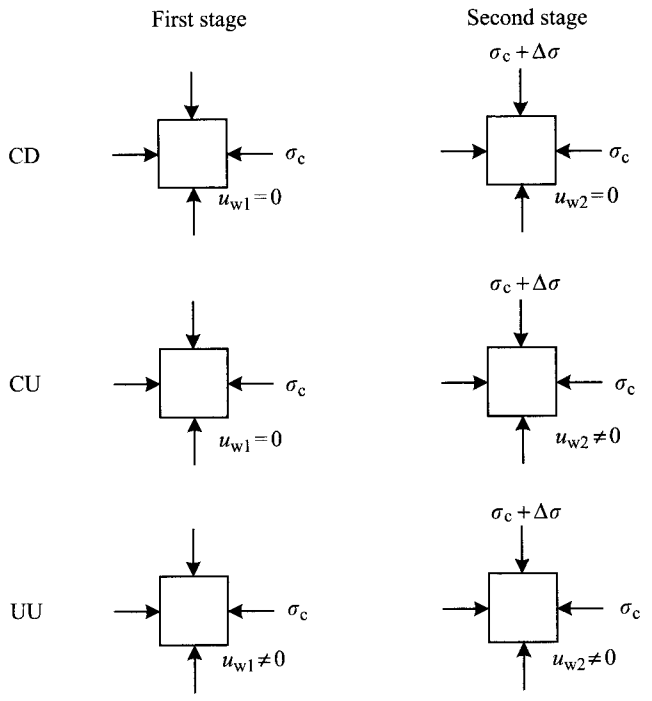

Figure 2.13 Loading patterns and drainage conditions of the CD, CU, and UU tests (u_{w1} and u_{w2} are excess porewater pressures).

2.6.2.2 *Direct shear test*

Figure 2.14 is the diagram of the basic configuration of a direct shear apparatus. Basically, inside the direct shear apparatus is a shear box, divided horizontally into two halves, to contain the soil specimen. The vertical force acts on the top cap of the specimen. Usually, the lower half of the shear box is fixed while thrust or tensile force acts on the upper half and the specimen inside is sheared. When shearing, we can measure the movement, the shear stress and the change of the thickness (or volume) of the specimen.

As shown in Figure 2.14, because of the high rigidity of the shear box, the lateral deformation of the soil specimen in the box under the action of normal and shear stresses is not produced. Thus, the stress conditions when shearing can be assumed as the plane strain condition.

Generally speaking, the direct shear test has the following weaknesses:

1 The soil is forced to shear on the horizontal plane, which is not always the weakest plane of the soil.
2 The uneven distribution of shear stress on the failure surface makes the stress near the edges greater than that in the center.
3 The soil specimen can not be encased with a rubber membrane and thus it is impossible to control the drainage condition when shearing.

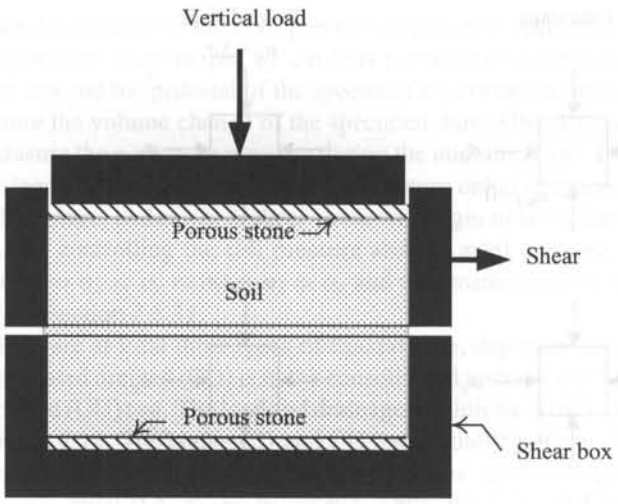

Figure 2.14 Direct shear test apparatus.

However, since soil specimens can be directly pressed into the shear box through a thin tube, to test those soils which do not have any cohesion, the direct shear test can be taken advantage of. Normally, the drained test (i.e. the CD test) is applied to sand to obtain the strength parameters (c', ϕ') because of sand's high permeability. Therefore, it is still useful to obtain the strength parameters of sand using the direct shear test though the test cannot control the draining condition.

Theoretically, we can perform the CD, CU, and UU tests using the direct shear test for clayey soils by controlling the testing speed. According to the principle of the CD test, it is workable to carry out the CD test on clayey soils using the direct shear test. However, the procedures are not simpler than those of the triaxial test and therefore the latter is more often adopted. Since the direct shear test cannot control the drainage condition and cannot measure the excess porewater pressure during the process of CU testing, the testing results are meaningless (please refer to Section 2.7.1), even though CU tests can be carried out to obtain the total strength parameters by manipulating the test speed (please refer to Section 2.8.3). What is more, as will be explained in Section 2.8.1, the undrained shear strength of a clayey soil is the shear stress on the failure surface by definition. The failure surface of the direct shear test is forced to be the horizontal plane. Thus, the results of the UU test on clayey soils from the direct shear test are questionable. Besides, the inability to control drainage of the direct shear test makes it a less favored choice for most people conducting the UU test on clayey soils.

2.6.2.3 *Direct simple shear test*

Considering the many weaknesses of the direct shear test, especially the inability for it to be applied to clayey soils, the direct simple shear apparatus was developed by modifying the direct shear apparatus as shown in Figure 2.15. The specimen of the direct simple apparatus can be either cylindrical or cubic, which is confined by a wire-reinforced rubber membrane

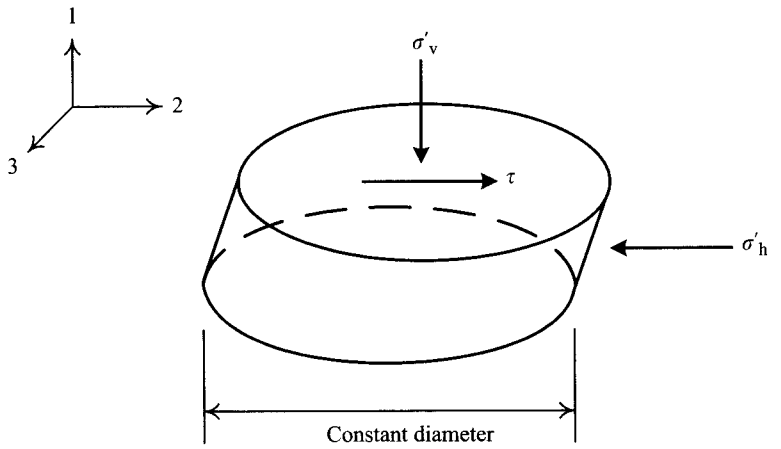

Before shearing $\sigma'_2 = \sigma'_3 = K_0\sigma'_v$

During shearing $\sigma'_2 \neq K_0\sigma'_v$ $\sigma'_3 = K_0\sigma'_v$

Figure 2.15 Direct simple shear test apparatus.

to prevent it from lateral deformation. Shear acts on the top of the specimen and a pure shear condition is thus generated.

Without lateral deformation produced, soil specimens in direct shear simple tests are subject to pure shear stress and are all in the state of plane strain. The direct simple shear test overcomes most of the weaknesses of the direct shear test: the failure surface being forced to be a horizontal plane with the inability to control drainage. The problem of the uneven distribution of stresses is also basically solved. Thus, the direct simple shear test is widely adopted in Europe and America. For further discussion of the testing results, please refer to Section 2.8.3.

2.6.3 *Stress paths*

Conventional triaxial CD and CU tests are isotropically consolidated and axially loaded as discussed in Section 2.6.2. Since the soil strength is related to the way it is loaded, in order to find out the in situ shear strengths of soils, the ways of loading in strength tests should simulate the in situ loading conditions. The methods of loading are not necessarily axial-directed. This is the so called stress path test. At any stage during the stress path test, the stress state of a point in the soil specimen can be expressed by the following equation:

$$q = \frac{\sigma_v - \sigma_h}{2} \tag{2.23}$$

$$p = \frac{\sigma_v + \sigma_h}{2} \tag{2.24}$$

where σ_v is the total vertical stresses and σ_h is the total horizontal stresses.

Depict every p and q at each stage on the p–q diagram, which denotes a serial process of shearing. The route of shearing is designated as the total stress path (TSP). Eqs 2.23 and 2.24 can also be rewritten in terms of the effective stress:

$$q = \frac{\sigma'_v - \sigma'_h}{2} \tag{2.25}$$

$$p' = \frac{\sigma'_v + \sigma'_h}{2} \tag{2.26}$$

Plot the values of p' and q at each stage and we have the route which is designated as the effective stress path (ESP). The Mohr failure envelope (which is a line tangent to the Mohr circles) can be transformed into the p–q diagram, which is called K_f line (Figure 2.16). Comparing the geometric relationship between the K_f line and the Mohr failure envelope, there exists the following relationship:

$$\sin\phi = \tan\psi \tag{2.27}$$

$$c = \frac{a}{\cos\phi} \tag{2.28}$$

where a and ψ are respectively the intercept on the q-axis and the angle of the K_f line with respect to the horizontal as shown in Figure 2.16.

Depict the TSP and the ESP for an undrained test onto the same p–q diagram and the changes of the porewater pressure during the test can be easily observed, which will help one to understand the strength behavior of soils. Concerning the TSP and ESP of the normally consolidated and overconsolidated soils under the drained or undrained conditions, see Section 2.9.

The stress path test can be carried out using special testing apparatus (e.g. the direct simple shear testing apparatus) or by increasing or decreasing the horizontal (confining pressure) and the vertical pressures in the triaxial test. Generally speaking, the commonly used triaxial stress path tests include the triaxial axial compression (AC), the axial extension (AE), the lateral compression (LC), and the lateral extension (LE). The loading methods for these tests are as follows:

AC tests, σ_v increases while σ_h remains the same.
LE tests, σ_v remains the same while σ_h decreases.

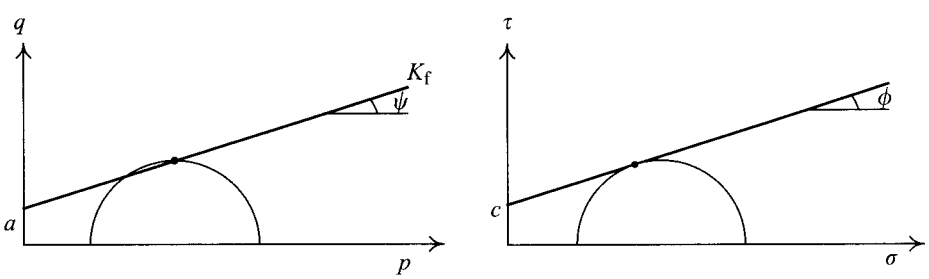

Figure 2.16 K_f-line and Mohr-Coulomb's failure envelope.

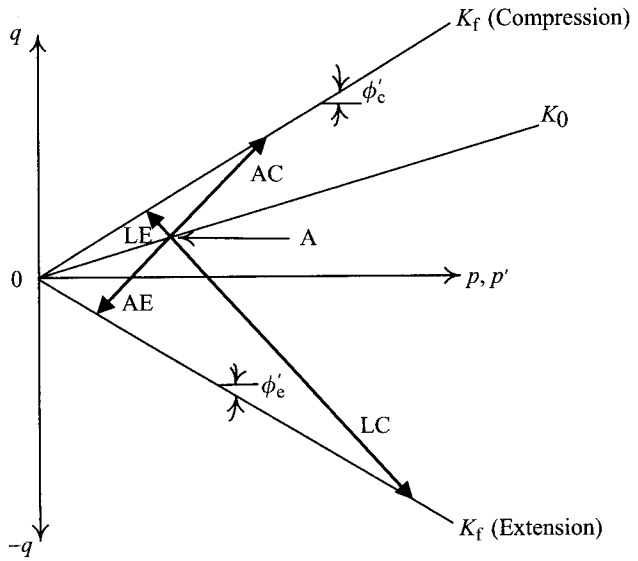

Figure 2.17 Drained stress paths for normally consolidated soils (or total stress paths).

AE tests, σ_v decreases while σ_h remains the same.
LC tests, σ_v remains the same while σ_h increases.

If the test has to simulate K_0-consolidated condition of the in situ soils, we usually make the specimen consolidated under K_0 condition and then load the deviator stress onto it. Figure 2.17 illustrates the total stress paths of the K_0-consolidated specimens for AC, AE, LC, and LE tests.

Ou *et al.* (1995) carried out a series of triaxial stress path tests on the Taipei silty clay. The stress paths included the four paths: AC, AE, LE, and LC. The test types included CD and CU tests. We found from the results that the effective friction angles are the same despite the differences in stress paths and drainage conditions as long as the deformation directions of the specimens are the same. For example, the effective friction angles of the AC and LE tests are the same while those of the AE and LC tests are equal also. Table 2.10 provides the results of the CK_0U tests under the plane strain condition on four different soils by Ladd *et al.* (1977). Their study shows that the effective friction angle obtained from axial compression tests (ϕ'_c) is larger than that from the axial extension test (ϕ'_e). However, the differences lessen with the increase of plasticity of soils.

2.7 Drained shear strength of soils

If the interior porewater is drained from soil during the shear test, excess porewater pressure will not be generated. Thus, when the soil fails, the shear stress acting on the failure surface is called the drained shear strength. Since the excess porewater pressure inside the soil is zero, the effective stress acting on the soil specimen equals the total stress and we can easily derive the shear stress on the failure surface from Mohr's circle as shown in Figure 2.9. Thus,

Table 2.10 Effective friction angle of undisturbed clay from CK_0U compression test and extension test (Ladd *et al.*, 1977)

Soil type	LL	*Compression test*		*Extension test*		*Reference*
	PI	ε_f(%)	ϕ'_c (deg)	ε_f(%)	ϕ'_e (deg)	
Undisturbed sensitive Haney clay	44 18	0.4	25.2	10.5	34.3	Vaid and Campanella (1974)
Reconstituted Boston blue clay	41 21	0.4	29	4.3	≤40	Ladd *et al.* (1971)
Undisturbed AGS CH clay	71 40	1.0	36.5	8.2	36.5	Unpublished data from University of British Columbia (1975)
San Francisco bay mud	88 45	3.6	38	10.2	35	Duncan and Seed (1966)

ε_f: Failure strain.

Table 2.11 Typical values of effective cohesion and effective angle of friction for some urban soils

Soil type	c' (kN/m^2)	ϕ' (degree)
San Francisco bay mud (CH)	0	32.5–35[1]
Boston blue clay (CL)	0	32–34[1]
Chicago silty clay (CL)	0	24–29
London clay (CH)	10	25
Mexico City clay (MH)	0	34–47
Bangkok clay (CH)	—	—
Singapore marine clay (CH)	0	22–25
Shanghai clay (CL)	0	30–35
Taipei silty clay (CL)	0	29–32[1]
Taipei silty sand	0	32.5–34

Note
1 Parameters at normally consolidated state.

concerning the characteristics of the drained shear strength, it is the effective cohesion (c') and the effective friction angle (ϕ') that are under consideration.

As discussed in Section 2.6.2, for undisturbed sands, c' and ϕ' are usually obtained from the direct shear test. Though completely undisturbed samples of sands are not easily obtained, the c' and ϕ', which are basically related to the friction properties of material, are relatively less affected by the disturbance of samples. For gravel soil, it is not suitable to obtain the parameters of strength from a laboratory test. Thus, the in situ direct shear test is often used instead. As discussed in Section 2.6.1, the parameter of strength ϕ' of the granular soil decreases with the increase of confining pressure. Thus, it follows that the strength should be represented in terms of the apparent cohesion and the apparent friction angle, or be expressed in ϕ'_0 and $\Delta\phi'$ as shown in Eq. 2.22. Table 2.11 lists c', ϕ' of sandy soils of some urban areas.

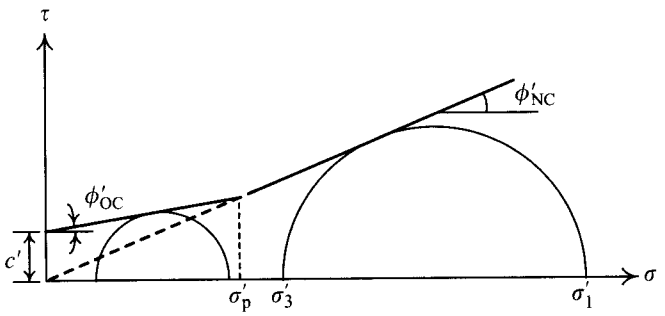

Figure 2.18 Failure envelopes for the overconsolidated soil and normally consolidated soil.

Furthermore, as discussed in Section 2.6.2, the direct shear test is not suitable to obtain c' and ϕ' of undisturbed clayey soils. The triaxial CD or CU test is usually adopted. Basically, since the triaxial CD test is directly related to the properties of friction among particles of clay, it can obtain c' and ϕ' of soils directly. As to the triaxial CU test, a type of undrained shear test, its results are also affected by the effective stress acting on the soils. If the porewater pressure is able to be measured during the test, the effective stress on soil can be known. The testing results can thus be expressed in terms of the effective stress and c' and ϕ' are thus obtained. Since the effective stress represents the intergranular contact stress among particles, the results of the triaxial CU test conducted following the above principles are also related to the properties of intergranular friction and thus the c', ϕ' should not be different from those obtained from the CD test.

The c' of normally consolidated soils equals 0. The c' of overconsolidated soils, having been compressed, does not equal 0. However, when the consolidation pressure or confining pressure in the CD/CU test is greater than the pre-consolidation pressure of the soil, the consolidation pressure or confining pressure becomes the maximum stress which has acted on the soil. Under such conditions, the soil reverts to the normal consolidation and $c' = 0$ as shown in Figure 2.18. The typical c' and ϕ' of clays for some urban areas are also listed in Table 2.11.

2.8 Undrained shear strength of saturated cohesive soils

2.8.1 *Concepts of undrained shear strength*

Let the interior porewater not be drained from soil during the shear strength test. Excess porewater pressure is thus generated. Therefore, when the soil comes to failure, the shear stress acting on the failure surface is called the undrained shear strength, as illustrated by τ_f in Figure 2.19a. The circle B in Figure 2.19c is the corresponding total stress Mohr's circle.

According to the principle of effective stress, in the undrained state, soils fail only when the effective stress Mohr's circle for the soil mass is tangent to the effective failure envelope and it has nothing to do with the total stress. As illustrated in Figure 2.19c, circle A is the effective Mohr's circle tangent to the effective failure envelope. Due to the inability of the

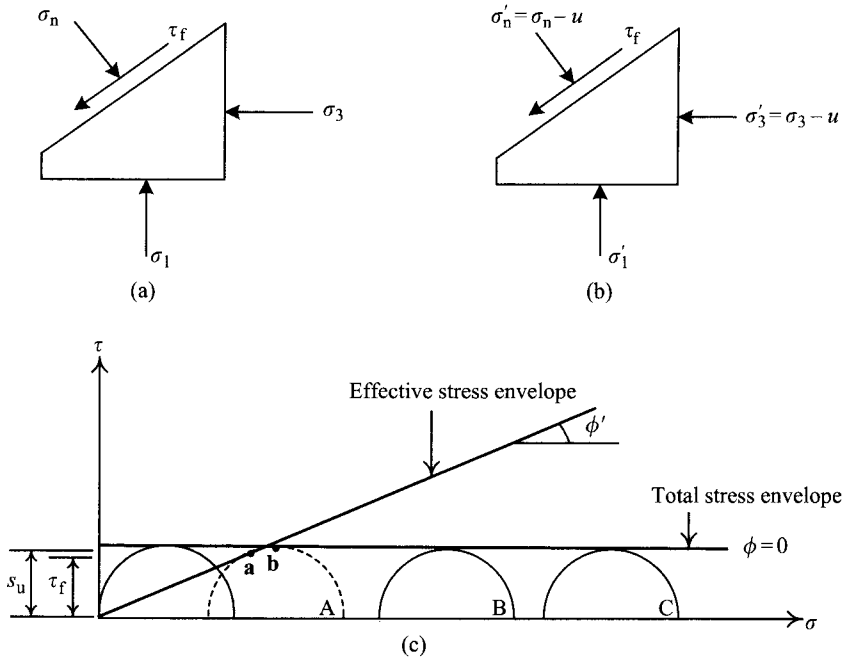

Figure 2.19 Basic principle of undrained shear strength.

porewater in soils to bear the shear stress, the shear stress on the failure plane in the effective stress state equals that in the total stress state, as shown by τ_f in Figure 2.19b. Since τ_f is identical, the size of the Mohr's circle of the effective stress should be the same as that of the total stress. Known from Figure 2.19c, the shear stress on the failure plane (point **a** in Figure 2.19c) can be expressed in the following form:

$$\tau_f = \frac{\sigma'_1 - \sigma'_3}{2} \cos\phi' = \frac{\sigma_1 - \sigma_3}{2} \cos\phi' \tag{2.29}$$

where τ_f denotes the shear stress on the failure plane, which can be defined as the undrained shear strength of the soil.

Observing the nearness of the top point (**b** in Figure 2.19c) to the tangent point (**a** in Figure 2.19c) of the Mohr's circle and on the other hand considering the great trouble needed to obtain the c' and ϕ' of a clay through tests necessary for the calculation of its undrained shear strength using Eq. 2.29, the value of the shear strength at the top point of the Mohr's circle is adopted to calculate the undrained shear strength of soils as follows:

$$s_u = \frac{\sigma_1 - \sigma_3}{2} \tag{2.30}$$

Though Eq. 2.30 gives some error in the computation of the undrained shear strength of soils, it has the merit of leaving out c' and ϕ' and is therefore frequently used in engineering design.

From the above discussions, we know that the principle of effective stress should be applied to the undrained shear strength of clayey soils, too. That is to say, the shear strength of soils, though in the undrained state, relates only to the effective stress acting on them and has nothing to do with the total stress. As far as the clayey soil is concerned, the void ratio or water content (in the saturated state) is the best representative of the effective stress of clayey soils. To any specific normally consolidated clayey soil, its $e - \log p$ or $w - \log p$ relationship is unique, and the same with the results of the consolidation test (see the line segment ABC in Figure 2.2).

Put a saturated clay to a triaxial UU test. At the first stage of loading, the soil in the undrained (i.e. unconsolidated) state, the void ratio or water content does not change, which means the effective stress acting on the soil at the first stage remains unchanged. Actually, the first-stage load acts totally on the porewater and the soil solids are not stressed. The reader is recommended to prove that the effective stress at this stage remains unchanged using Skempton's porewater pressure parameters.

During the second-stage loading, shear stress begins to act in the soil. When the soil reaches failure, the shear stress on the failure surface is called the (undrained) shear strength of the soil, whose magnitude is determined by the value of the effective stress or the void ratio after the first-stage loading. The reason is that the undrained shear strength is only related to the effective stress on it. The Mohr's circles of the effective stress and the total stress of the test results are shown as circles A and B in Figure 2.19c. Let another identical soil specimen (i.e. that with the same void ratio) be tested in the UU test. Have the confining pressure greater than that of circle B and conduct the undrained test. As discussed, though the confining pressure has increased now, the before-shear effective stress remains the same and the shear strength of the soil should be the same. Thus, the effective stress Mohr's circle is circle A as before and the size of the total stress Mohr's circle (circle C) does not change.

Since the slope of the total stress failure envelope (ϕ) equals 0, as shown in Figure 2.19c, considering the analytical expediency, the undrained shear strength is sometimes called s_u, $\phi = 0$ concept or method where s_u can be derived from Eq. 2.30.

However, there is a pitfall which needs to be explicated. Though the total stress failure envelope can be represented by Eq. 2.18, it seems workable to substitute $\phi = 0$ into the equation to obtain the undrained shear strength, which will be the same as that computed by Eq. 2.30. The procedure is wrong according to the principle of effective stress. Eq. 2.18 should not be used to compute the undrained shear strength.

2.8.2 Characteristics of undrained shear strength

The undrained shear strength of soil has the following characteristics:

1 Strength-depth relation: As discussed in the Section 2.8.1, the undrained shear strength of the soil relates only to the effective stress acting on it and has nothing to do with the total stress. For a normally consolidated clayey deposit, the effective stress increases with the increase of the depth. As a result, the undrained shear strength increases with the increase of the depth. However, for clayey soils near the ground surface, frequently influenced by the change of groundwater level, the desiccation, and the capillarity, the soil normally exhibits overconsolidated behavior. The void ratio of overconsolidated soil, having been compressed, is smaller than that of normally consolidated soil under the same effective stress. Thus, the undrained shear strength of overconsolidated soil is greater than that of normally consolidated

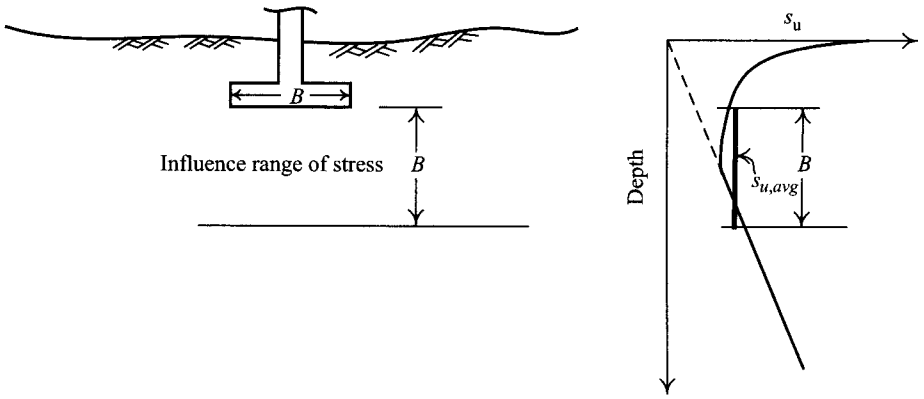

Figure 2.20 Profile of undrained shear strength and bearing capacity of footings.

soil under the same effective stress. Figure 2.20 displays the typical relationship between the undrained shear strength and the depth.

The average value of the undrained shear strengths within the range of the stress influence is often used for analysis. As shown in Figure 2.20, to analyze the bearing capacity of an individual footing with a width of B, the average undrained shear strength ($s_{u,avg}$) within the range equal to the foundation width from the foundation bottom is used to compute the bearing capacity, using Terzaghi's bearing capacity equation.

The variation of excess porewater pressure in underconsolidated soil is usually very uncertain. As a result, the effective stress may not increase with the increase of the depth. That is, the undrained shear strength of soil does not necessarily increase with the depth, either. Since the effective stress in underconsolidated clay is very low, the undrained shear strength of underconsolidated clay might also be very small and often exhibit constant value, not increasing with depth.

2 *Influence of sampling disturbance*: According to many studies (Ladd and Lambe, 1963; Seed *et al.*, 1964), the undrained shear strength of clay is particularly affected by sampling disturbance. The main source of disturbance is the relief of the total stress during the sampling process, which brings about a negative value of the porewater pressure within soil (due to the undrained condition, as illustrated in Example 2.4). The absolute value of the negative porewater pressure might decrease because of vibration or draining and decreases, in turn, the effective stress. The undrained shear strength obtained by the test might be smaller than the true in situ value.

3 *Anisotropic behavior*: Under an embankment, as shown in Figure 2.21, each point on the failure surface is subject to a different stress path. The directions of the major principal stress at points **a**, **b**, and **c**, as shown in Figure 2.21, are different. Thus, when conducting laboratory tests, letting the directions of loading be consistent with those of the major principal stress at points **a**, **b**, and **c** respectively, the resulting undrained shear strengths will diverge accordingly. Since the conventional boring and loading directions are both vertical, the conventional triaxial test (vertical sampling and vertical loading) can be represented by point **a** in Figure 2.21, where the obtained undrained shear strength is greater than those obtained by other stress path tests (**b** and **c** in Figure 2.21).

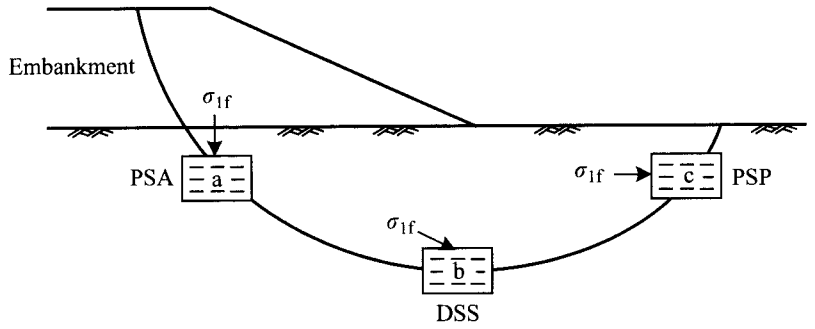

Figure 2.21 Failure of soft soil under an embankment.

4 Strain rate dependent: According to many studies (e.g. Bjerrum, 1971), when shearing in the undrained state, the slower the strain rate, the smaller is the undrained shear strength. The reason is that, with a low strain rate, creep is produced within soil and the excess pore-water pressure increases, which in turn decreases the undrained shear strength. Because the laboratory triaxial tests (UU and CU tests) have high strain rates, the specimens usually fail within one hour. However, the in situ undrained shearing strain rate at failure (as shown in Figure 2.21) is often much smaller than that applied in laboratory tests. Thus, the differences between the strain rates in the field and those in laboratory tests should be considered.

5 Normalized soil behavior: According to Ladd and Foote (1974), saturated clay with the same overconsolidation ratio may have similar stress-strain behavior though the effective stresses acting on the soil, which refers to the consolidated stress at the first loading stage in a CU test or the effective overburden stress on the specimen before sampling in a UU test, are different. If we normalize this stress-strain relation with respect to the effective stress, the normalized stress-strain relation will fall on a narrow band, like a unique stress-strain relation, which is often called the normalized soil behavior. Ladd and Foote also found that clays usually have the normalized behavior, except for those with a high degree of structure, such as quick clays or naturally cemented clays.

Figure 2.22a illustrates the normalized stress-strain behavior of Boston blue clay by the DSSCK$_0$U test. The strength and stiffness of clay with the same overconsolidation ratio can be represented by the normalized parameters, such as the normalized undrained shear strength (s_u/σ') and the normalized stiffness (E_u/σ'), etc., where σ' is the average principal stress (i.e. $\sigma' = (\sigma'_1 + \sigma'_2 + \sigma'_3)/3$) or the effective overburden pressure (σ'_v).

6 Plane strain: Basically, the failure pattern of the soil under an embankment, as shown in Figure 2.21, is in the plane strain condition. Thus, the stress states at point **a** are σ'_1, $\sigma'_2 (= K_0\sigma'_1)$, and σ'_3 while those in the conventional triaxial test are σ'_1, $\sigma'_2 (= \sigma'_3)$, and σ'_3. According to Ladd and Foote (1974), the undrained shear strength obtained from a triaxial test is smaller than that from a plane strain test under the same conditions.

7 Undrained behavior of unsaturated soil: The confining pressure on unsaturated soil will increase the effective stress of the soil and its strength accordingly. The larger the confining pressure, the larger the strength. When it reaches a certain magnitude, the specimen will approach to full saturation and its strength behavior thus exhibits $\phi = 0$. Figure 2.23 shows the results of the triaxial UU test on unsaturated soil.

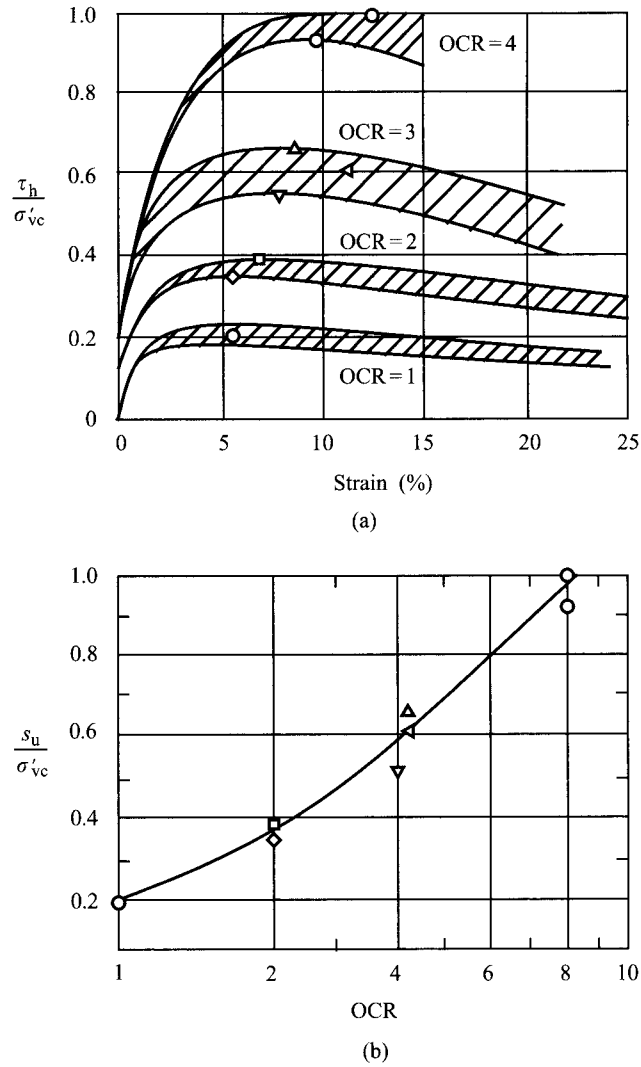

Figure 2.22 Normalized behavior of normally consolidated and overconsolidated Boston blue clay (Ladd and Foote, 1974) (τ_h = shear stress, σ'_{vc} = vertical consolidation stress, s_u = undrained shear strength).

2.8.3 Methods to obtain undrained shear strength

The undrained shear strength of a saturated soil can be determined by the following methods:

2.8.3.1 Triaxial UU test

Figure 2.24a illustrates a soil specimen sampled from a clayey layer located at a depth of z. With the in situ effective stresses σ'_v and σ'_h, the void ratio at the point is e. Sampled with a thin tube, the total stress on the sample is totally relieved, as shown in Figure 2.24b. Since

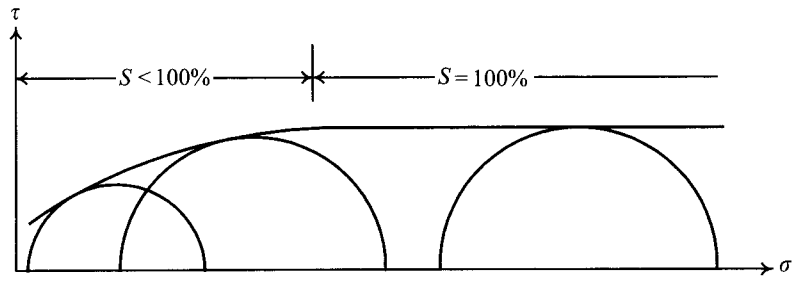

Figure 2.23 UU triaxial tests on saturated and unsaturated clay.

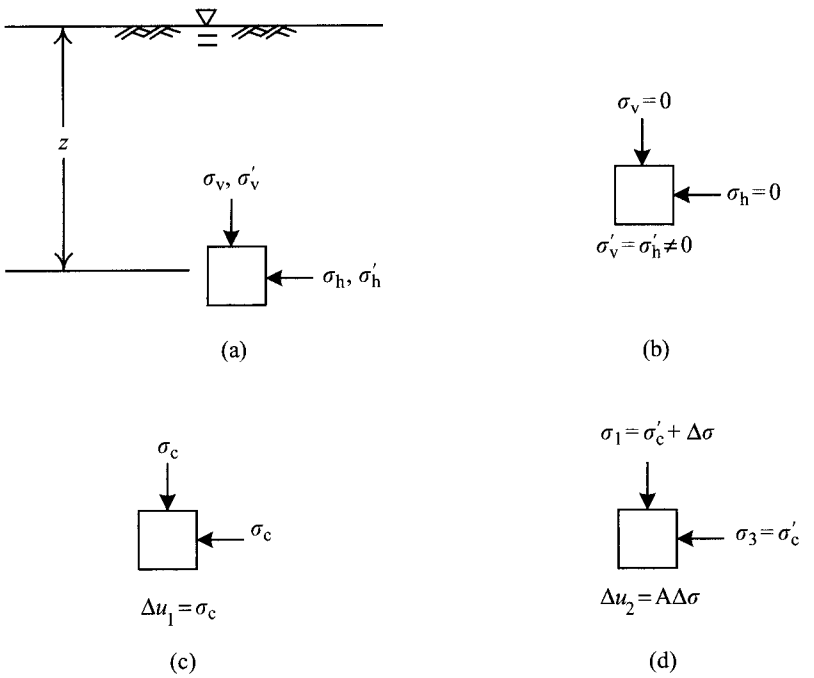

Figure 2.24 Undrained shear strength of saturated clay obtained from triaxial UU tests: (a) state of stresses at a depth of z, (b) state of stresses of the soil specimen after sampling, (c) loading at the first stage of the triaxial UU test (unconsolidated stage), (d) loading at the second stage of the triaxial UU test (undrained shear stage).

the voids in clay are extremely small, the thin-tube sampled soil is normally in the undrained state and no volume change will be produced. Thus, the void ratio or water content remains unchanged, so, it follows that the effective stress stays the same and its value is about equal to that of the in situ condition.

While adding the confining pressure to the soil, at the first stage, in the triaxial UU test, the confining pressure acts solely on the porewater because the soil is in the saturated undrained state. The incremental porewater pressure equals the confining pressure, that is, $\Delta u = \sigma_c$ (see Figure 2.24c). Thus, the increment of the effective stress is nil and the effective stress

on the soil stays almost the same as that in the in situ state. At the second stage, where the axial stress begins to act, since the effective stress on the soil sample before axial loading is close to that of the in situ soil, the obtained strength can therefore represent the undrained shear strength of the in situ soil. The changing of the porewater pressure and the effective stress due to sampling is as illustrated in Example 2.4.

Theoretically, to obtain the in situ undrained shear strength by way of lab tests, a completely undisturbed soil sample is necessary. Besides, the stress condition, the stress path and the strain rate of the in situ soil must be simulated in the lab tests. However, it is impossible that the soil not be disturbed during sampling and the results of the triaxial UU test are largely affected by the sampling disturbance. What's more, the soil sample is subjected to vertical loading and the triaxial UU test has a larger strain rate than that of the in situ soil at failure. With so much difference, how can the result of the triaxial UU test represent the undrained shear strength of the in situ soil? The reason is that the discrepancy can be made up for by self-compensation. The higher strain rate and the vertical loading of the triaxial UU test bring about a larger undrained shear strength. On the other hand, the triaxial stress state and the sampling disturbance lead to a lower value. The two groups of factors compensate for each other in such a way that the test result can suitably represent the in situ soil.

The unconfined compression test (UC test), also called the uniaxial test, is a special triaxial UU test with no confining pressure. As shown in Figure 2.19, the Mohr's circle of the effective stress obtained from the UC test on a saturated soil specimen is identical with that obtained from the triaxial UU test as long as the specimens have the same effective stress (or void ratio). Without being held by confining pressure, the UC test specimen is capable of standing by itself because a negative porewater pressure is generated in the specimen, which renders the effective stress on the specimen equivalent to that of the in situ soil. However, if the specimen has been disturbed, or its pores are relatively large, or a thin layer of pervious soil exists inside the specimen or there are fine cracks in the specimen, the negative porewater would dissipate, which in turn reduces the effective stress. Moreover, because the specimen is not restrained by the confining pressure, the undrained shear strength obtained from the unconfined compression test tends to be smaller.

The self-compensation effect of the triaxial UU test renders the obtained undrained shear strength capable of representing the in situ undrained shear strength as discussed above. Nevertheless, the effect is not always reliable: the extra amount does not necessarily equal the lowered amount. It counts on either the testing or sampling quality or both. Therefore, Ladd and Foote (1974) recommended adopting the CU test by the Stress History and Normalized Soil Engineering Properties (SHANSEP) approach.

2.8.3.2 *CU test*

The triaxial CU test produces a series of total stress Mohr's circles, which is able to form a failure envelope whose intercept on the y-axis c_T and slope ϕ_T can be determined, as shown in Figure 2.25. As discussed earlier, the Mohr-Coulomb equation represents only the effective failure envelope. If we substitute c_T and ϕ_T into Eq. 2.18, an erroneous result will follow.

The shear stress on the failure surface derived from the triaxial CU test or the shear stress at the apex of the effective Mohr's circle is called the undrained shear strength, as shown by point **a** or **b** in Figure 2.19c. Since the triaxial CU test undergoes consolidation process, the undrained shear strength relates more to the consolidation pressure of the test than the effective overburden pressure of in situ soil. If the consolidation pressure is greater than

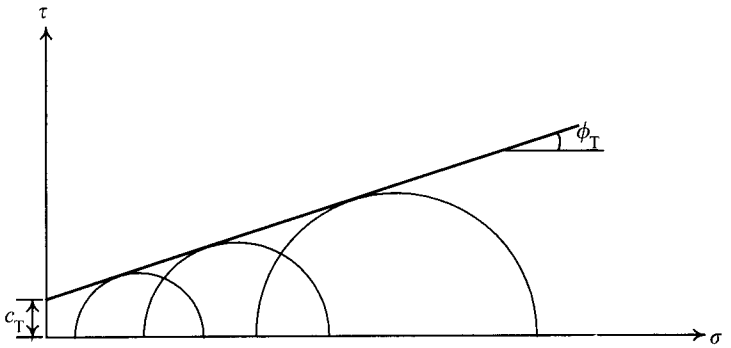

Figure 2.25 Total stress Mohr's circles and total stress envelope from the CU test.

the effective overburden pressure, it follows that the undrained shear strength relates only to the consolidation pressure and no longer correlates with the effective overburden pressure of in situ soil. Besides, whether the CU test can represent the undrained shear strength of the in situ soil depends on whether the testing can fully simulate the in situ stressed condition. The same as the UU triaxial test discussed earlier, the CU test has some problems to be resolved: the sampling disturbance, the rate of strain, the plane strain, and the stress path (i.e. the anisotropy of strength) etc.

Generally speaking, sampling disturbance can be eliminated either by recompression (Bjerrum, 1973) or the SHANSEP approach (Ladd and Foote, 1974). The former is to consolidate the specimen as close as possible to the in situ consolidation state before putting it to a shear test. It is mainly applied to structural soils (such as quick clays or cemented clays) or soil with high sensibility. The latter is applied to normalized soils, as will be discussed later. The strain rate of the CU test should be capable of simulating the in situ condition. The rate of strain can be determined by referring to the case histories before conducting the CU test. If the soil failure exhibits the characteristics of plane strain and strength anisotropy (e.g. the arc failure surface under the embankment in Figure 2.21), the CU test should simulate the condition of plane strain and the variation of strength along the failure surface.

Table 2.12 provides the values of the undrained shear strength obtained from the CU stress path test on normally consolidated Boston blue clay according to Ladd and Foote's study (1974). The plane strain axial compression test (PSA) results in the largest strength. The AC triaxial test (TC) results, though a little smaller, are close to the PSA test. The triaxial extension test (TE) yields the smallest strength. The ratio of the strength value from the plane strain lateral compression test (PSP) to that from TE test is about 1.2. The strength obtained from the direct simple shear test (DSS), a type of plane strain test, is about the average of those of PSA and PSP tests. Though different at each point on the failure surface under the embankment, as shown in Figure 2.21, the strength obtained by DSS test can generally represent the average strength on the failure surface. Thus, though sometimes data from a DSS test are not available, they can be obliquely derived from the above descriptions of their relations among TC, PSA, TE, and PSP tests.

As shown in Figure 2.21, the failure modes along the failure surface under the embankment include at least three modes: the PSA, the DSS, and the PSP. The strength obtained from

Table 2.12 Undrained shear strength of Boston blue clay from various strength tests (Ladd and Foote, 1974)

Soil type	s_u/σ'_{vc}	γ_f (%)	$s_u/s_{u,TC}$	*Mark*
CK_0U (PSA)	0.34	0.8	1.03	Plane strain compression test
CK_0U (TC)	0.33	0.5	1.00	Conventional triaxial compression test
CK_0U (DSS)	0.20	6	0.61	Direct simple tests
CK_0U (PSP)	0.19	8.5	0.57	Plane strain lateral compression test
CK_0U (TE)	0.155	15	0.47	Conventional triaxial extension test

γ_f: Shear strain at failure; σ'_{vc}: effective vertical pressure; definition of plane strain refers to Appendix E.

the DSS test is about the average of those from the PSA and PSP tests. Thus, the average undrained shear strength of the failure surface can be represented by the result of the DSS test. The method is more reliable than the triaxial UU test or the unconfined compression test and has been widely applied in many countries.

The SHANSEP approach is a method of eliminating the sampling disturbance. The SHANSEP approach (see Figure 2.26) can be described as follows (Ladd and Foote, 1974):

1 Divide the soil into several layers according to the results of subsurface exploration.
2 Establish the profile of the effective overburden pressure (σ'_{vo}) and the pre-consolidation pressure (σ'_{vp}), as shown in Figure 2.26a, on the basis of the unit weight, the in situ porewater pressure and the consolidation test.
3 According to the potential failure modes of the in situ soil, choose a suitable testing method which can best represent the failure modes of the in situ soil to conduct the CU test (e.g. PSA, PSP, or DSS).
4 Examine whether the soil has normalized properties by seeing whether it exhibits a similar behavior type, as shown in Figure 2.22a.
5 At the first loading stage of the CU test (i.e. the consolidation stage), consolidate the specimen to the virgin consolidation curve and then unload it to the pre-determined value of OCR before proceeding to the second stage (i.e. the shear test). As shown in Figure 2.26c, point **a** represents the initial state after sampling. The soil is consolidated to the virgin consolidation curve (point **c**) and then unloaded to point **d** where the CU test is going to be conducted. In this way, various values of normalized strength (s_u/σ'_v) with the corresponding OCR value can be obtained, as shown in Figure 2.26d.
6 With the OCR values and the effective overburden pressures (σ'_{vo}) at various depths (Figure 2.26a) and referring to Figure 2.26d, we can then compute the strengths at various depths, as shown in Figure 2.26b.

2.8.3.3 *Field vane shear test*

The device for the field vane shear test (FV test) consists of a connecting shaft and four vanes as shown in Figure 2.27a. The most commonly used vane is rectangular to obtain the average undrained shear strength in different directions. American Society for Testing and Materials (ASTM) also suggests other different shapes of vanes to obtain anisotropic undrained shear strength for specific directions.

As shown in Figure 2.27b, to conduct the field vane shear test, first bore to a depth 50 cm above the test depth and stay till the dirt is washed away, then press the shaft and the vanes

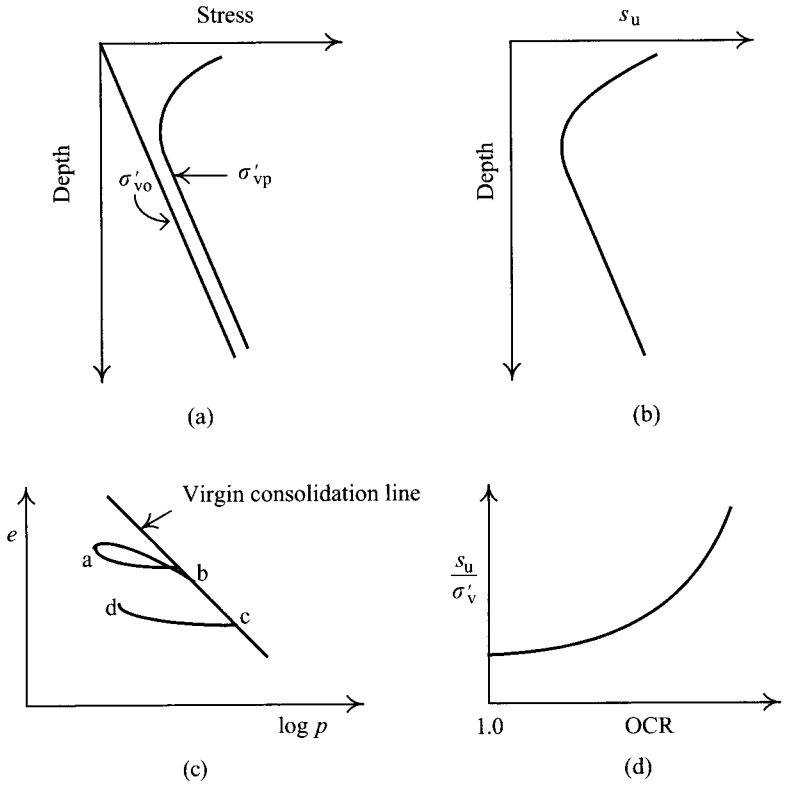

Figure 2.26 Procedure of the SHANSEP approach.

to the test depth. Install the torsion apparatus onto the connecting shaft and then have the torsion act on vanes with a constant rate to make them swirl till the soil within the vanes and outside them separate and fail. Thus, the torsion (T) at the failure is obtained.

The soil within the vanes is column shaped at failure. As shown in Figure 2.27a, the torsion should equal the sum of the resistant moments of the soil strength on the top of the column (M_T), on the bottom of the column (M_B), and on the side of the column, and can be expressed as follows:

$$T = M_T + M_B + M_S \tag{2.31}$$

Assume that the soil on the top, the bottom, and the side of the column has all failed with equal undrained shear strength, which implies that the undrained shear strengths in all directions are the same. Thus,

$$M_S = \pi DH\frac{D}{2}s_u \tag{2.32}$$

$$M_T = M_B = \frac{\pi D^2}{4}\frac{2}{3}\frac{D}{2}s_u \tag{2.33}$$

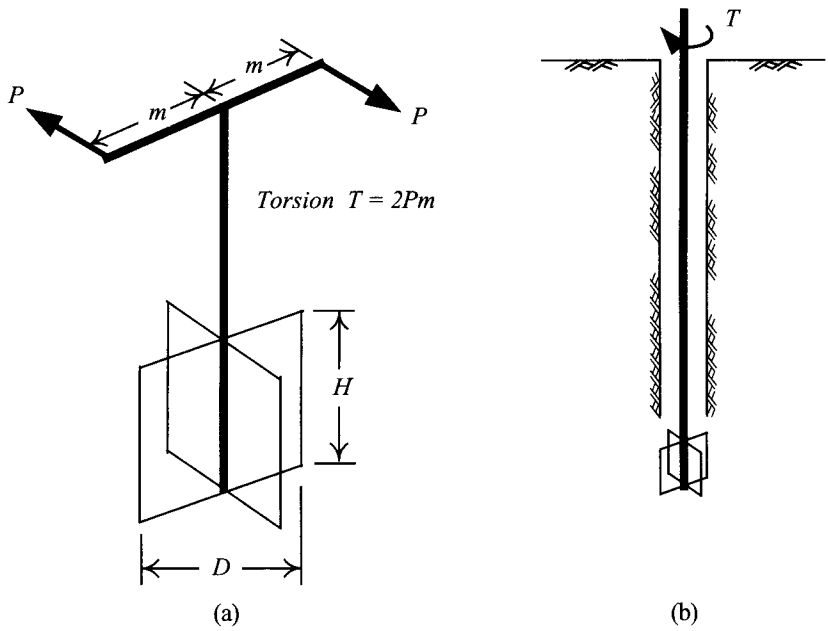

Figure 2.27 Field vane shear test: (a) FV test apparatus, (b) FV test apparatus in a boring hole.

Therefore,

$$T = s_u \left[\left(\pi DH \frac{D}{2} \right) + 2 \left(\frac{\pi D^2}{4} \frac{2}{3} \frac{D}{2} \right) \right] \tag{2.34}$$

Then,

$$s_u = \frac{T}{\pi (D^2 H/2 + D^3/6)} \tag{2.35}$$

where

s_u = undrained shear strength of soil,
D = diameter of the vanes,
H = height of the vanes.

As discussed above, the field vane shear test causes little disturbance to the in situ soil. The testing results also represent the average strength of soils in various directions. However, its result often overestimates the strength of in situ soil, according to Bjerrum's study (1972). Therefore, Bjerrum suggested that the result of the field vane shear test be modified to be applied to the design as follows:

$$s_{u,d} = \lambda s_{u,FV} \tag{2.36}$$

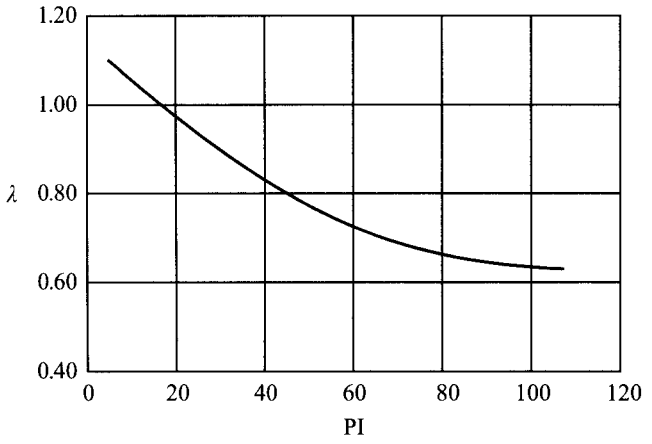

Figure 2.28 Relation between λ and PI for the field vane shear test (Bjerrum, 1972).

where

$s_{u,d}$ = undrained shear strength for design
$s_{u,FV}$ = undrained shear strength obtained from the field vane shear test
λ = modification factor, related to the PI values of soil, which can be determined by referring to Figure 2.28.

2.8.3.4 *Cone penetration test*

The cone penetration test is to push into soil a drilling rod with a mechanical or electrical cone and take the cone end resistance and side friction measurements. Some cone penetration tests can also measure the porewater pressure, in addition to end resistance and side friction. Such an apparatus is called a CPTU. From these data the type of the soil and its parameters of strength can be estimated.

Figure 2.29 illustrates the basic configuration of a CPTU apparatus. According to Robertson and Campanella (1989), the undrained shear strength of clayey soils can be obtained by the following equation:

$$s_u = \frac{q_t - \sigma_{vo}}{N_k} \tag{2.37}$$

$$q_t = q_c + u(1 - a) \tag{2.38}$$

where

s_u = undrained shear strength of soil
q_c = cone end resistance
u = porewater pressure
σ_{vo} = total overburden pressure

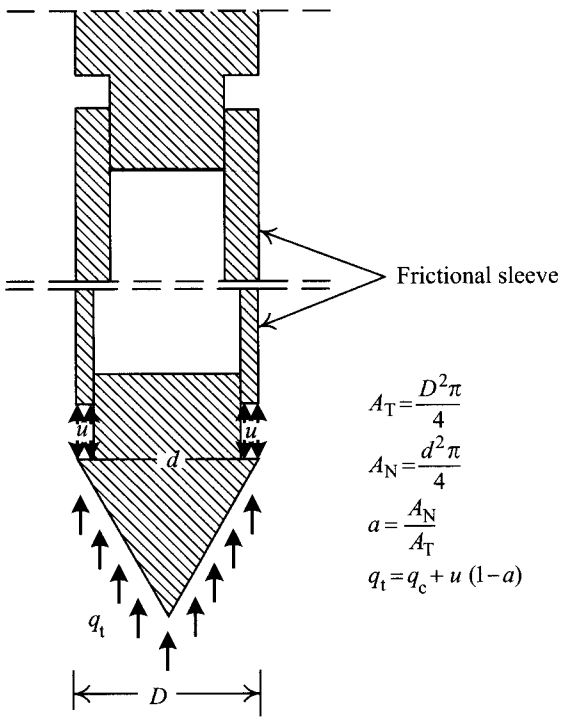

Figure 2.29 Configuration of a CPTU.

a = area ratio, which equals D^2/d^2 (see Figure 2.29)
D = diameter at the top of the CPTU cone
d = diameter at the place where the porewater pressure is measured
N_k = an empirical value that correlates to the value of OCR, the sensitivity and the stiffness of the soil collectively. Usually $N_k = 15 \pm 5$.

Since the N_k-value relates to the type of soil, to obtain the in situ undrained shear strength, a correlation between the result of the field vane shear test (or the UU triaxial test) and that of the CPT test is required to derive the N_k-value. Then, the value is used to obtain s_u for other CPTs.

Because of the continuity of CPT results, the results will not miss any soil layer no matter how thin it is. Thus, CPTs are used not only to obtain the parameters of strength, but also to classify layers of soil. The procedures are also simple. As a result, CPTs have been widely applied in recent years.

2.8.3.5 *Other methods and empirical formulas*

The undrained shear strength of saturated soils can also be obtained by a pressuremeter or lab vane shear test, etc. However, these methods are not commonly used. Therefore, this book will pass them over. Interested readers may refer to relevant literature.

2.9 Relationship between shear strength, volume change, and porewater pressure

Figure 2.30 shows the typical stress-strain behaviors of dense and loose sand respectively. As shown in the figure, the stress acting on loose sand increases up to the ultimate strength while its volume decreases, that is, the soil contracts. On the other hand, the stress acting on dense sand increases up to the peak strength first and then decreases with the increasing strain to the ultimate strength. The soil will contract first and then dilate. With the same type of sand, the values of the ultimate strength for the dense and loose states are nevertheless close. The reason is that the strain at the ultimate strength is rather large and the soil has been disturbed significantly. Under such conditions, the soil strength largely relates to the characteristics of intergranular friction (i.e. roughness of the soil particles).

Basically, normally consolidated soils (or lightly overconsolidated soils) have similar stress-strain behavior to loose sand. The void ratio-stress relation for a normally consolidated clay is unique and under isotropic consolidation the relational curve is called the virgin compression line (VCL), as shown by $e_0 - p'_0$ line (the subscript "0" marks the virgin consolidation state) in Figure 2.31. Shearing will cause the void ratio of normally consolidated

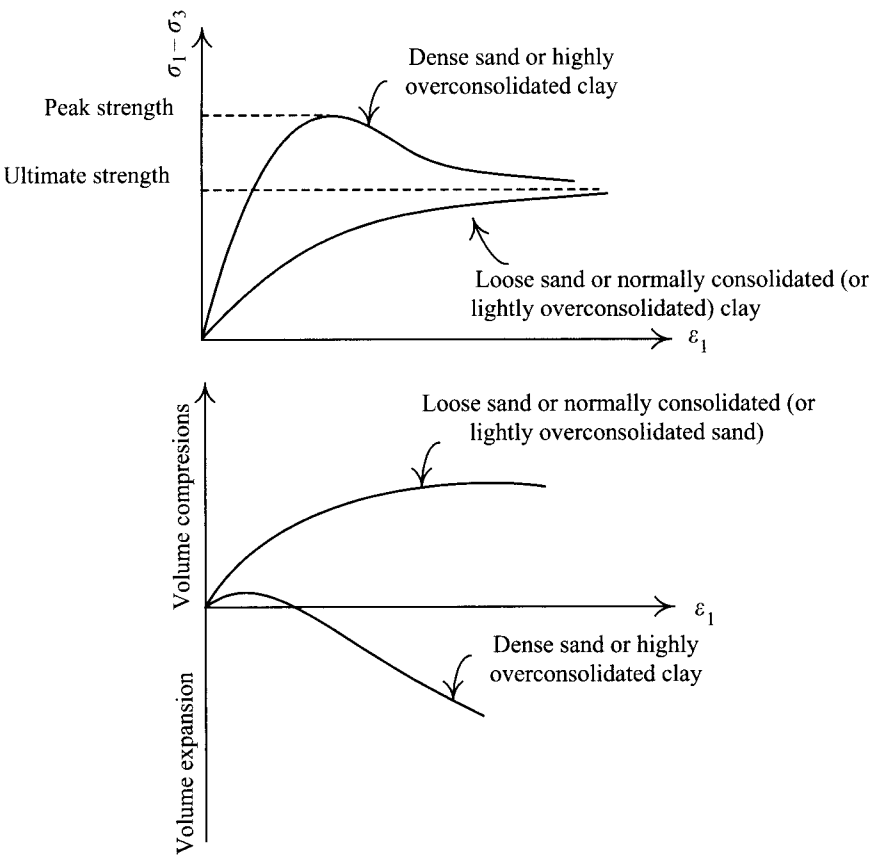

Figure 2.30 Drained stress-strain relations for sand and clay.

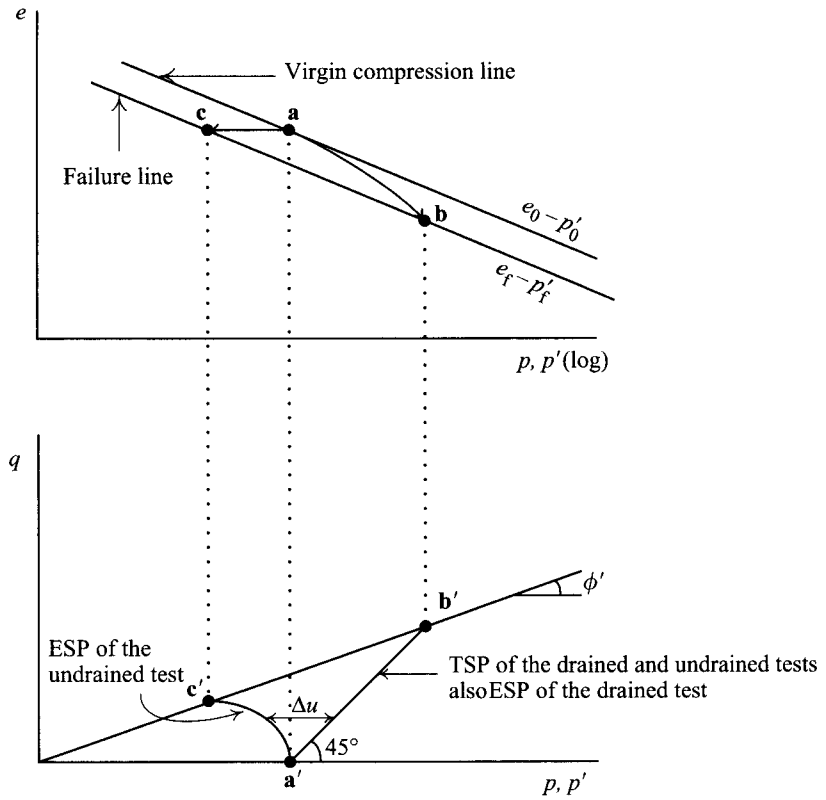

Figure 2.31 Relation between e_f, p'_f, and q_f for normally consolidated clay.

clay (or lightly overconsolidated clay) in the drained condition to decrease. The relation between the stress path and the void ratio is as shown by line segment **ab** in Figure 2.31. Because drained shearing tends to cause the saturated normally consolidated clay (or lightly overconsolidated clay) to contract, a positive porewater pressure will be produced with undrained shearing where the volume remains unchanged, as shown in Figure 2.31 and 2.32. The straight line **ac** in Figure 2.31 represents the unchanged volume of normally consolidated clay after undrained shearing. Curve **a′c′** refers to the effective stress path (ESP) while **a′b′** refers to the total stress path (TSP).

Because the excess porewater pressure in the drained test is nil, line **a′b′** in Figure 2.31 also represents the ESP for drained tests (it is also the TSP). With the q value with regard to **b′** larger than that with regard to **c′**, the undrained shear strength of normally consolidated (or lightly overconsolidated) clay is smaller than the drained shear strength of clay with the same consolidation pressure. That is to say, if a positive porewater pressure is generated in an undrained test (or if the volume decreases in a drained test), the shear strength under undrained conditions will be smaller than the shear strength under drained conditions with the same consolidation pressure. The undrained shear strength should then be adopted for design.

According to the principle of effective stress, soil failure relates solely to the effective stress on soils whereas failure has nothing to do with the total stress. Since the $e_0 - p'_0$

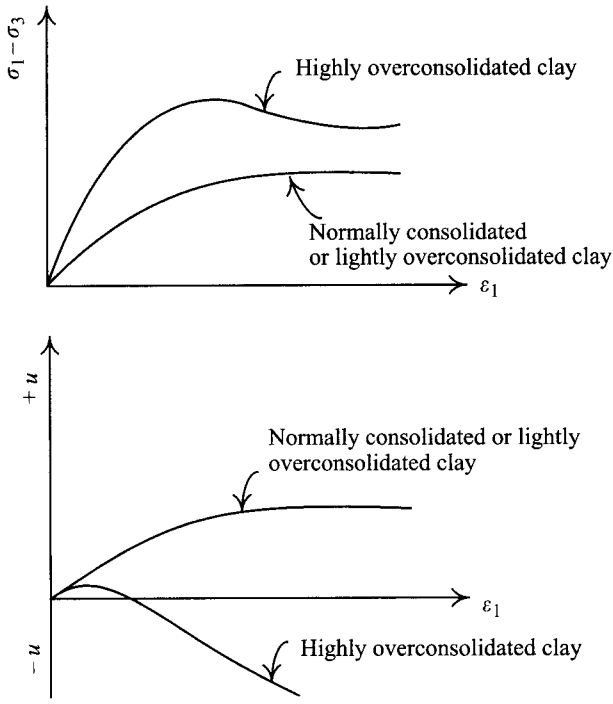

Figure 2.32 Undrained stress-strain relation and the porewater pressure-strain behavior for clay.

relation of clay in the normally consolidated state is unique, that is, the void ratio of normally consolidated clay can be representative of the effective stress on it, the relationship between the void ratio of normally consolidated clay at failure and the effective stress on it is also unique. Thus, both the $e_f - p'_f$ and the $e_f - q_f$ relations are unique (The subscript "f" refers to the failure condition), so, it follows that the $e_f - p'_f - q_f$ relation is unique, too, no matter which drainage condition or testing method is used. Figure 2.33 shows the $w_f - p'_f - q_f$ relation of Weald clay (Lambe and Whitman, 1969), where w_f refers to the water content at failure (note: the $w - e$ relation for a particular type of soil is unique).

The behavior of highly overconsolidated clay is similar to that of dense sand. As we know, drained shearing will cause the saturated highly overconsolidated clay to contract first and then dilate (see Figure 2.30), and therefore, undrained shearing will produce first positive and then negative porewater pressure, as shown in Figure 2.32. Point **a** in Figure 2.34 refers to the overconsolidated soil with preconsolidation pressure, P'_m. Undrained shearing does not change the volume as shown by line **ab** in the figure. The path of total stress during the process of shearing is shown by $\mathbf{a'c'}$ and that of effective stress by $\mathbf{a'b'}$.

From the above inference, line $\mathbf{a'd'}$ in Figure 2.34 represents both the ESP and the TSP in the drained test. The q value with regard to $\mathbf{b'}$ is larger than that with regard to $\mathbf{d'}$. As a result, highly overconsolidated clay has a larger undrained shear strength than the drained shear strength, with the same consolidation pressure. In other words, if the undrained test produces a negative porewater pressure (or the volume dilates in a drained test), the undrained shear strength will be larger than the drained shear strength with the same consolidation pressure. Therefore, the drained shear strength should be adopted for design.

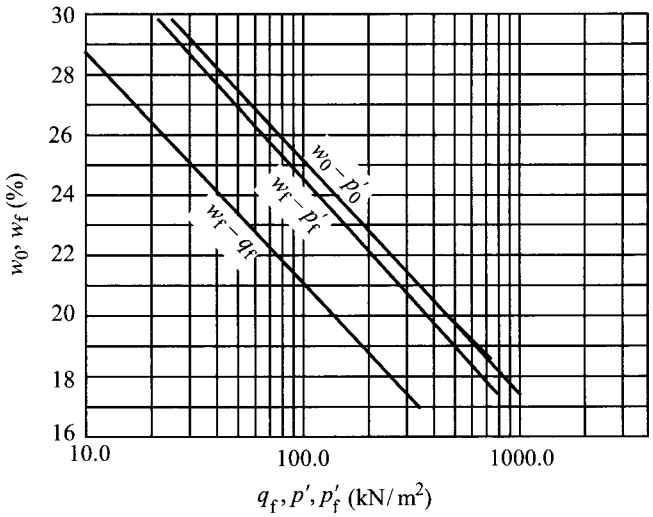

Figure 2.33 Relation between water content and state of stresses for Weald clay (Lambe and Whitman, 1969).

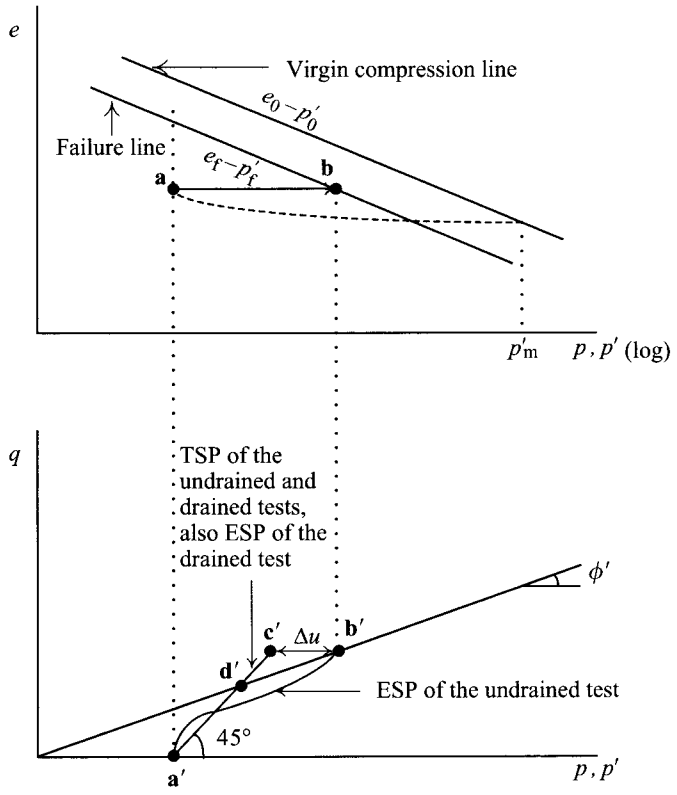

Figure 2.34 Relation between e_f, p'_f, and q_f for overconsolidated clay.

EXAMPLE 2.1
Conduct a series of triaxial CD tests on saturated clay. The effective cohesion and angle of internal friction thus determined are separately $c' = 98.1$ kN/m^2 and $\phi' = 30°$. Let another identical clay specimen be put to triaxial CU tests. We then obtain the following total-stress-related results: $c_T = 58.8$ kN/m^2, $\phi_T = 15°$. What is the angle of the failure surface of the soil at failure?

ANSWER
According to the principle of effective stress, the strength or deformation of a soil relates only to the effective stress whereas it has nothing to do with the total stress. c' and ϕ' are effective strength parameters while c_T and ϕ_T are the parameters of total stress. Thus, using Eq. 2.20, the angle between the failure surface and the horizontal can be obtained as follows:

$$\alpha_f = 45° + \frac{\phi'}{2} = 45° + \frac{30°}{2} = 60°$$

EXAMPLE 2.2
The friction angle of a saturated normally consolidated clay $\phi' = 30$. The major and minor principal stresses at failure of the UU test on the clay $\sigma_3 = 98.1$ kN/m^2, $\sigma_1 = 490.5$ kN/m^2. If the apex of the Mohr's circle is adopted as the undrained shear strength (i.e. $s_u = (\sigma_1 - \sigma_3)/2$), what will be the error for the method?

ANSWER
Referring to Figure 2.19, in the triaxial UU test, the effective Mohr's circle at failure should be tangent to the effective failure envelope. What they are tangent to represents the undrained shear strength. Use Eq. 2.29 and the shear stress on the failure surface (τ_f) can be computed as follows:

$$\tau_f = \frac{\sigma_1' - \sigma_3'}{2}\cos\phi' = \frac{\sigma_1 - \sigma_3}{2}\cos\phi' = \frac{490.5 - 98.1}{2}\cos 30° = 169.9 \text{ kN/m}^2$$

The shear strength at the apex of the Mohr's circle (s_u) is

$$s_u = \frac{490.5 - 98.1}{2} = 196.2 \text{ kN/m}^2$$

$$\text{Error} = \frac{196.2 - 169.9}{169.9} = 15.5\%$$

EXAMPLE 2.3
As shown in Figure 2.35, the ground is mainly composed of saturated clay. Suppose that an embankment is to be constructed on the ground in two stages. In the first stage of construction the embankment consolidates the soil completely. In the second stage, the embankment is constructed at such a speed that the soil through the whole process stays in the undrained state. Before construction (the first stage), what parameters are necessary for the stability analysis of the embankment in the second stage?

ANSWER
Before the first stage of construction, use the SHANSEP approach discussed in Section 2.8.3 and conduct a series of undrained CK_0UDSS tests on the soil specimen sampled at point **A** in Figure 2.35. Establish the s_u/σ_v'-OCR relation, as illustrated in Figure 2.26d. Then calculate

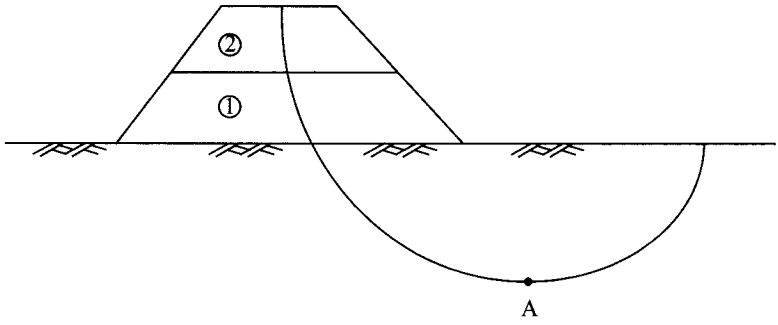

Figure 2.35 Embankment constructed in two stages.

the value of vertical stress (σ_v') at **A** after the first stage of construction. According to the OCR at **A**, the value of s_u/σ_v' at **A** can be obtained, referring to the corresponding figure, such as one like Figure 2.26d. Substitute σ_v' into s_u/σ_v' to obtain s_u, which can be used as the average s_u along the failure surface.

EXAMPLE 2.4

A ground is composed of normally consolidated Weald clay whose groundwater table is on the ground surface. $\gamma_{sat} = 17.66$ kN/ m^3, $K_0 = 0.5$, $c' = 0$, and $\phi' = 30°$. Sample the clay at the depth of 10 m. Due to sampling disturbance, a 15% of negative porewater pressure loss is estimated. Put the trimmed specimen to the UU triaxial test. When the confining pressure (σ_3) is equal to 78.5 kN/m^2, compute the undrained shear strength of the soil and the porewater pressure at failure.

ANSWER

The problem can be solved as follows:

1 *The in situ stress*: Before sampling

$$u_0 = 9.81 \times 10 = 98.1 \text{ kN/m}^2$$

$$\sigma_v = 17.66 \times 10 = 176.6 \text{ kN/m}^2$$

$$\sigma_v' = \sigma_v - u_0 = 176.6 - 98.1 = 78.5 \text{ kN/m}^2$$

$$\sigma_h' = K_0\sigma_v' = 0.5 \times 78.5 = 39.25 \text{ kN/m}^2$$

$$\sigma_h = \sigma_h' + u_0 = 137.34 \text{ kN/m}^2$$

2 *The after-sampling stress*: Since the total stress is relieved, the generated excess porewater pressure is

$$\Delta u = B\Delta\sigma_3 + AB(\Delta\sigma_1 - \Delta\sigma_3)$$

$$= (1.0)(-137.34) + (0.2)(1.0)(-176.6 + 137.34) = -145.2 \text{ kN/m}^2$$

$$u = u_0 + \Delta u = 98.1 - 145.2 = -47.1 \text{ kN/m}^2$$

Considering the 15% of negative porewater pressure loss during sampling, thus

$$\sigma_v' = \sigma_v - 0.85u = 0 - (-40.04) = 40.04 \text{ kN/m}^2$$

$$\sigma_h' = \sigma_h - 0.85u = 0 - (-40.04) = 40.04 \text{ kN/m}^2$$

3 *Triaxial UU test*: At the moment, the effective stress on the specimen (σ_3') is equal to $p_0' = 40.04$ kN/m^2. Though the total stress (σ_3) is known to be 78.5 kN/m^2, the strength of soil relates solely to the effective stress before shearing. According to the $w_0 - p_0'$ curve in Figure 2.33, when $p_0' = 40.04$ kN/m^2, w_0 is equal to 28.2%. Considering the test is the undrained test, the water content at failure would then equal that before failure. From the $w_f - p_f'$ and the $w_f - q_f$ curves, the effective stresses corresponding to $w_f = 28.2\%$ can be obtained, $p_f' = 32.5$ kN/m^2 and $q_f = 12$ kN/m^2. Thus, the undrained shear strength $s_u = q_f = 12$ kN/m^2. Also, two equations can be obtained:

$$\tfrac{1}{2}(\sigma_1' + \sigma_3') = 32.5 \text{ kN/m}^2$$

$$\tfrac{1}{2}(\sigma_1' - \sigma_3') = 12 \text{ kN/m}^2$$

The stresses at the failure are thus obtained as $\sigma_{1f}' = 44.5$ kN/m^2 and $\sigma_{3f}' = 20.5$ kN/m^2. The excess porewater pressure at the failure $\Delta u_f = 78.5 - 20.5 = 58.0$ kN/m^2.

EXAMPLE 2.5

Other conditions unchanged as in Example 2.4, suppose a loss of 25% of negative porewater pressure is estimated due to sampling disturbance. Estimate the undrained shear strength obtained by UU triaxial tests with a confining pressure of $\sigma_3 = 78.5$ kN/m^2.

ANSWER

Suppose 25% of the negative porewater pressure is lost during the process of sampling. Thus,

$$\sigma_v' = \sigma_v - 0.75u = 0 - (-35.3) = 35.3 \text{ kN/m}^2$$

$$\sigma_h' = \sigma_h - 0.75u = 0 - (-35.3) = 35.3 \text{ kN/m}^2$$

At the moment, the effective stress on the specimen $\sigma_c' = p_o' = 35.3$ kN/m^2. Thus, though the triaxial UU test is conducted with $\sigma_3 = 78.5$ kN/m^2, the strength of soil relates only to the before-shear effective confining pressure regardless of the value of σ_3. Refer to Figure 2.33 and the q_f can be found to be 10 kN/m^2. The undrained shear strength, $s_u = q_f = 10$ kN/m^2.

As found by Examples 2.4 and 2.5, sampling disturbance will cause the undrained shear strength to decrease.

2.10 Undrained shear strength of unsaturated cohesive soils

Unsaturated soils refer to those whose voids are not fully filled by water or where the degree of saturation is less than 100%. Unsaturated soils have suction, which can be classified into

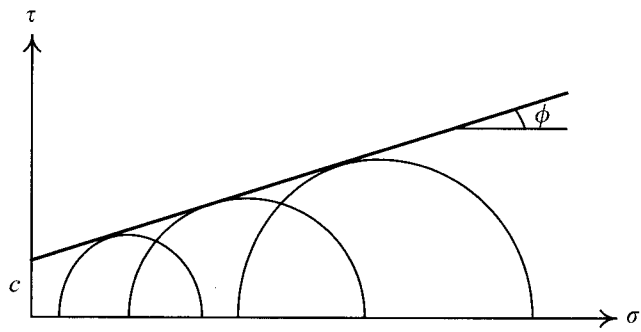

Figure 2.36 Test results of triaxial UU test on unsaturated clay.

matric suction and seepage suction. Since unsaturated soils are composed of solid materials (soil particles), gaseous matter (air), and liquids (porewater), a border zone between liquid water and air in the soil exists where a pressure difference will be generated. While the porewater pressure (u_w) is negative, the pore air pressure (u_a) is positive. The difference between these two ($u_a - u_w$) is designated as matric suction or capillary suction. On the other hand, materials or ions dissolved in water will lead water toward where concentration is higher and generate suction, known as seepage suction. Total suction is the sum of matrix suction and seepage suction. However, since the latter is usually much weaker than the former, matrix suction can be practically taken as the total suction.

Suction in the soil pulls particles together tightly and increases its effective stress and strength accordingly. Therefore, with the suction in the soil known, the undrained shear strength of unsaturated soils can be computed according to the effective stress. Literature relating to failure theories of unsaturated soils based on effective stress can be found, for example Fredlund (1997) etc. Nevertheless, since the measurement of suction requires a special instrument, the application of the above failure theories is comparatively inconvenient. UU triaxial tests are more commonly adopted to obtain the undrained shear strength.

Figure 2.36 illustrates the results of UU triaxial tests where the intercept (c) and the slope (ϕ) of the failure envelope are the parameters of strength. Due to the unsaturated state, ϕ is apparently not 0. The strength of the soil on the failure surface can be calculated using Eq. 2.18. Though the equation is expressed in total stress and does not answer to the principle of effective stress, some small discrepancy is allowed considering that not too much unsaturated soil is encountered in most of the deep excavation problems.

2.11 Soil properties at the TNEC site

The construction of the basement of the Taipei National Enterprise Center (TNEC) is a typical excavation using the top down construction method. The soil at the site is the typical Taipei soil. The author and his research group (Ou and Shiau, 1993; Ou *et al.*, 1998, 2000a,b) carried out detailed studies on the excavation. The contents included the soil properties of the site, the stress behavior of excavation, and the strain and displacement behavior. This section will introduce the soil properties of the construction site of TNEC. As to the process and procedures of excavation, please see Section 3.6. For stress, strain, and displacement

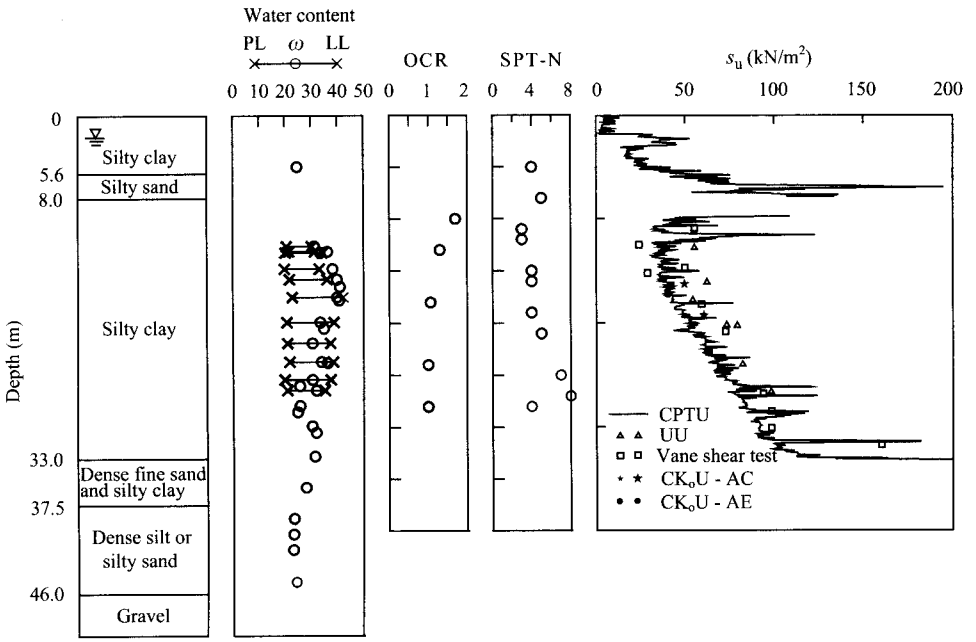

Figure 2.37 Geological data of the TNEC excavation.

behavior, please see Chapter 6. The related data are indexed in Appendix B. The information can be useful for the understanding of the soil properties of the site, which is essential for the understanding of excavation behavior.

In Chapter 3, Figure 3.33 shows the shape of the TNEC construction site. Figure 2.37 shows the profiles of the water contents, the Atterberg limits and the SPT-N values. As shown in the figure, the subsoil conditions at the TNEC construction site can be roughly divided into seven layers. Starting from the ground surface, they can be described as follows: the first layer is soft silty clay (CL), which ranges from ground level (GL)00 m to GL-5.6 m and whose N-value is around 2–4. The second layer, from GL-5.6 m to GL-8.0 m, loose silty fine sand with N-values between 4 and 11 and $\phi' = 28°$. The third layer, from GL-8.0 m to GL-33.0 m, is again soft silty clay (CL) whose N-value is around 2–5 and the PI is within the range of 9–23, with an average value of 17. This layer is the one which most affects the excavation behavior. The soil mainly contains 40–55% of silt and 45–60% of clay. The coefficient of permeability (k) is around 4×10^{-6} cm/sec. The coefficient of consolidation ranges from 3×10^{-3} cm^2/sec to 1.1×10^{-2} cm^2/sec. The fourth layer, ranging from GL-33.0 m to GL-35.0 m, is medium dense silty fine sand with N-value between 22 and 24 and $\phi' = 32°$. The fifth: medium soft clay; ranges from GL-35.0 m to GL-37.5 m. N = 9–11. The sixth: medium dense to dense silt or silty fine sand; ranges from GL-37.5 m to GL-46.0 m, N = 14–37 and $\phi' = 32°$. Below the sixth: dense Chingmei gravel soil and N is above 100.

Figure 2.37 also displays the profile of OCR. The relationship between OCR and the water content is fairly consistent as shown in the figure. Generally speaking, the greater the

OCR, the lower the water content. As can be observed, the soil within 15 m in depth is overconsolidated. It can be reasonably inferred as having to do with the fact that a five-storey building was at the construction site.

Figure 2.37 also provides the values of the undrained shear strength obtained from various triaxial tests and field tests. The ratios (s_u/σ'_v) of the undrained shear strength (s_u), obtained respectively from the field vane shear test and the UU triaxial test, to the effective overburden pressure (σ'_v) are 0.32 and 0.36, respectively. Those from the CK_0U-AC and CK_0U-AE tests are 0.32 and 0.21. The values of s_u from the cone penetration test (CPTU) are computed using Eq. 2.36 and 2.37 with the cone coefficient (N_k) = 15. As shown in the figure, the values of s_u from CPTU increase with the depth.

2.12 Summary and general comments

This chapter has explored the basic properties and the mechanical properties of soils, including the specific gravity, the Atterberg limit, the permeability, the compression index and the swelling index. Some typical values of some urban soils around the world are provided for comparison, useful for further understanding of the engineering characteristics of soil. In addition, they can be used for preliminary designs for deep excavations.

The chapter can be summarized as follows:

1 Based on the principle of effective stress, we have defined drained and undrained shear strength of soil. We also explained why the Mohr-Coulomb failure theory can only be applied with the effective stress, regardless of the total stress. As a result, the total stress parameters obtained from the CU triaxial test (c_T, ϕ_T) cannot be used for design.
2 In engineering practice, the parameters of the drained shear strength (c', ϕ') of undisturbed sandy soils can be obtained from the direct shear test. As for those of undisturbed saturated clay, the CD or CU triaxial test is often adopted.
3 The undrained shear strength of saturated clay can be obtained through the triaxial UU test, the unconfined compression test, or the field vane shear test.
4 The undrained shear strength of the saturated clay can also be obtained by the CU test with the provision that (1) the testing method has to conform to the failure mode of the in situ soil, (2) the testing rate has to be the same as the failure rate of the in situ soil considered, and (3) the SHANSEP approach or other methods are required to eliminate the influence of sampling disturbance.
5 According to the principle of effective stress, the relationship between the volume and the stress condition of saturated clay at failure is unique, regardless of the drainage condition or the test method. Thus, the $e_f - p'_f - q_f$ relation is also unique.
6 According to the principle of effective stress, the undrained shear strength of unsaturated clay can be obtained by measuring soil suction. However, in engineering practice, it is often derived from the triaxial UU test directly.

Problems

2.1 As shown in Figure P2.1, the depth of the groundwater level H_1 = 2.0 m; the moisture unit weight of clay γ_m = 11.8 kN/m^3; the saturated unit weight γ_{sat} = 17.7 kN/m^3.

The thickness of the clayey layer $H_2 = 40.0$ m. Under the clayey layer is a sandy layer where the piezometric level is the same as the groundwater level, that is, $H_3 = 38.0$ m. Compute and plot the total stress, the porewater pressure and the effective stress with depth.

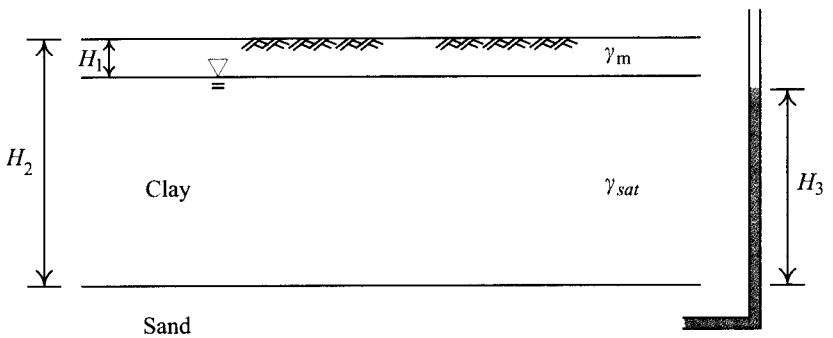

Figure P2.13

2.2 Same as above. Assume the piezometric pressure in the sandy soil is lowered and renders $H_3 = 30.0$ m. Compute (1) the variation of the total stress, porewater pressure, and effective stress with depth for the short-term condition after dewatering (2) the variation of the total stress, porewater pressure, and effective stress with depth for the long-term condition (when the seepage reaches the steady state condition)

2.3 Same as shown in Figure P2.1. Assume $\gamma_m = 13.2$ kN/m^3, $\gamma_{sat} = 20.6$ kN/m^3, $H_1 = 5.0$ m, and $H_2 = 50$ m this time. The piezometric level of the sandy layer is originally the same as the groundwater level ($H_3 = 45$ m) and then is lowered by 5 m ($H_3 = 40.0$ m) through dewatering. Compute the variation of the total stress, the porewater pressure, and effective stress in the clay layer for the short-term and long term conditions.

2.4 Assume a homogeneous normally consolidated clayey ground where the groundwater level is on the ground surface and the properties of clay are: $\gamma_{sat} = 20.6$ kN/m^3, $K_0 = 0.5$, $c' = 0$, $\phi' = 27°$, $c_T = 0$, and $\phi_T = 15°$. Assume a horizontal failure surface in the soil at the depth of 10 m is generated under undrained condition, with the vertical total stress unchanged. The excess porewater pressure at failure is 49.1 kN/m^2. Compute the undrained shear strength of the soil (i.e. shear stress on the failure surface).

2.5 Same as the previous problem. Assume the major principal stress (total stress) occurs in the vertical direction at failure whereas the horizontal total stress is unchanged during the testing. The porewater pressure at failure is unknown, though the parameter of porewater pressure is $A_f = 0.6$. Compute the undrained shear strength (i.e. shear stress on the failure surface).

2.6 If we perform a direct shear test on sand, with the before-test vertical stress on the shear box $\sigma_v = 981$ kN/m^2 and the shear stress on the failure surface $\tau_f = 63.77$ kN/m^2, compute the effective angle of friction and the major principal stress at failure.

2.7 According to the principle of effective stress, the failure or deformation of soil relates solely to the effective stress whereas it has nothing to do with the total stress. In the triaxial UU test, the pressure acting on the soil is the total stress rather than the effective stress. If so, why cannot the result of a triaxial UU test be used to obtain the shear strength of soil?

2.8 The results of a CU test on soil are as follows:

σ_3 (kN/m^2)	$(\sigma_1 - \sigma_3)_f$(kN/m^2)	Δu_f(kN/m^2)
196.2	114.8	107.9
392.4	237.4	224.7
784.8	459.1	446.4

Find: (1) The strength parameters under the effective stress? (2) Which type of soil is it (NC or OC)? (3) If we take another specimen of the same type of soil, what will be the porewater pressure when the confining pressure reaches 147.2 kN/m^2 and the deviator stress is 172.8 kN/m^2?

2.9 A triaxial CD test was performed on a saturated sample of overconsolidated clay with the pre-consolidation pressure equal to 147.2 kN/m^2. At failure, $\sigma'_{3f} = 294.3$ kN/m^2, $\sigma'_{1f} = 882.9$ kN/m^2. A triaxial CU test was performed on another sample of the same clay. At failure, the confining pressure (σ_{3f}) was 392.4 kN/m^2 and the axial stress at failure (σ_{1f}) is 784.8 kN/m^2. Find (1) the porewater pressure at failure for the CU test, (2) the angle between the failure surface and horizontal plane.

2.10 A ground is mainly composed of normally consolidated clay with the groundwater level at the ground surface and $\gamma_{sat} = 20.6$ kN/m^3, $K_0 = 0.45$, $c' = 0$, and $\phi' = 27°$. A sample at the depth of 12 m was taken and 16% of the negative porewater pressure is estimated lost during the sampling process. A triaxial UU test is performed on the sample with a confining pressure of 98.1 kN/m^2. Find (1) the undrained shear strength, (2) the porewater pressure at failure, (3) angle of the failure surface (assume the porewater pressure parameter during sampling and at failure are the same: $A = 0.3$).

2.11 Same as the previous problem. If the clay is Weald clay, c' and ϕ' unknown, and relation between the water content and stress path is as shown in Figure 2.33. Find (1) the major and minor principal stresses at failure, (2) the porewater pressure at failure.

2.12 The ratio of the undrained shear strength of clay, obtained from the triaxial CK_0U (axial compression) test, to the effective vertical overburden stress (s_u/σ'_v) is 0.25. Is it feasible to use the ratio directly for stability analysis of an excavation or bearing capacity analysis of a foundation? If not, how must it be modified?

2.13 Figure P2.13 is a profile of the undrained shear strength of a clayey ground. The groundwater level is 1.0 m below the ground surface. $\gamma_m = 11.77$ kN/m^3 above the groundwater level whereas $\gamma_{sat} = 17.66$ kN/m^3 below it. Use Terzaghi's bearing capacity equation to compute the net ultimate bearing capacity of a 3 m wide and 2 m deep strip footing.

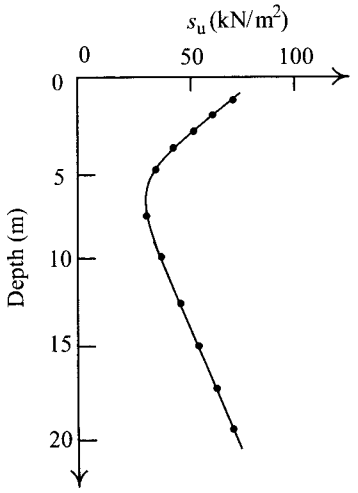

Figure P2.14

2.14 A 15 m high embankment is to be constructed on a normally consolidated clayey ground with the groundwater table at the ground surface (see Figure 2.35). In fear of the shear failure of the soil below the embankment, a stability analysis has to be performed. How should one obtain the undrained shear strength (1) Through the CU test? (2) Through the UU test? (3) Compare the strengths and shortcomings of the two methods.

Chapter 3

Excavation methods and lateral supporting systems

3.1 Introduction

Deep excavation or the construction of basements includes the construction of retaining walls, excavation, the installation of struts, the constructions of foundations and floor slabs, etc. With the great variety of excavation methods and lateral supporting systems, to come to the most appropriate design, we have to consider, in combination, the local geological conditions, the environmental conditions, the allowable construction period, the budget, and the available construction equipments and make an overall plan accordingly. Since the foundation construction, itself a field of specialty, involves many construction details and this book emphasizes analysis and design, this chapter will only introduce some of the most commonly used excavation methods and lateral supporting systems.

This chapter will also introduce the construction process of the TNEC (Taipei National Enterprise Center) excavation. Its geological data are discussed in Section 2.11. With the thorough documentation and studies of the excavation process, geological data and monitoring results, we can get further understanding of excavation behaviors.

3.2 Excavation methods

The following are some commonly used excavation methods: the full open cut method, the braced excavation method, the island excavation method, the anchored excavation method, the top-down construction method, and the zoned excavation method. The braced excavation method is the most commonly used among them. Selection of an appropriate excavation method necessarily considers many factors, such as construction budget, allowable construction period, existence of adjacent excavations, availability of construction equipment, area of construction site, conditions of adjacent buildings, foundation types of adjacent buildings, and so on. Experienced engineers are able to make good selections, based on these factors. This section will introduce the characteristics of the commonly used methods for reference.

3.2.1 Full open cut methods

The full open cut method can be further distinguished into the slope full open cut method and the cantilever method. As Figure 3.1 shows, the slope method does not use retaining walls or struts. Instead, the construction site is excavated with sloped sides. Since there is no strut to obstruct excavation, the cost is thereby quite cheap if the excavation is not too deep. However, in deep excavations or if the slopes are very gentle, the amount of excavated soil

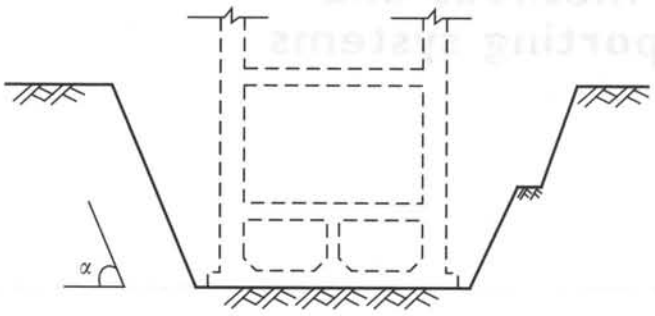

Figure 3.1 Sloped open cut method.

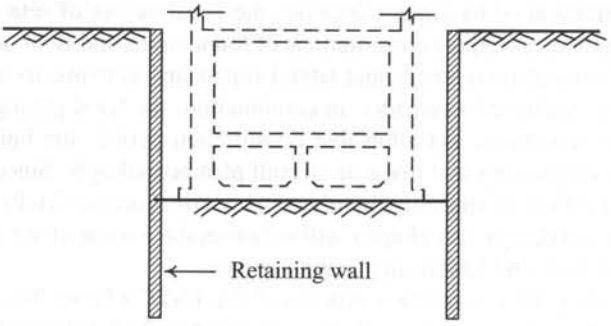

Figure 3.2 Cantilevered open cut method.

is tremendous and a great amount of soil will be needed to backfill after the construction is finished. Thus, the cost as a whole is not necessarily low.

Figure 3.2 illustrates the cantilever full open cut method. The stiffness of retaining walls is the sole source to keep them stable without the temporary installment of struts, which will obstruct excavation activities. The cantilever method, though requiring the construction of retaining walls, does not necessitate digging the slope and backfilling. Therefore, the cost may not be necessarily higher than that of the slope method. Which method is more economic and safer should be determined according to the results of analysis, design, and evaluation.

3.2.2 Braced excavation nethods

Installing horizontal struts in front of retaining walls to resist the earth pressure on the backs of walls is called the braced excavation method. Figure 3.3 shows the typical arrangement of horizontal struts. Figure 3.4 is the photo of a braced excavation. The bracing system of the braced excavation method includes struts, wales, end braces, corner braces, and center posts. The function of wales is to transfer the earth pressure on the back of retaining walls on to horizontal struts. End or corner braces can help shorten the span of wales without increasing the number of struts. For example, some distances between horizontal struts may slightly exceed allowable distances out of construction expediency; adding one more strut,

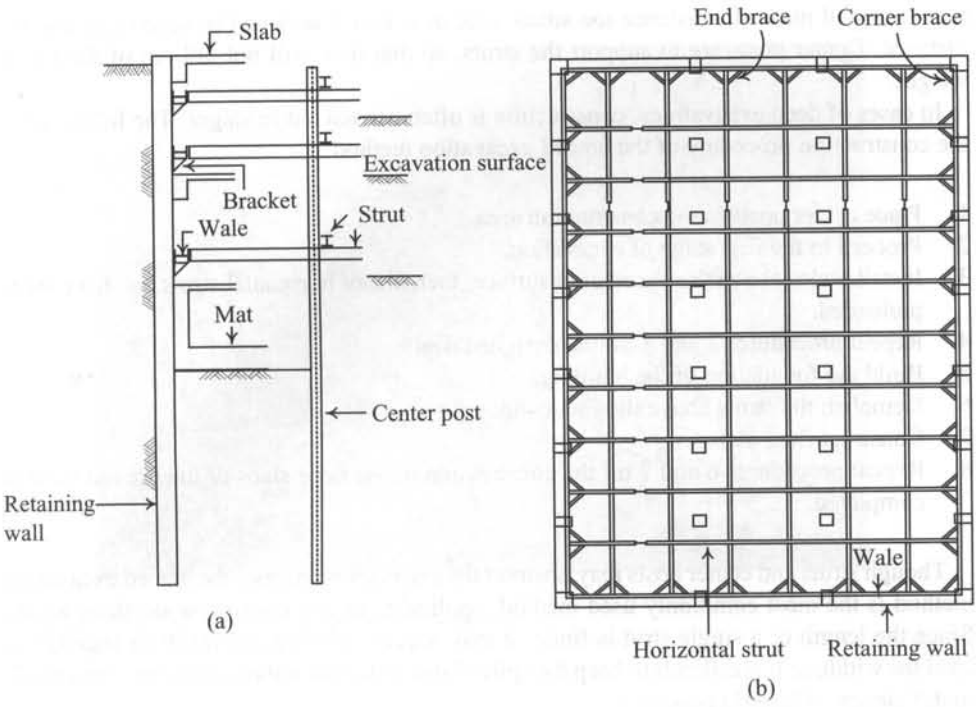

Figure 3.3 Braced excavation method: (a) profile and (b) plan.

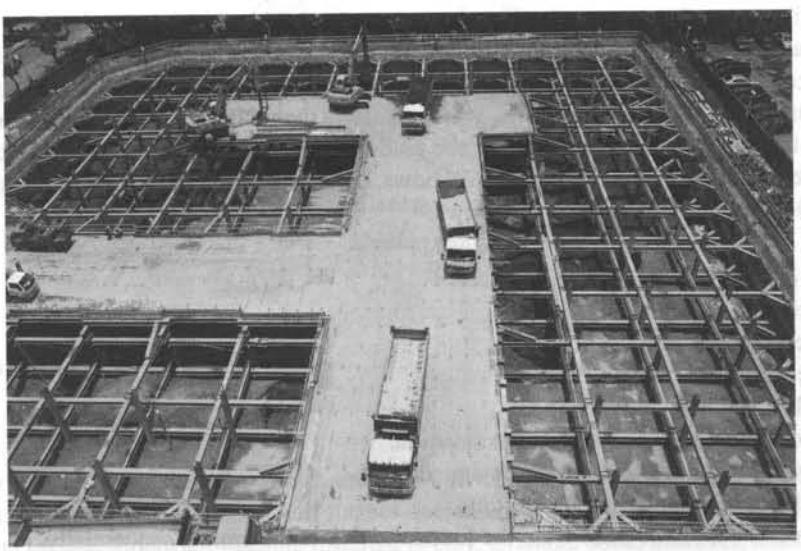

Figure 3.4 Photo of the braced excavation method.

however, will make the distance too small. End or corner braces can be used to adjust this distance. Center posts are to support the struts, so that they will not fall out of their own weight.

In cases of deep excavations, construction is often carried out in stages. The following is the construction procedure of the braced excavation method:

1 Place center posts in the construction area.
2 Proceed to the first stage of excavation.
3 Install wales above the excavation surface, then install horizontal struts and have them preloaded.
4 Repeat procedures 2 and 3 till the designed depth.
5 Build the foundation of the building.
6 Demolish the struts above the foundation.
7 Construct floor slabs.
8 Repeat procedures 6 and 7 till the construction of the floor slabs of the ground floor is completed.

Though struts and center posts may obstruct the excavation process, the braced excavation method is the most commonly used method, applicable to any excavation depth or width. Since the length of a single strut is finite, it may require splicing several struts together to span the width, as it is difficult to keep the spliced struts aligned and misalignment may result in deficiency of lateral resistance.

3.2.3 *Anchored excavation methods*

Braced excavation methods, as discussed in Section 3.2.2, use struts to offer lateral support against lateral earth pressure. Anchored excavation methods substitute anchors for struts to counteract the lateral earth pressure. Figure 3.5 is the photo of an anchored excavation.

The configuration of an anchor can be divided into (1) the fixed section—which offers anchoring force, (2) the free section—which transfers the anchoring force to the anchor head, and (3) the anchor head—which locks the tendons and transfers the anchoring force to the structure (see Figure 3.6). As Figure 3.7 shows, the construction procedure of the anchored excavation method is described as follows:

1 Set out the first-stage excavation.
2 Bore for anchors.
3 Insert tendons into the bores.
4 Inject grouts.
5 Preload anchors and lock them.
6 Proceed to the second stage of excavation.
7 Repeat procedures 2–6 till the designed depth.
8 Build the foundation of the building.
9 Construct the floor slabs from the foundation up to the ground sequentially.

The anchored excavation counts solely on soil strength to offer the anchoring force. The higher the soil strength, the stronger the anchoring force and vice versa. Granular soils (such

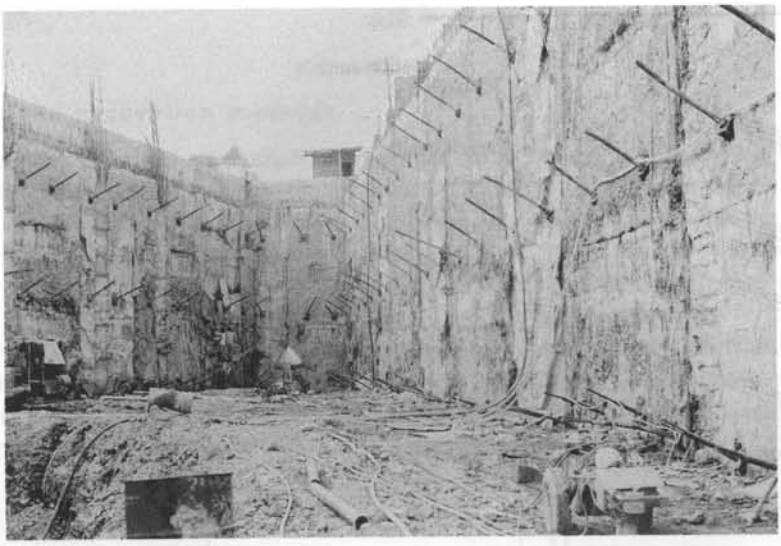

Figure 3.5 Photo of the anchored excavation method.

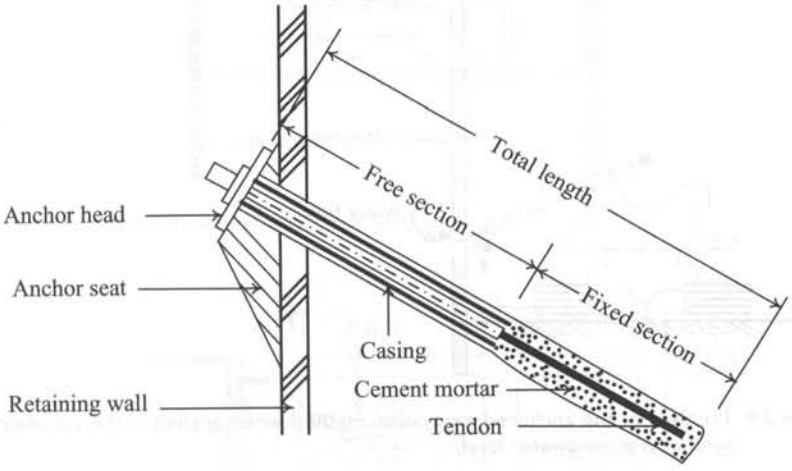

Figure 3.6 Basic configuration of an anchor.

as sandy soils or gravel soils) have high strengths and thus offer strong anchoring force while clay has weak strength and creep will further decrease the anchoring force. Therefore, the anchoring section should avoid being installed in clay. Granular soils, however, usually have rather high permeability, while clayey soils do not. Thus, an anchor installed in a granular soil with high groundwater level often encounters difficulty in sealing bores because of the higher water pressure outside the excavation area as shown in Figure 3.8. The anchored excavation

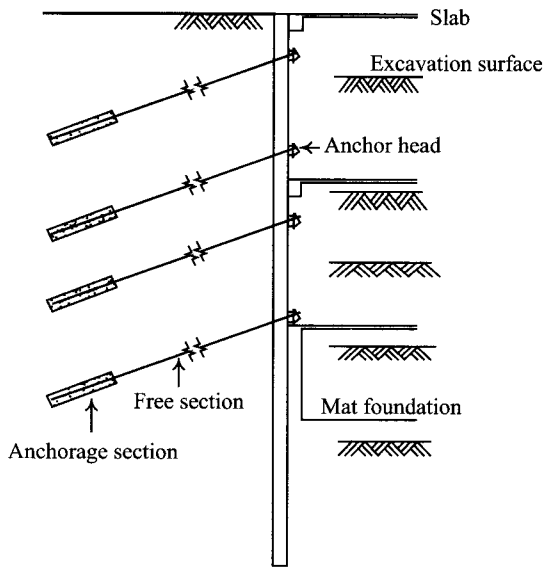

Figure 3.7 Profile of the anchored excavation method.

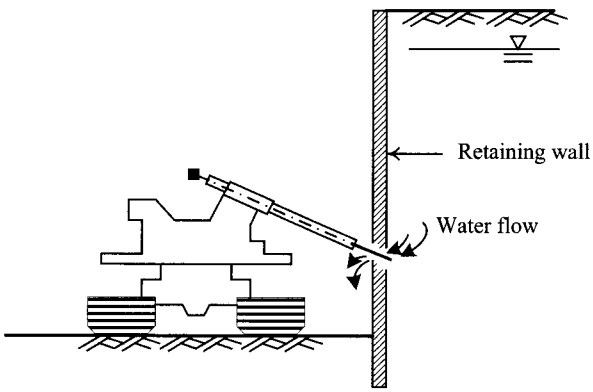

Figure 3.8 Problem of the anchored excavation method when applied in the cohesionless soil with high groundwater level.

method has the following merits notwithstanding:

1 High efficiency for excavation and underground structure construction.
2 Short construction period.
3 Fit for excavation projects with large areas and shallow depths.

The drawbacks of the anchored excavation method are:

1 This method of excavation is not applicable to weak soil layers.
2 When applied to a depth 10 m below the groundwater table in granular soils (such as sandy soils or gravel soils), anchors should be installed with care.

3 Large settlement may occur if the construction quality of anchors is not good enough.

3.2.4 *Island excavation methods*

The conception of island excavation methods can be explained as follows: excavate the central part of the site first and keep the soil near the retaining walls to form slopes; build the main structure in the central part; excavate the slope and install struts between the retaining walls and the main structure; dismantle the struts and build the other parts of the structure.

If the excavation depth is not too great, we can use rakers for strutting, as shown in Figure 3.9 and finish excavation in a single stage. If the excavation exceeds a certain depth, the removal of slopes will cause resort to the braced excavation method (Section 3.2.2) or the anchored excavation method (Section 3.2.3), that is, excavation and installation of struts or anchors proceeding by turns till the designed depth, as shown in Figure 3.10. Figure 3.11 offers a photo of the island excavation.

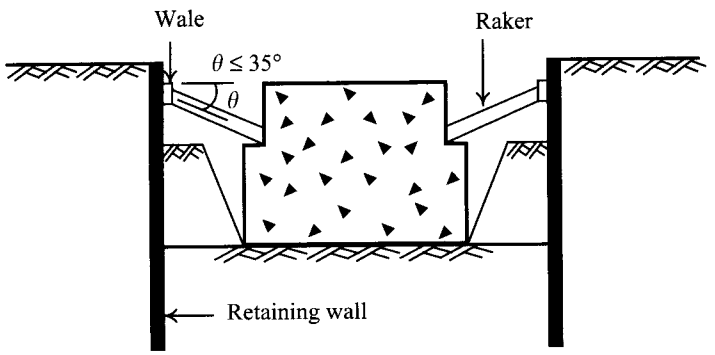

Figure 3.9 Island excavation method with single level of struts.

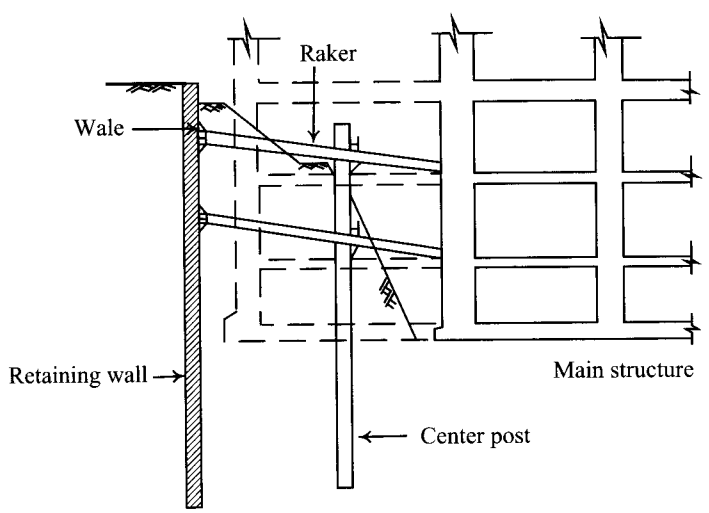

Figure 3.10 Island excavation method with multiple levels of struts.

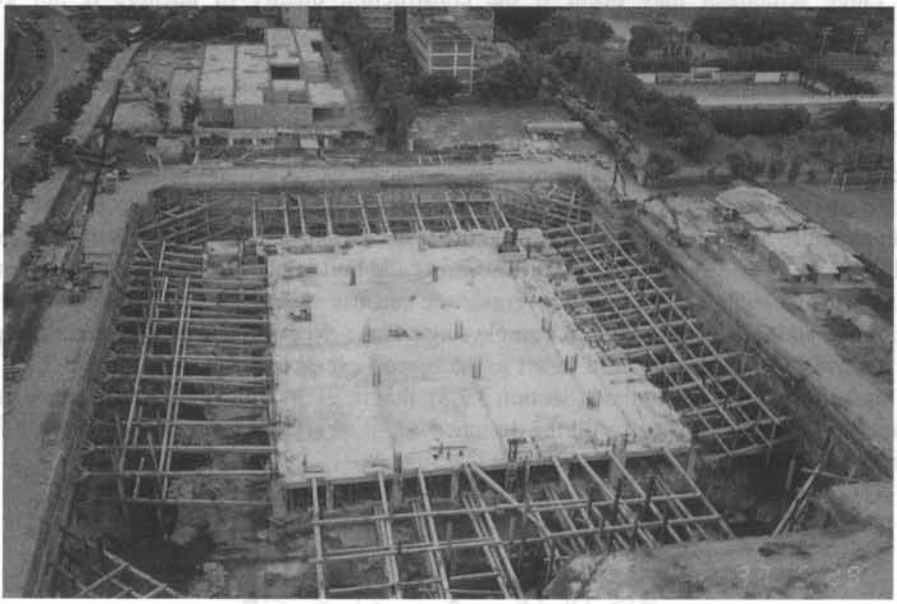

(a)

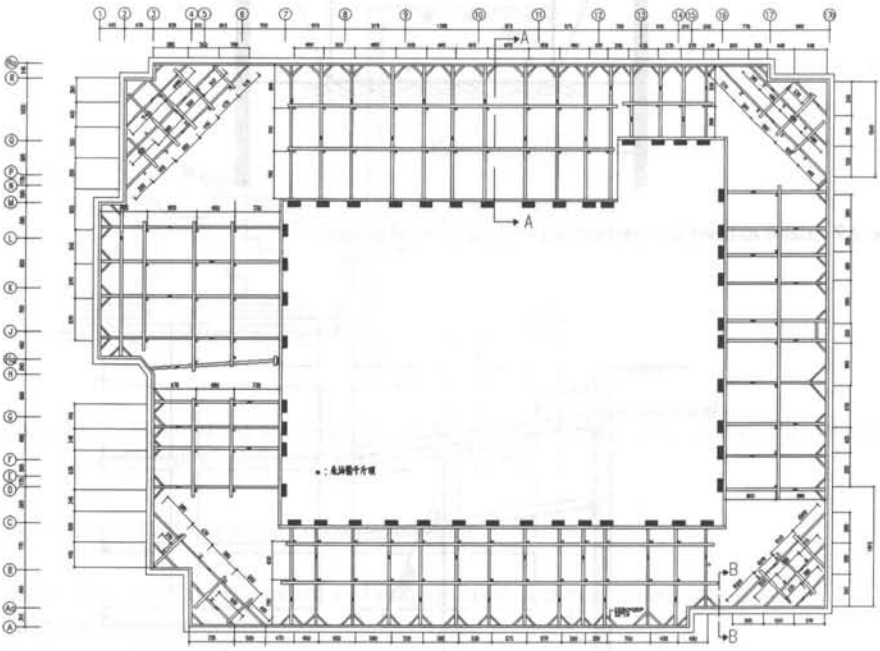

(b)

Figure 3.11 Photo and plan of the island excavation method.

If the island excavation method is to be applied to a certain site, the site has to be large enough and the construction method has to consider the location of the main structure. The widths and gradients of slopes have to be determined in such a way that they will not cause slope failures. Even though slope failures do not occur, the passive resistance offered by slopes is smaller than that in the normal state. This fact will bring about larger wall deflection or ground surface settlement. Therefore, analysis is required before excavation for the sake of adjacent property protection.

The most prominent strength of the island excavation method is the increase of efficiency and, accordingly, the shortened construction period. Compared to the braced excavation method, it requires fewer struts and reduces the cost of strut installation and dismantling. Used in large area excavations, it can avoid the drawbacks both of the braced excavation method where the larger span of struts may reduce the strut's resistance to lateral earth pressure and of the anchored method where high water pressures obstruct the anchor installation. The island excavation method can resolve most of those problems. The major shortcoming is possible water leakage or weak structural joints between the main structure in the center part and other structures in the surroundings. Besides, larger wall deflection and ground movement usually occur due to the lower passive resistance offered by slopes smaller than those in the normal state, especially in soft soil.

3.2.5 *Top-down construction methods*

Following the braced excavation method, excavation is carried out through to the designed depth and then raft foundations or foundation slabs are built; struts can then be removed floor by floor and floor slabs are built accordingly. Thus, the whole underground construction is finished. As such, the underground structure is constructed from bottom to top, which is the most conventional construction method and is generally called the bottom-up construction method. Precisely speaking, the anchored excavation method, the full open cut excavation method, and the braced excavation method all belong to the bottom-up construction method.

Contrary to the bottom-up construction method, the top-down construction method is to erect molds and construct floor slabs right after each excavation. The floor slabs are permanent structures, which replace temporary steel struts in the braced excavation method to counteract the earth pressure from the back of the retaining wall. In this way, the underground structure construction is finished with the completion of the excavation process. The construction of the underground structure is from the top to the bottom and is contrary to conventional foundation construction methods. The method is therefore called the top-down construction method.

The floor slabs used in the top-down construction method are heavier than the steel struts used in conventional excavation methods. In addition, the superstructure, which is constructed simultaneously during excavation, puts more weight on the column. Thus, the bearing capacity of the column has to be considered. As a result, pile foundations are often chosen to be used for the top-down construction method. The typical construction procedure of the top-down construction method is as follows (see Figure 3.12):

1 Construct the retaining wall.
2 Construct piles. Place the steel columns where the piles are constructed.
3 Proceed to the first stage of excavation.

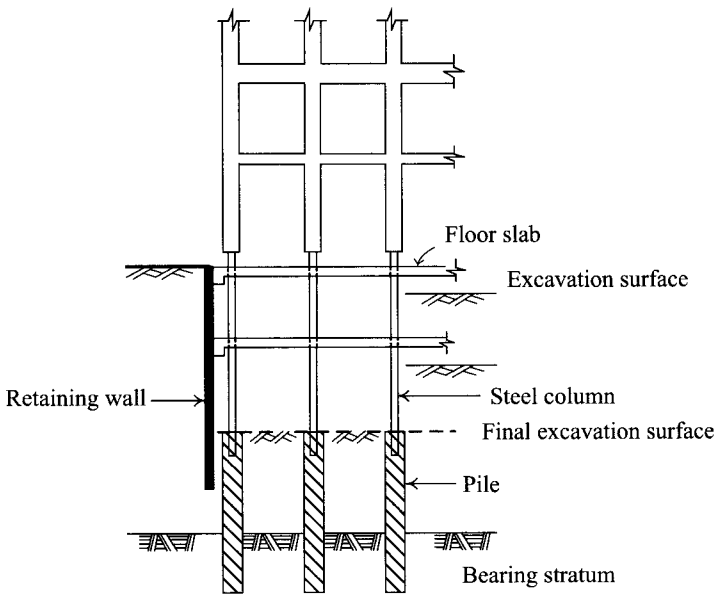

Figure 3.12 Top-down construction method.

4 Cast the floor slab of the first basement level (B1 slab).
5 Begin to construct the superstructure.
6 Proceed to the second stage of excavation. Cast the floor slab of the second basement level (B2 slab).
7 Repeat the same procedures till the designed depth.
8 Construct foundation slabs and ground beams, etc. Complete the basement.
9 Keep constructing the superstructure till finished.

The merits of the top-down construction method include:

1 The shortened construction period due to the simultaneous construction of the basement and the superstructure.
2 More operational space gained from the advanced construction of floor slabs.
3 The higher stiffness of floor slabs compared to steel struts improves the safety of excavation.

The drawbacks of the top-down construction method are:

1 Higher cost (due to the construction of pile foundations).
2 Since the construction period of the basement is lengthened, the lateral displacement of retaining walls or ground settlement may possibly increase due to the influence of creep, if soft soil layers are encountered.
3 The construction quality may be influenced because of the worsened ventilation and illumination under floor slabs.

3.2.6 Zoned excavation methods

The excavations that use diaphragm walls as retaining walls, because of the arching effect of concrete walls, have less deformation of the retaining walls or ground settlement at or around corners. Deformation on the shorter side of the excavation is less than that on the longer side of the excavation, as shown in Figure 3.13. Zoned excavation takes advantage of the above principle to reduce wall deformation or ground settlement during excavation.

As Figure 3.14 shows, divide the excavation into two areas, A and B, excavate area A to a certain depth while keeping area B intact. Area A is like a small-sized excavation with soil in area B left to support point ***b***. Thus, deformation at point ***a*** or ***b*** is less than that in a full area excavation. After excavating area A, install struts over the area and proceed to the excavation in area B, which is again a small-sized site with struts in area A to support point ***a***. Less wall deformation will then be generated accordingly at point ***a*** or ***b***. After the installation of struts in area B, repeat the same procedures and then proceed to the next stage of excavation till completion.

3.3 Retaining walls

3.3.1 Soldier piles

Types of steel for soldier piles include the rail pile, the steel H-pile (or W section) and the steel I-pile (or S section). The rail pile and the steel H-pile are more commonly used than

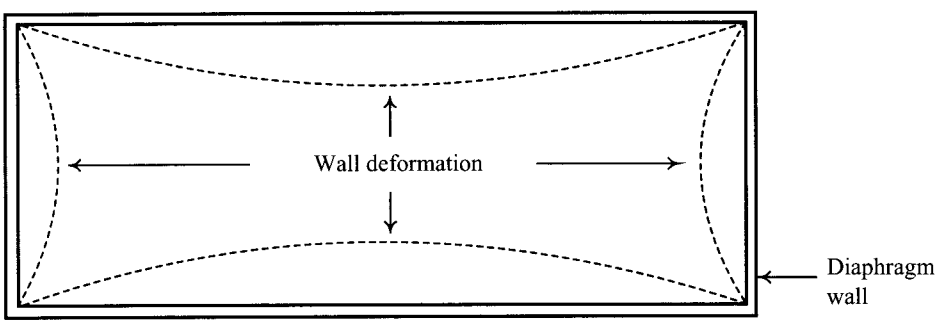

Figure 3.13 Plan of an excavation.

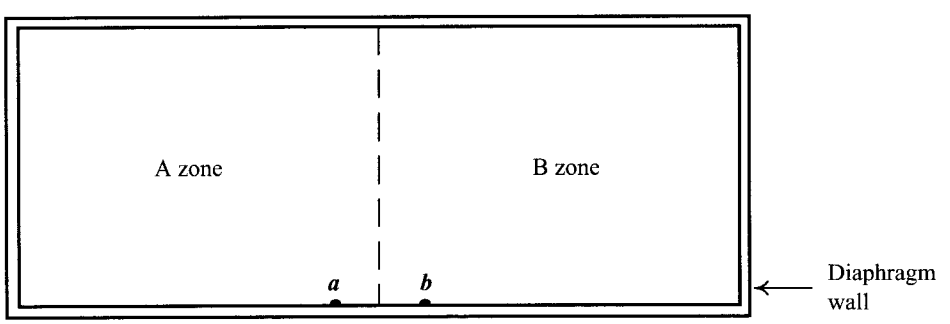

Figure 3.14 Plan of the zoned excavation method.

the steel I-pile. The commonly used sizes (dimensions) of these sections of the two types are offered in Appendix C, where this section of the rail pile is usually expressed in weight per unit length (kg/m).

It is optional to place laggings between soldier piles. Whether to place them or not depends on the in situ soil properties and strength characteristics. As Figure 3.15 illustrates, the construction procedure for soldier piles can be described as follows:

1 Strike soldier piles into soil. In non-urban areas, it will be all right to strike them into soil directly. In urban areas, however, static vibrating installation would be the better way to have soldier piles penetrated into the soil. If encountering a hard soil layer, pre-bore the soil.
2 Place laggings as excavation proceeds. Then backfill the voids between soldier piles and laggings.
3 Install horizontal struts in proper places during the excavation process.
4 Excavation completed, begin constructing the inner walls of the basement. Then remove struts level by level and construct floor slabs.

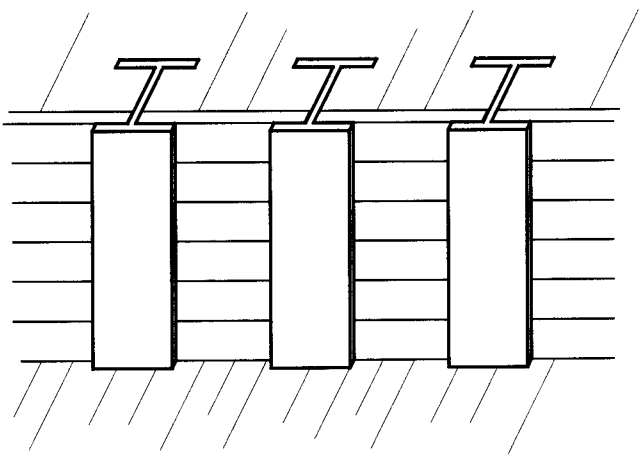

(a)

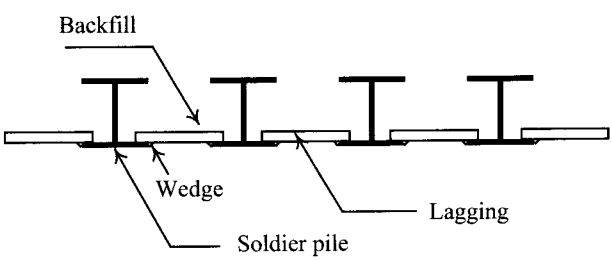

(b)

Figure 3.15 Soldier piles: (a) front view and (b) section view.

5 Complete the basement.
6 Pull out the piles.

The merits of soldier piles include:

1 Easier and faster construction with lower cost.
2 Piles can be easily pulled out.
3 It is necessary that less ground disturbance is caused when pulling out the piles, compared to pulling out sheet piles.
4 The pile tip can be strengthened with special steel materials for use in gravel soils.
5 Soldier piles are reusable.

The drawbacks of soldier piles include:

1 Sealing is difficult. In sandy soils with high groundwater level some dewatering measures may be necessary.
2 Installing soldier piles by striking will cause much noise and vibration. The latter will render sandy soils below the foundation denser in such a way that uneven settlement of the adjacent buildings may occur.
3 Backfilling is necessary if soldier piles are driven using pre-boring. Deficiency in backfilling will cause bad effects in the vicinity.
4 The voids between retaining walls and surrounding soil need filling.
5 Removing piles will disturb the surrounding soil.

Figure 3.16 is a photo of the soldier pile method.

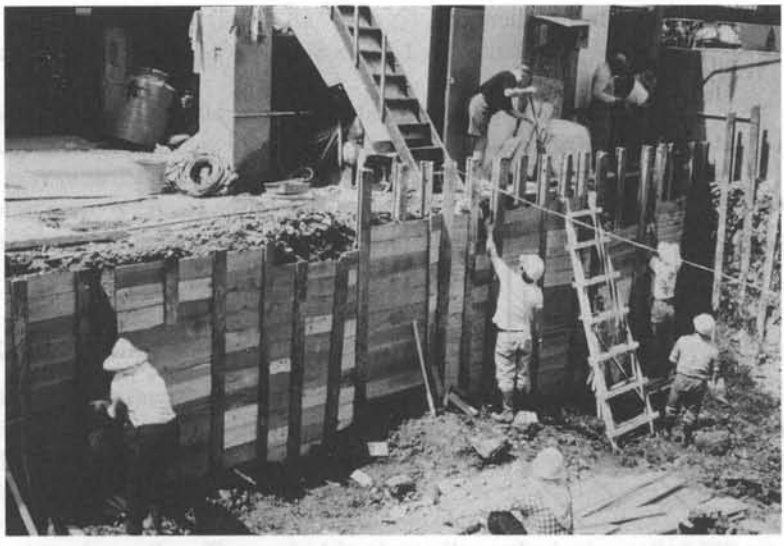

Figure 3.16 Photo of the soldier pile method.

3.3.2 *Sheet piles*

Sheet piles can be driven into soil by striking or static vibrating and have them interlocked or connected with one another. Figure 3.17 shows the front view of sheet piles and Figure 3.18 is a photo showing the sheet piles in an excavation. There are several shapes of sheet pile sections. Some commonly used include the U-section, Z-section, and the line-section, as shown in Figure 3.19. If the interlocking is well done, sheet piles can be quite efficient in water sealing. If not, leaking may occur at the joints. In clayey soils, having low permeability, sheet piles do not necessarily require perfect connection to prevent leaking. On the other hand, if they are used in sandy soils, with high permeability, any breach in sheet piles may well cause leaking. If leaks occur, sand in back of the retaining walls will very possibly flow out, which may cause settlement in turn. If leakages are too great, the excavation might be endangered. The construction method for sheet piles can be described as follows:

1 Drive sheet piles into soil by striking or static vibrating.
2 Proceed to the first stage of excavation.
3 Place wales in proper places and install horizontal struts.
4 Proceed to the next stage of excavation.
5 Repeat procedures 3 and 4 till the designed depth.
6 Complete excavation and begin to build the foundation of the building.
7 Build the inner walls of the basement. Dismantle the struts level by level and build the floor slabs accordingly.
8 Complete the basement.
9 Dismantle the sheet piles.

The merits of the steel sheet pile method are:

1 It is highly watertight.
2 It is reusable.
3 Has higher stiffness than soldier piles.

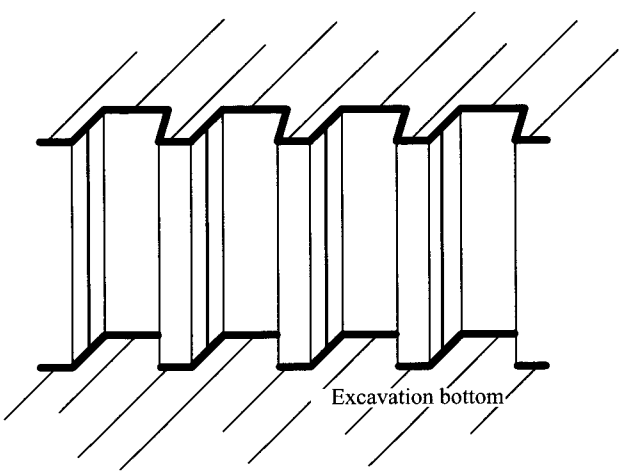

Figure 3.17 Steel sheet pile method.

Figure 3.18 Photo of the steel sheet pile method.

The drawbacks of the steel sheet pile method are as follows:

1 Lower stiffness than column piles or diaphragm walls.
2 Susceptible to settlement during striking or dismantling in a sandy ground.
3 Not easy to strike piles into hard soils.
4 A lot of noise is caused during striking.
5 Leaks cannot be completely avoided and sealing and grouting are probably necessary if leaks occur.

3.3.3 Column piles

The column pile method is to construct rows of concrete piles as retaining walls by either the cast-in situ pile method or the precast pile method. Figure 3.20 is a photo of the column pile wall. The cast-in situ method can be divided into three subtypes according to their construction characteristics:

1 Packed in place piles: The packed in place pile method, also called PIP pile method, can be described as follows: dig to the designed depth with a helical auger; while lifting the

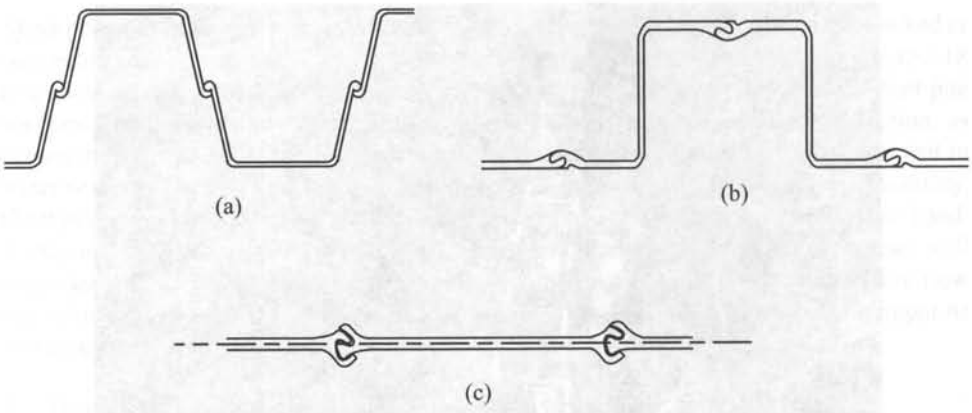

Figure 3.19 Sections of steel sheet piles: (a) U pile, (b) Z pile, and (c) straight pile.

Figure 3.20 Photo of column piles.

chopping bit gently, fill in prepacked mortar from the front end to press away the loosened soil to the ground surface; after grouting is finished, put steel cages or steel H-piles into the hole. The diameter of a PIP pile is around 30–60 cm. It often happens that PIP piles are not capable of being installed completely vertically, so connections are not always watertight, and connection voids often cause leaks of groundwater. Thus, if the PIP pile is adopted for the retaining wall in sandy soils with high groundwater level, sealing and grouting are often required. Figure 3.21 illustrates the construction of a PIP pile.

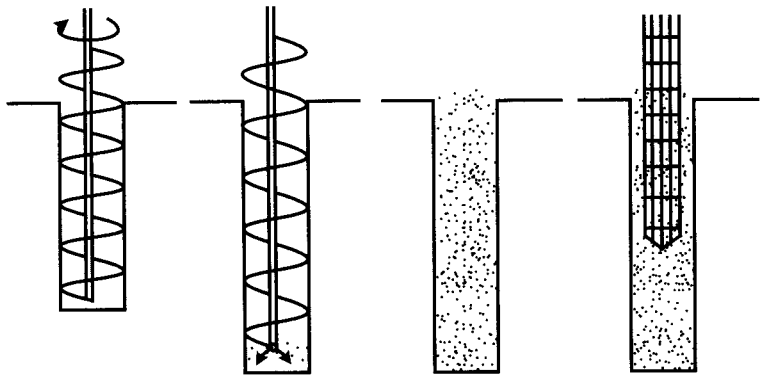

Figure 3.21 Construction procedure of a packed in place (PIP) pile.

2 *Concrete piles*: The construction of concrete piles can be described as follows: drill a hole to the designed depth by machine, put the steel cages into it, and fill it with concrete using Tremie tubes.

The reverse circulation drill method (also called the reverse method), which is to employ stabilizing fluid to stabilize the hole wall during drilling, is the most commonly used construction method for concrete piles. It is also feasible to build following the all casing method, which is to drill with simultaneous casing-installment to protect the hole wall. Since the wall is protected by casings, stabilizing fluid is not required. The cost of the all casing method is rather high. Nevertheless, it can be easily applied to cobble-gravel layers or soils with seepage whereas the reverse method cannot. The diameters of the concrete piles are around 60–200 cm.

3 *Mixed piles*: Mixed piles are also called MIP piles (mixed in place piles) or SMW (soil mixed wall). The method is to employ a special chopping bit to drill a hole with the concrete mortar sent out from the front of the bit to be mixed with soil. When the designed depth is reached, lift the bit a little, keeping swirling and grouting simultaneously, and let mortar mix with soil thoroughly. After pulling out the drilling rod, put steel cages or H-piles into the hole if necessary. Figure 3.22 illustrates the construction process for a mixed pile. Figure 3.23 shows MIP piles with H steels.

Precast methods use precast PC piles or steel pipes placed into soil by static pressing, pre-boring, or striking.

As illustrated in Figure 3.24, the patterns of column piles include the independent pattern, the S pattern, the line pattern, the overlapping pattern, and the mixed pattern. They can be described as follows:

1 *Independent pattern*: As shown in the figure, sealing is impossible with the independent pattern. Thus, excavation in permeable ground with high groundwater level requires dewatering in advance. The pattern, nevertheless, is especially fitting for soil with high strength, such as gravel soils.

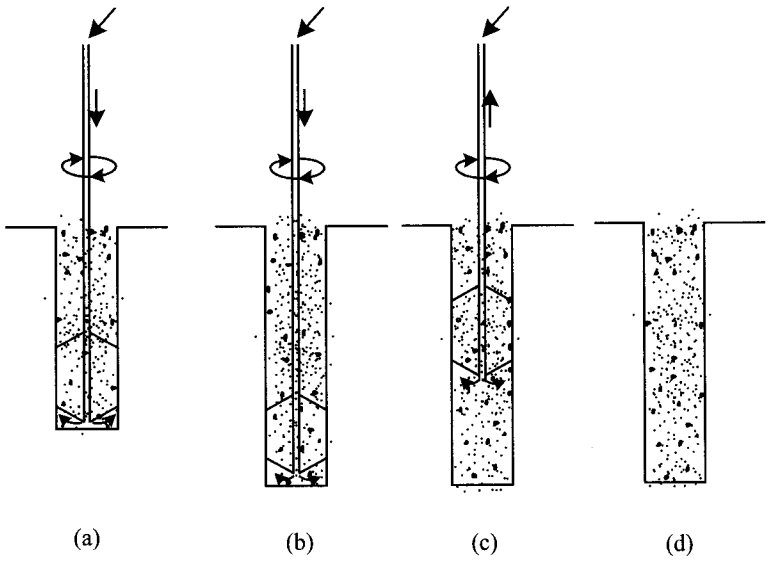

Figure 3.22 Construction procedure of a mixed in place (MIP) pile: (a) swirl the drilling rod and inject mortar into the soil from the bottom of the drilling rod, (b) drill to the designed depth and treat the soil simultaneously while keeping swirling, (c) withdraw the drilling rod and inject the mortar simultaneously, and (d) finish the improvement.

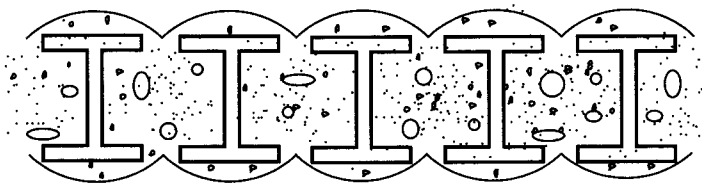

Figure 3.23 Soil mixed wall (SMW).

2 S pattern: The second row of piles fits into gaps in the first row, which have been arranged in the independent pattern. This pattern is also called the tangent piles. The method is relatively simple in construction. On the other hand, the sealing capability is weak because of the less orderly layout. Grouting is necessary for sealing.

3 Line pattern: Being one type of tangent piles, the piles are connected to one another to form a line. It is also one of the most commonly used patterns. Since sealing capability is not good, chemical grouting is often required to make up for the problem.

4 Overlapping pattern: As shown in Figure 3.24, after piles No. 1, 2, and 3 are completed, before they congeal, construct piles No. 4, 5, and 6 piles in order. The latter will cut through the former. They, therefore, are also called secant piles. The overlapping pile can only be cast in the field. Precast piles cannot be used for this type of pattern. The pattern is good for sealing.

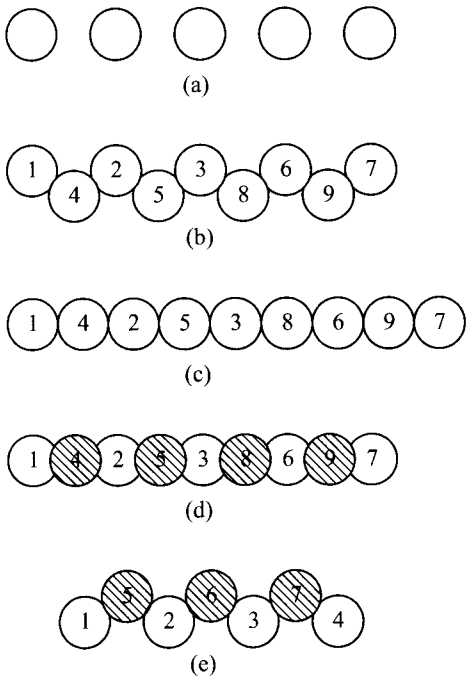

Figure 3.24 Layouts of column piles: (a) independent pattern, (b) S pattern, (c) line pattern, (d) overlapping pattern, and (e) mixed pattern.

5 *Mixed pattern*: The mixed pattern is the independent pattern along with jet grouting or MIP piles. If grouting quality is guaranteed, the sealing capability of the mixed pattern will be fairly good.

The merits of column piles are:

1 Less noise or vibration than produced by the installation of soldier piles or steel sheet piles.
2 Adjustable pile depth.
3 Greater stiffness than soldier piles or steel sheet piles.
4 When equipped with a special bit, they are also applicable to cobble-gravelly soils.
5 Easier construction on sandy ground.

The drawbacks of column piles are:

1 Without lateral stiffness in the direction parallel to the excavation side, no arching effect to prevent wall deformation exists.
2 Longer construction period than that for the soldier pile method or the steel sheet pile method.
3 Lower stiffness than diaphragm walls.
4 Highly susceptible to construction deficiency.

3.3.4 *Diaphragm walls*

Diaphragm walls are also called slurry walls. Since first adopted in Italy in the 1950s, they have been widely used around the world. With technological advances, more and more new methods and construction equipment have been developed. The basement wall (BW) method and Impresa Construzioni Opere Specializzate (ICOS) method, designed separately by a Japanese company and an Italian company are commonly used in some Asian countries. The Masago Hydraulic Long bucket (MHL) method, taking advantage of a bailing bucket to excavate the trenches of the diaphragm wall, are also used in many countries. As shown in Figure 3.25, the teeth of the steel bailing bucket can clutch soils and rocks and store them inside the bucket. Then, the full bucket is lifted out of the trench and soil and rocks inside are bailed out. Thus, stabilizing fluid need not be pumped out and mud separation equipment is saved. The method is easy in operation. The span of the bailing bucket is about 2.5–3.3 m.

The first stage of the constructing of diaphragm walls is to divide the whole length into several panels according to the construction conditions. The construction procedure of each panel is as follows: the construction of guided walls, the excavation of trenches, placing steel cages, and concrete casting, as shown in Figure 3.26. After excavating the trench, mud in the trench must be cleared from the trench. Concrete casting, the last stage of diaphragm wall panel construction, adopts the Tremie pipe to pour concrete into the trench and form a diaphragm wall panel. Figure 3.27 shows the construction procedure of a diaphragm wall panel, including excavating trenches, placing connection pipes (depending on the method), placing steel cages, and concrete casting. Figure 3.28 is a photo depicting the placing of a steel cage into the trench with a crane.

The joints between panels of a diaphragm wall have to be carefully treated so that they are watertight and are able to transmit bending moments and shear forces. There are many types of joints of diaphragm walls. There is no standard form. Some patent methods are available. The connection pipe method and the end-plate method are the commonly used joint methods. The former is highly watertight. On the other hand, its capability of transmitting bending moments and shear forces is not good enough. If the diaphragm walls are confined to the temporary use of soil retaining, the connection pipe method can serve the purpose well. If

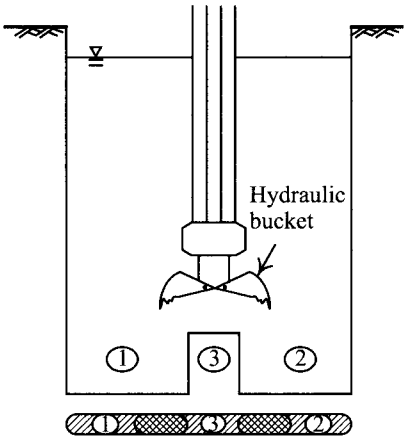

Figure 3.25 Trench excavation by the MHL method.

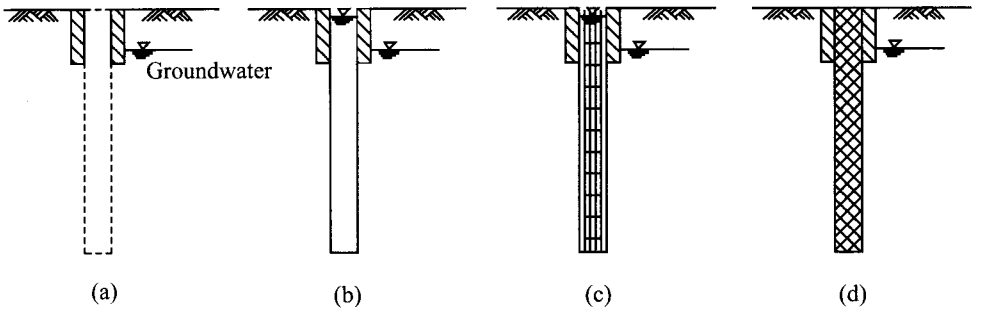

Figure 3.26 Construction procedure of a diaphragm wall panel: (a) construction of the guided wall, (b) excavation of the trench, (c) placement of reinforcements, and (d) concrete casting.

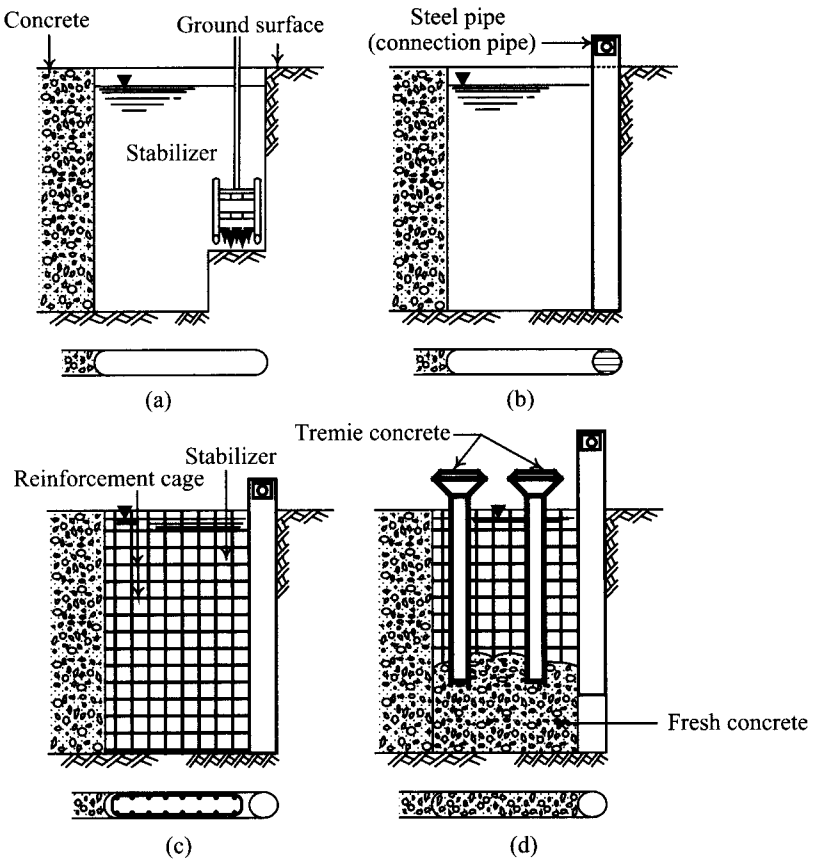

Figure 3.27 Procedure of construction of a diaphragm wall: (a) trench excavation, (b) steel pipe installation, (c) steel cage placement, and (d) concrete casting (redrawn from Xanthakos (1994)).

Figure 3.28 Photo of the diaphragm wall method.

they are meant for permanent structures, the end-plate method is recommended for its better capability to transmit bending moments and shear forces.

As shown in Figures 3.27 and 3.29, when the trench excavation of the primary panel is finished, put a connection pipe into the trench, then place the steel cage with a crane and pour concrete into the trench. Once the concrete has been poured, dismantle the connection pipe in two or three hours and proceed to the construction of the secondary panel.

Figure 3.30 illustrates the end-plate method where the joints between panels are lateral overlapping reinforcements connected to each other. The reinforcements of the primary panel extend outside the end plate to overlap with the reinforcements of the secondary panel. The end plate is a thick steel plate, 3–5 cm smaller than the thickness of diaphragm walls and some 30 cm deeper than the depth of diaphragm walls, to be embedded into the bottom soil of the trench to prevent lateral displacement of the end plate. The ends of the end plate are equipped with strong nylon fibers to make a blocking screen, together with the end plate, to prevent the grouting concrete from leaking into the evacuated trenches. This type of joint is capable of transmitting bending moments and shear forces. Theoretically speaking, it can be fairly water-tight under normal construction conditions. The actual results, however, are not satisfactory.

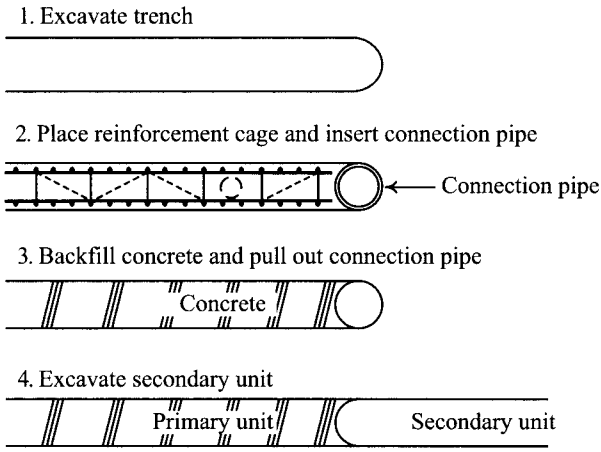

Figure 3.29 Joint of diaphragm walls: the connection pipe method.

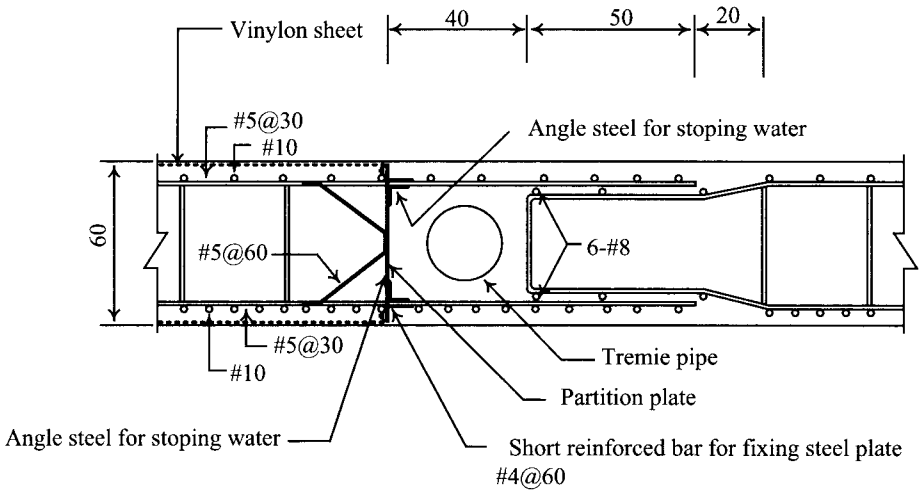

Figure 3.30 Joint of diaphragm walls: the end-plate method (unit: cm).

Many improvement measures have been developed (Lee, 1983, 1988), some of which require jet grouting near the joints to prevent the leaking of diaphragm walls during excavation.

To ensure the quality of diaphragm walls, many other construction details need to be taken care of. Concerning the construction details of diaphragm walls, interested readers are advised to read Xanthakos (1994).

The merits of diaphragm wall methods include:

1 Low vibration, low noise, high rigidity, and relatively small wall deformation.
2 Adjustable thickness and depth of the wall.
3 Good sealing capability.

4 May be used as a permanent structure.
5 The diaphragm wall and foundation slabs form a unity, such that the former can serve as pile foundations.

The drawbacks of the diaphragm wall method are:

1 Massive equipment is required, long construction period, and great cost.
2 The peripheral equipment (e.g. the sediment pool) occupies a large space.
3 This method is not applicable to cobble-gravelly grounds.
4 It is difficult to construct when encountering quick sand.

Though there are several merits in this method, and it involves matured construction technology, diaphragm walls as retaining walls have engendered quite a few excavation accidents. The reason is either geological uncertainty or bad quality control, or both. Engineers should keep studying how to improve the construction technology under different geological conditions by consulting case histories.

3.4 Strutting systems

Other than the gravity retaining walls (the retaining wall alone can rarely resist the lateral pressure), supplementary strutting systems are also required. The selection of the strutting system depends on, not only the magnitude of lateral pressure, but also on the period it will take to install the strutting system and the obstruction it may bring about on the construction.

According to the material a strut is made of, there are wood struts, Reinforced concrete (RC) struts, and steel struts. In countries that are abundant in wood, for the sake of saving costs, horizontal wooden struts are employed in excavations that are narrow and not deep. Wood struts are of relatively low cost but their compression strength, knots, cracks, and susceptibility to erosion lead to low axial stiffness. Besides, it is difficult to splice wood pieces with one another, they are not reusable, and the scarcity of wood in some countries also makes the wood strut an unwelcome choice.

The axial stiffness of RC struts is high and thus they are applicable to excavations of various shapes without causing stress relaxation. The RC strut, on the other hand, with its heavy weight, is not easy to dismantle. Also, preload cannot easily act on it. It takes some time for the strength of the RC strut to work.

As for steel struts, except that they cannot easily be used at sites of great topographical undulation or of great width, the merits of steel struts are many: easy to install and dismante, short construction period and low cost, easy to be preloaded. They have been widely accepted for strutting systems in many countries now.

According to the function of a strut, it is classified as an earth berm, a horizontal strut, a raker, an anchor, or as a top-down floor slab, etc. Figure 3.31 shows an earth berm, which is made by removing the soil in the central area while retaining an earth berm with a certain width for the lateral support of retaining walls. The earth berm is usually supplementary to island excavation methods. With the limitation of the width, the earth berm has accordingly limited lateral resistance and is useful only on grounds with high strength, and is rendered useless on soft ground.

Horizontal struts can be made of wood, RC, or steel, whose merits and drawbacks are as mentioned earlier.

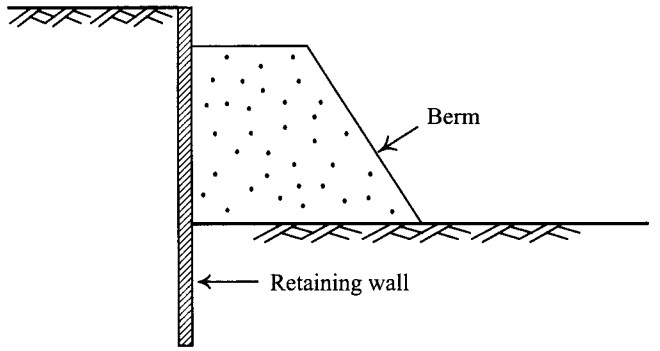

Figure 3.31 Earth berm as lateral support.

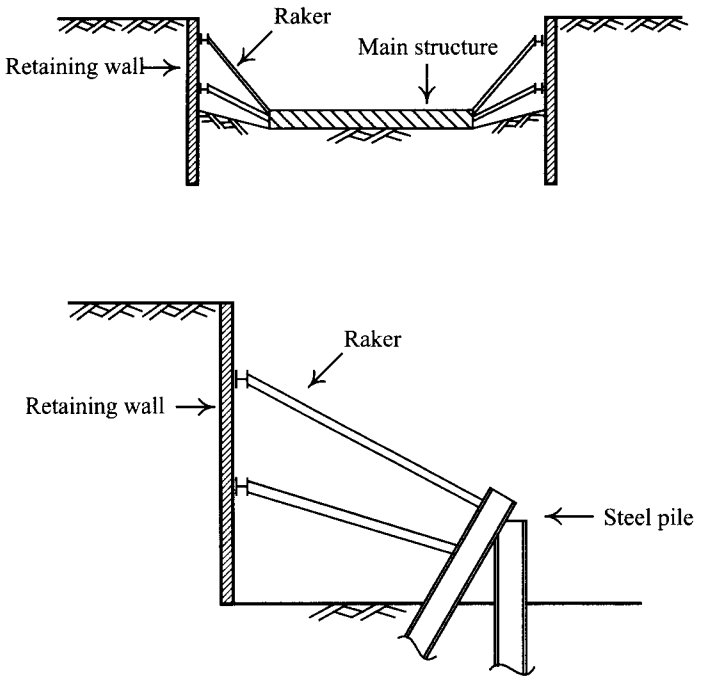

Figure 3.32 Rakers.

A raker is a type of strut and can also be made of wood, RC, or steel. Known from the systematic characteristics of a structure, the lateral support from the raker is smaller than that from the horizontal strut. Rakers are mostly employed in the island excavation method though they can also be used separately as shown in Figure 3.32. Anchors and top-down floor slabs are two other types of struts. Concerning their structures, applications and strengths and shortcomings, please see Sections 3.2.3 and 3.2.5.

Table 3.1 Application conditions for retaining walls

Wall type	*Soil type*			*Sealing and stiffness*		*Construction conditions*				*Excavation depth*	*Construction period*	*Budget*
	Soft clay	*Sand*	*Gravel soil*	*Sealing*	*Stiffness*	*Noise and vibration*	*Treatment of dump mud*	*Surface settlement*	*Underground obstruction*			
Soldier pile	×	○	○[1]	×	×	×[2]	◎	×	○	×	◎	◎
Steel sheet pile	○	◎	×	○	×	×[2]	◎	×	○	×	◎	◎
PIP pile	◎	○	×	○	◎	◎	×	○	×	○	×	○
Reinforced concrete column pile	◎	◎	×	◎	◎	◎	×	◎	×	◎	×	×
MIP pile	○	○	×	◎	○	◎	○	○	×	○	○	○
Diaphragm wall	◎	◎	○	◎	◎	◎	×	◎	×	◎	×	×

◎: good ○: acceptable ×: not good.

Notes
1 Should be applied along with special drill and striking device.
2 If driven into soil by static vibrating process, noise and vibration can be reduced.

3.5 Selection of the retaining strut system

The retaining strut system consists of retaining walls and strutting systems. The selection of retaining walls has to consider the excavation depth, geological conditions, groundwater conditions, adjacent building conditions, the site size, the construction period, and the budget, etc. The characteristics of retaining walls are as described in Section 3.3. Table 3.1 offers the application ranges of various retaining walls for design or construction reference.

Table 3.2 illustrates the nominal stiffness per unit length where the value of moment of inertia (I) is not reduced. A stress or deformation analysis, however, has to consider the decrease of stiffness of a soldier pile or a steel sheet pile because of repetitive use. A discount of 80% of the nominal stiffness is often suggested.

The f_c'-value of a PIP pile is about 170 kg/cm^2 while that of a concrete pile, a reverse circulation drill pile, or a diaphragm wall is about 210 kg/cm^2 or more. Their Young's modulus can be derived from $E = 15,000\sqrt{f_c'}$ kg/cm^2. Considering the cracks in the retaining wall due to bending moment, the moment of inertia may be reduced by 30–50%. Since the compressive strength of a mixed pile is very small, about 5 kg/cm^2, its stiffness can be estimated solely on the basis of the stiffness of the H- steel. Listed in the sixth column of Table 3.2 are the stiffness ratios where the inverse values represent the deformation ratios under the same construction condition (i.e. same excavation depth, strut location, and strut stiffness, etc.). For example, the deformation of a SP-III steel sheet pile is 6.63 (5.3/0.8) times as great as a 50 cm thick diaphragm wall.

The selection of the strutting system is highly related to the excavation method and thus, there are not many choices for selection. This section will not go into further discussion of the topics.

Table 3.2 Nominal stiffness (before reduction)

Retaining wall		E (kg/cm^2)	I (cm^4/m)	EI (t-m^2/m)	*Stiffness ratio*
Method	*Type and dimension*				
Soldier pile[1]	H 300 × 300 × 10 × 15	2.04 × 10^6	20,400	4,160	1.0
	H 350 × 350 × 12 × 19	2.04 × 10^6	40,300	8,220	2.0
Steel sheet pile[2]	SP-III	2.04 × 10^6	16,400	3,350	0.8
	SP-IV	2.04 × 10^6	31,900	6,500	1.6
Column pile[3]	30 cm (diameter)	2.10 × 10^5	132,500	2,780	0.7
	80 cm (diameter)	2.10 × 10^5	2,513,300	52,780	12.7
MIP pile[4]	SMW method H 400 × 200 × 8 × 13	2.04 × 10^6	59,250	12,090	2.9
Diaphragm wall[5]	50 cm thick	2.1 × 10^5	1,041,700	21,900	5.3
	100 cm thick	2.1 × 10^5	8,333,300	175,000	42.0

Notes

1 The distance between H-steels is 1.00 m. The stiffness of the soldier pile can be reduced by 20% in analysis.

2 The stiffness of the sheet pile can be reduced by 20% in analysis.

3 f_c' for PIP piles is about 170 kg/cm^2; f_c' for reinforced concrete column piles is about 280 kg/cm^2; in the table f_c' is assumed to be 210 kg/cm^2, which can be reduced by 30–50% in analysis.

4 f_c' for MIP piles is about 5 kg/cm^2, that is, the stiffness of the MIP can be ignored and only the stiffness of H-piles is to be considered. The distance between H-piles in the table is 40 cm.

5 f_c' is assumed to be 210 kg/cm^2. The stiffness can be reduced by 30–50% in analysis.

3.6 Case history of the TNEC excavation

The author and collaborators (1998, 2000a,b) have conducted thorough investigations of the excavation of TNEC (Taipei National Enterprise Center). The objects of the investigations include the soil properties of the site, the stress behavior of excavation, and the strain and displacement behaviors of soil. The excavation of TNEC is a typical case of the top-down construction method. Since the process has been thoroughly documented, the excavation of TNEC is an ideal object for case study. Engineers can obtain information on the excavation depth for each stage, distances between the excavation surface and floor slab, the period of each stage, etc., for design or construction reference. Synthetically studying the soil properties introduced in Section 2.11, the excavation process to be discussed in this section and the monitoring results of stress and deformation caused by excavation (Chapter 6), we can further understand excavation behavior in general. Besides, these data are useful for verification of analysis methods (Chapters 7 and 8). The related data of the excavation of TNEC are as indexed in Appendix B.

Figure 3.33a is the plan of the construction site of TNEC. As shown in the figure, the site was basically a trapezoid 60–105 m long and 43 m wide. There were six buildings A, B, C, D, E, and F in the neighborhood of the site. C and D were old four-story RC apartments with individual footings. A, B, E, and F were high rise buildings with mat foundations. On A, B, D, and E were installed tiltmeters. Three in-wall inclinometer casings were installed on the southern diaphragm of the site, the eastern one of which was also equipped with many rebar stress meters and earth/water pressure cells on this section. To the south of the site were placed many ground settlement marks, serial extensometers and in-soil inclinometer casings. Concerning the details of the allocation of the instruments, please refer to the author's previous studies (Ou *et al.*, 1998, 2000a,b).

The construction of the diaphragm wall of TNEC started on August 13, 1991 and was completed on November 10, 1991. The monitoring devices, including earth/water pressure cells, rebar stress meters and inclinometer casings, were installed as the diaphragm wall were being built. For the convenience of description, take the first day that diaphragm wall construction started as the base, the completion day of the diaphragm wall construction would be the 89th day. Figure 3.34 and Table 3.3 show separately the illustration of the top down construction process and the schedule of the construction operation. Known from Table 3.3, the excavation is divided into 16 construction stages where the 1st, 3rd, 5th, 7th, 9th, 11th, and the 13th are excavation stages and the 2nd, 4th, 6th, 8th, 10th, 12th, 14th, and the 15th are strut installation or floor slab construction stages. The table also records the detailed start and end time of each stage.

With the completion of the diaphragm wall, the construction of foundation piles and steel columns proceeded, which are necessary to the top-down construction method. The construction of foundation piles was finished on the 155th day. Then, piezometers and heave gauges were installed in the excavation area. When all monitoring instruments had been set up, the excavation operation was initiated on the 156th day.

As Table 3.3 shows, on the 156th day the excavation operation started. The first stage was the first excavation operation with the excavation depth down to GL-2.8 m. The excavation period was six days, that is, the completion day of the first stage was the 162nd day. Then followed the second stage, which was the installation of the first level of struts. The struts were H300 × 300 × 10 × 15 steel with 6–11 m long horizontal spans whose average was 8.0 m. A preload of 784.8 kN onto each strut was exerted. All finished, the second excavation operation (the 3rd construction stage) was started, whose excavation depth was down to GL-4.9 m. The

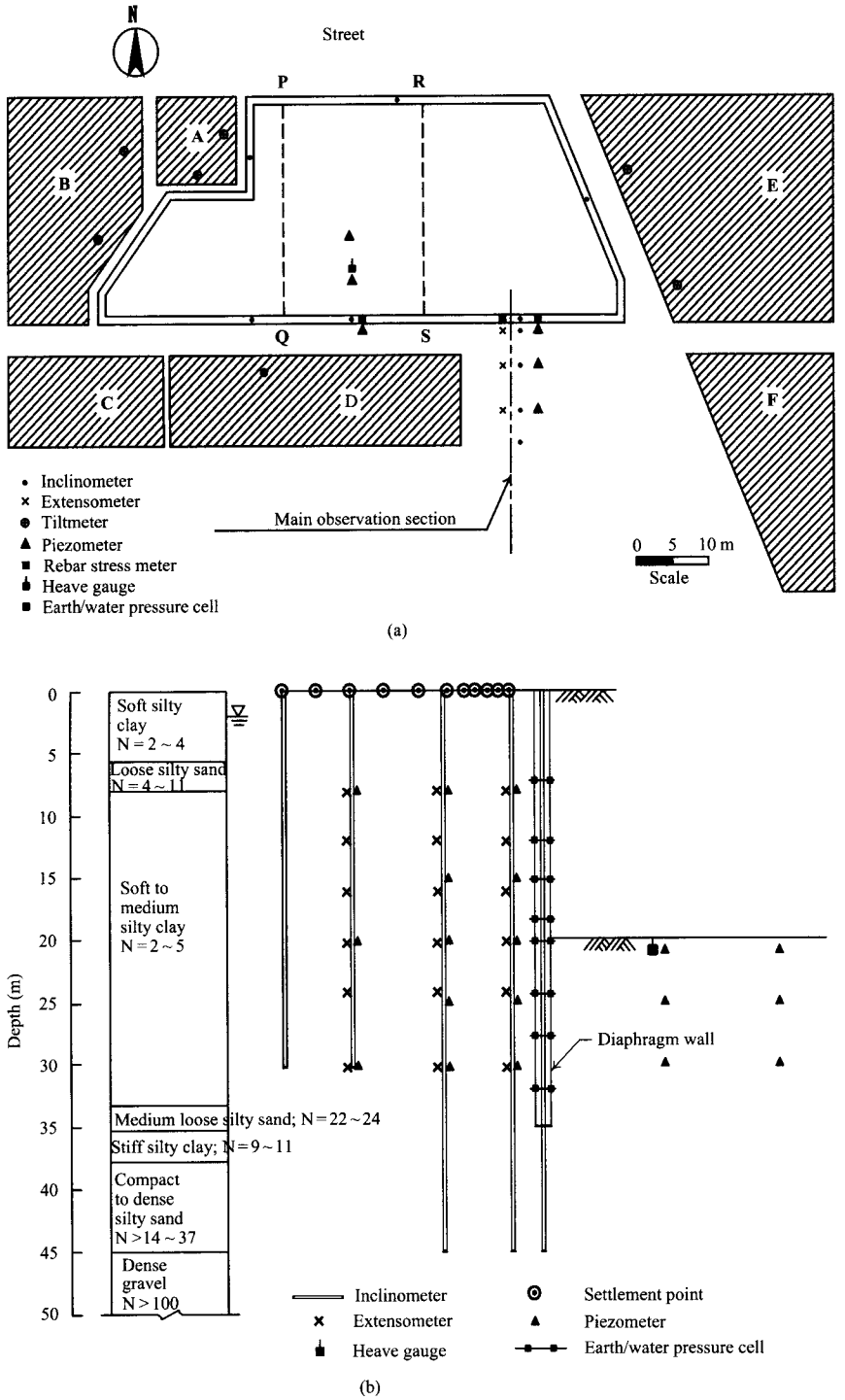

Figure 3.33 Excavation of the Taipei National Enterprise Center: (a) plan and (b) profile.

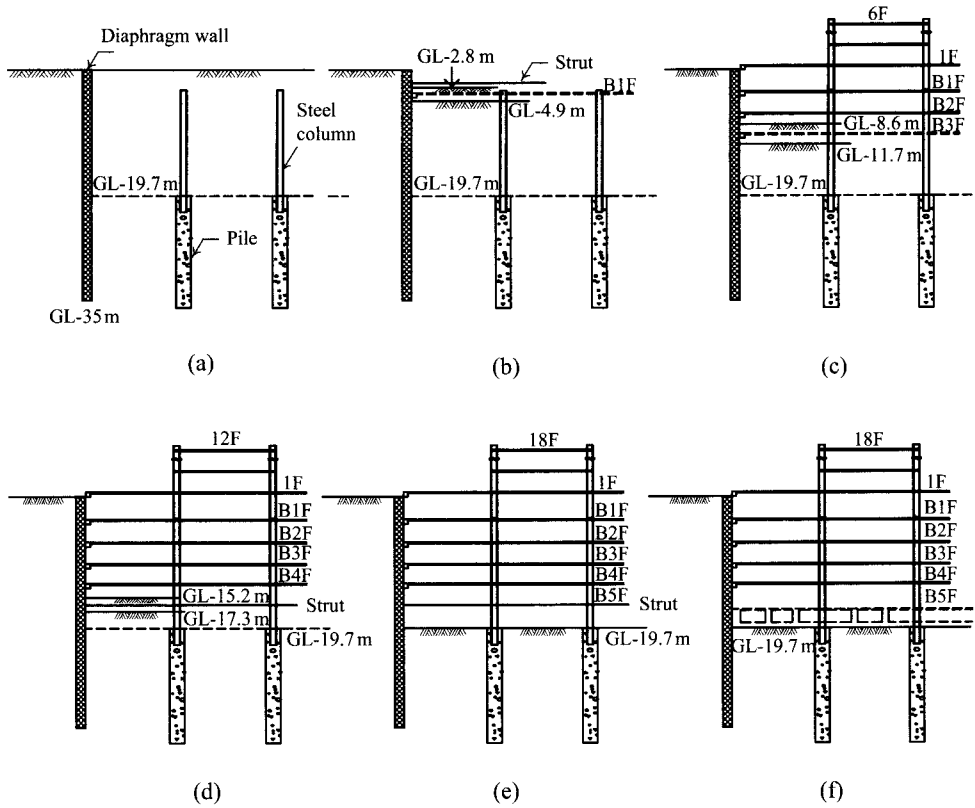

Figure 3.34 Construction procedure of the Taipei National Enterprise Center (see Table 3.3 for the description of the construction procedure).

operation took seven days to finish. Reaching the GL-4.9 m deep, 10 cm thick layer of pure cement was splashed onto the excavation surface. Formworks were set up for the construction of the B1F floor slab at GL-3.5 m. As the B1F floor slab was finished and had reached a certain degree of strength, the construction began to proceed upward (i.e. superstructure construction) and downward (i.e. basement construction) simultaneously. The 1F floor slab and the superstructure were built while at the same time the third excavation operation (the 5th stage) was started, whose depth was down to GL-8.6 m. After that, the excavation and the construction of floor slabs were repeated till the completion of the construction of the B4F floor slabs (the 10th stage).

After the 10th stage, considering that the deformation of the retaining walls had accumulated up to 8.0 cm (see Figure 6.9 in Chapter 6), to reduce the wall deformation, the zoned excavation method was adopted. That is, the central area would be excavated (the area PQRS in Figure 3.33) first. The central area was excavated to the depth of GL-17.3 m while at the depth of GL-16.5 m the second level of steel struts was set up. The east and west parts were excavated following the installation of the struts in the central area. Then the struts of the side areas were also installed. Thus, the 11th and 12th stages were further divided into 11A, 11B,

Table 3.3 Excavation process of TNEC

Stage	*Day*	*Excavation activities*
	−29 ~	Installed devices outside of the excavation zone, including in-soil inclinometers, extensometers, observation wells, and electronic piezometers
	1–89	Constructed the diaphragm wall, including installation of the earth/water pressure cells, in-wall rebar strain meters, and in-wall inclinometers
	89–147	Constructed piles and the steel columns
	147–155	Installed devices inside of the excavation zone, including the piezometers and heave gauges
1	156–162	Excavated to the depth of GL-2.80 m
2	164–169	Installed struts H 300 × 300 × 10 × 15 at the depth of GL-2.0 m. The preload of each strut = 784.8 kN
3	181–188	Excavated to the depth of GL-4.9 m
4A	217	Constructed B1F floor slab at the depth of GL-3.5 m
4B	222–238	Dismantled the first level of strut and constructed the 1F floor slab. Started the construction of the superstructure
5	233–255	Excavated to the depth of GL-8.6 m
6	279	Constructed the B2F floor slab at the depth of GL-7.1 m
7	318–337	Excavated to the depth of GL-11.8 m
8	352	Constructed the B3F floor slab at the depth of GL-10.3 m
9	363–378	Excavated to the depth of GL-15.2 m
10	400	Constructed the B4F floor slab at the depth of GL-13.7 m
11A	419–423	Excavated the central zone to the depth of GL-17.3 m
12A	425–429	Installed struts H 400 × 400 × 13 × 21 at the depth of GL-16.5 m in the central zone. The preload of each strut = 1177 kN
11B	430–436	Excavated the side zones to the depth of GL-17.3 m
12B	437–444	Installed struts H 400 × 400 × 13 × 21 in the two side zones at the depth of GL-16.5 m. The preload of each strut = 1177 kN
13	445–460	Excavated to the depth of GL-19.7 m
	457	Finished the superstructure
14	464–468	Cast the foundation slab
15	506–520	Constructed the B5F floor slab at the depth of GL-17.1 m
16	528	Dismantled the second level of struts

Note
The first day of the construction of the diaphragm wall is the datum, that is, the first construction day.

12A, and 12B stages. The second level of steel struts was H400 × 400 × 13 × 21 steel whose spans ranged from 2.5 to 6.0 m with an average of 3.4 m. Each strut was preloaded to 1,177 kN. The 7th excavation operation (the 13th construction stage) followed, reaching the final excavation bottom, which was GL-19.7 m deep. On the final excavation bottom was built the raft foundation. The construction of the raft foundation was divided into two stages: first the building of the raft foundation, then the building of the B5F floor slab (the 15th construction stage). When the concrete of the B5F floor had hardened, the second level of steel struts was removed (the 16th construction stage) and the whole excavation operation was finished.

The excavation of the foundation of TNEC lasted 372 days, from the 156th day, the beginning of the excavation operation, to the 528th days, the dismantling of the second level of steel struts. Counted from the beginning of the construction of the diaphragm wall (August 13, 1991), the total time of excavation was 528 days, as listed in Table 3.3.

During the construction of the diaphragm wall, the adjacent building, A, slanted slightly. To resolve the problem, after the completion of the diaphragm wall and before excavation (between the 102nd day and 124th day), some measures of ground improvement were taken: jet grouting between building A and the excavation site was performed. Nevertheless, the measures did not succeed. On the contrary, they brought about further slanting of building A. The ground improvement measures were held back temporarily (concerning the reasons, please refer to Section 11.4). Besides, considering the soil at the site was mostly clayey soil, only sumps were set up at the excavation zone and then the gathered water was pumped away.

3.7 Summary and general comments

The commonly used excavation methods introduced in this chapter, including the full open cut method, the braced excavation method, the anchored excavation method, the island excavation method, the top-down construction method, and the zoned excavation method, have their separate strengths and drawbacks. In practical application, one or several of them may be adopted independently or together according to the local geological conditions, the environmental conditions, available equipment, and the allowable construction period and budget. This is a challenge to the knowledge and experience of engineers.

This chapter also introduces retaining walls, including soldier piles, steel sheet piles, column piles, and diaphragm walls. Each method has its strengths and shortcomings. The first consideration in selecting the most suitable method is whether the construction of the retaining wall is possible under the local geological conditions. The second is how well the retaining wall is capable of sealing. Last, stress and deformation analyses are required to safeguard the safety of the retaining wall. How to select the most economical and safe retaining wall is another challenge to engineers. As to the strutting system, the room for selection is quite limited since its choice depends greatly on the selection of the excavation method. The commonly used methods include steel struts, anchors, top-down floor slabs, and earth berms.

At the end of this chapter is introduced the excavation process of TNEC, which is a typical case in Taiwan and was thoroughly documented concerning its geological data and excavation monitoring results. It is suggested to cross study the detailed information on the excavation, including the locations of the floor slabs, the distance between a floor slab and the excavation bottom, the excavation depth of each excavation stage and the time it took, along with the geological data described in Chapter 2 and the monitoring results that will be discussed in Chapter 6 in order to obtain more understanding of excavation behaviors.

Problems

3.1 List a table to elucidate the strengths and drawbacks of the full open cut method, the braced excavation method, the anchored excavation method, the island excavation method, and the top-down construction method in terms of geological conditions (sandy soils, clayey soils, and gravel soils), construction periods, excavation depths, and excavation widths.

3.2 List a table to elucidate the strengths and drawbacks of the soldier pile, the sheet pile, the column pile, and the diaphragm wall from the viewpoint of geological conditions (sandy soils, clayey soils, and gravel soils), construction period, excavation depth, and sealing capability.

3.3 According to the construction characteristics of solider piles and sheet piles, what kinds of excavation calamites and property damage might be produced in using them as retaining walls?
3.4 According to construction characteristics of PIP column piles, what kinds of excavation calamites and property damages might be produced in using them as retaining walls?
3.5 What kinds of excavation calamites and property damages might be produced if the diaphragm wall is used as a retaining wall in sandy soils with high groundwater pressure?
3.6 From literature, references, or excavations in progress, find an excavation case which adopts a different excavation method other than the six methods introduced in this chapter and elucidate its excavation process.
3.7 Elucidate the commonly used construction methods of diaphragm walls from literature or references and explain their applicability.
3.8 Elucidate the construction process of the MHL method of diaphragm wall construction.
3.9 Elucidate the construction process of the ICOS method of diaphragm wall construction.
3.10 Elucidate the construction process of the BW method of diaphragm wall construction.
3.11 Explore the strengths and drawbacks and applicability of the MHL, ICOS, and BW methods according to literature and references.
3.12 Explicate the construction process of the reverse circulation drill method.

Chapter 4

Lateral earth pressure

4.1 Introduction

Problems of deep excavation, no matter if stability analysis (Chapter 5), stress analysis or deformation analysis (Chapters 6–8), entail the distribution of earth pressures. Though introductory books on soil mechanics or foundation engineering have discussed quite a few earth pressure theories along with many examples, a systematic organization is lacking. Some important points may not be sufficiently emphasized. In actual analyses, a wrong choice of earth pressure theory may lead to an uneconomical or even unsafe design. This chapter is going to do systematic organization and to simplify the complicated calculations for excavation analyses and design. Most of the methods introduced here have been frequently used in engineering practice though they have not been introduced in general textbooks. Common examples of the calculation of earth pressures, since many exist in books on soil mechanics and foundation engineering, are not to be discussed in the chapter but will be left in the exercise problems at the end of the chapter. The exercise problems are mostly those that have been encountered in engineering practice.

4.2 Lateral earth pressure at rest

Figure 4.1 shows a vertical retaining wall whose height is H. Suppose friction does not exist between the retaining wall and the soil. When the wall is not allowed to move, the stresses at depth, z, below the ground surface are under elastic equilibrium with no shear stress. Supposing the vertical effective overburden stress is σ'_v, and lateral effective stress σ'_h, then:

$$\sigma'_h = K_0 \sigma'_v \tag{4.1}$$

where K_0 = coefficient of lateral earth pressure at rest.

The total lateral stress is

$$\sigma_h = \sigma'_h + u \tag{4.2}$$

where u is porewater pressure, the sum of the static water pressure and excess porewater pressure.

For cohesionless soils, K_0 can be estimated by Jaky's (1944) equation:

$$K_0 = 1 - \sin \phi' \tag{4.3}$$

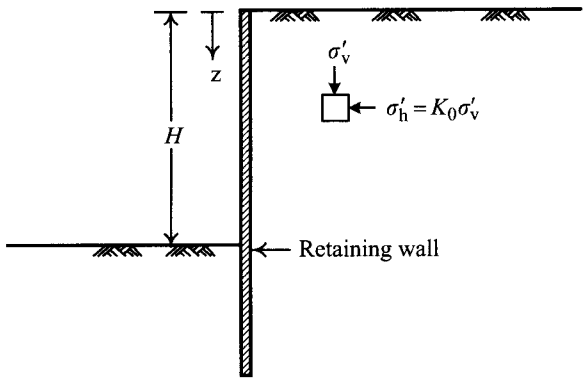

Figure 4.1 Lateral earth pressure at rest.

where ϕ' = effective internal angle of friction (also called the effective angle of shearing resistance or the drained angle of shearing resistance).

When cohesionless soils are in the unloading or preconsolidated states (i.e. overconsolidated), K_0 can be expressed by the following equation (Alpan 1967; Schmidt 1967):

$$K_{0,OC} = K_{0,NC}(OCR)^{\alpha} \tag{4.4}$$

where $K_{0,OC}$ = coefficient of lateral earth pressure at rest of overconsolidated soils with overconsolidation ratio, OCR; $K_{0,NC}$ = coefficient of lateral earth pressure at rest of a normally consolidated soil; α = empirical coefficient, $\alpha \approx \sin\phi'$.

Ladd *et al.* (1977) suggested that K_0 of normally consolidated cohesive soils can also be estimated by Eq. 4.3. For overconsolidated soils, Ladd *et al.* (1977) suggested that K_0 can be obtained by Eq. 4.4, where the α-value decreases slightly with the increase of the plasticity index (PI). For example, when PI = 20, α = 0.4; when PI = 80, α = 0.32. The α-value does not actually vary much. When applied to practical cases, we can select an appropriate α-value according to the above experimental results.

Generally speaking, for normally consolidated cohesive or cohesionless soils, Eq. 4.3 can produce quite satisfactory results. For overconsolidated soils, nevertheless, cohesive and cohesionless alike, the results from Eq. 4.4 are relatively inaccurate. One of the reasons is that the formation process of overconsolidated soils is complicated. To obtain the most appropriate K_0-value, the best way is to carry out an in situ test.

4.3 Rankine's earth pressure theory

Rankine (1857) developed a theory of lateral earth pressure in conditions of failure in front of and in back of a retaining wall on the basis of the concept of plastic equilibrium.

As Figure 4.2a shows, the parameters of soil strength both in front of and in back of the retaining wall are c and ϕ. Suppose there exists no friction between the retaining wall and the soil and the earth pressure both in front of and in back of the retaining wall is at K_0 before

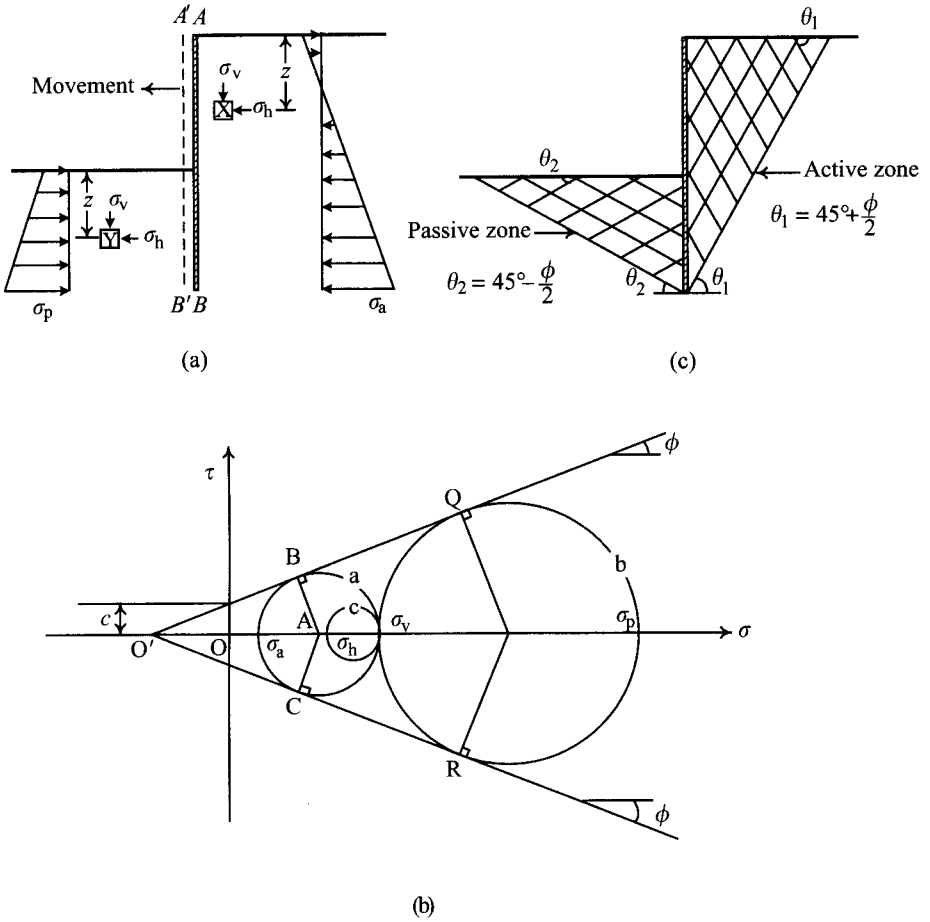

Figure 4.2 Rankine's earth pressure theory.

the retaining wall moves. The vertical stress, σ_v, at X and Y near the wall and at depth, z, below the ground surface are the same and the stress conditions can be represented by the Mohr's circle (circle **c**) in Figure 4.2b. Due to the earth pressure on the back of the retaining wall, the wall is pushed away to A′B′. The horizontal stress decreases while the vertical stress condition is unchanged. The Mohr's circle grows larger and will intersect at a point with the failure envelope when the soil at X is at failure. The type of failure is called active failure and the lateral earth pressure on the retaining wall is called active earth pressure, as is represented by σ_a on circle **a**. Therefore

$$\sin\phi = \frac{AB}{AO'} = \frac{AB}{OO' + OA} = \frac{(\sigma_v - \sigma_a)/2}{c\cot\phi + (\sigma_v + \sigma_a)/2}$$

which can be simplified as follows:

$$\sigma_a = \sigma_v \frac{1-\sin\phi}{1+\sin\phi} - 2c\frac{\cos\phi}{1+\sin\phi} \tag{4.5}$$

$$= \sigma_v \tan^2\left(45° - \frac{\phi}{2}\right) - 2c\tan\left(45° - \frac{\phi}{2}\right)$$

$$= \sigma_v K_a - 2c\sqrt{K_a} \tag{4.5a}$$

where K_a = Rankine's coefficient of lateral active earth pressure = $\tan^2(45° - \phi/2)$.

According to Mohr's failure theory, there forms a failure zone behind the retaining wall, which is called the active failure zone where the soil is all at failure. The failure surfaces all form angles of $(45° + \phi/2)$ with the horizontal (see Figure 4.2c). From Figure 4.2b, the earth pressure distribution behind the retaining wall can be obtained at the theoretical level as shown in Figure 4.2a.

Figure 4.2a shows that the earth pressure behind the wall pushes the wall forward. In front of the wall, at depth z below the ground surface, the lateral stress at Y increases while the vertical stress σ_v stays constant. Thus, the corresponding Mohr's circle grows smaller. When the lateral stress exceeds σ_v, however, the Mohr's circle begins to grow larger. When the Mohr's circle intersects at a point with the failure envelope, the soil at Y will fail. The above type of failure is called passive failure and the lateral earth pressure acting on the front of the wall is called passive earth pressure, which can be represented by σ_p on circle **b**. Following similar derivations used in Eq. 4.5, we can obtain:

$$\sigma_p = \sigma_v \tan^2\left(45° + \frac{\phi}{2}\right) + 2c\tan\left(45° + \frac{\phi}{2}\right) \tag{4.6}$$

$$= \sigma_v K_p + 2c\sqrt{K_p} \tag{4.6a}$$

where K_p is called Rankine's coefficient of lateral passive earth pressure = $\tan^2(45° + \phi/2)$.

Similarly, according to Mohr's failure theory, the failure zone where passive failures happen is called the passive failure zone. The soil in the area is all at failure, whose failure surfaces form angles of $45° - \phi/2$ with the horizontal plane, as shown in Figure 4.2c.

Suppose the wall moves forward by such a great distance that the soil before the wall is completely at passive failure (see Section 4.5.1). The distribution diagram of the passive earth pressures before the wall is also as shown in Figure 4.2a.

According to the principle of effective stress, soil failures are exclusively related to the effective stress, and they have nothing to do with the total stress. Thus, Mohr's circles of failure should be expressed in terms of the effective stress and the failure envelope in Figure 4.2b should be expressed in terms of the effective cohesion (c') and the effective internal angle of friction (ϕ'). Eqs 4.5 and 4.6 should be rewritten in terms of the effective stress as follows:

$$\sigma'_a = \sigma'_v \tan^2\left(45° - \frac{\phi'}{2}\right) - 2c'\tan\left(45° - \frac{\phi'}{2}\right) \tag{4.7}$$

$$= \sigma'_v K_a - 2c'\sqrt{K_a} \tag{4.7a}$$

$$\sigma'_p = \sigma'_v \tan^2\left(45° + \frac{\phi'}{2}\right) + 2c' \tan\left(45° + \frac{\phi'}{2}\right) \tag{4.8}$$

$$= \sigma'_v K_p + 2c'\sqrt{K_p} \tag{4.8a}$$

where the coefficients of the active and the passive earth pressure are separately $K_a = \tan^2(45° - \phi'/2)$ and $K_p = \tan^2(45° + \phi'/2)$.

The angle between the active failure surface and the horizontal plane is $45° + \phi'/2$ and that between the failure passive surface and the horizontal plane is $45° - \phi'/2$.

As Figure 4.3a shows, suppose the soil in front of and in back of the wall is all saturated and both σ_v and the undrained shear strength (s_u) of soil at X and Y are the same (Note: as a matter of fact, the soil at X and Y may not be the same). The soil is at the K_0-condition initially, corresponding to Mohr's circle **a**. Due to the gradual movement toward A′B′, σ_h decreases little by little (σ'_h decreases as well). Shear begins to act on X (under undrained conditions) and excess porewater pressure is produced. When the corresponding Mohr's circle of σ'_h and σ'_v (circle **b**) intersects at a point with the failure envelope, the soil will fail. If we suppose the

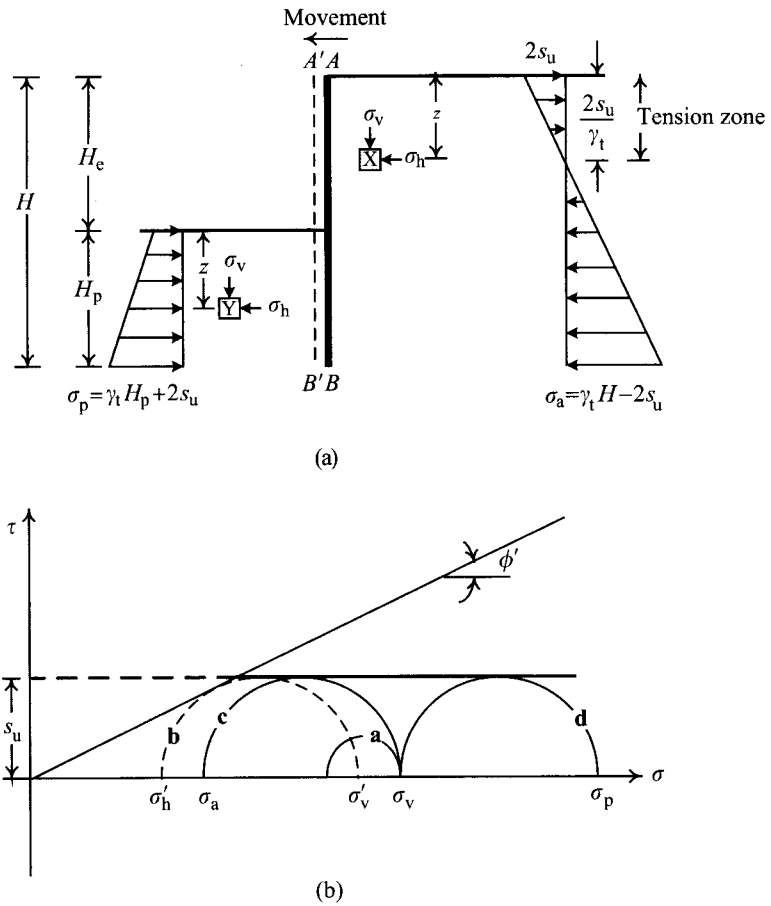

Figure 4.3 Active and passive earth pressures under undrained conditions.

corresponding Mohr's circle of total stress at failure is circle **c**, according to the geometric relationships as shown in Figure 4.3b, the active earth pressure on the wall is:

$$\sigma_a = \sigma_v - 2s_u \tag{4.9}$$

where s_u is the undrained shear strength.

According to Eq. 4.9, we can obtain the theoretical distribution of earth pressure as shown in Figure 4.3a. Soil, however, can not actually bear tension. It needs modification for practical applications. For more discussion, please see Section 4.6.

Concerning the soil at Y in front of the wall, the movement of the wall from AB to A′B′ increases the lateral earth pressure σ_h (σ_h' increases as well), and makes the Mohr's circle grow smaller. When σ_h exceeds σ_v, the Mohr's circle begins to grow larger. Shear begins to act on the soil and produces excess porewater pressure with the increase of σ_h. When the Mohr's circle of the effective stress, constituted by the σ_h' and σ_v', intersects at a point with the Mohr failure envelope, the soil will fail. What is noteworthy, the s_u values at X and Y are the same, as shown in Figure 4.3a. Thus, the corresponding Mohr's circles of the effective stress of X and Y at failure should be identical as well, though the major effective principal stress and the minor effective principal stress are reversed. The passive earth pressure can be obtained from the geometric relationships in Figure 4.3b as follows:

$$\sigma_p = \sigma_v + 2s_u \tag{4.10}$$

According to Eq. 4.10, we can obtain the distribution of passive earth pressures in front of the wall, as shown in Figure 4.3a.

Suppose Eqs 4.5 and 4.6 could apply to the total stress. Observing the failure envelope of total stress in Figure 4.3b parallels the x-axis, its slope is zero, that is, $\phi = 0$. It seems workable to substitute $\phi = 0$ into Eqs 4.5 and 4.6 and the results of σ_a and σ_p will turn out to be identical with those from Eqs 4.9 and 4.10. The procedure is certainly erroneous according to the principle of effective stress but the results are correct.

According to the principle of effective stress, soil behaviors relate only to the effective stress and have nothing to do with the total stress. Eqs 4.5 and 4.6 can only apply to effective stress and have no explanatory value for total stress. At the theoretical level, both the active and passive earth pressures of saturated clay should conform to the principle of effective stress and should only be derived according to it. Though Eqs 4.9 and 4.10 are expressed in total stress, they are derived following the principle of effective stress, as shown in Figure 4.3. Concerning the related theory, please refer to Section 2.8.1 in Chapter 2.

The Mohr failure envelope of total stress obtained from the UU test on unsaturated cohesive soils does not parallel the x-axis, that is, $\phi \neq 0$. Theoretically, the active and passive earth pressure on the retaining wall should also be computed following the principle of effective stress. However, for simplification, the lateral earth pressures are usually computed by Eqs 4.5 and 4.6 in engineering practice, considering the theoretical complication of unsaturated cohesive soils, studies of which are to be done yet.

Rankine's earth pressure theory applies, originally, only to problems under specific conditions: vertical and smooth wall backs, homogeneous soil, level grounds, and no surcharge. Real excavation problems, however, are seldom that pure and simple. Some modifications are necessary when applying the theory to practical cases (see Section 4.6).

4.4 Coulomb's earth pressure theory

Coulomb's earth pressure theory (1776) assumes that soil in back of the retaining wall is homogeneous and cohesionless, the failure surface is a plane, the wedge between the wall and the failure surface is rigid material, and the weight of the wedge, the reaction of the soil and the reaction of the wall are in equilibrium.

Figure 4.4a shows a retaining wall of height H, retaining a soil with an angle of friction ϕ and an angle of friction between the wall and soil δ. BC is an assumed failure surface, which intersects with the horizontal plane at an angle of α. Figure 4.4b illustrates the force polygon formed by the reaction of the wall against the wedge (P), the reaction of soil against the wedge (R), and the weight of soil (W). The directions of P and R are determined, assuming that the wall has a tendency to fall forward and the wedge ABC downward. As shown by the force polygon in Figure 4.4b, we can derive the following equation:

$$\frac{W}{\sin(90^\circ + \theta + \delta - \alpha + \phi)} = \frac{P}{\sin(\alpha - \phi)} \tag{4.11}$$

$$P = \frac{W \sin(\alpha - \phi)}{\sin(90^\circ + \theta + \delta - \alpha + \phi)} \tag{4.12}$$

$$= \frac{1}{2}\gamma H^2 \left[\frac{\cos(\theta - \alpha)\cos(\theta - \beta)\sin(\alpha - \phi)}{\cos^2\theta \sin(\alpha - \beta)\sin(90^\circ + \theta + \delta - \alpha + \phi)} \right] \tag{4.12a}$$

where γ is unit weight of soil, parameters γ, ϕ, δ, θ, β, H are constants. α is a variable because BC is an assumed failure surface. P varies with α; the minimum of P represents the active earth pressure P_a, that is,

$$\frac{dP}{d\alpha} = 0 \tag{4.13}$$

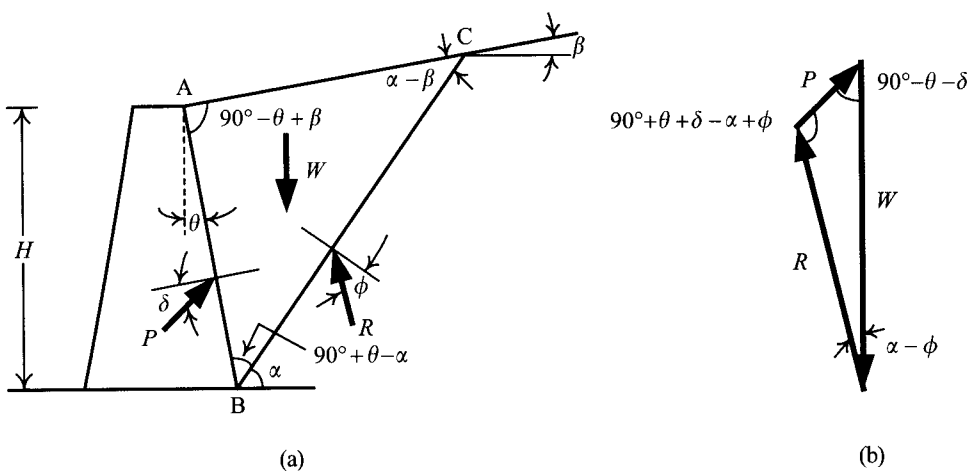

Figure 4.4 Coulomb's active earth pressure.

Substitute the critical α-value derived from the above equation in Eq. 4.12a and we will obtain the active earth pressure (P_a) as follows:

$$P_a = \tfrac{1}{2}\gamma H^2 K_a \tag{4.14}$$

$$K_a = \frac{\cos^2(\phi - \theta)}{\cos^2\theta\cos(\delta + \theta)\left[1 + \sqrt{\dfrac{\sin(\delta + \phi)\sin(\phi - \beta)}{\cos(\delta + \theta)\cos(\theta - \beta)}}\right]^2} \tag{4.14a}$$

where K_a is Coulomb's coefficient of active earth pressure. When $\theta = 0$, $\beta = 0$, and $\delta = 0$, $K_a = \tan^2(45° - \phi/2)$, which is identical with Rankine's.

Figure 4.5 illustrates passive soil failure in back of the retaining wall, which is pushed outward by an external force. BC in the figure is an assumed failure surface. The directions of the soil reaction force (R) and the reaction of the wall (P) are determined on the basis that the wall is pushed against soil and the wedge (ABC) moves upward. Following similar methods used in obtaining the active earth pressure, the passive earth pressure (P_p) can be derived and expressed by the following equation:

$$P_p = \tfrac{1}{2}\gamma H^2 K_p \tag{4.15}$$

$$K_p = \frac{\cos^2(\phi + \theta)}{\cos^2\theta\cos(\delta - \theta)\left[1 - \sqrt{\dfrac{\sin(\phi + \delta)\sin(\phi + \beta)}{\cos(\delta - \theta)\cos(\beta - \theta)}}\right]^2} \tag{4.15a}$$

where K_p is Coulomb's coefficient of passive earth pressure.

When $\theta = 0$, $\beta = 0$, and $\delta = 0$, Eq. 4.15a can be rewritten as $K_p = \tan^2(45° + \phi/2)$, which is identical with that of Rankine.

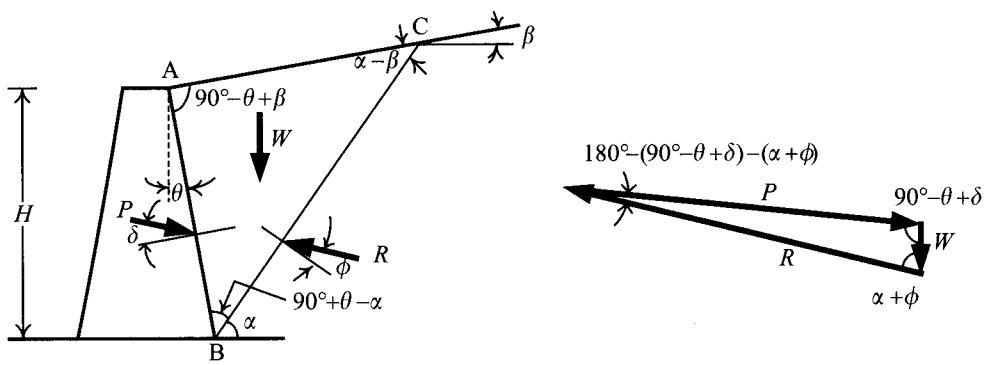

(a) (b)

Figure 4.5 Coulomb's passive earth pressure.

4.5 General discussion of various earth pressure theories

4.5.1 Displacement and earth pressure

According to the loading conditions of soil, when the soil's strained state changes from K_0 to active failure, the direction of its principal stresses will remain unchanged. From K_0 to passive failure, its direction will change by a rotation of 90°. That is, σ_1 is originally vertical ($\sigma_1 = \sigma_v$) and then changes to be horizontal ($\sigma_1 = \sigma_h$). Both the major and minor principal stresses rotate by 90°.

Thus, the strain for soil to come to passive failure is greater than that for it to reach active failure. As to problems concerning retaining walls, there have been many experiments that explore the relationships between wall displacement and earth pressure. Figure 4.6 and Table 4.1 are the synthetic results from experiments on rigid gravity walls provided by NAVFAC DM7.2 (1982). As shown in Table 4.1, the necessary wall displacement inducing passive conditions for cohesionless soils is four times larger than that inducing active conditions. For cohesive soils, the relationship is about two times.

Concerning problems of deep excavation, since the rigidity of the wall is much smaller than that of the gravity retaining wall, under the working load, displacement at the bottom of the wall (see Figure 4.7) may be too small to induce passive failure. Thus it is reasonable to infer that the actual earth pressure near the wall bottom is smaller than the passive earth pressure. However, the displacement of the retaining wall near the excavation surface is actually large enough to cause passive failure of soil in the vicinity of the excavation surface. Thus, the actual distribution of earth pressure on the passive side is as illustrated in Figure 4.7b. On the other hand, with the smaller displacement necessary to produce active failure, active failure may well occur in soil generally outside of the excavation area (Ou *et al.*, 1998).

4.5.2 Comparisons of Rankine's and Coulomb's earth pressure theories

As discussed in Section 4.4, the results obtained from Rankine's and Coulomb's earth pressure theories are identical under the same conditions (smooth wall surfaces, level grounds, and homogeneous cohesionless soils) though the two theories are quite differently based. As described in Section 4.3, Rankine's earth pressure theory is based on the principle of the plasticity equilibrium of the strained soil. That is to say, soil at any point within the failure zone (also called the wedge) is indiscriminately at failure and thereby there are infinite failure surfaces. On the other hand, Coulomb's theory is derived according to the principle of force equilibrium. As a result, there is only one failure surface, which is a plane, assuming that the wedge between the failure surface and the retaining wall is rigid.

The actual conditions, however, may not conform to the hypothetical terms: the wall surface may be rough and the ground surface in back of the wall may be of irregular shape with certain load. Rankine's theory can hardly apply under these conditions. Coulomb's theory can cope with these complicated conditions, though it is difficult to obtain a theoretical solution. Solutions to active and passive earth pressures, nevertheless, can be attained by Culmann's (1875) graphic method. Apparently, Coulomb's theory is more readily applicable. Practical cases, however, don't always work out that way. It depends on whether the hypotheses

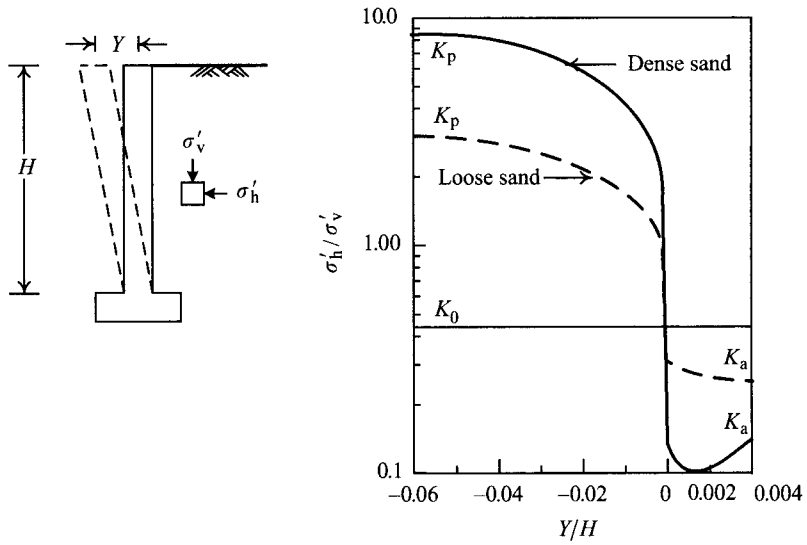

Figure 4.6 Effect of wall movement on earth pressure (Y is the lateral movement at the top of the wall and H is the wall height) (NAVFAC DM7.2, 1982).

Table 4.1 Magnitudes of wall rotation to reach failure (NAVFAC DM7.2, 1982)

Soil type	*Y/H*	
	Active	*Passive*
Dense cohesionless	0.0005	0.002
Loose cohesionless	0.002	0.006
Stiff cohesive	0.01	0.02
Soft cohesive	0.02	0.04

Note
Y is the movement at the wall top and H is the height of the wall (see Figure 4.6).

of Coulomb's earth pressure theory are in accordance with the field conditions, as will be discussed in the next section.

4.5.3 *Reliability of earth pressure theories and other solutions*

Whether Rankine's or Coulomb's earth pressure theories are reliable to represent the actual earth pressure depends on how close the hypotheses of the two theories are to the field condition. According to many studies and experiments (Peck and Ireland, 1961; Rowe and Peaker, 1965; Mackey and Kirk, 1967; James and Bransby, 1970; Rehnman and Broms, 1972), since

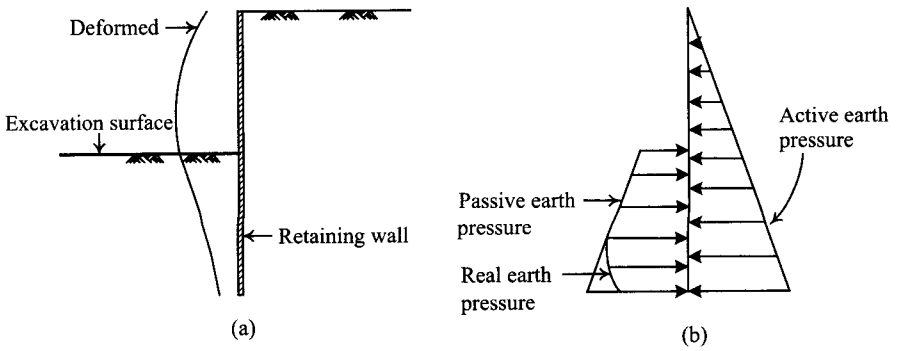

Figure 4.7 Excavation-induced deformation of a retaining wall and the distribution of lateral earth pressure: (a) wall deformation and (b) distribution of lateral earth pressure.

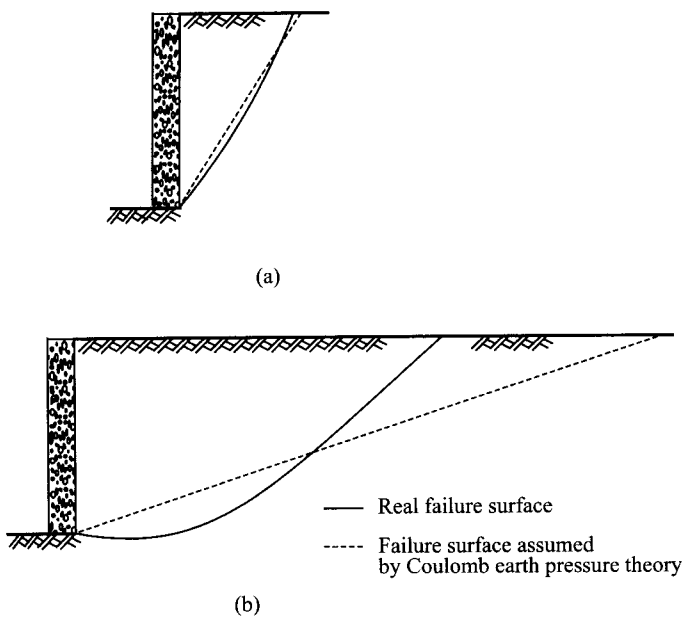

Figure 4.8 Real failure surfaces and failure surfaces assumed by Coulomb's earth pressure theory: (a) active condition and (b) passive condition.

there exists friction between retaining walls and soil, the failure surfaces of active failure and passive failure are both curved surfaces rather than planes. As Figure 4.8 shows, the actual active failure surface and Coulomb's assumed one are close. On the other hand, the actual passive failure surface can be rather different from that assumed by Coulomb's. The less the friction between the retaining wall and the surrounding soil, the closer the failure surface to a plane.

Many theories of active and passive earth pressure are developed on the assumption that the passive failure surface (as line segment BC in Figure 4.5a) is a curve function. For

example, Caquot and Kerisel (1948) assumed that it was an elliptical curved surface, James and Bransby (1970) assumed it to be a log spiral, Terzaghi and Peck (1967) assumed it to be another log spiral. Basically speaking, the better the assumed function of the curved surface represents the actual failure surface, the closer the derived earth pressure will be to the real earth pressure. None of the theories can be expressed in a simple equation. Among them, Caquot and Kerisel's assumed failure surface is quite close to the actual one and the derived coefficients of earth pressure are expressed by many tables to be readily applied. Thus, the coefficients of the active and passive earth pressures derived from the Coquot-Kerisel theory are seen to be very close to the real ones and are widely adopted in engineering practice (e.g. NAVFAC DM7.2, 1982; Padfield and Mair, 1984).

Figures 4.9 and 4.10 are, separately, the coefficients of the active and passive earth pressures induced from Rankine's, Coulomb's, and Caquot-Kerisel's theories on the assumptions of level ground and vertical walls (for the directions of P_a and P_a, see Figure 4.11). As shown in Figure 4.9, we can see when $\delta = 0$ (δ is the friction angle between the wall and the surrounding soil), the coefficients of active earth pressure obtained from Rankine's, Coulomb's, and Caquot-Kerisel's theories will be identical. When $\delta > 0$, the coefficient from Rankine's will come out the largest while Coulomb's and Caquot-Kerisel's will be close. The difference between Coulomb's coefficient of active earth pressure and Caquot-Kerisel's grows smaller and smaller with the decrease of δ. As we note, Caquot-Kerisel's coefficient of active earth pressure and Coulomb's will almost always come out identical when $\delta \leq 0.67\phi'$. In applications, K_a can be obtained, with δ and ϕ' known, by referring to Figure 4.9. The horizontal component of the earth pressure $\sigma_{a,h} = \gamma H K_{a,h} = \gamma H K_a \cos\delta$ and $P_{a,h} = (\gamma H^2 K_a \cos\delta)/2$ can then be computed accordingly.

From Figure 4.10, we can see that Rankine's, Coulomb's, and Caquot-Kerisel's coefficients of passive earth pressure are all the same, when $\delta = 0$. If $\delta > 0$, K_p, computed according to Rankine's earth pressure theory, will be the smallest, while that computed according to Coulomb's the largest. If $\phi' > 40°$, Coulomb's K_p will come out unreasonably large especially when $\delta = \phi'$. Observed from Figure 4.10, if $\delta \leq 0.5\phi'$, Coulomb's coefficient of passive earth pressure and Caquot-Kerisel's will be close. In applications, K_p can be obtained, with δ and ϕ' known, by referring to Figure 4.10. The horizontal component of the earth pressure $\sigma_{p,h} = \gamma H K_{p,h} = \gamma H K_p \cos\delta$ and $P_{p,h} = (\gamma H^2 K_p \cos\delta)/2$ can then be computed accordingly.

For problems of excavation, considering that the active earth pressure is usually the main force leading to the failure of retaining walls, Caquot-Kerisel's active earth pressure should be adopted for analysis and design since it is regarded as most close to the real active earth pressure. Slightly smaller than Caquot-Kerisel's, almost the same under most circumstances, Coulomb's coefficient of active earth pressure is also workable for analysis and design. For conservative reasons, Rankine's coefficient of active earth pressure is recommended for it is the largest among the three without significant difference from Caquot-Kerisel's.

The passive earth pressure is usually the force resisting failure. Caquot-Kerisel's passive earth pressure is regarded as the real passive earth pressure and is therefore the most favored choice. Rankine's coefficient of passive earth pressure deviates much from the real value, usually too small, to be applicable. When $\delta < 0.5\phi'$, Coulomb's does not differ significantly from Caquot-Kerisel's and is workable. On the other hand, when $\delta \geq 0.5\phi'$, it is so much larger than Caquot-Kerisel's that it is unsafe to adopt for analysis and design.

As to related problems of analysis and design, please see Chapter 5.

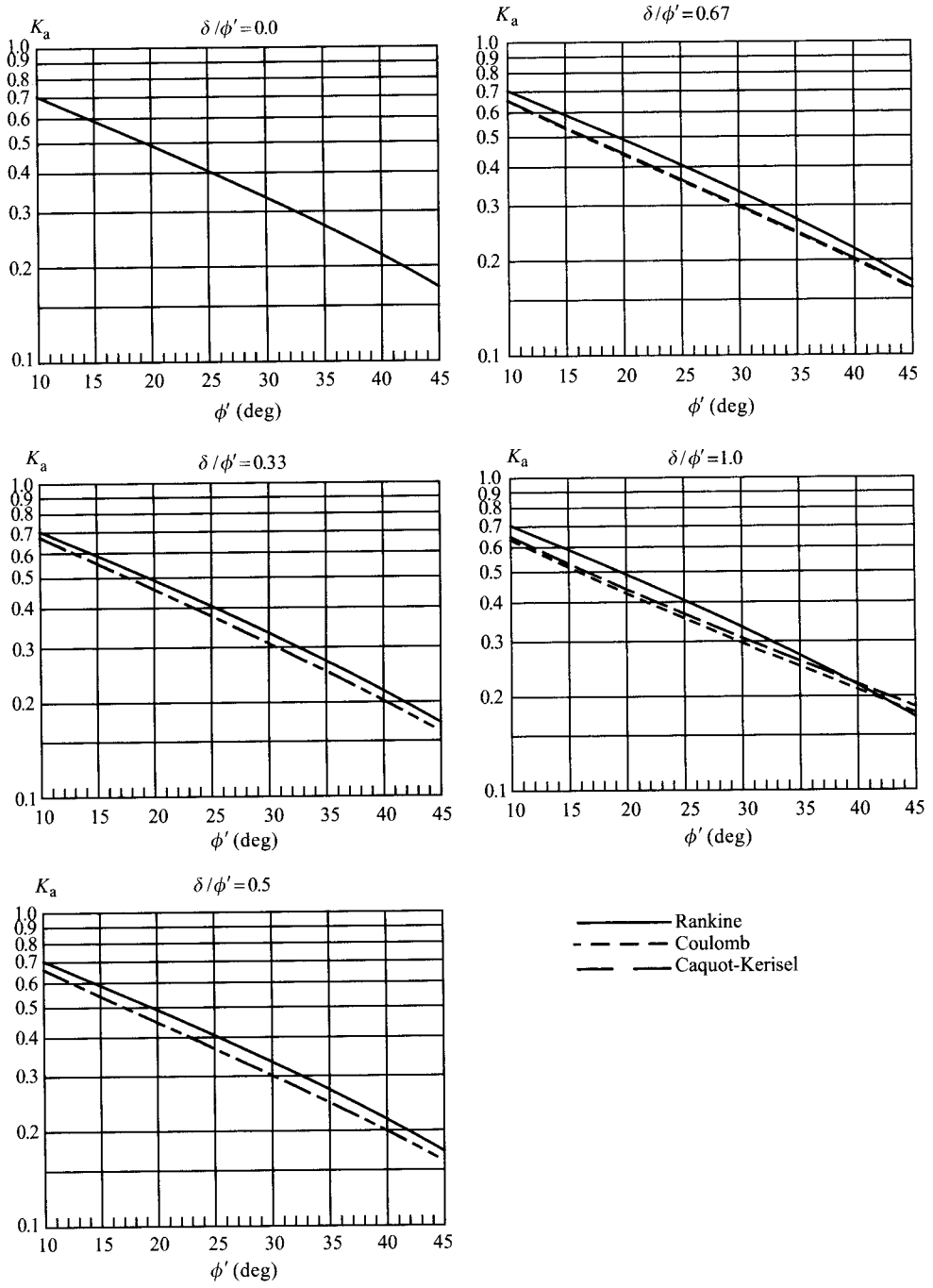

Figure 4.9 Coefficients of Rankine's, Coulomb's, and Caquot-Kerisel's active earth pressure (horizontal component $K_{a,h} = K_a \cos \delta$).

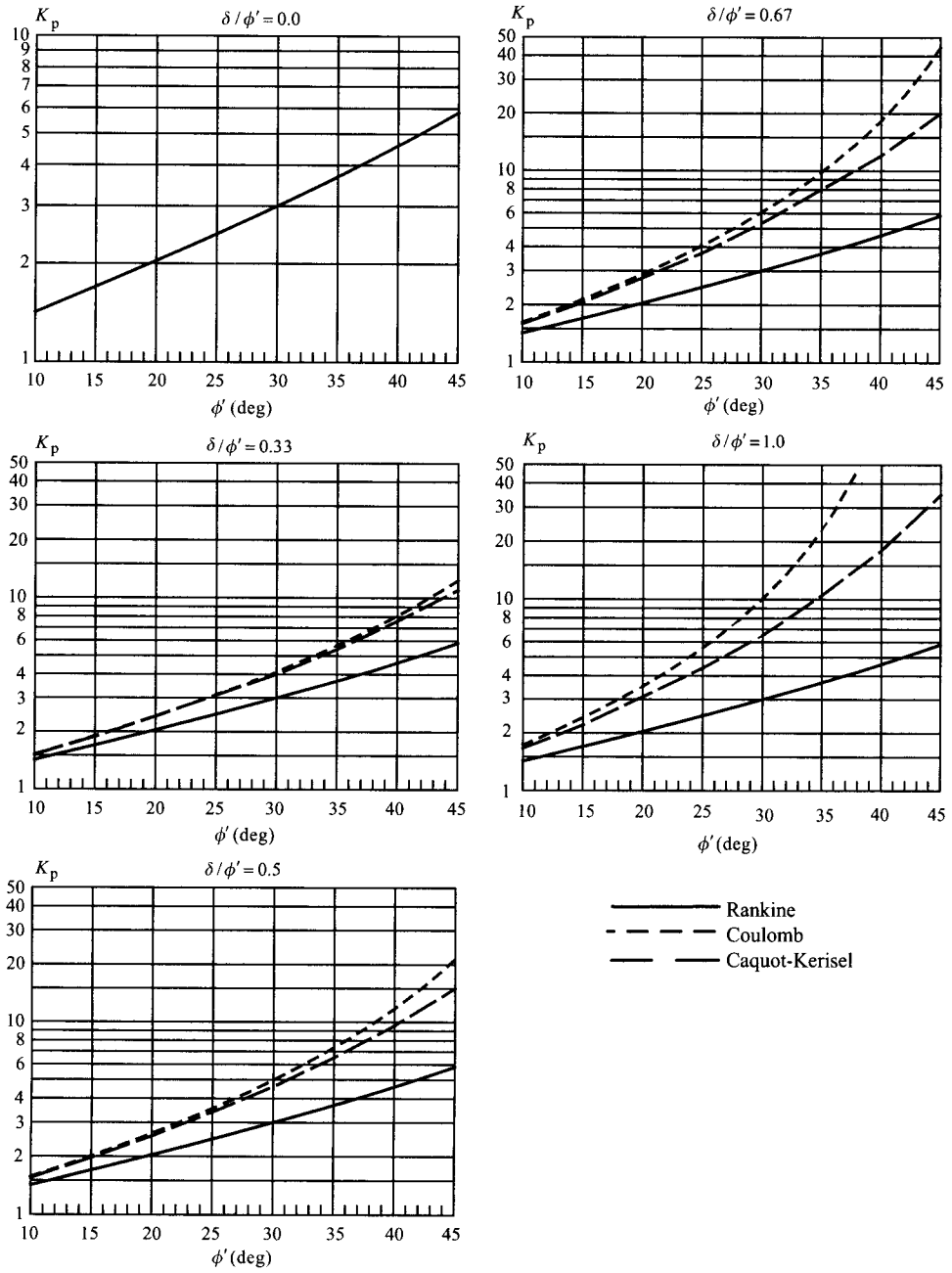

Figure 4.10 Coefficients of Rankine's, Coulomb's, and Caquot-Kerisel's passive earth pressure (horizontal component $K_{p,h} = K_p \cos \delta$).

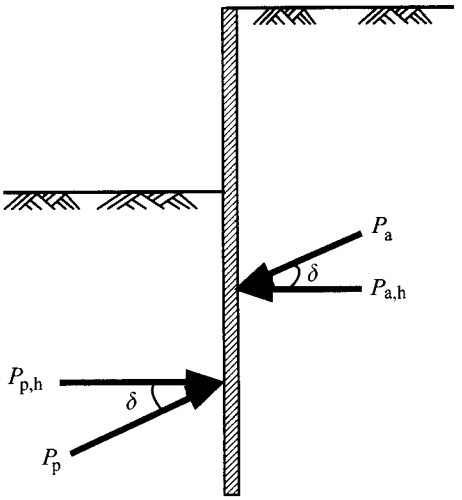

Figure 4.11 Active and passive forces of level cohesionless soils on a vertical wall.

4.6 Earth pressure for design

Theoretically speaking, Rankine's earth pressure can be applied both to cohesive and cohesionless soils. Nevertheless, it is unable to consider the adhesion or friction between retaining walls and soil. On the other hand, Coulomb's and Caquot-Kerisel's earth pressure can take into consideration the friction between retaining walls and soil, though they can only apply to cohesionless soils. Following Padfield and Mair's (1984) suggestion, this section will adopt Rankine's earth pressure theory and Caquot-Kerisel's coefficient of earth pressure together to calculate earth pressure for problems of deep excavation. Though the section mainly focuses on deep excavations, the methods are generally applicable to other problems of geotechnical engineering.

4.6.1 Cohesive soils

As to the short-term behavior of cohesive soils, their earth pressures should be obtained following the total stress method while the parameters of soil strength should be derived from the UU test, the FV test, or the CPT test. If the cohesive soil is 100% saturated, it should be analyzed assuming $\phi = 0$. Considering the adhesion between retaining walls and soil (i.e. the surface of the retaining wall is not smooth), the earth pressures for design can be expressed as follows (Padfield and Mair, 1984):

$$\sigma_a = \sigma_v K_a - 2cK_{ac} \tag{4.16}$$

$$K_{ac} = \sqrt{K_a\left(1 + \frac{c_w}{c}\right)} \tag{4.17}$$

$$\sigma_p = \sigma_v K_p + 2cK_{pc} \tag{4.18}$$

$$K_{pc} = \sqrt{K_p\left(1 + \frac{c_w}{c}\right)} \tag{4.19}$$

where

σ_a = total active earth pressure (horizontal) acting on the retaining wall
σ_p = total passive earth pressure (horizontal) acting on the retaining wall
c = cohesion intercept
ϕ = angle of friction, based on the total stress representation
c_w = adhesion between the retaining wall and soil
K_a = coefficient of active earth pressure
K_p = coefficient of passive earth pressure.

When cohesive soils are completely saturated, $\phi = 0$ and c equals the undrained shear strength s_u; that is, $K_a = K_p = 1$, $K_{ac} = K_{pc} = \sqrt{1 + c_w/s_u}$ where the value of c_w can be estimated by the following equation:

$$c_w = \alpha s_u \tag{4.20}$$

where α is a reduction factor, which relates to the soil strength, the construction method of the retaining wall, and the roughness of its surface.

Adhesion between the retaining wall (note: for excavation) and the surrounding soil is not well studied. There exist, nevertheless, many studies on adhesion between pile foundations and soil. Striking and casting in situ are two common construction methods for pile foundations. The pile material can be steel or concrete, etc. Thus, it may be feasible to apply the studies on pile foundations to retaining walls for deep excavations. The suggested relations between α and s_u/σ_v' by API (the American Petroleum Institute, 1993) and the study results of bored piles in Taipei (Lin and Lin, 1999) are shown in Figure 4.12, and can be used to estimate the α-value.

According to Eqs 4.16 and 4.18, the distribution of earth pressures in front of and in back of the retaining wall should be similar to Figure 4.3a, where the resultants of $\sigma_a$and σ_p are all perpendicular to the retaining wall (referring to the conditions where the ground is level). From Figure 4.3a, we can see that there exists a tension zone in the cohesive soils in back of the wall. A tension crack will occur if the soil is subject to long-term tensile stress. The depth of a tension crack can be estimated by Eq. 4.16 with $c_w = 0$. Let the lateral earth pressure be 0, then

$$\sigma_a = \gamma z K_a - 2c\sqrt{K_a} = 0 \tag{4.21}$$

The depth of a tension crack is

$$z_c = \frac{2c}{\gamma\sqrt{K_a}} \tag{4.22}$$

where z_c = depth of a tension crack.

Once tension cracks are produced, the soils are no longer able to bear tensile stress. Thus, to be conservative, we often suppose that there already exist tension cracks in the design. Rain and environmental factors will further make cracks full of moisture, so that they begin to push

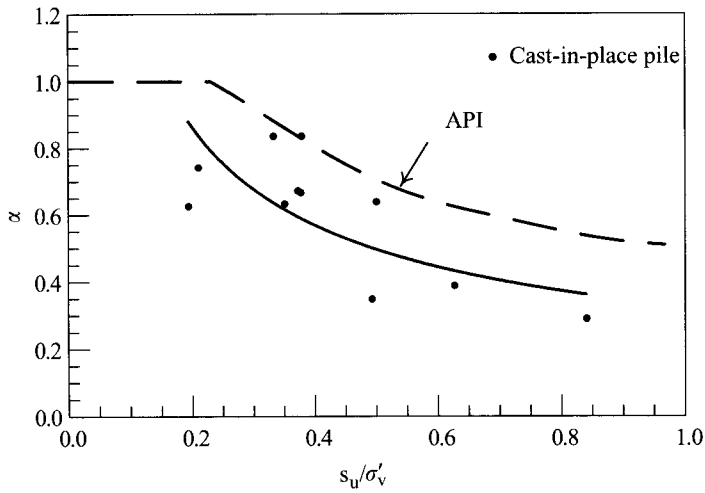

Figure 4.12 Relation between adhesion and undrained shear strength of clay.

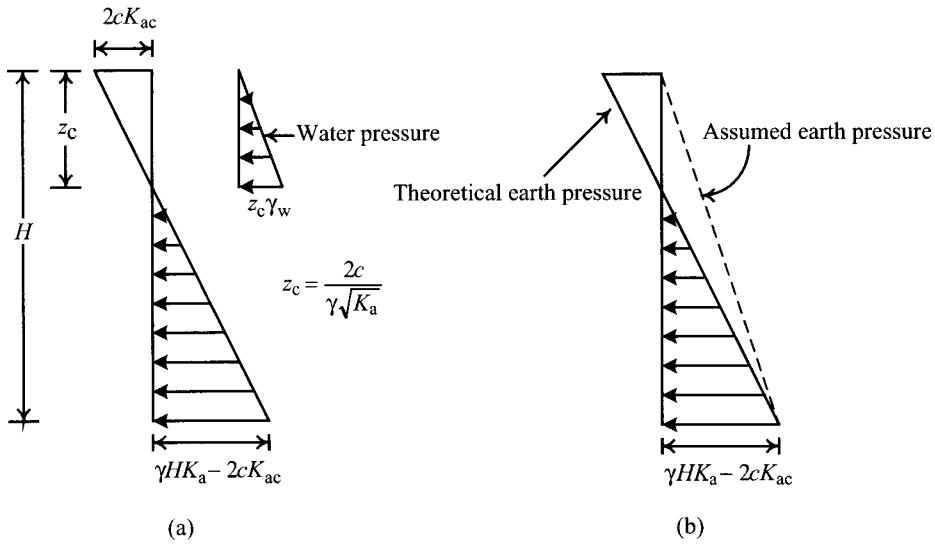

Figure 4.13 Distribution of lateral earth pressure for the cohesive soil.

the retaining wall as shown in Figure 4.13a. For problems of deep excavation, considering the possibilities that soil creep in the tension zone may lead more soil to jostle against the retaining wall, the distribution of earth pressure may be as illustrated in Figure 4.13b.

The long-term behavior of cohesive soils should be analyzed on the basis of the complete dissipation of the excess porewater pressure. The distribution of earth pressure is to be estimated the same way as that of cohesionless soils, as will be discussed in the following section.

4.6.2 Cohesionless soils

The excess porewater pressure of cohesionless soils dissipates quickly as soon as shearing occurs. As a result, the analysis should follow the effective stress method. Supposing there exists friction between the retaining wall and the surrounding soil, the earth pressure for design can be represented as follows (Padfield and Mair, 1984):

$$\sigma'_a = K_a(\sigma_v - u) - 2c'K_{ac} \tag{4.23}$$

$$K_{ac} = \sqrt{K_a\left(1 + \frac{c'_w}{c'}\right)} \tag{4.24}$$

$$\sigma_a = \sigma'_a + u \tag{4.25}$$

$$\sigma'_p = K_p(\sigma_v - u) + 2c'K_{pc} \tag{4.26}$$

$$K_{pc} = \sqrt{K_p\left(1 + \frac{c'_w}{c'}\right)} \tag{4.27}$$

$$\sigma_p = \sigma'_p + u \tag{4.28}$$

where

σ'_a = effective active earth pressure acting on the retaining wall
σ'_p = effective passive earth pressure acting on the retaining wall
σ_a = total active earth pressure
σ_p = total passive earth pressure
K_a = Caquot-Kerisel's coefficient of active earth pressure
K_p = Caquot-Kerisel's coefficient of passive earth pressure
c' = effective cohesion intercept
ϕ' = effective angle of friction
c_w = effective adhesion between the retaining wall and soil
u = porewater pressure.

For most cohesionless soils, $c' = 0$, $c'_w = 0$; therefore, $K_{ac} = K_a$, $K_{pc} = K_p$. K_a and K_p can be determined referring to Figures 4.9 and 4.10, given the values of ϕ' and δ. To obtain the horizontal component of active earth pressure ($\sigma_{a,h}$), $K_{a,h}$ should substitute for K_a in Eqs 4.23–4.25 and $K_{p,h}$ should substitute for K_p in Eqs 4.26–4.28 to obtain the horizontal component of passive earth pressure ($\sigma_{p,h}$), where $K_{a,h} = K_a \cos\delta$ and $K_{p,h} = K_p \cos\delta$.

Clough (1969) studied the characteristics of friction between concrete and sand using the direct shear test and found that the friction angle (δ) between concrete and sand is around $0.83\phi'$ (where ϕ' stands for the friction angle of sand). Potyondy (1961) employed a smooth steel mold to cast concrete, which was in turn employed to explore the characteristics of friction between concrete and sand by tests, and found $\delta = 0.8\phi'$. Chapter 5 will explore further reasonable friction angles (δ) between retaining walls and soils.

A tension zone or a tension crack zone will not occur in cohesionless soils because $c' = 0$. Sometimes a value of c' may be found which is other than 0 in design, the reason for which might be that c' is an apparent earth pressure or a deviation due to regression analysis of test results. Whichever is the case, there cannot exist a tension zone or a tension crack zone in cohesionless soils and some necessary modifications are required.

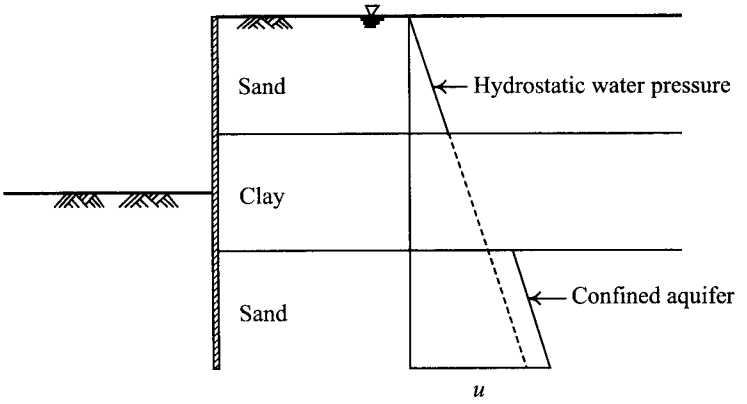

Figure 4.14 Distribution of water pressures for alternated layers.

4.6.3 Alternated layers

To compute the distribution of earth pressures for alternated layers composed of both cohesive and cohesionless soils, the total stress analysis should be adopted for (short-term behavior of) cohesive soils, the water pressure will not be considered while doing the effective stress analysis for cohesionless soils, the water pressure is to be computed separately. Note that cohesive soils do not necessarily have static water pressure because of the influences of geology formation, the environment change, and past dewatering history. If working with the long-term behavior, the effective stress analysis should be applied to both cohesive and cohesionless soils and the water pressure should be computed separately. Figure 4.14 illustrated a typical formation of alternated and a "possible" distribution of porewater pressure.

4.6.4 Sloping ground

According to Rankine's earth pressure theory, the coefficients of the earth pressure for sloping ground (Bowles, 1988) can be computed as follows:

$$K_a = \cos\beta \frac{\cos\beta - \sqrt{\cos^2\beta - \cos^2\phi}}{\cos\beta + \sqrt{\cos^2\beta - \cos^2\phi}} \tag{4.29}$$

$$K_p = \cos\beta \frac{\cos\beta + \sqrt{\cos^2\beta - \cos^2\phi}}{\cos\beta - \sqrt{\cos^2\beta - \cos^2\phi}} \tag{4.30}$$

where ϕ is the angle of friction and β is the slope of the ground.

Thus, the active and passive earth pressures, and their resultants acting on the retaining wall as shown in Figure 4.15 are:

$$\sigma_a = \gamma z K_a \tag{4.31}$$

$$P_a = \tfrac{1}{2}\gamma H^2 K_a \tag{4.32}$$

$$\sigma_p = \gamma z K_p \tag{4.33}$$

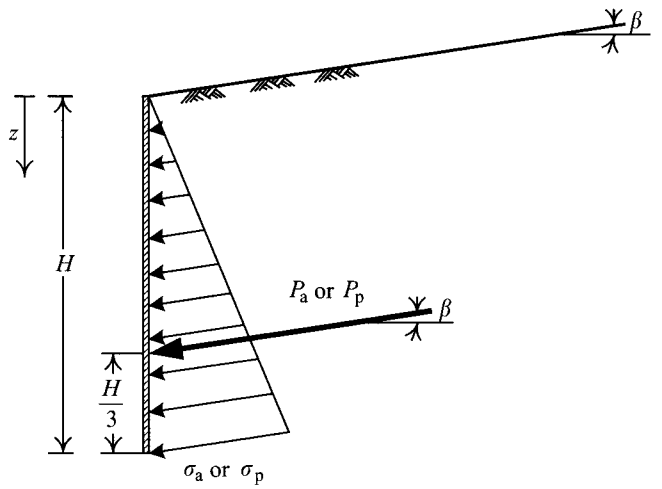

Figure 4.15 Earth pressure for sloping ground.

$$P_p = \tfrac{1}{2}\gamma H^2 K_p \tag{4.34}$$

where

γ = unit weight of soil
H = height of the retaining wall
σ_a = active earth pressure
σ_p = passive earth pressure
P_a = resultant of active earth pressure
P_p = resultant of passive earth pressure.

In problems of deep excavation, only the horizontal components are relevant and they are:

$$\sigma_{a,h} = \gamma z K_a \cos\beta \tag{4.35}$$

$$P_{a,h} = \frac{1}{2}\gamma H^2 K_a \cos\beta \tag{4.36}$$

$$\sigma_{p,h} = \gamma z K_p \cos\beta \tag{4.37}$$

$$P_{p,h} = \frac{1}{2}\gamma H^2 K_p \cos\beta \tag{4.38}$$

Figure 4.16 shows the comparison of coefficients of horizontal active earth pressure derived from Rankine's, Coulomb's, and Caquot-Kerisel's earth pressure theories for the conditions of $\beta/\phi' = 1.0$ and $\delta/\phi' = 1.0$. As shown in the figure, the coefficients of Rankine's earth pressure come out the largest and those of Coulomb's and Caquot-Kerisel's theories are almost identical. Apparently, the active earth pressure on the back of the retaining wall can be computed by Eq. 4.14, that is, Coulomb's earth pressure theory. Inside the excavation zone the ground is mostly level, so the passive earth pressure can be obtained from Caquot-Kerisel's

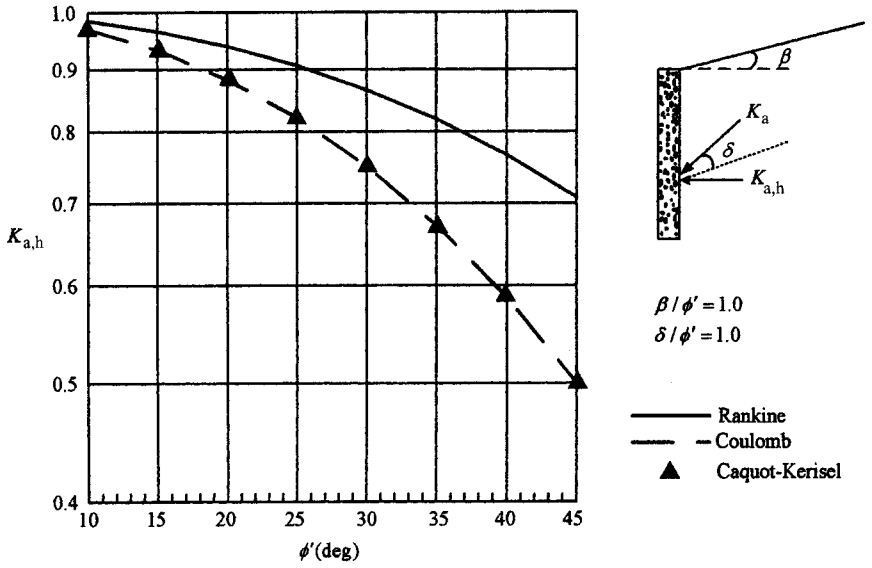

Figure 4.16 Coefficients of Rankine's, Coulomb's, and Caquot-Kerisel's horizontal active earth pressure.

earth pressure theory as Figure 4.10 shows (see Section 4.5.3). Besides, NAVFAC DM 7.2 also provides the passive earth pressure of a sloping ground according to Caquot-Kerisel's earth pressure theory. Seldom confronted in deep excavation, the question will not be further discussed here.

4.6.5 Surcharge

As shown in Figure 4.17, the uniformly distributed load, q, extensively acts on the ground surface while p acts on the excavation bottom. The load-induced active and passive earth pressures on the retaining wall are separately:

$$\sigma_a = qK_a \tag{4.39}$$

$$\sigma_p = pK_p \tag{4.40}$$

where

K_a = Caquot-Kerisel's coefficient of active earth pressure, which can be determined by referring to Figure 4.9,
K_p = Caquot-Kerisel's coefficient of passive earth pressure, which can be determined by referring to Figure 4.10.

If the load is neither uniformly nor extensively distributed, the thrust of load against the wall will then be a problem of the theory of elasticity. According to Gerber (1929) and

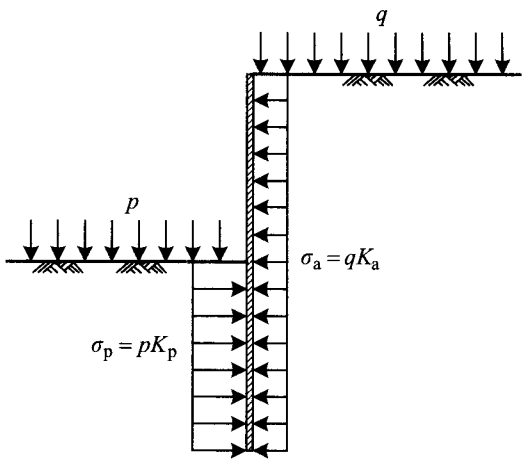

Figure 4.17 Lateral earth pressure produced by uniformly distributed load.

Spangler (1938), the distribution of earth pressure (σ_h) against the wall caused by a point load Q_p can be expressed in m, n as follows:

$$m \leq 0.4$$

$$\sigma_h = \frac{0.28Q_p}{H^2}\frac{n^2}{(0.16+n^2)^3} \tag{4.41}$$

$$m > 0.4$$

$$\sigma_h = \frac{1.77Q_p}{H^2}\frac{m^2n^2}{(m^2+n^2)^3} \tag{4.42}$$

Figure 4.18a illustrates the dimensionless diagram of earth pressure distribution derived from the above equation where m is separately made 0.2, 0.4, and 0.6. The corresponding resultant of earth pressure (P_h) and the point of action R are marked in the figure. Figure 4.18c is the diagram of the earth pressure (σ_h) at depth z below the ground surface (the AA section in Figure 4.18a) where $\sigma_{h,\theta}$ is

$$\sigma_{h,\theta} = \sigma_h \cos^2(1.1\theta) \tag{4.43}$$

Figure 4.19a illustrates the earth pressure distribution caused by a line load paralleling the retaining wall (Q_ℓ), whose earth pressure and earth pressure resultant can be expressed as follows:

$$m \leq 0.4$$

$$\sigma_h = \frac{0.203Q_\ell}{H}\frac{n}{(0.16+n^2)^2} \tag{4.44}$$

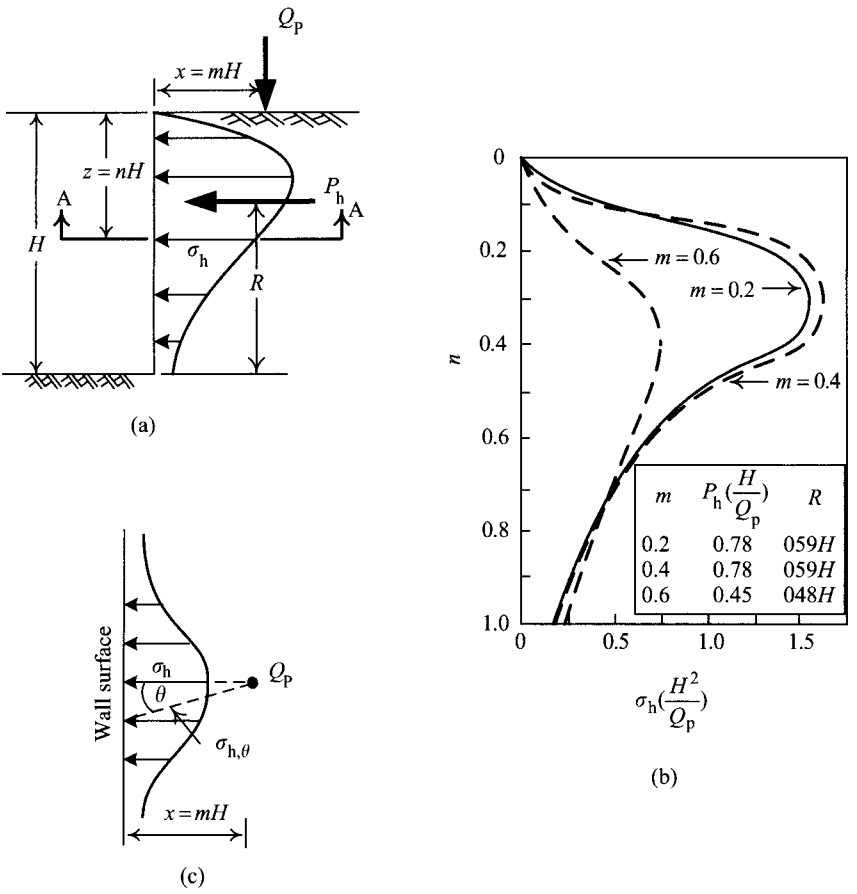

Figure 4.18 Lateral earth pressure produced by a point load Q_p: (a) notations, (b) vertical profile of lateral stress distribution, and (c) horizontal profile of lateral stress distribution.

$m > 0.4$

$$\sigma_h = \frac{1.28Q_\ell}{H}\frac{m^2 n}{(m^2+n^2)^2} \tag{4.45}$$

and their resultant is

$$P_h = \frac{0.64Q_\ell}{(m^2+1)} \tag{4.46}$$

Figure 4.19b illustrates the dimensionless diagram of earth pressure distribution derived from the above equation where m is separately made 0.1, 0.3, 0.5, and 0.7. The corresponding point of action R is also marked in the figure.

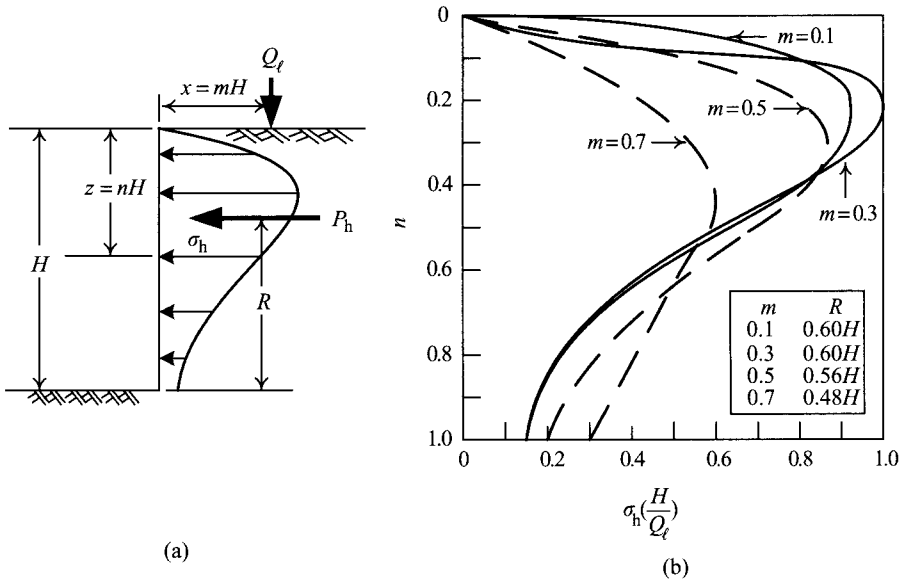

Figure 4.19 Lateral earth pressure produced by a line load Q_ℓ: (a) notations and (b) vertical profile of lateral stress distribution.

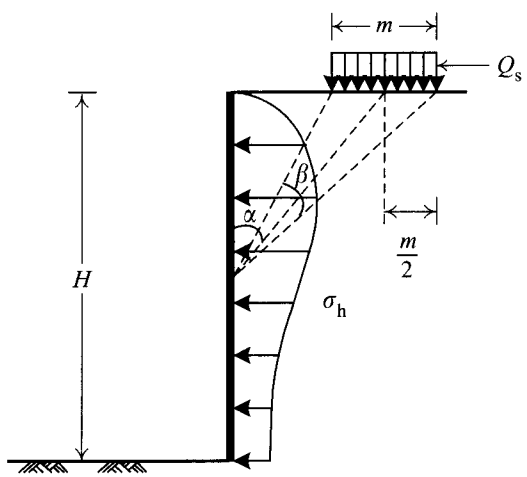

Figure 4.20 Lateral earth pressure produced by a strip load Q_s.

Figure 4.20 illustrates a strip load (Q_s) paralleling the retaining wall. According to the theory of elasticity, the lateral earth pressure (σ_h) at depth z is

$$\sigma_h = \frac{Q_s}{H}(\beta - \sin\beta\cos 2\alpha) \tag{4.47}$$

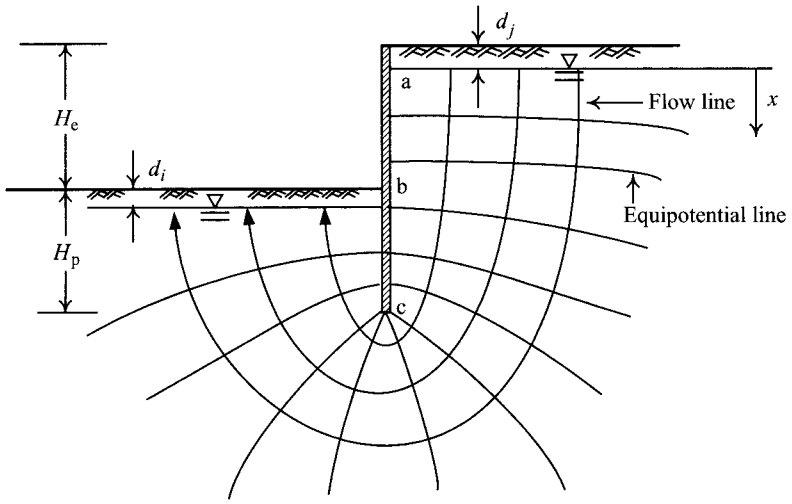

Figure 4.21 Seepage in an excavation zone.

Considering the restraining effect of the retaining wall, the earth pressure acting on the wall can be modified from Eq. 4.47 to the following:

$$\sigma_h = \frac{2Q_s}{H}(\beta - \sin\beta\cos 2\alpha) \tag{4.48}$$

4.6.6 Seepage

Cohesionless soils have a high degree of permeability. As a result, the difference of the water levels between the excavation bottom and the area outside the excavation in cohesionless soils will cause seepage. Cohesive soils exhibit undrained behavior in the short-term condition. That is to say, no seepage is to be considered. In the long run, cohesive soils may also produce seepage and can be analyzed in the same way as cohesionless soils.

Seepage will affect the water pressures inside and outside the excavation zone and also the effective stresses. In deep excavations, seepage caused by the difference of water level is two-dimensional and the corresponding variation of water pressure can be estimated by flow net or using the finite element method. Figure 4.21 is a typical diagram of the flow net.

Generally speaking, excavation will encounter various soil layers. The subsurface soil may not be homogeneous or isotropic. Considering the difficulty of the depiction of a non-homogeneous and non-isotropic flow net, for the sake of simplification, we sometimes assume that the behavior of seepage is one dimensional, that is, the head loss per unit length of a flow path is the same.

As shown in Figure 4.22a, the difference of the total heads between the upstream water level (outside the excavation zone) and the downstream water level is $(H_e + d_i - d_j)$. The length of the path of the water flowing from the upstream water level along the retaining wall down to the downstream water level is $(2H_p + H_e - d_i - d_j)$. Assuming that the datum of the elevation

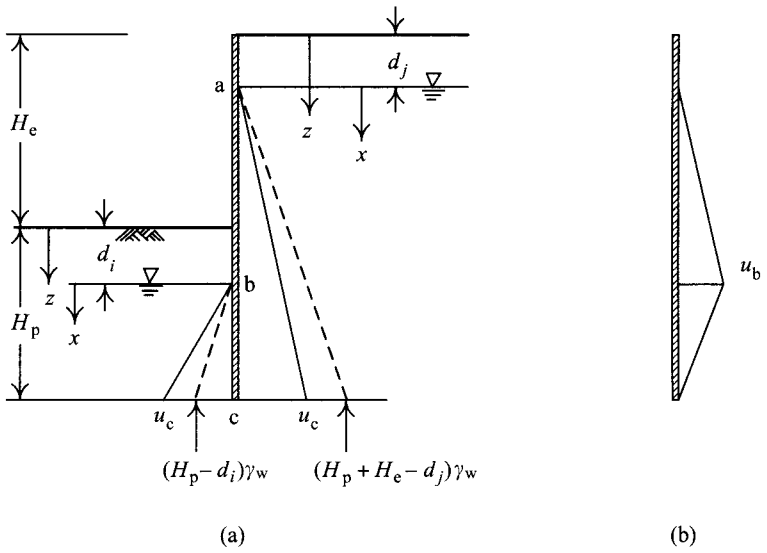

Figure 4.22 Simplified analysis method for seepage: (a) distribution of water pressure and (b) net water pressure.

head is set to be the same with the upstream water level, the total head (h) at a distance of x from the upstream water level would be:

$$h = 0 - \frac{x(H_e + d_i - d_j)}{2H_p + H_e - d_i - d_j} = -\frac{x(H_e + d_i - d_j)}{2H_p + H_e - d_i - d_j} \tag{4.49}$$

Let h_e be the elevation head and h_p the pressure head. The pressure head at a distance of x from the upstream water level would be:

$$h_p = h - h_e = \frac{-x(H_e + d_i - d_j)}{2H_p + H_e - d_i - d_j} - (-x) = \frac{2x(H_p - d_i)}{2H_p + H_e - d_i - d_j} \tag{4.50}$$

Thus, the water pressure, u_x, at a distance of x from the upstream water level would be:

$$u_x = \frac{2x(H_p - d_i)\gamma_w}{2H_p + H_e - d_i - d_j} \tag{4.51}$$

The water pressure at the bottom of the retaining wall, u_c, would be:

$$u_c = \frac{2(H_p + H_e - d_j)(H_p - d_i)\gamma_w}{2H_p + H_e - d_i - d_j} \tag{4.52}$$

When actually conducting an excavation analysis, the distribution of water pressure is usually expressed in the net water pressure (please see Section 5.5). The largest net water pressure is to be found at b, whose value would be:

$$u_b = \frac{2(H_e + d_i - d_j)(H_p - d_i)\gamma_w}{2H_p + H_e - d_i - d_j} \tag{4.53}$$

As shown in Figure 4.22a, seepage will decrease the porewater pressure on the active side (lower than the hydrostatic water pressure) and increase it on the passive side (higher than the hydrostatic water pressure). As discussed earlier, we can derive the rates of increase of porewater pressure per unit length on the active and passive sides as follows:

$$\mu_a = \frac{u_c}{H_p + H_e - d_j} \tag{4.54}$$

$$\mu_p = \frac{u_c}{H_p - d_i} \tag{4.55}$$

where μ_a and μ_p represent the rates of increase of the porewater pressure per unit length on the active and passive sides, respectively.

Thus, the water pressures x below the water level at the active and passive sides are separately $u_x = \mu_a x$ (the active side) and $u_x = \mu_p x$ (the passive side).

Therefore, μ_a and μ_p can be seen as the modified unit weights of water on the active side and passive side, respectively. As a result, the total lateral earth pressure at a depth of z below the ground surface on the back of the wall would be:

$$\sigma_h = \sigma'_v K_a + u \tag{4.56}$$

$$= \left[\sigma_v - \frac{(z - d_j)}{H_p + H_e - d_j} u_c\right] K_a + \frac{(z - d_j)}{H_p + H_e - d_j} u_c \tag{4.57}$$

Similarly, the total lateral earth pressure at a distance of z below the ground surface on the front of the wall would be:

$$\sigma_h = \sigma'_v K_p + u \tag{4.58}$$

$$= \left[\sigma_v - \frac{(z - d_i)}{H_p - d_i} u_c\right] K_p + \frac{(z - d_i)}{H_p - d_i} u_c \tag{4.59}$$

4.6.7 Earthquakes

Earthquakes will engender lateral and vertical acceleration, which will in turn increase the active earth pressure outside the retaining wall and decrease the passive earth pressure inside the wall. The Mononobe–Okabe equation is generally adopted (Okabe, 1926; Mononobe, 1929) to compute the active and passive earth pressures under the influence of earthquakes. As shown in Figure 4.23, the active and passive earth pressures (P_{ae}, P_{pe}) under the influence of earthquakes can be computed by the following equations:

$$P_{ae} = \frac{1}{2}\gamma H_1^2 (1 - k_v) K_a \tag{4.60}$$

$$K_a = \frac{\cos^2(\phi - \alpha_a - \theta)}{\cos\theta \cos^2\alpha_a \cos(\delta + \alpha_a + \theta)\left\{1 + \left[\frac{\sin(\phi + \delta)\sin(\phi - \beta_a - \theta)}{\cos(\delta + \alpha_a + \theta)\cos(\beta_a - \alpha_a)}\right]^{1/2}\right\}^2} \tag{4.61}$$

$$P_{pe} = \frac{1}{2}\gamma H_2^2 (1 - k_v) K_p \tag{4.62}$$

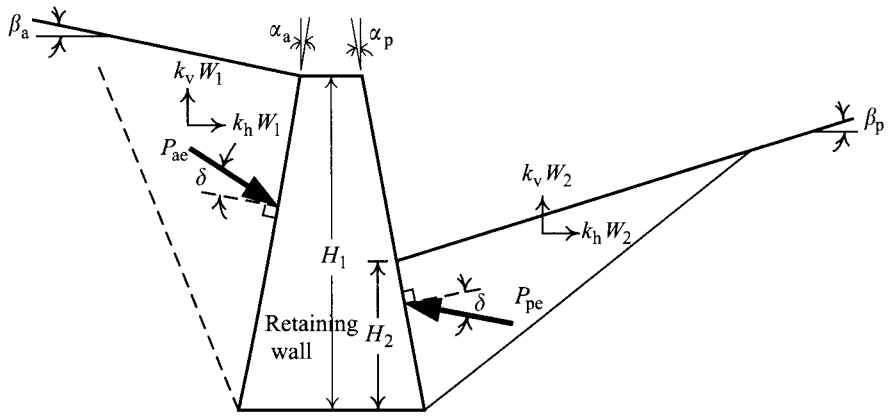

W_1: Weight of wedge in the active zone

W_2: Weight of wedge in the passive zone

Figure 4.23 Active and passive earth pressure under the influence of earthquakes.

$$K_p = \frac{\cos^2(\phi + \alpha_p - \theta)}{\cos\theta \cos^2\alpha_p \cos(\delta - \alpha_p + \theta)\left\{1 - \left[\frac{\sin(\phi + \delta)\sin(\phi + \beta_p - \theta)}{\cos(\delta - \alpha_p + \theta)\cos(\beta_p - \alpha_p)}\right]^{1/2}\right\}^2} \tag{4.63}$$

where $\theta = \tan^{-1}[k_h/(1 - k_v)]$; k_h and k_v are the horizontal and vertical coefficients of earthquake, which are defined as follows:

$$k_h = \frac{\text{the horizontal acceleration of earthquake } (a_h)}{\text{the acceleration of gravity } (g)} \tag{4.64}$$

$$k_v = \frac{\text{the vertical acceleration of earthquake } (a_v)}{\text{the acceleration of gravity } (g)} \tag{4.65}$$

Some building codes have suggested that the horizontal coefficient of earthquake (k_h) for design be half of the horizontal peak acceleration of the site. With lateral displacement restrained, nevertheless, the dynamic earth pressure caused by an earthquake will be greater than the displacement without restraint. With the lateral displacement completely restrained, k_h can be estimated as 1.5 times as great as the horizontal peak acceleration of the site. The vertical coefficient of earthquake (k_v) for design can be assumed to be half of the vertical acceleration of the earthquake at the site. As for earthquakes occurring far away, however, the influence of vertical earthquake can be reasonably ignored, that is, $k_v = 0$. The peak acceleration of the site should be determined on the basis of design criteria of service life and risk analysis.

Location of action of the dynamic active pressure on the retaining wall depends on the type of the earthquake-induced displacement of the wall. There are three types of displacement

of a retaining wall: overturning about the wall toe, sliding along the wall base and rotating about the wall top. The first type, however, is the only one generally considered.

According to the characteristics of the earth pressure distribution, the static active and passive earth pressures act at distances of $H_1/3$ and $H_2/3$ from the base of the wall, respectively. The increment of active earth pressure ($P_{ae} - P_a$) and that of passive earth pressure ($P_{pe} - P_p$) due to earthquake act at distances of $2H_1/3$ and $2H_2/3$ from the base of the wall, respectively.

Besides, based on many tests, Bowles (1988) suggested that δ be assumed to be 0 in the dynamic condition.

If the wall rotates about the wall toe when earthquakes occur, the location of the dynamic active earth pressure resultant can be determined as follows:

1 Compute the increment of the active earth force ΔP_{ae}:

$$\Delta P_{ae} = P_{ae} - P_a \tag{4.66}$$

2 Locate P_a at a distance of $H_1/3$ from the base of the wall.
3 Locate ΔP_{ae} at a distance of $2H_1/3$ from the base of the wall.
4 Compute the location of P_{ae}, resultant of P_e and ΔP_{ae}:

$$\bar{z} = \frac{P_a(H/3) + \Delta P_{ae}(2H/3)}{P_{ae}} \tag{4.67}$$

The location of the dynamic passive earth pressure resultant can be determined similarly.

In design, the influence of earthquakes on the safety of a retaining wall as a permanent structure should be considered. In deep excavations, the outer walls of a basement are permanent structures. The design should thereby take into consideration the influence of earthquakes. If the diaphragm walls also serve as the outer walls of a basement, the influence of earthquakes should be considered accordingly. Otherwise, the influence of earthquakes can be ignored. As for temporary retaining structures such as soldier piles, steel sheet piles, and column piles, earthquake effects are ignorable.

4.7 Summary and general comments

The chapter can be summarized as follows:

1 For those retaining walls to which displacement does not occur, such as the outer wall of a basement, the lateral earth pressure at rest is to be adopted for design. The coefficients of at-rest lateral earth pressure for normally consolidated cohesive soils and cohesionless soils can be estimated by Jaky's equation. For overconsolidated soils, though some empirical equations for the coefficients of at-rest lateral earth pressure are also available, in situ tests are preferable.
2 Rankine's earth pressure theory cannot consider friction or adhesion between the retaining wall and soil. Coulomb's earth pressure theory, on the other hand, can. Though the two theories are differently based, the obtained earth pressures are the same when both assume a vertical and smooth wall back. Both theories assume the failure surfaces as planes, not conforming to reality, and thereby their results cannot represent real earth pressures.

3 Friction between the retaining wall and soil considered, failure surfaces are curved surfaces. Thus, Rankine's active earth pressure would overestimate the real earth pressure very slightly whereas its passive earth pressure would underestimate the real value. Caquot-Kerisel's earth pressures, both the active and the passive ones, are the closest to the real values and are regarded as the real earth pressures.

4 In problems of excavation, the active earth pressure is the main force engendering failure. Caquot-Kerisel's active earth pressure, regarded as the real earth pressure, is to be adopted for design. Coulomb's active earth pressure is smaller than Caquot-Kerisel's, but the difference is insignificant. Therefore, Coulomb's active earth pressure can be used for design, too. To be conservative, Rankine's active earth pressure is to be recommended for it is the largest among the three and does not differ significantly from Caquot-Kerisel's.

5 The passive earth pressure is often the force to resist failure. Caqout-Kerisel's earth pressure is the first choice for analysis and design since it is regarded as the real earth pressure. Rankine's earth pressure is too small and differs significantly from the real value. Thus, Rankine's is not to be adopted. When $\delta \leq 0.5\phi'$, Coulomb's coefficient of passive earth pressure is similar to that of Caqout-Kerisel's and is also feasible for analysis and design. When $\delta > 0.5\phi'$, on the other hand, Coulomb's coefficient of passive earth pressure is obviously larger than Caqout-Kerisel's and will render the design unsafe.

6 Seepage will decrease the water pressure on the active side and increase it on the passive side, and will in turn affect the effective stress and the lateral earth pressure on the retaining wall. The seepage analysis can be conducted with the flow net method or the finite element method. To simplify the analysis, it is also workable to assume that the seepage is one dimensional.

Problems

4.1 Figure P4.1 shows a two story basement. The soil is silty sand and the groundwater level $H = 3.0$ m. $\gamma = 18$ kN/m^3, $\gamma_{sat} = 22$ kN/m^3, $c' = 0$, $\phi' = 34°$. Compute the total lateral force on the outer wall of the basement (including the resultant and the location of line of action).

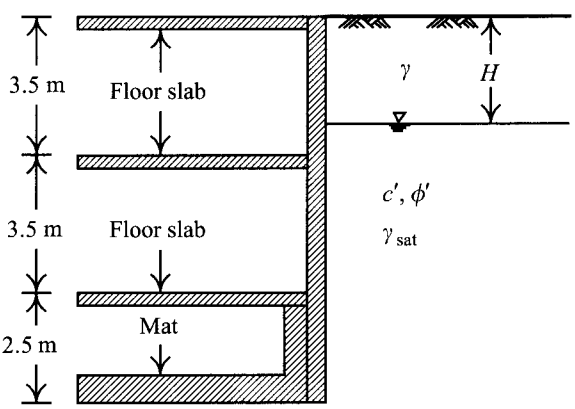

Figure P4.1

4.2 Same as above. Assume that the soil is normally consolidated clay this time. $H = 2.5$ m, $\gamma = 16$ kN/m^3, $\gamma_{sat} = 20$ kN/m^3, $c' = 0$, $\phi' = 32°$, and $s_u = 55$ kN/m^2. Compute the total lateral force on the outer wall of the basement (including the resultant and the location of line of action).

4.3 Assume the soil as shown in Figure P4.3 is sand and the groundwater level is very deep. $H_e = H_p = 13.0$ m, $c' = 0$, $\phi' = 34°$, and $\gamma = 18$ kN/m^3. Compute the active earth pressure using the following earth pressure theories separately (including the resultant and the location of line of action).

a Rankine's earth pressure theory
b Coulomb's earth pressure theory ($\delta = \phi'$)
c Caquot-Kerisel's earth pressure theory ($\delta = \phi'$)

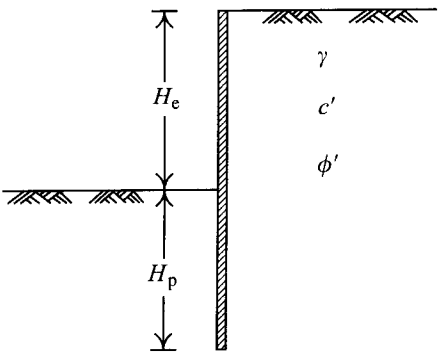

Figure P4.3

4.4 Same as above. If $\delta = \phi'/2$ this time, compute the active earth pressure using Rankine's, Coulomb's, and Caquot-Kerisel's earth pressure theories again.

4.5 Same as Problem 4.3. Compute the passive earth pressure.

4.6 Same as Problem 4.4. Compute the passive earth pressure.

4.7 Assume that the ground as shown in Figure P4.7 consists of clayey soils. $H_1 = 4.0$ m, $s_u = 100$ kN/m^2, $\gamma_{sat1} = 18$ kN/m^3, and $\gamma_{sat2} = 18$ kN/m^3, and $s_u/\sigma'_v = 0.3$. (a) Use Rankine's earth pressure theory (b) use Eq. 4.16 with $c_w = 0.5s_u$ to compute the total active earth pressure (including the resultant and the location of line of action).

4.8 Redo Problem 4.7 assuming $c_w = s_u$ this time.

4.9 Same as Problem 4.7. (a) Use Rankine's earth pressure theory (b) use Eq. 4.18 with $c_w = 0.5s_u$ to compute the total passive earth pressure (including the resultant and the location of line of action).

4.10 Figure P4.10 shows a retaining wall and the soil profile. $H_e = H_p = 9.5$ m, $H_1 = 4.0$ m, $c' = 0$, $\phi' = 32°$, $\gamma = 16$ kN/m^3, $\gamma_{sat} = 18$ kN/m^3, and $s_u/\sigma'_v = 0.35$. The sandy layer has porewater pressure $u = 300$ kN/m^2. Compute the active and passive earth pressures and their locations of line of action using Rankine's earth pressure theory.

4.11 Same as above. Assume that the earth pressure in the sandy layer is computed according to Caquot-Kerisel's theory. The active and passive earth pressures for the clayey layer are computed following Eqs 4.16 and 4.18 ($c_w = 0.5s_u$). Compute the lateral forces on the active and passive sides.

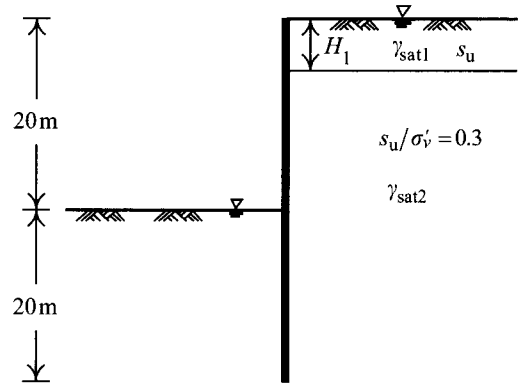

Figure P4.7

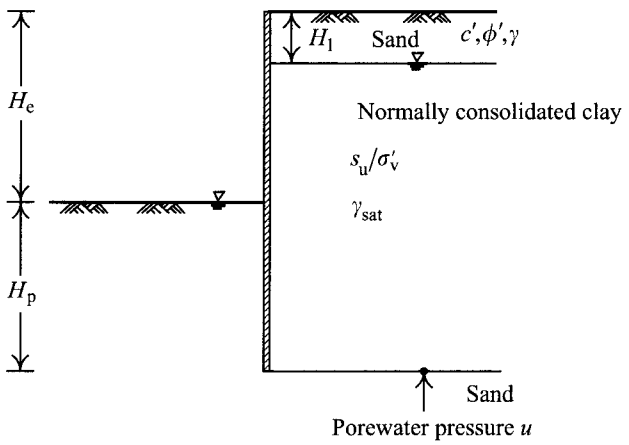

Figure P4.10

4.12 Redo Problem 4.10. Assume that $H_e = H_p = 15$ m, $H_1 = 5.0$ m, $c' = 0$, $\phi' = 35°$, $\gamma = 14$ kN/m^3, $\gamma_{sat} = 20$ kN/m^3, and $s_u/\sigma'_v = 0.30$. The porewater pressure in the sandy layer is $u = 300$ kN/m^2.

4.13 Figure P4.13 shows a clayey layer with a line load of Q_ℓ. The soil above the groundwater level is saturated. $H_e = H_p = 10$ m, $d_j = 1.0$ m, $\gamma_{sat} = 18$ kN/m^3, $s_u = 20$ kN/m^2, $Q_\ell = 500$ kN/m, $d = 3.0$ m. Compute the earth pressure induced by the line load and compare the result with Rankine's active earth pressure.

4.14 Same as the previous problem. Assume that the clayey layer is acted on by a point load $Q_p = 500$ kN. Compute the earth pressure on the section nearest to the point load Q_p. Compare the result with Rankine's active earth pressure, too.

4.15 Redo Problem 4.13. Assume that $H_e = H_p = 15$ m, $d_j = 1.0$ m, $\gamma_{sat} = 20$ kN/m^3, $s_u = 20$ kN/m^2, $Q_\ell = 900$ kN/m, $d = 2.0$ m.

4.16 Figure P4.16 shows a retaining wall and the soil profile. Assume that $H_e = H_p = 10$ m, $d_i = 0.5$ m, $d_j = 1.0$ m, $\gamma = 18$ kN/m^3, $\gamma_{sat} = 22$ kN/m^3, $c' = 0$, $\phi' = 34°$.

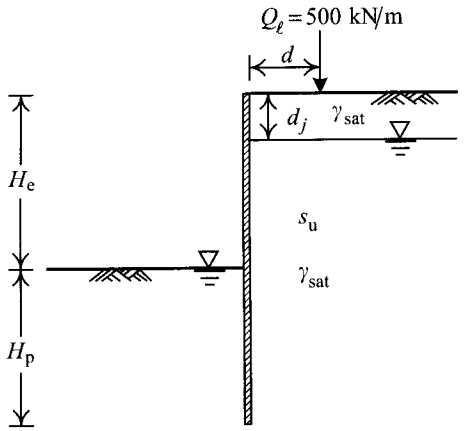

Figure P4.13

According to Caquot-Kerisle's theory, compute the total lateral force, including the resultant and the location of the line of action under the following conditions (assuming $\delta = \phi'$):

a If no seepage occurs.
b If seepage occurs, use the simplified method (assuming that the seepage is one dimensional).
c If seepage occurs, draw the flow net to compute the water pressure.

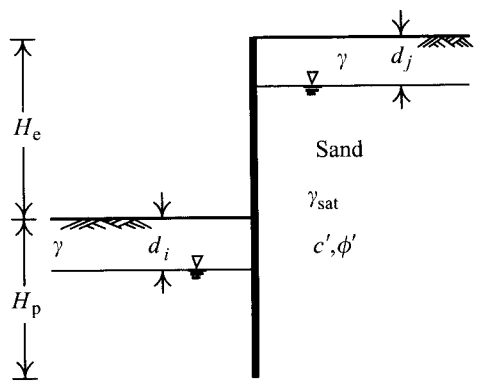

Figure P4.16

4.17 Redo Problem 4.16. Assume $H_e = H_p = 15$ m, $d_i = 0.5$ m, $d_j = 3.0$ m, $\gamma = 12$ kN/m^3, $\gamma_{sat} = 20$ kN/m^3, $c' = 0$, $\phi' = 34°$.

4.18 Redo Problem 4.16. Use Rankine's theory this time.

Chapter 5

Stability analysis

5.1 Introduction

Failures or collapses of excavations are disastrous at excavation sites. At worst they endanger the workers and adjacent properties. Their influence range is usually large: much ground settlement may arise and adjacent properties within the influence range of settlement may be damaged significantly. Since they are so crucially influential, to avoid failures or collapses is of the first importance and stability analyses are therefore required.

Failure of an excavation may arise from the stress on the support system exceeding the strength of its materials, for example, when the strut load exceeds the buckling load of struts or the bending moment of the retaining wall exceeds the limiting bending moment, etc. Please see Chapter 10 for more detailed discussions. Failure can also arise from the shear stress in soil exceeding the shear strength. The methods of analyzing whether the soils at the excavation site are able to bear the stress generated by excavation are called stability analyses, and are the main subject matter of this chapter.

Stability analyses include overall shear failure analysis, sand boiling analysis, and upheaval analysis. The overall shear failure analysis can be further divided into push-in and basal heave failure analyses. This chapter will introduce these methods for analyses and their applications in detail.

5.2 Types of factors of safety

There are basically three methods to determine the factor of safety for stability analysis: the strength factor method, the load factor method, and the dimension factor method, which are explained as follows:

1 Strength factor method: The method considers the soil strength involving much uncertainty and has the strength reduced by a factor of safety. If the factor of safety for the strength factor method is represented as FS_s, the parameters for the effective stress analysis are as follows:

$$\tan \phi'_m = \frac{\tan \phi'}{FS_s} \tag{5.1a}$$

$$c'_m = \frac{c'}{FS_s} \tag{5.1b}$$

The parameter for the undrained analysis is

$$s_{u,m} = \frac{s_u}{FS_s} \tag{5.2}$$

After conducting a force equilibrium or a moment equilibrium analysis with the after-reduction parameters c'_m, ϕ'_m or $s_{u,m}$ derived as above, we can design the penetration depth. The method locates the factor of safety at the source where the largest uncertainty arises and is therefore quite a reasonable method. Since the after-reduction parameters will lead to a smaller K_p and a larger K_a, the distribution of earth pressures on the retaining wall will be skewed. As a result, the method is applicable only to stability analysis and cannot be applied to deformation analysis or stress analysis (see Chapters 6–8).

2 *Load factor method*: The factor of safety for the load method, FS_ℓ, can be defined as follows:

$$FS_\ell = \frac{R}{D} \tag{5.3}$$

where R represents the resistant force and D is the driving force. R and D can be either the resistant moment and the driving moment, or the bearing force and the external force. FS_ℓ considers uncertainty arising from the soil strength, the analysis method, and external forces synthetically. The factors of safety adopted in this chapter are mainly derived from the load factor method.

3 *Dimension factor method*: Suppose that retaining walls are in the limiting state and the soil strengths are fully mobilized. With the force equilibrium (the horizontal force equilibrium, the moment equilibrium or other type of force equilibrium), the penetration depth of retaining walls in the limiting state can be found. The penetration depth for design is:

$$H_{p,d} = FS_d H_{p,cal} \tag{5.4}$$

where FS_d = factor of safety for the dimension factor method

$H_{p,cal}$ = penetration depth computed from the limit equilibrium.

The factor of safety is usually defined as a ratio of the resistant force to driving force or as a factor to reduce the strength. Eq. 5.4 is too much empirically oriented and cannot properly express the meaning of the factor of safety, leading to unreasonable results and is not recommended. If applied, cross checking by other methods is necessary.

5.3 Overall shear failure

When the shear stress at a point in soil exceeds or equals the shear strength of soil at the point, the point is in the failure state or limiting state. When many failure points connect up into continuities and form a plane, the failure surface is thus produced. Once the failure surface is produced, the excavation failure or collapse will occur. This is called the overall shear failure.

The push-in and the basal heave are two main overall failure modes of excavation. As shown in Figure 5.1a, the push-in is caused by the earth pressures, reaching the limiting state, on both sides of the retaining wall, which is thereby moved, a large distance, toward the excavation zone (especially the part embedded in soil) until reaching the full-zone failure. The analysis views the retaining wall as a free body and the external forces on the wall and internal forces of the wall are in equilibrium. The factor of safety against push-in or

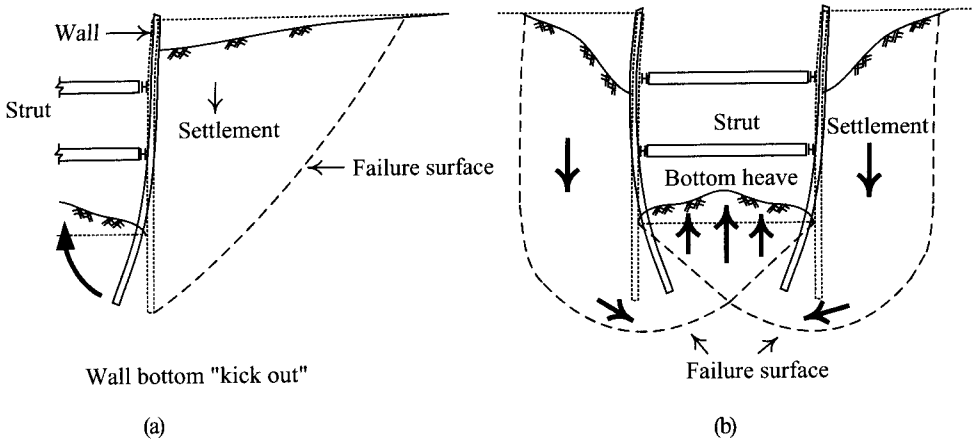

Figure 5.1 Overall shear failure modes: (a) push-in and (b) basal heave.

penetration depth of the wall can thus be obtained. When push-in is caused, with different extents of movement of the embedded part of the retaining wall, the earth pressure on the retaining wall varies. Thus there are the fixed earth support method and the free earth support method for analysis, which are to be introduced in Section 5.4.

The basal heave arises from the weight of soil outside the excavation zone exceeding the bearing capacity of soil below the excavation bottom, causing the soil to move and the excavation bottom to heave so much that the whole excavation collapses. Figure 5.1b is a possible form of basal heave. When analyzing the basal heave, we should assume several possible basal heave failure surfaces and find their corresponding factors of safety according to mechanics. The surface having the smallest factor of safety is the most likely potential failure surface or critical failure surface. With the variable forms of critical failure surfaces, there exist many analyzing methods. Details of analyses will be discussed in Section 5.5.

As discussed above, the mechanisms of push-in and basal heave are different. Basically, push-in refers to the stability of the retaining wall. Push-in also causes soil near the wall to heave. As to basal heave, it refers to the stability of the soil below the excavation bottom and its failure surface may pass through the bottom of the retaining wall or through the soil below the bottom of the retaining wall. When basal heave occurs, the soil around the excavation bottom will mostly heave. Nevertheless, when it occurs to a soft clay ground, the earth pressure on both sides of the wall may also reach the limiting state, from which it follows that a push-in failure is also possible.

5.4 Free earth support method and fixed earth support method

There are two analysis methods for the push-in failure: free earth support method and fixed earth support method. As shown in Figure 5.2a, the free earth support method assumes that the embedment of the retaining wall is allowed to move to a certain distance under the action of lateral earth pressure. Therefore, the earth pressure on the retaining wall in the limiting state can be assumed as shown in Figure 5.2b.

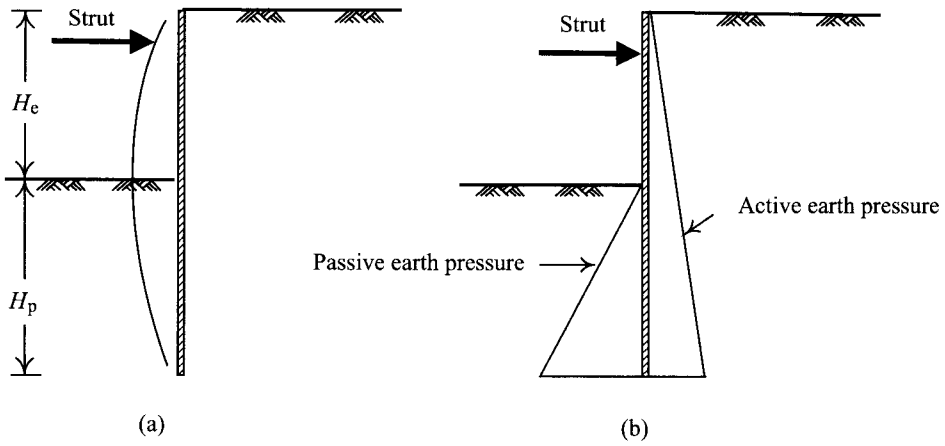

Figure 5.2 Free earth support method: (a) deformation of the retaining wall and (b) distribution of earth pressure.

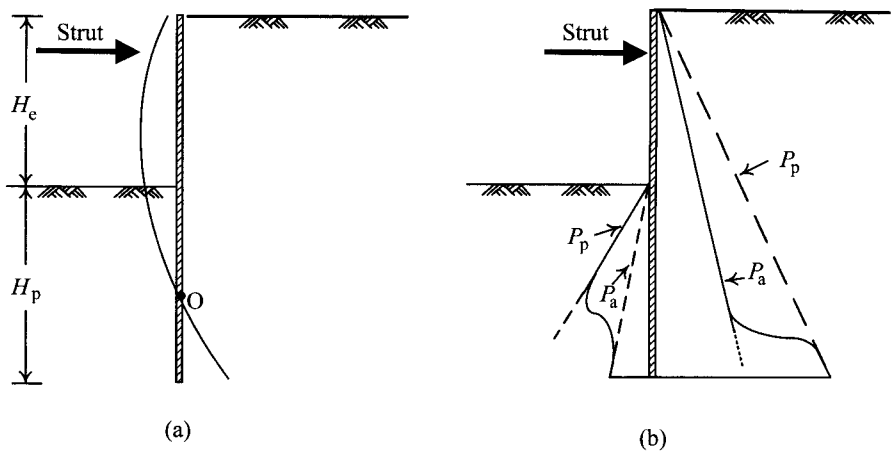

Figure 5.3 Fixed earth support method: (a) deformation of the retaining wall and (b) distribution of earth pressure.

The fixed earth support method is to assume that the embedment of the retaining wall seems to be fixed at a point below the excavation surface. The embedded part may rotate about the fixed point, as shown in Figure 5.3a. Thus, when the retaining wall is in the limiting state, the lateral earth pressure around the fixed point on the two sides of the retaining wall does not necessarily reach the active or passive pressures, as shown in Figure 5.3b.

If a cantilever wall is designed based on the free earth support method, no fixed point is supposed to exist in the embedded part of the wall, as discussed above. The external forces, only passive and active forces, on the retaining wall are not to come to equilibrium. Therefore, the free earth support method is not applicable to cantilever walls. On the other hand, if the

free earth support method is applied to a strutted wall, the forces acting on the wall will include both the passive and active forces and the strut load. With external forces on the wall coming to equilibrium, the method is applicable to a strutted wall. On the other hand, if we apply the fixed earth support method to a strutted wall, the penetration depth of the wall will be too large to be economical.

5.5 Overall shear failure of strutted walls

5.5.1 Push-in

As discussed in Section 5.4, for a strutted wall, the free earth support method is the commonly used analysis method. As shown in Figure 5.4a, the earth pressures on the outer and the inner sides of the retaining wall in the braced excavation will reach the active and the passive earth pressures respectively in the limiting state. Take the retaining wall below the lowest level of strut as a free body and conduct a force equilibrium analysis (Figure 5.4b), and we can then find the factor of safety against push-in as follows:

$$F_p = \frac{M_r}{M_d} = \frac{P_p L_p + M_s}{P_a L_a} \tag{5.5}$$

where

F_p = factor of safety against push-in
M_r = resisting moment
M_d = driving moment
P_a = resultant of the active earth pressure on the outer side of the wall below the lowest level of strut
L_a = length from the lowest level of strut to the point of action P_a
M_s = allowable bending moment of the retaining wall

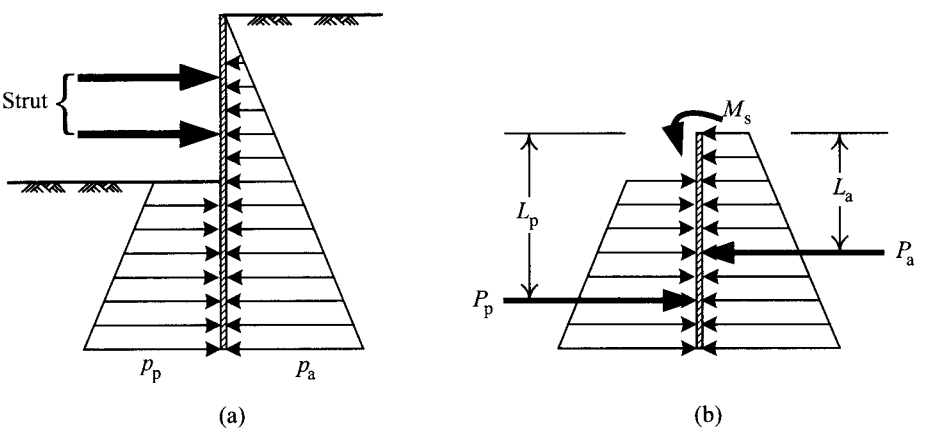

Figure 5.4 Analysis of push-in by gross pressure method: (a) distribution of gross earth pressure and (b) force equilibrium of the retaining wall as a free body.

P_p = resultant of the passive earth pressure on the inner side of the retaining wall below the excavation surface

L_p = length from the lowest level of strut to the point of action P_p.

Equation 5.5 is generally called the gross pressure method. JSA (1988) and TGS (2001) suggested $F_p \geq 1.5$. Nevertheless, when assuming $M_s = 0$, $F_p \geq 1.2$. Eq. 5.5 can be used either to obtain the factor of safety against push-in for a certain depth of wall or the required penetration depth of a retaining wall with a certain value of safety factor.

For cohesive soils with s_u = constant and $2s_u/\gamma H_e \geq 0.7$ (i.e. s_u comparatively large and not varying with the increase of depth, or shallow excavations), the results from the gross pressure method would come out illogical, that is, the deeper the penetration depth of the retaining wall, the smaller the factor of safety, as shown in Figure 5.5 (Burland and Potts, 1981; Ou and Hu, 1998). Thus, the gross pressure method is not applicable to cohesive soils with a constant s_u-value and $2s_u/\gamma H_e$ too large. However, the method is good enough for cohesive soils when $2s_u/\gamma H_e < 0.7$. Ou and Hu (1998) also found that the results of the gross pressure method will not come out illogical when applied to cohesive soils with s_u/σ'_v = constant or s_u increasing with the increase of depth.

For cohesionless soils with ϕ' smaller than 22°, the penetration depth using the gross pressure method would come out too large, according to Burland and Potts (1981).

From the conclusions of Chapter 4, Eqs 4.16 and 4.18 can be adopted for the earth pressures on a retaining wall in cohesive soils. Both equations have to consider the adhesion (c_w) between the wall and soil, which can be estimated by the following equation:

$$c_w = \alpha s_u \tag{5.6}$$

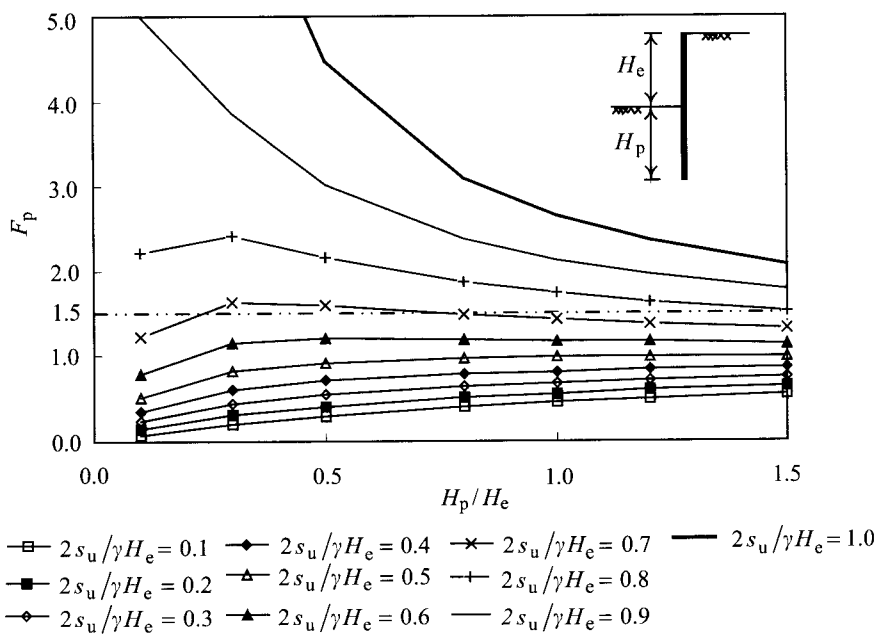

Figure 5.5 Relations between factors of safety against push-in obtained by the gross pressure method and penetration depths (s_u = constant).

where s_u is the undrained shear strength of clay and α is the strength reduction factor.

As discussed in Section 4.6, α relates to the soil strength, the construction method of the retaining wall, and the roughness of the wall. α can be determined by consulting the studies of pile foundations. For example, the value of α in Figure 4.12.

Ou and Hu (1998) also carried on a series of stability analysis studies on some case histories of excavations in soft clay in Taipei, Singapore, San Francisco, and Chicago. The results show that, if we assume that the adhesion (c_w) between diaphragm walls and clay is equal to 0.67 s_u and that between steel sheet piles and clay is equal to 0.5 s_u, the factors of safety for the cases where failures occurred are all lower than 1.0 while those where failures did not occur are all greater than 1.0, as shown in Figure 5.6.

Taking the excavation profile and geological conditions of the TNEC (Taipei National Enterprise Center) for example, Table 5.1 provides some required penetration depths of the retaining wall, given various c_w-values. As for the geological conditions of TNEC, please refer to Figure 2.37; the excavation plan and profile, Figure 3.33. The excavation depth of TNEC was 19.7 m and its retaining wall was a 90 cm thick, 35 m deep diaphragm wall. The excavation and the basement construction adopted the top-down construction method, and the lowest level of struts was 3.2 m above the excavation surface. The soil at the site was mainly composed of normally consolidated clay. To simplify the analysis, we assume the site was equally composed of normally consolidated clay whose ratio of undrained shear strength to effective overburden pressure (s_u/σ'_v) was 0.32, the groundwater level was 2 m below the ground surface, and the saturated unit weight was 18.6 kN/m^3. The required penetration depths of the retaining wall with $c_w = 0$, $c_w = 0.5\ s_u$, $c_w = 0.67\ s_u$, and $c_w = s_u$ were computed using Eq. 5.5, as illustrated in Table 5.1, from which we can see that the penetration depth of a retaining wall closely relates to the c_w-value. Suppose we assume

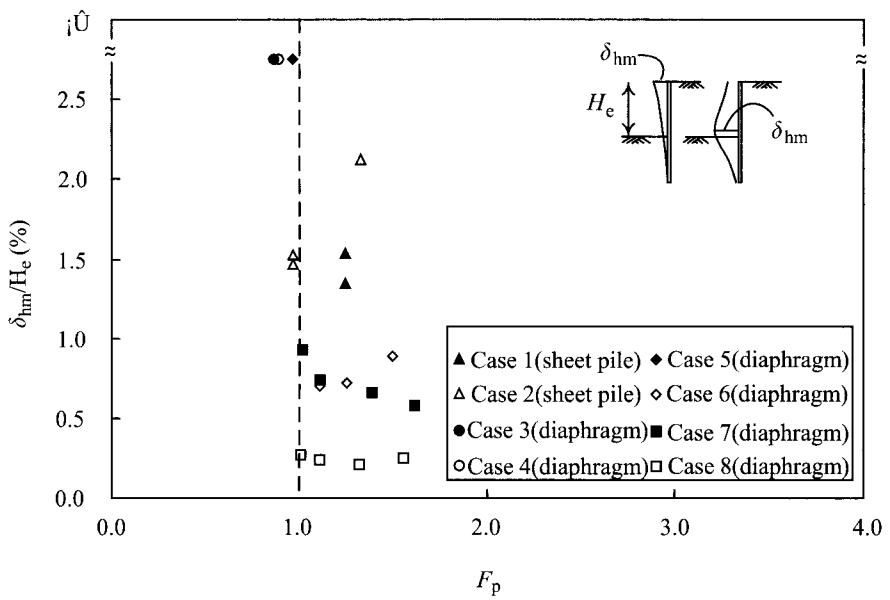

Figure 5.6 Factors of safety against push-in for excavations in clayey soils, where Cases 3, 4, and 5 are failure cases and the others are safe cases (assuming $c_w = 0.67s_u$ for diaphragm walls, $c_w = 0.5s_u$ for sheet piles).

Table 5.1 Relationship between depth of the diaphragm wall (or penetration depth) for the assumed excavation case and c_w

	$F_p = 1.2$	$F_p = 1.3$	$F_p = 1.5$
$c_w = 0.0$	50.4(30.7)	60.4(40.7)	96.6(76.9)
$c_w = 0.33s_u$	39.5(19.8)	45.3(25.6)	63.1(43.4)
$c_w = 0.50s_u$	35.7(16.0)	40.3(20.6)	53.7(34.0)
$c_w = 0.67s_u$	32.7(13.0)	36.4(16.7)	46.8(27.1)
$c_w = 1.00s_u$	28.4(8.7)	30.9(11.2)	37.7(18.0)

Note
Numbers in ( ) represent the "penetration depth."

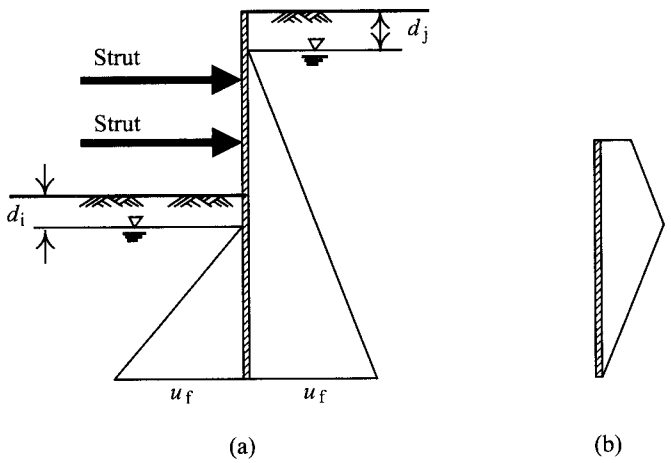

Figure 5.7 Distribution of water pressure due to seepage: (a) distribution of water pressure and (b) net water pressure (note: u_f = water pressure due to seepage).

$F_p = 1.2$, $M_s = 0$, and $c_w = 0$, we will obtain the wall penetration depth of 30.7 m, which is far from reasonable. If we let $c_w = 0.67\ s_u$ and $F_p = 1.2$, then the required penetration depth will be 13.0 m, which is closer to the empirical value and to the actual penetration depth of TNEC. Note that the actual penetration depth should also be determined according to the analysis of basal heave (please see Section 5.5.2).

From the above discussion, we can reasonably assume $c_w = 0.67\ s_u$ (for diaphragm walls) or $c_w = 0.5\ s_u$ (for steel sheet piles), and the factor of safety is around 1.2 when analyzing the push-in failure in clayey soils.

To estimate the factor of safety, for a purely sandy ground (cohesionless soils) with a high groundwater level, though the gross pressure method can be used along with either the gross water pressure distribution or the net water pressure distribution, the latter is more reasonable according to Padfield and Mair's study (1984), as shown in Figure 5.7.

We have concluded in Chapter 4 that for cohesionless soils, Caquot-Kerisel's or Coulomb's active earth pressure should be adopted for the active earth pressure acting on the retaining wall. Both Caquot-Kerisel's and Coulomb's coefficient of active earth pressure correlate with δ closely. To be conservative, Rankine's active earth pressure is also recommendable.

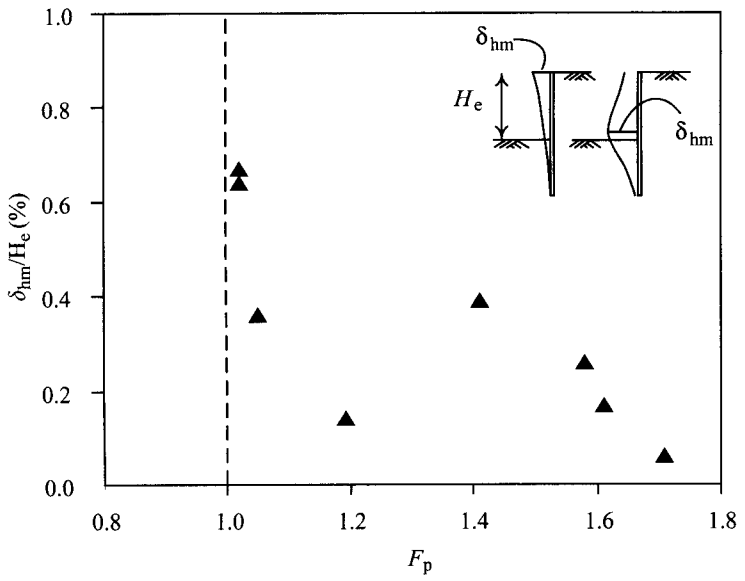

Figure 5.8 Factors of safety against push-in for excavations in sand (all cases are safe, $\delta = \phi'$ is assumed).

As for the passive earth pressure, Caquot-Kerisel's is preferable. When $\delta < \phi'/2$ (δ is the friction angle between the retaining wall and soil), Coulomb's passive earth pressure coefficient is quite close to Caquot-Kerisel's.

Section 4.5.3 has summarized some findings on values of δ and concluded that between concrete (cast in steel mold) and sand, δ is about $0.8\phi'$. Ou and Hsiao (1999) investigated nine no failure excavation case histories located in Taiwan to explore the reasonable factor of safety against push-in and found, only when assuming $\delta = \phi'$ (in sandy soils), the factors of safety in the nine case histories were larger than 1.0, as shown in Figure 5.8. In fact, in the process of trench excavation and concrete casting of the construction of diaphragm walls, the borders between trenches and soil are often rugged and the assumption that $\delta = \phi'$ seems to be reasonable for sandy soils. However, to be conservative in analysis, we usually assume $\delta = (0.5 \sim 0.67)\phi'$ instead. For analysis and design, to assume $F_p = 1.2$ is supposed to be reasonable.

As shown in Figure 5.9a, the active and passive earth pressures on the two sides of the retaining wall are expressed in terms of net values. By conducting a force equilibrium analysis of the net forces on the retaining wall below the lowest level of strut, viewed as a free body (Figure 5.9b), we will thus derive an equation similar to Eq. 5.5 to compute the factor of safety against push-in. The method is called the net pressure method. Nevertheless, according to Burland and Potts (1981) and Ou and Hu (1998), any slight difference of the penetration depth will lead to a large change in the factor of safety computed from the net pressure method. That is to say, the factor of safety is too sensitive to the penetration depth and the net pressure method is not good for stability analysis of the push-in failure.

Some engineers prefer to assume $F_p = 1.0$ first and then use Eq. 5.5 to determine the preliminary penetration depth and then added 20–40% to be the penetration depth for design.

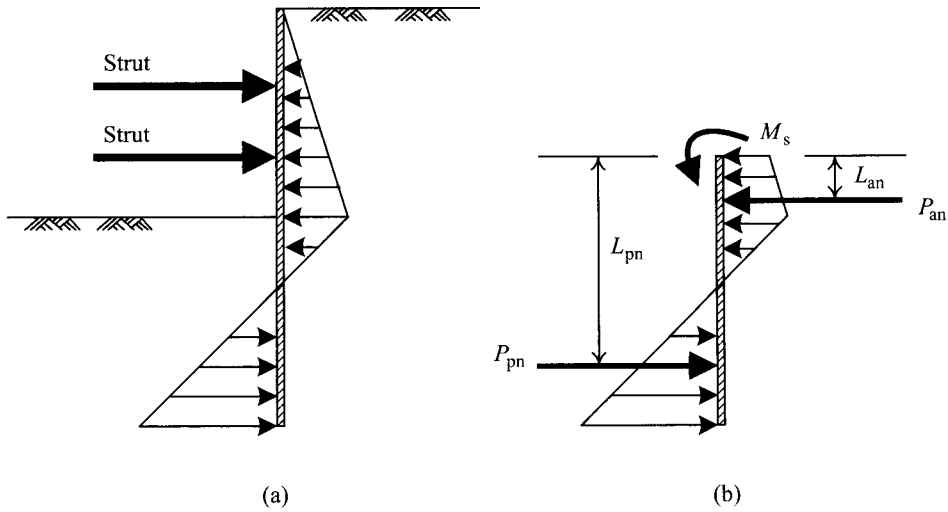

Figure 5.9 Analysis of push-in by the net pressure method: (a) distribution of net earth pressure and (b) force equilibrium of the retaining wall as a free body.

The method is the dimension factor method, as discussed in Section 5.2. According to Burland and Potts' study (1981), the factor of safety obtained following the dimension factor method does not conform to the definition of the factor of safety and may lead to unreasonable results.

Some prefer to reduce the passive earth pressure by a factor of safety. For example, $K_{p,design} = K_p/F_p$. Then, compute the penetration depth by way of the horizontal force equilibrium and the moment equilibrium. This is another way of following the strength factor method (as discussed in Section 5.2). Though the method is logical, when applied to practical design, appropriate factors of safety should be carefully determined.

5.5.2 *Basal heave*

The analyses of the basal heave failure are only applicable to clayey soils and the reasons will be given at the end of this section.

Since $\phi = 0$ for clay, the failure surfaces of bearing capacity failures in clay (e.g. the slope stability problems, the ultimate bearing capacity problems of foundations, etc.) are circular arc surfaces. The basal heave failure due to excavation is also a kind of bearing capacity failure and might also have a main circular arc failure surface. The analysis method for basal heave varies with the assumed shapes of failure surfaces near the ground or excavation surface, though the main failure surface is still a circular arc. As discussed in Section 5.3, the analysis method for basal heave assumes many possible failure surfaces and finds their corresponding factors of safety according to mechanics. The one with the smallest factor of safety is the most likely potential failure surface. Many analysis methods have been proposed for basal heave, the most commonly applied of which are Terzaghi's method, Bjerrum and Eide's method, and the slip circle method. This section will categorize these methods into the bearing capacity method, the negative bearing capacity method, and the slip circle method according to their characteristics.

5.5.2.1 Bearing capacity method

As shown in Figure 5.10, the soil weight above the level of the excavation surface (plane **abc**) can be seen as the load to cause excavation failure. Supposing a trial failure surface caused by the soil weight within the width of B_1 acts on plane **abc** as is shown in Figure 5.10a, we can find the ultimate load for the width of B_1 following Terzaghi's bearing capacity method with the shear strength along side **bd** considered. The ratio of the ultimate load to the weight of soil within the width of B_1 is the factor of safety for the trial failure surface. Then increase the value of B_1 (which denotes increasing of the size of trial failure surfaces) and find the corresponding factor of safety accordingly until the trial failure surface covers the whole excavation (i.e. $B_1 = B/\sqrt{2}$), as shown in Figures 5.10b and 5.10c. Since the weight of B_1-wide soil on each side of the excavation zone may produce failures, the schematic diagram to calculate the factor of safety will be as illustrated in Figure 5.10d. Following the principle of virtual work, the factor of safety induced from Figure 5.10c and that from Figure 5.10d would be identical. The factor of safety against basal heave (F_b) for the excavation is the smallest one among the safety factors corresponding to the trial failure surfaces.

Figure 5.11 is the profile of a hypothetical excavation case, where the undrained shear strength (s_u) is constant. Following the bearing capacity method, we can obtain the relationship between trial failure surfaces (represented by X/H_e) and their corresponding factors of safety, as shown in Figure 5.12. From the figure we can see that the factor of safety falls with the rising of X (i.e. the expansion of the trial failure surfaces). When X rises to two times the

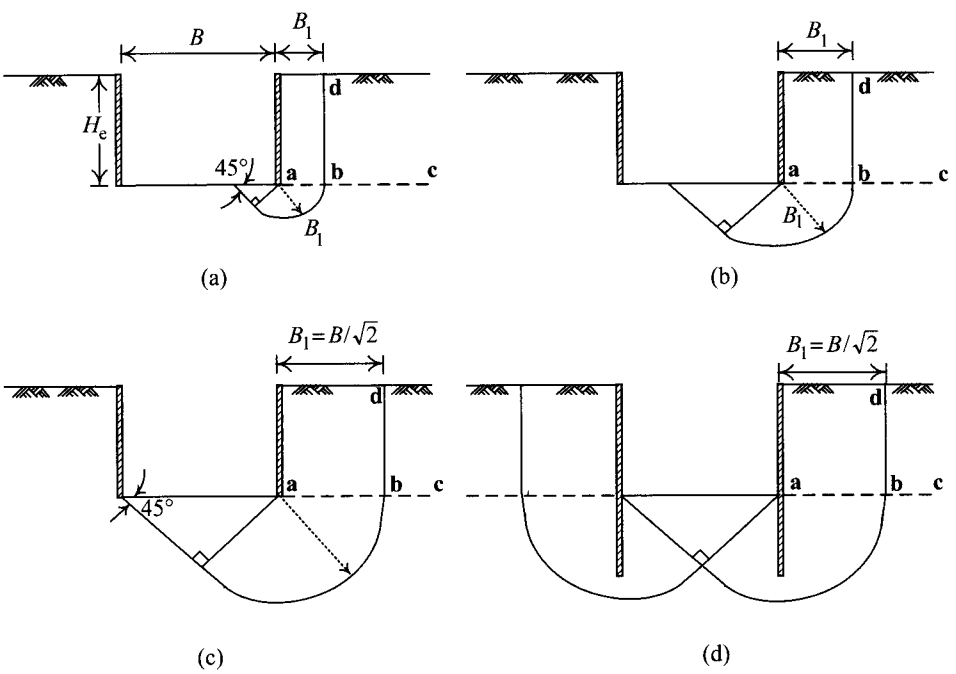

Figure 5.10 Analysis of basal heave by bearing capacity method: (a) a B_1 wide trial failure surface, (b) a second B_1 wide trial failure surface, (c) a third B_1 wide trial failure surface, and (d) both sides of the excavation produce failure surfaces.

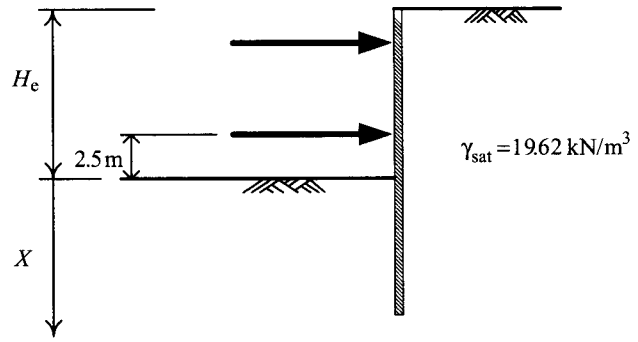

Figure 5.11 Excavation profile of the assumed excavation case.

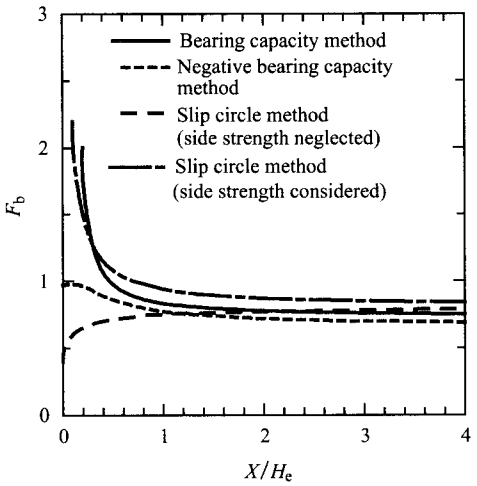

Figure 5.12 Relations between failure circle sizes and factors of safety against basal heave obtained by the bearing capacity method, negative bearing capacity method, and the slip circle method (s_u = 25 kN/m^2).

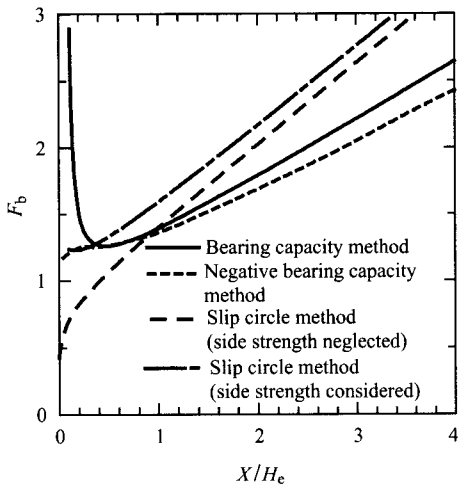

Figure 5.13 Relations between failure circle sizes and factors of safety against basal heave obtained by the bearing capacity method, negative bearing capacity method, and the slip circle method ($s_u/\sigma'_v = 0.3$).

excavation depth, the factor of safety will be approaching a constant. Figure 5.13 is a similar excavation profile with s_u/σ'_v constant. From the figure we can see that F_b also falls with the increase of X. When X comes to a certain value, F_b will be the smallest and then will grow again. It follows that when the trial failure surface covers the whole excavation zone, that is, $X = B/\sqrt{2}$, F_b will not necessarily be its smallest.

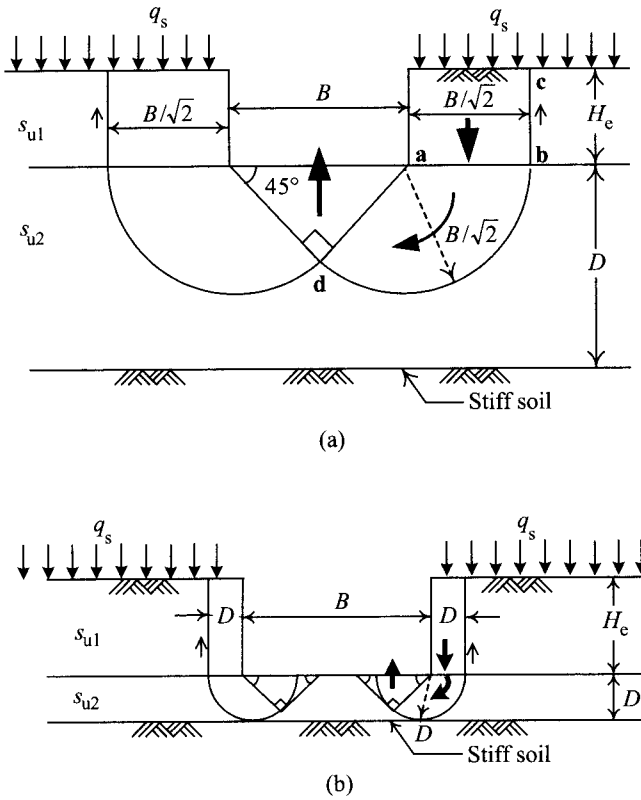

Figure 5.14 Analysis of basal heave using Terzaghi's method: (a) $D \geq B/\sqrt{2}$ and (b) $D < B/\sqrt{2}$.

Terzaghi (1943) did not adopt the above method, where the smallest factor of safety is taken to be the factor of safety against basal heave. Instead, he directly assumed the trial failure surface where $B_1 = B/\sqrt{2}$ (i.e. $X = B/\sqrt{2}$) is the critical failure surface and its corresponding factor of safety is the factor of safety against basal heave, as shown in Figure 5.14. According to Terzaghi's bearing capacity theory, the bearing capacity of saturated clay under plane **ab** can be denoted as $P_{max} = 5.7s_u$. When the soil weight above plane **ab** is greater than the soil bearing capacity, the excavation will fail. Besides, the failure surface will be restrained by stiff soils. Let D represent the distance between the excavation surface and the stiff soil. We can discuss Terzaghi's method in two parts: $D \geq B/\sqrt{2}$ and $D < B/\sqrt{2}$:

When $D \geq B/\sqrt{2}$

As shown in Figure 5.14a, the formation of a failure surface is not restrained by the stiff soil. Suppose the unit weight of the soil is γ. The soil weight (containing the surcharge q_s) ranges B_1 on plane **ab** will then be:

$$W = (\gamma H_e + q_s)(B_1 \times 1) = (\gamma H_e + q_s)\frac{B}{\sqrt{2}} \tag{5.7}$$

The ultimate load, Q_u, of the saturated clay below plane **ab** will be:

$$Q_u = 5.7s_{u2}(B_1 \times 1) = (5.7s_{u2})\frac{B}{\sqrt{2}} \tag{5.8}$$

When a basal heave failure occurs, vertical plane **bc** can offer shear resistance ($s_{u1}H_e$) and the factor of safety against basal heave (F_b) will be:

$$F_b = \frac{Q_u}{W - s_{u1}H_e} = \frac{5.7s_{u2}B/\sqrt{2}}{(\gamma H_e + q_s)B/\sqrt{2} - s_{u1}H_e} = \frac{1}{H_e} \cdot \frac{5.7s_{u2}}{\gamma + (q_s/H_e) - (s_{u1}/0.7B)} \tag{5.9}$$

where s_{u1} and s_{u2} represent respectively the undrained shear strengths of the soils above and below the excavation surface; q_s denotes surcharge on the ground surface.

When $D < B/\sqrt{2}$

Under such a condition, the failure surface will be restrained by the stiff soil, as shown in Figure 5.14b, and its factor of safety (F_b) will be:

$$F_b = \frac{Q_u}{W - s_{u1}H_e} = \frac{5.7s_{u2}D}{(\gamma H_e + q_s)D - s_{u1}H_e} = \frac{1}{H_e} \cdot \frac{5.7s_{u2}}{\gamma + (q_s/H_e) - (s_{u1}/D)} \tag{5.10}$$

For most excavation cases, Terzaghi's factor of safety (F_b) should be greater than or equal to 1.5 (Mana and Clough, 1981; JSA, 1988).

Assuming that the penetration depth of the retaining wall is deep enough, the failure surface may be formed as illustrated in Figure 5.15a, which is one of the possible failure modes. According to the analysis on the basis of the principle of virtual work, the factor of safety for a failure surface as illustrated in Figure 5.15a is close to that of Eqs 5.9 and 5.10. The only difference is that the failure surface in Figure 5.15a ranges wider (with the extra failure surface **be**) and the average soil strength on the failure surface is higher than that in Figure 5.15b (assuming the undrained shear strength of clay increases with the increase of depth).

As shown in Figure 5.15b, assuming the penetration depth of the retaining wall is not deep enough, the calculation of the factor of safety will still follow Eqs 5.9/5.10. That is to say, the value of the factor of safety against basal heave has nothing to do with the existence of

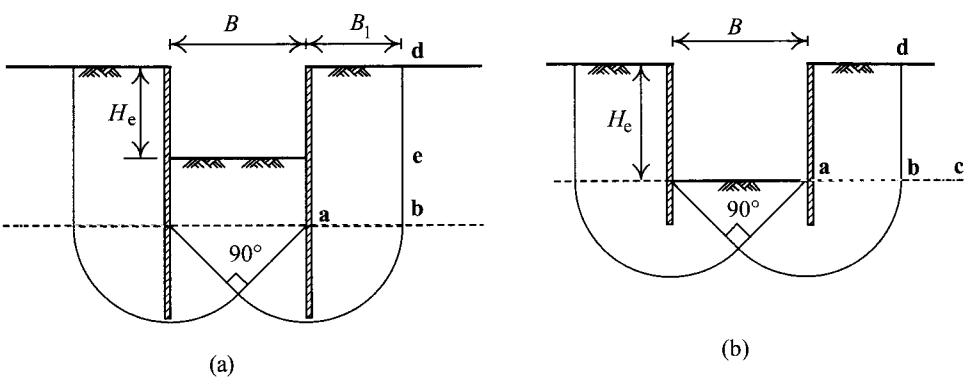

Figure 5.15 Relation between the embedded part of the retaining wall and the failure surface: (a) large penetration depth and (b) small penetration depth.

the retaining wall according to the equations. However, theoretically speaking, the retaining wall with high stiffness may be capable of restraining basal heave failures. Thus, the actual factor of safety should be greater than the result from Eq. 5.9 or 5.10 though there does not exist a suitable way to estimate it.

The bearing capacity method or Terzaghi's method is suitable for shallow excavations, where the excavation width (B) is larger than the excavation depth (H_e). For deep excavations, $B < H_e$, the bearing capacity method or Terzaghi's method may not yield reasonable results because the method assumes that the failure surface extends up to the ground surface and that the shear strength of clay is fully mobilized all the way to the ground surface, neither of which is necessarily true for deep excavations.

5.5.2.2 *Negative bearing capacity method*

The negative bearing capacity method assumes that the unloading behavior caused by excavation is analogous to the building foundation being subject to an upward loading and that the shape of the failure surface is similar to the failure mode of the deep foundation. Then, using the bearing capacity equation for the deep foundation, we can obtain the ultimate unloading pressure. The factor of safety is the ratio of the ultimate unloading pressure to the unloading pressure. As shown in Figure 5.16, assuming various failure surfaces to analyze (representing different B_1-values) and finding their separate corresponding factors of safety, the smallest factor of safety among them is the factor of safety against basal heave for the excavation.

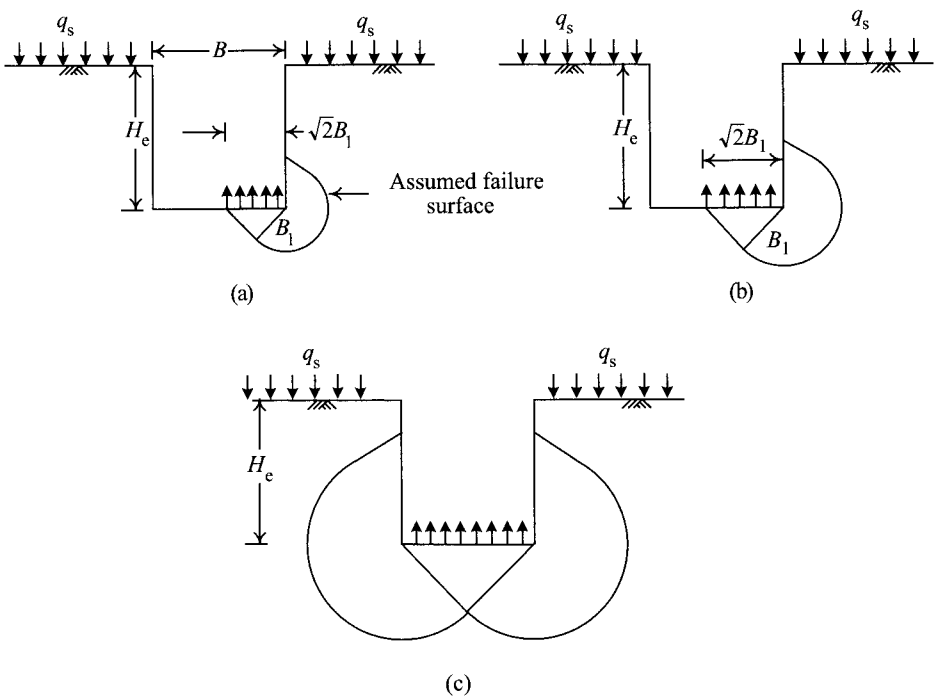

Figure 5.16 Analysis of basal heave failure by negative bearing capacity method: (a) a $\sqrt{2}B_1$ wide failure surface, (b) another $\sqrt{2}B_1$ wide failure surface, and (c) Failure surface covers the whole excavation bottom.

Figures 5.12 and 5.13 also illustrate the changing tendencies of the factor of safety against basal heave with the size of the trial failure surfaces for s_u = constant or s_u/σ'_v = constant respectively, following the negative bearing capacity method (as for the excavation profile, please see Figure 5.11), where the bearing capacity factor, N_c, can be determined according to Skempton (1951), as shown in Figure 5.17. N_c can also be calculated by the following equation:

$$N_{c(\text{rectangular})} = N_{c(\text{square})}\left(0.84 + 0.16\frac{B}{L}\right) \tag{5.11}$$

As shown in Figures 5.12 and 5.13, we can see that for soils where s_u = constant, the factors of safety against basal heave derived from the negative bearing capacity method will decrease with the increase of the size of the trial failure surfaces (which means X increases). For soils where s_u/σ'_v = constant, the factors of safety against basal heave derived from the negative bearing capacity method will increase with the increase of the size of the trial failure surfaces.

Like Terzaghi's method, Bjerrum and Eide (1956) did not yield the factor of safety against basal heave by finding the smallest, as just mentioned. Instead, they assumed the failure surface where the radius of the circular arc is equal to $B/\sqrt{2}$ is the critical failure surface and the corresponding factor of safety is the one against basal heave (see Figure 5.16c). The factor of safety can be expressed as follows:

$$F_b = \frac{N_c \cdot s_u}{\gamma \cdot H_e + q_s} \tag{5.12}$$

where q_s is the surcharge on the ground surface and N_c is Skempton's bearing capacity factor as shown in Figure 5.17.

Since N_c has taken into account the effects of the embedment depth of foundations and excavation size, Eq. 5.12 is equally valid for shallow and deep excavations, as well as rectangular excavations.

According to Reddy and Srinivasan's study (1967), NAVFAC DM 7.2 (1982) modified Bjerrum and Eide's method to apply the method to the excavations where there are stiff soils below the excavation surfaces or there are two layers of soils. As shown in Figure 5.18, the

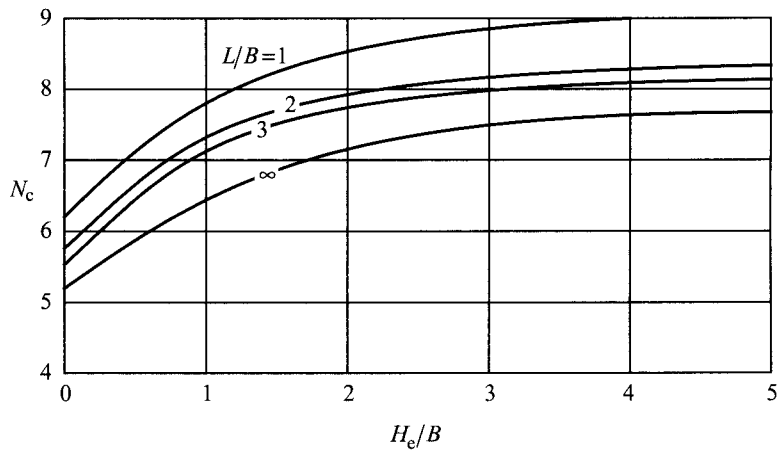

Figure 5.17 Skempton's bearing capacity factor (Skempton, 1951).

Extended Bjerrum and Eide's method can be expressed as follows:

$$F_b = \frac{s_{u1} N_{c,s} f_d f_s}{\gamma H_e} \tag{5.13}$$

where

γ = unit weight of the soil
H_e = excavation depth
s_{u1} = undrained shear strength of the upper clay
s_{u2} = undrained shear strength of the lower clay
$N_{c,s}$ = bearing capacity factor that does not consider the excavation depth. This can be determined according to Figure 5.18a or 5.18b with the values of D/B (the ratio of the distance from the excavation surface to the lower soils to the excavation width) and s_{u2}/s_{u1} given
f_d = depth correction factor, which can be found in Figure 5.18c
f_s = shape correction factor, which can be estimated by the following equation:

$$f_s = 1 + 0.2\frac{B}{L} \tag{5.14}$$

where B refers to the excavation width and L the excavation length.

Like Terzaghi's method, when there exists stiff soil below the excavation surface, the failure surfaces assumed by Bjerrum and Eide's method and by the Extended Bjerrum and Eide's method would also be restrained by the stiff soil. The stiff soil may be stiff clays, sandy soils or gravel soils. To conduct the stability analysis of the basal heave failure, we can use Eq. 5.13, where $N_{c,s}$ can be found in Figures 5.18a or 5.18b. The latter is a simplified version of the former, assuming that the failure circle will be tangent to the lower soils when s_{u2}/s_{u1} is very large.

If the penetration depth of the retaining wall is deep enough, Bjerrum and Eide's method computes the factor of safety in a way similar to Terzaghi's method. That is to say, the failure surface will be formed in a deeper level, similar to what is illustrated in Figure 5.15a. Under such conditions, Eq. 5.12 is still workable to estimate the factor of safety with the slight differences of average soil strengths on failure surfaces. When the H_p is not large enough, the calculation of the factor of safety will still follow Eqs 5.12/5.13. That is to say, the value of the factor of safety against basal heave has nothing to do with the existence of the retaining wall according to the equations.

The negative bearing capacity method or Bjerrum and Eide's method take into account the effects of excavation shape, width, and depth. Therefore, the methods are applicable to various shapes of excavations, shallow excavations as well as deep excavations.

For most excavations, the factor of safety obtained according to Bjerrum and Eide's method (F_b) should be larger than or equal to 1.2 (JSA, 1988).

5.5.2.3 *Slip circle method*

Let the trial failure surfaces of the basal heave failure be assumed to be basically circular arcs, and separately compute the ratios of the resistant moments to the driving moments for the trial circular arc failure surfaces. The smallest factor of safety among them is then the factor of safety against basal heave for the excavation. The method is designated as the slip circle

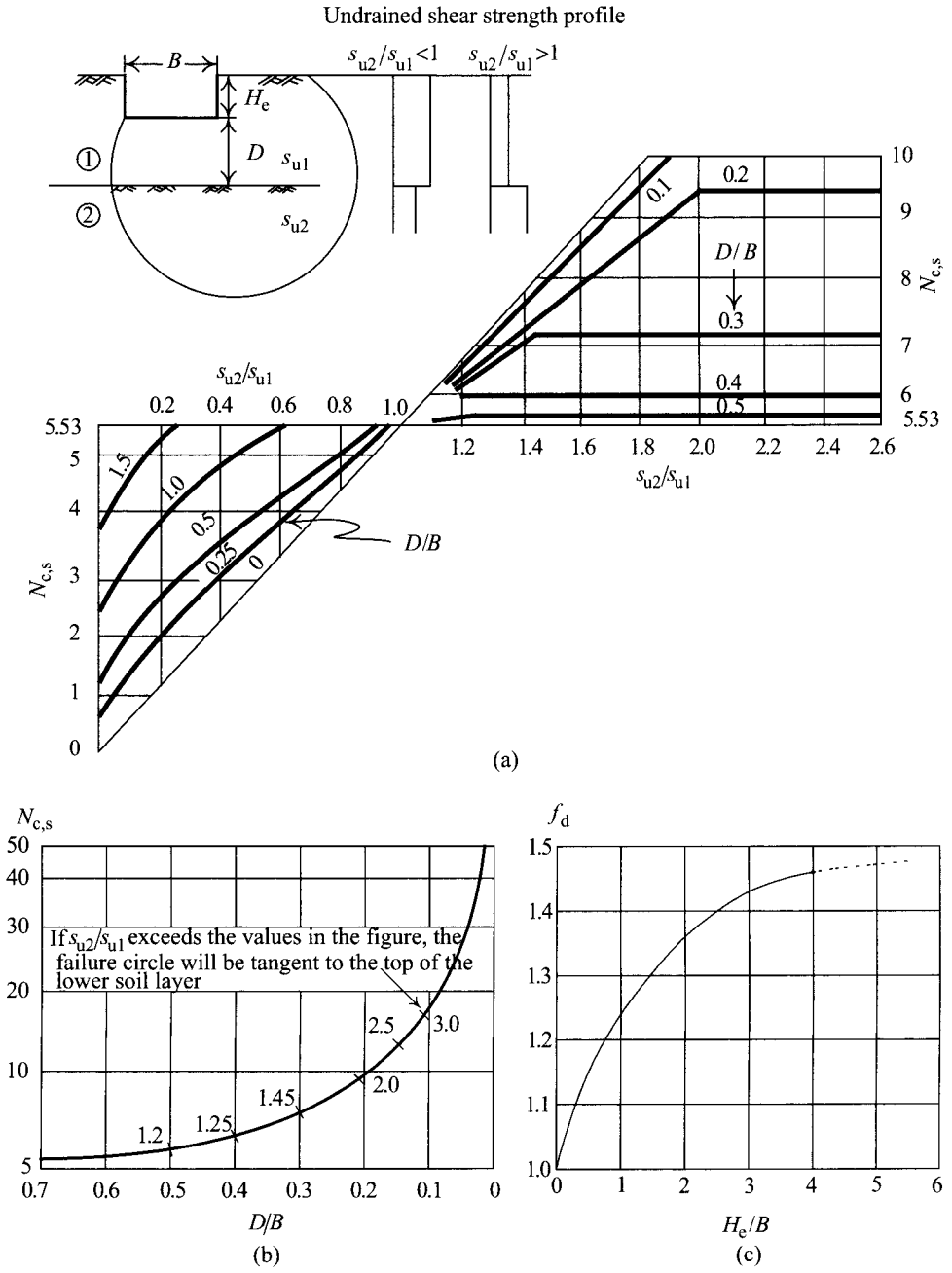

Figure 5.18 Extended Bjerrum and Eide's method: (a) $N_{c,s}$ for failure circles passing two soil layers, (b) $N_{c,s}$ for failure circles tangent to the top of the lower soil layer, and (c) f_d modified by the width (NAVFAC DM7.2, 1982; Reddy and Srinivasan, 1967).

method. The center of the circle with the slip circle method can be set at the lowest level of strut, at the excavation surface, or not to be set at any specific position, for example, points A, B, O as shown in Figure 5.19. The slip circle method, without setting the center at a specific position, is to try out the circles for various positions and sizes and to find the corresponding factors of safety. The circle with the smallest factor of safety is the critical circle.

Theoretically, the critical circle has the smallest factor of safety though few adopt it for analysis, considering it causes a lot of complication in computation. According to the analysis results, the factor of safety corresponding to the failure circle whose center is set at the lowest level of strut (point O) is smaller than that at the excavation surface (point B) and is close to the factor of safety of the critical circle (Liu *et al.*, 1997). Thus, the circular arc failure surface whose center is set at the lowest level of strut is often adopted for analysis.

Suppose the failure surface of the basal heave failure is a combination of a circular arc which centers at the lowest level of strut and a vertical plane above the lowest level of struts, as shown in Figure 5.20a. Let the shear strength on the vertical failure plane (line **bc** in Figure 5.20a) be ignored, and take the retaining wall and soil below the lowest level of struts as well as above the circular arc as a free body, as shown in Figure 5.20b. If we regard the soil weight above the excavation surface in back of the retaining wall as the driving force and

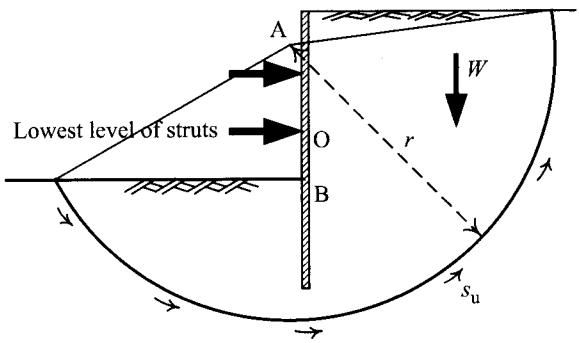

Figure 5.19 Location of the center of a failure circle for slip circle method.

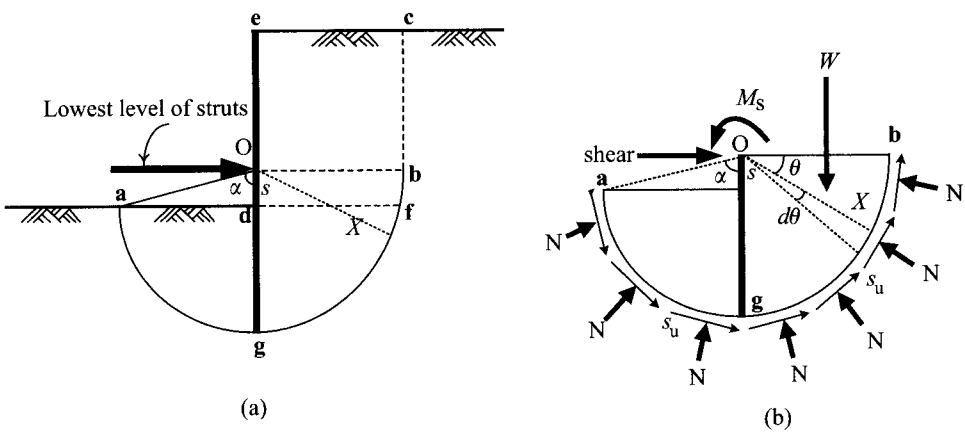

Figure 5.20 Analysis of basal heave by the slip circle method: (a) the failure surface and (b) forces acting on the free body.

the shear strength along the failure surface as the resistant force, the factor of safety against basal heave, the ratio of the resistant moment to the driving moment with regard to the point at the lowest level of strut will be:

$$F_b = \frac{M_r}{M_d} = \frac{X \int_0^{(\pi/2)+\alpha} s_u (X d\theta) + M_s}{W \cdot (X/2)} \tag{5.15}$$

where

M_r = resistant moment
M_d = driving moment
M_s = allowable bending moment of the retaining wall
s_u = undrained shear strength of clay
X = radius of the failure circle
W = total weight of the soil in front of the vertical failure plane and above the excavation surface, including the surcharge on the ground surface.

Equation 5.15 is a commonly used slip circle method. The original source of the slip circle method is untraceable. Nevertheless, TGS (2001) and JSA (1988) adopted the method in their building codes. Both assume that $M_s = 0$ and recommend that the factor of safety against basal heave (F_b) should be greater than or equal to 1.2. According to design experience in some countries, the value is quite reasonable. In fact, the allowable bending moment value of the retaining wall M_s is far less than the resistance created by shear strength. Thus, to simplify computation, it is reasonable to assume that $M_s = 0$.

Figures 5.12 and 5.13 also illustrate separately the changing tendencies of the factor of safety against basal heave with the size of the trial failure surface for s_u = constant or s_u/σ_v' = constant, following the slip circle method. We can see from the figures that, as far as soils with s_u = constant are concerned, the factor of safety against basal heave increases with the increase of the radius of the trial failure circle (i.e. X increases). When the radius of the trial failure circle is greater than the excavation depth, the factor of safety against basal heave slightly increases with the increase of X. The factor of safety against basal heave with s_u/σ_v' = constant increases noticeably with the increase of the radius of the trial failure circle.

As Figure 5.21 shows, when the radius of the trial failure circle exceeds the excavation width, the factor of safety should increase significantly for both s_u = constant and s_u/σ_v' = constant.

In analysis, we should try out different radii of circles and find the one with the smallest factor of safety as the critical circle, which represents the factor of safety against basal heave. In fact, a failure circle cannot pass through the embedded part of a retaining wall. Thus, for soils with constant strength or strength increasing with depth, the circle passing through the bottom of a retaining wall is the critical circle with the smallest factor of safety. Therefore, it is rational to let $X = s + H_p$, where s is the distance between the lowest level of strut and the excavation surface and H_p the penetration depth of a retaining wall. Eq. 5.15, therefore, can be used to compute the penetration depth of a retaining wall. Nevertheless, if there exist soft soils below the bottom of a retaining wall, the circle passing through the bottom of a retaining wall is not necessarily the critical failure circle, with the smallest factor of safety. Thus, we have to try out different values of X to find the failure circle with the smallest factor of safety, as shown in Figure 5.22.

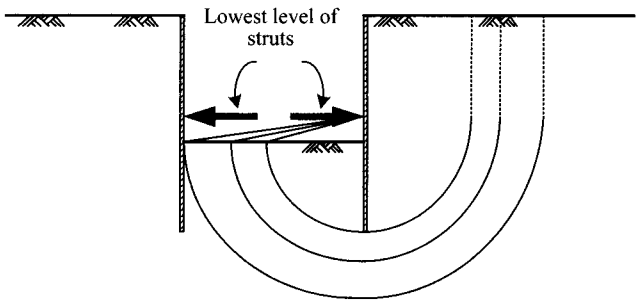

Figure 5.21 Factor of safety increasing when the failure circle exceeding the excavation width.

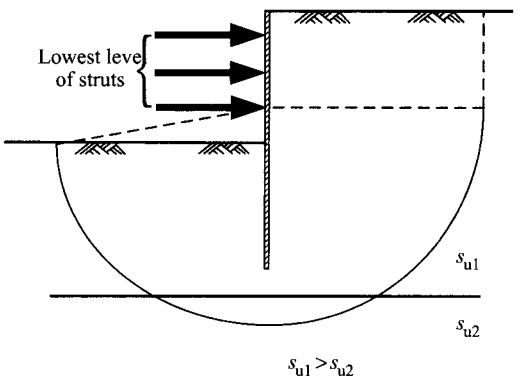

Figure 5.22 Analysis of basal heave in layered soft soils.

5.5.2.4 *Comparisons of the various analysis methods for basal heave failure*

The above section has introduced three methods to analyze a basal heave failure: the bearing capacity method/Terzaghi's method, the negative bearing method/Bjerrum and Eide's method, and the slip circle method. Terzaghi's method and Bjerrum and Eide's method are separate special cases of the bearing capacity method and the negative bearing capacity method, assuming the radius of the critical circle to be $B/\sqrt{2}$. The slip circle method, on the other hand, assumes many different failure circles and finds the one with the smallest factor of safety to be the critical failure circle. Both Figures 5.12 and 5.13 show the factor of safety with the slip circle method increases with the increase of the radius of the trial failure circle, as seems contrary to the tendencies with the bearing capacity method or the negative bearing capacity method. The main reason is that the slip circle method neglects the shear strength on the vertical failure plane whereas the other two methods do not. Figures 5.12 and 5.13 also provide the results of the slip circle method with the side shear strength considered. We can see from the figures that the changing tendencies of the factor of safety against basal heave failure using the modified slip circle method and those using the bearing capacity and the negative bearing capacity methods are similar, though the values are different. The reason

for the difference of the values is that the assumed shape of the failure surface with the slip circle method is different from those of the other two.

Seen from the changing tendencies of the factors of safety, the values derived from the negative bearing capacity method are more reasonable. When the radius of a trial failure circle is small, the factor of safety derived from the bearing capacity method is unreasonably high whereas that from the slip circle method is unreasonably low. Thus, Bjerrum and Eide's method is frequently used to analyze the factor of safety against basal heave in many European and American countries.

The changing tendencies of the factors of safety deduced from the slip circle method are opposite to the actual tendencies. Besides, the factor of safety is unreasonably low with a small radius of the trial failure circle. Nevertheless, the method is still useful for stability analysis of basal heave. The main reason is the consideration of being conservative. Since the induced factor of safety is unreasonably low when the radius of a trial failure circle (i.e. the penetration depth) is small, the penetration depth should be designed deeper and the radius of the trial failure circle will grow larger accordingly (because a failure circle does not pass through the retaining wall). When the penetration depth exceeds $0.8H_e$ (i.e. the radius of the trial failure circle exceeds $0.8H_e$), the factor of safety according to the slip circle method would approach a reasonable one. Actually, excavations in soft soils mostly have the penetration depth larger than $0.8H_e$.

In many Asian countries, the slip circle method is used to estimate the factor of safety against basal heave and a value larger than 1.2 is recommended. Many excavation case histories and design experiences have proved the limit well founded in terms of both safety and economy.

5.5.2.5 Applicability to sandy soils

We have explained that failure surfaces of bearing failures in clayey soils are circular arcs from the outset. Belonging to bearing failure, most of basal heave failure surfaces are circular arcs, too. We also explained that the methods introduced in this section are only applicable to clayey soils. In fact, the ultimate bearing failure in sandy soils is also a type of bearing failure. Therefore, it is reasonable to assume that similar methods can be applied to the "basal heave failure" mode for excavations in sandy soils. However, since $\phi \neq 0$ for sandy soils, the failure surface of bearing failures are log spirals rather than circular arcs. If $\phi \neq 0$, surface **bd** in Figure 5.14a would not be a circular arc and both Terzaghi's and Bjerrum and Eide's methods would render the solutions too complicated. Similarly, because surface **agf** in Figure 5.20 is not a circular arc, the direction of the action line of the reaction, N, unknown, would not pass through the center of the trial failure circle. The slip circle method would then be rendered difficult to apply.

Thus we know why the analysis of basal heave failure is only applicable to clayey soils. On the other hand, the bearing capacity of sandy soils is quite large, so that a bearing failure is unlikely to occur. Therefore, it is not necessary to examine the possibility of occurrence of basal heave failure for excavations in sandy soils.

5.5.3 Case study of overall shear failure

The excavation case was located in Taipei. The width of the excavation was 17.6 m; the length was 100.1 m; the depth was 13.45 m. The excavation adopted a 70 cm thick, 24 m deep diaphragm wall as the retaining wall. There were four levels of struts and the excavation

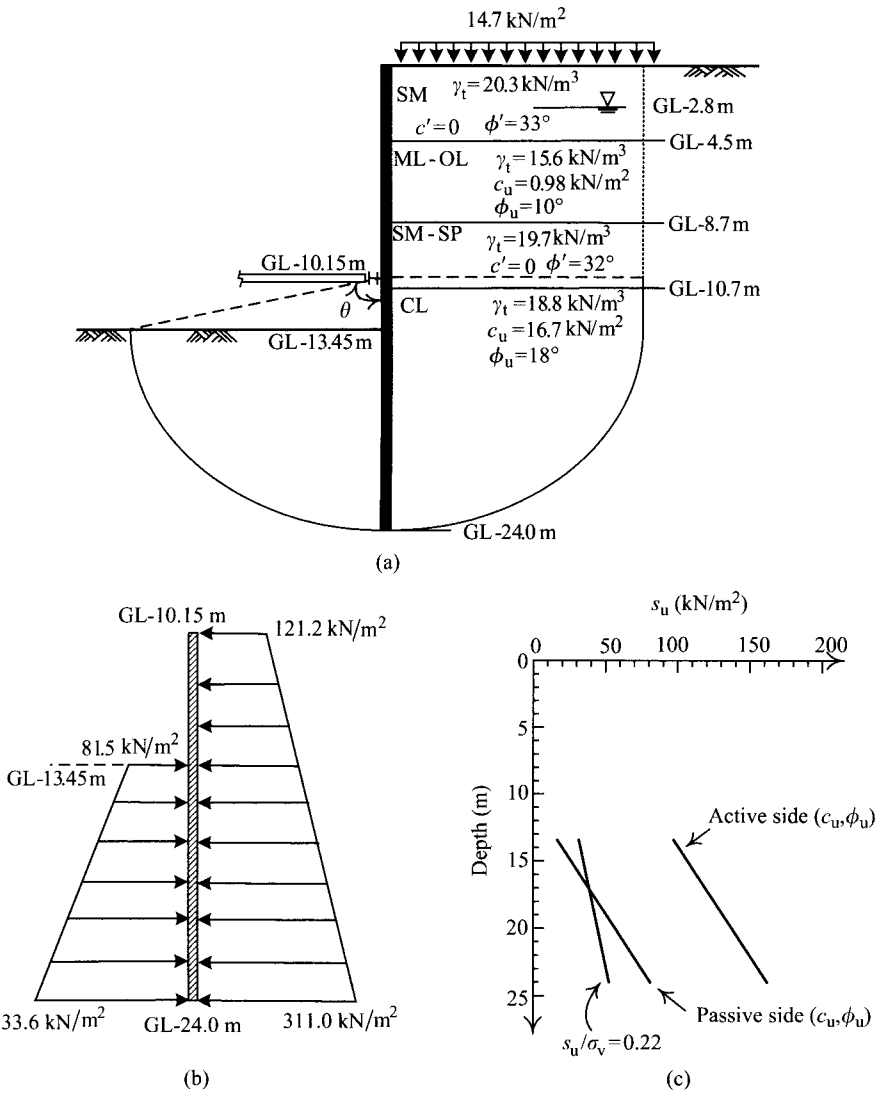

Figure 5.23 Stability analysis of an excavation case history: (a) excavation and geological profiles, (b) distribution of earth pressure for the push-in analysis, and (c) the undrained shear strength used in the analysis.

was carried out in five stages. The excavation profile and the related soil test data are as illustrated in Figure 5.23a. The construction collapsed seriously one hour and a half after the completion of excavation and caused great damage to not only the construction site and the adjacent properties but also the roads, the culverts, and the public facilities such as the running water system.

c_u and ϕ_u in Figure 5.23a were the total stress strength parameters of the clayey soils, obtained from the triaxial CU test and adopted by the original designer, who assumed no

adhesion or friction exists between the retaining wall and the soil. According to Eq. 5.5, the designer then computed the factor of safety against push-in to be 1.5, and the factor of safety against basal heave would be 2.3 according to Eq. 5.15.

Based on the author's studies, the normalized undrained shear strength of the soil for the site was about $s_u/\sigma'_v = 0.22$.

To simplify the analyses and be conservative, we assume the soil below the lowest level of struts (GL-10.15 m) to be a clayey layer, the adhesion between the retaining wall and the soil $c_w = 2s_u/3$ and the normalized undrained shear strength $s_u/\sigma'_v = 0.22$. The active earth pressure and the passive earth pressure of the clayey soil on the diaphragm wall can be estimated following Eqs 4.16 and 4.18, respectively. Then we can find the total stress, the pore water pressure, the undrained shear strength and the active (or passive) earth pressure at each depth.

At the depth of GL-10.15 m

$$\sigma_v = 20.3 \times 4.5 + 15.6 \times 4.2 + 19.7 \times 1.45 = 185.5 \text{ kN/m}^2$$

$$u = (10.15 - 2.8) \times 9.81 = 72.1 \text{ kN/m}^2$$

$$\sigma'_v = \sigma_v - u = 113.3 \text{ kN/m}^2$$

$$s_u = 0.22\sigma'_v = 0.22 \times 113.3 = 24.9 \text{ kN/m}^2$$

$$\sigma_{h,a} = \sigma_v K_a - 2s_u\sqrt{K_a\left(1 + \frac{c_w}{s_u}\right)} = 185.5 - 2(24.9)\sqrt{1 + \frac{2}{3}} = 121.2 \text{ kN/m}^2$$

At the depth of GL-13.45 m

Before excavation—

$$\sigma_v = 185.5 + 19.7 \times 0.55 + 18.8 \times 2.75 = 248.0 \text{ kN/m}^2$$

$$u = (13.45 - 2.8) \times 9.81 = 104.5 \text{ kN/m}^2$$

$$\sigma'_v = \sigma_v - u = 143.5 \text{ kN/m}^2$$

$$s_u = 0.22\sigma'_v = 0.22 \times 143.5 = 31.6 \text{ kN/m}^2$$

After excavation was started, $\sigma_v = 0$ on the passive side, but s_u-value stayed unchanged. Thus,

$$\sigma_{h,p} = \sigma_v K_p + 2s_u\sqrt{K_p\left(1 + \frac{c_w}{s_u}\right)} = 0 + 2(31.6)\sqrt{1 + \frac{2}{3}} = 81.5 \text{ kN/m}^2$$

At the depth of GL-24.0 m

The active side—

$$\sigma_v = 248.0 + 18.8 \times 10.55 = 446.3 \text{ kN/m}^2$$

$$u = (24 - 2.8) \times 9.81 = 208.0 \text{ kN/m}^2$$

$$\sigma'_v = \sigma_v - u = 238.3 \text{ kN/m}^2$$

$$s_u = 0.22\sigma'_v = 0.22 \times 238.3 = 52.4 \text{ kN/m}^2$$

$$\sigma_{h,a} = \sigma_v K_a - 2s_u\sqrt{K_a\left(1 + \frac{c_w}{s_u}\right)} = 446.3 - 2(52.4)\sqrt{1 + \frac{2}{3}} = 311.0 \text{ kN/m}^2$$

The passive side—

s_u stayed constant after excavation was started,

$$\sigma_v = 18.8 \times (24.0 - 13.45) = 198.3 \text{ kN/m}^2$$

$$\sigma_{h,p} = \sigma_v K_p + 2s_u\sqrt{K_p\left(1 + \frac{c_w}{s_u}\right)} = 198.3 + 2(52.4)\sqrt{1 + \frac{2}{3}} = 333.6 \text{ kN/m}^2$$

Figure 5.23b shows the earth pressures on both sides of the retaining wall. According to Eq. 5.5, we obtain the factor of safety against push-in as

$$F_b = \frac{81.5 \times 10.55 \times ((10.55/2) + 3.3) + (333.6 - 81.5) \times 10.55 \times 0.5 \times (10.55 \times (2/3) + 3.3)}{121.2 \times 13.85 \times (13.85/2) + (311.0 - 121.2) \times 13.85 \times 0.5 \times 13.85 \times (2/3)}$$

$$= 0.89$$

Similarly, we can compute the factor of safety against basal heave according to Eq. 5.15. Assuming again the soil below the lowest level of struts is clay, the average value of the undrained shear strengths (the active side) of the soil between GL-10.15 m and GL-24.0 m would be

$$s_{u,a} = \frac{24.9 + 52.4}{2} = 38.7 \text{ kN/m}^2$$

The average value of the undrained shear strengths of the soil between GL-13.45 m and GL-24.0 m would be

$$s_{u,p} = \frac{31.6 + 52.4}{2} = 42.0 \text{ kN/m}^2$$

The radius of the failure circular arc would be

$$24 - 10.15 = 13.85 \text{ m}$$

The central angle of the failure circular arc on the active side would be

$$\theta = \frac{\pi}{2} = 1.57$$

The central angle of the failure circular arc on the passive side would be

$$\theta = \cos^{-1}\left(\frac{3.3}{13.85}\right) = 1.33$$

The factor of safety against circular arc failure would be

$$F_b = \frac{13.85 \times 1.33 \times 42.0 \times 13.85 + 13.85 \times 1.57 \times 38.7 \times 13.85}{\sigma_{v(\text{GL-13.45})} \times 13.85 \times (13.85/2)} = \frac{22370}{23786} = 0.94$$

Besides, with the width of the excavation $B = 17.6$ m, $B/\sqrt{2}$ was larger than the penetration depth (10.55 m). When computing the factor of safety against basal heave following Terzaghi's method, the assumed failure surface will pass below the bottom of the

retaining wall as shown in Figure 5.15b. Thus, the average undrained shear strength of soil within the range of the failure circle can be calculated as follows:
Of soil $13.45 + (B/\sqrt{2}) = 25.9$ m deep below the ground surface

$$\sigma_v = 248.0 + 18.8 \times (25.90 - 13.45) = 482.1 \text{ kN/m}^2$$

$$\sigma'_v = \sigma_v - u = 482.1 - (25.90 - 2.8) \times 9.81 = 255.5 \text{ kN/m}^2$$

$$s_u = 0.22\sigma'_v = 0.22 \times 255.5 = 56.2 \text{ kN/m}^2$$

The average undrained shear strength within the range of the failure circle would be

$$s_u = (31.6 + 56.2)/2 = 43.9 \text{ kN/m}^2$$

As computed earlier, the total stress outside the excavation zone at the depth equaling the excavation surface would be

$$\sigma_v = 248.0 \text{ kN/m}^2$$

To simplify the analysis and be conservative, we assume the soil above the excavation surface is clay and has soil shear strength expressed as $s_u/\sigma'_v = 0.22$. The average undrained shear strength of the soil outside the excavation zone and above the excavation surface would be

$$s_u = \frac{0.22\sigma'_{v(\text{GL-13.45})}}{2} = \frac{31.6}{2} = 15.8 \text{ kN/m}^2$$

The factor of safety according to Terzaghi's method would be

$$F_b = \frac{Q_u}{W - s_{u1}H_e} = \frac{5.7 \times 43.9 \times (17.6/\sqrt{2})}{248.0 \times (17.6/\sqrt{2}) - 15.8 \times 13.45} = \frac{3118}{2874} = 1.08$$

With $H_e/B = 0.76$, $L/B = 5.7$ given, we would have $N_c = 6.2$, according to Figure 5.17. Therefore, the factor of safety following Bjerrum and Eide's method would be

$$F_b = \frac{s_u N_c}{\gamma H_e + q_s} = \frac{43.9 \times 6.2}{248.0} = 1.10$$

The factor of safety for this case is, as above computed, always smaller than 1.0 or slightly larger than 1.0 no matter if it is computed by push-in failure analysis or basal heave failure analysis based on the slip circle method, Terzaghi's method, or Bjerrum and Eide's method. The above computation did not involve the surcharge on ground surface 14.7 kN/m^2 (please refer to Figure 5.23a) yet. If it is considered, the factor of safety will be even smaller. We can thus see why the excavation failed.

The relation between the undrained shear strength of soil below the excavation surface and the depth, as above computed, is shown in Figure 5.23b. Assuming the failure surface to be horizontal and the undrained shear strength of soil below the lowest level of strut calculated following the equation $\tau = c_u + \sigma_v \tan \phi_u$ and total strength parameters c_u, ϕ_u, we may also compute the variation of the undrained shear strength with the depth. Figure 5.23b shows the comparison of the undrained shear strengths from $s_u/\sigma'_v = 0.22$ and those from total strength parameters c_u, ϕ_u. We can see from the figure that the total stress strength parameters (c_u and ϕ_u) would slightly overestimate the undrained shear strengths of the soil on the passive side but significantly overestimate those on the active side, which would lead to underestimation

of the penetration depth of the diaphragm wall. Therefore, the factors of safety against push-in and basal heave, as originally computed for design, are separately 1.5 and 2.3. Besides, it is necessary to assume the angle of the failure surface, which is in this case temporarily presupposed as horizontal, if analyzed on the basis of the total stress. In fact, it is s_u and $\phi = 0$ rather than c_u and ϕ_u that should be adopted as the strength parameters for clay in analysis according to the discussion in Section 2.8, Chapter 2.

EXAMPLE 5.1

Assume a 9.0 m deep excavation in a sandy ground and the lowest level of struts is 2.5 m above the excavation surface. The level of groundwater outside the excavation zone is ground surface high while that within the excavation zone is as high as the excavation surface. The unit weight of saturated sandy soils $\gamma_{sat} = 20\ kN/m^2$, the effective cohesion $c' = 0$, and the effective angle of friction $\phi' = 30°$. Because of the difference between the levels of groundwater, seepage will occur. Assume that the friction angles (δ) between the retaining wall and soil on both the active and passive sides are $0.5\phi'$ and the factor of safety against push-in, $F_p = 1.5$. Compute the required penetration depth (H_e).

SOLUTION

Let z represent the depth from the ground surface and x the depth from the groundwater level (see Figure 4.21)

1 Determine the coefficient of the earth pressure:
Compute both the active and passive earth pressures following Caquot-Kerisel' s earth pressure theory. When $\delta = 0.5\phi'$, the coefficients of active and passive earth pressure can be found from Figures 4.9 and 4.10 to be 0.3 and 4.6 separately. Thus, the coefficients of the horizontal active and passive earth pressure would be

$$K_{a,h} = 0.3\cos\delta = 0.3\cos 0.5\phi' = 0.29$$

$$K_{p,h} = 4.6\cos\delta == 4.6\cos 0.5\phi' = 4.4$$

2 Compute the effective active earth pressure on the wall:
At the lowest level of strut ($z = 6.5$ m, $x = 6.5$ m)—

$$\sigma'_{a,h} = \sigma'_v K_{a,h}$$

$$\sigma_v = 20 \times 6.5 = 130\ kN/m^2$$

According to Eq. 4.51, the porewater pressure at x away from upstream water level would be

$$u = \frac{2x(H_p - d_i)\gamma_w}{2H_p + H_e - d_i - d_j} = \frac{2 \times 6.5 \times H_p \times 9.81}{2H_p + 9} = \frac{63.77H_p}{H_p + 4.5}$$

$$\sigma'_{a,h} = (\sigma - u)K_{a,h} = \left(130 - \frac{63.77H_p}{H_p + 4.5}\right) \times 0.29 = 37.7 - \frac{18.49H_p}{H_p + 4.5}$$

At the bottom of the retaining wall ($z = 9 + H_p$, $x = 9 + H_p$)—

$$\sigma_v = 20 \times (9 + H_p) = 180 + 20H_p$$

$$u = \frac{2x(H_p - d_i)\gamma_w}{2H_p + H_e - d_i - d_j} = \frac{2 \times (9 + H_p) \times H_p \times 9.81}{2H_p + 9} = \frac{9.81H_p^2 + 88.29H_p}{H_p + 4.5}$$

$$\sigma'_{a,h} = \left(180 + 20H_p - \frac{9.81H_p^2 + 88.29H_p}{H_p + 4.5}\right) \times 0.29$$

$$= 52.2 + 5.8H_p - \frac{2.84H_p^2 + 25.60H_p}{H_p + 4.5}$$

3 Compute the lateral effective passive earth pressure on the wall:
At the bottom of the retaining wall—

$$\sigma_v = 20 \times H_p = 20H_p$$

$$u = \frac{9.81H_p^2 + 88.29H_p}{H_p + 4.5}$$

$$\sigma'_{p,h} = \left(20H_p - \frac{9.81H_p^2 + 88.29H_p}{H_p + 4.5}\right) \times 4.4 = 88H_p - \frac{43.16H_p^2 + 388.48H_p}{H_p + 4.5}$$

4 Compute the maximum net water pressure (at the excavation surface):
According to Eq. 4.53, the maximum net water pressure would be

$$u_b = \frac{2(H_e + d_i - d_j)(H_p - d_i)\gamma_w}{2H_p + H_e - d_i - d_j} = \frac{2 \times 9 \times H_p \times 9.81}{2H_p + 9} = \frac{88.29H_p}{H_p + 4.5}$$

5 The effective earth pressure on both sides of the wall and the distribution of the net water pressure are as shown in Figure 5.24.

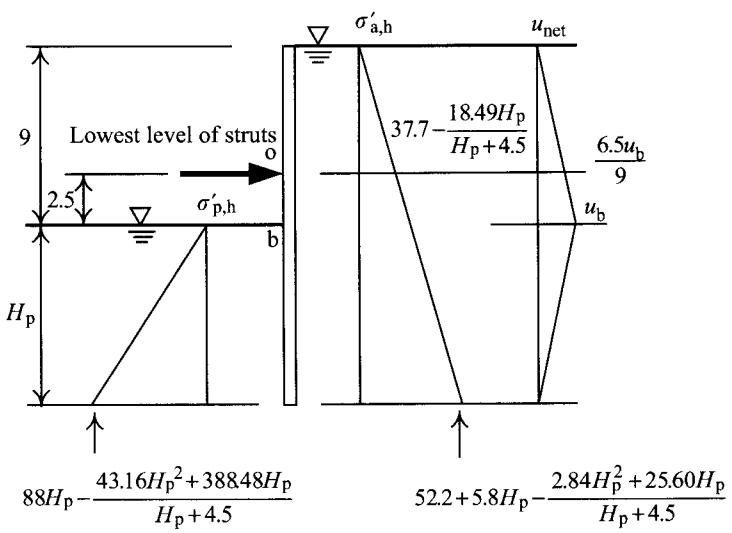

Figure 5.24 Distribution of lateral earth pressure.

6 Compute the driving moment (M_d) and the resistant moment (M_r) for the free body below the lowest level of struts

$$
\begin{aligned}
M_d &= P_{a,h} L_a \\
&= \left(37.7 - \frac{18.49H_p}{H_p + 4.5}\right) \times \frac{(H_p + 2.5)^2}{2} + \left(14.5 + 5.8H_p - \frac{2.84H_p^2 + 7.11H_p}{H_p + 4.5}\right) \\
&\quad \times \frac{2(H_p + 2.5)^2}{2 \times 3} + \frac{u_b H_p}{2} \times \left(2.5 + \frac{H_p}{3}\right) + \frac{6.5u_b}{9} \times \frac{2.5^2}{2} + \frac{2.5u_b}{9} \times \frac{2 \times 2.5^2}{2 \times 3} \\
&= \left(23.68 + 1.93H_p - \frac{0.95H_p^2 + 11.62H_p}{H_p + 4.5}\right)(H_p + 2.5)^2 \\
&\quad + (0.17H_p^2 + 1.25H_p + 2.84)u_b \\
M_r &= P_{p,h} L_p \\
&= \left(88H_p - \frac{43.16H_p^2 + 388.48H_p}{H_p + 4.5}\right) \times \frac{H_p}{2} \times \left(2.5 + \frac{2H_p}{3}\right) \\
&= \left(44H_p^2 - \frac{21.58H_p^3 + 194.24H_p^2}{H_p + 4.5}\right)\left(2.5 + \frac{2H_p}{3}\right)
\end{aligned}
$$

7 Determine the penetration depth (H_p)

$$F_b = \frac{M_r}{M_d} = 1.5$$

Then we have $H_p = 7.25$ m

EXAMPLE 5.2

An excavation in clay goes 9.0 m into the ground ($H_e = 9.0$ m). The groundwater outside the excavation zone is at the ground surface level while that within the excavation zone is at the level of the excavation surface. $\gamma_{sat} = 17.0$ kN/m^3. The undrained shear strength $s_u = 45$ kN/m^2. Suppose the excavation width $B = 10$ m and the excavation length $L = 30$ m. Compute the factor of safety against basal heave according to Terzaghi's method and Bjerrum and Eide's method, respectively.

SOLUTION

In this example, the surcharge $q_s = 0$

According to Terzaghi's method,

$$F_b = \frac{1}{H_e} \cdot \frac{5.7s_u}{\gamma - (s_u/0.7B)} = \frac{1}{9}\left[\frac{5.7 \times 45}{17 - 45/(0.7 \times 10)}\right] = 2.7$$

According to Bjerrum and Eide's method,

$$\frac{L}{B} = \frac{30}{10} = 3.0$$

$$\frac{H_e}{B} = \frac{9}{10} = 0.9$$

According to Figure 5.17, we have $N_c = 7.1$

$$F_b = \frac{s_u N_c}{\gamma_t H_e} = \frac{45 \times 7.1}{17 \times 9} = 2.09$$

EXAMPLE 5.3
Same as Example 5.2 except assume there exists a stiff clayey layer 3.0 m below the excavation surface and the undrained shear strength of the clay is 90 kN / m^2. Compute the factor of safety against basal heave according to Terzaghi's method and Bjerrum and Eide's method, respectively.

SOLUTION
According to Terzaghi's method,

$$F_b = \frac{1}{H_e} \cdot \frac{5.7 s_u}{\gamma - (s_u/D)} = \frac{1}{9}\left[\frac{5.7 \times 45}{17 - (45/3.0)}\right] = 14.25$$

According to Extended Bjerrum and Eide's method,

$$\frac{s_{u2}}{s_{u1}} = \frac{90}{45} = 2.0$$

$$\frac{D}{B} = \frac{3}{10} = 0.3$$

$$\frac{D}{H_e} = \frac{3}{9} = 0.33$$

According to the above three equations, consult Figures 5.18a or 5.18b and we have $N_{c,s} = 7.15$

$$\frac{H_e}{B} = \frac{9}{10} = 0.9$$

According to the above equation, consult Figure 5.18c and we have $f_d = 1.22$

$$\frac{B}{L} = \frac{10}{30} = 0.3$$

According to Eq. 5.14, we have $f_s = 1.06$. Thus,

$$F_b = \frac{s_{u1} N_{c,s} f_d f_s}{\gamma H_e} = \frac{45 \times 7.15 \times 1.22 \times 1.06}{17 \times 9} = 2.72$$

5.6 Overall shear failure of cantilever walls

Theoretically speaking, the overall shear failure analysis of a cantilever wall should include analyses of push-in failure and basal heave failure. However, the stability of the cantilever wall is rather weak and its application is usually confined to sand, gravelly soils or stiff clays.

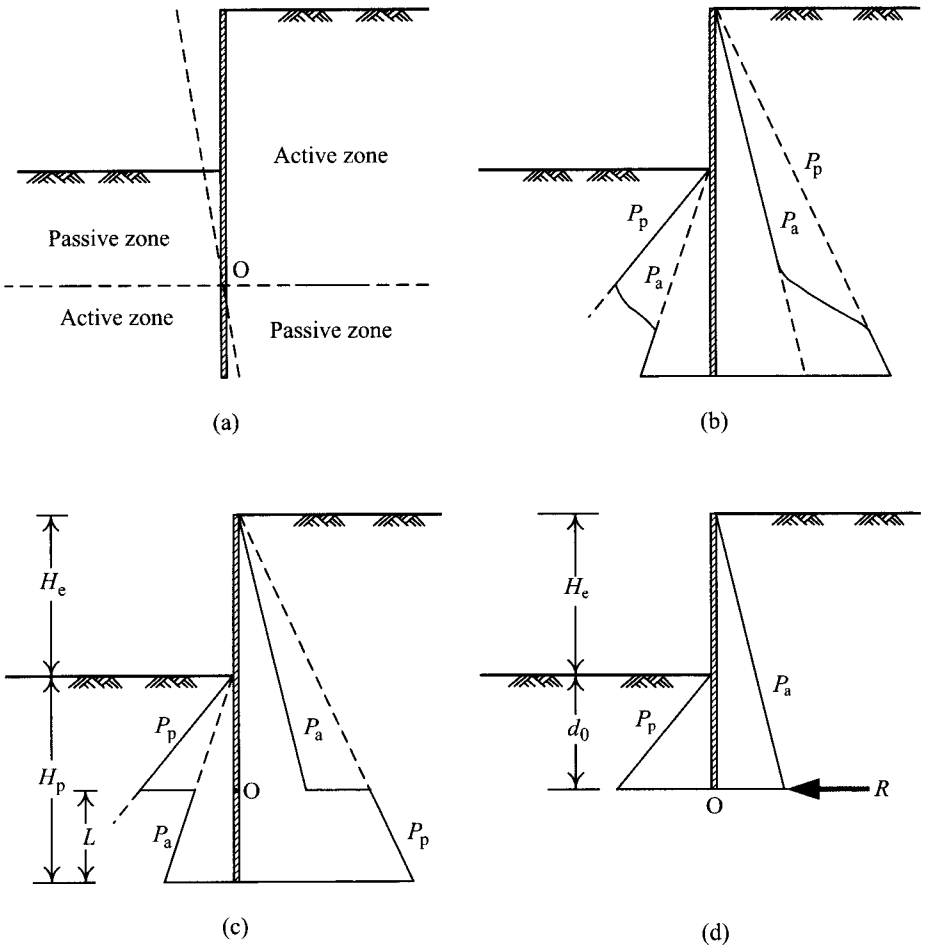

Figure 5.25 Analysis of a cantilever wall by gross pressure method: (a) deformation of the retaining wall, (b) real distribution of lateral earth pressure, (c) idealized distribution of lateral earth pressure, and (d) simplified analysis method.

On soft clay, the cantilever wall is not reliable enough to be adopted. Since no basal heave failure is found happening in sandy gravel soils or stiff clays, as far as the cantilever wall is concerned, only analysis of push-in failure is required.

The stability of a cantilever wall counts on the soil reaction at a specific fixed point. The design is therefore confined to the fixed earth support method and the free earth support method is inapplicable. Figure 5.25a illustrates a cantilever wall rotating about point O in a limiting state. Figure 5.25b shows the earth pressure on the retaining wall. For the simplification of analysis, assume the active and passive earth pressures above and below point O are fully mobilized and therefore the earth pressure distribution is discontinuous around point O as shown in Figure 5.25c.

See the earth pressure distribution as shown in Figure 5.25c, H_p and L are unknown. With the horizontal force equilibrium and the moment equilibrium, we would obtain the required penetration depth. Since both the horizontal force equilibrium and the moment equilibrium will generate quadratic and cubic equations, it is not easy to solve the equations directly. The trial-and-error method is not less complicated to solve. It is necessary to simplify the analysis method for practical use.

Figure 5.25d illustrates the simplified earth pressure distribution where the concentration force, R, represents the difference between the passive earth pressure from outside the excavation zone and the active earth pressure from inside the excavation zone below the turning point O. It is necessary that R exists to keep the horizontal force equilibrium. Based on the moment equilibrium against point O, we can find the value d_0. Because of the simplification of the analysis, d_0 should be slightly smaller than the actually required penetration depth and has to be increased properly (generally, 20%). The increment has to be examined to make R satisfy the horizontal force equilibrium as shown in Figure 5.25d. The detailed computing process can be found in Example 5.4. The simplified analysis method as shown in Figure 5.25d has been commonly adopted in engineering design (Padfield and Mair, 1984).

Excavation in a sandy ground with groundwater on both sides of the retaining wall should be analyzed in terms of the distribution of net water pressure as discussed in Section 5.5.1, viewed as the driving force, following the method shown in Figure 5.25d. In clayey soils, even though groundwater there exists, water pressure is not to be considered since the undrained analyses have had the water pressure considered automatically.

To compute the penetration depth following the gross earth pressure method, the load factor method is usually adopted to estimate the factor of safety. Sometimes the strength factor or the dimension factor methods are used. The strengths and shortcomings of these methods are as discussed in Section 5.2.

Figure 5.26 shows the net earth pressure distribution. According to the characteristics of the deformation of the cantilever wall, we can see the earth pressures at point **b** (excavation surface) on the front and back of the retaining wall should achieve the passive earth and the active earth pressures, respectively. The net value of the earth pressure at the point is CD (Figure 5.26b). Point **c** is close to point **b** and the earth pressures on the front and back of the wall should also achieve the passive and active earth pressures separately. Thus, the net earth pressure at point **c** should be

$$\sigma_{h,c} = [\gamma H_e + \gamma(z - H_e)]K_a - \gamma(z - H_e)K_p = \gamma H_e K_a - \gamma(z - H_e)(K_p - K_a) \tag{5.16}$$

where

γ = unit weight of the soil
K_a = coefficient of the active earth pressure
K_p = coefficient of the passive earth pressure.

We can see from the above equation that the slope of line CF is $1{:}\gamma(K_p - K_a)$ (the vertical: the horizontal). The net earth pressure with the slope $1{:}\gamma(K_p - K_a)$ maintains till point **d**, where the passive and active earth pressures "begin" not to be fully mobilized. Assuming the lateral movement of the bottom of the wall is large enough, the soil in front and back of the wall will reach the active and passive states, respectively, the net value of the earth pressure here is BG. The soil strength between points **f** and **d** in front and in back of the wall may not be fully mobilized and to simplify the analysis, we assume the net earth pressures

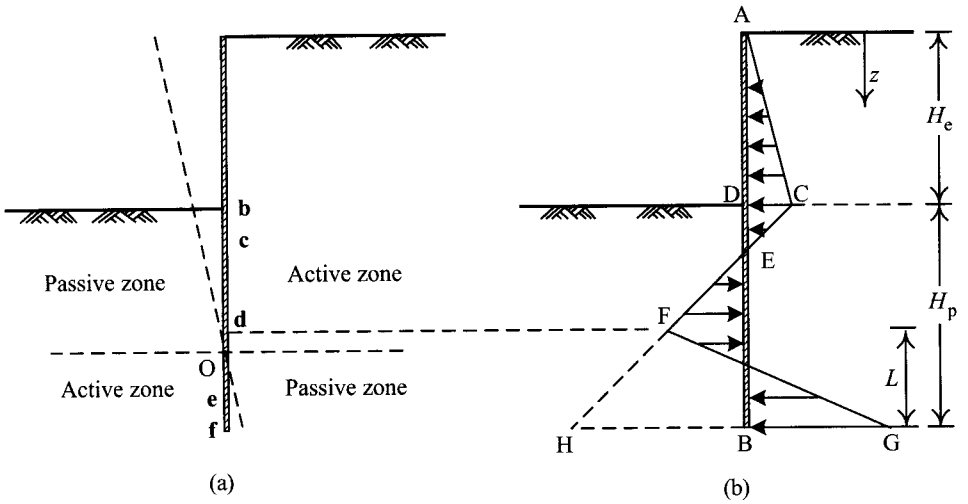

Figure 5.26 Analysis of a cantilever wall by net pressure method: (a) deformation of the wall and (b) distribution of net earth pressure.

between points **d** and **f** are of a linear relation, as line FG. Figure 5.26b shows an assumed net earth pressure distribution. According to the relation of the horizontal force equilibrium in Figure 5.26b, we know

$$\text{Area ACE} - \text{Area EFHB} + \text{Area FHBG} = 0.$$

We can find L according to the above equation. Substitute L in the moment equilibrium equation with regard to point **f** and we have the quadratic equation with H_p as a single unknown variable. To solve H_p, the trial-and-error method is recommended. When performing trial and error, we usually begin from $H_p = 075H_e$. As for the detailed calculation, please refer to Example 5.5.

The earth pressure distribution of a cantilever wall in sand is similar to that in Figure 5.26b. As for one in clay, refer to Figure 5.27. The computation of the penetration depth is as just discussed.

Though in Section 5.5.1 we have mentioned that the net pressure method is not applicable to the stability analysis of strutted walls, the net pressure method just introduced, however, is not the real net pressure method as introduced in Section 5.5.1. Therefore, no unreasonable penetration depth has been found by using the method introduced. The "net pressure method" introduced, therefore, is still applicable to the analysis of the penetration depth of cantilever walls. Both Das (1995) and Bowles (1988) adopt the net pressure method and the dimension factor method to estimate the penetration depth of a cantilever wall.

EXAMPLE 5.4

Figure 5.28 shows a 4.0 m deep excavation with a cantilever wall. The groundwater level is very deep. The unit weight of soil is $\gamma = 20\ \text{kN/m}^3$. The effective strength parameters are $c' = 0$ and $\phi' = 25°$. Adopt the simplified gross pressure method to compute the penetration depth instead.

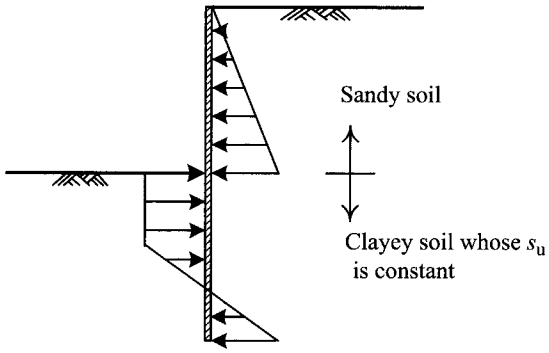

Figure 5.27 Distribution of net earth pressure for a cantilever wall in clay.

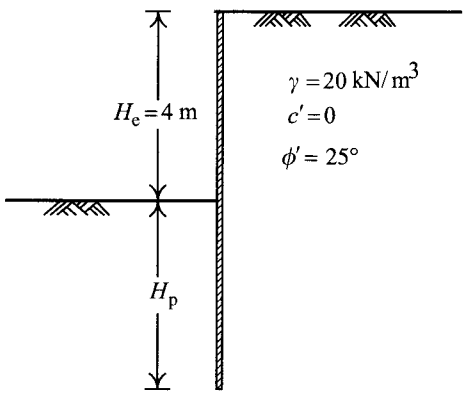

Figure 5.28 Excavation of a cantilever wall.

SOLUTION

Suppose that the friction angles between the retaining wall and soil on the active and passive sides are respectively, $\delta = 2\phi'/3$ and $\delta = \phi'/2$. According to Caquot-Kerisel's earth pressure theory (consult Figures 4.9 and 4.10), we have the coefficients of the active and passive earth pressure as 0.37 and 3.55, respectively. Thus, the coefficient of the horizontal active earth pressure $K_{a,h} = 0.37\cos(2\phi'/3) = 0.36$ and the coefficient of the horizontal passive earth pressure $K_{p,h} = 3.55\cos(\phi'/2) = 3.47$. According to the earth pressure distribution and its explanation in Figure 5.25, the gross pressure distribution on the wall is as shown in Figure 5.29, where P_{fa} and P_{fp} are the resultants of the active and passive earth pressures, respectively. Their values and arms are separately

$$P_{fa} = \frac{1}{2} \cdot K_{a,h} \cdot \gamma \cdot (H_e + d_0)^2$$

$$P_{fp} = \frac{1}{2} \cdot K_{p,h} \cdot \gamma \cdot d_0^2$$

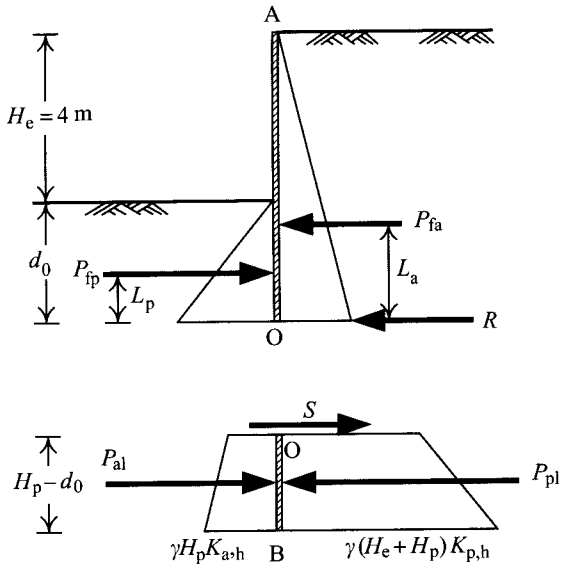

Figure 5.29 Simplified gross pressure analysis method.

$$L_a = \frac{1}{3} \cdot (H_e + d_0)$$

$$L_p = \frac{1}{3} \cdot d_0$$

Assuming the factor of safety to be 1.5, take the moment with regard to point O. Then we have

$$F_p = \frac{M_r}{M_d} = \frac{P_{fp} \cdot L_p}{P_{fa} \cdot L_a} = 1.5$$

Thus,

$$d_0 = 4.7 \text{ m}$$

Considering the inaccuracy due to simplification, the required penetration depth for design should be 1.2 times as large as d_0. Therefore,

$$H_p = 1.2d_0 = 5.6 \text{ m}$$

According to Figure 5.29, compute the shear force, S, below point O of the retaining wall

$$S = K_{p,h}\gamma \left[\frac{(d_0 + H_e) + (1.2d_0 + H_e)}{2} \right] (1.2 - 1)d_0 - K_{a,h}\gamma \frac{d_0}{2}(1 + 1.2)(1 - 1.2)d_0$$

$$= 563.2 \text{ kN}$$

As shown in Figure 5.29, the shear force, R, to maintain the equilibrium of the retaining wall above point O is

$$R = P_{fp} - P_{fa}$$

$$R = \frac{1}{2} \cdot K_{p,h} \cdot \gamma \cdot d_0^2 - \frac{1}{2} \cdot K_{a,h} \cdot \gamma \cdot (H_e + d_0)^2 = 494.0 \text{ kN}$$

With $S > R$, the penetration depth, 5.6 m, supports the assumption.

EXAMPLE 5.5

Same as Figure 5.28, compute the required penetration depth following the net pressure method instead.

SOLUTION

The coefficients of the horizontal active and passive earth pressures are still $K_{a,h} = 0.36$ and $K_{p,h} = 3.47$, respectively. According to the earth pressure distribution and the explanation in Figure 5.26, the net pressure distribution is as illustrated in Figure 5.30. First, we have to find the point at which the net pressure is none. As shown in the figure, the earth pressure at the depth of z from the ground surface would be

$$p_a = [\gamma H_e + \gamma(z - H_e)]K_{a,h} = 7.2z$$

$$p_p = \gamma(z - H_e)K_{p,h} = 69.4z - 277.6$$

The point where the net pressure is none (point C) can be found as follows:

$$p = p_a - p_p = [\gamma H_e + \gamma(z - H_e)]K_{a,h} - \gamma(z - H_e)K_{p,h} = 0$$

After reduction, we have

$$-62.2z + 277.6 = 0$$

$$z = 4.46 \text{ m}$$

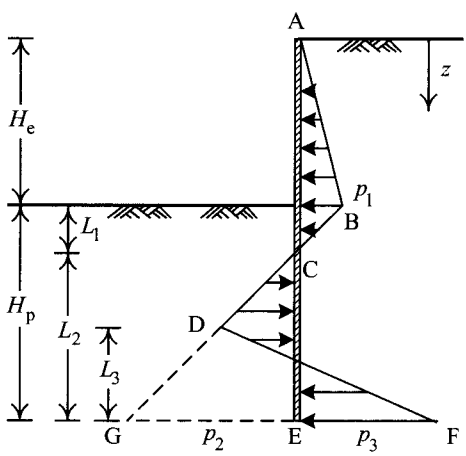

Figure 5.30 Distribution of net earth pressure.

$$L_1 = z - H_e = 0.46 \text{ m}$$

$$p_1 = \gamma H_e K_{a,h} = 28.8 \text{ kN/m}^2$$

As discussed in Section 5.6, the slope of line BD is $1{:}\gamma(K_p - K_a)$ (the vertical: the horizontal). Thus,

$$p_2 = L_2(K_{p,h} - K_{a,h})\gamma = 62.2L_2$$

$$p_3 = \gamma H_e K_{p,h} + (K_{p,h} - K_{a,h})\gamma(L_1 + L_2) = 306.2 + 62.2L_2$$

The area of ΔABC would be

$$P_f = \frac{1}{2}(H_e + L_1)p_1 = \frac{1}{2}\gamma H_e K_{a,h}(H_e + L_1) = 64.2 \text{ kN/m}$$

The earth pressure on the retaining wall should satisfy the horizontal force equilibrium. Therefore, we have the area of ΔABC−the area of ΔGEC+ the area of ΔDGF=0

$$P_f - \frac{1}{2}p_2L_2 + \frac{1}{2}L_3(p_2 + p_3) = 64.2 - 31.1L_2^2 + \frac{1}{2}L_3(124.4L_2 + 306.2) = 0$$

After reduction, we have

$$L_3 = \frac{62.2L_2^2 - 128.4}{124.4L_2 + 306.2}$$

The point of action ($\bar{z}$) (the distance from point C) of the resultant (P_f, the area of ΔABC) would be

$$\bar{z} = \frac{\frac{1}{2}p_1H_e(L_1 + (H_e/3)) + \frac{1}{2}p_1L_1\frac{2L_1}{3}}{P_f}$$

$$\bar{z} = 1.64 \text{ m}$$

Since $\sum M_E = 0$, we have

$$P_f(L_2 + \bar{z}) - \left(\frac{1}{2}p_2L_2\right)\frac{L_2}{3} + \frac{1}{2}L_3(p_2 + p_3)\frac{L_3}{3} = 0$$

After reduction, we have

$$L_2 = 3.38 \text{ m}$$

$$H_p = L_2 + L_1 = 3.38 + 0.46 = 3.84 \text{ m}$$

Because the calculation in this example does not follow the real net pressure method, it is not workable to adopt the factor of safety of the load factor method to compute the penetration depth as in the previous example. Instead, the factor of safety of the dimension factor method is used to compute the required penetration depth, which is

$$H_p = 1.5 \times 3.84 = 5.76 \text{ m}$$

As illustrated by the above two examples, the penetration depths computed with the simplified gross pressure method and the net pressure method are 5.6 and 5.76 m, respectively. The difference between the two is little. Therefore, the simplified gross pressure method is most commonly adopted.

5.7 Upheaval

If below the excavation surface there exists a permeable layer (such as sand or gravel soils) underlying an impermeable layer, the impermeable layer has a tendency to be lifted by the water pressure from the permeable layer. The safety, against upheaval, of the impermeable layer should be examined. As shown in Figure 5.31, the factor of safety against upheaval is

$$F_{up} = \frac{\sum_i \gamma_{ti} \cdot h_i}{H_w \cdot \gamma_w} \tag{5.17}$$

where

F_{up} = factor of safety against upheaval
γ_{ti} = unit weight of soil in each layer above the bottom of the impermeable layer
h_i = thickness of each soil layer above the bottom of the impermeable layer
H_w = head of the water pressure in the permeable layer
γ_w = unit weight of the groundwater.

The factor of safety against upheaval F_{up} should be larger than or equal to 1.2.

To safeguard the safety of excavation construction, the possibilities (of the occurrence) of upheaval at each stage of excavation should be analyzed. If drilling within the excavation zone is required (e.g. in order to place piezometers or build a well), the possible paths of water flow should be verified and the possible upheaval induced by drilling should be prevented to secure the excavation. Please see Section 5.8.2.

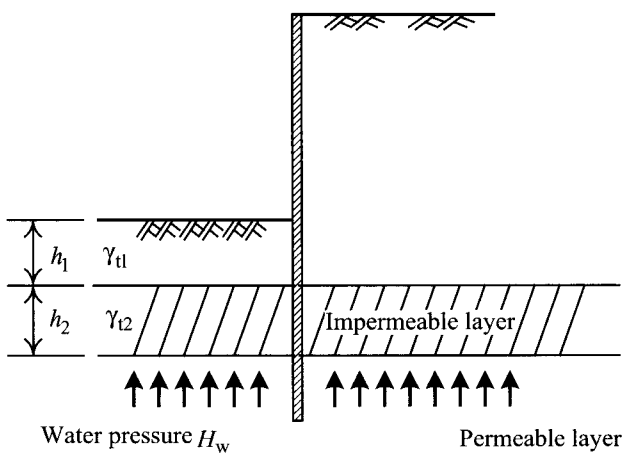

Figure 5.31 Analysis of upheaval.

5.8 Sand boiling

5.8.1 Mechanism and factors of safety

As shown in Figure 5.32, suppose there exists an upward water flow passing through a sandy layer. The total stress, σ, at the depth of z (point C) would be

$$\sigma = H_1\gamma_w + z\gamma_{sat} \tag{5.18}$$

where γ_{sat} = saturated unit weight of soil.

Water pressures at points A and B are separately $H_1\gamma_w$ and $(H_1 + H_2 + h)\gamma_w$. Suppose the water pressure between A and B distributes linearly. The water pressure at point C would be

$$u = \left(H_1 + z + \frac{h}{H_2}z\right)\gamma_w \tag{5.19}$$

The effective stress at point C would be

$$\sigma' = \sigma - u = (H_1\gamma_w + z\gamma_{sat}) - \left(H_1 + z + \frac{h}{H_2}z\right)\gamma_w$$

$$= z(\gamma_{sat} - \gamma_w) - \frac{hz}{H_2}\gamma_w = z\gamma' - \frac{hz}{H_2}\gamma_w \tag{5.20}$$

As shown in the above equation, the upward water flow may cause the effective stress at point C to be 0, which means that the soil is unable to bear any load, and the phenomenon is

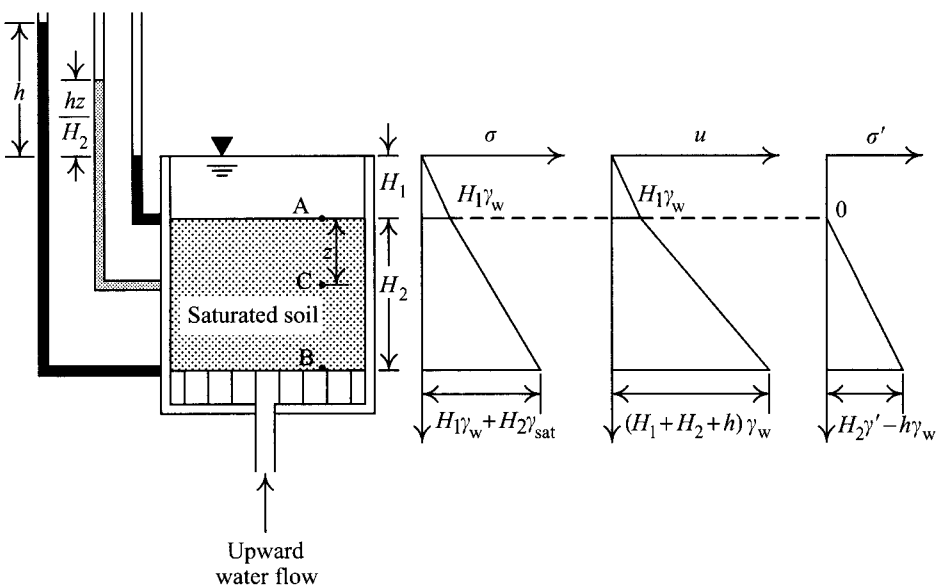

Figure 5.32 Total stresses, effective stresses, and change of porewater pressure in sandy soils acted on by an upward water flow.

called sand boiling. Thus,

$$\sigma' = 0 = z\gamma' - \frac{hz}{H_2}\gamma_w \tag{5.21}$$

$$\frac{h}{H_2} = \frac{\gamma'}{\gamma_w} \tag{5.22}$$

The hydraulic gradient when the effective stress equals 0 is called the critical hydraulic gradient, i_{cr}, which can be expressed as follows

$$i_{cr} = \frac{(h/H_2)z}{z} = \frac{h}{H_2} = \frac{\gamma'}{\gamma_w} \tag{5.23}$$

Besides, according to the phase relationship of soil, the submerged unit weight is

$$\gamma' = \left(\frac{G_s - 1}{1 + e}\right)\gamma_w \tag{5.24}$$

where G_s is the specific gravity and e is the void ratio. The critical hydraulic gradient is then

$$i_{cr} = \frac{G_s - 1}{1 + e} \tag{5.25}$$

Since the G_s-value of sand is about 2.65 and its e-value is between 0.57 and 0.95, the critical hydraulic gradient for most sands is close to 1.0 according to the above equation.

Figure 5.33 shows watertight sheet piles. When the exit gradient (point **A** in the figure) is close to the critical hydraulic gradient, sand boiling occurs. Harza (1935) defines the factor of safety against sand boiling as follows

$$F_s = \frac{i_{cr}}{i_{max(exit)}} \tag{5.26}$$

where $i_{max(exit)}$ is the maximum hydraulic gradient at the exit of seepage, which can be obtained with the flow net method.

Terzaghi (1922) found, according to many model tests with single rows of sheet piles, that the phenomenon of piping occurs within a distance of about $H_p/2$ from the sheet piles (H_p refers to the penetration depth of the sheet piles). Thus, to analyze the stability of single rows of sheet piles, we can take the soil column $H_p \times H_p/2$ in front of the sheet pile as an analytic object, as shown in Figure 5.33. The uplift force on the soil column would be

$$U = (\text{the volume of the soil column}) \times (i_{av}\gamma_w) = \tfrac{1}{2}H_p^2 i_{avg}\gamma_w \tag{5.27}$$

where i_{avg} is the average hydraulic gradient of the soil column. The downward force of the soil column (i.e. the submerged weight) is

$$W' = \frac{1}{2}H_p^2(\gamma_{sat} - \gamma_w) = \frac{1}{2}H_p^2\gamma' \tag{5.28}$$

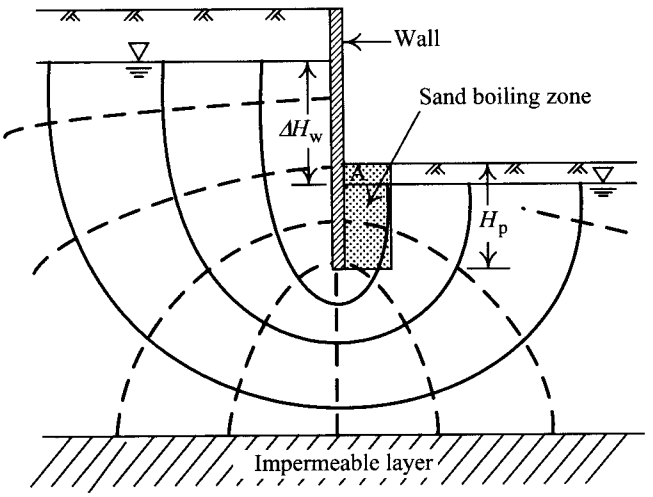

Figure 5.33 Seepage in soil below sheet piles.

Therefore, the factor of safety is

$$F_s = \frac{W'}{U} = \frac{\gamma'}{i_{avg}\gamma_w} \tag{5.29}$$

According to Eq. 5.29, provided the computed factor of safety is too small, we can consider placing filters at the exits of seepage. Assuming the weight of the filters is Q, the factor of safety will be

$$F_s = \frac{W' + Q}{U} \tag{5.30}$$

In general, the required F_s for the above equation should be greater than or equal to 1.5 (JSA, 1988; TGS, 2001).

As this equation shows, if sand boiling or piping occurs, in addition to evacuating the workers and equipment as soon as possible, the possible remedial measures include dewatering to reduce the water pressure and dumping permeable soils onto the excavation surface to increase the value of the numerator in the equation.

Marsland (1953) conducted a series of model tests to explore the phenomenon of piping in excavations in sand and obtained the results, which were later adopted by NAVFAC DM7.1 (1982), as shown in Figure 5.34. Figures 5.34a and 5.34b show the results with the impermeable layers located infinitely deeply and with the impermeable layer within a finite depth, respectively. NAVFAC DM 7.1 suggested that the reasonable factor of safety against piping in an excavation be around 1.5–2.0. We can see from the figure that as long as the allowable factor of safety (F_s), the excavation depth (H_e), and the distance of the excavation surface to the impermeable layer (D) are known, we can obtain the required penetration depth of the retaining wall (H_p) against piping.

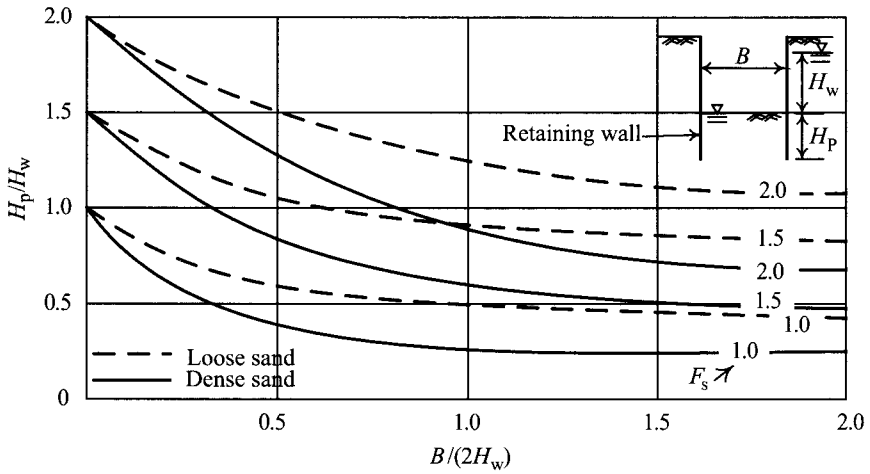

(a)

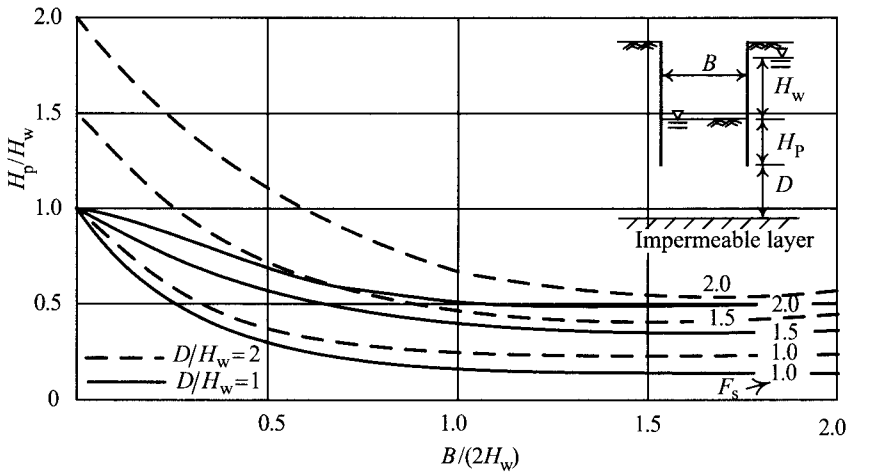

(b)

Figure 5.34 Relations between wall penetration depths and factors of safety against sand boiling: (a) dense and loose sands with the impermeable layer located at the infinite depth and (b) dense sand with the impermeable layer located at a finite depth (Marsland, 1953; NAVFAC DM7.1, 1982).

As shown in Figure 5.35, if we assume the datum is at the downstream level, the total head at the elevation of downstream (point **d**) will be

$$h_{t,d} = h_e + h_p = 0 + 0 = 0 \tag{5.31}$$

where h_e is the elevation head and h_p = pressure head.

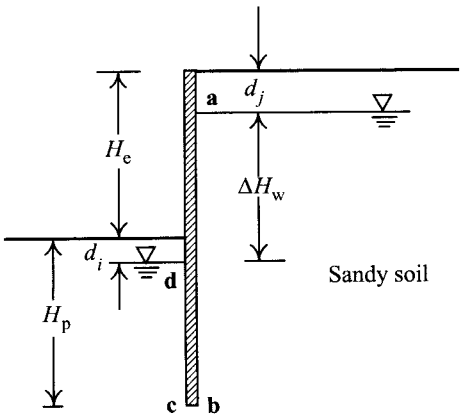

Figure 5.35 Analysis of sand boiling.

The total head at the upstream elevation (point **a**) will be

$$h_{t,a} = h_e + h_p = H_e + d_i - d_j + 0 = H_e + d_i - d_j \tag{5.32}$$

The difference of the total heads between upstream and downstream levels will be

$$\Delta H_w = h_{t,a} - h_{t,d} = H_e + d_i - d_j \tag{5.33}$$

Suppose the seepage is one dimensional and the hydraulic gradients for each depth along the flow path **abcd** are equal. The hydraulic gradient will be

$$i_{avg} = \frac{\Delta H_w}{H_e - d_j + d_i + 2(H_p - d_i)} = \frac{\Delta H_w}{H_e + 2H_p - d_i - d_j} \tag{5.34}$$

The factor of safety against boiling will be

$$F_s = \frac{i_{cr}}{i_{avg}} = \frac{\gamma'(H_e + 2H_p - d_i - d_j)}{\gamma_w \Delta H_w} \tag{5.35}$$

The required F_s for the above equation should be greater than or equal to 1.5.

We can see from the above discussion that the factor of safety against boiling can be estimated by Harza's method (Eq. 5.26), by Terzaghi's method (Eq. 5.29), by Marsland's method (Figure 5.34) or by the simplified one-dimensional seepage method (Eq. 5.35). The results of these methods don't come out the same. Since there are not many case histories regarding sand boiling, it is difficult to judge which method is better. The most reliable way is to try all of them and choose the conservative one.

For excavations, NAVFAC DM7.1 (1982) suggested that a reasonable factor of safety be around 1.5–2.0. If a rock fill dam or a great dam is at question, by which many people's lives may be endangered, Harr (1962), Kashef (1987), and Holtz and Kovacs (1981) all suggested the factor of safety be greater than $4.0 \sim 5.0$.

5.8.2 Case study

Figure 5.36a shows the excavation profile and the geological profile of the Sieman Station of the Taipei Rapid Transit System. The excavation was 23.25 m wide, 560 m long, and 24.5 m deep. The retaining-strut system was a diaphragm wall 100 cm thick and 44.0 m deep with eight levels of struts. As shown in the figure, 49.1 m down from the ground surface is a gravel layer known as the Chingmei formation. Above it are six alternated layers of sand and clay known as the Sungshan formation.

After the last stage of excavation, the foundation slabs partly cast and the rest laid with the steel reinforcements, the engineers found one of the piezometers placed in the retaining wall damaged and unable to take any measurement. According to the contract, a new one was to be placed. The contractor thus was going to place a new one in the excavation zone 6.2 m away from the west retaining wall as shown in Figure 5.36b. To install it, a drill machine was employed to drill from the excavation surface (elevation EL.+80 m). When drilling reached 20.5 m below the excavation surface (EL.+59.5 m), groundwater began springing out along the drill hole. At first, since there was not much water, the contractor put a 9.00 m long steel case onto the hole and stopped it as shown in Figure 5.36c.

About four hours later, the sump 5.00 m south of the drill hole, began springing sandy water in great amounts, as shown in Figure 5.36c. The contractor then placed sand bags and grouted around the water source. The situation, however, got worse. The roads outside the excavation zone began cracking and settling. In addition to grouting, the contractor also blocked the roads and refilled coarse soils into the excavation zone to stabilize the excavation. For the detailed process, please see the document (Chou and Ou, 1999).

As shown in Figure 5.36, the silty sand layer (Sungshan **I** formation) right above the Chingmei formation was a permeable layer, whose water pressure should be close to the water pressure of the Chingmei gravel formation, that is, EL.+88.0 m. At the beginning of drilling, the water level in the drilling hole was at most as high as the excavation surface (EL.+80.0 m). When drilling to EL.+59.5 m, though the drilling was working in the clayey layer (Sungshan **II** formation), either because the drilling had actually gone as far as the Sungshan **I** formation or the water pressure in the drilling hole was lower than that of the Sungshan**I** formation so that the water pressure from the Sungshan **I** formation broke through the last 0.1 m thick clayey layer, and water began flowing from the drilling hole.

The steel case placed onto the drilling hole caused the water level in the hole to go up by 8.00 m (to El.+88.0 m). Theoretically, the water pressure in the drilling hole should have been balanced with that in the Sungshan **I** formation or that in the Chingmei Gravel formation. However, due to the steel case not reaching the impermeable layer, with a 4.0 m deep sump just 5.0 m away from the drilling hole, the water in the hole took a short cut to the sump. The exit hydraulic gradient at the bottom of the sump thus became so large as to exceed the critical hydraulic gradient. Sand boiling from the bottom of the sump thus occurred.

Obviously, as these discussions have shown, when drilling within a construction zone that has been excavated, due to the overburden pressure decreasing, a builder has to be especially careful to prevent failures when there exists a permeable layer. Applying a steel case to obstruct the flow of the groundwater along the drilling hole has to take care of the occurrence of boiling. The methods to prevent such accidents are to lengthen the water path to lower the hydraulic gradient (e.g. by having the case go deeper) or to extend the steel case to reach an impermeable layer. The latter method has to consider the thickness of the impermeable layer to prevent upheaval.

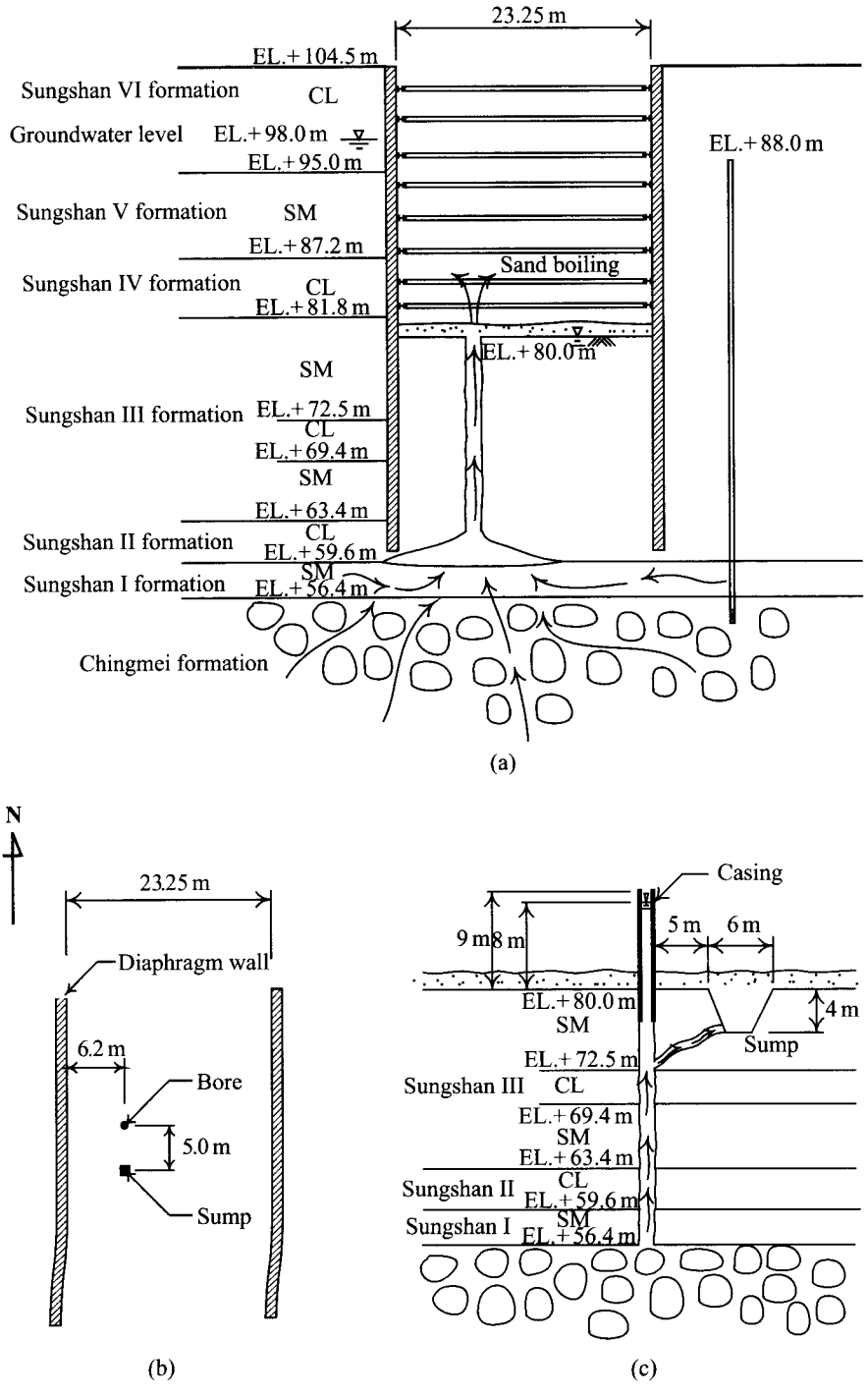

Figure 5.36 Excavation of Siemen Station of Taipei Rapid Transit System: (a) excavation and geological profiles, (b) plan view, and (c) process of sand boiling (Chou and Ou, 1999).

5.9 Summary and general comments

This chapter explores the stability analysis of retaining walls and the factors of safety against overall shear failure, sand boiling, and upheaval. A case history of the overall shear failure and another of boiling are studied in this chapter. Table 5.2 is a summary of the stability

Table 5.2 Stability analysis methods for strutted walls and the required minimum factors of safety

	Overall shear failure		*Sand boiling*	*Upheaval*
	Push-in	*Basal heave*		
Sand or gravel	Gross pressure method {Eq. 5.5, $F_p \geq 1.2$, assuming $M_s = 0$}[1]	—	Harza's method {Eq. 5.26, $F_s \geq 2.0$}[4] Terzaghi's method {Eq. 5.30, $F_s \geq 1.5$}[1,5] Marsland's method {Fig. 5.34, $F_s \geq 1.5 \sim 2.0$}[4] Simplified 1-D seepage method {Eq. 5.35, $F_s \geq 2.0$}[1,5]	—
Clay	Gross pressure method {Eq. 5.5, $F_p \geq 1.2$, assuming $M_s = 0$}[1]	Terzaghi's method {Eq. 5.9 or 5.10, $F_b \geq 1.5$}[1,2] Bjerrum and Eide's method {Eq. 5.12 or 5.13, $F_b \geq 1.2$}[4] Slip circle method {Eq. 5.15, $F_b \geq 1.2$}[1]	—	—
Alternated layers of sand (or gravel) and clay	Gross pressure method {Eq. 5.5, $F_p \geq 1.2$, assuming $M_s = 0$}[1]	Terzaghi's method {Eq. 5.9 or 5.10, $F_b \geq 1.5$}[1–3] Bjerrum and Eide's method {Eq. 5.12 or 5.13, $F_b \geq 1.2$}[4,3] Slip circle method {Eq. 5.15, $F_b \geq 1.2$}[1,3]	Short-term behaviors can be ignored while long-term behaviors may need consideration. The analysis methods are the same as those for sand and gravel	{Eq. 5.17, $F_{up} \geq 1.2$}[1]

Notes
1 The methods and factors of safety are suggested by TGS (2001) and JSA (1988).
2 The factor of safety is suggested by Mana and Clough (1981).
3 It is only when clay is the dominant soil layer that the analysis of basal heave is required.
4 The factor of safety is suggested by NAVFAC DM 7.1 (1982).
5 TGS (2001) and JSA (1988) suggest the conservative value obtained by Terzaghi's method or the simplified 1-D seepage method be adopted for design.

Table 5.3 Stability analysis methods for cantilevered walls and the required minimum factors of safety

	Overall shear failure	*Sand boiling*	*Upheaval*
Sand or gravel	Gross pressure method {Figure 5.25c, $F_p \geq 1.5$}[3] Simplified gross pressure method {Figure 5.25d, $F_p \geq 1.5$}[3] Net pressure method {Figure 5.26, $F_p \geq 1.5$}[2]	Harza's method {Eq. 5.26, $F_s \geq 2.0$}[2] Terzaghi's method {Eq. 5.30, $F_s \geq 1.5$}[1] Marsland's method {Figure 5.34, $F_s \geq 1.5$–2.0}[2] Simplified one-dimensional seepage method {Eq. 5.35 $F_s \geq 2.0$}[1]	—
Clay	Gross pressure method {Figure 5.25c, $F_p \geq 1.5$}[3] Simplified gross pressure method {Figure 5.25d, $F_p \geq 1.5$}[3] Net pressure method {Figure 5.26, $F_p \geq 1.5$}[2]	—	—
Alternated layers of sand (or gravel) and clay	Gross pressure method {Figure 5.25c, $F_p \geq 1.5$}[3] Simplified gross pressure method {Figure 5.25d, $F_p \geq 1.5$}[3] Net pressure method {Figure 5.26, $F_p \geq 1.5$}[2]	—	{Eq. 5.17, $F_{up} \geq 1.2$}[1]

Notes
1 The methods and factors of safety are suggested by TGS (2001) and JSA (1988). They also suggest using the conservative value obtained by Terzaghi's method or the simplified 1-D seepage method.
2 The factors of safety are suggested by NAVFAC DM7.1 (1982).
3 The methods and factors of safety are suggested by Padfield and Mair (1984).

analyses for strutted walls. Table 5.3 is a summary for cantilever walls. This chapter can be summarized as follows:

1 The computation of factors of safety for stability analyses can follow the dimension factor method, the strength factor method, or the load factor method. The first method is too empirically oriented, so that it cannot represent the real factor of safety and is therefore not recommended generally. If it must be adopted, other methods are required for cross checking. Both the strength factor method and the load factor method are reliable for the computation of factors of safety. The selection of a more reasonable method and factor of safety depends on engineering experience, learned from design experience and case histories, no matter if they are successful or not.
2 The free earth support method and the fixed earth support method are two commonly used methods for the design of retaining walls. Generally speaking, the design of a cantilever wall can only adopt the fixed earth support method while that of a strutted wall can adopt either of them. The fixed earth support method is too expensive to be

adopted for the design of strutted walls and the free support method can obtain reasonable results.

3 The overall shear failure of a retaining wall can be further classified into push-in failure and basal heave failure. Having different mechanisms, they should be analyzed by different methods. The methods to analyze the push-in failure are the gross pressure method and the net pressure method, the latter of which is less reasonable. As for the gross pressure method, though still partly unreasonable, the method is suitable for the analysis of excavation in soft clay or deep excavations. Analysis of sandy soils, with high groundwater levels, following the gross pressure method, should adopt the net water pressure distribution. The commonly used methods to analyze basal heave failure are the bearing capacity method /Terzaghi's method, the negative bearing capacity method/Bjerrum and Eide's method, and the slip circle method. Terzaghi's method is a special case of the bearing capacity method and Bjerrum and Eide's method is a special case of the negative bearing capacity method. The center of the failure circle for the slip circle method can be placed at the lowest level of the strut or at the excavation surface, the former of which is more commonly adopted. Though the three methods are different and assume different failure circles, they all can apply to the basal heave failure. The slip circle method has been used in many Asian countries.

4 To excavate in a sandy soil one should consider push-in and sand boiling. In clayey soils, push-in and basal heave. In alternated layers of sand (or gravel) and clay, push-in and upheaval. If the clayey layer is thick enough, basal heave is also to be considered. When analyzing basal heave, the soils below the excavation surface can be expediently assumed to be pure clay and an appropriate soil parameter should be adopted for analysis.

5 There exist many methods to estimate the factor of safety against sand boiling, each having different results. Since there are not many case histories regarding sand boiling, it is not easy to judge which method is more suitable or reasonable. The most workable way is to go through all of these methods and find the most conservative one for design. The penetration depth of a retaining wall is usually determined according to the results of stability analyses because sand boiling is normally not a main control factor.

Problems

5.1 As shown in Figure P5.1, no groundwater exists inside or outside the excavation zone. Assume the friction angle between the retaining wall and soil $\delta = 0$. Use the factor of safety FS $= 1.5$ to compute the required penetration depth following the dimension factor method.

5.2 Same as Problem 5.1. Assume the penetration depth as computed above. Compute the factor of safety following the load factor method. Compare the result with the factor of safety as given in Problem 5.1.

5.3 Same as Problem 5.1. Use the factor of safety FS $= 1.5$ to compute the required penetration depth following the strength factor method.

5.4 As shown in Figure P5.4, an excavation with the groundwater level outside the excavation zone at the ground surface and that inside at the excavation surface. If the friction angle between the retaining wall and soil $\delta = 0.5\phi'$, compute the required penetration depth against push-in.

5.5 Figure P5.5 shows an excavation. Compute the required penetration depth against basal heave with $F_b = 1.2$ as well as push-in with $F_p = 1.2$, considering c_w/s_u equal to 0.67.

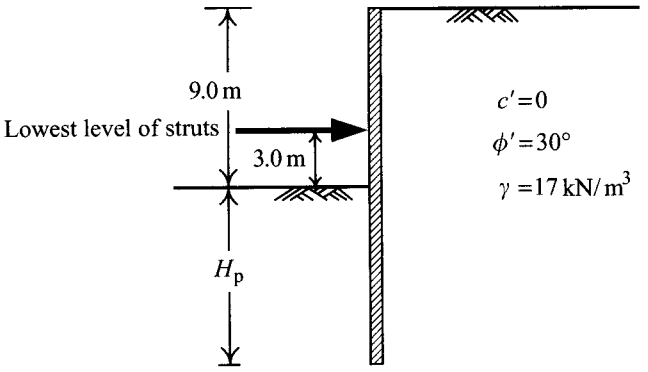

Figure P5.1

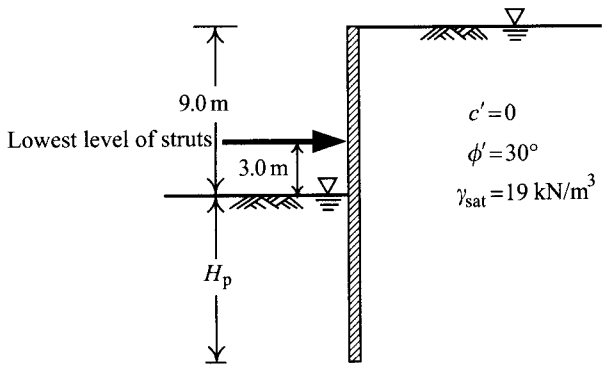

Figure P5.4

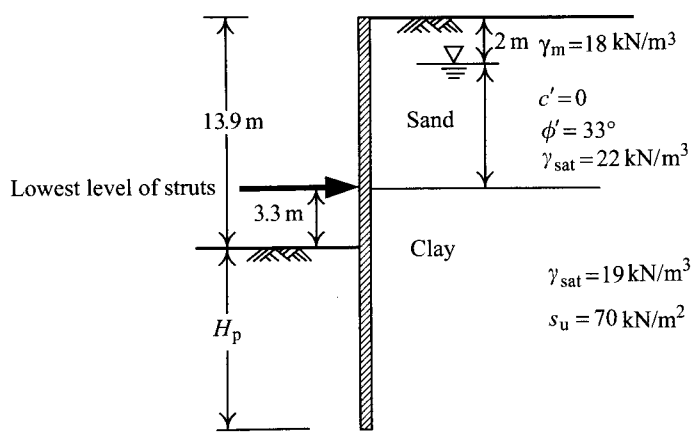

Figure P5.5

5.6 Same as the previous problem. Assume the penetration depth to be $H_p = 15$ m. Use the same method as in Problem 5.5 to compute the factor of safety against basal heave. Re-compute the factor of safety for $H_p = 20$ m. Does the factor of safety increase with the increase of the penetration depth?

5.7 Same as Problem 5.6. Assume the excavation width $B = 20$ m, the excavation length $L = 100$ m. Use the slip circle method and Terzaghi's method to compute the factor of safety against basal heave for $H_p = 15$ m and $H_p = 20$, respectively.

5.8 Same as Problem 5.6. Assume the excavation width $B = 20$ m and the excavation length $L = 100$ m. Use Bjerrum and Eide's method to compute the factor of safety against basal heave for $H_p = 15$ m and $H_p = 20$ m, respectively.

5.9 Assume an excavation as shown in Figure P5.9. The undrained shear strength of clay has the normalized behavior. Compute the required penetration depth of the

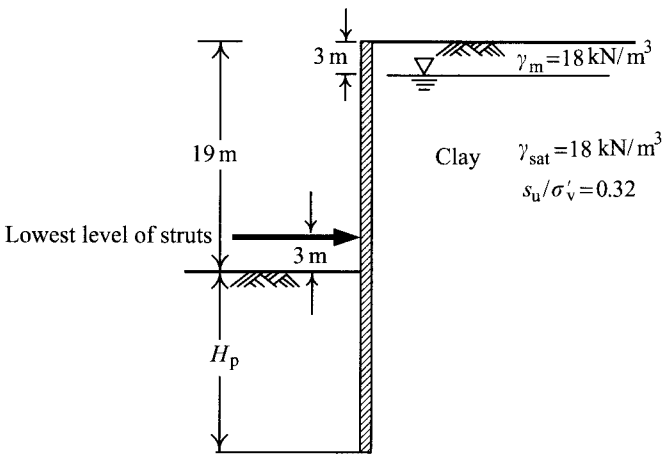

Figure P5.9

retaining wall against basal heave with $F_b = 1.2$ as well as push-in with $F_p = 1.5$, considering the adhesion or friction between the retaining wall and soil.

5.10 Same as Problem 5.9. Assume the penetration depth $H_p = 15$ m and $H_p = 20$ m, respectively. Compute the factors of safety against basal heave using the slip circle method. Does the factor of safety increase with the increase of the penetration depth?

5.11 Same as Problem 5.9. Assume the excavation width $B = 20$ m and the excavation length $L = 100$ m. Compute the factor of safety against basal heave for $H_p = 15$ m and $H_p = 20$ m, respectively, using Terzaghi's method.

5.12 Same as Problem 5.9. Assume the excavation width $B = 20$ m and the excavation length $L = 100$ m. Use Bjerrum and Eide's method to compute the factor of safety against basal heave when $H_p = 15$ m and $H_p = 20$ m, respectively.

5.13 See in Figure P5.13. Assume the excavation width $B = 50$ m and the excavation length $L = 100$ m. The penetration depth of the diaphragm wall $H_p = 15$ m. A gravel soil exists 39 m below the ground surface. Use the slip circle method, Terzaghi's method, and Bjerrum and Eide's method, respectively, to compute the factor of safety against basal heave.

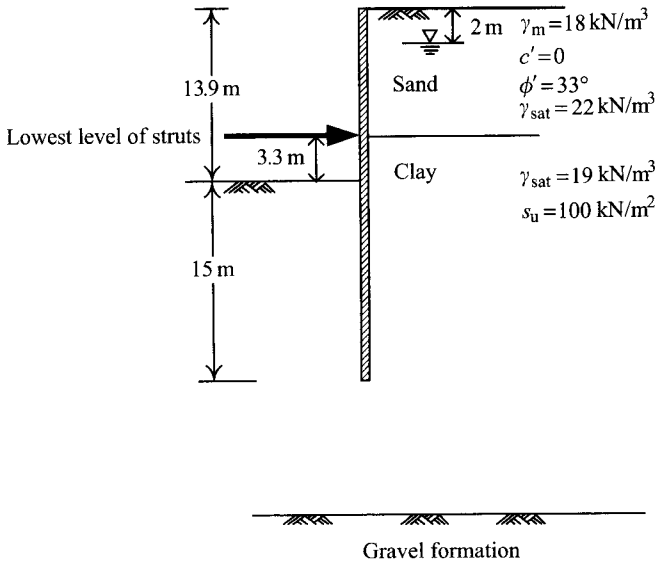

Figure P5.13

5.14 See Figure P5.14. Between 45 m and 60 m depth from the ground surface is a soft soil. Assume $B = 50$ m and the excavation length $L = 100$ m. The penetration depth $H_p = 18$ m. Use the slip circle method to compute the factor of safety against basal heave.

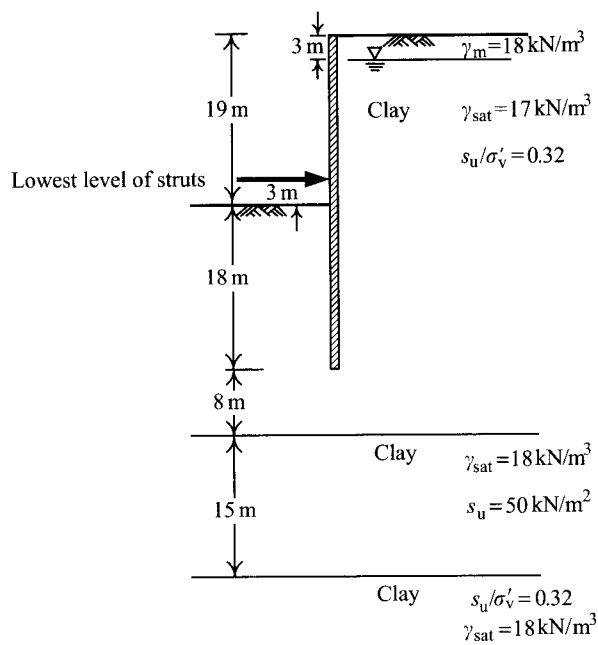

Figure P5.14

5.15 Same as the previous problem. Use Terzaghi's method and Bjerrum and Eide's method, respectively, to compute the factor of safety against basal heave.

5.16 See Figure P5.16. Assume the retaining wall is a diaphragm wall. Compute the factor of safety against sand boiling using (1) the simplified one-dimensional seepage method, (2) Marsland's method, (3) Terzaghi's method, and (4) Harza's method.

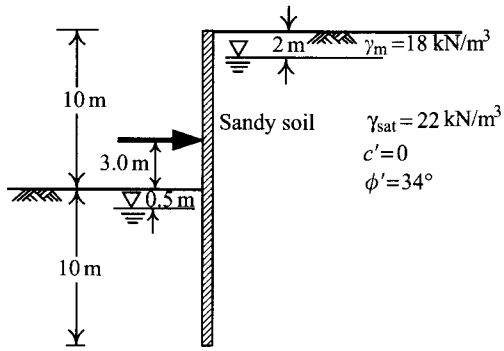

Figure P5.16

5.17 Figure P5.17 is a cantilever wall in saturated sandy soil. The groundwater levels inside and outside the excavation zone are at the excavation surface and the ground surface, respectively. The excavation depth $H_e = 3.5$ m. The saturated unit weight of sand $\gamma_{sat} = 22$ kN/m^3. The effective stress parameters $c' = 0$, $\phi' = 35°$. The friction angles between the wall and soil inside and outside the excavation zone are the same, $\delta = 2\phi'/3$. Compute the required penetration depth with the factor of safety to be 1.5 using the simplified gross earth pressure method (to simplify analysis, the seepage effect is to be ignored).

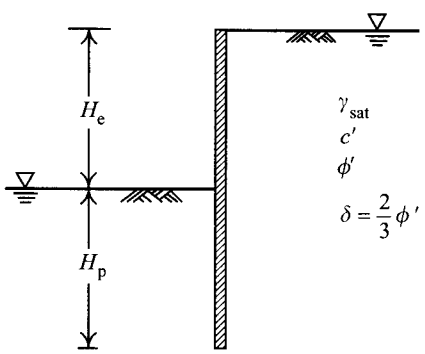

Figure P5.17

5.18 Here is an excavation site as shown in Figure P5.18. Assume the water pressure in the soil is in the hydrostatic condition. The depths for each excavation stage are 2, 5, 8.5, 11, 14, 17, and 20 m, respectively. To avoid sand boiling or upheaval during the process of excavation, make dewatering plans for each excavation stage.

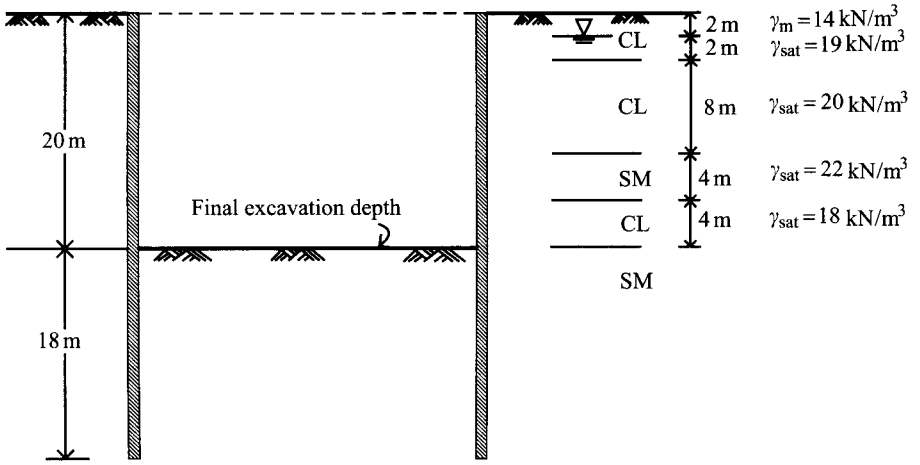

Figure P5.18

5.19 Same as Problem 5.17. Use the net earth pressure method to compute the required penetration depth for the retaining wall with the factor of safety to be 1.5 (to simplify analysis, the seepage effect is to be ignored).

5.20 Figure P5.20 shows a cantilever wall. Assume the groundwater level is at the interface between sand and clay. $H_e = 3.3$ m, $\gamma = 17.6$ kN/m^3, $c' = 0$, $\phi' = 34°$ for sand. $\gamma_{sat} = 22$ kN/m^3, $s_u = 60$ kN/m^2 for clay. Assume there exists no friction between sand and the wall. Nor does there exist adhesion between clay and the wall. Compute the required penetration depth, with the factor of safety to be 1.5, using the simplified gross earth pressure method.

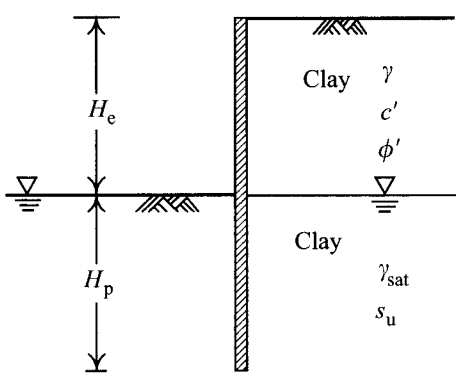

Figure P5.20

5.21 Same as the previous problem. Compute the required penetration depth with the factor of safety to be 1.5 using the net earth pressure method.

5.22 Figure P5.22 shows a cantilever wall. Assume the groundwater level is at the ground surface. $H_e = 3.0$ m, $P = 600$ kN/m, $\gamma_{sat} = 19.2$ kN/m^3, $s_u = 70$ kN/m^2. Assume no adhesion exists between the wall and clay. Compute the required penetration depth with the factor of safety to be 1.5 using the simplified gross earth pressure method.

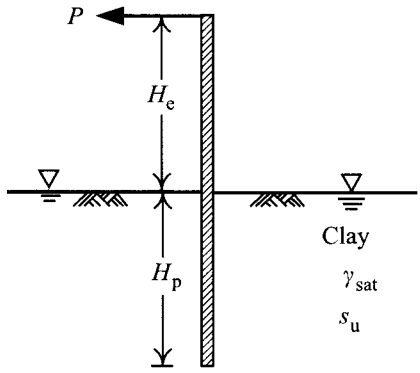

Figure P5.22

5.23 Same as the previous problem. Compute the required penetration depth with the factor of safety to be 1.5 using the net earth pressure method.

Chapter 6

Stress and deformation analysis

Simplified method

6.1 Introduction

The analyses necessary for an excavation design include stability analysis, introduced in Chapter 5, and stress and deformation analyses, which will be explored in the following three chapters. As introduced in Chapter 5, the aim of the stability analysis is to avoid collapse of an excavation due to the insufficiency of the strength of soils. Stress analysis is necessary for the design of structural components and deformation analysis aims at diagnosing the wall deflections and soil movements caused by excavation to protect adjacent properties. The contents of stress analyses that will be introduced in this chapter are strut load and wall bending moment. Nevertheless, stress analyses should also include those for detailed design of structural components, such as bracing struts, wales, and center posts, etc., which will be explored in Chapter 10.

The stress and deformation engendered by excavation may arise from either unbalanced forces or construction defects. The former are produced by the clearance of soil in the excavation site. The larger the unbalanced forces, the greater the movements of soils within the influence range of excavation. Construction defects can cause, in less serious situations, extra wall deflection, greater ground settlement and excavation bottom movement or, in serious conditions, collapses of excavations and damage to adjacent buildings and public facilities. The magnitude of stress and deformation due to construction defects cannot be predicted through theoretical simulation or empirical formulae. Such conditions can only be prevented by the improvement of construction quality. Some commonly found construction defects and their influences will be discussed in Section 11.7, Chapter 11. This chapter will be confined to ground surface settlement caused by the construction of diaphragm walls, excavation-induced deformation behaviors (including retaining wall deformation, ground surface settlement, and excavation bottom movement), and the stress of retaining walls and struts, under normal construction conditions (i.e. no over-excavation or construction defects).

The stress and deformation analysis methods for excavation include the simplified method and the numerical method. The latter can be further classified into the beam on elastic foundation method and the finite element method, which will be introduced in Chapters 7 and 8, respectively. In this chapter only the simplified method will be introduced.

Generally speaking, simplified methods employ the monitoring results of excavation case histories and then sort them into the stress and deformation characteristics of retaining walls and soils. The characteristics are useful not only to help understand the actual excavation behavior but to offer information for excavation-induced stress and deformation analyses.

As far as the wall deformation and ground surface settlement are concerned, the simplified method, which is inferred from field measurement results, represents the effect of every relevant element on deformation. Therefore, it can lead to effective predictions, without much complexity, for similar excavation projects, in terms of soil conditions, construction methods, and engineering designs. Besides, some people have also conducted systematic parametric studies using numerical methods and induced the deformation characteristics of excavation, which can be used for the prediction of wall deformation and ground settlement. Easy to apply, the methods inferred in this way are also called the simplified method. The results of deformation analyses following the simplified method are generally quite good for common excavations.

The strut-retaining system of an excavation is, in nature, a highly static indeterminate structure and thereby is difficult to analyze by hand calculation unless the loading pattern, boundary conditions, and analysis method are simplified. The stress analysis methods that will be introduced in this chapter are induced from accumulated experience or observations of designers and are more applicable to common excavations. As for special excavations (e.g. large scale or great depth), the numerical method, introduced in Chapters 7 and 8, is recommended instead, considering that the simplified method is lacking in solid theoretical support.

This chapter will largely take advantage of the measurement data from the Taipei National Enterprise Center (TNEC) excavation to explain excavation behaviors. The indices of soil data, construction process, and monitoring results from the TNEC are included in Appendix B.

6.2 Analysis of settlement induced by the construction of diaphragm walls

As discussed in Chapter 3, the construction of a diaphragm wall first partitions the wall into several panels. The construction process of each panel includes guided trench excavation, guided wall construction, trench excavation (for diaphragm wall), reinforcement placement and concrete casting (please see Section 3.3.4, Chapter 3).

The depth of a guided trench is generally about 2–3 m, sometimes 5 m. Before concreting guided walls, guided trenches, not strutted, are open ditches. The maximum settlement induced by excavation of the guided trench occurs at the verge of the trench. The settlement decreases with the distance from the trench. Considering that both measurement of and literature on this field are almost nonexistent and that no significant settlement occurs during this stage (Woo, 1992), this chapter will not delve into the subject.

The stress condition of soil in the vicinity of trenches during diaphragm wall construction is rather complicated. Take the construction of a single panel of a diaphragm wall for example. To keep the trench wall from falling, it is necessary to fill the panel with stabilizing fluid during the excavation process of the trench panel. Under normal construction conditions, excavating a trench panel filled with bentonite will cause the stress states of the soil around the trench panel to change from the original K_0 to the balanced state of the fluid pressure. However, the fluid pressure is normally not equal to the original earth and water pressures in the trench panel, but is usually smaller. The trench excavation will decrease the total lateral stress of the soil within a specific range around the trench, and thereby produce lateral movement of the soil in the vicinity of the trench. Ground settlement is thus produced. During concrete casting, the lateral pressure in the panel during this stage should be greater than the fluid pressure during the stage of excavation because the unit weight of concrete is greater than that of stabilizing fluid. Therefore, the lateral movement caused at the previous stage

will be pushed back and decrease in amount while the amount of ground settlement does not change significantly.

The soil deformation behavior caused by trench excavation is not the same as that caused by main excavation. The reasons for the differences are the differences in excavation geometric shapes and the strutting methods. The ratio of the depth of a trench panel to its width and that of the depth to length are both much larger than those in main excavations. What's more, there is the influence of stabilizing fluid, employed to counteract the lateral earth pressure and to ensure the stability of trench walls. Nevertheless, in spite of the differences in geometric shapes and construction techniques, the excavation of a trench panel is also a type of excavation, producing deformations, though fewer and with smaller influence range. The shape of ground surface settlement is basically similar to that induced by main excavation. Besides, because the retaining wall is the combined whole of many connected diaphragm wall panels, settlement will be accumulated panel by panel and the final deformation gets more serious accordingly.

Though the problems of ground displacement induced by the construction of diaphragm walls have gradually drawn attention from engineers, there are few study results available due to the complexity of the construction process and the fact that monitoring results are almost nonexistent. In the 1980s, there were some in situ monitoring projects and some results were obtained. Nevertheless, most of them were confined to the deformation induced by the construction process of a single panel, for example, those carried out in Oslo and in Singapore. As for the monitoring of the final deformation after the completion of a whole retaining wall, there is almost no literature. According to the monitoring results of the rapid transit system in Hong Kong (Cowland and Thorley, 1985), after the completion of the diaphragm walls and before the main excavation, the accumulated deformation can achieve 40–50% of the total deformation after the completion of the main excavation. Clough and O'Rourke (1990) found that the ratio of the maximum settlement induced by the construction of diaphragm walls to the depth of the trench is 0.15%, according to many in situ monitoring results, as shown in Figure 6.1. We can see that soil settlement in the vicinity of diaphragm wall panels, induced by their construction, is significant and that caution is strictly required to protect adjacent properties.

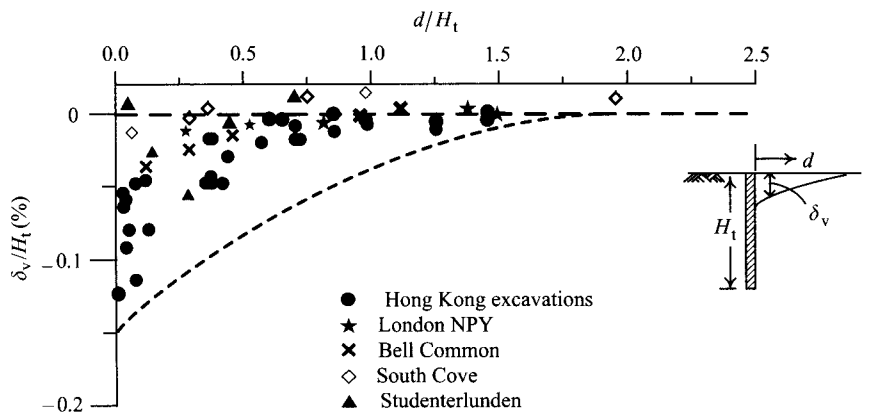

Figure 6.1 Envelope of ground surface settlements induced by trench excavations (Clough and O'Rourke, 1990).

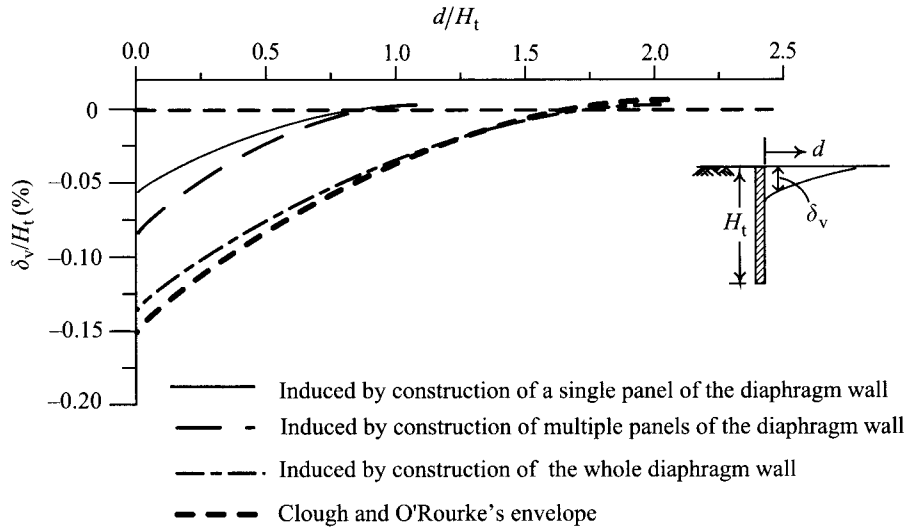

Figure 6.2 Envelopes of ground surface settlement induced by the diaphragm wall construction (Ou and Yang, 2000).

Ou and Yang (2000) studied the monitoring results of the settlement induced by the construction of the diaphragm walls for the excavations in the Taipei Rapid Transit System and found that, under normal construction conditions, the maximum settlement induced by a single panel was about 0.05 H_t% (H_t is the depth of a trench) and the maximum settlement mostly occurred within 0.3 H_t from the trench panel, as shown in Figure 6.2. The main influence range of settlement was 0.5 H_t from the trench panel and little settlement occurred beyond 1.0 H_t from the trench panel. The concrete casting did not cause significant settlement. In sand-clay alternated layers, the maximum settlement induced by a single trench panel is 10–15 mm, in Singapore marine clay, 24 mm (Poh and Wong, 1998).

Ou and Yang (2000) also found that the maximum accumulated settlement after the completion of several test panels was 0.07 H_t% (Figure 6.2) and its location and influence range were basically similar to those of single-panel induced settlement. The maximum amount of accumulated settlement after the completion of the whole diaphragm wall was greater than that induced by a single test panel as well as that by multiple test panels. The maximum amount of total settlement was about 0.13 H_t%, occurring within a distance of 0.3H_t from the diaphragm wall. The above maximum amount of total settlement was less than that of Clough and O'Rourke's (1990) envelope (0.15 H_t%). Settlement became less observable beyond the distance of 1.5–2 H_t from the diaphragm wall.

6.3 Characteristics of wall movement induced by excavation

The magnitude of wall movement is determined by the excavation-induced unbalanced forces, the stiffness of the retaining-strutting system, the excavation stability, etc. The unbalanced forces are synthetic results of many factors such as the excavation width, the excavation

depth, the preload, etc. The relations of these factors with the deformation of a retaining wall can be inferred theoretically. For example, the thicker the retaining wall, the narrower and the shallower the excavation, the stronger the strut stiffness, the larger the preload; and the greater the safety factor of stability, the smaller the wall deformation. Some factors have complicated relations with the deformation and this section is going to explore them in detail.

6.3.1 Safety factors of stability

The smaller the factor of safety, the weaker the stability of the excavation. If an excavation fails due to insufficiency of safety factor, it follows, a great amount of displacement of the retaining wall will be produced. Thus, we can see that the deformation of a retaining wall relates closely to the factor of safety. In Figure 6.3, compiled by Clough and O'Rourke (1990), are summarized many excavation case histories. As shown in the figure, the smaller the factor of safety against basal heave (F_b), the larger the deformation of the retaining wall. As the factor of safety approaches 1.0, the excavation is on the verge of failing and a large amount of deformation is produced. The relation between the factor of safety against push-in failure and wall deformation is similar to Figure 6.3.

6.3.2 Excavation width

Clough and O'Rourke (1990) found that the wider the excavation, the larger the deformation of the retaining wall. As a matter of fact, for a typical excavation the wider excavation, the larger are the unbalanced forces; the larger the unbalanced forces, the greater is the wall deformation. Moreover, the factor of safety against basal heave for soft clay decreases with

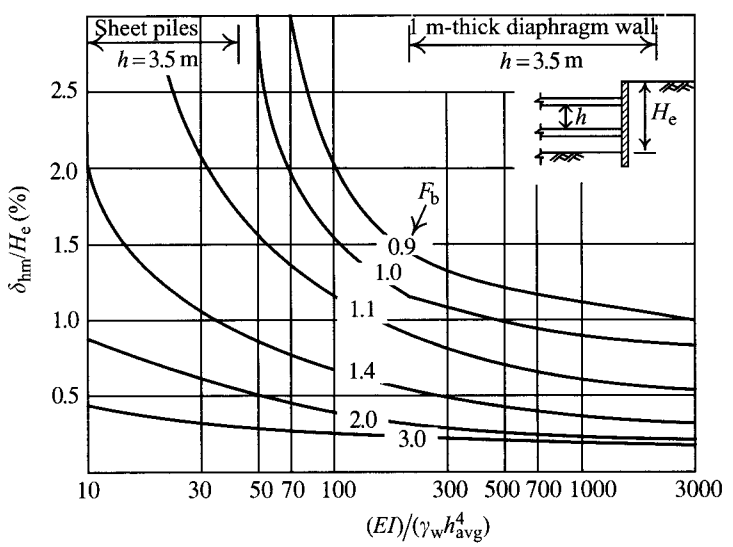

Figure 6.3 Relationships between the maximum deflections of walls, stiffness of strutting systems, and factors of safety against basal heave (*EI* denotes wall stiffness, γ_w denotes unit weight of water, $EI/(\gamma_w h_{avg}^4)$ represents system stiffness of wall-retaining system) (Clough and O'Rourke, 1990).

the increase of the excavation width (please see Section 5.5.2, Chapter 5). As elucidated in Section 6.2.1, the deformation of a retaining wall increases with the decline of the factor of safety.

6.3.3 Excavation depth

Figure 6.4 shows the relationship between the deformations of excavations in the Taipei area and their excavation depths (Ou *et al.*, 1993). As shown in the figure, in most of the case histories, the deformation of a retaining wall deteriorates with the increase of the excavation depth. The deformation of a retaining wall in soft clay is generally greater than that in sand. We can see from the figure that the maximum deformation (δ_{hm}) can be estimated with the following equation:

$$\delta_{hm} = (0.2\text{–}0.5\%)H_e \tag{6.1}$$

where H_e = excavation depth.

The upper limit of the δ_{hm}-value is recommended for soft clay while the lower limit should be used for sand. An averaged value is suggested for alternating layers of sand and clay. If the top-down excavation method is employed in soft clay, the δ_{hm}-value may exceed the above maximum value. For an explanation of this, please refer to Section 6.6.

6.3.4 Wall penetration depth

Figure 6.5 shows the analytic relationship between wall deformations engendered by a 20 m-deep excavation and penetration depths using the finite element method. As shown in the figure, if the normalized strength of the soil is $s_u/\sigma'_v = 0.36$, the deformations for wall penetration depth $H_p = 15$ m and $H_p = 20$ m are the same. When $H_p = 10.0$ m, though the deformation increases a little, the excavation system is still basically stable.

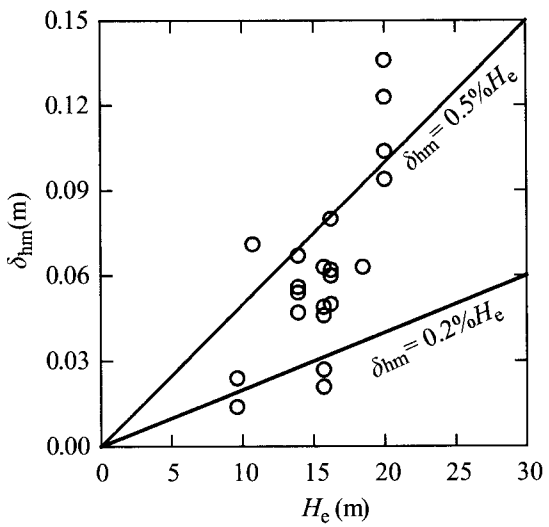

Figure 6.4 Relationships between maximum wall deflections and excavation depths (Ou *et al.*, 1993).

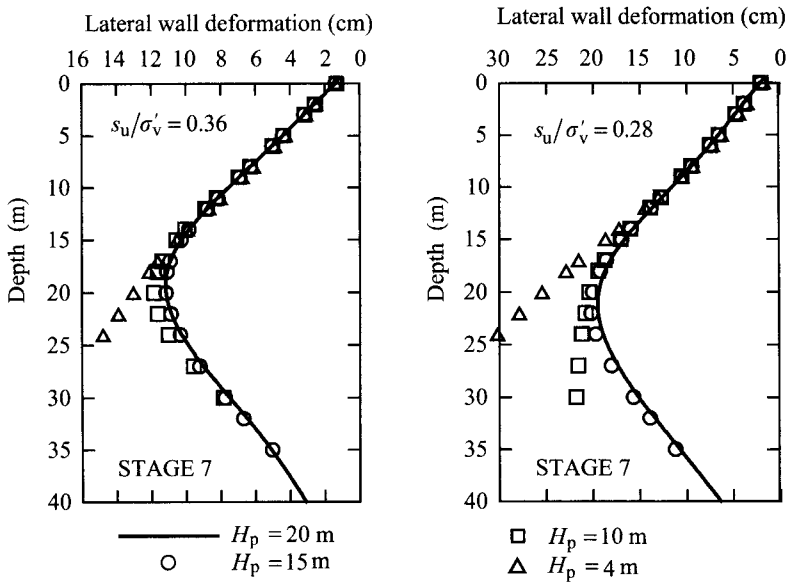

Figure 6.5 Relationships between penetration depths and wall deflections.

When $H_p = 4.0$ m, at the bottom of a retaining wall occurs the phenomenon of "kicking," shows that heave failure has been produced and the deformation increases rapidly.

Figure 6.5 also shows the relationships between the deformations and penetration depths with the normalized strength $s_u/\sigma'_v = 0.28$ under the same excavation conditions. As shown in the figure, the deformation is slightly larger for H_p=15 m than that for $H_p = 20$ m. When $H_p = 10.0$ m, the phenomenon of kicking at the bottom of the retaining wall grows worse and the excavation fails.

We can see from the above discussion that as long as the retaining wall is in a stable state, the growth of the penetration depth does not affect the deformation of the retaining wall.

6.3.5 *Wall stiffness*

Theoretically, the deformation of a retaining wall will decrease with the increase of the stiffness of the retaining wall. However, the amount of decrease does not have a linear relationship with the increment of stiffness. The increase of wall thickness or wall stiffness to reduce wall deformation is certainly effective, but only to a certain extent (Hsieh, 1999). Thus, to decrease the deformation by way of increasing the thickness of the retaining wall will not be very effective.

6.3.6 *Strut stiffness*

As shown in Figure 6.6a, with the start of the first stage of excavation, wall movement will be produced and form a cantilever shape. The second stage of excavation starts after the installation of the first level of struts. If the stiffness of the struts is high enough, the compression

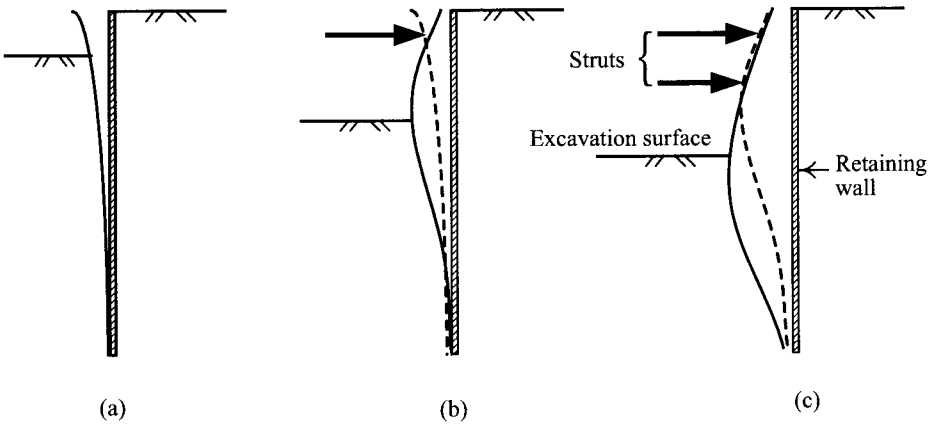

Figure 6.6 Relationship between the shape of wall deformation and high strut stiffness: (a) first stage of excavation, (b) second stage of excavation, and (c) third stage of excavation.

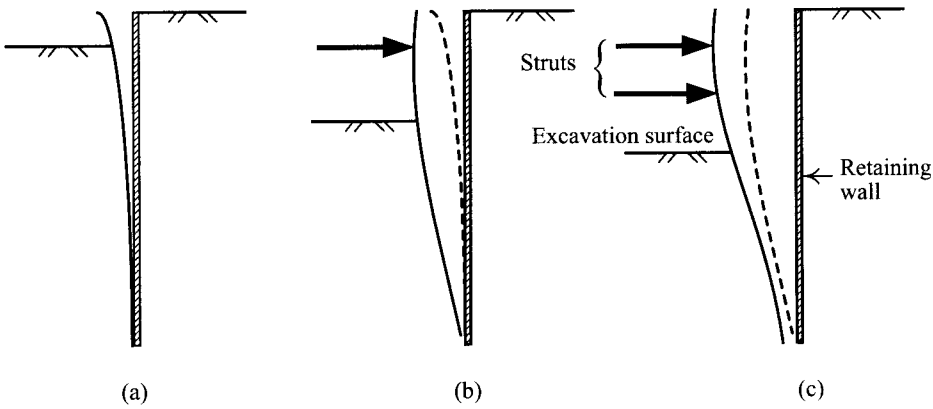

Figure 6.7 Relation between the shape of wall deformation and low strut stiffness: (a) first stage of excavation, (b) second stage of excavation, and (c) third stage of excavation.

of the struts will be rather small, so that the retaining wall will rotate about the contact point between the struts and the wall, and wall deformation is thus generated. The maximum wall deformation will occur near the excavation surface as shown in Figure 6.6b. With the completion of the second level of struts, the third stage of excavation starts. Suppose the stiffness of the second level of struts is also strong enough. The retaining wall will continue rotating about the contact point with the second level of the struts, and wall deformation is produced again. The location of the maximum deformation will be near the excavation surface (Figure 6.6c). If the soil below the excavation surface is soft soil, the resisting force to prevent the retaining wall from pushing in will be weak and the location of the maximum deformation will be mostly below the excavation surface. Inferred from the same extrapolation, excavation in stiff soils (such as sand) will mostly produce the maximum deformation above the excavation surface. Actually, the locations of the maximum deformations are found near the excavation surfaces in most of the excavations in Taipei (Ou *et al.*, 1993).

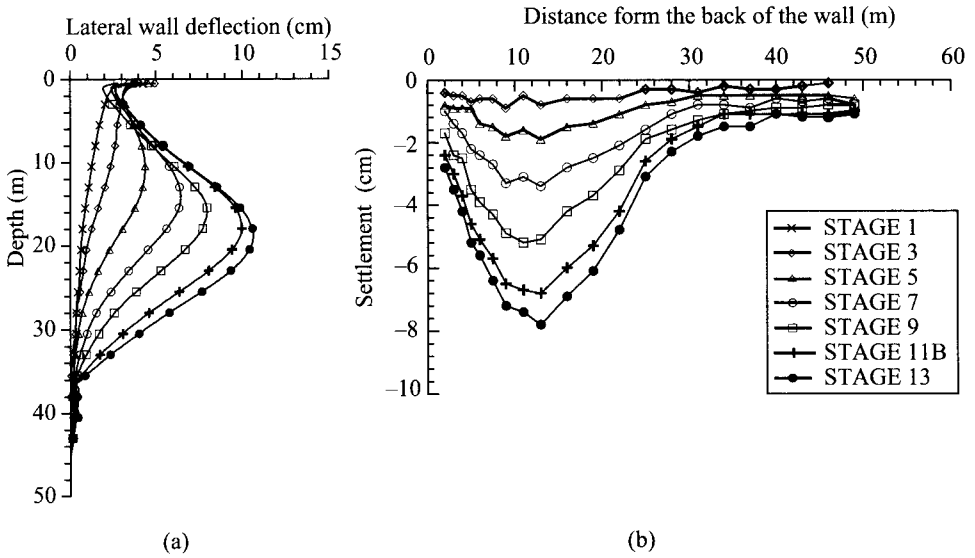

Figure 6.8 Lateral wall deflections and ground surface settlements of the TNEC excavation: (a) lateral wall deflections and (b) ground surface settlements (Ou *et al.*, 1998).

As shown in Figure 6.7, with the stiffness of struts not high, the compression of the struts should be quite large. There will be larger wall displacement around the contact points during the second and the third stages of excavation. The final deformation pattern of the retaining wall will be close to that of the cantilever type and the maximum deformation will be produced at the top of the retaining wall.

Figure 6.8a is a diagram of the lateral deformation of the retaining wall at each excavation stage of the TNEC excavation (Ou *et al.*, 1998). Since the top-down construction method was employed in this case, the axial stiffness of floor slabs was quite high and the deformation behavior was similar to that shown in Figure 6.6, in which the maximum deformation occurs near the excavation surface.

6.3.7 *Strut spacing*

The problem of strut spacing can be distinguished into that of horizontal spacing and vertical spacing. Narrowing the horizontal spacing can increase the stiffness of the struts per unit width. The effect will be the same as discussed in Section 6.3.6 and the problem will not be further explored here.

Shortening the vertical spacing of struts can effectively decrease the deformation of a retaining wall because the stiffness of the strut system is raised. The stiffness raised, the deformation of a retaining wall also declines. Put another way, since the deformation of a retaining wall is the accumulated result throughout all the excavation stages, with the unsupported length generated in each stage reduced due to the shortening of the vertical spacing, the deformation of a retaining wall will decline as a result. The "unsupported length" refers to the distance between the lowest level of strut and the excavation surface.

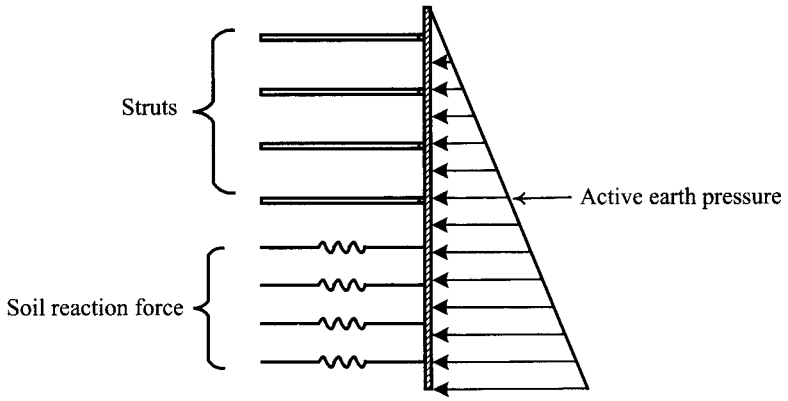

Figure 6.9 Relationship between earth pressures, strut loads, and reactions of soil.

As for the detailed mechanism of the unsupported length affecting excavation deformation, please see Section 11.4.1 in Chapter 11.

6.3.8 *Strut preload*

When applying the braced excavation method (or the anchored excavation method), preload is often exerted onto struts. Suppose the struts are placed at shallower levels. Thus, under normal conditions (with the preload not too small), the preload will be capable of pushing the retaining wall out. If the struts are placed at deeper levels, with the earth pressure growing with the depth, the preload of struts will not be able to push the wall outward easily (Ou *et al.*, 1998).

Actually, no matter whether the preload is capable of causing a retaining wall to move, preload is always helpful to reduce the displacement of a retaining wall or the ground settlement. The reason for this can be explained by Figure 6.9. As explicated in Section 5.4, the design of a braced excavation is based on the concept of the free earth support method. Therefore, the retaining wall will inevitably move toward the excavation zone once excavation is started and the phenomenon will make the earth pressure in back of the retaining wall approach the active pressure. Figure 6.9 shows the way the struts and soil resist, collectively, against the active earth pressure from outside the retaining wall. According to the concept of the force equilibrium of the wall, when the struts bear more lateral earth pressure because of preload, the soil below the excavation surface will then bear less pressure, which leads to less wall deformation or ground settlement.

6.4 Characteristics of ground movement induced by excavation

Observing the shapes or types of ground surface settlement (as shown in Figures 6.6 and 6.7), we can see that soil in back of the retaining wall moves forward and down with the retaining wall deforming under normal conditions and ground settlement will thus be produced. Thus, the factors causing wall deformation will also produce ground settlement. This section will

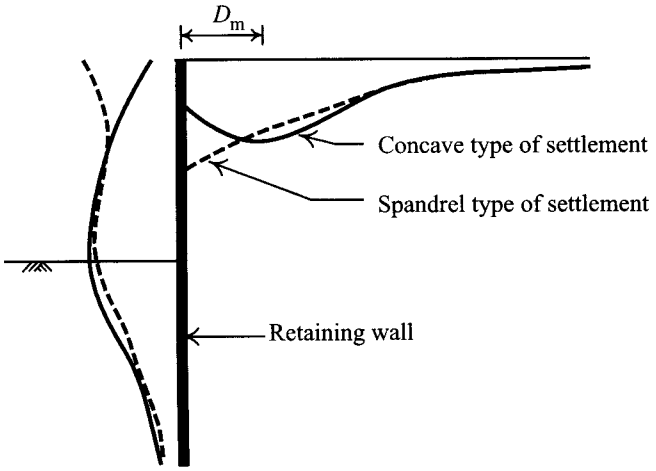

Figure 6.10 Types of ground surface settlements.

not introduce the influence factors repeatedly (they are the stiffness of struts, the preload, the factor of safety of stability, the excavation depth, and the excavation width, etc.). This section will focus on the characteristics of ground surface settlement.

6.4.1 Shapes and types of ground surface settlement

The author found that the shapes or types of the ground surface settlement engendered by excavation can be categorized into the spandrel type and the concave type, as shown in Figure 6.10 (Hsieh and Ou, 1998). The main factors responsible for these two types of ground surface settlements are the magnitude and shape of deformation of a retaining wall.

If the first stage of excavation has generated more deflection of the retaining wall than the later excavation stages or excavation has continued to produce the cantilever type of deflection in the later stages, the spandrel type of settlement will be more likely to occur and the maximum ground surface settlement will be found near the retaining wall. If the wall has a deep inward movement as shown in Figure 6.6, the maximum ground surface settlement will be found located at a distance in back of the wall, that is, a concave type of settlement will be produced.

Under normal construction conditions, excavation in soft clay will produce more deflection of the retaining wall and tend to bring about deep inward movement, which likely leads to the concave type of settlement. Excavation in sandy grounds or stiff clay, on the other hand, will produce less deformation of the retaining wall and the spandrel type of settlement may be produced (Clough and O'Rourke, 1990).

As discussed earlier, the shape of ground surface settlement is supposed to correlate with the area of the cantilever component and the area of the deep inward component of the lateral wall movement. To predict the type of ground surface settlement based on the shape of lateral wall movement, the author defined A_c as the area of the cantilever component and A_s as the area of the total wall movement subtracting the area of the cantilever component

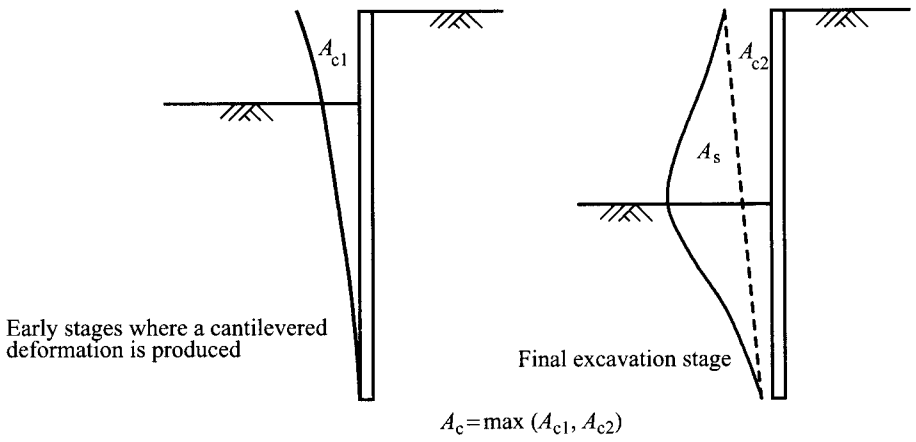

Figure 6.11 Definitions of the area of the deep inward part and the cantilevered part of wall deformation.

(Hsieh and Ou, 1998), as shown in Figure 6.11. A_c is determined as follows:

$$A_c = \max(A_{c1}, A_{c2}) \tag{6.2}$$

where A_{c1} is the area of the cantilever deformation of the wall at the beginning of excavation and A_{c2} is the area of the cantilever component of the lateral wall deformation at the final stage of excavation.

To study the relationship between the shape of the lateral wall displacement and that of ground surface settlement, the author took the monitoring results of 16 ground surface settlement cases of the concave type and seven of the spandrel type to compute their A_c and A_s and established the relationships between the type of ground surface settlement and the shape of the lateral wall movement. The relationships between A_c and A_s of the 16 case histories are as shown in Figure 6.12, where the following tendencies can be observed: when A_s is greater than $1.6A_c$, the shape of ground surface settlement will tend to be the concave type. Otherwise, it is of the spandrel type.

Therefore, to predict the type of ground surface settlement, we can refer to the relationship between A_c and A_s. When $A_s < 1.6A_c$, we can predict that the ground surface settlement will be of the spandrel type. When $A_s \geq 1.6A_c$, we can predict the ground surface settlement will be of the concave type.

6.4.2 *Influence zones of settlement*

Peck (1969b) proposed that the influence zone of settlement should be two or three times of the excavation depth. Clough and O'Rourke (1990) proposed excavation in sandy soils may induce an influence zone of settlement about twice of the excavation depth. As for stiff to very stiff clay, three times the excavation depth. Soft or medium soft clay, twice the excavation depth. In addition to the above, there are various other suggested values of the influence zone (Nicholson, 1987, for example). However, most of them are lacking in formal

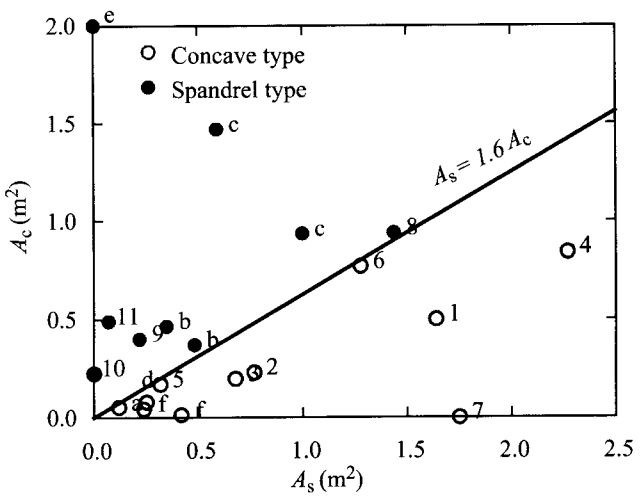

Figure 6.12 Relationship between the type of ground surface settlement and shapes of lateral wall deflection (English letter labels refer to excavation cases from other countries while Arabic numbers labels refer to cases from Taiwan) (Hsieh and Ou, 1998).

definitions of the influence zone and the excavation depth is the only parameter in estimating the influence zone. Nevertheless, according to the author's numerical analyses and studies of the characteristics of ground settlement from excavation case histories, the influence zone of ground settlement does not relate exclusively to the excavation depth. It also relates to the excavation width, the location of the hard soil, etc.

As discussed earlier, the types of settlement induced by excavation include the spandrel type and the concave type. The author (Hsieh and Ou, 1998) has proposed the conception of the primary influence zone (PIZ) and the secondary influence zone (SIZ) on the basis of the principles of mechanics and regression analysis of excavation case histories. We claim that the influence zone may extend very far and the distribution of the settlement curve includes the primary influence zone and the secondary influence zone no matter whether the settlement belongs to the spandrel type or the concave type. The curve is steeper in the primary influence zone where buildings receive more influence. In the secondary influence zone the slope of the curve is gentler and the influence on buildings is less. The range of the secondary influence zone is approximately equal to that of the primary influence zone. Settlement might still happen beyond the secondary influence zone. However, its magnitude is so gentle that it is beyond perception or evenly distributed. Under normal conditions, its influence on buildings is ignorable.

Take the ground surface settlement of the TNEC excavation, as shown in Figure 6.8b, as an example to illustrate the characteristics of influence zones.

1 As soon as excavation was started, settlement began occurring and its influence zone was large. The excavation depth of the third stage was 4.9 m while the influence zone, for settlement, reached as far as 50 m away from the retaining wall. At this stage, no distinction between the primary influence zone and the secondary influence zone was discerned.

2 At the fifth stage of excavation (excavation depth = 8.6 m), the primary influence zone, which was about as far as 32 m away from the retaining wall, began to be distinguishable from the settlement trough.
3 After the fifth stage, though the excavation depth kept growing, the range of the primary influence zone was not enlarged accordingly.

According to this observation, the excavation depth should not be the only parameter to affect the settlement influence range. Ou and Hsieh (Ou and Hsieh, 2000; Ou *et al.*, 2005) therefore established a simplified method, proved by finite element analyses as well as case histories as displayed in Section 6.8.5, to determine the settlement influence zone based on the potential failure zones. The method is described as follows.

According to the loading behavior of soil, strain in soil will increase greatly when soil is going to fail or has failed. The movement or strain within the primary influence zone is rather large and we can reasonably assume the primary influence zone is the potential failure zone. According to the elucidation of the mechanism of overall shear failure in Chapter 5, failure due to excavation can be mainly divided into push-in failure and basal heave failure. The former may happen in sand, clay, or any other type of soil (hard soils not included) while the latter happens only in soft clay.

Since the design of the strutted wall is based on the conception of the free earth support method, not only the bottom of the retaining wall has movement but also the soil below the wall bottom may exhibit movement. If we suppose that the movement of the soil is not restricted (i.e. hard soils are very far underneath), the formation of the active failure in back of the retaining wall will not be obstructed and the active failure zone will be about twice as wide as the excavation depth ($2\ H_e$). When the hard soil is shallow enough to restrict the movement of the soil, the range of the active failure zone will be about the same as the depth of the hard soil. Under such conditions, the potential failure zone based on the push-in failure mode can be determined as follows:

$$\mathrm{PIZ}_1 = \min(2H_e, H_g) \tag{6.3}$$

where H_g = depth of the hard soil.

Excavation in soft clay can also induce basal heave. As shown in Figure 6.13, the potential basal heave failure surface can be the one with the wall top as axis and the excavation width as radius (B in Figure 6.13). If the formation of the potential basal heave failure surface is not restricted by sandy or hard soil, the range of the potential basal heave failure in back of the wall will be close to the excavation width. If the sandy or the hard soil is located shallower, the potential basal heave failure surface will then be tangential to the sandy or hard soil and the potential basal heave failure range in back of the wall will be close to the distance to the soft clay bottom from the ground surface. Thus, the potential failure zone based on the basal heave failure mode can be determined as follows:

$$\mathrm{PIZ}_2 = \min(H_f, B) \tag{6.4}$$

where H_f is the depth of the soft clay bottom, and B is the excavation width.

Both PIZ_1 and PIZ_2 are potential failure zones. The primary influence zone of excavation-induced settlement is the maximum of the potential failure zones. Thus, the primary influence

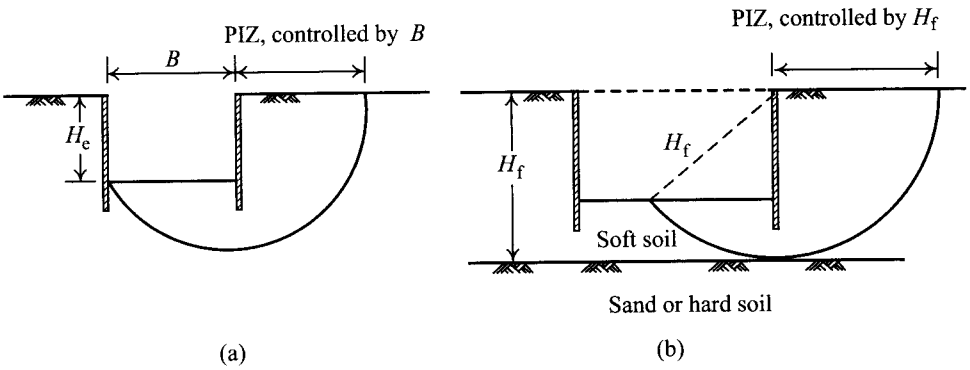

Figure 6.13 Primary influence zone produced by potential basal heave failure surfaces.

zone is the larger of PIZ_1 and PIZ_2:

$$PIZ = \max(PIZ_1, PIZ_2) \tag{6.5}$$

6.4.3 Locations of the maximum settlement

As shown in Figure 6.10, the maximum ground surface settlement of the spandrel type occurs near the retaining wall. Earlier documents (Nicholson, 1987; Ou *et al.*, 1993) claimed the maximum ground surface settlement of the concave type would occur at a distance of 0.5 H_e from the wall. Nevertheless, observing the typical settlement curve of excavation in the Taipei area, as shown in Figure 6.8, the location of the maximum ground surface settlement is determined with the starting of excavation and does not change with the increase of the excavation depth. Thus, neither Nicholson's nor the author's earlier study conforms to the actual conditions.

According to parametric studies using the finite element method (Ou and Hsieh, 2000; Ou *et al.*, 2005), the location of the maximum settlement of the cantilevered type can be determined by the equation: D_m = PIZ/3 (Note: definition of D_m can be referred to in Figure 6.10). As elucidated earlier, the primary influence zone (PIZ) is determined as soon as the excavation is started and the location of the maximum settlement (D_m), which does not move with the continuation of excavation, is determined accordingly, too. The result conforms to the measurement (see Figure 6.8b).

6.4.4 Magnitude of the maximum settlement

Clough and O'Rourke (1990) established the relationship between the maximum settlement and the excavation depth in stiff clays, sandy soils, and soft to medium soft clays, based on many case histories. Nevertheless, since the excavation depth is not the only factor affecting settlement, the derived relationship varies from one case history to another.

Since the factors affecting the deformation of a retaining wall are also those affecting ground surface settlement, there should exist a certain relationship between the maximum wall deformation and the maximum ground surface settlement. Figure 6.14 shows relationships between the maximum wall deformations and ground surface settlements, which were

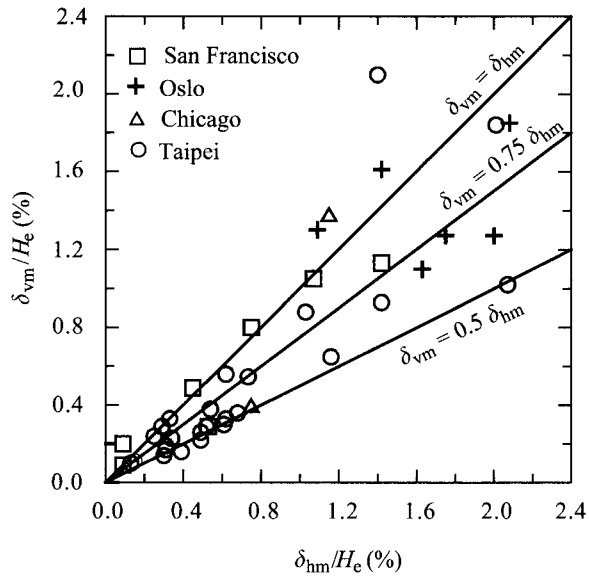

Figure 6.14 Maximum ground surface settlement and lateral wall deflection (Ou *et al.*, 1993).

obtained from excavation case histories in Taipei, Chicago, San Francisco, and Oslo (Mana and Clough, 1981; Ou *et al.*, 1993). We can find from the figure that $\delta_{vm} = (0.5 \sim 0.75)\delta_{hm}$ for most of the cases, with the lower limit for sandy soils, the upper limit for clays, and somewhere between the two for alternating soils of sand and clay. As for very soft soils, δ_{vm} might run beyond $1.0\delta_{hm}$.

Thus, to estimate the maximum ground surface settlement, we can follow the beam on elastic foundation method or the finite element method to compute the maximum value of excavation-induced deformation of a retaining wall and then estimate the maximum settlement with the help of Figure 6.14 (note: for the reason for not employing the finite element method to directly compute the ground settlement, please refer to Section 8.11). Since the analyses with either the beam on elastic foundation method or the finite element method have had the factors affecting the deformation of a retaining wall considered (such as the soil sampling quality, the safety factor of stability, the strut system, etc.), the computed maximum wall deformation will be quite accurate.

6.4.5 *Relationships between ground surface settlements and soil movements*

The magnitude and distribution of settlements introduced so far refer to those of the ground surface. Actually, most foundations are placed at a certain depth below the ground surface. How to estimate the settlement of the foundations will be something interesting which remains to be resolved. Due to the absence of reliable study results, some engineers assume that the maximum excavation-induced settlement occurs on the ground surface and the settlement decreases with growing depth.

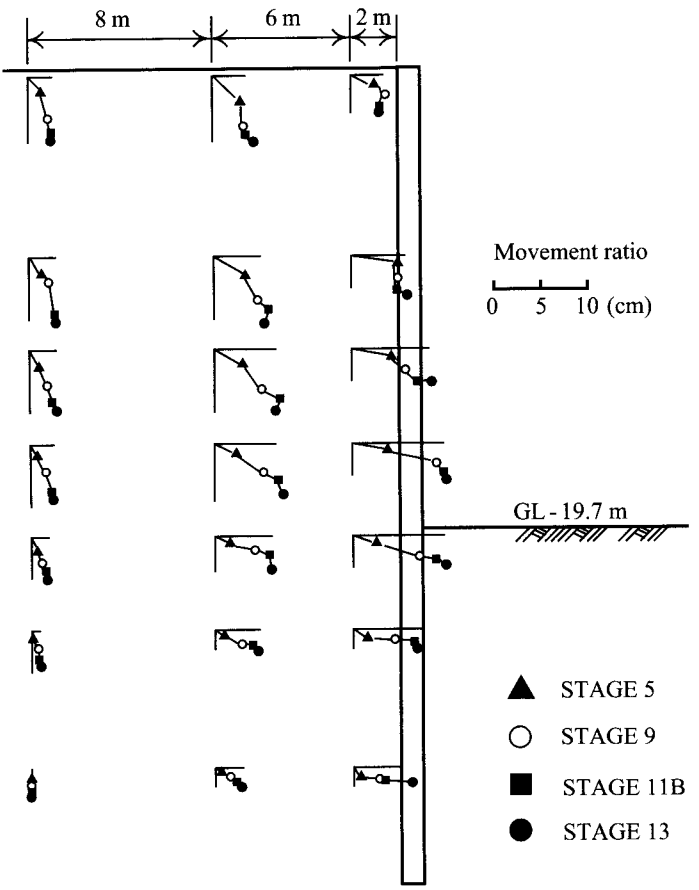

Figure 6.15 Displacement vectors at points in soil outside of the TNEC excavation zone (Ou *et al.*, 2000).

Figure 6.15 provides the measurement values of the displacement vectors of soil below the ground surface and in back of the retaining wall at the last stage of the TNEC excavation (Ou *et al.*, 2000). We can see from the figure that the soil settles downward and moves toward the excavation zone. The soil in back of the retaining wall and around the same level as the excavation surface moves toward the excavation zone (horizontally) more than moving down (vertically). The vertical displacements of the soil above the excavation surface are basically close. On the other hand, the vertical displacements of the soil below the excavation surface decrease with the increase of the depth from the excavation surface. Data provided in Figure 6.15 can be used to decide the settlement of embedded foundations.

6.5 Characteristics of excavation bottom movement induced by excavation

The sources of excavation bottom movement include elastic unloading due to removal of soil, the lateral displacement of the embedded part of the retaining wall, or the plastic deformation

of the soil below the excavation surface (Figure 6.16). According to the mechanism of the occurrence of movement, we can see the maximum movement occurs near the excavation surface and the magnitude of movement decreases with growing depth from the excavation surface.

Generally speaking, the center post in excavations mainly bears the weight of struts and is not to be embedded deeply into soil. If the heave of the center post out of the excavation bottom movement makes the struts placed on the center post arch upward, the failure of the strut system may occur as a result of too much displacement, as shown in Figure 6.17.

The measurement of excavation bottom movement is difficult (see Chapter 12) and few studies are available. Figure 6.18 provides the measurement values of the excavation bottom movement occurring in the T1, T2, K1, and K2 areas of the Taipei area (soils in the K1 and K2 areas are basically soft clay while those in T1 and T2 areas are alternating soils of sand and clay, and sandy soils are more common). Figure 6.19 provides the monitoring results of excavation bottom movement of the TNEC excavation. The two figures can be used for initial design.

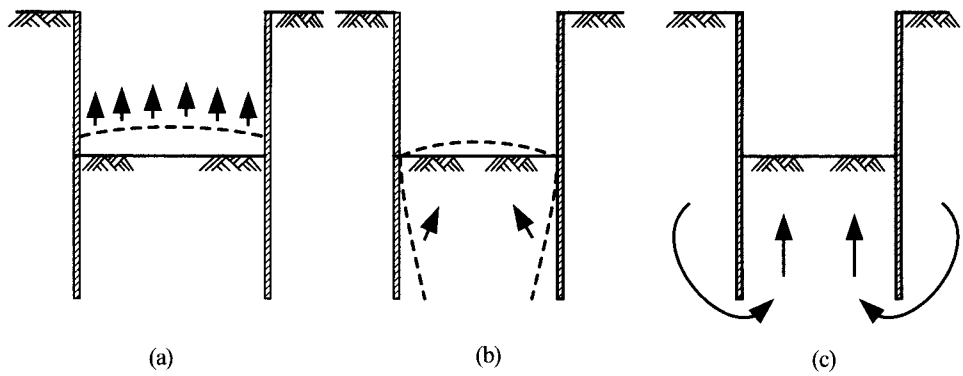

Figure 6.16 Mechanism of excavation bottom movement: (a) due to elastic unloading, (b) due to lateral movement of the retaining wall, and (c) due to plastic basal heave.

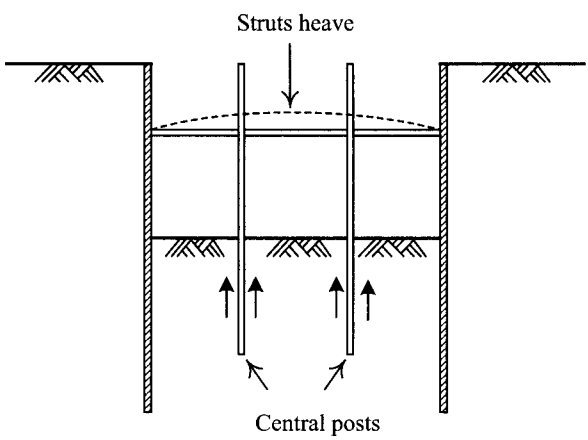

Figure 6.17 Influence of the heave of the central post on the strutting system.

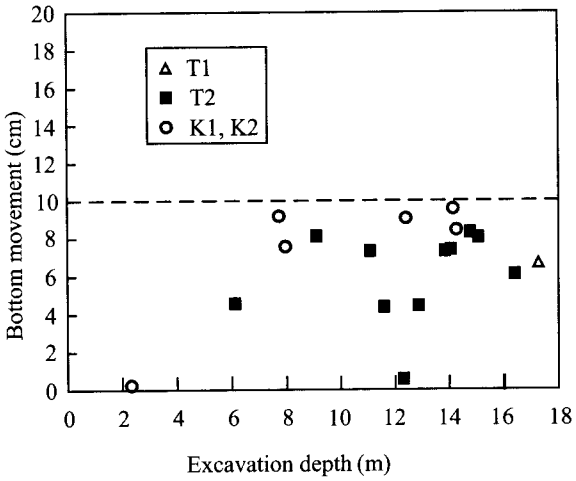

Figure 6.18 Relations between excavation bottom heaves and excavation depths (Woo and Moh, 1990).

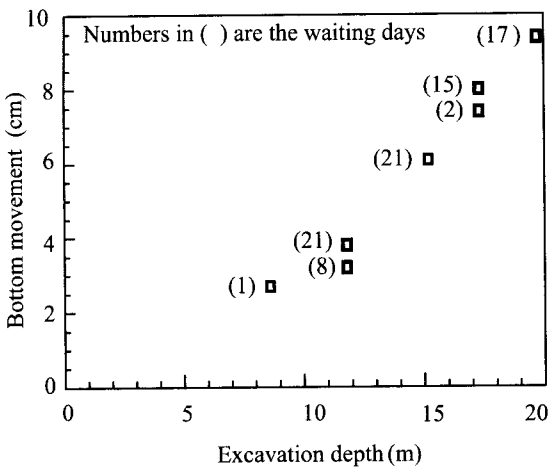

Figure 6.19 Excavation bottom movement and excavation depth of the TNEC excavation (Ou *et al.*, 1998).

6.6 Time dependent movement

The top-down construction method requires long periods to erect molds, cast floor slabs and wait for them to gain enough strength before proceeding to the next stage of excavation. Sometimes, for the convenience of construction, the next stage of excavation is not to be started until the construction of the superstructures has come to a scheduled stage. Take the TNEC excavation for example, each stage took a waiting period of 30–60 days (the waiting time refers to the period between the completion of an excavation stage and the start of the

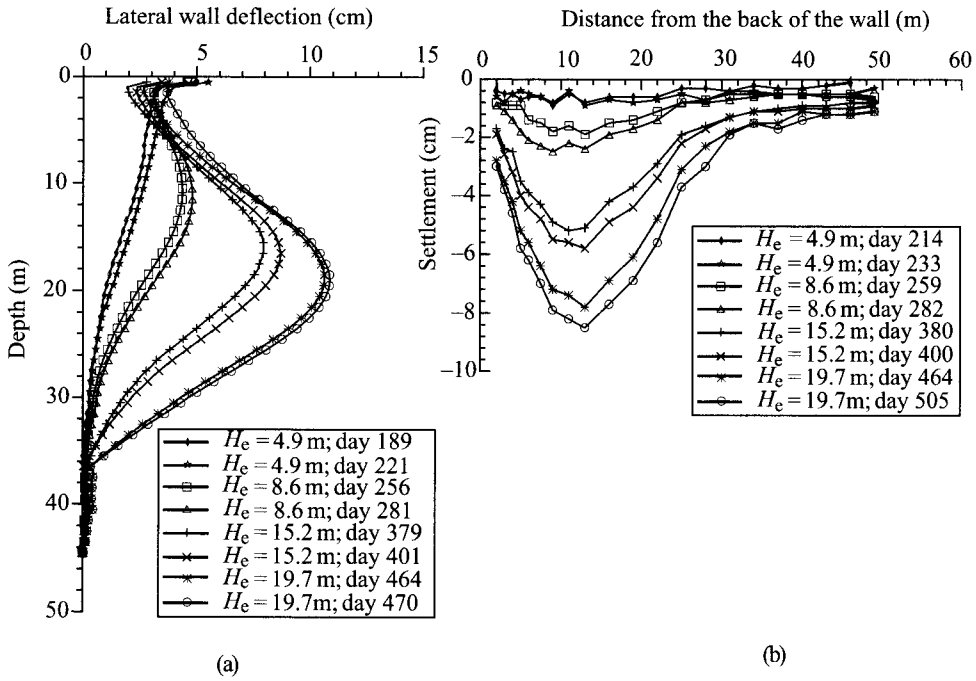

Figure 6.20 Time-dependent lateral wall deflection and ground surface settlement of the TNEC excavation: (a) wall deflection and (b) ground surface settlement (Ou *et al.*, 1998).

next). As the field measurements showed, during the waiting periods, the lateral displacement of the retaining wall, the ground surface settlement, and the movement of the excavation bottom all increased, though no excavation activity was being conducted. The author infers the reason for the phenomena is perhaps either the dissipation of excess porewater pressure or soil creep, especially the latter. No simple formula is available to predict the influence of creep on deformation so far. This section will therefore be confined to the introduction of the characteristics of the influence of creep on deformation and the available monitoring results, which can be used by engineers in design.

Figure 6.20 shows a significant increase of displacement of the retaining wall during waiting periods. If we take the excavation depth of 8.6 m for example, the period between the 256th day and the 281st day of construction, the maximum deflection increased from the original 4.40–4.81 cm. Figure 6.21 shows the relationship between the maximum wall deflection rates $(\Delta\delta/\Delta t)_{max}$ and the excavation depths. The maximum wall deflection rate is defined as the maximum wall deflection increment divided by the waiting time. We can see from the figure that the deeper the excavation the higher the deflection rate. Besides, inclinometer casings were also installed in the soil outside the excavation zone and the monitoring results showed that the characteristics of the lateral deflection rate of the soil were similar to those of the retaining wall. The farther the soil is from the retaining wall, the lower the lateral deflection rate is. The reason may be that the stress level grows smaller with the increase in distance from the retaining wall (the stress level is the ratio of the shear stress in soil to the shear strength. At failure, the stress level equals 1.0). The lower the stress level

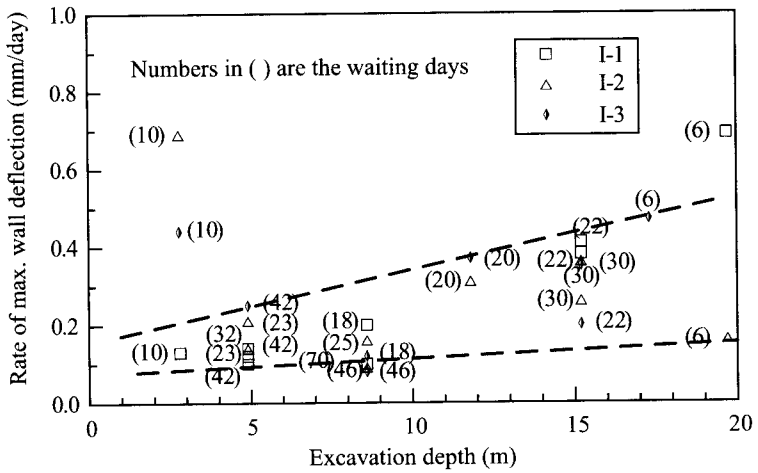

Figure 6.21 Relationships between the rates of maximum wall deflection and excavation depths of the TNEC excavation (Ou *et al.*, 1998).

is, the less obvious the creep behavior is. Ou *et al.* (1998) found from case studies of the TNEC excavation that the deflection of the wall generated during the waiting periods added up to 30–35% of the total deflection, a fairly high percentage.

Mana and Clough (1981) found that when the factor of safety against basal heave is small, creep often happens, based on case studies of excavations in Chicago and San Francisco. Their study also pointed out that the deflection rate of walls was about 0.3–30 mm/day in these cases, which is far larger than the rate at the TNEC excavation. The reason for the significant difference should have a lot to do with the stress level of the soil. As far as the objects of Mana and Clough's study are concerned, the steel sheet pile was employed as the retaining system. Though the excavation depths were relatively small, between 9.1 and 13.5 m, the lateral deflections of the retaining walls were all so large that the soil in the vicinity of the excavation zone could be seen to be on the verge of failure. Thus, the stress levels were much larger than those in the TNEC excavation and thereby higher deflection rates were produced.

Figure 6.20b shows the settlements during the waiting periods in the various excavation stages. We can see that the settlement grew with the increase of waiting time for a certain excavation depth. Their tendencies were similar to the deformation behaviors of the retaining wall. Figure 6.22 shows the relationship between the rate of ground surface settlement ($\Delta s/\Delta t$) of the soil 13 m from the retaining wall and the excavation depth. The settlement rate refers to the change of settlement during the waiting time divided by the waiting time. As shown in the figure, the settlement rate ($\Delta s/\Delta t$) grows larger with the increase of excavation depth. Ou *et al.*'s study also found that the settlement produced during the waiting periods added up to 43% of the total settlement, which is a significant proportion.

Figure 6.19 also shows that the magnitude of excavation bottom movement increases with waiting time. If we judge from the causes of soil movement, we can tell that the rate of creep-induced movement increases with the increase of excavation depth and decreases with the increase of the safety factor against basal heave failure.

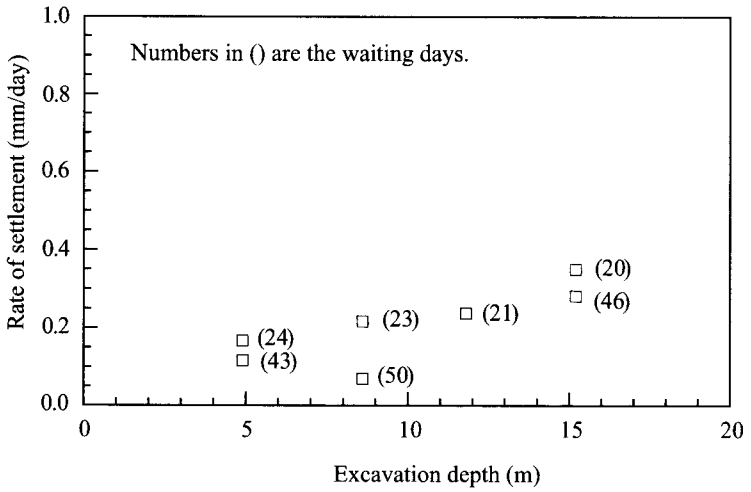

Figure 6.22 Relationships between the rates of ground surface settlement and excavation depths of the TNEC excavation (Ou *et al.*, 1998).

6.7 Analysis of wall deformations induced by excavation

As discussed in Section 6.3, in addition to soil-related factors, factors influencing the deformation of a retaining wall are the excavation width, the excavation depth, the safety factor of stability, the penetration depth of a retaining wall, the strut stiffness, and the strut preload, etc. Thus, Clough and O'Rourke (1990) established Figure 6.3 for the estimation of the maximum wall deformation for excavations in soft to medium soft clay on the basis of finite element parametric studies. The influence factors in the figure include the safety factor of stability and the stiffness of the strut retaining system (inclusive of the vertical distance of struts and the stiffness of the retaining wall), etc.

Though Figure 6.3 can be used to estimate the excavation-induced deformation of a retaining wall, it does not cover all of the influence factors. Moreover, extra parameters are required when using Figure 6.3. As a result, Figure 6.3 is too complicated to be applied for the preliminary estimation of wall deformation. According to the author's experience, Figure 6.4 or Eq. 6.1 is more useful for preliminary estimation. For a clayey soil, the upper limit in the figure or the equation is to be adopted. For a sandy soil, the lower limit. For an alternating soil of sand and clay, a middle value.

6.8 Analysis of ground surface settlements induced by excavation

This section will introduce empirical formulas to predict ground surface settlement and the characteristics of soil movement. Though many empirical formulas have been proposed, only four of the most well-known ones among them are to be discussed for reference and application without a comprehensive introduction to all of the available formulas.

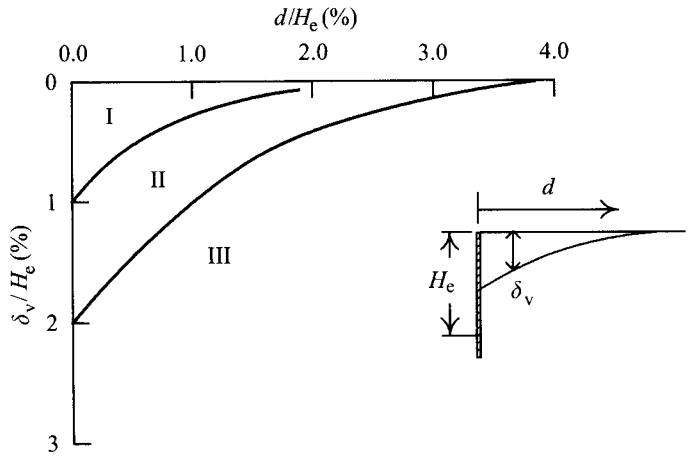

Figure 6.23 Peck's method (1969) for estimating ground surface settlement.

6.8.1 Peck's method

Peck (1969b) was the first to propose a method to predict excavation-induced ground surface settlement, based on field observations. He mainly employed the monitoring results of case histories in Chicago and Oslo and established the relation curves between the ground surface settlement (δ_v) and the distance from the wall (d) for different types of soil, as shown in Figure 6.23. The method classifies soil into three types according to the characteristics of soil:

Type I: Sand and soft to stiff clay, average workmanship
Type II: very soft to soft clay

1 Limited depth of clay below the excavation bottom
2 Significant depth of clay below the excavation bottom but $N_b < N_{cb}$.

Type III: very soft to soft clay to a significant depth below the excavation bottom and $N_b \geq N_{cb}$.

where N_b, the stability number of soil, is defined as $\gamma H_e/s_u$, where γ is the unit weight of the soil, H_e is the excavation depth, and s_u is the undrained shear strength of soil, and N_{cb} is the critical stability number against basal heave.

Since Peck's method took the monitoring results of case histories before 1969, most of which employed steel sheet piles or soldier piles with laggings as the retaining wall, quite different from the more advanced design and construction methods (e.g. the diaphragm wall method which offers higher stiffness) employed in excavation projects in recent years, the relation curves proposed by Peck are not necessarily applicable to all excavations.

Basically, the curves derived from Peck's method are envelopes. Since Peck's method is the first to derive an empirical formula to predict the ground surface settlement induced by excavation and is simple to apply, it is still used by some engineers.

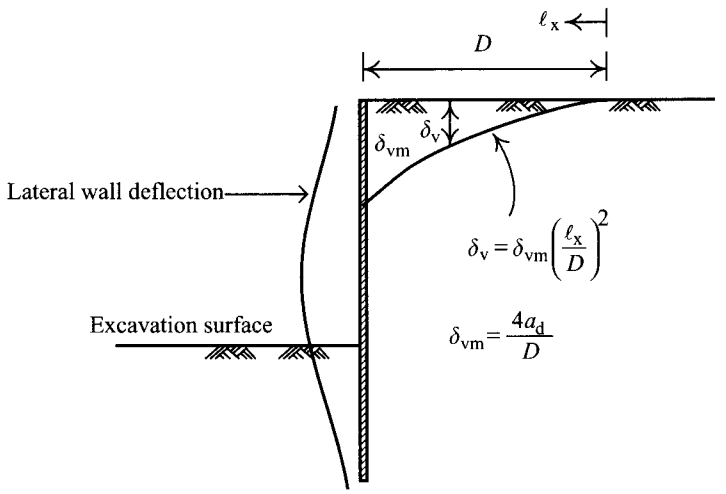

Figure 6.24 Bowles's method (1986) for estimating ground surface settlement.

6.8.2 Bowles's method

Bowles (1986) suggested a procedure to estimate excavation-induced ground surface settlements, which can be described as follows (Figure 6.24):

1 Compute the lateral displacement of the wall using the finite element method or the beam on elastic foundation method.
2 Compute the area of the lateral wall deflection (a_d).
3 Estimate the influence range of ground surface settlement (D) following Capse's method (1966):

$$D = (H_e + H_d)\tan\left(45° - \frac{\phi}{2}\right) \tag{6.6}$$

where H_e = the excavation depth; $H_d = B$ if $\phi = 0$ and $H_d = 0.5B\tan(45° + \phi/2)$ if $\phi \geq 0$, where B = the excavation width and ϕ = the parameter of soil strength.
4 Suppose the maximum ground surface settlement is located at the intersection of the wall and ground surface. Estimate the maximum ground surface settlement (δ_{vm}):

$$\delta_{vm} = \frac{4a_d}{D} \tag{6.7}$$

5 Suppose the ground surface settlement exhibits parabolic distribution. The settlement (δ_v) at ℓ_x can be computed as follows:

$$\delta_v = \delta_{vm}\left(\frac{\ell_x}{D}\right)^2 \tag{6.8}$$

where ℓ_x = distance from a point at the distance of D from the wall and δ_v = the settlement at the distance of ℓ_x.

Theoretically, excavating in undrained saturated soft soils, the area of lateral wall displacement should be about that of ground surface settlement (Milligan, 1983). Thus, δ_{vm} should equal $3a_d/D$ instead of $4a_d/D$. The value of δ_{vm} following Bowles's method is 1.33 times larger than that derived from the theoretical derivation. Bowles did not explain the reasons for using $4a_d/D$ rather than $3a_d/D$.

The method proposed by Bowles is obviously only applicable for the spandrel type of ground surface settlement.

6.8.3 Clough and O'Rourke's method

Clough and O'Rourke (1990) proposed various types of envelopes of excavation-induced ground surface settlements for different soils on the basis of case studies. According to their studies, excavation in sand or stiff clay will tend to produce triangular ground surface settlement. The maximum settlement will be found near the retaining wall. The envelopes of ground surface settlement are as shown in Figures 6.25a and 6.25b, whose influence ranges are separately $2H_e$ and $3H_e$ where H_e is the final excavation depth. Excavation in soft to medium clay will produce a trapezoidal envelope of ground surface settlement, as shown in Figure 6.25c. The maximum ground surface settlement occurs in the range of $0 \leq d/H_e \leq 0.75$ while $0.75 \leq d/H_e \leq 2.0$ is the transition zone where settlement decreases from the largest to almost none. Basically, the curves in Figure 6.25 are also envelopes.

6.8.4 Ou and Hsieh's method

Ou and Hsieh (Ou and Hsieh, 2000; Ou *et al.*, 2005) developed a method to predict the ground surface settlement on the basis of studies of the type of ground surface settlement, the influence zone, the location of the maximum settlement, and the maximum settlement. We proposed settlement curves for the spandrel and the concave types, as shown in Figure 6.26.

Line segment **ab** in Figure 6.26a, with a steeper slope, represents the primary influence zone, which will generate a larger angular distortion as far as the adjacent structures are concerned. Thus, it is necessary to examine the safety of the adjacent structures as long as values of δ_{vm} is large. Line segment **bc** represents the secondary influence zone and has a less steep slope. Under normal conditions, settlement in the SIZ has less influence on structures.

According to Figure 6.26b, the settlement curve of the concave type can be described in three line segments. Line segment **abc** represents the primary influence zone and line segment **cd** the secondary influence zone. Their separate influences on structures are the same as described in the spandrel type.

According to Ou and Hsieh's method, the excavation-induced ground surface settlement in back of the wall can be predicted based on the following procedure:

1 Estimate the maximum lateral displacement of the wall (δ_{hm}): the methods include the simplified method (Eq. 6.1 or Figure 6.3), the finite element method, or the beam on elastic foundation method.

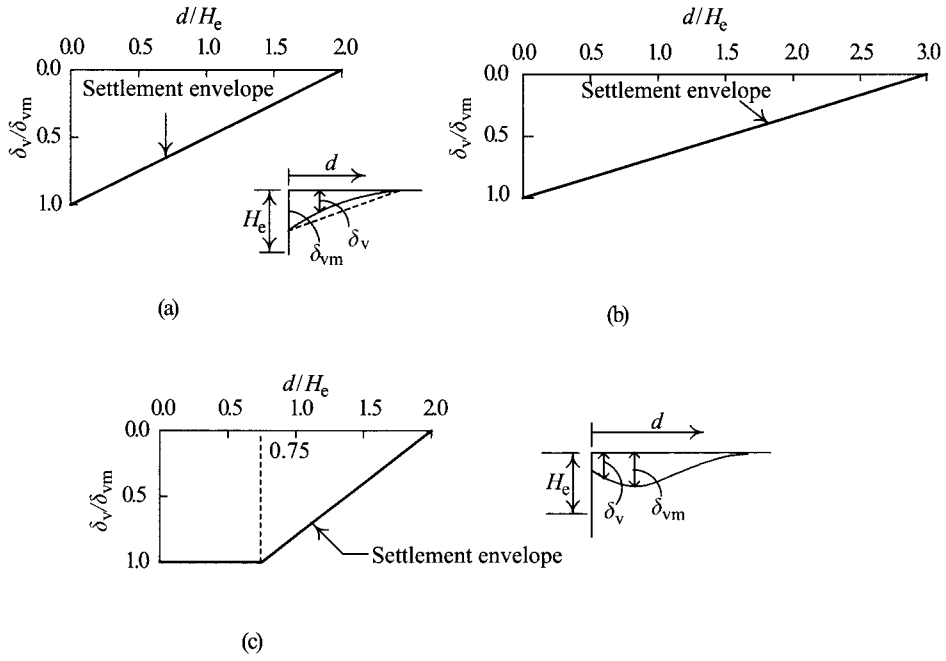

Figure 6.25 Clough and O'Rourke's method (1990) for estimating ground surface settlement: (a) sand, (b) stiff to very stiff clay, and (c) soft to medium soft clay.

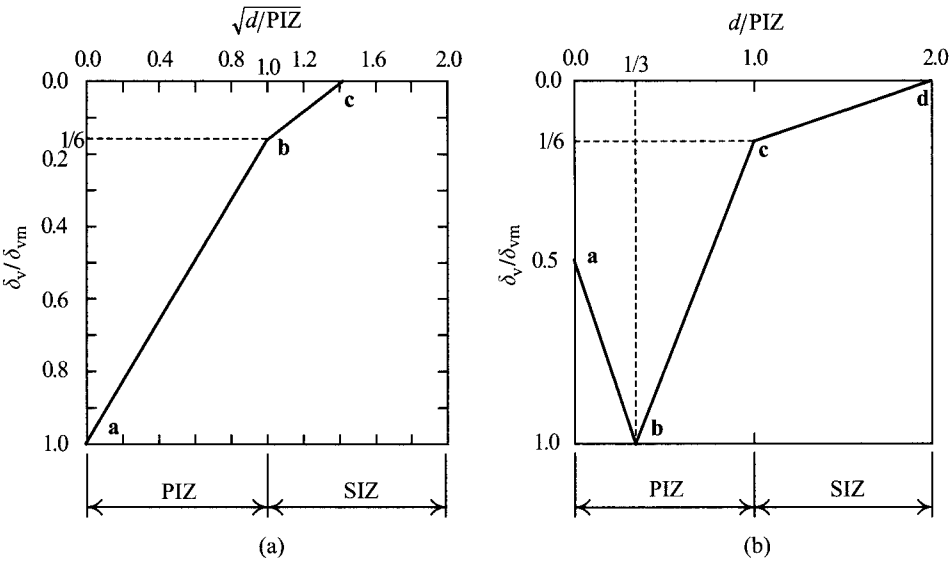

Figure 6.26 Ou and Hsieh's method for estimating ground surface settlement (Ou and Hsieh, 2000; Ou *et al.*, 2005).

2 Determine the type of ground surface settlement: Compute the lateral wall displacement from either the finite element method or the beam on elastic foundation method. Then with the help of Figure 6.12 we can basically determine the type of ground surface settlement. Or we can take advantage of the monitoring results of settlement at the initial excavation stage because the type of settlement profile emerging at the initial stages often lasts to the final stage.
3 Estimate the value of δ_{vm} on the basis of the relations between the maximum settlement (δ_{vm}) and the maximum lateral displacement (δ_{hm}) as shown in Figure 6.14.
4 According to the type of ground surface settlement determined at the second step, compute various settlements occurring in different positions in back of the wall.

6.8.5 Comparison of the various analysis methods

This section will compare the predicted ground surface settlement profile and angular distortions using Peck's method, Bowles's method, Clough and O'Rourke's method, and Ou and Hsieh's method separately with the measurement data of three excavation case histories. For the convenience of comparison, both Ou and Hsieh's and Clough and O'Rourke's methods will adopt the measurement value for δ_{vm}. As for Bowles's method, we will follow its own formula to estimate the δ_{vm}-value. The settlement profile in Peck's method will be computed adopting the boundary curve between Zone I and Zone II (the 1%-curve).

The first case history is the TNEC excavation. The excavation was 40 m wide. The retaining wall was a 35 m deep and 90 cm thick diaphragm wall. The final excavation depth was 19.7 m. The basement was constructed using the top-down construction method, which included 16 construction stages (note: seven excavation stages). As for the soil properties, the construction process, and the monitoring results of the TNEC excavation, please see the index in Appendix B.

Concerning the push-in failure, twice the excavation depth, $2H_e$, is 39.4 m, and regarding the cobble-gravel soil is regarded as a hard soil, $H_g = 46$ m, $PIZ_1 = 39.4$ m. If we regard the soil between GL-33 m and GL-35 m as hard soils, $PIZ_1 = 33$ m. With the depth of the bottom of the soft soil (H_f) being 33 m, $B = 40$ m, $PIZ_2 = 33$ m. Thus, if we follow Ou and Hsieh's method, we will conclude the primary influence zone (PIZ) is 39.4 or 33 m. Now set PIZ at 39.4 m for analysis. Figure 6.27a shows the settlement profile computed from Ou and Hsieh's method satisfactorily conforms to the field measurement. If we compute the settlement with PIZ = 33 m alternatively, the results will be even better. The settlement profile derived from Clough and O' Rourke's method can lead to a satisfactory settlement envelope as far as the primary influence zone is concerned, though the secondary influence zone is obviously ignored.

The second case history is located in the K1 zone of the Taipei Basin. The excavation was 60 m long and 35 m wide. The diaphragm wall was 31 m deep and 80 cm thick. The final excavation depth was 18.45 m. The braced excavation method was adopted with seven excavation stages. The locations of the temporary steel struts and the soil profile are as shown in Figure 6.27b, according to which we have the following data: $2H_e = 36.9$ m, $H_g = 31$ m, $PIZ_1 = 31$ m; $B = 35$ m, $H_f = 31$ m, $PIZ_2 = 31$ m. Thus, we can conclude the primary influence zone is 31 m (PIZ = 31 m).

Figure 6.27b also shows the comparisons between the measured settlement profile and those computed separately from Clough and O'Rourke's method and Ou and Hsieh's methods. As shown in the figure, the settlement profile derived from Ou and Hsieh's method is

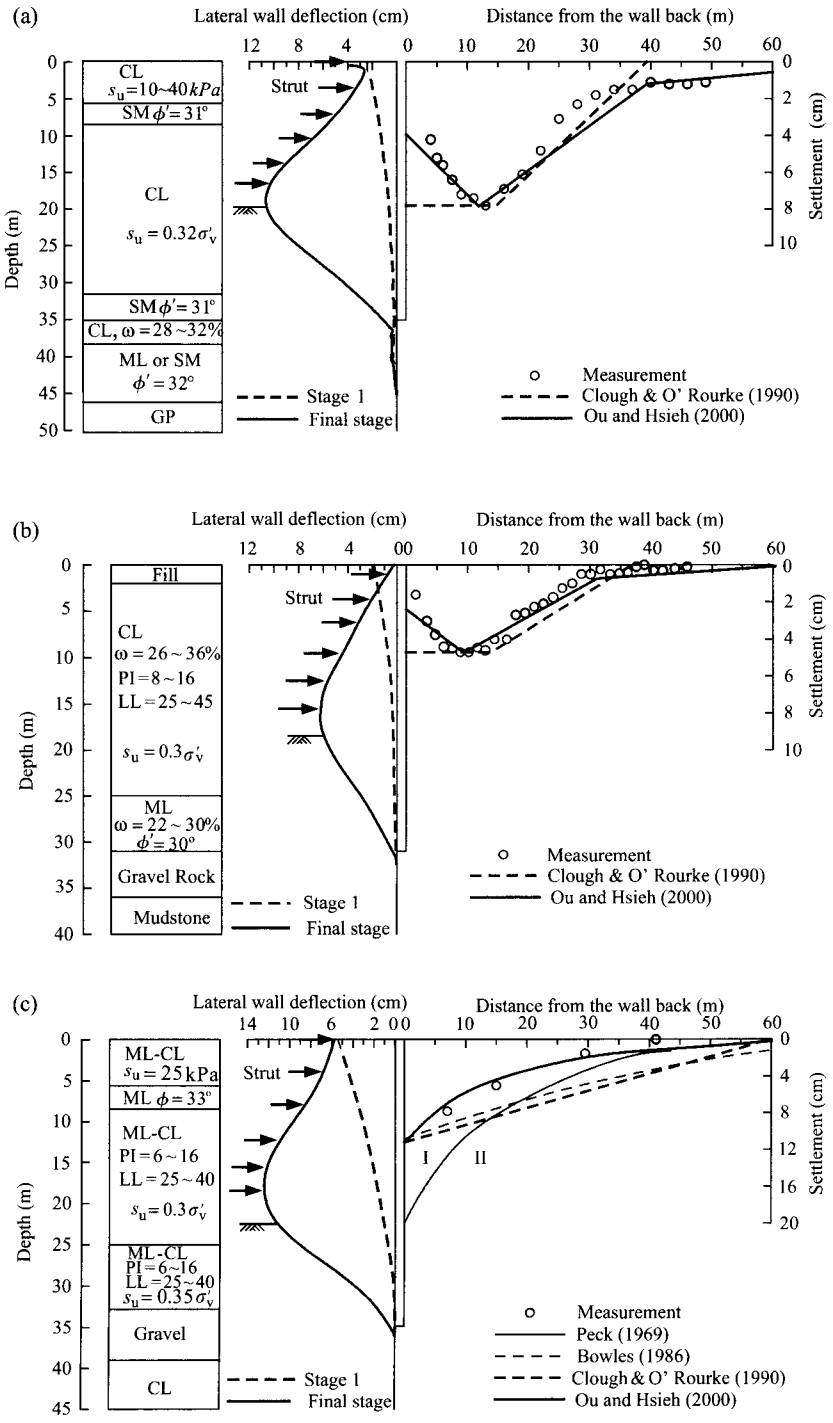

Figure 6.27 Comparisons of predicted and observed ground surface settlements: (a) Case I: the excavation of TNEC, (b) Case II: the excavation of a building, and (c) Case III: the excavation of a building.

close to the field measurement. On the other hand, the results computed using Clough and O'Rourke's method do not satisfactorily correspond to field measurements: only the settlement in the primary influence zone is enveloped and that in the secondary influence zone is quite neglected.

The third excavation case is also located in the K1 zone of the Taipei Basin. The structure has 41 floors of superstructure and 5 levels of basement. The area of the excavation site, basically a trapezoid 133–136.5 m long and 63.8–88.15 m wide, was about 10,000 m^2. The diaphragm wall was 32 m deep and 70 cm thick with the final excavation depth of 20.0 m. The top-down construction method was adopted. The locations of the lateral supports (i.e. concrete floor slabs) and the soil profile are as shown in Figure 6.27c.

We can obtain the following data from Figure 6.27c: $2H_e = 40$ m, $H_g = 32$ m, $PIZ_1 = 32$ m; $B = 64$ m, $H_f = 32$ m, $PIZ_2 = 32$ m. Thus, the range of the primary influence zone (PIZ) is 32 m. Figure 6.27c also provides the comparisons between the settlement profile computed separately from the four prediction methods and field measurement. As shown in the figure, Peck's method, represented by the 1%-curve, obviously overestimates the settlements. Bowles's method is good in estimating the maximum settlement δ_{vm} but overestimates the settlements in back of the wall and the influence range significantly. Clough and O'Rourke can hardly predict the actual conditions of settlement. The settlement profile derived from Ou and Hsieh's method satisfactorily conforms to the field monitoring results.

Angular distortion is a main factor causing damage of structures when ground settles. Thus, this section will compute the angular distortion on the basis of the monitoring results of the above three case histories and compare the results with the computed values of Ou and Hsieh's method and other empirical formulas to examine their applicability.

As shown in Figure 6.28, the definition of the angular distortion (β_{12}) between the footings F_1 and F_2 induced by settlement is given as follows:

$$\beta_{12} = \frac{\delta_{12}}{L_{12}} \tag{6.9}$$

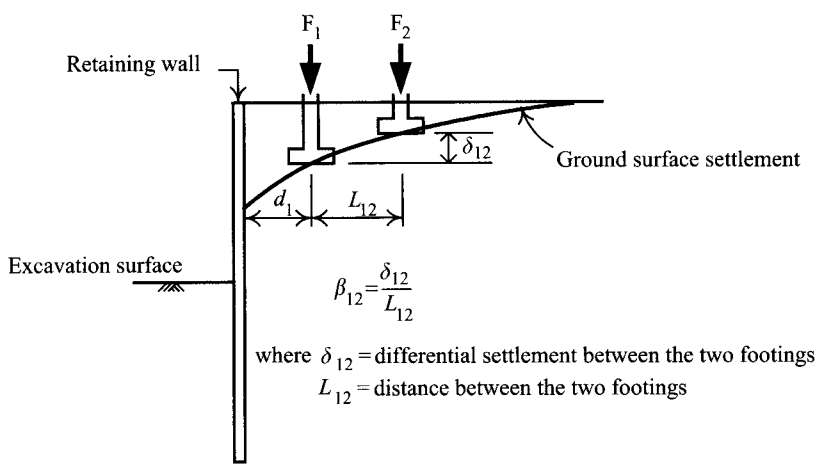

Figure 6.28 Angular distortions of footings near an excavation.

Table 6.1 Comparisons of the predicted and observed angular distortions at the final excavation stage of the case

Case	*Observation and prediction method*	d_1/H_e			
		0.0	0.5	1.0	1.5
Case I	Observation	1/200	1/5,000	1/300	1/750
	Clough and O'Rourke	0	1/7,350	1/320	1/320
	Ou and Hsieh	1/300	1/4,100	1/400	1/400
Case II	Observation	1/150	1/870	1/660	1/1,400
	Clough and O'Rourke	0	1/6,800	1/530	1/530
	Ou and Hsieh	1/390	1/540	1/520	1/750
Case III	Observation	1/180	1/370	1/450	1/820
	Clough and O'Rourke	1/540	1/540	1/540	1/540
	Bowles	1/430	1/485	1/555	1/660
	Ou and Hsieh	1/125	1/390	1/530	1/1,100

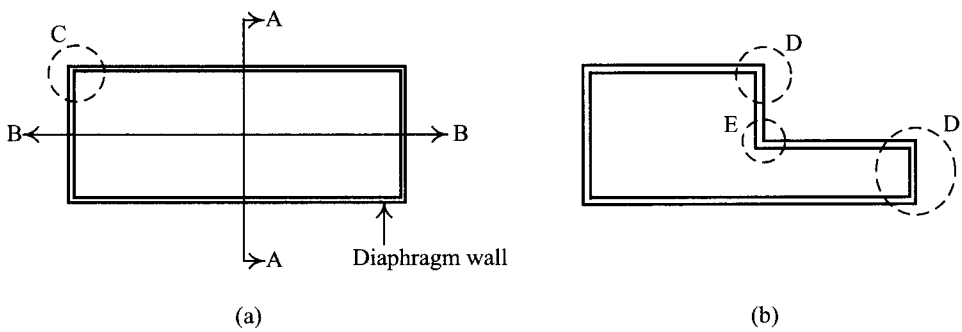

Figure 6.29 Zones of plane strain behavior and three-dimensional behavior in excavations (a) rectangular excavation and (b) irregular excavation.

where δ_{12} is the differential settlement of the two footings and L_{12} is the distance between them.

Table 6.1 offers the values of angular distortion with relation to the locations of F_1 (represented by d_1/H_e) for the three cases, given $L_{12} = 5$ m. As shown in the table, Ou and Hsieh's method obtains good results in predicting the value of angular distortion and is better than other methods.

6.9 Three-dimensional excavation behavior

Figure 6.29a shows a rectangular excavation where the deformations of the diaphragm wall near the central section of the longer side (the A–A section) are about the same. Thus, the behavior can be seen as two-dimensional plane strain behavior (as for the definition of plane strain, see Appendix D). The deformation behavior at the central section of the shorter side (the B–B section), affected by concrete arching effect, is three dimensional and the displacements of the diaphragm wall and soil are both smaller than those at the A–A section. The behaviors of the retaining wall and soil near the corner are also three dimensional (area C in the figure) and the displacements should be much smaller than those at the central section. Area D in Figure 6.29b is also under the influence of the arching effect and the displacements

of the wall and soil are smaller than those in the central section. As for area E, the conditions are opposite: the displacement of the wall and soil should be larger than in area D.

The characteristics of wall deformation, ground settlement, excavation bottom movement, and the related empirical formulas explicated earlier in this chapter all refer to the two-dimensional plane strain behavior and are not necessarily true in the vicinity of corners. With lateral stiffness, diaphragm walls have three-dimensional behaviors. Other retaining methods, such as the soldier pile, the steel sheet pile, and the column pile, do not have three-dimensional behaviors since they do not possess any lateral stiffness. Three-dimensional analysis is required to obtain correct results for excavations possessing three-dimensional behavior. The beam on elastic foundation method that will be introduced in Chapter 7 is also a two-dimensional plane strain method. The only method capable of analyzing three-dimensional problems is the finite element method.

Ou *et al.* (1996) explored the three-dimensional behaviors of an excavation using a three-dimensional finite element analysis program and obtained the plane strain ratio (PSR) of the wall displacement in terms of the width-length ratio of the excavation and the distance from the corner, as shown in Figure 6.30a. The definition of the width-length ratio (B/L) is given as shown in Figure 6.30b while that of the plane strain ratio is given by

$$\text{PSR} = \frac{\delta_{\text{hm,d}}}{\delta_{\text{hm,ps}}} \tag{6.10}$$

where

PSR = plane strain ratio
$\delta_{\text{hm,d}}$ = maximum wall deflection at the distance of d from the corner
$\delta_{\text{hm,ps}}$ = maximum wall deflection under the plane strain condition.

In analysis, the maximum displacement of the wall in the plane strain condition $\delta_{\text{hm,ps}}$ has to be determined first, using the methods explicated in Sections 6.7, 6.8, and Chapters 7 or 8, and then one should consult Figure 6.30 for PSR for the section, given the width-length ratio of the excavation and the distance from the corner. The maximum deflection, $\delta_{\text{hm,d}}$, on the section can then be computed by $\delta_{\text{hm,d}} = \text{PSR} \times \delta_{\text{hm,ps}}$.

6.10 Stress analysis

6.10.1 Struts—the apparent earth pressure method

To design a strutting system, one first has to analyze the load on the strut during excavation. The strut load can be calculated following the finite element method, the beam on elastic foundation method, or the apparent earth pressure method, the last of which will be introduced in the present section.

Peck (1969b) measured the strut loads in excavations located in Chicago, Oslo, and Mexico. Assuming the load on each level of struts is produced by the soil pressure within the range covering half the vertical span between the upper strut and the current one and half the vertical span between the current one and the lower strut, he back calculated the earth pressures from the measured strut load. The thus obtained earth pressure envelopes were then classified into three earth pressure diagrams, which are called the apparent earth pressure. Figure 6.31a illustrates the procedure of calculating the apparent earth pressure.

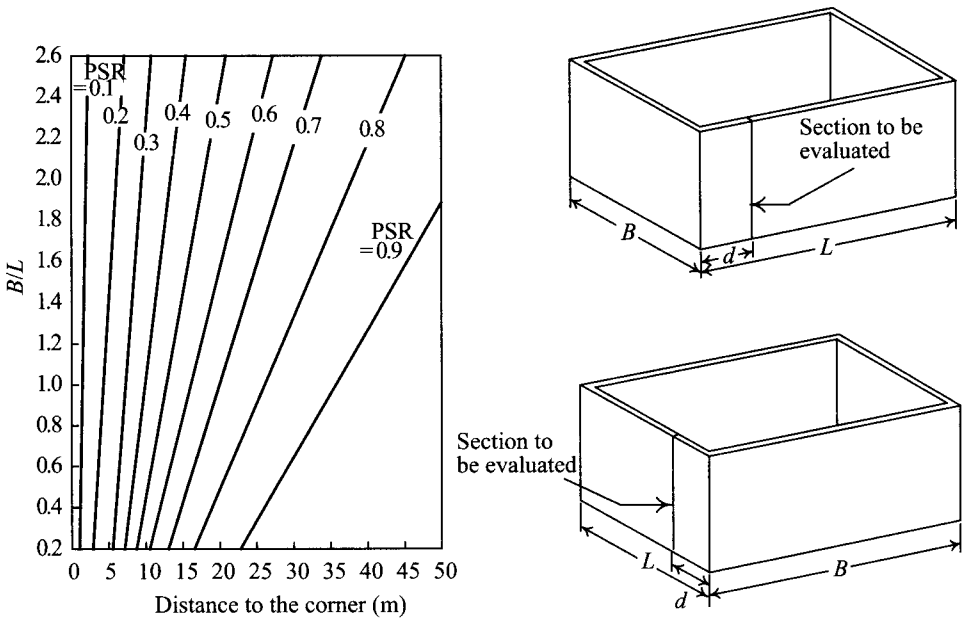

Figure 6.30 Relationship between the plane strain ratio and the aspect ratio of an excavation: (a) PSR, the width-length ratio, and the distance from the corner and (b) symbol explanation (Ou *et al.*, 1996).

Figure 6.32 shows diagrams of the apparent earth pressure established by Peck (1969b). As shown in the figure, when the soil in back of the wall mainly consists of sandy soils, the apparent earth pressure p_a will be:

$$p_a = 0.65\gamma H_e K_a \tag{6.11}$$

where

γ = unit weight of sandy soils
H_e = excavation depth
K_a = Rankine's coefficient of earth pressure = $\tan^2(45° - \phi/2)$.

Equation 6.11 adopts the effective stress method for the calculation of the apparent earth pressure, that is, the friction angle of soil refers to the drained friction angle or the effective friction angle (ϕ'); the unit weight of soil above the groundwater level refers to the moisture unit weight of soil(γ_m); the earth pressure and the water pressure below the groundwater

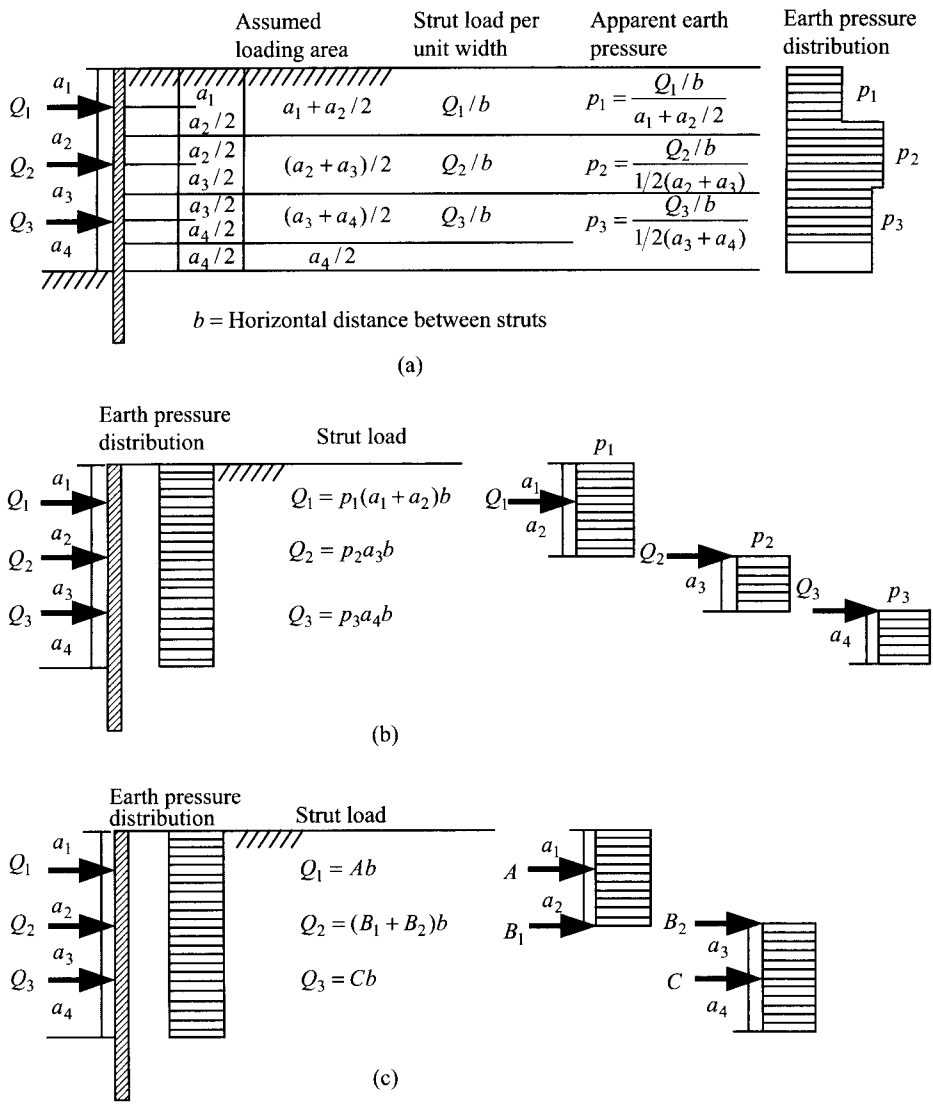

Figure 6.31 Calculation of strut load: (a) half method, (b) underneath pressure method, and (c) simply supported method.

level should be calculated separately and the unit weight of soil be taken as the submerged unit weight (γ').

If the soil in back of the wall is soft to medium soft clay (i.e. $\gamma H_e/s_u > 4$), the apparent earth pressure, p_a, would be the larger of

$$p_a = \gamma H_e \left(1 - m\frac{4s_u}{\gamma H_e}\right) \quad \text{or} \quad p_a = 0.3\gamma H_e \tag{6.12}$$

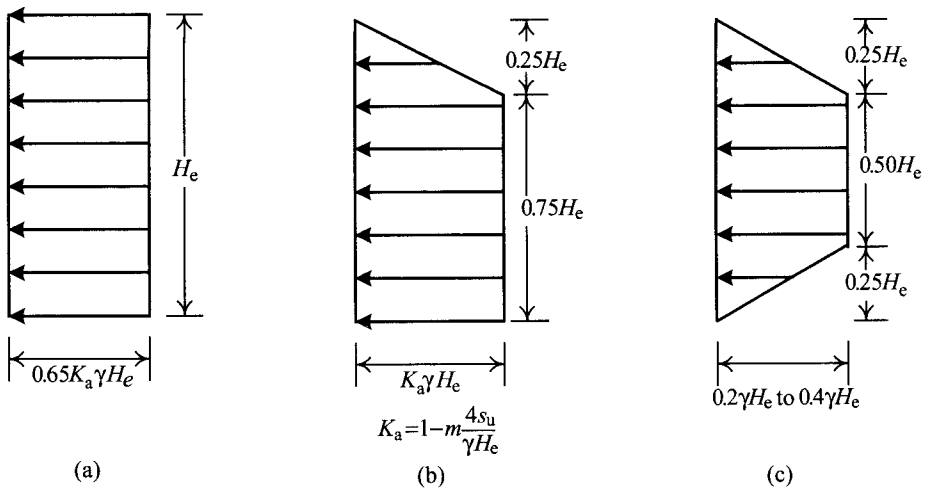

Figure 6.32 Peck's apparent earth pressure diagram: (a) sand, (b) soft to medium soft clay ($\gamma H_e/s_u > 4$), and (c) stiff clay ($\gamma H_e/s_u \leq 4$).

where

s_u = undrained shear strength of soil within the range of the excavation depth,

m = an empirical coefficient, which is related to the stability number $N_b = \gamma H_e/s_{u,b}$, where $s_{u,b}$ = undrained shear strength of soil between the excavation bottom and the influence depth of excavation. The larger is N_b, the more possible is the occurrence of large displacement at the bottom of the retaining wall. Peck (1969b) suggested $N_b \leq 4$, $m = 1.0$; $N_b > 4$, $m < 1.0$.

Equation 6.12 should be used based on the total stress method, that is, it assumes $\phi = 0$ without the porewater pressure considered.

If the soil in back of the wall is stiff clay ($\gamma H_e/s_u \leq 4$), the apparent earth pressure p_a would be:

$$p_a = 0.2\gamma H_e \sim 0.4\gamma H_e (\text{the average is } 0.3\gamma H_e). \tag{6.13}$$

Similarly, Eq. 6.13 should be used based on the total stress method. Nor does it have the porewater pressure considered. In addition to Peck's diagrams of the apparent earth pressure, Terzaghi and Peck (1967), and many other investigators have also recommended similar types of diagrams. Peck's diagrams of apparent earth pressures are the most commonly applied in engineering design, though.

As for alternating layers of sand and clay, two ways of calculating the apparent earth pressure are available. The first is to judge which, sand or clay, is the dominant soil within the range of the excavation depth, and then consult Figure 6.32 to calculate the apparent earth pressure. The other is to apply the concept of the equivalent cohesion to calculating the apparent earth pressure (Peck, 1943). As shown in Figure 6.33a, the equivalent strength of

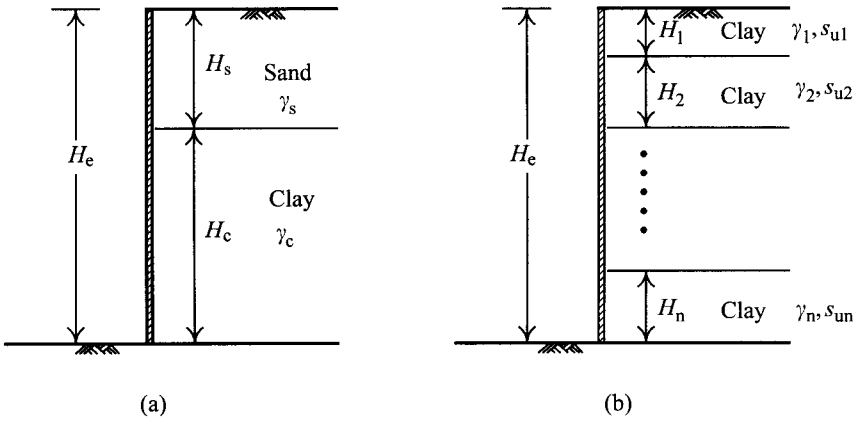

Figure 6.33 Multiple layers in excavations: (a) sand and clay and (b) multilayered clay.

alternating layers can be calculated as follows:

$$s_{avg} = \frac{1}{2H_e}\left[\gamma_s K_s H_s^2 \tan\phi_s + 2(H_e - H_s)n' s_u\right] \tag{6.14}$$

where

H_e = excavation depth
γ_s = unit weight of sand
H_s = height of the sandy soil layer
K_s = coefficient of lateral earth pressure
ϕ_s = friction angle of sand
s_u = undrained shear strength of clay
n' = coefficient of progressive failure (whose value is between 0.5 and 1.0 and has an average of 0.75).

The average unit weight of the alternating layers is

$$\gamma_{avg} = \frac{1}{H_e}\left[\gamma_s H_s + (H_e - H_s)\gamma_c\right] \tag{6.15}$$

where γ_c = unit weight of clay.

Similarly, for layered clayey strata, the concept of equivalent values can also be used to calculate the strut load, as shown in Figure 6.33b. The equivalent strength of clay would be

$$s_{avg} = \frac{1}{H_e}(s_{u1}H_1 + s_{u2}H_2 + \cdots + s_{un}H_n) \tag{6.16}$$

where $s_{u1}, s_{u2}, \ldots, s_{un}$ = undrained shear strength of the 1st, 2nd, nth layer, respectively.
$H_1, H_2, \ldots, H_n$ = height of the 1st, 2nd, nth layer, respectively.

The equivalent unit weight of clay would be

$$\gamma_{avg} = \frac{1}{H_e}(\gamma_1 H_1 + \gamma_2 H_2 + \cdots + \gamma_n H_n) \tag{6.17}$$

where $\gamma_1, \gamma_2, \ldots, \gamma_n$ = unit weight of the 1st, 2nd, nth layer, respectively.

Providing the equivalent strength (or the cohesion) and the equivalent unit weight as derived above, consult Peck's diagrams of the apparent earth pressures and choose a proper distribution of earth pressures. We then have the strut load. There are three methods for the calculation of the strut load: the half method, the underneath pressure method, and the simply supported method.

The half method assumes the load on each level of struts is the resultant of the earth pressure within the range covering half the vertical span between the upper and current struts and half the vertical span between the current and lower struts. The calculating procedure of the half method is the reverse procedure of Figure 6.31a. The underneath pressure method assumes the load of a strut is the resultant of the earth pressures below the strut. The method considers the load on the strut is small when the strut is freshly installed and it will increase with the advance of excavation. The load on the strut will change little after the installation of the next strut, whereas the load on the next strut stays small since it is newly installed. The underneath pressure method is to deal with such conditions as shown in Figure 6.31b. The simply supported method assumes the support of the strut to the wall is hinged. The calculating process is as shown in Figure 6.31c.

Since the apparent earth pressure method is highly empirically oriented, accuracy would be doubtful. The half method is the most commonly adopted because of the simplicity in calculation.

From the above discussion we can see that the apparent earth pressure is the earth pressure derived from the strut load rather than from the true earth pressure. Thus, the apparent earth pressure is only used to calculate the strut load. Though some engineers adopt the apparent earth pressure for the calculation of the stress/bending moment of the retaining wall, it is incorrect.

Since the apparent earth pressure diagram was established 20 or 30 years ago, both excavation scale and depth have become larger, and some people doubt the applicability, considering that excavation depth and retaining systems having remarkably advanced. According to many documents and empirical experience, nevertheless, the apparent earth pressure method is still useful for excavations not deeper than 10 m. As for deep excavations (over 20 m), the applicability of the method needs more examination.

6.10.2 *Cantilevered walls—the simplified gross pressure method*

As explained in Section 5.4, the design of a cantilevered wall is based on the fixed earth support method, that is, the embedded part of the wall is assumed to be fixed at a certain depth. Thus, in the limiting state, the active earth pressure above the excavation surface can develop fully whereas the passive and active earth pressures near the fixed point can not, as shown in Figure 5.25. On the other hand, under working load, though the active earth pressure above the excavation surface may still fully develop, the passive as well as the active earth pressures near the fixed point are not fully developed. It is therefore difficult to estimate the distribution of earth pressure on the retaining wall. To be conservative and simplify the

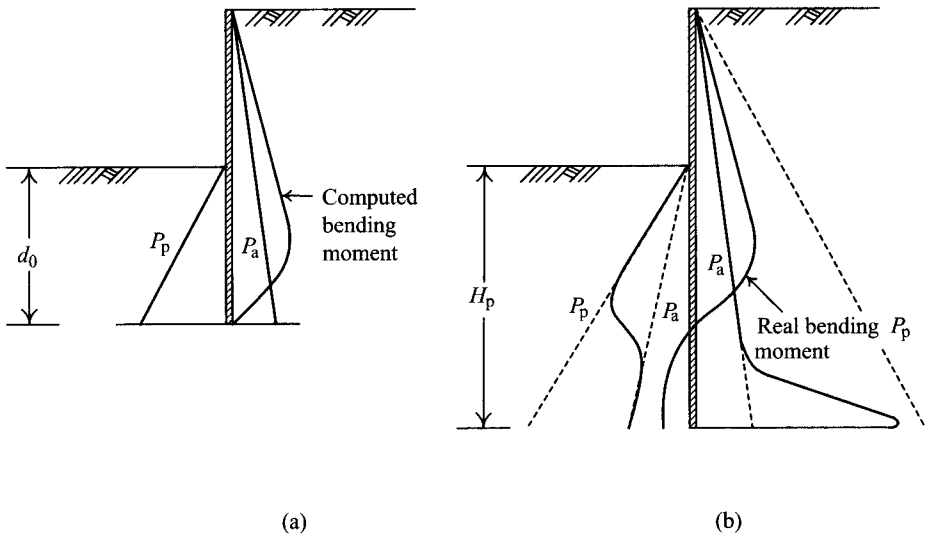

Figure 6.34 Computation of bending moment of cantilever walls: (a) bending moment computed from simplified analysis and (b) real bending moment.

procedure of computing the stress of cantilevered walls, we may assume the earth pressure is in the limiting state.

With the earth pressure on the wall known, we can then adopt the simplified gross pressure method for the analysis of the stress of a cantilevered wall (Padfield, and Mair, 1984), as shown in Figure 6.34a (please also see Section 5.6). The earth pressure distribution must not include the safety factors or the distribution of earth pressures will be distorted. Though the depth of the wall used for analysis, as shown in Figure 6.34a, is not as deep as designed (Figure 6.34b), the maximum bending moment of the wall thus derived is closest to the real value, as shown in Figure 6.34b. If sheet piles or soldier piles are to be adopted, we can design according to the maximum bending moment without knowing the distribution of bending moments. If the retaining wall is an RC wall (such as diaphragm walls or column piles), the bending moment derived from the simplified method has to be modified. The way to perform modification is as illustrated in Example 6.3.

The stress analyses of cantilevered walls can also follow the net pressure method as introduced in Section 5.6. To analyze the stress/bending moment of a cantilevered wall using the net pressure method is similar to that of using the gross pressure method and is not to be discussed here.

6.10.3 Strutted walls—the assumed support method

The design of a strutted wall is usually based on the concept of the free earth support method. Thus, in the limiting state, both the active and passive earth pressures can fully develop. If multilevel strutted walls are regarded as continuous beams, though the earth pressures on the wall are given, the stress/bending moment of the strutted wall may not be able to be computed by way of simple structural mechanics or hand calculation. Moreover, under working load,

the active earth pressure on the back of the wall may be fully developed whereas the passive earth pressure rarely is. As a result, if we adopt the method of hand calculation to solve the problem, we have to first simplify the boundary conditions and loading pattern.

The assumed support method simplifies the interaction between the soil and wall as the lateral earth pressure on the wall, and the soil resisting against the wall movement as centered on an assumed support point. The retaining wall is simulated as a simply supported beam or continuous beam to solve the problem by simple structural mechanics. With the merits of simple computation of the highly indeterminate beam, in the past the assumed support method was often adopted to obtain the stress/bending moment of the wall for deep excavation problems. Because many high-level analysis methods have been coded into computer programs, the assumed support method has lost its standing in engineering design. It can, nonetheless, still be helpful in some small scale excavation projects in case computer programs are not available. The procedure can be described in three parts:

6.10.3.1 Distribution of lateral earth pressure

As explained in Chapter 5, the design of a strutted wall is based on the concept of the free earth support method and the earth pressure on the back of the wall can be assumed as the active earth pressure. The distribution of the earth pressures should be as close as possible to the real earth pressure distribution, so, it follows that no safety factors, which will distort the real distribution, are to be included.

Following the conclusions of Chapters 4 and 5, Caquot-Kerisel's or Coulomb's active earth pressure (with the values of the two similar, see Section 4.5.3 or Figure 4.9) can be regarded as the true active earth pressure for cohesionless soil, providing a reasonable friction angle δ between the wall and soil is assumed. The adhesion between the wall and soil should be included in the estimation of the earth pressure for cohesive soil. On the other hand, since Rankine's active earth pressure is slightly larger than that of Caquot-Kerisel's and the assumed support method is a highly empirically oriented method, Rankine's earth pressure is often used, considered as being conservative. In the case of sandy soils with high groundwater levels, the water pressure should be considered in analysis, as explained in Chapter 5.

Some books may assume the earth pressure on the back of the wall to be Peck's apparent earth pressure, as show in Figure 6.32, when dealing with the stress/bending moment of the wall. The assumption is, however, incorrect. The reason is that the apparent earth pressure is only used for the calculating of the strut load and can not be used to calculate the stress of the wall.

6.10.3.2 Location of the assumed support

Retaining walls will move toward the excavation zone due to the lateral earth pressure and the soil from inside will produce passive resistance accordingly. If the passive earth pressure is viewed as a concentrated reaction force, the action point of this concentrated reaction force is designated as the assumed support. The determination of the assumed support can follow one of the methods as below:

1 At each stage of excavation, with the moments produced by the active and passive earth pressures with respect to the lowest level of struts respectively in equilibrium, the

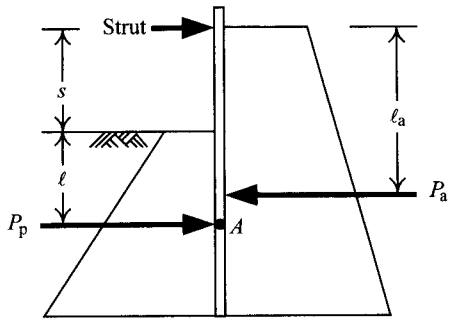

A is the location of the assumed support

Figure 6.35 Determination of the location of the assumed support by way of the moment equilibrium of earth pressures below the lowest level of struts.

action point of the passive earth resultant would be the assumed support. As shown in Figure 6.35, the location of the assumed support (ℓ) is determined as follows:

$$\ell = \frac{P_a \ell_a}{P_p} - s \tag{6.18}$$

2 According to the stiffness of soil, the location of the assumed support can be determined as illustrated below:

	Sandy soils	*Clayey soils*	*The locations of the assumed supports*
Dense soils	$N > 50$	$N > 15$	ℓ = 0–0.5 m
Medium dense soils	$10 \leq N \leq 50$	$4 \leq N \leq 15$	ℓ = 1.0–2.0 m
Soft soils	$N < 10$	$N < 4$	ℓ = 3.0–4.0 m

where N = standard penetration number ℓ = depth of the assumed support from the excavation surface. If a dense soil layer is right below a soft layer, as shown in Figure 6.36, ℓ is then the distance from the boundary of the dense layer to the assumed support.

6.10.3.3 Computation procedure

With the distribution of earth pressures and location of the assumed support both determined, the retaining wall can be seen as a simply supported beam or a continuous beam, and the stress, bending moment and deformation of the retaining wall can be obtained using simple structural mechanics. If the retaining wall is simulated as a continuous beam, the computation of stresses of the wall is complicated. Using a complicated method to solve the problem is meaningless if it cannot increase the analysis accuracy. Instead, the simply supported beam model is more often adopted.

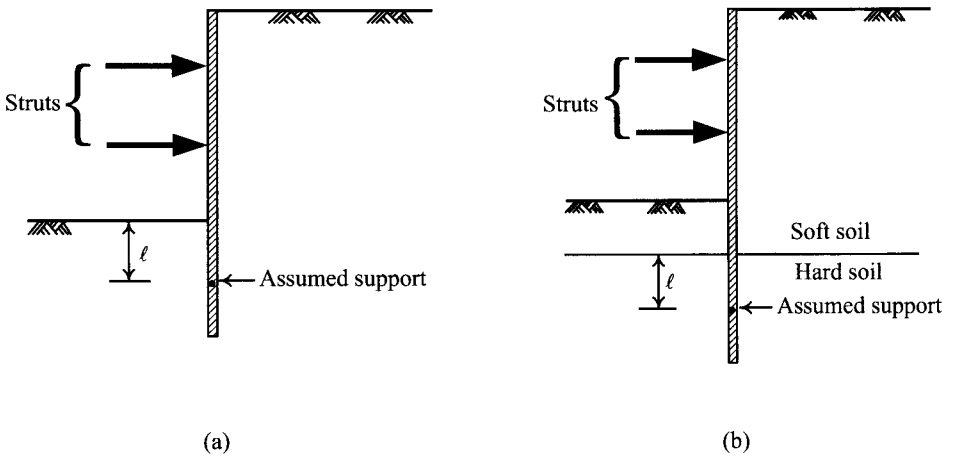

Figure 6.36 Locations of the assumed support: (a) homogeneous soil and (b) soft clay above a stiff layer.

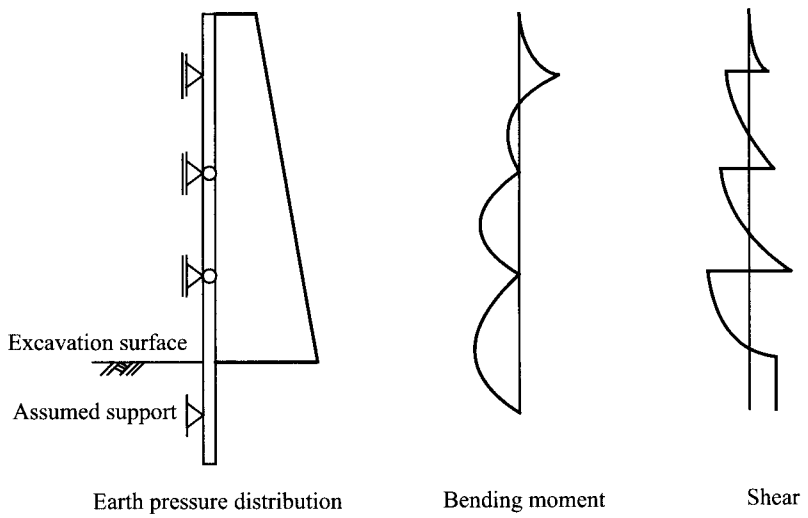

Figure 6.37 One-stage loading simply supported beam method (the simply supported beam model).

To analyze the stress/bending moment of the wall with the simply supported beam model, the earth pressure can be assumed to be added onto the retaining wall once for all. The method is designated as the one-stage loading method, as shown in Figure 6.37.

The analysis based on the simply supported beam model is also able to simulate the procedure of excavation by loading the lateral earth pressure on a simply supported beam stage by stage and then compute the stress/bending moment and deformation of the wall at each stage, which are then added up to get the total stress/bending moment and deformation, after

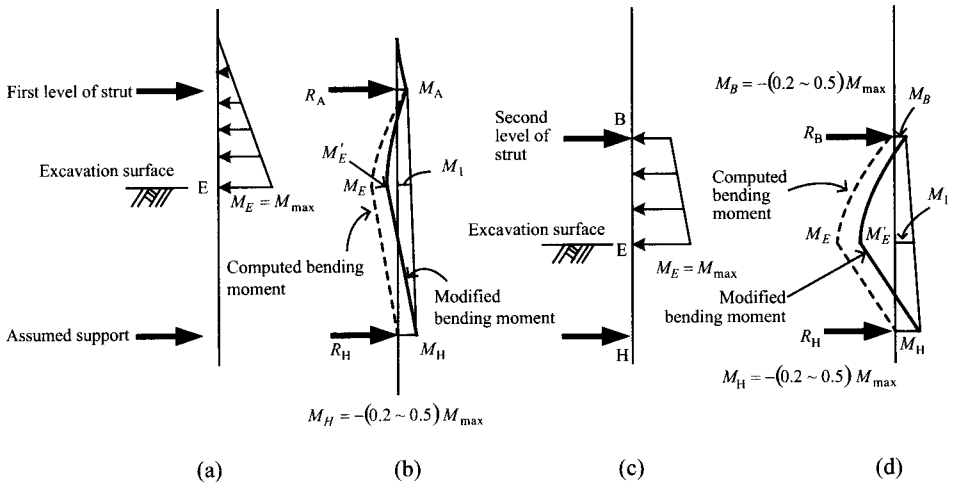

Figure 6.38 Phased loading assumed support method: (a) earth pressure distribution at the second excavation stage, (b) computation of bending moment at the second excavation stage, (c) earth pressure distribution at the third excavation stage, and (d) computation of bending moment at the third excavation stage.

excavation is finished. The method is designated as the phased loading method. The following are the principles of computation for the wall using the assumed support method with phased loading. There are also other structural analysis methods to compute the stress/bending moment of the wall. Whichever one chooses, the method should avoid complexity. The procedure of using the assumed support method is as follows:

1 Compute the bending moment for the second stage of excavation using the simply supported beam method as illustrated in Figures 6.38a and 6.38b.
2 The computing of the bending moment after the second stage: take the distribution of lateral earth pressure below the lowest level of struts to the excavation surface for each excavation stage. The computing of the bending moment is the same as shown in Figures 6.38c and 6.38d.
3 The bending moment in the position where the assumed support is located can be assumed to be 20–50% of the maximum bending moment at the stage. The greater is the soil strength in the position where the assumed support is located, the greater is the bending moment. The bending moment at the fulcrum of the strut can be similarly assumed to be 20–50% of the maximum bending moment at the stage. With the bending moments at the assumed support and at the fulcrum of the strut both determined, modify the calculated bending moments by way of the method as shown in Figure 6.38. The modified maximum bending moment would be $M'_E = M_E - M_1$.
4 As shown in Figure 6.39, to compute the bending moment of the wall at the stage of strut demolition and floor slab construction, the strut above the one to be demolished and the floor slab or the base slab can be viewed as two fulcrums, the span between which is considered as a simply supported beam. The axial load of the strut to be demolished can be viewed as a concentrated force acting on the simply supported beam, whose acting

direction is the same with that of the lateral earth pressure. The concentrated force is the sum of the strut load at the final stage of excavation and increment of strut load generated by demolition of the struts at the previous stage. The strut load at the final stage can be computed with the apparent earth pressure diagram. For example (refer to Figure 6.39), the concentrated force due to demolition of the third level of the struts (strut C) after the raft foundation construction is the strut load as computed with the apparent earth pressure diagram. The concentrated force due to demolition of the second level of struts (strut B) is the sum of the strut load as computed with the apparent earth pressure diagram and the axial increment produced by demolition of the third level of struts (strut C).

5 The bending moment or shear of the simply supported beam can be easily computed using structural mechanics. However, to match the actual boundary conditions, the bending moment at the upper fulcrum (where the upper struts are) can be assumed to be 30% of the maximum bending moment whereas that at the lower fulcrum (where the floor slabs are supported) can be assumed to be 50% of the maximum bending moment. With the bending moments at the fulcrums determined, modify the calculated values. The modified maximum bending moment would be $M'_C = M_C - M_1$ or $M'_B = M_B - M_2$ (refer to Figure 6.39).

Figure 6.40 is the calculating procedure for the assumed support method. Please note that only the bending moment and the shear derived from the method can be used for the design of a retaining wall. Though also feasible for the computing of wall deformation, with poor accuracy, the method may not work well for the protection of the adjacent property in deep excavations.

EXAMPLE 6.1

Figure 6.41 is the excavation profile of a building (Building P) in Taipei. The length of the excavation was 40 m, the width was 34 m, and the excavation depth was 12.3 m. The retaining wall was a 60 cm thick and 23 m deep diaphragm wall. The excavation was carried out in five stages. There were four levels of struts: with the completion of each excavation, one level of struts was then built. The type of the first level of struts was H steel H250 × 250 × 9 × 14, the second, H300 × 300 × 10 × 15; the third and the fourth, H350 × 350 × 12 × 19. The average distance between struts was 4.4 m. Figure 6.42 shows the wall deformations at the excavation stages measured at the central section of the longer side (the 40 m long side). Estimate the type of excavation-induced ground surface settlement.

SOLUTION

According to the figure of the lateral deformation of the wall, we have $A_{c1} = 3.7$ cm-m, $A_{c2} = 6.0$ cm-m. Thus, $A_c = \max(A_{c1}, A_{c2}) = 6.0$ cm-m, $A_s = 88$ cm-m; since $A_s \geq 1.6A_c$, the type of ground surface settlement can be predicted to be the concave type.

EXAMPLE 6.2

In Figure 6.43 are the excavation profile and geological profile of a building (Building Q) in Taipei. The excavation depth was 14.1 m. Four levels of struts were installed. The subsurface soils at the site consisted mainly of clayey soils. The groundwater level was 3 m below the ground surface. Compute the strut load following Peck's apparent earth pressure method.

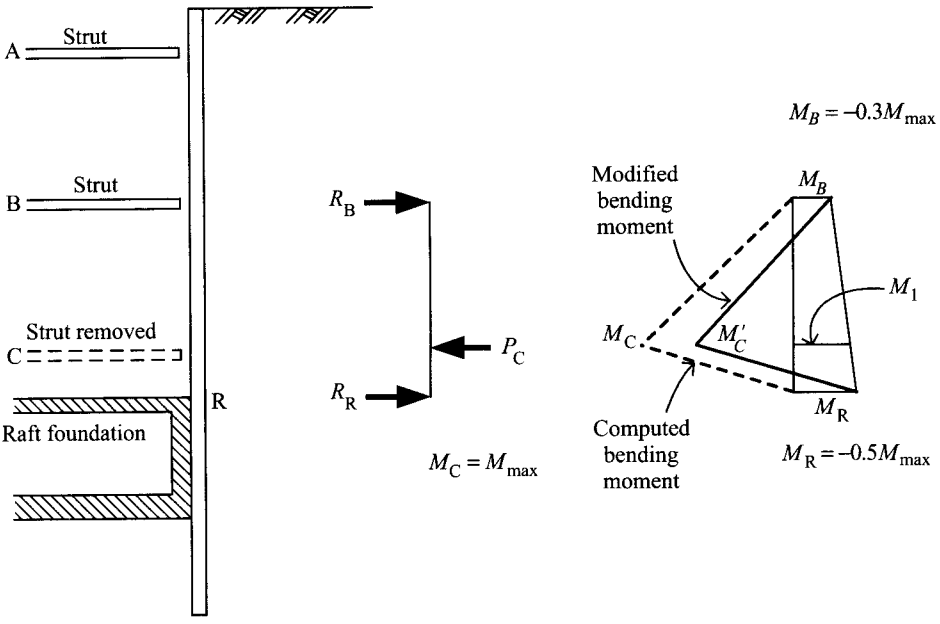

(a)

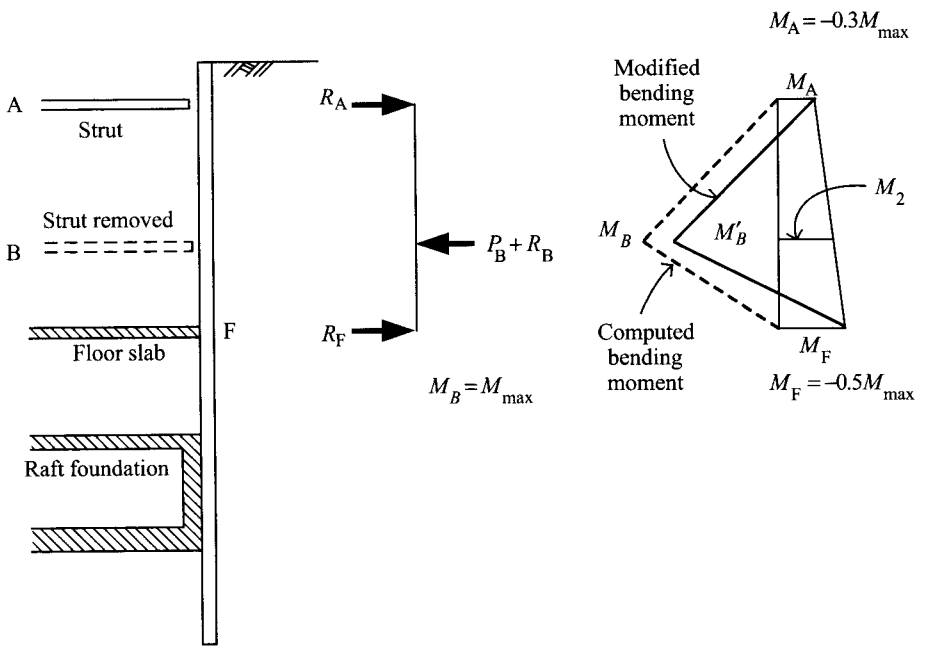

(b)

Figure 6.39 Phased loading assumed support at the stage of strut demolition (R_B, R_R, R_A, R_F are reaction forces due to demolition of the struts; P_C, P_B are strut loads at the final stage of excavation and can be computed using the apparent earth pressure diagram).

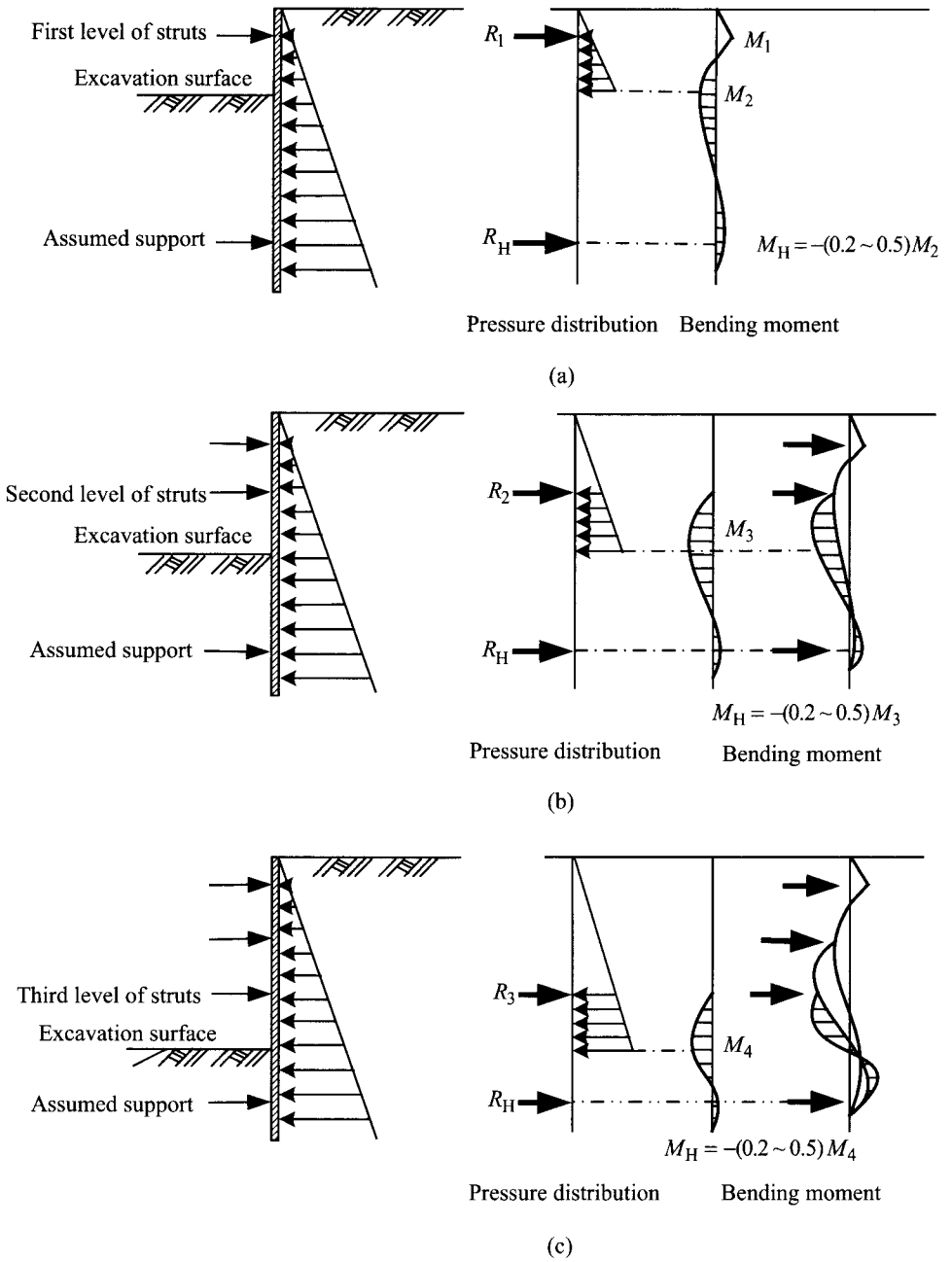

Figure 6.40 Computing procedure for the assumed supported method.

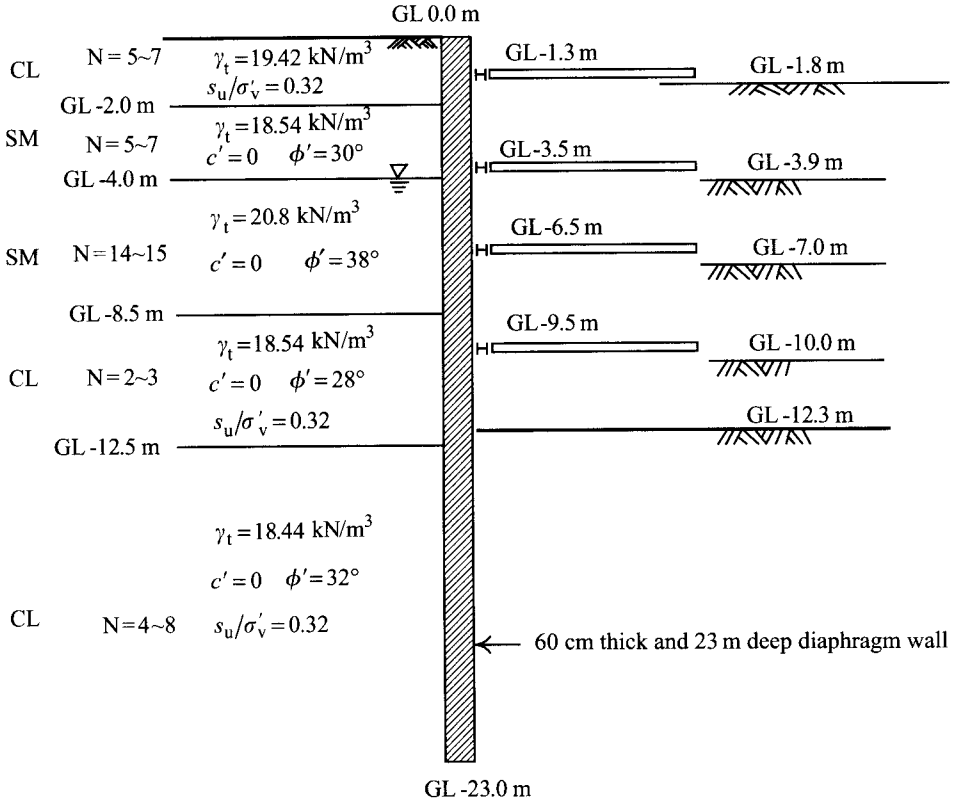

Figure 6.41 Soil and excavation profile of Building P in Taipei.

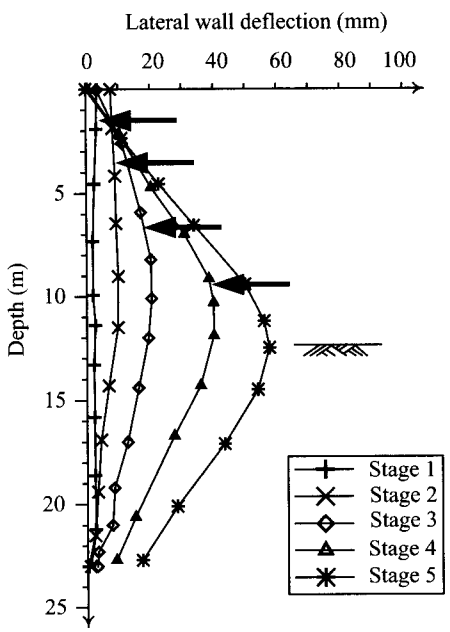

Figure 6.42 Lateral wall deflection in the excavation of Building P in Taipei.

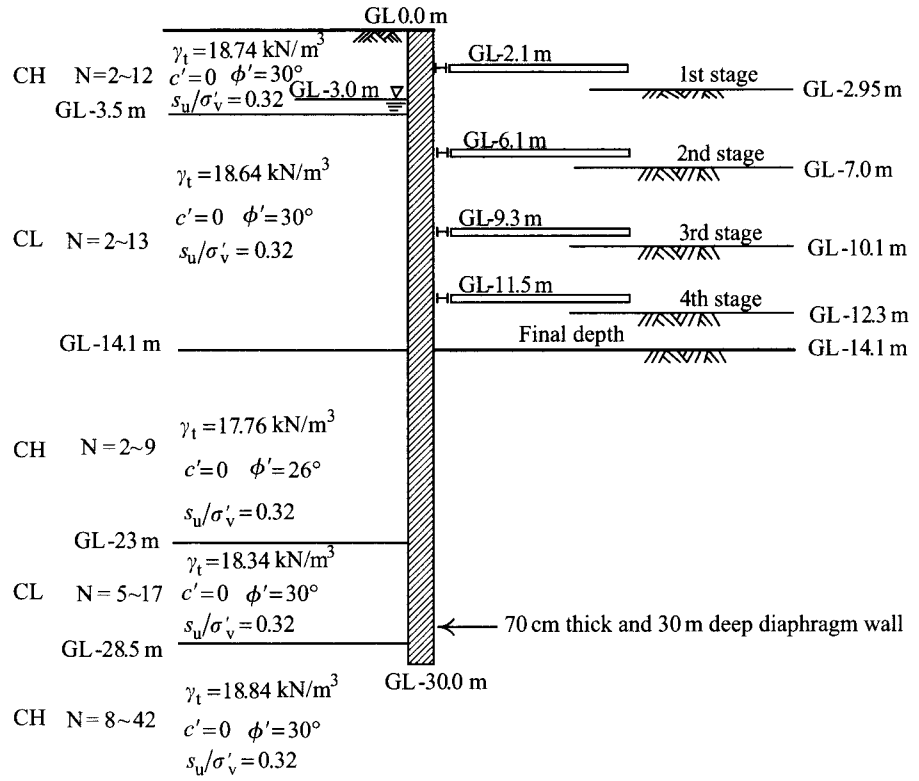

Figure 6.43 Soil and excavation profile of Building Q in Taipei.

SOLUTION

Suppose the soil above the excavation surface was clay whose normalized undrained shear strength is $s_u/\sigma'_v = 0.32$. The average unit weight of soil is $\gamma = 18.64$ kN/m^3. We can compute the undrained shear strength at the depth of 7.05 m (14.1 m/2) below the ground surface as follows:

$$\sigma_v = 18.74 \times 3.5 + 18.64 \times (7.05 - 3.5) = 131.8 \text{ kN/m}^2$$

$$u = 9.81 \times (7.05 - 3.0) = 39.7 \text{ kN/m}^2$$

$$\sigma'_v = \sigma_v - u = 131.8 - 39.7 = 92.1 \text{ kN/m}^2$$

$$s_u = 0.32\sigma'_v = 29.5 \text{ kN/m}^2$$

$$\gamma H_e/s_u = 18.64 \times 14.1/29.5 = 8.9 > 4.0$$

The soil at the site can then be categorized as soft to medium soft clay according to Peck's apparent earth pressure diagrams. The influence depth of excavation can be defined to be as

deep as the excavation width. Since the excavation width $B = 28.8$ m, the influence depth is about from the excavation surface down to $14.1 + 28.8 = 42.9$ m below it. Then the stress in the soil at a depth of 28.5 m ($14.1 + 28.8/2$) is

$$\sigma_v = 131.8 + 18.64 \times 7.05 + 17.76 \times (23 - 14.1) + 18.34 \times (28.5 - 23)$$
$$= 522.2 \text{ kN/m}^2$$
$$u = 9.81 \times (28.5 - 3.0) = 250.2 \text{ kN/m}^2$$
$$\sigma'_v = \sigma_v - u = 522.2 - 250.2 = 272 \text{ kN/m}^2$$
$$s_u = 0.32\sigma'_v = 87 \text{ kN/m}^2$$
$$N_b = \gamma H_e / s_{u,b} = 18.64 \times 14.1/87 = 2.97$$

According to Eq. 6.12, we can reasonably assume that $m = 1.0$, given the value of N_b.

$$p_a = \gamma H_e - 4s_u = 18.64 \times 14.1 - 4 \times 29.5 = 144.6 \text{ kN/m}^2$$

or

$$p_a = 0.3\gamma H_e = 78.8 \text{ kN/m}^2.$$

The apparent earth pressure is $p_a = 144.6$ kN/m^2. The distribution of earth pressure is as shown in Figure 6.44. According to the half method, the load on each level of struts would be

The load on the 1st level of struts $= 144.6 \times 3.5/2 + 144.6 \times (2 + 2.1 - 3.5) = 339.8$ kN/m
The load on the 2nd level of struts $= 144.6 \times (4.0/2 + 3.2/2) = 520.6$ kN/m
The load on the 3rd level of struts $= 144.6 \times (3.2/2 + 2.2/2) = 390.4$ kN/m
The load on the 4th level of struts $= 144.6 \times (2.2/2 + 2.6/2) = 347$ kN/m

EXAMPLE 6.3
Assume a cantilevered wall in a sandy soil, as shown in Figure 6.45a. Compute bending moment and shear using the simplified gross pressure method.

SOLUTION
Assume the friction angles between the retaining wall and soil in the active side and passive side are respectively $\delta = 2\phi'/3$ and $\delta = \phi'/2$. According to Caquot-Kerisel's earth pressure (consult Figures 4.9 and 4.10), we can obtain the coefficients of the active and passive earth pressures, which are 0.37 and 3.55, respectively. Thus, the coefficient of the horizontal active earth pressure would be $K_{a,h} = 0.37\cos(2\phi'/3) = 0.36$ and that of the horizontal passive earth pressure would be $K_{p,h} = 3.55\cos(\phi'/2) = 3.47$. Since there exists a difference between the water levels inside and outside the retaining wall, the after seepage water pressure and effective stress should be taken into account. The seepage-induced water pressure can be estimated using the method introduced in Section 4.6.6.

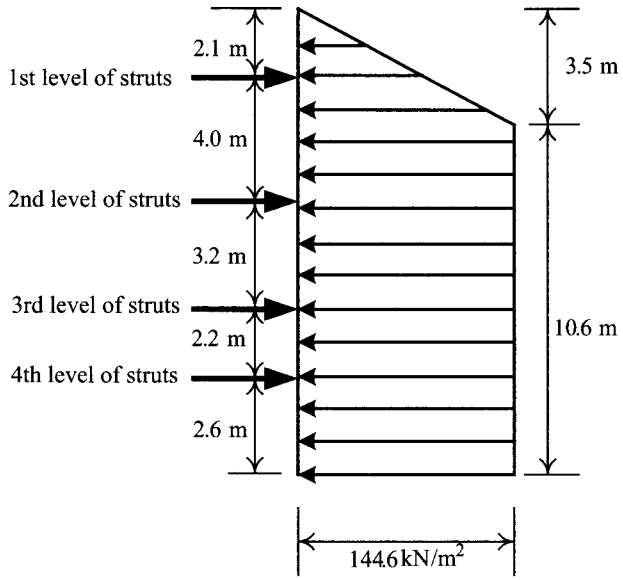

Figure 6.44 Distribution of apparent earth pressure and locations of struts.

According to the elucidations in Section 6.10.2, the distribution of earth pressure distribution for the stress analysis of a retaining wall has to exclude the factor of safety. Thus, we can compute the depth of the turning point d_0 for $F_p = 1.0$ using the simplified gross pressure method introduced in Section 5.6 and obtain $d_0 = 5.7$ m. Then, compute the distributions of the active and passive earth pressures and that of the water pressure following the methods introduced in Chapter 4. The results are as shown in Figure 6.45b. Given the distribution of earth pressures, the shear and bending moment at a point below the ground surface can be easily computed, as illustrated in Table 6.2. Figure 6.45c is the computed shear diagram. Figure 6.45d is the computed bending moment diagram. If the diagram is to be adopted for the design of reinforced concrete wall, we can assume the distribution of bending moments below the turning point to be the dotted line in Figure 6.45d.

6.11 Summary and general comments

The stress and deformation analysis of a retaining wall can adopt the simplified method, the beam on elastic foundation method, or the finite element method. This chapter introduces simplified methods, most of which are empirical formulas or diagrams based on the monitoring results of excavations. Since an excavation can be viewed as a full scale test, with the geological conditions and excavation methods similar, simplified methods based on past experience are feasible to make reasonable predictions.

Simplified methods for ground settlement induced by diaphragm wall construction are rare because of insufficient monitoring data. This chapter, however, offers some study results from the literature and the author's study of the Taipei Rapid Transit System for readers' reference.

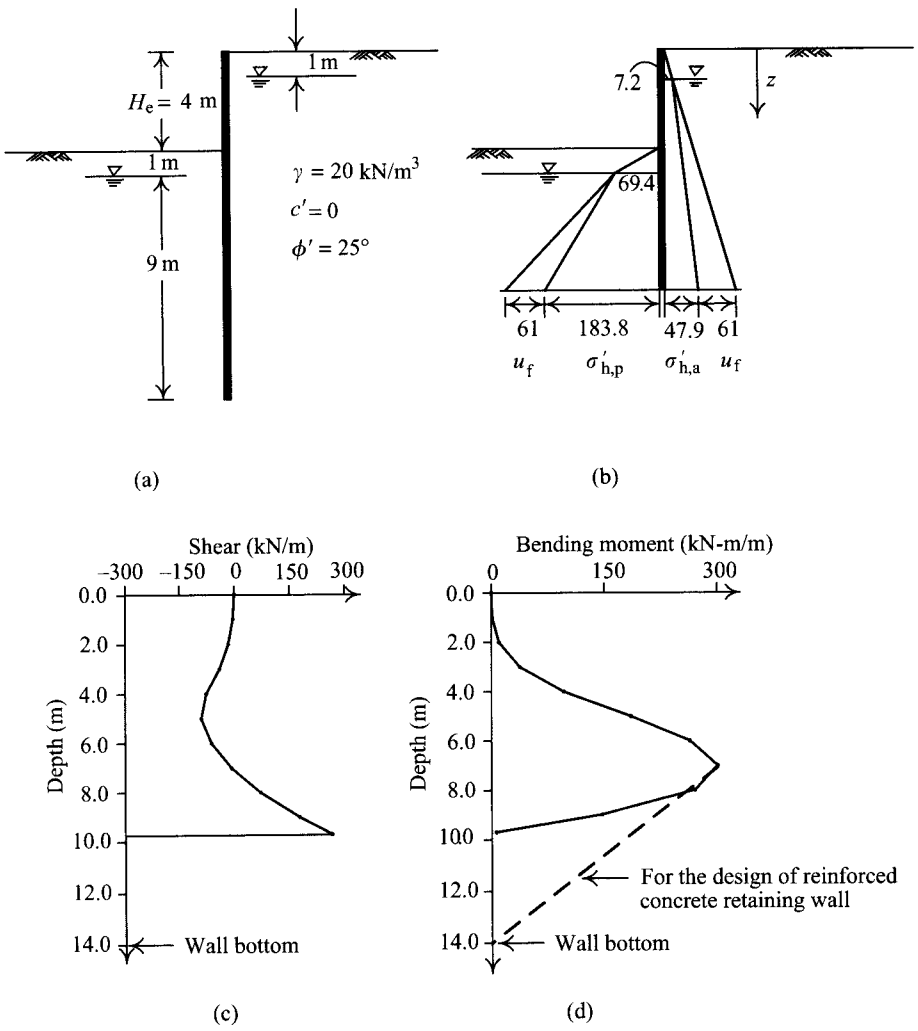

Figure 6.45 Cantilevered wall excavation: (a) excavation profile, (b) distribution of earth pressure for the simplified gross pressure method, (c) shear diagram, and (d) bending moment diagram.

This chapter also introduces, in detail, the characteristics of wall deformation, the ground surface settlement, and the excavation bottom movement and the related mechanisms of movements on the basis of both monitoring results and parametric studies using the numerical method. Since neither the beam on elastic foundation method nor the finite element method (see Chapters 7 and 8) are fully capable of predicting wall deformation or ground surface settlement, it is recommended to supplement the numerical analysis with the methods introduced in this chapter. Though many advanced and high level programs for excavation analysis have been developed, simplified methods still retain their irrefutable value in the prediction

Table 6.2 Shears and bending moments at different depths of retaining wall

Depth from ground surface (m)	*Shear* (kN/m)	*Bending moment* (kN-m/m)
0	0	0
1	−4	1
2	−17	10
3	−41	38
4	−77	96
5	−90	185
6	−62	263
7	−7	300
8	72	270
9	178	147
9.7	267	6

of wall deformation and ground surface settlement. Sometimes the results of the beam on elastic method or the finite element method also need examination by the simplified method.

The strut load can be computed using the apparent earth pressure method. The apparent earth pressure is obtained by way of back calculation from the measured strut load. With the excavation scale much larger than before and the excavation depth deeper, whether the apparent earth pressure method is still applicable in the computing of strut load has aroused many doubts. The recommendation is to limit the method to shallow excavations.

For a cantilevered wall, the real distribution of earth pressures under working load is difficult to obtain. To be conservative and simplify the calculation, the earth pressure in the limiting state can be adopted for the stress analysis of a cantilevered wall. Both the gross pressure method and the net pressure method are applicable to compute shear and bending moment of a cantilevered wall.

The shear and bending moment of a strutted wall can be computed using the assumed support method. No solid theory can be followed to locate the assumed support. Instead, it is necessary to locate it by empirical methods. Though the method is capable of calculating the stress and deformation of a wall, the deformation thus obtained is not accurate enough. For shallow excavations, the method is basically good enough in the calculation of the stress of the wall.

Problems

6.1 According to the mechanism of movements in excavations, explain the factors affecting the magnitude of ground surface settlement.

6.2 According to the mechanism of ground surface settlement, explain the causes of the spandrel and concave types of settlements.

6.3 Explain the influence of time on wall deformations, ground surface settlement, and excavation bottom movement.

6.4 Consider a five-level basement of a building (Building R), which was constructed with the top-down construction method. Figure P6.4 shows the excavation profile and the

soil conditions. The excavation was a trapezoid in plan with the length of 133–136.5 m and the width of 63.8–88.15 m. The excavation depth was 20.0 m. The diaphragm wall was 70 cm thick and 32 m deep. As shown in the figure, after the first stage of excavation of 5.0 m, the 1FL and B1FL floor slabs were simultaneously built. A level of floor slabs was constructed after each excavation stage. When the B5FL floor slab was finished, the distance between the floor slabs and the last excavation surface was 6.1 m. With such a long unsupported length, excavation was then advanced to the depth of GL-16.9 m in order to install temporary steel struts, H350 × 350 × 12 × 19 (Properties of H steel, please refer to Appendix C), with a horizontal span of 3 m, at GL-16.4 m. Use Ou and Hsieh's method to estimate the excavation-induced ground surface settlement profile for each excavation stage (note: the thickness of a floor slab is 15 cm and the strut span for the last level of struts is 3 m; we can use the simplified method to estimate the maximum wall deflection and judge the type of ground surface settlement based on the geological condition).

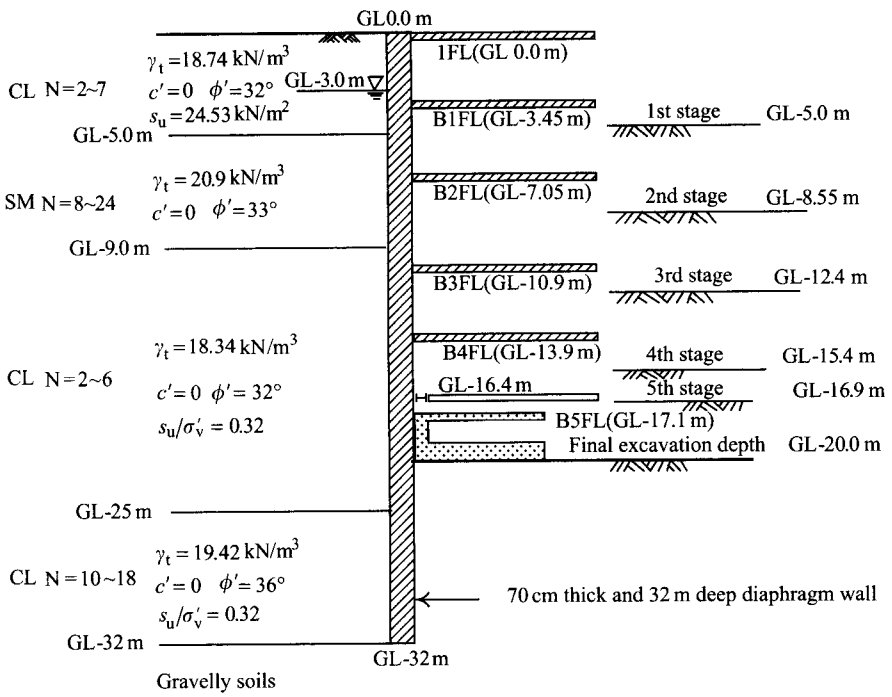

Figure P6.13

6.5 Same as the previous problem. Use Clough and O'Rourke's method to estimate the excavation-induced ground settlement profiles for all excavation stages.

6.6 Same as the previous problem but use Bowles's method to estimate the ground surface settlement profiles for all the excavation stages this time.

6.7 Compare the results of Problems 6.4–6.6 with the ground surface settlement tendencies in the excavation of TNEC (see Figure 6.8b) and explain which method to estimate the ground surface settlement is more rational and why?

6.8 Same as Problem 6.4. Assume in back of the retaining wall exists an individual footing 10 m from the wall. The base of the footing is 3 m deep below the ground surface. According to the results of Problem 6.4, estimate the settlement of the footing when the excavation reached the final depth.

6.9 Assume in back of the retaining wall, as shown in Figure P6.4, exist two individual footings which are separated by 5 m. One is 10 m from the wall while the other is 15 m from the wall. Use Ou and Hsieh's method, Clough and O'Rourke's method, and Bowles's method to estimate the angular distortion of the foundation at the final stage of the excavation.

6.10 Same as shown in Figure P6.4, use Ou and Hsieh's method, Clough and O'Rourke's method, and Bowles's method to compute the ground surface settlement at the final stage of excavation and then use the method introduced in Section 6.2 to estimate the ground surface settlement caused by the construction of the diaphragm wall. Plot the total settlement profile.

6.11 Figure P6.11 shows the excavation profile, soil conditions, and the location of groundwater for a building in Taipei (Building S). The excavation was 89 m long, 36 m wide in plan. The excavation depth was 13.7 m. The diaphragm wall was 70 cm thick and 28.5 m deep. There were four levels of struts. A level of struts was installed after each excavation stage. The first and second levels of struts were temporary steel struts H300 × 300 × 10 × 15, with a horizontal span of 5.2 m. The third level was temporary steel struts 2H300 × 300 × 10 × 15 (double struts), with a horizontal span of 5.2 m.

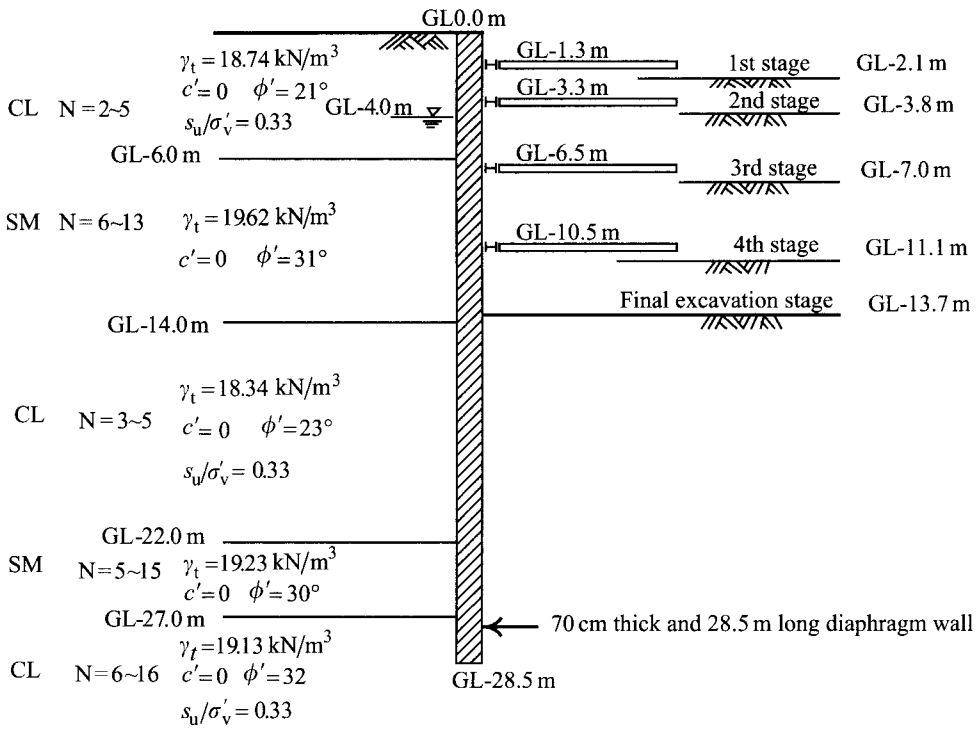

Figure P6.11

The fourth level was temporary steel struts 2H350 × 350 × 12 × 19 (double struts), also with a horizontal span of 5.2 m. Use Ou and Hsieh's method to estimate the ground surface settlement profile for each excavation stage.

6.12 Same as the previous problem. Estimate the ground surface settlement profile for each excavation stage using Clough and O'Rourke's method.

6.13 Same as Problem 6.11, use Bowles's method to estimate the ground surface settlement profile for each excavation stage this time.

6.14 Compare the results of Problems 6.11–6.13 with the tendency of the ground surface settlement in the TNEC excavation (see Figure 6.8b) and evaluate which method is the most rational. Why?

6.15 Same as Problem 6.11, assume in back of the retaining wall exists an individual footing 6 m from the wall this time. The base of the footing is 3 m deep below the ground surface. According to the result of Problem 6.11, estimate the settlement of the footing after the completion of the last excavation stage.

6.16 Assume two individual footings, 4 m from each other, are located 10 m and 14 m in back of the retaining wall as shown in Figure P6.11. Use the calculated results with Ou and Hsieh's method, Clough and O'Rourke's method, and Bowles's method separately to estimate the angular distortions after the completion of the last excavation stage.

6.17 As shown in Figure P6.11, use Ou and Hsieh's method, Clough and O'Rourke' method, and Bowles's method separately to compute the final ground surface settlement and use the method introduced in Section 6.2 to estimate the ground surface settlement caused by the construction of the diaphragm wall. Then plot the total ground surface settlement profile.

6.18 The top down construction method is characterized by using concrete floor slabs as lateral supports during excavation. The distance between floor slabs and the excavation surface should be at least 1.5 m. After the completion of each excavation stage, excavation is usually suspended for a period before proceeding to the next stage. On the other hand, the bottom-up method is characterized by using H steel as lateral struts. The distance between struts and the excavation surface is usually 0.5 m. When using the bottom-up excavation method, it is not necessary to wait before proceeding to the next stage. The axial stiffness of a floor slab is far larger than that of a H steel. Under the same excavation conditions, which will generate larger ground surface settlement when excavating in soft clay? Why?

6.19 Figure P6.19 shows the plan of an excavation and its adjacent building. Assume the excavation profile is as shown in Figure P6.4 and the soil is sandy soil. The ground water level is 2 m deep below the ground surface. The effective stress parameters for

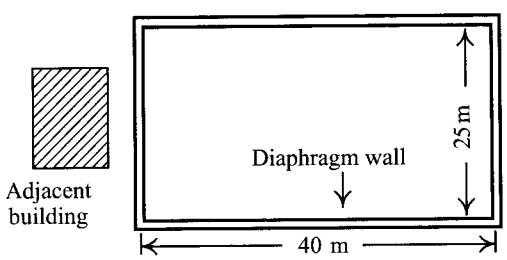

Figure P6.13

the sand: $c' = 0$, $\phi' = 32°$. Use the simplified method to estimate the maximum ground surface settlement at the section where the adjacent building is located.

6.20 Figure P6.20 shows the plan of an excavation and its adjacent building. Assume the excavation profile is as shown in Figure P6.11 and the soil is clayey soil. The groundwater level is 2 m below the ground surface. The normalized undrained shear strength $s_u/\sigma'_v = 0.3$. Use the simplified method to estimate the maximum ground surface settlement at the section where the adjacent building is located.

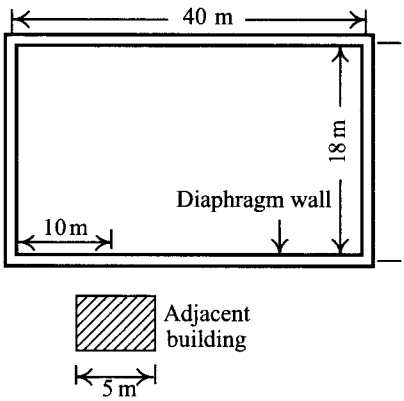

Figure P6.20

6.21 Assume an excavation as shown in Figure P6.11. The soil is clay. The groundwater level is 2 m below the ground surface. The moisture unit weight and saturated unit weight of clay is $\gamma_m = 16$ kN/m^3, $\gamma_{sat} = 18$ kN/m^3, respectively. The normalized undrained shear strength $s_u/\sigma'_v = 0.3$. Use Peck's apparent earth pressure method and the half method to compute the strut load.

6.22 Same as the previous problem except that the soil is sandy soil this time. The groundwater level is 2 m below the ground surface. The moisture unit weight and the saturated unit weight of sand are $\gamma_m = 15$ kN/m^3, $\gamma_{sat} = 19$ kN/m^3, respectively. The effective stress parameters: $c' = 0$, $\phi' = 32°$. Use Peck's apparent earth pressure method and the half method to compute the strut load.

6.23 Assume an excavation profile as shown in Figure P6.11. The soil condition is also identical with that as shown in the figure, alternating layers of sand and clay. Use Peck's apparent earth pressure method and the half method to compute the strut load.

6.24 Same as Problem 6.21, use the assumed support method with one-stage loading to compute the bending moment of the retaining wall this time.

6.25 Same as Problem 6.21, use the assumed support method with phased loading to compute the bending moment of the retaining wall this time.

6.26 Same as Problem 6.22, use the assumed support method with one-stage loading to compute the bending moment of the retaining wall this time.

6.27 Same as Problem 6.22, use the assumed support method with phased loading to compute the bending moment of the retaining wall this time.

6.28 See Problem 5.17 and Figure P5.17. Assume $H_p = 7.0$ m. Use the net earth pressure to compute the bending moment and shear of the retaining wall.

6.29 Same as the previous problem. Use the simplified gross earth pressure method to compute the bending moment and shear of the retaining wall this time.

6.30 See Problem 5.20 and Figure P5.20. Use the simplified gross earth pressure method to compute the bending moment and shear of the retaining wall.

6.31 Same as the previous problem, use the net earth pressure method to compute the bending moment and shear of the retaining wall this time.

Chapter 7

Stress and deformation analysis

Beam on elastic foundation method

7.1 Introduction

Under normal excavation conditions, the stress on and deformation of walls, or ground surface settlement relate to the unbalanced forces acting on the walls, the stiffness of the wall-strut system, the stability of the excavations and so on. The unbalanced forces are in turn related to the soil conditions, ground water levels, water pressures, the excavation width, the excavation depth, the excavation area, etc. To analyze excavation-induced deformation using the numerical method, the analysis method has to simulate all these factors rationally. The finite element method and the beam on elastic foundation method are two commonly used numerical methods. Theories concerning the finite element method are quite complicated and some of them are not fully developed. The finite element analysis normally requires enormous preprocessor and postprocessor time, computation time, and analysts have to be well equipped with comprehensive geotechnical knowledge and experience. Thus, the method is not widely adopted in the analysis and design of excavations. The beam on elastic foundation method, on the other hand, is simpler in its analysis model. With succinct input parameters, it does not take much time for processing and therefore is favored by most engineers. Nevertheless, the simplicity of the beam on elastic foundation method requires more delicacy and prudence when dealing with complicated excavation problems so that mistakes can be avoided.

Sections 7.2 and 7.3 will introduce the basic principles and formulation of the beam on elastic foundation method. For college students and engineers designing excavations, these sections can be skipped. For graduate students planning to explore the contents of the beam on elastic foundation method or to develop related computer programs, the basic principles of the finite element method that will be introduced in Chapter 8 and the present section are important references.

There exist many commercial computer programs using the beam on elastic foundation method for excavation analysis. Some of them are not based on the principles of soil mechanics. Their users' manuals may not explain well on what principles they are based. Thus, much confusion is caused. At the end, this chapter also introduces the application of computer programs and offer simple methods for verifying the basic principles on which a computer program is based in order to establish a correct analysis method. Readers are strongly advised to execute a computer program by themselves to fully understand the contents that will be introduced in this section.

As elucidated in Chapter 6, a complete stress analysis for structural design of excavations includes detailed stress analyses of many structural components such as the end brace, corner brace, wale (see Figure 3.3), the central post, etc. These contents will be introduced in Chapter 10.

7.2 Basic principles

In foundation engineering, the soil-structure interaction problem is often simulated as a series of springs to simplify analysis. Among them, Winkler's model (Winkler, 1867) is most widely applied.

As shown in Figure 7.1, the basic assumption of the Winkler model is—given that the foundation is a structure with stiffness and soils are of elastic foundation, their interaction can be simulated as a series of individual springs. The spring constant is the ratio of stress (p) to displacement (δ), which can be expressed as follows:

$$k_s = \frac{p}{\delta} \tag{7.1}$$

where the constant k_s is called the coefficient of subgrade reaction, the modulus of subgrade reaction, or the soil spring constant, the unit of which is (force) × (dimension)$^{-3}$. The strength of the Winkler model is that it greatly simplifies analysis, for it assumes the elements are individually acting without interaction.

As shown in Figure 7.2a, the beam on elastic foundation analysis of an excavation assumes the retaining wall to be a beam on an elastic foundation, which is simulated as a series of soil springs and the earth pressures on both sides of the wall before excavation are taken to be the at-rest earth pressure (K_0-condition) (see Figure 7.2b).

After excavation is started, unloading induced by excavation will cause unbalanced forces between the two sides of the wall and make the wall deform. The amount of the unbalanced force is the difference between the at-rest earth pressure on the two sides of the wall when the wall is kept unmoved, as shown as the difference between p_{02} and p_{01} in Figure 7.2c.

Acted on by the unbalanced forces, the beam is displaced, and will change the distribution of earth pressures. The earth pressure from outside is decreased to $p_0 - k_h\delta$ (k_h is the horizontal coefficient of subgrade reaction and δ is the lateral displacement of the wall) with the increase of displacement. The minimum lateral earth pressure is the active earth pressure. The earth pressure from inside is increased to $p_0 + k_h\delta$ due to the inward displacement of the wall. When soil springs develop up to the passive condition, the soil reaction on the passive side ceases increasing and stays at the passive earth pressure. This state is called the plastic state (see Figure 7.2d). When the reaction forces of soil springs are smaller than the passive earth pressure at a point, this is called the elastic state.

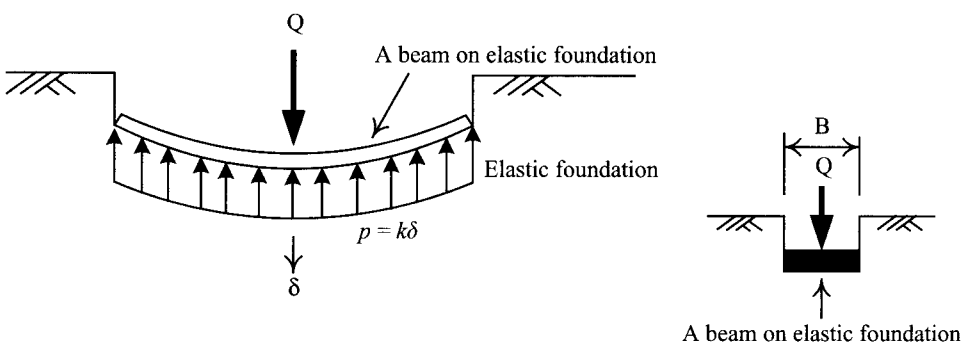

Figure 7.1 Winkler's model.

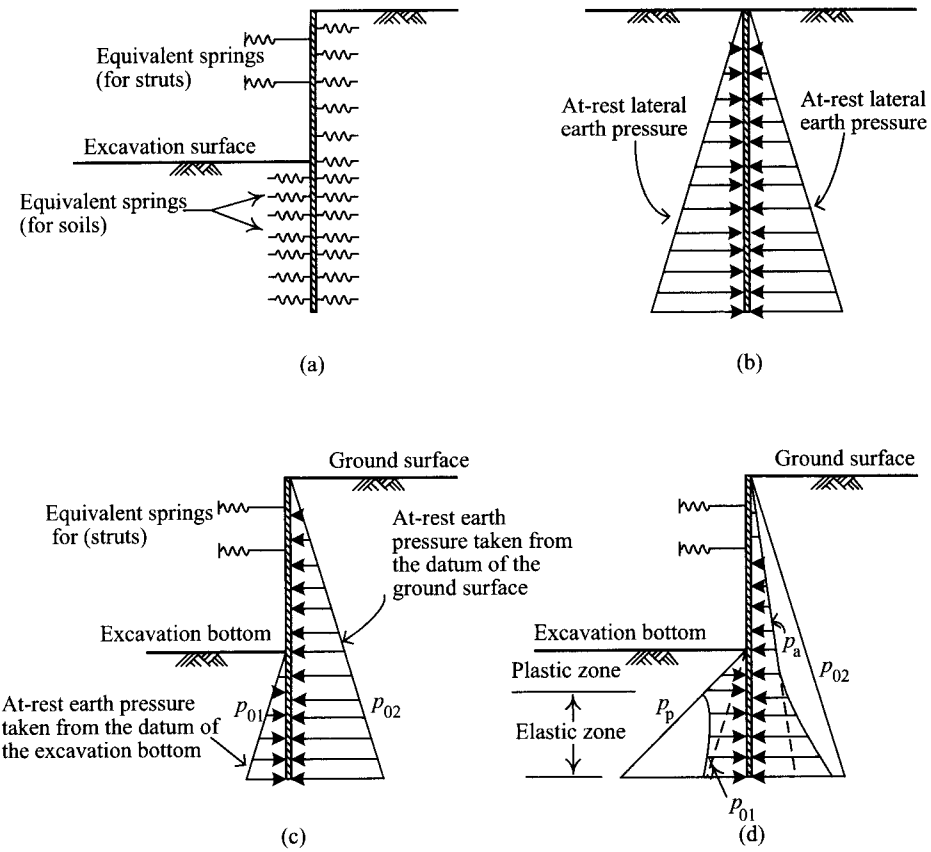

Figure 7.2 The beam on elastic foundation method: (a) springs placed at both sides of the continuous beam, (b) at rest earth pressure before excavation, (c) distribution of earth pressures on both sides of the retaining wall before wall movement, and (d) distribution of earth pressures on both sides of the wall after wall movement.

Figure 7.3 illustrates another model of beam on elastic foundation. In Figure 7.3a, the pressure acting on the back of the wall is assumed to be the active earth pressure and the resistance from inside is simulated as a series of soil springs. At each excavation stage, the active earth pressure on the back of the wall should be balanced by the internal struts and soil springs. The magnitude of the force of soil springs is the coefficient of subgrade reaction k_h multiplied by the displacement at the place. When the soils are acted on by a force smaller than the passive earth pressure at the place, this is called the elastic state. Once the displacement of the wall is large enough to develop the soil springs to the passive earth pressure, the soil reaction on the passive side ceases increasing and stays at the passive earth pressure, and is called the plastic state (see Figure 7.3b).

To consider the influence of excavation width on analysis, the active earth pressures below the excavation bottom are assumed to converge with the increase of depth till pressure convergence point is zero (Miyoshi, 1977). According to the concept of Boussinesq's pressure

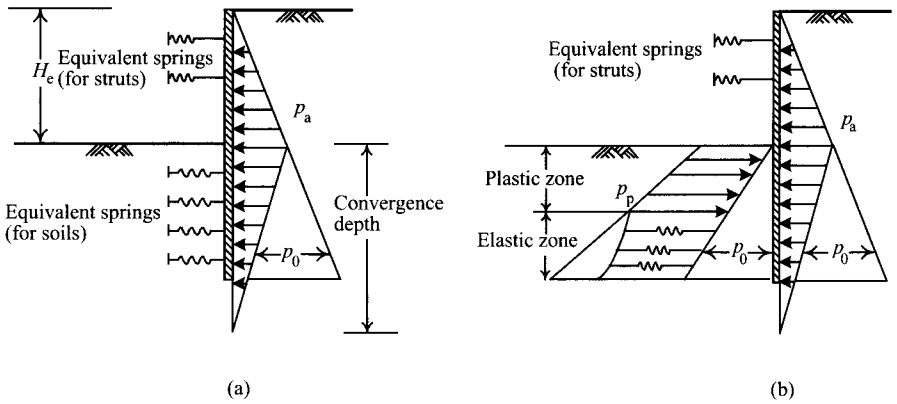

Figure 7.3 Another model of the beam on elastic foundation method: (a) springs placed at the front of the continuous beam and (b) distribution of earth pressure.

bulb, the unloading force (induced by soil removal) has an influence on the vertical plane of the wall to the depth equaling an excavation width. Therefore, the depth of the converging point can be assumed to be below the excavation bottom at a depth equaling an excavation width without going through hard soils. The passive soil reaction is thus equal to the passive earth pressure subtracting the earth pressure, p_0 (see Figure 7.3 b).

7.3 Formulation

Though the beam on elastic foundation method can be used in hand calculation, with the development of computers, most of the analysis methods are coded into computer programs, some of which have been made into commercial software. The theories of beam on elastic foundation, however, are still not complete in application and the analysis principles of these computer programs are not without dispute either. There is still much room for improvement. This section will introduce the process of mechanical computation. The part using the principle of the finite element method to introduce the mechanical computation of the beam on elastic foundation method can be ignored for undergraduate students and engineers dealing with excavation in practice. Graduate students intending to thoroughly explore the contents of the beam on elastic foundation method or develop related computer programs are recommended to refer to Chapter 8, in addition to studying this section.

According to the conception of the finite element method, the retaining wall is simulated as a continuous beam of a unit width, which will be partitioned into many beam elements. Each beam element can be further classified into basic beam elements and beam on elastic foundation elements, depending on whether there exist soil springs. The stiffness matrix is elucidated as follows:

1 Basic beam elements: A basic beam element refers to a beam element without soil springs. As shown in Figure 7.4, a beam element has four degrees of freedom. Assuming the displacement of any point on the beam in the y direction is v, the displacement equation will be

$$v = c_1 + c_2x + c_3x^2 + c_4x^3 \tag{7.2}$$

The boundary values

$$v(0) = q_1, \qquad v'(0) = -q_1' = -\theta_1$$
$$v(\ell) = q_2, \qquad v'(\ell) = -q_2' = -\theta_2$$

Thus, we can infer the displacement at x is

$$v(x) = [v][f_1, f_2, f_3, f_4] \cdot \begin{bmatrix} q_1 \\ \theta_1 \\ q_2 \\ \theta_2 \end{bmatrix} \tag{7.3}$$

where

$$\begin{aligned} f_1 &= \frac{1}{\ell^3}(2x^3 - 3x^2\ell + \ell^3) \\ f_2 &= \frac{1}{\ell^3}(-x^3\ell + 2x^2\ell^2 - x\ell^3) \\ f_3 &= \frac{1}{\ell^3}(-2x^3 + 3x^2\ell) \\ f_4 &= \frac{1}{\ell^3}(-x^3\ell + x^2\ell^2) \end{aligned} \tag{7.4}$$

The above equation can be transformed into a matrix whose form is $v = [f] \cdot [q]$ where $[f]$ is called the displacement shape function. According to the principle of virtual work (see Section 8.2), we can infer that the stiffness matrix of the beam element is

$$\begin{aligned} [K_b] &= \int_V [B]^T \cdot [C] \cdot [B] dV \int_0^L \left[\frac{d^2 f}{dx^2}\right]^T EI \left[\frac{d^2 f}{dx^2}\right] dx \\ &= \begin{bmatrix} 12EI/\ell^3 & -6EI/\ell^2 & -12EI/\ell^3 & -6EI/\ell^2 \\ -6EI/\ell^2 & 4EI/\ell & 6EI/\ell^2 & 2EI/\ell \\ -12EI/\ell^3 & 6EI/\ell^2 & 12EI/\ell^3 & 6EI/\ell^2 \\ -6EI/\ell^2 & 2EI/\ell & 6EI/\ell^2 & 4EI/\ell \end{bmatrix} \end{aligned} \tag{7.5}$$

where E is the elastic modulus of the wall and I is the moment of inertia.

2 *Beam on elastic foundation elements*: A beam on elastic foundation element is a beam element that takes the reaction of soil springs into consideration, as shown in Figure 7.5. The range of application includes:

1 The model as shown in Figure 7.2 takes all beam elements as beam on elastic foundation elements while that as shown in Figure 7.3 takes only the beam elements below the excavation bottom as beam on elastic foundation elements.
2 Under the influence of preload of struts, all the beam elements on the retaining wall should be viewed as beam on elastic foundation elements in analysis, as shown in Figure 7.6.

When considering beam on elastic foundation elements, their displacement shape function is the same as that of basic beam elements. The k_h value is the coefficient of the horizontal

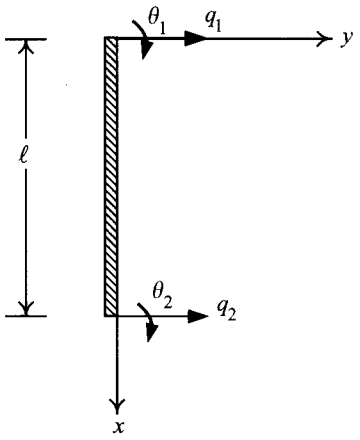

Figure 7.4 Basic beam element.

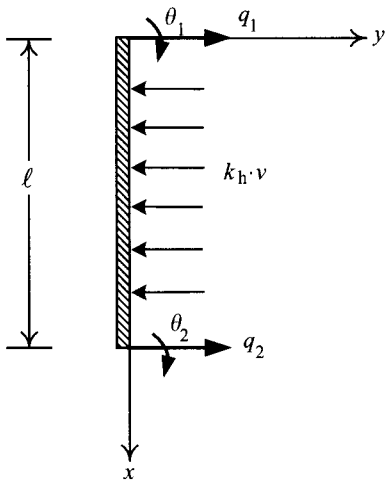

Figure 7.5 Beam on elastic foundation element.

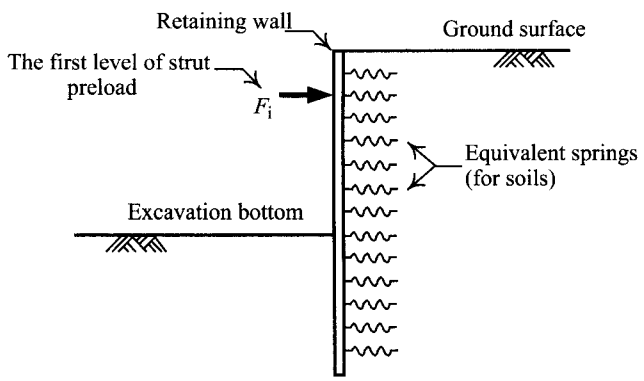

Figure 7.6 Wall acted on by strut preload as beam on elastic foundation beam.

subgrade reaction. According to the principle of virtual work, we can obtain the internal virtual strain energy as follows:

$$\delta U = \int [\delta\varepsilon]^{\mathrm{T}}[\sigma]\mathrm{d}V = \int [\delta v]^{\mathrm{T}} k_{\mathrm{h}}[v]\mathrm{d}V \tag{7.6}$$

and the external virtual work is

$$\delta W = [\delta q]^{\mathrm{T}} \cdot [P] \tag{7.7}$$

The internal virtual strain energy equals the external virtual work. Thus, since $\delta U = \delta W$, we have

$$\int [\delta q]^{\mathrm{T}} [f]^{\mathrm{T}} k_{\mathrm{h}} [f][q] \mathrm{d}V = [\delta q]^{\mathrm{T}} \cdot [P] \tag{7.8}$$

$$k_{\mathrm{h}} \int [f]^{\mathrm{T}} [f] \mathrm{d}V \cdot [q] = [P] \tag{7.9}$$

$$[K_{\mathrm{r}}] \cdot [q] = [P] \tag{7.10}$$

$$[K_{\mathrm{r}}] = k_{\mathrm{h}} \int [f]^{\mathrm{T}} [f] \mathrm{d}V \tag{7.11}$$

where $[K_{\mathrm{r}}]$ is the stiffness matrix for the soil springs of a beam on elastic foundation element.

For a beam on elastic foundation element with a length of ℓ, $[K_{\mathrm{r}}]$ would be

$$[K_{\mathrm{r}}] = \frac{k_{\mathrm{h}} \ell}{420} \begin{bmatrix} 156 & -22\ell & 54 & 13\ell \\ -22\ell & 4\ell^2 & -13\ell & -3\ell^2 \\ 54 & -13\ell & 156 & 22\ell \\ 13\ell & -3\ell^2 & 22\ell & 4\ell^2 \end{bmatrix} \tag{7.12}$$

The stiffness matrix of a beam on elastic foundation element is to combine the stiffness matrices of soil springs and beams, and is expressed as follows:

$$[K_{\mathrm{e}}] = [K_{\mathrm{b}}] + [K_{\mathrm{r}}] \tag{7.13}$$

$$[K_{\mathrm{e}}] = \begin{bmatrix} (12EI/\ell^3) + (K_{\mathrm{r}})_{11} & (-6EI/\ell^2) + (K_{\mathrm{r}})_{12} & (-12EI/\ell^3) + (K_{\mathrm{r}})_{13} & (-6EI/\ell^2) + (K_{\mathrm{r}})_{14} \\ & (4EI/\ell) + (K_{\mathrm{r}})_{22} & (6EI/\ell^2) + (K_{\mathrm{r}})_{23} & (2EI/\ell) + (K_{\mathrm{r}})_{24} \\ \text{symmetric} & & (12EI/\ell^3) + (K_{\mathrm{r}})_{33} & (6EI/\ell^2) + (K_{\mathrm{r}})_{34} \\ & & & (4EI/\ell) + (K_{\mathrm{r}})_{44} \end{bmatrix} \tag{7.14}$$

The external forces acting on a beam element should be transformed into the element nodal forces, which can be computed by the following equation:

$$[P] = \int_0^{\ell} [f]^{\mathrm{T}} w(x) dx \tag{7.15}$$

where $[f]$ is the displacement shape function and $w(x)$ is the lateral earth pressure, which distributes linearly with depth (see Figure 7.7) and can be expressed as follows:

$$w(x) = A_0 + \frac{(A_1 - A_0)}{\ell} \cdot x \tag{7.16}$$

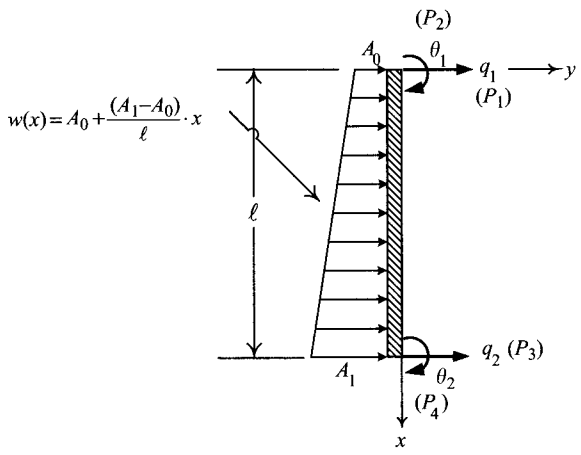

Figure 7.7 Lateral earth pressure on a beam element transformed into equivalent nodal forces.

The equivalent nodal force at each degree of freedom is as follows:

$$P_1 = \int_0^{\ell} f_1 w(x)dx = \left(\frac{7}{20}A_0 + \frac{3}{20}A_1\right)\cdot \ell$$

$$P_2 = \int_0^{\ell} f_2 w(x)dx = -\left(\frac{1}{20}A_0 + \frac{1}{30}A_1\right)\cdot \ell^2$$

$$P_3 = \int_0^{\ell} f_3 w(x)dx = \left(\frac{3}{20}A_0 + \frac{7}{20}A_1\right)\cdot \ell$$

$$P_4 = \int_0^{\ell} f_4 w(x)dx = \left(\frac{1}{30}A_0 + \frac{1}{20}A_1\right)\cdot \ell^2 \tag{7.17}$$

If we combine the stiffness matrices of the basic beam elements, beam on elastic foundation elements of a retaining wall, and the structural components, the global stiffness matrix, $[K]$, can then be obtained. If we superpose the equivalent nodal forces of all the beam elements, the result can be represented by a matrix $[P_0]$. If we use $[q]$ to represent nodal displacements, the force-displacement relation of the retaining wall can then be expressed by the following equation:

$$[K]\cdot[q] = [P_0] \tag{7.18}$$

The above global stiffness matrix comprises the stiffness of the structural components, such as struts, anchors, and beams, and therefore the above equation refers to a condition where the struts already exist before excavation. Actually, struts are installed on the wall which has already deformed in the previous excavation stage and the above factor should be considered accordingly. This can be solved by adding the auxiliary forces to the right part of Eq. 7.18. The value of the auxiliary forces is the stiffness of the strut multiplied by the

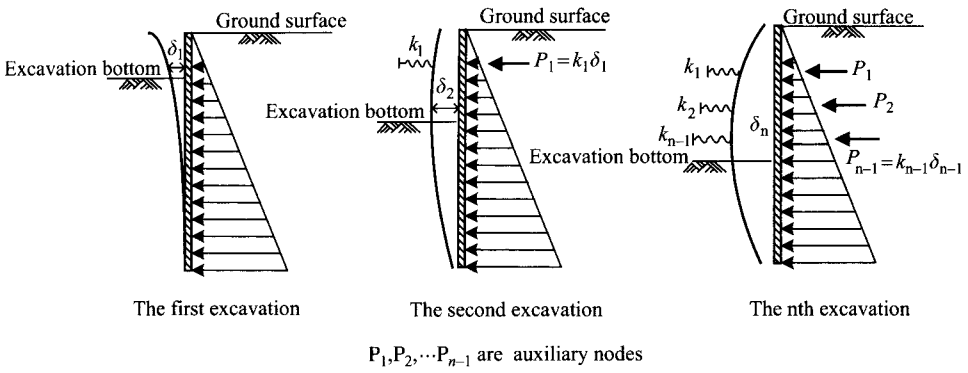

Figure 7.8 Auxiliary forces.

wall displacement in the previous excavation stage, as shown in Figure 7.8. Thus, the above equation can be rewritten into the following:

$$[K] \cdot [q] = [P_0] + [P_{\text{aux}}] \tag{7.19}$$

The displacement, $[q]$, at each node in an excavation stage can then be solved according to the above equation. With the displacement at each node known, the bending moment and shear of each beam element can then be found accordingly. The solution procedure for the beam on elastic foundation method can be diagrammed as in Figure 7.9. What's noteworthy is that, when the soil reaction force is larger than the capacity (Q_j, that is, the passive earth pressure), it follows that the soil springs are at the plastic stage and should be analyzed on the basis of nonlinear iteration.

7.4 Distribution of lateral earth pressures

The distribution of earth pressures on a retaining wall should be as close to the actual distribution of earth pressures on the wall as possible. The actual earth pressure relates to whether the assumed failure plane is the actual one. The closer the assumed failure surface to the true failure surface, the more accurate the derived earth pressure. The distribution of earth pressures cannot contain any safety factor. Otherwise, the distribution will be distorted. The related theories and the reasonable values of earth pressures for design are introduced in Chapter 4. In this section only a summary elucidation is given.

As discussed in Section 4.5, for granular soils such as sandy soils or gravelly soils, the relations between the actual earth pressure, Rankine's earth pressure, and Coulomb's earth pressure are as follows:

$$P_a \text{ (Rankine)} > P_a \text{ (actual earth pressure)} > P_a\text{(Coulomb)}$$

$$P_p\text{(Coulomb)} > P_p\text{(actual earth pressure)} > P_p \text{ (Rankine)}$$

As shown above, if Rankine's earth pressures are adopted for both sides of a wall, the analysis result will come out too conservative. If Coulomb's earth pressures are adopted

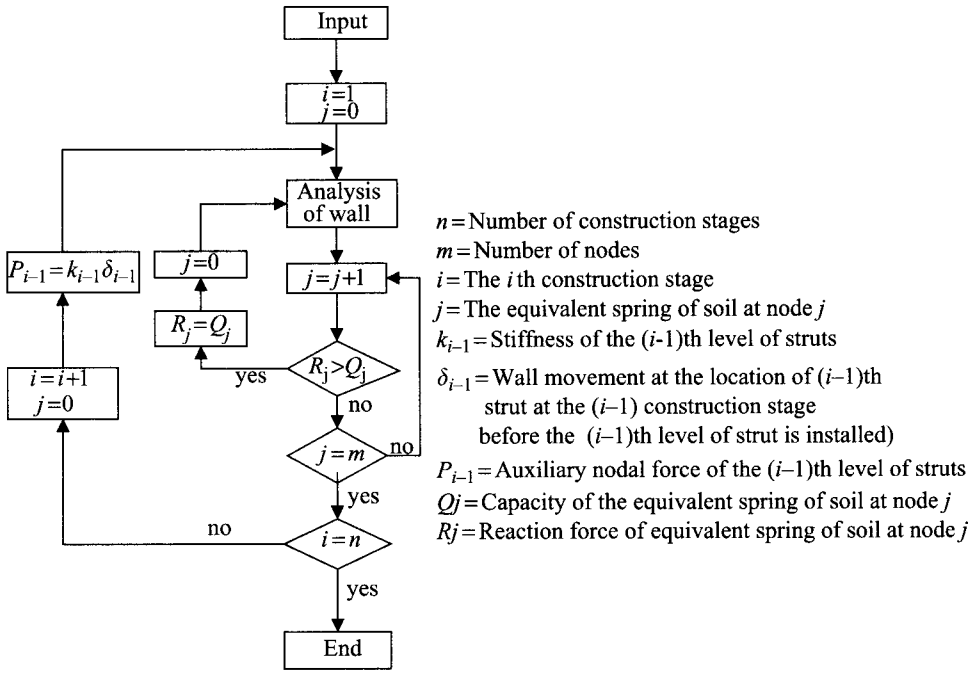

Figure 7.9 Flow chart of analysis of the beam on elastic foundation method.

for both sides, on the other hand, the result may lead to insecure design. The failure surface derived from Caquot-Kerisel's earth pressure theory is the closest to the actual failure surface. Therefore, the earth pressure distribution on the two sides of the wall should follow Caquot-Kerisel's earth pressures.

According to Figure 4.9, Coulomb's coefficients of active earth pressure are rather close to Caquot-Kerisel's. Therefore, Coulomb's coefficients can also be used to compute the true active earth pressure. Rankine's coefficients of active earth pressure are a little larger than Caquot-Kerisel's. With not much difference, for the consideration of simplification, Rankine's coefficients of active earth pressure can be used to compute the active earth pressure.

If the friction angle (δ) between the retaining wall and soils is smaller than $0.5\phi'$, as shown in Figure 4.10, Caquot-Kerisel's coefficients of passive earth pressure are close to Coulomb's. Thus, Coulomb's coefficients of passive earth pressure can also be adopted to compute the actual passive earth pressure. When $\delta \geq 0.5\phi'$, on the other hand, Coulomb's coefficients of passive earth pressure are significantly larger than Caquot-Kerisel's and will make the design tend to be unsafe if adopted in analysis.

According to Section 4.6.2, the earth pressures on the active and passive sides of the wall for cohesionless soils can be obtained by using Eqs 4.23–4.28. The active and passive earth pressures relate closely to the friction angle (δ) between the retaining wall and soils. As discussed in Section 5.5, the friction angle between a diaphragm wall and soils can be

assumed to be $\delta = \phi'$. If being conservative, we can instead assume $\delta = (0.5–0.8)\phi'$. The friction angle between sheetpiles and soils can be $\delta = (1/3–1/2)\phi'$.

According to Section 4.6.1, the earth pressures on the active and passive sides of the wall for cohesive soils can be obtained using Eqs 4.16–4.19. The active and passive earth pressures relate closely to the adhesion (c_w) between the retaining wall and soils. As discussed in Section 5.5, the adhesion between a diaphragm wall and clay can be assumed to be $c_w = 0.67s_u$ and that between sheetpiles and soils $c_w = 0.5s_u$ where s_u is the undrained shear strength of soils.

7.5 Estimation of coefficient of subgrade reaction

Following Terzaghi's study (Terzaghi, 1955), the factors influencing the coefficient of subgrade reaction include the dimension, the shape, and the depth of the foundation. That is to say, the coefficient of subgrade reaction is not a basic soil parameter but relates to the foundation system.

Many investigators have proposed methods of estimating the coefficient of subgrade reaction on the basis of test results, the theory of elasticity, or experience. For example, Vesic (1961) derived the coefficient of subgrade reaction for an infinitely long and B wide beam acted on by a concentrated load (see Figure 7.1) as

$$k_s = 0.65 \cdot \sqrt[12]{\frac{E_s B^4}{E_b I}} \frac{E_s}{B(1 - v_s^2)} \tag{7.20}$$

The value of $\sqrt[12]{(E_s B^4)/(E_b I)}$ multiplied by 0.65 would approach 1.0. Therefore, for practical purposes, the above equation can be approximated as follows:

$$k_s \approx \frac{E_s}{B(1 - v_s^2)} \tag{7.21}$$

where

E_s = secant Young's modulus of soils
E_b = Young's modulus of the beam
V_s = Poisson's ratio of the soil
B = width of the beam
I = inertia moment of the beam.

Some engineers substitute the excavation width for B in Eq. 7.20 or 7.21 to estimate the coefficient of horizontal subgrade reaction for excavation analysis. However, comparing Winkler's model as shown in Figure 7.1 with the profile of an excavation (e.g. Figure 7.10), we can see that it is not suitable to substitute the excavation width for B in Eq. 7.20 or 7.21. Vesic's equation for the coefficient of subgrade reaction, though with a rigorous theoretical basis, cannot readily serve as an equation for estimating the coefficient of subgrade reaction for excavation analysis.

Terzaghi (1955) also proposed the coefficient of subgrade reaction for anchored sheetpiles should be related to the penetration depth, which could be regarded as the loaded area. If the penetration depth is shallow and the pile bottom is not restrained, the retaining wall will

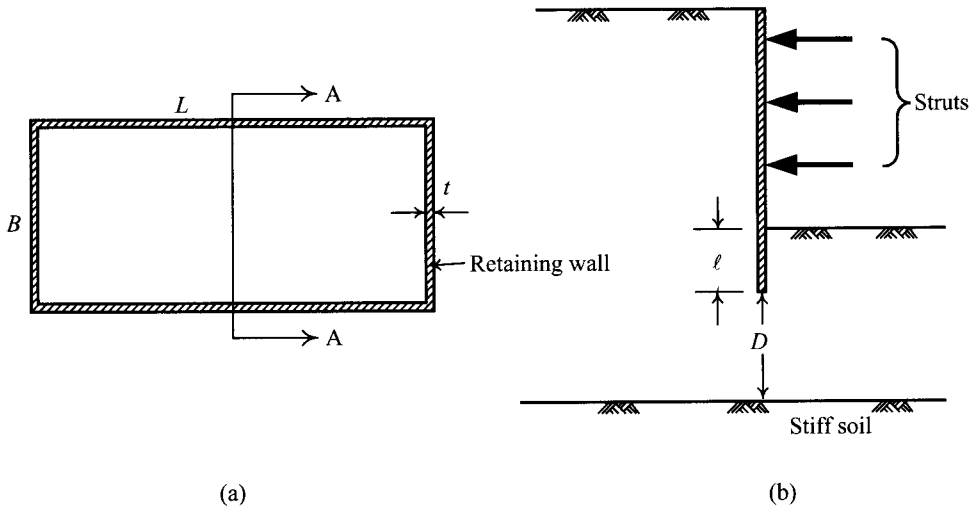

Figure 7.10 Excavation with the retaining wall ℓ deep into ground: (a) plan and (b) profile at the A-A section.

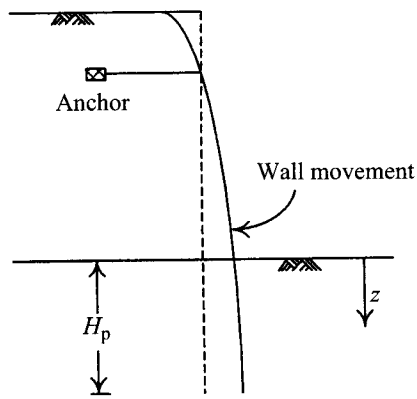

Figure 7.11 Deflection of a free earth support wall.

behave as a free earth support wall does, as shown in Figure 7.11. Therefore, the coefficients of subgrade reaction in sandy soils and stiff clays can be estimated by the following equations, respectively, as

$$\text{Sandy soils:} \quad k_h = \ell_h \frac{z}{H_p} \tag{7.22}$$

$$\text{Stiff clays:} \quad k_h = \ell_{h1} \frac{1}{H_p} \tag{7.23}$$

where

ℓ_h = soil constant, which relates only to the relative density of the soils surrounding the sheetpile.
z = depth below the excavation bottom on the passive side.
k_{h1} = coefficient of horizontal subgrade reaction when the penetration depth is 1 foot.
H_p = penetration depth of the sheetpile.

Since excavations are usually carried out in stages, the penetration depth, that is, the loaded area, decreases with the progress of excavation. Therefore, k_s for the soils in front of the retaining wall would increase with the progress of excavation if Young's modulus and Poisson's ratio of the soils remain unchanged, according to Eqs 7.22 and 7.23.

On the other hand, because sand usually exhibits drained behaviors, the effective stress in front of the wall and below the excavation surface should decrease with the progress of excavation and the strength and Young's modulus of soils in turn decreases with the progress of excavation. As a result, the coefficient of subgrade reaction should decrease with the progress of excavation. However, the effective stress in clay does not vary with the decrease of the overburden pressure under the undrained condition. Neither the undrained shear strength nor Young's modulus changes with the progress of excavation, as shown in Figure 7.12. As a result, the coefficient of subgrade reaction remains unchanged.

Based on the discussions above, k_s for the soils in front of the wall used for excavation analysis has the following characteristics:

1 k_s is related to the penetration depth (loaded area), Young's modulus, and Poisson's ratio.
2 For sandy soils, following the progress of excavation, k_s will decrease because of the decrease of the effective overburden pressure and on the other hand, k_s will increase due to the decrease of penetration depth.
3 For clayey soils, following the progress of excavation, k_s will remain unchanged even though total overburden pressure decreases with the excavation depth because the clayey soils are under the undrained condition and on the other hand, k_s will increase because of the decrease of the penetration depth.

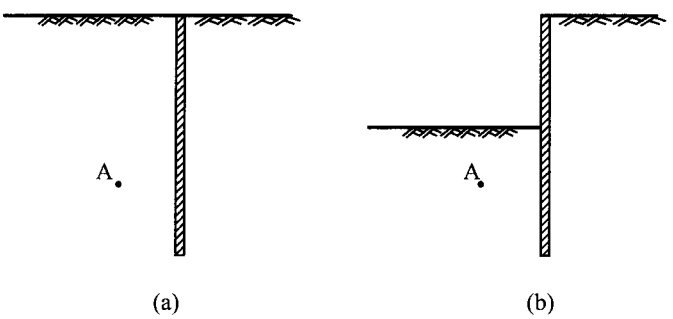

Figure 7.12 Undrained shear strength and Young's modulus in clay remain unchanged after excavation: (a) before excavation and (b) after excavation.

Currently, there are no equations available which are able to consider all of the influencing factors, such as penetration depth and basic soil properties. However, some investigators have proposed empirical equations to estimate k_h, correlated with the strength parameters of soils and other basic soil parameters.

The author performed a series of back analyses of many excavation histories and proposed the following empirical formula to estimate k_h by

$$\text{For clay} \quad k_h = (40\text{–}50)s_u \tag{7.24}$$

$$\text{For sand} \quad k_h = (700\text{–}1000)N \tag{7.25}$$

where

k_h = coefficient of subgrade reaction. The unit is kN/m^3
s_u = undrained shear strength of soils. The unit is kN/m^2
N = SPT value.

7.6 Estimation of structural parameters

As discussed in Section 3.3.1, soldier piles commonly used in excavations are H steels and rail piles. For the dimensions and related properties of H steels and rail piles, please refer to books on steel structures or steel structure design manuals. The nominal Young's modulus for solider piles is 2.04×10^6 kg/cm^2. Theoretically, the stiffness (EI) does not need reduction in analysis. Considering the repeated use of solider piles, which decreases their stiffness as a result, therefore, the nominal Young's modulus is usually reduced by 20%.

The nominal Young's modulus for sheetpiles is also 2.04×10^6 kg/cm^2. Some people consider that sheetpiles are not rigidly jointed together and advise the nominal moment of inertia per unit width be reduced by 40%. The author, however, does not think it necessary to take the question of joining into consideration since it is an analysis on the basis of plane strain, that is, only the vertical stiffness is to be considered. Therefore, the nominal stiffness is recommended for use. Considering the repeated use of sheetpiles, however, the stiffness can be assumed to be 80% of the nominal value in analysis. When analyzing the three dimensional behaviors of sheetpiles, on the other hand, the joining should be considered and a suitable reduction factor for the horizontal stiffness should be taken into account.

Young's modulus for diaphragm walls is basically determined according to the compressive strength of concrete. According to the ACI Code, the Young's modulus for concrete can be estimated using the equation: $E = 15,000\sqrt{f'_c}$ kg/cm^2 where f'_c is the 28th-day compressive strength of concrete. Considering the possibility of bending moment-induced cracking in concrete and the reduction of the sectional modulus accordingly, the stiffness (EI) is usually reduced by 20–40% in analysis.

Figure 7.13 is the wall bending moments in the main observation section of the TNEC excavation. The solid line refers to the bending moments obtained from the rebar strain meters embedded inside the diaphragm wall. Because the cracking of the diaphragm wall will influence the measurement results of the rebar strain meter, the computed bending moments contain the effect of cracking of the diaphragm wall. The dotted line in the figure represents the bending moment computed from the deformation curve of the diaphragm wall. The computation is as follows: First, compute the radius of the curvature by differentiating twice the multinomial function simulating the deformation curve. Assuming EI is not reduced,

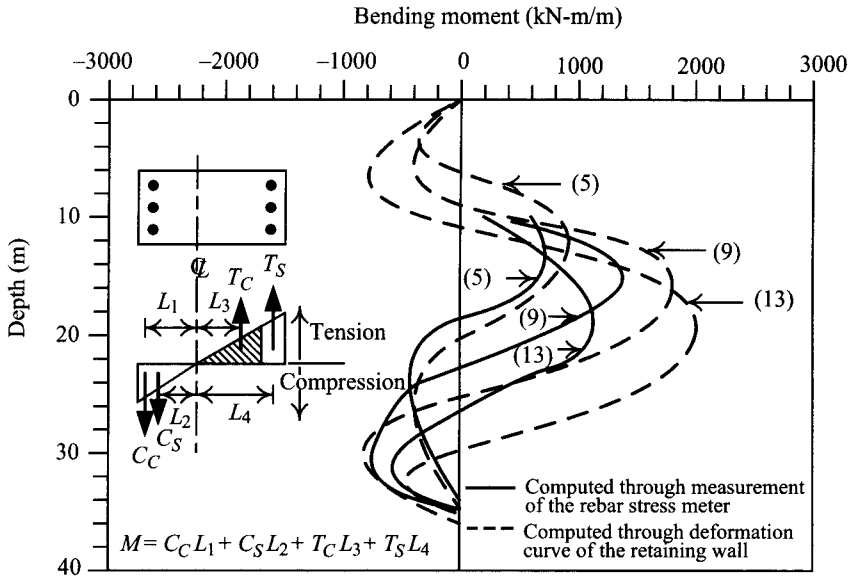

Figure 7.13 Variations of bending moments of the diaphragm wall in the TNEC excavation.

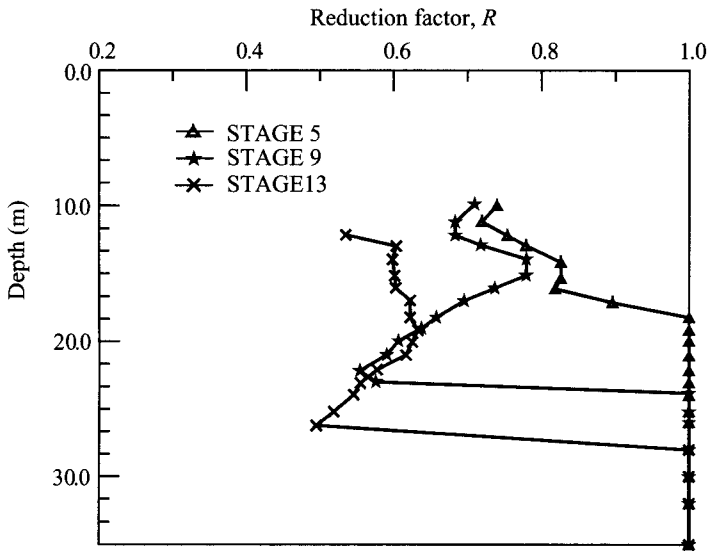

Figure 7.14 Reduction factors of bending moments for the diaphragm wall in the TNEC excavation.

the moment at a certain depth of the diaphragm wall can be obtained using the equation: $M = EI/r$, where r is the radius of curvature.

The bending moment computed from the wall deformation curve excludes the effect of the diaphragm wall cracking. The ratios of the bending moments from rebar strain meters to those from wall deformation curves are then the reduction factors (R), as shown in Figure 7.14. From

the figure, we can see that the reduction factors at different depths are different. Basically, the reduction factors at the top and bottom of the wall are close to 1.0 and that near the excavation bottom is as low as 0.5. In analysis, we can then assign different reduction factors for different depths of the diaphragm wall.

As elucidated in Section 3.3.3, column piles can be distinguished into packed-in-place (PIP) piles, reinforced concrete piles, and mixed piles. Reinforced concrete piles can further be classified into reverse circulation drill piles and all casing piles. The value of f_c' for PIP piles is about 170 kg/cm^2 and that for reinforced concrete piles is about 280 kg/cm^2. In analysis, it can be reduced by 30–50%. Which value of the reduction factor is to be taken, however, depends on the construction quality of the column pile. Besides, if considering the different degrees of cracking of concrete at different depths of the column pile, we can assign different reduction factors at different depths of the column pile, which is similar to the approach for diaphragm walls.

The value of f_c' for mixed piles is about 5 kg/cm^2. With rather low strength, the stiffness of mixed piles can be ignored and we can, instead, only consider the stiffness of the H steel (or W section) within mixed piles.

Struts or floor slabs only bear axial forces. Thus, they can be simulated as springs, whose stiffness can be estimated as follows:

$$k = \frac{AE}{L} \tag{7.26}$$

where

A = cross-sectional area of a strut or floor slab
E = Young's modulus
L = length of the strut or floor slab, usually half of the excavation width.

In the field, struts are installed by splicing H steels together, which are thus not easily lined up straight to achieve nominal axial stiffness. What's more, the bending phenomena caused by heave of the center posts will reduce their axial stiffness. In analysis, the axial stiffness of a strut has to be reduced.

The axial stiffness of floor slabs of the top-down construction method has also to be reduced. The reasons are two. One involves whether the compressive strength of concrete in the field agrees with the design strength. The other is cracking due to concrete shrinkage.

Under the same conditions, the axial stiffness of floor slabs is less affected by construction quality, compared to struts. The axial stiffness of floor slabs is thus less reduced. According to experience, the stiffness of a floor slab is about 80% of the nominal value whereas that of a steel strut is 50–70% of the nominal value.

7.7 Analysis methods for excavations

7.7.1 *Direct analysis and back analysis*

Input the soil parameters obtained from soil tests into the computer program and the thus derived results represent the behaviors of the excavation. The method is called direct analysis. In theory, if the soil model and soil parameters can thoroughly simulate the soil behaviors, the direct analysis can obtain reasonable and accurate results.

The stress-strain behaviors of soils are in nature anisotropic and are influenced by stress paths. The existing testing methods may not fully simulate the behaviors of in situ soils. The available soil models may not appropriately simulate soil behaviors, either. Therefore, the soil parameters obtained from soil tests sometimes have to be adjusted. If the adjustment procedure has a certain regularity, reproducibility, and consistency and is also applicable to any soil and construction conditions, the method is also called the direct analysis method.

On the other hand, we can take measurement data as an object, modify the parameters of the soil model to make the analysis results match the measurements and then use the same soil parameters for the prediction of excavations with similar geological conditions, construction situations, and procedures, which usually results in satisfactory results. The analysis method is called back analysis. Back analysis can also be applied to staged construction. That is, one uses the observations at the initial stages as an object to back analyze the soil parameters, which are then used for the prediction of behaviors at the final or critical construction stage. The method can also obtain fairly satisfying results. As early as 1969, Peck utilized the method to analyze geotechnical problems, and designated it as the observational method.

Actually, any soil model usually requires some parameters. Besides, soils below the ground surface are usually multilayered. As a result, if we assume all of the parameters are unknown, to carry out a back analysis will be time-consuming and expensive. A reasonable way is to focus on those parameters that cannot be obtained from tests or cannot be reasonably estimated. Those parameters that are relatively reliable should be obtained from soil tests. For example, with the beam on elastic foundation method, the s_u value of saturated clay can be obtained from soil tests. The only parameter that has to be back analyzed is k_h. The procedure of back analysis can then be simplified substantially.

7.7.2 Drained analysis, undrained analysis, and partially drained analysis

Drained analysis is to assume that, in analysis, the excess porewater pressure has been all dissipated (i.e. $u_e = 0$) and the volume of soils thereby changes. Drained analysis is mainly applied to granular soils such as sandy soils or gravel soils. It is also applied to the analysis of long-term behaviors of clayey soils. That is to say, the analysis has to adopt the effective stress analysis and the required parameters in analysis are effective parameters, that is, c' and ϕ'.

The undrained analysis, instead, assumes that the excess porewater is not dissipated ($u_e \neq 0$) and the total stress analysis is adopted accordingly. Suppose the soils are in the saturated state, no volume change can be observed under the undrained condition. The parameter to be used in analysis would be s_u and $\phi = 0$. The undrained analysis for unsaturated clay adopts the test results of the triaxial UU tests where c_T and ϕ_T are directly adopted.

In some cases, the clay is neither totally drained nor completely undrained. Instead, it is in between the two conditions, called the partially drained behavior. The analysis of the partially drained behavior of clay can be carried out through undrained analysis, which takes advantage of the known excess porewater at each stage. To obtain the porewater pressure at a certain stage, one of the methods is to install a piezometer to measure the porewater pressure, which may partially dissipate at a construction stage. Then use the equation, $\sigma' = \sigma - u$, to derive the effective stress of the soils. Given the effective stress of soils, according to the normalized behavior of soils (s_u/σ'_v = constant), the undrained shear strength of the soils can then be obtained. Then carry out an undrained analysis of the excavation for each stage to obtain the partially drained behavior of soils. Another method is to obtain the undrained

shear strengths for each stage by way of laboratory or in situ shear strength tests first, which are then used for undrained analysis to analyze the partially drained behavior.

7.8 Computation of ground surface settlement

The beam on elastic foundation method can only yield the deformation of a retaining wall but is not capable of producing the ground settlement. As discussed in Chapter 6 about the characteristics of ground settlement, under normal conditions, the soils behind a retaining wall move forward and downward and the soils are thus settled. That is, the factors influencing wall deformation also influence ground settlement. These factors include strut stiffness, strut preload, safety factor for stability, excavation depth, excavation width, etc. The beam on elastic foundation method takes these factors all into consideration and thus is capable of analyzing wall deformation. Since deformation of a retaining wall relates closely to ground settlement, we can estimate the ground settlement on the basis of the computed wall deformation (see Section 6.8).

Chapter 6 introduces Peck's method, Bowles's method, Clough and O'Rourke's method, and Ou and Hsieh's method to estimate ground settlement. The last three methods have to estimate the lateral deformation or the maximum lateral deformation of the retaining wall before analysis. The ground surface settlement caused by excavation can be classified into the spandrel and concave types. Peck's method does not separate the two types. Bowles' method can only predict the spandrel type of ground surface settlement. Though separating the spandrel and concave types, Clough and O'Rourke's method cannot offer a quantified method to distinguish the two. Ou and Hsieh's method, on the other hand, offers a quantified method to distinguish between the spandrel and concave types.

In prediction, Bowles's method can only be used with the lateral wall deformation given. Clough and O'Rourke's method needs the maximum lateral wall deformation. Ou and Hsieh's method needs the lateral wall deformation. These data can all be obtained using the beam on elastic foundation method. According to the case studies (see Figure 6.27), Ou and Hsieh's method can reasonably predict the excavation-induced ground surface settlement (see Section 6.8.4). In this section, we will elucidate the procedure of prediction using Ou and Hsieh's method as follows:

1 Predict the lateral wall deformation using the beam on elastic foundation method.
2 The lateral wall deformation known, compute the areas of the cantilevered part (A_c) and the deep inward movement (A_s). Determine the type of ground surface settlement with the help of Figure 6.12.
3 Estimate the maximum ground surface settlement (δ_{vm}) according to its relation with the maximum lateral wall deformation (δ_{hm}), as shown in Figure 6.14.
4 According to the settlement type determined in step 2, compute the ground surface settlements in different positions behind the retaining wall using Figure 6.26.

The above analysis process, including the analysis of wall deformation, the computation of A_c and A_s, the judgment of the settlement type, the ranges of the main and secondary influence zones, and the computation of the ground surface settlement profile, are all elucidated in detail in Chapter 6 and built into the computer program VEX.

If readers want to predict ground surface settlement using the beam on elastic foundation method together with other empirical methods or simplified methods, they can consult

the above methods, making some modifications perhaps, and should obtain reasonable results.

7.9 Limitations of the beam on elastic foundation method

Basically, the beam on elastic foundation method is an analysis method based on the plane strain condition (whose definition is given in Appendix D). As discussed in Section 6.9, however, in excavations with short sides, influenced by the corner effect, the deformations of the retaining wall or the ground surface settlements will be smaller than those in the plane strain condition. In analysis, we can first analyze the wall deformation under the plane strain condition using the beam on elastic foundation method and then modify the analysis result using the concept of plane strain ratio (PSR) and Figure 6.30. Or, we can also assume the corners of the retaining wall are restrained and adopt the techniques of structural analysis to analyze the difference between the deformation of the "object section" and that of the section under the plane strain condition. Then modify the results of the beam on elastic foundation method.

Figure 7.15a illustrates soil improvement over the whole excavation area within a certain depth. From the excavation profile as shown in Figure 7.15b, we can compute the distribution of earth pressures as shown in Figure 7.15c, adopting the parameters of the treated soils within the range of the depth where the soil is treated. Figure 7.16a shows the condition where only a part of the excavation site is treated. As shown in Figure 7.16b, the excavation profile, though the deformation of the retaining wall and ground surface settlement in the central section are under the plane strain condition, the strength parameters needed for the computation of earth pressures and coefficient of subgrade reaction may not be computed directly from the parameters of the treated soils. They are not necessarily obtained through weighting with regard to comparative areas, either. The finite element method certainly can be used to analyze the excavation behavior.

Besides, it is not easy to draw analogies between the mechanical characteristics for counterfort walls or cross walls (see Chapter 11) and beams on elastic foundation. That is, the correctness of analyzing the deformation of counterfort wall or cross wall using the beam on elastic foundation needs more study.

7.10 Application of computer programs

There are some commercial computer programs available for excavation analysis using the beam on elastic foundation method. Some of them are not clear in their coding logic. Some are only built on a specific earth pressure theory, which may not be appropriate for excavation analysis. Some are merely coded in terms of effective stress. Therefore, it is necessary to examine the applicability of the computer programs before analysis.

Soil properties are complicated. The existing soil models and the parameters from existing test techniques may not be able to completely simulate the true soil behavior. However, most geotechnical experts believe that if we can improve the theories to ensure rationality and obtain better parameters closer to actual ones, the actual excavation behaviors can be further approached. The VEX program mentioned in this book is based on rigorous theories and is consistent with geotechnical principles. Readers are invited to test its applicability. If readers adopt computer programs other than VEX, they can adopt the following test procedures to check their function and modify the analysis methods accordingly so that the results can be rational, reproducible, and consistent.

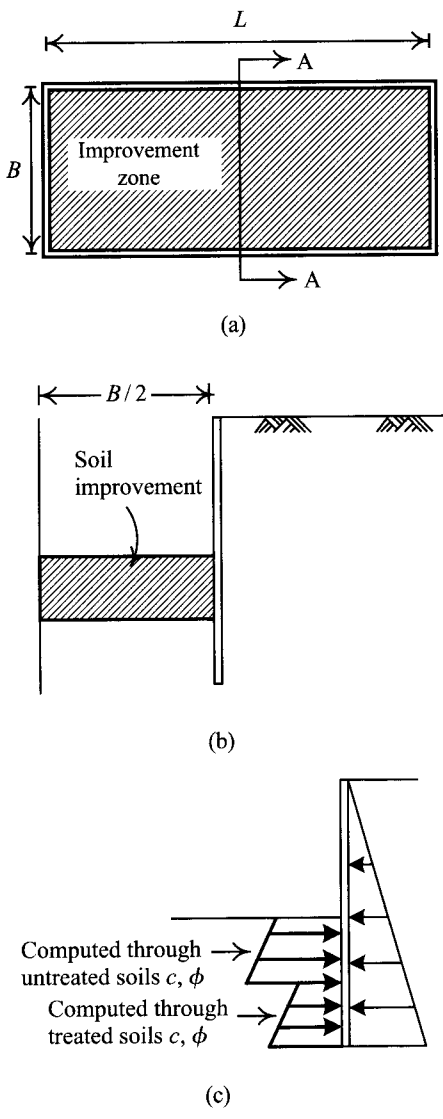

Figure 7.15 Soil improvement implemented to the whole site: (a) plan, (b) profile, and (c) distribution of earth pressure.

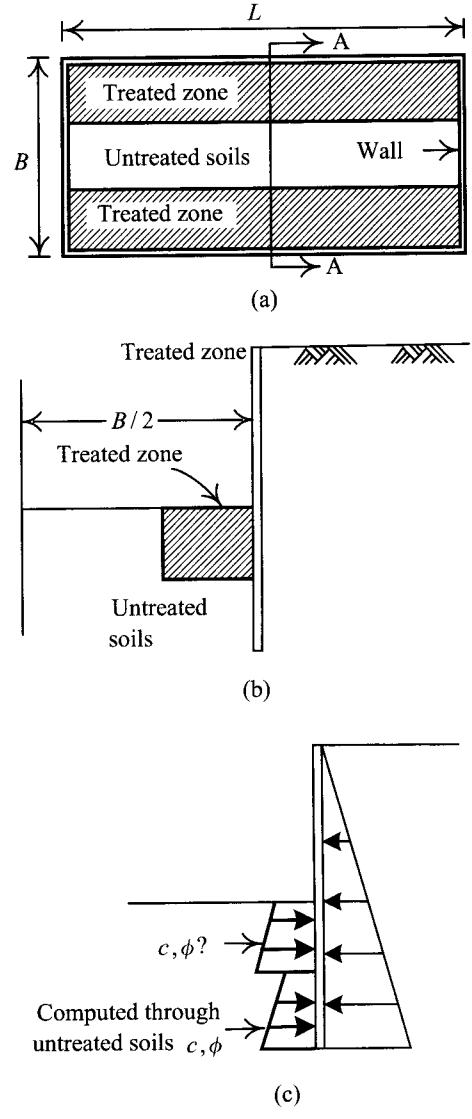

Figure 7.16 Soil improvement implemented to a part of the excavation zone: (a) plan, (b) profile, and (c) distribution of earth pressure.

7.10.1 *Confirmation of the type of stress used in computer programs*

Some excavation analysis computer programs using the beam on elastic foundation method are available on the market. Some of them are coded on the sole basis of the effective stress

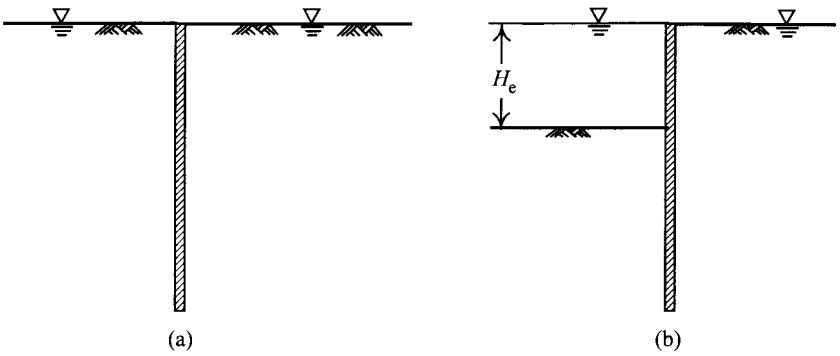

Figure 7.17 Example for the examination of types of stresses used in computer programs: (a) conditions before excavation and (b) excavate to a certain depth and without lowering groundwater level.

analysis method and some are based on both the effective stress and total stress analysis methods. Most of them do not explain on what their stress computations are based, so users may well input wrong parameters or apply wrong simulation procedures. To prevent such mistakes, how the stress is computed in the computer program has to be confirmed first.

Those computer programs coded on the sole basis of the effective stress analysis method require γ_m (the moisture unit weight of soil) and γ' (the submerged unit weight of soil) as well as general soil parameters c, ϕ, K_a, and K_p, etc. Such computer programs will take γ_m automatically for soils above the groundwater level in computation. For soils below the groundwater table, they usually separate the earth pressure and porewater pressure in computation. That is, they will take γ' automatically to compute the earth pressure no matter whether cohesive soils or cohesionless soils are encountered. As a result, the lateral pressures on the retaining wall below the groundwater level include the effective earth pressure computed from γ' and water pressure.

To check whether the computer program is coded on the sole basis of the effective stress analysis method, one can follow the procedures below. Assume there is an excavation site in clayey soils (see Figure 7.17a). Set its groundwater level. Run the computer program to compute the earth pressure on the retaining wall for excavation depth (H_e). In addition to s_u and $\phi = 0$, feed the computer program with γ_m and γ'. In analysis, no dewatering within the excavation zone is carried out, which follows that the groundwater level does not change if the computer program is coded on the sole basis of the effective stress analysis method, as shown in Figure 7.17b. Use hand calculation to check whether the earth pressure derived from the computer program is the same as that using γ_{sat} (i.e. total stress analysis) or γ' (i.e. effective stress analysis). If it comes out to be the latter, the computer program can be confirmed to be coded on the sole basis of the effective stress analysis method.

7.10.2 *Application of the computer program coded on the sole basis of the effective stress*

Using computer programs coded on the sole basis of the effective stress analysis method (where the earth pressures are separately computed in terms of soils and water) to make an

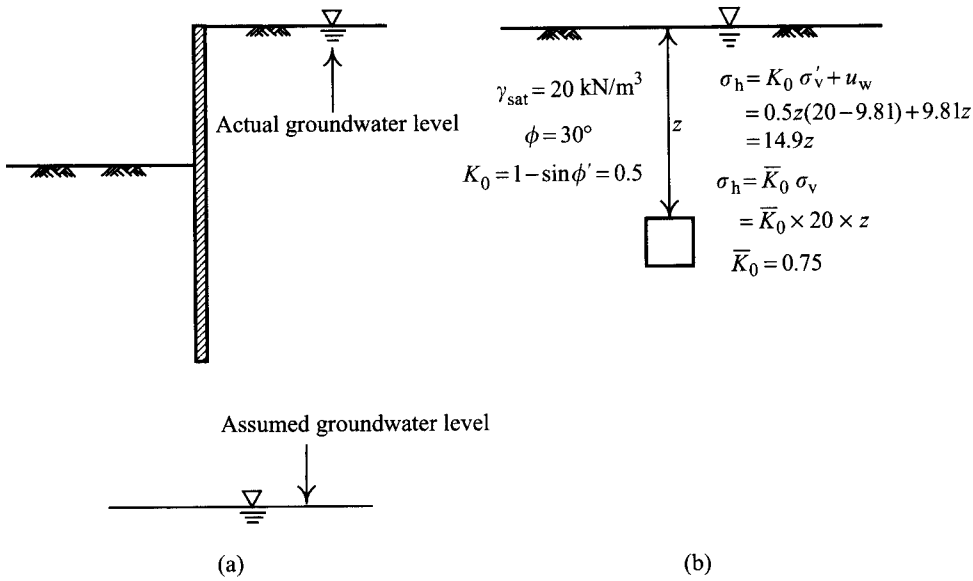

Figure 7.18 Undrained analysis using an effective-stress-based computer program: (a) assume the groundwater level to be very deep and (b) modify the coefficient of the at-rest earth pressure.

undrained analysis of clay has to notice not to violate the basic principles of soil mechanics. Some common mistakes include confusion between the parameters c' and ϕ' (based on effective stresses) and c_T and ϕ_T (based on the total stresses); a wrong simulation of dewatering in clayey layers, etc. Basically, it is the saturated unit weight γ_{sat}, s_u, $\phi = 0$ that is to be adopted for the computation of lateral earth pressures of saturated clay below the groundwater level.

There are two ways to analyze the undrained behavior of soils with computer programs coded on the sole basis of the effective stress analysis method. One is to assume the groundwater level at an infinite depth from the bottom of the retaining wall (see Figure 7.18a), in which case the parameters of the total stresses are $c = s_u$, $\phi = 0$, $K_a = K_p = 1$, and γ_{sat} is taken for the unit weight of soils. The coefficient of at-rest earth pressure should be modified as the ratio of the total lateral earth pressure to the total overburden pressure. As shown in Figure 7.18b, if we assume the saturated unit weight of clay to be 20 kN/m^3, the groundwater level is at the ground surface and $K_0 = 0.5$, the modified coefficient of at-rest earth pressure is then $\overline{K_0} = 0.75$.

The other way is to assume dewatering with the proceeding of excavation. That is, to activate the dewatering command of the computer program and to make the groundwater level to be lowered to the excavation surface, and then assume the distribution of water pressures within and outside of the excavation to be hydrostatic and that there is no seepage produced, as shown in Figure 7.19.

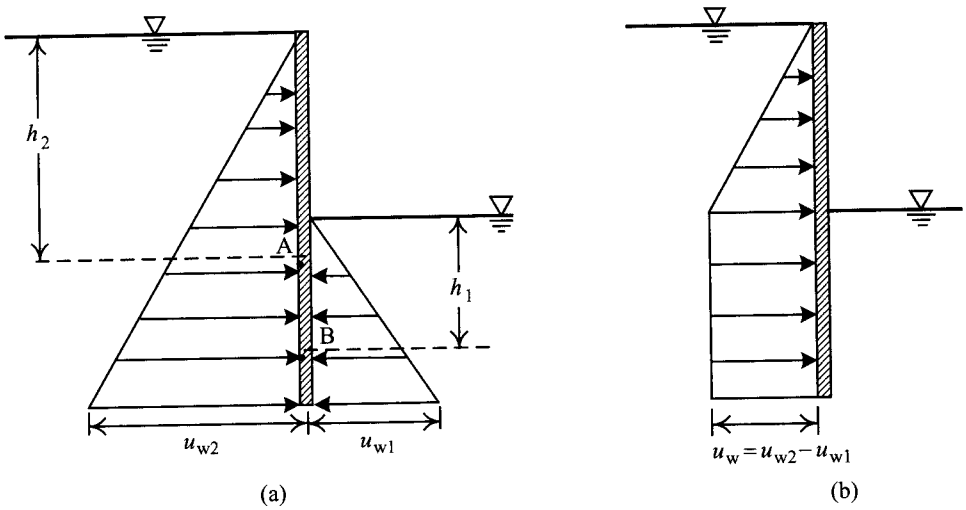

Figure 7.19 Analysis of excavation in clay assuming dewatering with the progress of excavation: (a) assumed water pressures and (b) net water pressures.

If we assume the parameters fed into the computer program are $c = s_u, \phi = 0, K_a = K_p = 1$, and $K_0 = 0.5$, through the computer simulation, the active earth pressure at a certain point A behind the retaining wall will be:

$$\begin{aligned}\sigma_{h,a} &= \sigma'_{h,a} + u_w \\ &= K_a\sigma'_v - 2s_u + u_w \\ &= \gamma' h_2 - 2s_u + r_w h_2 \\ &= \gamma_{sat} h_2 - 2s_u \\ &= \sigma_v - 2s_u\end{aligned}$$

where

$\sigma_{h,a}$ = total active earth pressure
$\sigma'_{h,a}$ = effective active earth pressure
σ'_v = effective overburden pressure
σ_v = total overburden pressure
K_a = coefficient of active earth pressure
u_w = hydrostatic water pressure.

As shown above, σ_a can represent the active earth pressure at a certain point, A, behind the retaining wall under the undrained condition.

Similarly, the passive earth pressure at a certain point, B, in front of the retaining wall will be:

$$\begin{aligned}\sigma_{h,p} &= \sigma'_{h,p} + u_w \\ &= K_p\sigma'_v + 2s_u + u_w \\ &= \gamma' h_1 + 2s_u + r_w h_2 \\ &= \gamma_{sat} h_2 + 2s_u \\ &= \sigma_v + 2s_u\end{aligned}$$

where

$\sigma_{h,p}$ = total passive earth pressure
$\sigma'_{h,p}$ = effective passive earth pressure
K_p = coefficient of passive earth pressure.

The σ_p value can represent the passive earth pressure at a certain point, B, in front of the retaining wall under the undrained condition. Actually, since the permeability of clay is very low, dewatering is not necessary during excavation. This technique of activating the dewatering command of computer programs is merely used for analysis without considering the field reality. It is merely used to simulate the undrained behavior.

The earth pressure obtained from the above two methods both imply the concept of the total stress analysis (or undrained analysis). The author analyzed excavations in clayey layers using the two techniques and found that the deformations obtained from the above two methods are quite close. However, the application of the first method where the groundwater level is assumed to be at an infinite depth is limited, for example, in alternating layers of clay and sand.

The technique of staged dewatering is to be used under the assumption of hydrostatic porewater pressure distribution. This technique can also be used for alternating layers of sand and clay, with the same assumption about porewater pressure distribution. Figure 7.20 shows a distribution of water pressures (expressed in net water pressure) when analyzing alternating soils using the technique. Though the water pressure in clay, which may possess a

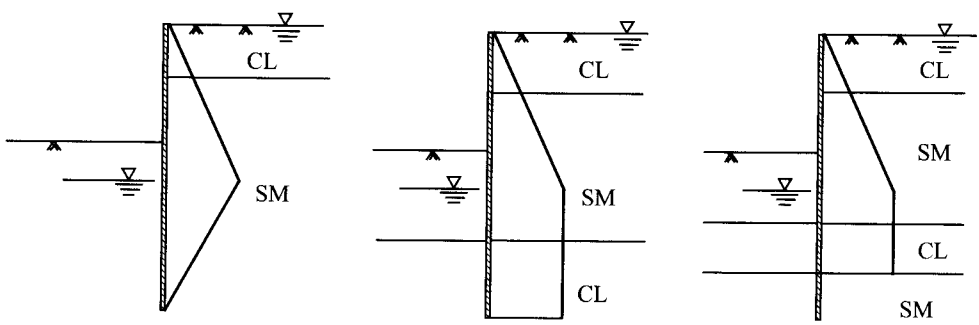

Figure 7.20 Assumed distribution of water pressures (represented by net water pressures) of alternating layers for effective-stress-based computer programs.

certain amount of excess porewater pressure, is not necessarily in the hydrostatic condition, it is still necessary to feed the computer program with the hydrostatic water pressure rather than the real water pressure. The reason is that this is simply a technique of analysis. s_u, influenced by the effective stress of soils which the real porewater pressure also contributes to, is derived from soil tests and thereby the analysis based on s_u has taken the influence of the real porewater pressure into consideration.

7.10.3 Application of the computer program coded on the double basis of effective and total stresses

The computer programs coded doubly using both the effective stress and total stress methods can be used to simulate the undrained behavior of saturated clays using the total stress analysis method (undrained analysis method) and analyze the drained behavior of cohesionless soils using the effective stress analysis. These computer programs can reasonably simulate the effects of simultaneous soil and porewater removal without activating the dewatering command to lower the groundwater level when analyzing excavations in clay.

7.10.4 Confirmation of the type of earth pressure theory built into computer programs

The earth pressures on a retaining wall have to be derived from earth pressure theories suitable for excavation analysis and design. Still, some computer programs are built on earth pressure theories that are not often used in the analysis of excavations. To avoid irrational results, users should refer to the user's manual to make sure which earth pressure theory the computer program is based on. If necessary, modify the input parameters to be close to the earth pressure theory introduced in Section 7.4 in this chapter.

7.10.5 Verification through case histories

Before analyzing and making predictions for an actual excavation project, we should first analyze excavation case histories to ensure the correctness of the use of the computer program, and rationality of input parameters, especially the coefficient of subgrade reaction. Then proceed to the analysis of the excavation project.

The excavation of TNEC has good observation data, high quality soil tests, and a complete record of excavation procedure. With its full records of deformations and stresses, TNEC is quite suitable to be used for case examination of computer programs. The index of the related data of TNEC is as listed in Appendix B. As well, the book also shows three more excavations, Building P (see Example 6.1), Building R (see Problems 6.4 and 7.17), and Building S (Problems 6.11 and 7.14), with their excavation profiles, geological data, and observed deformations of the retaining wall for case examination.

EXAMPLE 7.1

Figure 7.21 shows the excavation profile and stages of an excavation. The excavation width is 30 m and the excavation depth is 8 m. The soil is overconsolidated clay. OCR is about 1.5; the index of plasticity is about 17. The groundwater level is at the ground surface. The saturated unit weight of soil $\gamma_{sat} = 18\ kN/m^3$; the undrained shear strength $s_u = 40\ kN/m^2$. Compute the coefficients of subgrade reaction for all the stages.

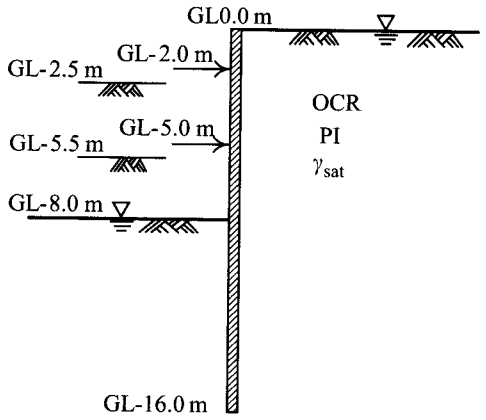

Figure 7.21 Profile of an excavation in clay and the excavation stages.

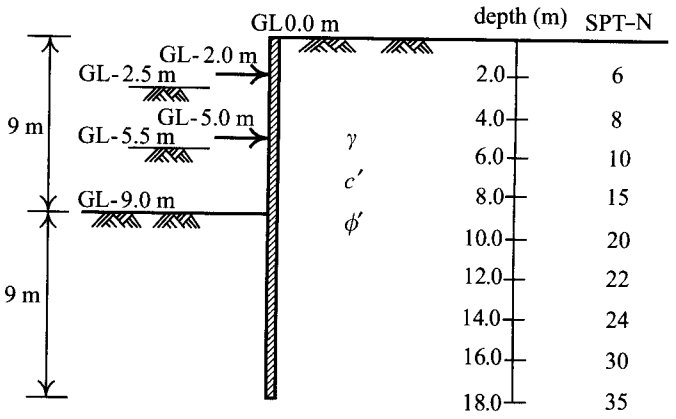

Figure 7.22 Profile of an excavation in sand and the excavation stages.

SOLUTION

The coefficient of subgrade reaction should change with the excavation depth though the undrained shear strength and Young's modulus remains unchanged. For simplification, we use Eq. 7.24 to compute as $k_h = (40–50)s_u = (40–50) \times 40 = 1,600–2,000$ kN/m^3
The value computed from Eq. 7.24 is a constant and does not change with the excavation depth.

EXAMPLE 7.2

Figure 7.22 shows the profile and stages of an excavation. The soil is sandy and the N values from the standard penetration test are as shown in the figure. The unit weight of soil $\gamma = 15$ kN/m^3 and the effective strength parameters $c' = 0$, $\phi' = 32°$. Compute the coefficient of subgrade reaction for the site.

SOLUTION

Young's modulus and the coefficient of subgrade reaction of sandy soils change with the denseness, strength of soils, and the overburden pressure. On the other hand, the coefficient of subgrade reaction should increase with the excavation depth. For simplification, we ignore these factors and adopt Eq. 7.25 to compute the coefficient of subgrade reaction for different depths as:

At a depth of 4 m
$k_h = (700 \sim 1000)N = (700 \sim 1000) \times 8 = (5,600 \sim 8,000)\ \text{kN/m}^3$
At a depth of 10 m
$k_h = (700 \sim 1000)N = (700 \sim 1000) \times 20 = (14,000 \sim 20,000)\ \text{kN/m}^3$
At a depth of 14 m
$k_h = (700 \sim 1000)N = (700 \sim 1000) \times 24 = (16,800 \sim 24,000)\ \text{kN/m}^3$
At a depth of 18 m
$k_h = (700 \sim 1000)N = (700 \sim 1000) \times 35 = (24,500 \sim 35,000)\ \text{kN/m}^3$
k_h does not change with the excavation depth but changes with the SPT-value.

EXAMPLE 7.3

Suppose an excavation with a diaphragm wall in soft clay. A computer program based on the beam on elastic foundation method is to be used for analysis. From the user's manual, the active and passive earth pressures in the computer program are as follows:

$$\sigma_a = K_a\sigma_v - \frac{c}{\tan\phi}\left[\frac{\cos\delta - \sin\phi\cos\gamma}{1+\sin\phi} \cdot e^{-(\gamma-\delta)\tan\phi}\cos\delta - 1\right]$$

$$\sigma_p = K_p\sigma_v + \frac{c}{\tan\phi}\left[\frac{\cos\delta + \sin\phi\cos\gamma}{1-\sin\phi} \cdot e^{(\gamma+\delta)\tan\phi}\cos\delta - 1\right]$$

where K_a and K_p represent the coefficients of the active and passive earth pressures respectively. σ_v = the overburden pressure; c = cohesion; δ = the friction angle between the wall and soils; $\sin\gamma = \sin\delta/\sin\phi$, where γ is between 0° and 90°. If we use Caquot and Kerisel's earth pressure theory, introduced in Section 4.6, how should we modify the input parameters?

SOLUTION

Since the excavation is in clay, with $\phi = 0$ and $K_a = K_p = 1$, the above equations can be simplified as

$$\sigma_a = K_a\sigma_v - c\left[\frac{\pi}{2} + 1\right] = K_a\sigma_v - 2.57c = \sigma_v - 2.57c$$

$$\sigma_p = K_p\sigma_v + c\left[\frac{\pi}{2} + 1\right] = K_p\sigma_v + 2.57c = \sigma_v + 2.57c$$

According to the discussion in Section 5.5 in this book, the adhesion between a diaphragm wall and soft clay can be assumed $c_w = 2c/3$. Besides, according to Section 4.6, the active

and passive earth pressures of soft clay on a diaphragm wall are

$$\sigma_a = K_a\sigma_v - 2c\sqrt{\left(1+\frac{c_w}{c}\right)K_a} = \sigma_v - 2.58c$$

$$\sigma_p = K_p\sigma_v + 2c\sqrt{\left(1+\frac{c_w}{c}\right)K_p} = \sigma_v + 2.58c$$

As discussed above, when feeding the computer program with parameters $\phi = 0$ and $K_a = K_p = 1$, the earth pressures computed by the computer program will be close to the commonly computed earth pressure with the assumption $c_w = 2c/3$.

7.11 Summary and general comments

Due to a relatively simple analytic model, simple input parameters and quick computation time, the beam on elastic foundation method has been widely used in the analysis and design of deep excavations. Because of its easier model, however, it is not readily adopted for simulations of more complicated excavations. The analysis results are sometimes not reasonable. This chapter has introduced two beam on elastic foundation models for reference and this chapter is summarized as follows:

1 The coefficient of subgrade reaction is not a basic property of soils because it closely relates to not only the stiffness of soils but the structural stiffness and the loading area. Terzaghi's study shows that it is inversely proportional to the penetration depth of the retaining wall. Vesic's coefficient of subgrade reaction of beams on elastic foundation acted on by a centralized load, though based on a vigorous theoretical foundation, is not applicable to excavations because its loading pattern can not be analogized to excavation. Currently, there are no such equations able to consider all of the influencing factors, such as penetration depth and basic soil properties. However, for practical application, the author provided some other empirical equations for the estimation of coefficients of subgrade reaction of sandy and clayey soils.
2 Affected by bending moment, the concrete of a diaphragm wall may crack and its section modulus may be thereby decreased. Thus, the section modulus in analysis is usually reduced by 20–40%. According to field measurements, however, the bending moments of the diaphragm wall varied with depth and the section modulus should be reduced discriminately. Basically, the top and bottom of the diaphragm wall are the places where the reduction rate should be the lowest whereas the wall near the excavation bottom requires the highest reduction rate. In analysis, we can assign different reduction rates for different depths. Basically, Young's moduli of sheetpiles and soldier piles are not affected by the cracking or bending moment and their section moduli are not supposed to be reduced either. If considering the repeated use of sheetpiles and soldier piles, however, reduction is still necessary. The stiffness is usually reduced by 20%.
3 The struts are normally installed by splicing H steel together and thus are not easily lined up straight. Besides, the bending moment induced by the heave of center posts also contributes to the decrease of the axial stiffness. As a result, in analysis, the axial stiffness should be reduced. For top down construction, the floor slabs are cast with concrete and are affected by cracking and concrete shrinkage, which may decrease nominal axial

stiffness. According to experience, in analysis, the stiffness of floor slabs adopted is about 80% of the nominal values and that of steel struts 50–70% of the nominal values.

4 The beam on elastic foundation method can only produce the deformation of a retaining wall but not the ground surface settlement. Used along with the simplified analysis method introduced in Chapter 6, the results derived from the beam on elastic foundation method can also be used for the computation of the ground surface settlement.

5 If using commercial computer programs based on the beam on elastic foundation, it is necessary, before applying them, to make sure of the analysis logic, the earth pressure theories, and the computation method of stresses. Otherwise, mistakes might occur. This chapter provides suitable methods of building reasonable analysis methods.

Problems

Note: Most of the problems in this chapter must take advantage of computer programs based on the beam on elastic foundation method. The author provides the limited function of computer program VEX, which can be obtained from the website (http://web.ntust.edu.tw/~ou/). Or readers can use other computer programs.

7.1 Figure P7.1 shows the profile and stages of an excavation. The excavation depth is 8 m. The soil is overconsolidated clay whose OCR is about 1.5. The groundwater level is at the ground surface. The plastic index is about 25. The saturated unit weight of soil $\gamma_{sat} = 19.6\ kN/m^3$. The undrained shear strength $s_u = 54.0\ kN/m^2$. Estimate the coefficient of subgrade reaction for the soil in front of the wall.

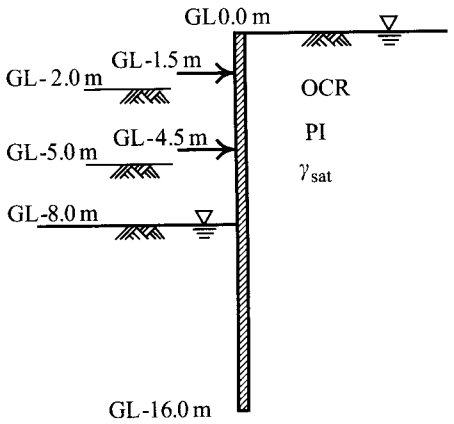

Figure P7.1

7.2 Suppose the stiffness of the first and second levels of struts are 25,000 kN/m/m and 35,000 kN/m/m (the reduced stiffness) and the stiffness of the retaining wall (the reduced value) is 180,000 kN-m^2/m. Analyze the excavation-induced deformation of the retaining wall using the coefficient of subgrade reaction estimated in Problem 7.1

and the VEX computer program (or other computer programs based on the beam on elastic foundation method) and compare the result with that obtained from the empirical equation in Chapter 6 to judge the rationality of the result.

7.3 Figure P7.3 shows the profile and stages of an excavation. The excavation depth is 7 m and the soil is over-consolidated clay whose OCR is about 1.5. The groundwater level is at the ground surface. The plasticity index is about 20. The unit weight of the soil $\gamma_{sat} = 16.7$ kN/m^3. The undrained shear strength $s_u = 34.3$ kN/m^2. Estimate the coefficient of subgrade reaction for the soil in front of the wall.

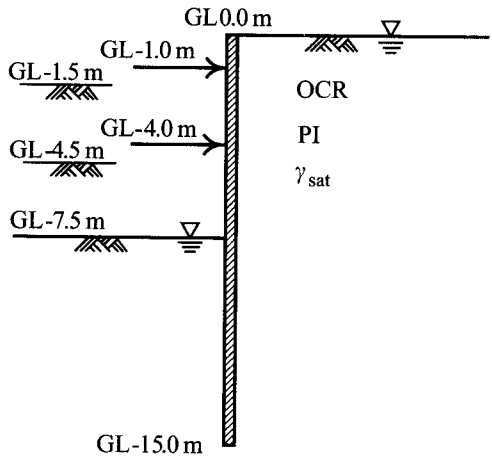

Figure P7.3

7.4 Suppose the stiffnesses of the two levels of struts are the same. Both are 35,000 kN/m/m (the reduced value). The stiffness of the retaining wall (reduced value) is 160,000 kN-m^2/m. Analyze the excavation-induced deformation of the retaining wall using the coefficients of subgrade reaction computed in Problem 7.3 and the VEX computer program (or other computer programs based on the beam on elastic foundation method) and compare the result with those obtained from the empirical equation in Chapter 6 to judge the rationality of the result.

7.5 Same as Figure P7.1 except the soil is normally consolidated clay whose OCR = 1. The plasticity index is about 25. The saturated unit weight of the soil $\gamma_{sat} = 17.7$ kN/m^3. The normalized undrained shear strength $s_u/\sigma'_v = 0.3$. Estimate the coefficient of subgrade reaction for the soil in front of the wall.

7.6 Same as above except the stiffnesses of the first and second levels of struts are 30,000 kN/m/m and 40,000 kN/m/m (reduced values), respectively. The stiffness of the retaining wall (EI) is 200,000 kN-m^2/m (reduced value). Analyze the excavation-induced deformation of the retaining wall using the coefficient of subgrade reaction computed in Problem 7.5 and the VEX computer program (or other computer programs

based on the beam on elastic foundation method) and compare the result with that obtained from the empirical equation in Chapter 6 to judge the rationality of the result.

7.7 Same as Figure P7.3 except the soil is normally consolidated clay whose OCR = 1. The plasticity index is about 25. The saturated unit weight of the soil $\gamma_{sat} = 17.7$ kN/m^3. The normalized undrained shear strength $s_u/\sigma'_v = 0.32$. Estimate the coefficient of subgrade reaction for the soil in front of the wall.

7.8 Same as above, but now supposing the stiffnesses of the two levels of struts are both 45,000 kN/m/m (reduced values). The stiffness of the retaining wall (EI) is 190,000 kN-m^2/m (reduced value). Analyze the excavation-induced deformation of the retaining wall using the coefficient of subgrade reaction computed in Problem 7.7 and the VEX computer program (or other computer programs based on the beam on elastic foundation method) and compare the result with that obtained from the empirical equation in Chapter 6 to judge the rationality of the analysis.

7.9 Assume the profile and stages of an excavation are as shown in Figure P7.1. The excavation depth is 8 m. The soil is sandy and the groundwater level is at the ground surface. The saturated unit weight of the soil $\gamma_{sat} = 21.6$ kN/m^3. The effective strength parameters $c' = 0$ and $\phi' = 32°$. The SPT-N value at a depth of 12 m below the ground surface before excavation $N = 15$. Estimate the coefficient of subgrade reaction for the soil in front of the wall (to simulate the actual conditions, the seepage should be considered in analysis).

7.10 Same as above. Assume the stiffnesses of the first and second levels of struts are 20,000 and 30,000 kN/m/m (reduced values). The stiffness of the retaining wall (EI) is 150,000 kN-m^2/m (reduced value). Analyze the deformation of the retaining wall using the coefficient of subgrade reaction obtained in Problem 7.9 and the VEX computer program and compare the result with the empirical equations introduced in Chapter 6 to judge the rationality of the analysis result.

7.11 Assume the profile and stages of an excavation are as shown in Figure P7.3. The excavation depth is 7 m. The soil is sandy and the groundwater level is at the ground surface. The saturated unit weight of the soil $\gamma_{sat} = 19.6$ kN/m^3 and the effective strength parameters $c' = 0$ and $\phi' = 33°$. The SPT-N value at GL-13 m before excavation is $N = 10$. Estimate the coefficient of subgrade reaction for the soil in front of the wall.

7.12 Same as above. Now assume the stiffness of the struts is 30,000 kN/m/m and that of the retaining wall (EI) is 150,000 kN-m^2/m (both reduced values). Analyze the deformation of the retaining wall using the coefficient of subgrade reaction derived from Problem 7.11 and the VEX computer program (or other computer programs based on the beam on elastic foundation method) and compare the result with the empirical equations introduced in Chapter 6 to judge the rationality of the analysis.

7.13 Same as Example 6.1. Figure 6.41 shows the profile and stages of the excavation of Building P in Taipei. The staged deformations of the retaining wall are as shown in Figure 6.42. Estimate the coefficient of subgrade reaction and analyze the excavation-induced deformation using the beam on elastic foundation method. Then compare the result with the observation value.

7.14 Same as Problem 6.11. Figure P6.11 shows the geological and excavation profiles for the Building S excavation. Figure P7.14 is the figure of the measured lateral deformations of the retaining wall in the central section of the longer side (89 m side) of the site. Estimate the coefficient of subgrade reaction and analyze the excavation-induced deformation using the beam on elastic foundation computer program. Compare the result with empirical value.

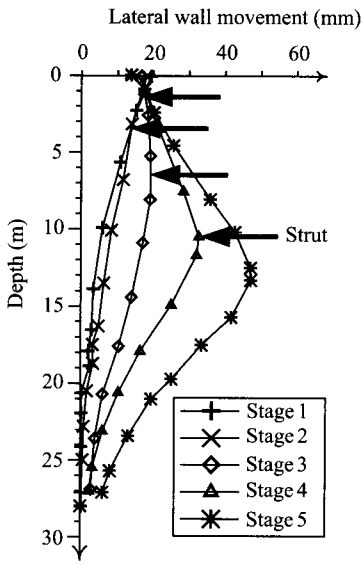

Figure P7.14

7.15 Same as Example 7.3. Assume the retaining wall is a sheetpile. Are there any parameters that should be modified before feeding the computer program to make the earth pressure theory used in the computer program be similar with the commonly used theory? (Note: According to Section 5.5, the adhesion between sheetpiles and soft clays can be rationally assumed $c_w = c/2$.)

7.16 Same as Example 7.3. Assume the soils within the site are sandy and the retaining wall is a diaphragm wall. Explicate how to feed the parameters to make the earth pressure theory used in the computer program be similar with the commonly used theory. (Note: according to Section 5.4, the friction between a diaphragm wall and sandy soils can be rationally assumed $\delta = 2\phi/3$.)

7.17 Same as Problem 6.4. Figure P6.4 shows the excavation profiles of the top-down construction of Building R in Taipei along with geological profile. Figure P7.17 shows

the measured lateral displacements of the retaining wall in the central section of the longer side of the site. Analyze the lateral displacements of the retaining wall using the beam on elastic foundation computer program with the suggested method introduced in this chapter and compare the results with the observed deformations.

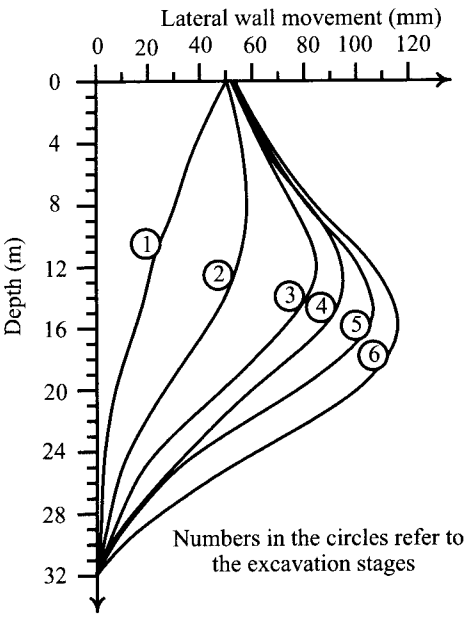

Figure P7.17

Chapter 8

Stress and deformation analysis

Finite element method

8.1 Introduction

As explained in Chapter 7, under normal excavation conditions, excavation-induced stress and deformation are engendered by unbalanced forces acting on the wall due to the removal of soils within the excavation zone. The magnitude of unbalanced forces is influenced by many factors: the conditions of soil layers, the table and pressures of groundwater, the excavation depth, the excavation width and so on. Theoretically, the finite element method is capable of simulating these factors and therefore the results derived from the method would be more accurate than those derived from simplified methods (Chapter 6) or the beam on elastic foundation method (Chapter 7). The theories on which the finite element method is based, however, are rather complicated and the data to be processed both before and after analysis are enormous. What's more, some of the theories are not fully developed. To apply a program based on the finite element method, analysts are required to be well equipped with comprehensive geotechnical knowledge and experience. All this adds confusion and trouble for analysts.

Considering the complexity of the finite element method and that any small neglect is likely to lead to wrong results, the results of the finite element method should be examined by other methods, the simplified methods, for example, to ensure the reasonability of the results.

Besides, some researchers write the governing equation in the form of an explicit finite difference equation and solve it by way of dynamic relaxation. The method solves the velocity and movement through the movement equation by assigning a damping value close to the critical damping. The strain rate is then obtained from velocity and used to solve the new stress increment. The process continues till the unbalanced forces are in equilibrium or the system reaches a steady state. The main theory on which the finite difference method is based is not the same as that of the finite element method. However, other theories, such as constitutive laws of soil, drained or undrained behaviors, determination of soil parameters, simulations of excavation, etc., are identical with the finite element method. If readers are to adopt the finite difference method to analyze deep excavation, the present chapter, except for Section 8.2, can also be used for reference.

As for the methods of analyzing excavation (see Section 8.8.1), direct analysis and back analysis of the finite element method are similar to the beam on elastic foundation method. In terms of stress type (see Section 8.8.2), the finite element method can be split into the total stress analysis and the effective stress analysis methods. Concerning the analysis of drained conditions (see Section 8.8.3), the finite element method can also be divided into the undrained

analysis method, drained analysis method, and the partially drained analysis method. With the finite element method, the undrained behaviors of clayey soils can be analyzed by total stress analysis, effective stress analysis, and coupled analysis. With the beam on elastic foundation method, the undrained behaviors of clayey soils can only be analyzed by undrained analysis (or total stress analysis).

Although many of the theoretical descriptions in this chapter are complicated, they are necessary knowledge for excavation analyses using the finite element method, and are also applicable to other problems concerning geotechnical engineering. Readers are advised to run programs according to the contents of this chapter to examine the correctness of analyses.

Although this chapter tries to elucidate the application of the finite element method on deep excavation in details, there remains much to be explored. For readers interested in the method, please see the related references. Besides, considering the complexity of the analysis process of the finite element method and the comprehensive knowledge required by analysts, this chapter is recommended for readers above the graduate level.

8.2 Basic principles

This section explains the basic principles of the finite element method. In an excavation, find a section whose behaviors meet the plane strain condition, the central section in most cases, as shown in Figure 8.1a. Take the profile of this section and divide the soils and structures within the excavation influence range into many meshes, each of which is called an element (see Figure 8.1b). According to the properties of the material of each element, establish its stress-strain relation, which is called the constitutive law. The constitutive law of an isotropic material can be expressed as follows:

$$\{\sigma\} = [C]\{\varepsilon\} \tag{8.1}$$

where

$\{\sigma\}$ = stress matrix. The sign { } refers to a column matrix
$\{\varepsilon\}$ = strain matrix
$[C]$ = stress-strain relational matrix.

Under the condition of plane strain, the matrices are

$$\{\sigma\} = \begin{Bmatrix} \sigma_{xx} \\ \sigma_{yy} \\ \tau_{xy} \end{Bmatrix} \tag{8.2}$$

$$\{\varepsilon\} = \begin{Bmatrix} \varepsilon_{xx} \\ \varepsilon_{yy} \\ \gamma_{xy} \end{Bmatrix} \tag{8.3}$$

$$[C] = \frac{E}{(1+\nu)(1-2\nu)} \begin{bmatrix} (1-\nu) & \nu & 0 \\ \nu & (1-\nu) & 0 \\ 0 & 0 & (1-2\nu)/2 \end{bmatrix} \tag{8.4}$$

E and ν in Eq. 8.4 are Young's modulus and Poisson's ratio, respectively.

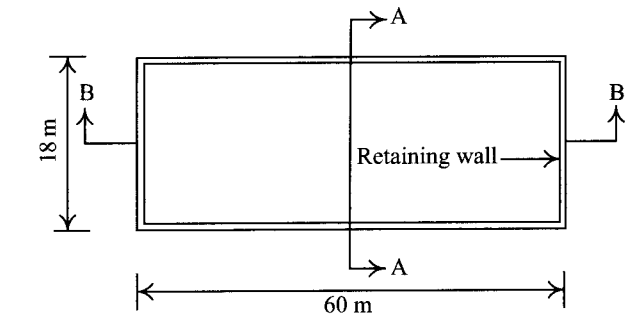

(a)

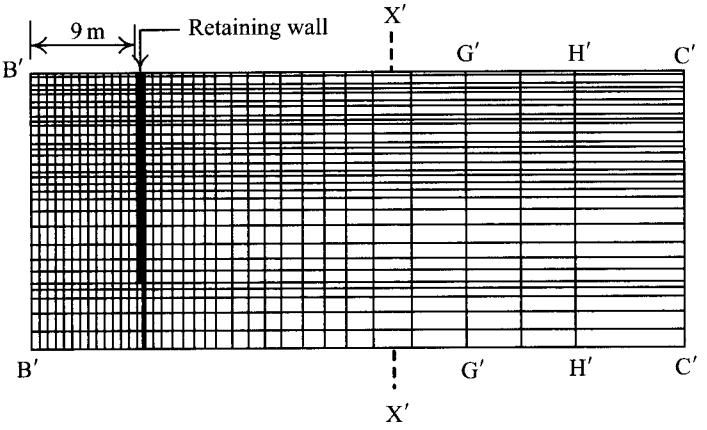

(b)

Figure 8.1 Finite element analysis of an excavation: (a) plan and (b) meshes of the section A–A.

As shown in Figure 8.2, the relation between the displacement at any point within the element and that of the nodal point of the element can be expressed as follows:

$$\{u\} = [f]\{q\} \tag{8.5}$$

where $[f]$ = displacement shape function.

According to the theory of elasticity, the strain and displacement at a point within the element have a relation which can be expressed as follows:

$$\{\varepsilon\} = [d]\{u\} = [d][f]\{q\} = [B]\{q\} \tag{8.6}$$

where $[d]$ = linear partial differential operator, such as $\partial/\partial x$, $\partial/\partial y$, etc., $[B] = [d][f] =$ relational matrix between the strain and the nodal displacement.

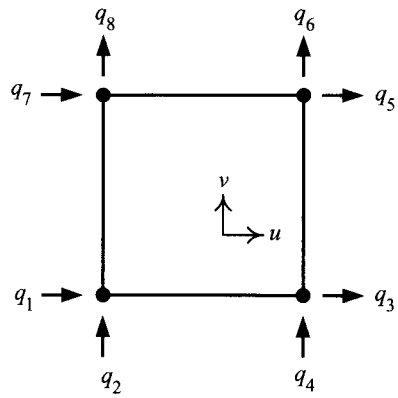

Figure 8.2 Four-node element.

According to the principle of virtual work, we can derive the stiffness matrix of the element to be:

$$[K_e] = \int_V [B]^T [C][B] \mathrm{d}V \tag{8.7}$$

After establishing the relational matrices for all the elements, combine them into the global stiffness matrix $[K]$. Then compute the excavation- or load-induced external forces, which are then transformed into the external force of the nodal points. The following equation can then be established:

$$[K]\{q\} = \{P\} \tag{8.8}$$

where

$\{q\}$ = nodal displacement matrix
$[K]$ = global stiffness matrix
$\{P\}$ = matrix of excavation-induced external force or equivalent nodal load at nodal points.

The nodal displacement $\{q\}$ can then be solved by way of the Gauss elimination method or other numerical methods. Using Eq. 8.5, we can then obtain the displacement at any point within the element. By means of Eq. 8.6, the strain at any point within the element can be obtained. Lastly, use Eq. 8.1 for obtaining the stresses at any point within the element. As a result, we can obtain the deformation, the stress, the strain, the bending moment of the retaining wall, the ground surface settlement, and the movement of the excavation bottom.

When the displacement shape function $[f]$ is quadratic, differentiated by the partial differential operator $[d]$, the matrix $[B]$ becomes linear, which shows that the strain within the element changes linearly. The element within which the strain changes linearly is called the low order element. Otherwise, those within which strains do not change linearly are called high order elements.

Since the order of the shape functions of high order elements is higher than those of the low order elements, the number of nodes of high order elements is larger than that of low order elements. High order elements are more capable of coping with the rapid change of stress or strain within an element and are thereby more accurate than low order elements.

The commonly used deformation parameters, in addition to E and ν in $[C]$ in Eq. 8.4, can also be represented by the shear modulus G, the bulk modulus B, and the constrained modulus M. Their definitions are as shown in Figure 8.3 and explained as follows:

As shown in Figure 8.3a, under the compressive force, E and ν are separately defined as

$$E = \frac{\sigma_1}{\varepsilon_1} \tag{8.9}$$

$$\nu = -\frac{\varepsilon_2}{\varepsilon_1} = -\frac{\varepsilon_3}{\varepsilon_1} \tag{8.10}$$

Figure 8.3b shows the strains ε_1, ε_2, and ε_3 produced under the action of the stresses, σ_1, σ_2, and σ_3. Thus, the bulk modulus is

$$B = \frac{\sigma_{avg}}{\varepsilon_v} = \frac{\sigma_1 + \sigma_2 + \sigma_3}{3\varepsilon_v} \tag{8.11}$$

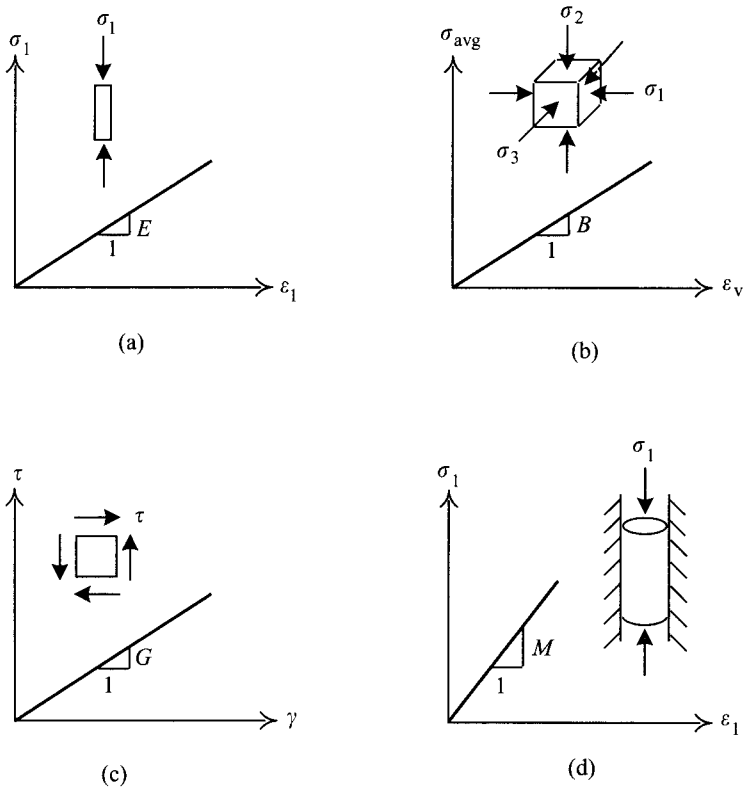

Figure 8.3 Definitions of various deformation moduli: (a) Young's modulus, (b) bulk modulus, (c) shear modulus, and (d) constrained modulus.

where

ε_v = volumetric strain = $\Delta V/V \approx \varepsilon_1 + \varepsilon_2 + \varepsilon_3$
ΔV = change of the volume
V = volume.

Figure 8.3c shows the shear strain produced under the action of the shear stress, τ. Thus, the shear modulus is

$$G = \frac{\tau}{\gamma} \tag{8.12}$$

where γ = shear strain.

Figure 8.3d displays the axial load, σ_1, on the material while the lateral strain is restrained. That is, the lateral strain is 0. The constrained modulus is

$$M = \frac{\sigma_1}{\varepsilon_1} \tag{8.13}$$

According to the theory of elasticity, the relationship between the deformation parameters E, v, G, B, and M can be derived, as shown in Table 8.1. That is, $[C]$ in Eq. 8.4 can also be expressed by any two parameters among E, v, G, B, and M. Thereby, the matrix $[C]$ in Eq. 8.4 is also often expressed in G and B as follows:

$$[C] = \begin{bmatrix} (3B+4G)/3 & (3B-2G)/3 & 0 \\ (3B-2G)/3 & (3B+4G)/3 & 0 \\ 0 & 0 & G \end{bmatrix} \tag{8.14}$$

In the plane strain excavation analysis, the commonly used elements can be categorized into the plane strain elements, the bar elements, and the beam elements, etc. They are explained as follows:

8.2.1 Plane strain elements

In terms of shape, plane strain elements are usually categorized into triangular elements and quadrilateral elements. As shown in Figure 8.4, the commonly used triangular elements are the constant strain triangular elements (CST elements), also called the T3 elements (Triangular with 3 nodes) where the strain variation is constant, and the linear strain elements (LST elements), also called the T6 elements (Triangular with 6 nodes) where the strain varies linearly. The commonly used quadrilateral elements are Q4 elements and Q8 elements. The former consist of 4 nodes for each and strains change linearly. They are thereby called low order elements. The latter have 8 nodes for each and the strain changes nonlinearly. They thus belong to high order elements, as shown in Figure 8.5.

In general excavation analysis, the plane strain elements are used to simulate soils and structural materials. High order plane strain elements, such as a Q8 element, are more recommended, considering the accuracy of analysis. Usually, the accuracy of a Q8 element is better than that of four Q4 elements, as shown in Figure 8.6.

Table 8.1 Relations between elastic deformation parameters (after Chen and Saleeb, 1982)

	G	E	M	B	λ	ν
G, E	B	E	$\frac{G(4G-E)}{3G-E}$	$\frac{GE}{9G-3E}$	$\frac{G(E-2G)}{3G-E}$	$\frac{E-2G}{2G}$
G, M	G	$\frac{G(3M-4G)}{M-G}$	M	$M-\frac{4G}{3}$	$M-2G$	$\frac{M-2G}{2(M-G)}$
G, B	G	$\frac{9GB}{3B+G}$	$B+\frac{4G}{3}$	B	$B-\frac{2G}{3}$	$\frac{3B-2G}{2(3B+G)}$
G, λ	G	$\frac{G(3\lambda+2G)}{\lambda+G}$	$\lambda+2G$	$\lambda+\frac{2G}{3}$	λ	$\frac{\lambda}{2(\lambda+G)}$
G, ν	G	$2G(1+\nu)$	$\frac{2G(1-\nu)}{1-2\nu}$	$\frac{2G(1+\nu)}{3(1-2\nu)}$	$\frac{2G\nu}{1-2\nu}$	ν
E, B	$\frac{3BE}{9B-E}$	E	$\frac{B(9B+3E)}{9B-E}$	B	$\frac{B(9B-3E)}{9B-E}$	$\frac{3B-E}{6B}$
E, ν	$\frac{E}{2(1+\nu)}$	E	$\frac{E(1-\nu)}{(1+\nu)(1-2\nu)}$	$\frac{E}{3(1-2\nu)}$	$\frac{\nu E}{(1+\nu)(1-2\nu)}$	ν
B, λ	$\frac{3(B-\lambda)}{2}$	$\frac{9B(B-\lambda)}{3B-\lambda}$	$3B-2\lambda$	B	λ	$\frac{\lambda}{3B-\lambda}$
B, M	$\frac{3(M-B)}{4}$	$\frac{9B(M-B)}{3B+M}$	M	B	$\frac{3B-M}{2}$	$\frac{3B(2M-1)+M}{3B(2M+1)-M}$
B, ν	$\frac{3B(1-2\nu)}{2(1+\nu)}$	$3B(1-2\nu)$	$\frac{3B(1-2\nu)}{1+\nu}$	B	$\frac{3B\nu}{1+\nu}$	ν

Note
λ is Lame parameter. For its definition, please see books on theory of elasticity. It is, though, rarely used in geotechnical analyses.

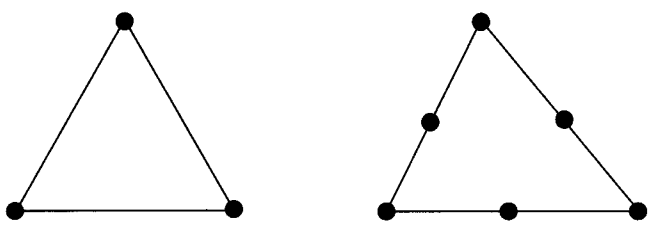

(a) (b)

Figure 8.4 Triangular elements: (a) CST element and (b) LST element.

8.2.2 Bar elements

Bar elements, also called truss elements, are used to simulate struts, anchors, or other members bearing only axial stress, as shown in Figure 8.7. Each node of a bar element has only one degree of freedom. A bar element of low order has two nodes while one of high order has three nodes. In general excavation analyses, two node bar elements can achieve good accuracy.

Figure 8.5 Quadrilateral elements: (a) Q4 element and (b) Q8 element.

Figure 8.6 Comparison of accuracy between a Q8 element and four Q4 elements.

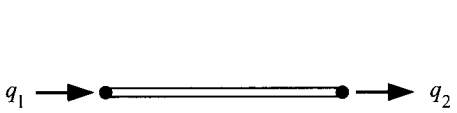

Figure 8.7 Two-node bar element.

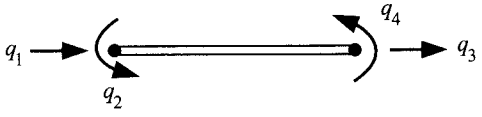

Figure 8.8 Two-node beam element.

8.2.3 Beam elements

Beam elements, also called flexural elements, are used to simulate members subjected to moment, as shown in Figure 8.8. Each node of a beam element has two degrees of freedom. A beam element of low order has two nodes while one of high order has three nodes. In general excavation analyses, the two node beam element can achieve good accuracy.

8.2.4 Interface elements

The finite element method is based on continuum mechanics and is incapable of effectively evaluating the loading and displacement conditions induced by relative displacement between materials. Retaining walls used in excavation are stiff while the adjacent material, soil, is relatively soft. When the retaining wall deforms, relative displacement may be generated between the soil and the wall. To simulate the relative displacement between soil and structures during excavation, interface elements are sometimes used in analysis.

As shown in Figure 8.9, an interface element is an element connecting structures and soil, with or without thickness, which has a quite large normal stiffness but relatively small

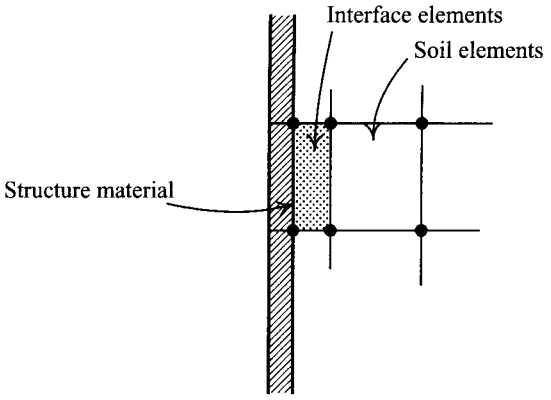

Figure 8.9 Interface element.

shear stiffness so that it can simulate the relative displacement between soil and structures. Concerning the studies of interface elements, readers can refer to the literature (Goodman *et al.*, 1968; Pande and Sharma, 1979; Sachdeva and Ramakrishnan, 1981; Desai and Nagaraj, 1988; Sharman and Desai, 1992).

Though interface elements can rationally simulate the relative displacement between soil and structures, since extra parameters, which are not easily obtained from conventional soil tests, will be introduced, and numerical instability during analysis often occurs, they have to be used especially carefully. If interface elements are not to be adopted, the soil in the vicinity of the structure can be considered to divide into fine elements. When the retaining wall is deformed, these fine soil elements can easily attain the plastic state, which will then produce larger deformation. Therefore, a rational analysis result is also attainable.

This section only succinctly elucidates the basic principles of the finite element method. As for other inferring processes and important related theories, please refer to related publications. This book will not go into them.

8.3 Stress-strain relationship and constitutive laws of soils

Figure 8.10 shows the typical soil stress-strain relation where soil has the characteristics of nonlinear, plastic, and confining pressure-related behaviors. According to the principle of effective stress, the stress-strain relation of soil relates to the stress path, and sometimes even to the time. The soil model in excavation analyses should fully consider these soil properties. The hyperbolic model, the elasto-plastic model, and the Cam-clay model are the commonly used models in geotechnical engineering. They are introduced in the following sections.

8.3.1 Elastic incremental model—the hyperbolic model

The elastic incremental model is to add loads stage by stage, simulating the stress-strain relation for each stage load, based on linear elasticity so that the nonlinear stress-strain relation of soils can be simulated. According to Eq. 8.1, the incremental stress-strain relation can be

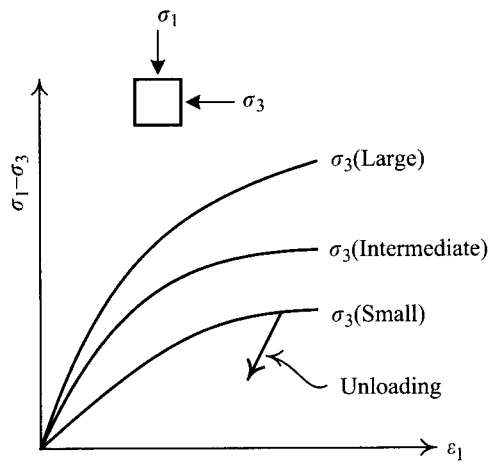

Figure 8.10 Typical stress-strain relations of soils.

expressed as follows:

$$\{\Delta\sigma\} = [C]\{\Delta\varepsilon\} \tag{8.15}$$

where

$\{\Delta\sigma\}$ = stress increment matrix
$\{\Delta\varepsilon\}$ = strain increment matrix
$[C]$ = stress-strain relation matrix.

There are many elastic incremental models. Among them, the hyperbolic model is the most widely applied one. Therefore, this section will only introduce the hyperbolic model. Readers interested in other elastic incremental models can refer to the related literature (e.g. Desai and Siriwardane, 1984).

Basically, the hyperbolic model is used to simulate the soil stress-strain curve using hyperbolic functions, by observing the characteristics of the soil stress-strain curve, such as the slope, degree of bending, and the ultimate strength. Duncan and Chang (1970), based on Konder's study (Konder, 1963), proposed that the soil stress-strain behaviors be expressed in hyperbolic curves, as shown in Figure 8.11. The hyperbolic curves can be expressed by the following equation.

$$\sigma_1 - \sigma_3 = \frac{\varepsilon}{1/E_i + \varepsilon/(\sigma_1 - \sigma_3)_{\text{ult}}} \tag{8.16}$$

where

σ_1 = major principal stress
σ_3 = minor principal stress
ε = axial strain

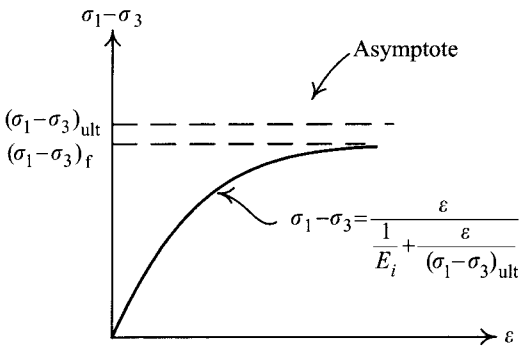

Figure 8.11 Hyperbolic model.

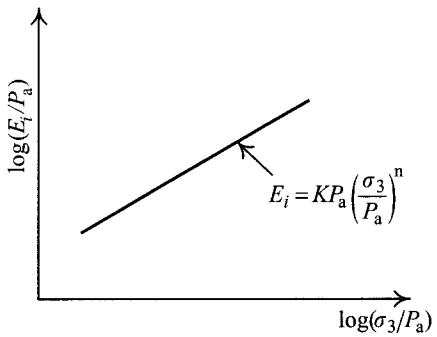

Figure 8.12 Relation between the initial Young's modulus and confining pressure.

E_i = initial tangent modulus
$(\sigma_1 - \sigma_3)_{ult}$ = asymptote of the stress-strain curve, representing the ultimate strength.

Under drained conditions, the stress-strain relation and the confining pressure are related. Janbu (1963) thus proposed the relation between E_i and σ_3 as follows (see Figure 8.12):

$$E_i = KP_a\left(\frac{\sigma_3}{P_a}\right)^n \tag{8.17}$$

where

P_a = atmospheric pressure = 1.033 kg/cm^2 = 101.3 kN/m^2 = 2116.2 lb/ft^2
K = dimensionless stiffness modulus number
n = dimensionless stiffness modulus exponent.

Figure 8.10 also shows that E_i increases with the increase of σ_3. Assume $(\sigma_1 - \sigma_3)_f$ to be the stress difference at failure, $(\sigma_1 - \sigma_3)_f$ and $(\sigma_1 - \sigma_3)_{ult}$ have the following relation:

$$(\sigma_1 - \sigma_3)_f = R_f(\sigma_1 - \sigma_3)_{ult} \tag{8.18}$$

where R_f = failure ratio. For most types of soil, R_f ranges between 0.5 and 0.9.

According to the Mohr-Coulomb failure theory, the relation between $(\sigma_1 - \sigma_3)_f$ and σ_3 can be expressed as

$$(\sigma_1 - \sigma_3)_f = \frac{2c\cos\phi + 2\sigma_3 \sin\phi}{1 - \sin\phi} \tag{8.19}$$

where c and ϕ are the strength parameters of soil.

For cohesionless soils, the angle of shear resistance decreases in proportion to the logarithm of the confining pressure. That is, the angle of shear resistance of soil under any confining pressure can be expressed as

$$\phi = \phi_0 - \Delta\phi \log_{10}\left(\frac{\sigma_3}{P_a}\right) \tag{8.20}$$

where ϕ_0 is the angle of shear resistance under the confining pressure of one atmospheric pressure and $\Delta\phi$ is the slope of the $\phi - \log_{10}(\sigma_3/P_a)$ curve.

Substitute Eqs 8.17, 8.18, and 8.19 in Eq. 8.16, and differentiate it with respect to strain, and then we can obtain the tangent elastic modulus E_t for any stress state as follows:

$$E_t = \left[1 - \frac{R_f(1 - \sin\phi)(\sigma_1 - \sigma_3)}{2c\cos\phi + 2\sigma_3 \sin\phi}\right]^2 KP_a\left(\frac{\sigma_3}{P_a}\right)^n = [1 - R_f \cdot \mathrm{SL}]^2 KP_a\left(\frac{\sigma_3}{P_a}\right)^n \tag{8.21}$$

where $\mathrm{SL} = (\sigma_1 - \sigma_3)/(\sigma_1 - \sigma_3)_f$, which is called the stress level. The stress level represents how close the soil is to the failure state. When SL = 0, it means the soil is in the zero loading state. When SL = 1, it indicates that the soil is in the failure state.

When soil is in the state of unloading or reloading, the elastic Young's modulus (E_{ur}) will be independent of strain but relates to the confining pressure (σ_3), as shown in Figure 8.13. E_{ur} can be expressed as follows:

$$E_{ur} = K_{ur}P_a\left(\frac{\sigma_3}{P_a}\right)^n \tag{8.22}$$

where K_{ur} = dimensionless unloading/reloading stiffness modulus number.

Though the soil stress-strain relation is nonlinear, the stress-strain relation at each load stage can be simulated as linear elastic if loading is divided into many stages and Young's modulus for the load stage can be expressed in E_t, as shown in Figure 8.14. Though the soil stress-strain relation is inelastic (i.e. plastic), the permanent deformation can be obtained by the model with the introduction E_{ur} into it. Thus, the hyperbolic model can simulate the characteristics of the nonlinearity and plasticity of soil.

According to Eqs 8.4 and 8.7, to establish the stiffness matrix of an element, the required parameters are E (representing E_t or E_{ur}) and ν. According to Eqs 8.16 or 8.21, if using the hyperbolic model to describe the stiffness matrix at a stress level or in a stress state, the required parameters are c, ϕ_0, $\Delta\phi$, K, n, K_{ur}, R_f, and ν.

Since the hyperbolic model, dividing the load into several stages and for each stage load substituting E_t (or E_{ur}) and ν into $[C]$ in Eq. 8.4 in analysis, uses the theory of elasticity without involving the plasticity theory, the hyperbolic model is usually categorized as an elastic model.

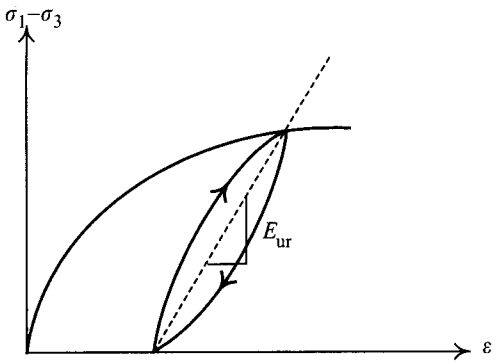

Figure 8.13 Unloading-reloading Young's modulus.

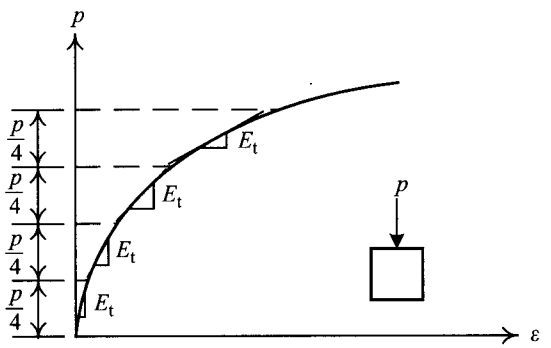

Figure 8.14 Variation of the tangent Young's modulus with strain.

8.3.2 *Linear elastic elastoplastic model*

Figure 8.15 shows the commonly used linear elastic elastoplastic model. Basically, the linear elastic elastoplastic model uses the linear elastic model to simulate the soil stress-strain relation till the yielding point **a** is achieved. Then the plastic model is used to simulate the behaviors after the yielding point, which is defined by a yielding function. In a stress space, a yielding function forms a surface, which is called the yielding surface. In the theory of plasticity, along the stress paths within the yielding surface only elastic strain is produced. When the stress state is on the yielding surface, stress paths moving toward the interior of the yielding surface will also produce elastic strain. Only when the stress path moves outward from the yielding surface is plastic strain produced.

Assume F in Figure 8.16 is a yielding surface in the two dimensional stress space and only elastic strain is produced along the stress paths **ab** and **cd,** whereas along **ef** plastic strain is produced. When soil is unloaded from any point on line **ab** in Figure 8.15a, its behavior will be similar to that on **ab** in Figure 8.16, that is, only elastic strain is produced.

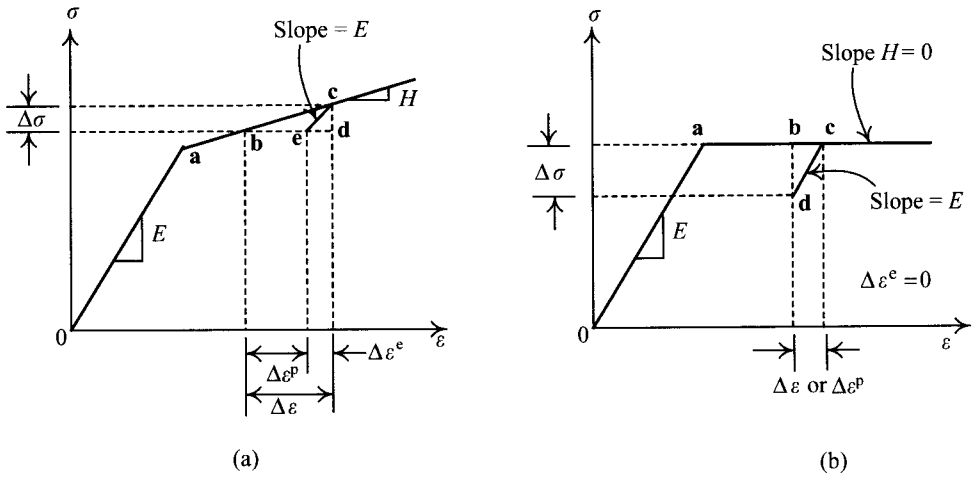

Figure 8.15 Commonly used plastic models: (a) linear elastic elastoplastic model and (b) linear elastic perfectly plastic model.

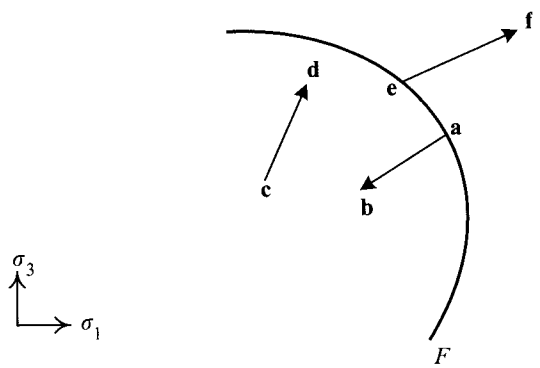

Figure 8.16 Yielding surface and stress paths.

As shown in Figure 8.15a, when soil is subjected to a small stress increment $\Delta\sigma$ (from **b** to **c** in the figure), both elastic strain and plastic strain increments will be produced. The elastic strain increment is the strain between **c** and **e** (i.e. line **ed**), produced by unloading to the original stress. The plastic strain increment ($\Delta\varepsilon^p$) is the total strain increment reduced by the elastic strain increment. Since both elastic strain and plastic strain are produced when the stress changes from **b** to **c**, it is therefore called elastoplastic behavior. Materials exhibiting elastoplastic behavior are called elastoplastic materials. A model capable of simulating elastoplastic behaviors is called an elastoplastic model. Usually, before achieving the yielding point, the behavior can be simulated by the linear elastic model. Therefore, a model simulating both linear elasticity before the yielding point and elastoplasticity after reaching the yielding point is called a linear elastic elastoplastic model.

As shown in Figure 8.15b, if the stress-strain curve after the yielding point is horizontal (i.e. the slope $H = 0$), the stress, changing from **b** to **c**, only produces plastic strain without any elastic strain. This type of behavior, material, and model are called perfectly plastic behavior, perfectly plastic material, and perfectly plastic model, respectively.

As shown in Figure 8.15, between the total strain increment ($\Delta\varepsilon$), the elastic strain increment ($\Delta\varepsilon^{e}$), and the plastic strain increment ($\Delta\varepsilon^{p}$) exists the following relation:

$$\Delta\varepsilon = \Delta\varepsilon^{e} + \Delta\varepsilon^{p} \tag{8.23}$$

Considering the three dimensional stress and strain conditions, expressing the above equation in matrix, we can derive:

$$\{\Delta\varepsilon\} = \{\Delta\varepsilon^{e}\} + \{\Delta\varepsilon^{p}\} \tag{8.24}$$

According to the theory of elasticity, we have

$$\{\Delta\varepsilon^{e}\} = [C]^{-1}\{\Delta\sigma\} \tag{8.25}$$

where $[C]$ is the stress-strain relational matrix (see Eq. 8.1). If we substitute the above equation into Eq. 8.24, we have

$$\{\Delta\varepsilon\} = \{\Delta\varepsilon^{e}\} + \{\Delta\varepsilon^{p}\} = [C]^{-1}\{\Delta\sigma\} + \{\Delta\varepsilon^{p}\} \tag{8.26}$$

Therefore,

$$[C]\{\Delta\varepsilon\} = \{\Delta\sigma\} + [C]\{\Delta\varepsilon^{p}\} \tag{8.27}$$

$$\{\Delta\sigma\} = [C]\{\Delta\varepsilon\} - [C]\{\Delta\varepsilon^{p}\} \tag{8.28}$$

Assume the yielding function of the soil is F and the plastic potential function is Q. According to the flow rule, Eq. 8.28 can be rewritten into the following

$$\{\Delta\sigma\} = \left\{[C] - \frac{\{\alpha\}\{\beta\}^{T}}{N}\right\}\{\Delta\varepsilon\} = \{[C] - [C^{p}]\}\{\Delta\varepsilon\} = [C^{ep}]\{\Delta\varepsilon\} \tag{8.29}$$

where

$$[C^{ep}] = [C] - [C^{p}] \tag{8.30}$$

$$\{\alpha\} = [C]\begin{Bmatrix} \partial Q/\partial\sigma_1 \\ \partial Q/\partial\sigma_2 \\ \partial Q/\partial\sigma_3 \end{Bmatrix} \qquad \{\beta\} = [C]\begin{Bmatrix} \partial F/\partial\sigma_1 \\ \partial F/\partial\sigma_2 \\ \partial F/\partial\sigma_3 \end{Bmatrix} \tag{8.31}$$

$$N = \{\beta\}^{T}\begin{Bmatrix} \partial Q/\partial\sigma_1 \\ \partial Q/\partial\sigma_2 \\ \partial Q/\partial\sigma_3 \end{Bmatrix} \tag{8.32}$$

where σ_1, σ_2, and σ_3 represent the major, intermediate, and minor principal stresses. N is a constant.

In the theory of plasticity, when $F = Q$, called the associated flow rule and $[C^p]$ in Eq. 8.29 then becomes a symmetrical matrix. Since $[C]$ is already a symmetrical matrix $[C^{ep}]$ and the stiffness matrix $[K]$ become symmetrical matrices, too (see Eq. 8.7). If $[K]$ is a symmetrical matrix, the required computer memory and computing time are much reduced when performing the finite element analysis.

When $F \neq Q$, it is called the non-associated flow rule, which is better capable of simulating soil behaviors. $[C^{ep}]$ is not a symmetrical matrix and will take more computer memory and time to compute in analysis.

The associated flow rule, however, cannot fully simulate the soil behaviors and is less accurate than the non-associated flow rule.

According to Eqs 8.29, 8.30, 8.31, and 8.32, to determine $[C^{ep}]$ or $[K]$ one has to determine not only the linear elastic E and v in $[C]$ but also the yielding function, F (assuming the associated flow rule). In most analyses, the failure criterion is often adopted as the yielding function, some commonly used failure criteria are the Mohr-Coulomb criterion, the von Mises criterion, the Tresca and the Drucker-Prager criteria. If the Mohr-Coulomb criterion is adopted as the yielding function and the slope of line segment **ac** (Figure 8.15) is assumed H, the required parameters would be only five: E, v, c, ϕ, and H.

In the elastoplastic model, some commonly used yielding functions are also the Mohr-Coulomb function, the von Mises function, the Tresca and the Drucker-Prager functions. Some of them have properties such that the yielding stress or strength increases with the increase of the average principal stress. These are called effective yielding surfaces. Some have constant yielding stress that does not change with the average principal stress and are called total yielding surfaces.

For drained analysis, it is the effective yielding surface that should be adopted. For undrained analysis, the total yielding surface should be adopted. The undrained analysis can also use effective yielding surface, where the values of E and v have to be decided carefully so that the analysis results will conform to the undrained behavior, that is, the volumetric strain should be 0. The undrained behaviors of clayey soils can also be analyzed using the porewater pressure-related coupled analysis. This type of analysis is an effective stress analysis, which can take into account the porewater pressure dissipation during analysis. The required parameter, in addition to the above-mentioned ones, is the coefficient of permeability.

The introductions to the above analyses are in Section 8.8. Interested readers can also refer to the related literature (Finno, 1983; Borja, 1990; Ou and Lai, 1994). For beginners, we advise using the Mohr-Coulomb yielding function and the effective stress analysis for sandy or gravelly soils, and the Mohr-Coulomb yielding function with $\phi = 0$ or the Tresca yielding function for saturated clayey soils.

8.3.3 Cam-clay model and other high order models

The Cam-clay model is derived according to critical state soil mechanics. First, define the mean effective stress (p') and the deviator stress (q) on the basis of the test results of the laboratory triaxial test:

$$p' = \tfrac{1}{3}(\sigma_1' + \sigma_2' + \sigma_3') \tag{8.33}$$

$$q = \sigma_1' - \sigma_3' \tag{8.34}$$

where σ_1', σ_2', σ_3' are the major, intermediate and minor principal stresses.

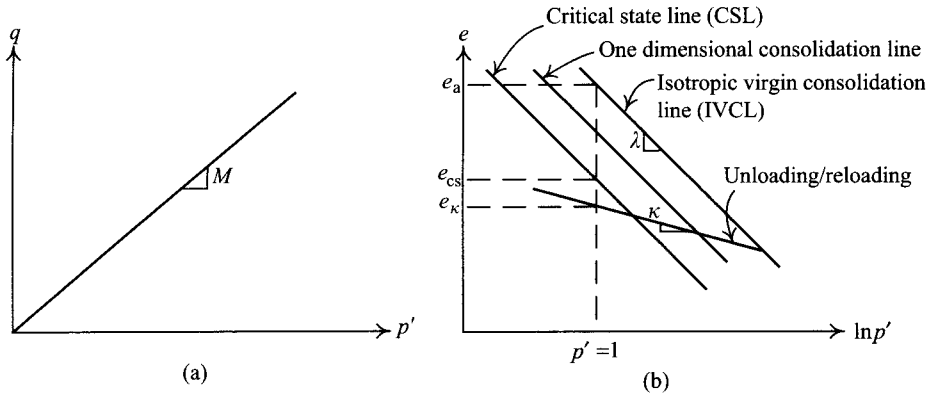

Figure 8.17 Definitions of various parameters in critical state soil mechanics: (a) $p' - q$ relation in the critical state and (b) critical state line and the consolidation line.

The critical state of soil refers to the state where volumetric strain is not further produced with the increase of shear strain at large shear strain. The state is usually either the failure state or the ultimate state. The critical state can be expressed by the following two equations:

$$q = Mp' \tag{8.35}$$

$$e = e_{cs} - \lambda \ln p' \tag{8.36}$$

where

e = void ratio
e_{cs} = void ratio when $p' = 1$ on the critical state line
M = slope of the critical state line on the $p' - q$ plane
λ = slope of the critical state line on the $e - \ln p'$ plane.

Assume the soil consolidation is in the isotropic consolidation state ($\sigma_1 = \sigma_2 = \sigma_3$). The $e - p'$ curve obtained from the isotropic consolidation is called the virgin isotropic consolidation line, as shown in Figure 8.17. It can be expressed by the following equation:

$$e = e_a - \lambda \ln p' \tag{8.37}$$

where e_a is the void ratio when p' = one unit and λ = the slope. In the $e - p'$ coordinate, the critical state line, the virgin one-dimensional consolidation line, and the isotropic virgin consolidation line parallel one another.

The unloading/reloading line represents the soil in the overconsolidated state. No plastic strain would be generated in the soil in this state. That is, the soil would be in the elastic condition. If we designate the slope as k, the unloading/reloading equation can be expressed as follows:

$$e = e_\kappa - \kappa \ln p' \tag{8.38}$$

where e_κ = void ratio when p' = one unit. κ is the slope of the unloading/reloading line.

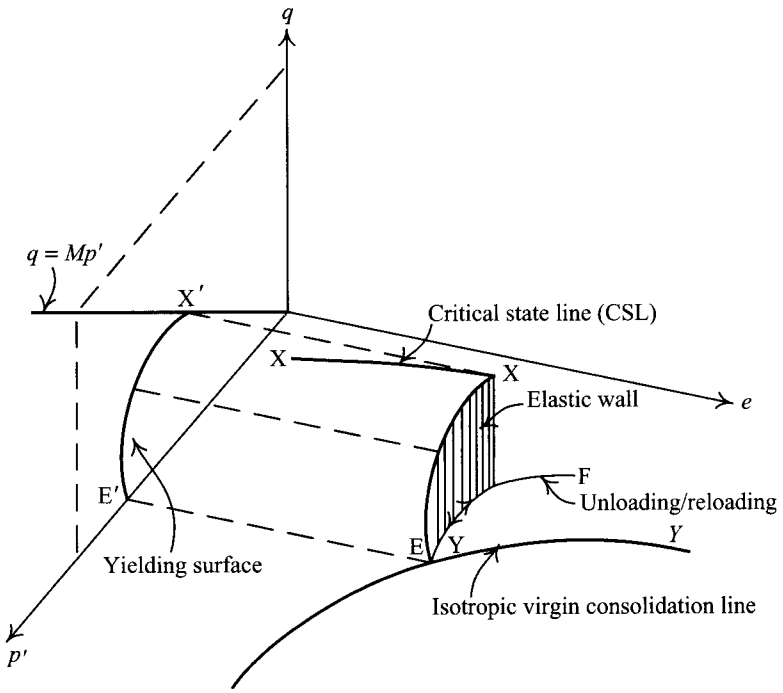

Figure 8.18 State boundary surface.

Critical state soil mechanics assumes there exists a single state boundary surface for normally consolidated or lightly overconsolidated soils in the $e - p' - q$ space, as shown in Figure 8.18. The state boundary surface intersects the plane $q = 0$ along line YY, which is called the virgin isotropic consolidated line. The border line of the state boundary surface is line XX. The state boundary surface represents the stress states in the various ultimate conditions (the coordinates of the stress states are e, p', q). That is, the stress states of soil exist only on or below the state boundary surface.

Assume the stress state of soil is on the swelling line (EF), only elastic deformation is produced, that is, no plastic deformation is produced. Furthermore, all paths that remain on the curved vertical plane above the swelling line EF, but below the state boundary surface, will only induce elastic deformation. Thus, this curve plane is called the elastic wall. Line EX, the state boundary surface intersecting with the elastic wall, is then projected onto the plane of $e = 0$, which forms line E′X′. E′X′ is generally defined as a yielding surface. As discussed above, if the state boundary surface is known, we can then derive the yielding function.

The Cam-clay model derives the state boundary surface and the yielding function on the basis of energy dissipation of soil after it has sheared. Depending on the assumption of the energy dissipation, the model can be divided into the original Cam-clay model and the modified Cam-clay model. With rational assumptions, the latter has become one of the most widely adopted analysis models in geotechnical engineering. According to Roscoe and Burland (1968), the equations for the state boundary surface with the modified Cam-clay

model are

$$\frac{p}{p_e} = \left(\frac{M^2}{M^2 + q^2/p^2}\right)^{(1-\kappa/\lambda)} \tag{8.39}$$

$$p_e = \exp\left(\frac{e_a - e}{\lambda}\right) \tag{8.40}$$

The yielding equation

$$p = p_0\left(\frac{M^2}{M^2 + q^2/p^2}\right) \tag{8.41}$$

where p_0 is the p-value when $q = 0$.

With the yielding equation given above, we can then obtain the constitutive law for the Cam-clay elastoplastic model according to Eqs 8.29–8.32. As discussed above, the parameters related to the state boundary surface or the yielding surface are M, λ, and κ. Thus, if the Cam-clay model is adopted as the yielding equation, in addition to E and v, the extra required input parameters are M, λ, and κ.

The Cam-clay model or the modified Cam-clay model can simulate the elastoplastic behaviors after loading. They are thereby, elastoplastic models also. Though the derivation of the Cam-clay model is theoretically rigorous, having the theoretical basis and having it confirmed by soil tests, it is still limited in application because it does not consider the anisotropic and overconsolidated behaviors of soil. Therefore, some high order elastoplastic models have been developed, for example, the anisotropic bounding surface model, the MIT-E3 model, etc. These high order models can analyze soil behaviors more accurately and rationally.

As discussed above, the Cam-clay model, the anisotropic bounding surface model (Finno and Harahap, 1991), the MIT-E3 model (Whittle *et al.*, 1993), and other high order effective stress models can all rationally simulate nonlinearity and plasticity. The required parameters such as M, λ, and κ are hardly disturbed during the process of sampling. As discussed in Section 8.3.2 regarding the elastoplastic analysis, the models can be used for drained analysis, undrained analysis, and coupled analysis.

8.4 Stress-strain relationship of structural materials and structural models

The structural materials used in excavations include retaining walls, struts, wales, central posts, etc. This chapter will only discuss retaining walls and struts. As for wales and central posts, please refer to Chapter 10.

The yielding stress of the retaining wall and struts is usually very high and can be analyzed using linear elastic models. That is, Young's modulus and Poisson's ratio are assumed to be constants.

Either plane strain elements or beam elements can be used for the analysis of retaining walls. If beam elements are adopted, the bending moment of the retaining wall can be found at each node of the elements. If plane strain elements are adopted instead, the bending moment of the retaining wall can be computed through the stresses at the integration points within the element. For example, a Q8 plane strain element has 9 integration points. The relative

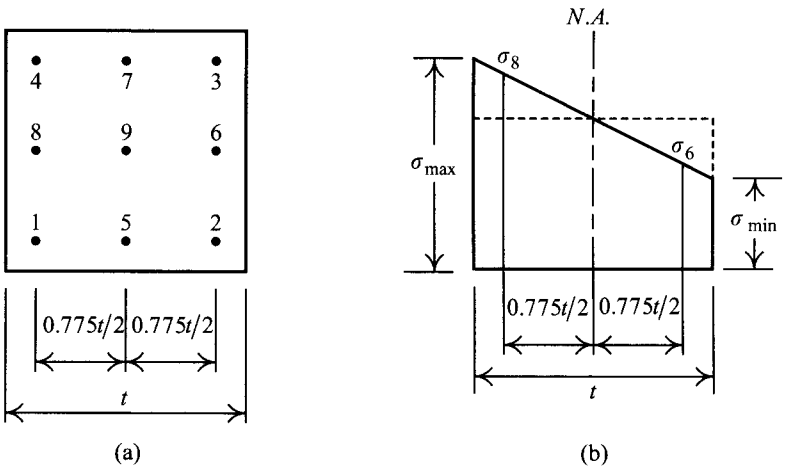

Figure 8.19 Computation of the bending moment of the retaining wall: (a) locations of the integration points and (b) stress distribution on the section.

positions of the integration points are as shown in Figure 8.19a. The finite element method can directly obtain the stresses at these 9 integration points. Figure 8.19b shows the typical distribution of stresses due to bending in the central section of the retaining wall. The stress includes the axial stress caused by the self-weight of concrete and the stress induced by the bending moment. Taking a unit width for computation, the wall bending moment (M_{wall}) and the flexural stress ($\sigma_{\max}$) at the outer fiber of the wall have the following relation:

$$M_{\text{wall}} = \frac{\sigma_{\max} t^2}{6} \tag{8.42}$$

where t = thickness of the wall.

If the stresses at no.6 and 8 integration points are used to compute the wall bending moment, the above $\sigma_{\max}$ can be computed by the following equation:

$$\sigma_{\max} = \frac{\sigma_8 - \sigma_6}{2 \times 0.775} \tag{8.43}$$

where σ_8 is the horizontal stress at no. 8 integration point and σ_6 is the horizontal stress at no. 6 integration point.

If the computer outputs do not provide the stresses at the integration points, or only provide the stresses at the center of the element, the retaining wall should then be divided into two lines (see Figure 8.20) and then compute bending moments through the stresses at the centers of the elements using the method above.

8.5 Determination of initial stresses

In the nonlinear finite element analysis, the magnitude of the initial stresses is one of the crucial factors to the analysis result. The initial stresses have to be determined at the beginning

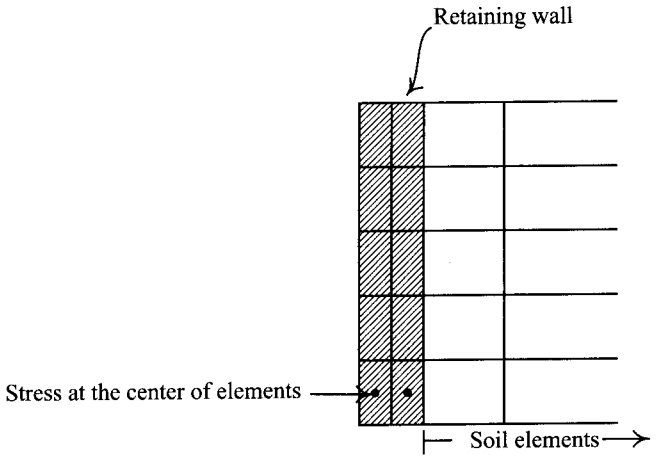

Figure 8.20 Double elements used for the retaining wall.

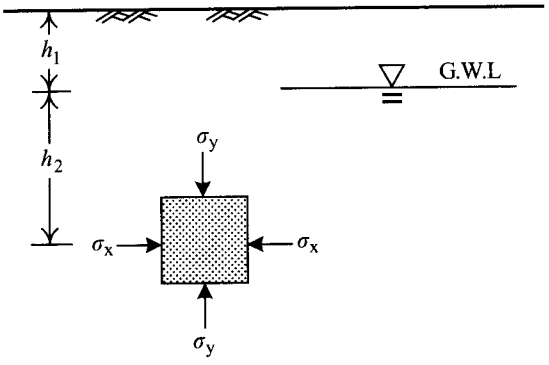

Figure 8.21 Computation of the initial stresses.

of analysis. There are two methods for the computation of the initial stresses: the direct input method and the gravity generation method. They are introduced as follows:

8.5.1 Direct input method

As shown in Figure 8.21, compute the vertical stress (σ_y) and the horizontal stress (σ_x) at a point in the ground in a free field surface:

$$\sigma_y = \gamma_m h_1 + \gamma_{sat} h_2 \tag{8.44}$$

$$\sigma_y' = \sigma_y - u \tag{8.45}$$

$$\sigma_x' = K_0 \sigma_y' \tag{8.46}$$

$$\sigma_x = \sigma_x' + u \tag{8.47}$$

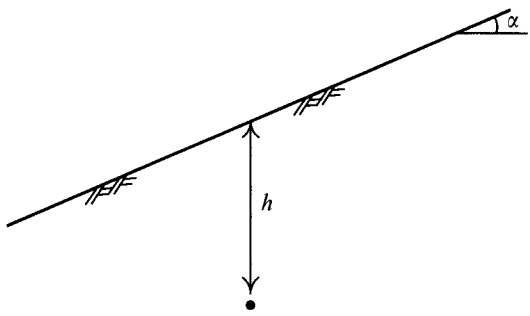

Figure 8.22 The stresses in sloping ground.

where γ_m and γ_{sat} are the moisture unit weight and the saturated unit weight of soil, respectively. u is the porewater pressure; K_0 is the coefficient of at-rest earth pressure; h_1 and h_2 are the depth of the groundwater level and the depth between the point and the groundwater level, respectively.

As shown in Figure 8.22, the initial stresses in sloping ground with no groundwater is

$$\sigma_y' = \gamma_m h \tag{8.48}$$

$$\sigma_x' = K_0 \sigma_y' \tag{8.49}$$

$$\tau_{xy} = \frac{1}{2}\gamma_m h \sin\alpha \tag{8.50}$$

If there is groundwater seepage, the porewater pressure can be estimated using the flow net method and then σ_y' and σ_x' can be determined accordingly. The shear stress $\tau_{xy} = 0.5\gamma' h \sin\alpha$.

8.5.2 Gravity generation method

Assume the boundaries of the excavation profile are all rollers (this is a temporary assumption to compute the initial stresses. When starting analysis, it should be set to what it should be). Assign suitable E and ν to each element. Considering the lateral strain of each element in the initial state is 0, according to the theories of elasticity, we can infer that $\nu = K_0/(1 + K_0)$. E can be an arbitrary large number. Then have the body forces act throughout the whole area and use the finite element method to solve the initial stresses for each element.

Considering that the values of E and ν are not easily determined, a modification can be made by determining the stresses for each element by way of the direct input method first and then by having the body forces act throughout all elements. The stresses of an element can be transformed into the equivalent internal nodal forces and the body force can be transformed into the equivalent external nodal force. The difference between the internal nodal force and the external nodal force can be expressed as follows:

$$\{R\} = \int_V [B]^T \{\sigma\} dV - \int_V [f]^T \{\gamma\} dV \tag{8.51}$$

where

$\{R\}$ = residual force matrix
$[B]$ = strain-displacement matrix
$\{\sigma\}$ = initial stress matrix
$\{f\}$ = displacement shape function matrix
$\{\gamma\}$ = unit weight of soil.

The stresses of the elements are solved repeatedly with the residual forces acting at the nodes until the residual forces $\{R\}$ equal to 0. The stresses are then the initial stresses.

8.6 Modeling of an excavation process

The conception of simulating excavations using the finite element method can be illustrated by Figure 8.23. As shown in Figure 8.23a, before excavation, the initial stresses of the soil are in equilibrium. Once excavation is started, the stresses on the excavation surface and the wall above the excavation surface shall become 0. Thus, an excavation simulation can be described as follows:

1 Compute the initial stress state on the designed excavation surface (Figure 8.23b).
2 According to the stress state obtained above, compute the equivalent nodal force (P_{eq}).
3 Load forces of $-P_{eq}$ on the excavation surface.
4 Reduce the stiffness of the soil that is to be excavated to 0 (or to a very low value).
5 Compute the displacement, stress, and strain in the unexcavated area caused by $-P_{eq}$.

Following Brown and Booker's study (1985), the equivalent nodal force on the excavation surface in Step 2 can be computed as follows

$$\{P_{eq}\} = \int_{V_i} [B]^T \{\sigma_{i-1}\} dV - \int_{V_i} [f]^T \{\gamma\} dV \tag{8.52}$$

where

P_{eq} = the equivalent nodal force on the excavation surface
i = the present excavation stage
$i-1$ = the previous excavation stage
V_i = the volume in the present excavation stage
σ_{i-1} = the stress in the previous excavation stage.

The first item in the above equation represents integration of the nodal forces derived from the stresses at the integration points in the previous excavation stage (the stresses before excavation) over the volume in the ith stage (the volume after excavation). The second item represents integration of the nodal forces derived from gravity over the volume in the ith stage (the volume after excavation). Subtract the latter from the former, and we can then obtain the equivalent nodal forces on the excavation surface.

If dewatering is carried out in the excavation zone, due to the change of the water pressure before and after excavation, a stress increment $\{U\}$ will be generated. The stress increment

can be transformed into the equivalent nodal force. Eq. 8.52 can then be rewritten into the following

$$\{P_{eq}\} = \int_{V_i} [B]^T \{\sigma_{i-1}\} dV - \int_{V_i} [f]^T \{\gamma\} dV + \int_{V_i} [B]^T \{U\} dV \tag{8.53}$$

where U = change in the water pressure due to dewatering.

The equivalent nodal forces can thus be obtained from Eq. 8.53. The changes of stresses and strains for soil elements can be obtained by loading the equivalent nodal forces on the excavation area and perform finite element analysis.

8.7 Mesh generation

The shape of the element used in an analysis can strongly affect the results obtained. The following are the commonly adopted rules for mesh generation:

8.7.1 Shape of the element

Elements used in finite element analysis should avoid irregular shapes. It is better to be as regular as possible, because elements in irregular shapes will cause numerical instability or inaccuracy of numerical analysis. Whether an element is a good shape can be evaluated by its aspect ratio. The aspect ratio is the ratio of the length to the width of an element (L/B), as

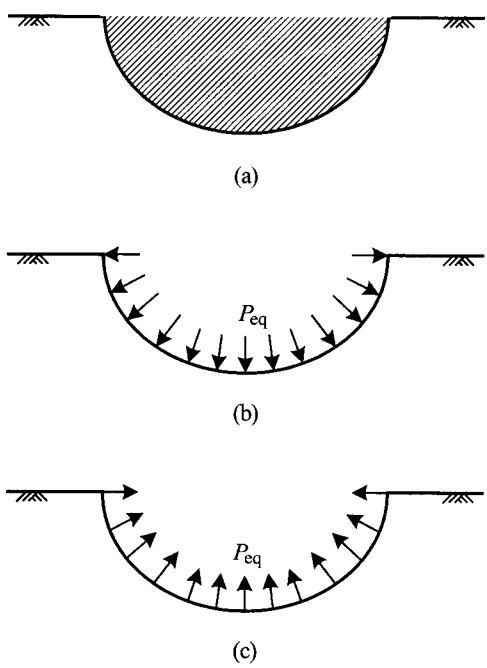

Figure 8.23 Simulation of excavation: (a) before excavation, (b) stresses on the excavation surface, and (c) unloading forces.

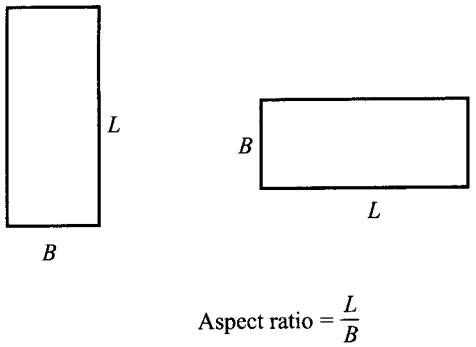

Figure 8.24 Definition of the aspect ratio.

shown in Figure 8.24. The closer to 1.0 is the aspect ratio, the better is the shape. That is, the square or an equilateral triangle is the best choice. Elements with angles of 90° (quadrangles) or 60° (triangles) are also good elements. Since neither squares nor equilateral triangles are easily found, elements with an aspect ratio within the range $1.0 \leq L/B \leq 2.0$–2.5 can be viewed as good ones.

The shape of an element will influence the analytical accuracy of the element and the surrounding elements. It is therefore necessary to place good elements in crucial areas. In less crucial areas some elements not so good can be placed. For example, if the retaining wall is an important object of analysis, good elements should be placed in its surroundings. On the other hand, the boundary areas are not important areas, some elements not that good can be placed there.

8.7.2 Density of mesh

In principle, the mesh in the area of stress concentration, of rapid strain changing, the crucial areas, and the object zones should be finer. The retaining wall is a rigid structure and soil is comparatively a soft material. The mesh in the transition zone between the wall and the surrounding soils should, therefore, be as fine as possible, since a larger stress gradient will be generated there. The farther from the wall, the lower can be the density of mesh.

Since the unloading forces caused by excavation act directly on the excavation bottom in the excavation zone, the density of mesh in the excavation zone will greatly affect the analysis results. Thus, the density of mesh in the excavation zone should be as fine as possible, as shown in Figure 8.25 (Ou *et al.*, 1996a).

8.7.3 Boundary conditions

If considering the symmetry of an excavation and taking a half for analysis as shown in Figure 8.1, the symmetric boundary (line B′–B′ in Figure 8.1b) should be equipped with rollers to restrain the lateral displacement and allow vertical displacement. According to Ou and Shiau (1998), to analyze movement in an excavation, rollers will be more efficient than hinges placed on line C′–C′ (Figures 8.1b and 8.26a). Also, the rollers should be placed

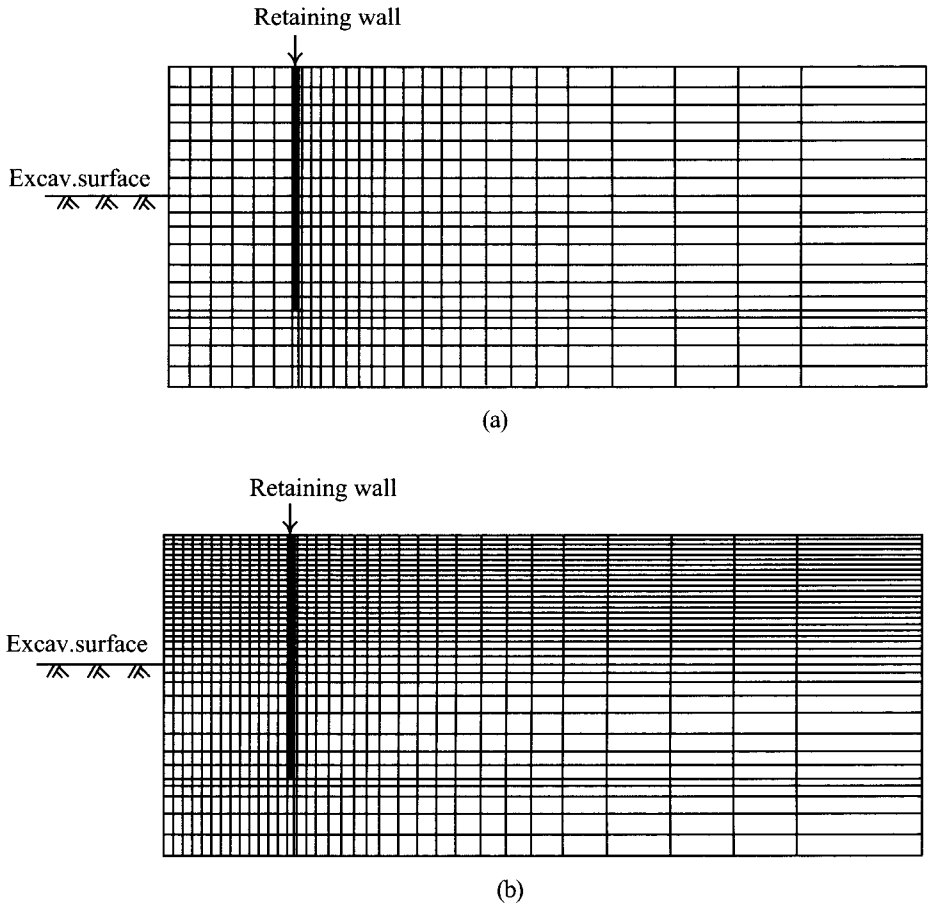

Figure 8.25 The finite element meshes used in the analysis of excavation: (a) bad mesh and (b) good mesh.

at a distance more than three excavation depths from the retaining wall for the analysis of wall deformation. To analyze ground settlement, the rollers should be placed at a distance more than four excavation depths from the retaining wall (Figure 8.27). In principle, the farther to the retaining wall is the boundary, here designated as C′–C′, the better are the analysis results, though it takes more computation time. On the base either rollers or hinges can be placed. In general, the hinges or rollers should be placed on hard soils or several meters below the retaining wall bottom.

The location of the boundary of mesh can also be determined from convergence study of the finite element analysis. As shown in Figure 8.1b, assume the boundary is line G′–G′ first and then carry out the analysis. Extend the boundary to line H′–H′ and perform the analysis again. If the two analyses come out similar in stress, strain, or displacement along, for example, X′–X′, it means that the boundary can be set at G′–G′ or H′–H′. Otherwise, the boundary should be moved to C′–C′.

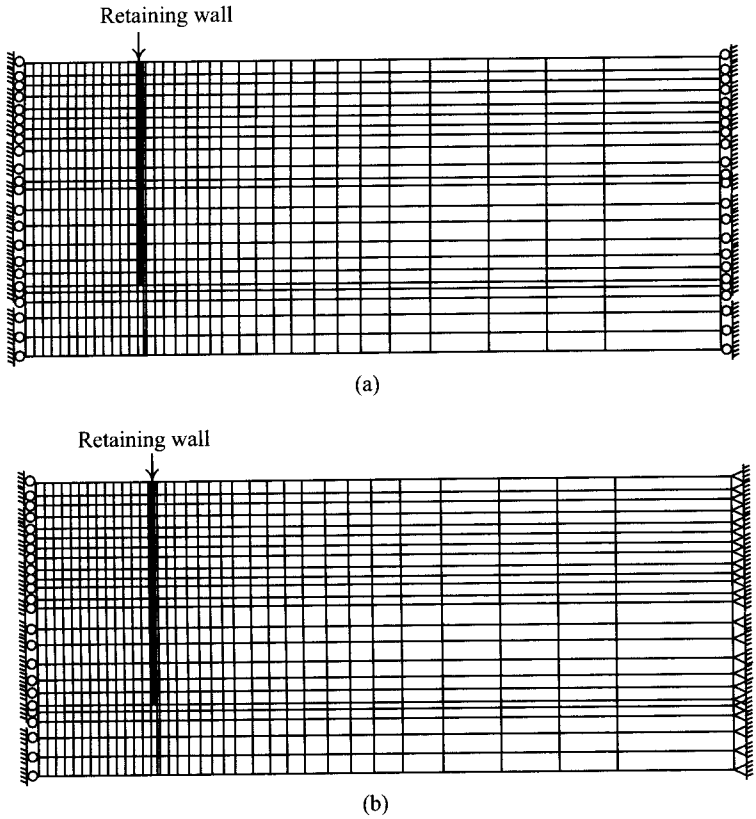

Figure 8.26 Boundary conditions of the finite element mesh: (a) boundary outside the excavation zone is allocated with rollers and (b) boundary outside excavation zone is allocated with hinges.

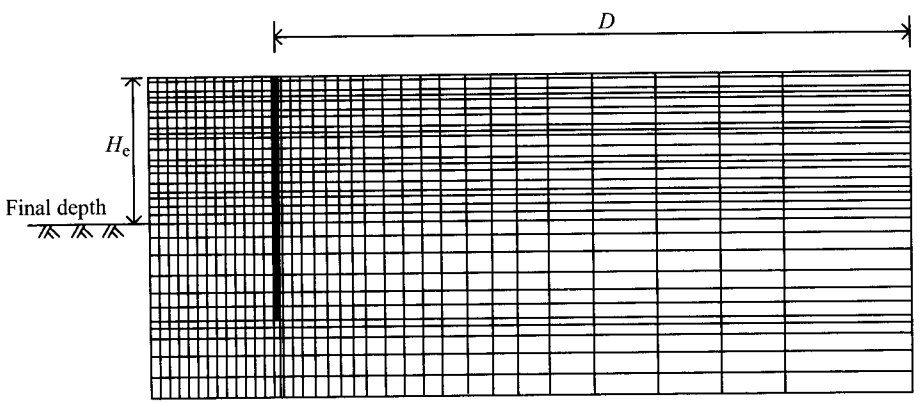

Ground settlement: $D \geq 4H_e$

Wall deflection: $D \geq 3H_e$

Figure 8.27 Distance of the boundary required for the analysis of wall deflection or ground settlement.

8.8 Excavation analysis method

8.8.1 Direct analysis and back analysis

The conception of direct or back analysis using the finite element method is identical to that using the beam on elastic foundation method (see Section 7.7.1) and the detailed descriptions will not be repeated here.

Since the finite element method is based on a rigorous theory and its soil models are better than beam on elastic foundation methods in simulating soil stress-strain relations, the accuracy of the direct analysis of the retaining wall deformation should be better than that based on the beam on elastic foundation method.

As discussed in Section 7.7.1 in Chapter 7, when performing back analysis using the beam on elastic foundation method, it is only the coefficient of subgrade reaction k_h that is required. The application is quite simple. When performing back analysis using the finite element method, however, it is very complicated and requires more soil parameters.

Take the hyperbolic model for example. For any single type of soil, there are eight input parameters: c, ϕ_0, $\Delta\phi$, K, n, R_f, ν, and K_{ur}. If performing back analysis of multilayered soils, assuming all the parameters are unknown, the analysis is time-consuming and expensive. As discussed in Section 7.7.1, it is more reasonable to back analyze those parameters that can not be obtained directly from soil tests or rationally derived. For example, the parameters c, ϕ_0, and $\Delta\phi$ of saturated clay required for the hyperbolic model can be obtained from soil tests while the parameters n, R_f, and ν can be rationally derived separately. The only parameters that need back analysis are K and K_{ur}. Thus, the computation is substantially simplified. For further explication, please see Section 8.9.2 in the present chapter or refer to the related literature (Ou and Lai, 1994; Ou and Tang, 1994; Ou *et al.*, 1996b).

8.8.2 Total stress analysis and effective stress analysis

The total stress analysis generally refers to analyses where the total stress is used and the input parameters are total stress parameters such as s_u and $\phi = 0$ (for saturated clay), or c_T and ϕ_T (for unsaturated clay). The stresses thus obtained are then the total stress. The effective stress analysis refers to the analyses where the effective stress is used and the input parameters are effective parameters such as c' and ϕ'. The stresses obtained from the analysis are then the effective stress.

In the beam on elastic foundation method introduced in the previous chapter, the analyses can be split into drained analysis, undrained analysis, and partially drained analysis. The corresponding type of stress used in these methods is the effective stress, the total stress, and the total stress, respectively. Therefore, the undrained behavior can only be analyzed by the total stress method.

In the finite element method, drained analysis should be done with the effective stress while undrained analysis can be carried out with either the total stress or effective stress.

For example, if the hyperbolic model is expressed by the effective stress, c' and ϕ' being the input parameters, $\{\Delta\sigma\}$ in Eq. 8.15 will then imply the effective stress. The method is an effective stress analysis. If the hyperbolic model is expressed by the total stress, $\{\Delta\sigma\}$ in Eq. 8.15 will then represent the total stress because E_t and ν in $[C]$ are obtained from the hyperbolic model expressed by the total stress. The method is a total stress analysis.

Similarly, if the yielding function in the elastoplastic model is expressed by the effective stress, $\{\Delta\sigma\}$ in Eq. 8.29 will then imply the effective stress. If the yielding function in the elastoplastic model is expressed by the total stress, $\{\Delta\sigma\}$ in Eq. 8.29 will then imply the total stress.

8.8.3 Drained analysis, undrained analysis, and partially drained analysis

Drained analysis refers to methods where the excess porewater pressure is assumed to be completely dissipated in analysis (i.e. $u_e = 0$) and the soil goes through a volume change accordingly. Drained analyses are mainly applied to granular soils and the long-term behavior of clayey soils. Thus, effective stress analysis and effective stress parameters should be adopted. Undrained analysis refers to methods where the excess porewater is not dissipated at all in analysis ($u_e \neq 0$). If the soil is in the saturated state, the volume change would be none.

In the hyperbolic model, the undrained analysis for short-term behavior of saturated clay has to adopt the total stress analysis. That is, the analysis should adopt s_u and assume $\phi = 0$. The undrained analysis of unsaturated clay directly adopts the results of the triaxial UU test, c_T and ϕ_T. For granular soils, it is only the effective stress analysis that has to be adopted. That is, c' and ϕ' are the required parameters.

In the elastoplastic model, the undrained analysis for short-term behavior of saturated clay can adopt either the effective stress analysis or the total stress analysis. If adopting the effective stress analysis, the yielding function has to be capable of representing the fact that the soil strength increases with the increase of the average effective stress (p'). The yielding function can be the Mohr-Coulomb model (input parameters c' and ϕ'), the Drucker-Prager model, the Cam-clay model, etc. The input parameters are all the effective stress parameters and the stiffness of porewater also has to be fed. If adopting the total stress analysis, the yielding function should be capable of simulating the fact that the soil strength does not increase with the increase of the average total stress (p). The yielding function can be the Mohr-Coulomb model (s_u, $\phi = 0$), the von Mises model, the Tresca model, etc. The input parameters are all the total stress parameters.

In some cases, the behaviors of clay are neither completely drained nor perfectly undrained. Rather, they are in between. They are partially drained behaviors. The partially drained behaviors of clay can be analyzed using the method introduced in Section 7.7.2 or the coupled analysis as introduced in the following section.

As for the parameters of drained analysis, undrained analysis, and partially drained analysis, please refer to Section 8.9.

8.8.4 Coupled analysis

In the method just mentioned, analysis is restricted to either drained or undrained analysis. However, real soil behavior is often time related, with porewater pressure response and rate of loading. To account for such behavior, it is necessary to couple the continuity of equation or general consolidation equation with the constitutive and equilibrium equations. The method is then called the coupled analysis, which is subsumed in effective stress analysis, that is, the effective stress parameters are required in analysis. In addition to the parameters of soil models, the coupled analysis also requires the coefficient of permeability and loading time.

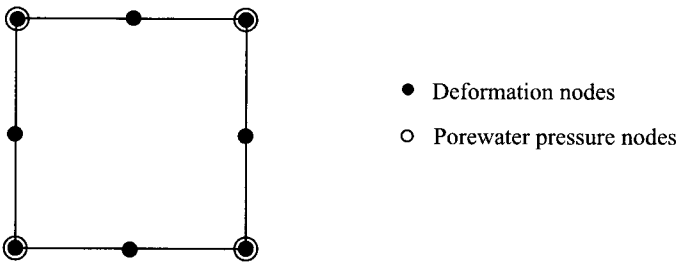

Figure 8.28 A commonly used element for the coupled analysis (eight deformation nodes and four porewater pressure nodes).

The coupled method uses displacement and porewater pressure as unknowns and therefore results in both displacement and porewater pressure degrees of freedom at element nodes. As a result, it can compute the displacements and stresses of a soil element as well as the porewater pressures based on the effective stress. Figure 8.28 shows a commonly used element for coupled analysis. The element has eight displacement nodes, four of which are simultaneously porewater pressure nodes.

If using the coupled method to analyze completely undrained behavior, we could simply set the time of loading at a very short time. For example, assume there is a site to be excavated 4 m deep. The coupled method simply sets the 4 m excavation to be finished within a very short time when considering the undrained condition. If considering the drained condition, we can set the excavation time for a very long period. When considering partially drained behavior, set the excavation time in between (the actual excavation time).

8.8.5 Plane strain analysis and three-dimensional analysis

Though in general engineering practice, plane strain analysis is capable of obtaining a rational result, the wall deformation and ground settlement on the section of the shorter side (B–B section in Figure 8.1a) or that near the corner are three-dimensional behaviors and plane strain analysis would overestimate the deformation or settlement. Three-dimensional analysis can solve the problems.

Figure 8.29 shows wall deformation at the corner in the Haihaw Financial Center excavation from plane strain analysis, three-dimensional analysis and field measurement. As shown in the figure, plane strain analysis will overestimate, whereas three-dimensional analysis will obtain rational results. Besides, the wall deformation and ground surface settlement in excavations with soil improvement or property protection measures such as counterfort walls or cross walls (see Section 11.6) also constitute three-dimensional behavior. In such cases, only three-dimensional analysis can obtain rational results.

In three dimensional analysis, the stress state at a point has six components: σ_{xx}, σ_{yy}, σ_{zz}, τ_{xy}, τ_{yz}, τ_{zx}. The theories of finite element analysis, the soil models, and others are all similar to those for the plane strain analysis. In practice, the element of the retaining wall and soil used in the three-dimensional analysis is usually an 8-noded low order hexahedron element, which is called a H8 (8-noded hexahedron) element, the solid element, or brick element, as shown in Figure 8.30a. A 20-node high order element (Figure 8.30b), though more accurate, is usually

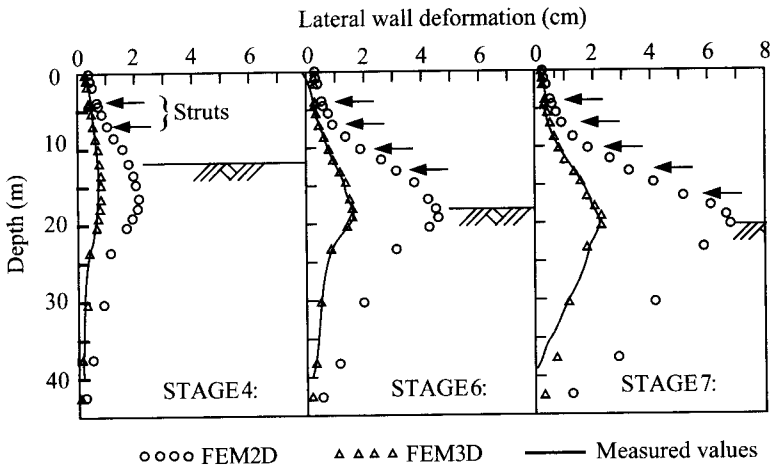

Figure 8.29 Comparisons of the wall deflection from plane strain analysis, three dimensional analysis and field measurement, respectively in a corner of the Haihaw Financial Center excavation.

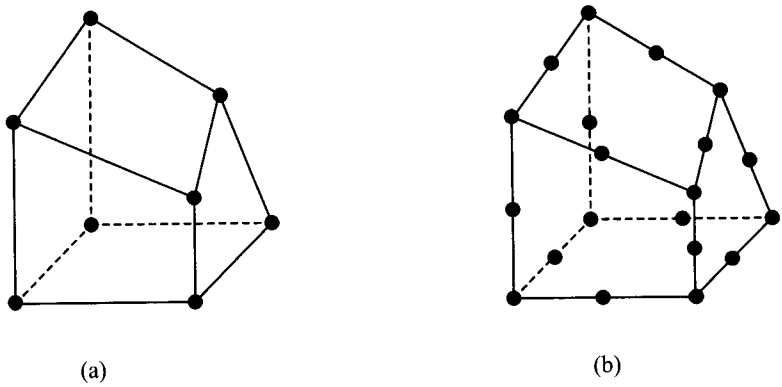

Figure 8.30 Three dimensional elements: (a) with 8 nodes and (b) with 20 nodes.

not adopted because it requires too much computer memory and is very time consuming in computation. Figure 8.31 is the mesh, containing 7,200 three-dimensional elements, used by the Ou *et al.* (1996a) for the three-dimensional analysis of an excavation.

8.9 Determination of soil parameters

8.9.1 Parameters for elastic deformation

From Table 8.1, we can see that in elastic analysis, when $\nu = 0.5$, $B = \infty$, G would equal $E/3$. $B = \infty$ means that the volume change is 0, from which it follows that the soil behavior

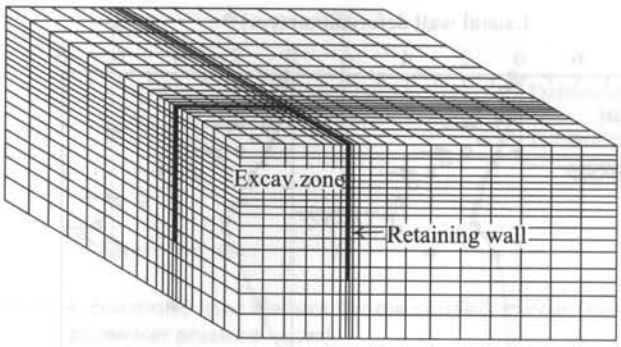

Figure 8.31 Meshes for the three dimensional finite element analysis.

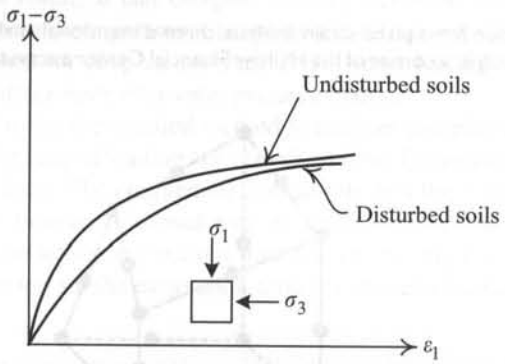

Figure 8.32 Stress-strain curves for undisturbed and disturbed soils.

is undrained behavior, according to the definition of the bulk modulus. From Eq. 8.4 or 8.14, we can see that when $B = \infty$ or $\nu = 0.5$, there exist some infinitely large terms in $[C]$, which will cause numerical instability. According to the parametric studies, the condition of zero volume change or undrained state of soil can be achieved by assuming $\nu = 0.49$ in Eq. 8.4 or transforming it into the B-value, and substituting it into Eq. 8.14. From the definition of shear modulus, we can infer that the porewater in soil cannot bear shear stress and the shear modulus in the drained state should equal that in the undrained state, that is, $G = G'$.

8.9.2 Parameters for the hyperbolic model

In theory, the eight parameters of the hyperbolic model can all be obtained through the results of the conventional triaxial test. However, because of the disturbance caused in the process of sampling, the stress-strain curve would not be identical to that under undisturbed conditions, as shown in Figure 8.32. The parameters obtained through the conventional triaxial test may not be directly adopted as the parameters for the hyperbolic model in excavation analyses.

Table 8.2 Range of the Poisson's ratio

Soil type	ν_s
Saturated clay (undrained)	0.5
Unsaturated clay (undrained)	0.35–0.4
Silty sand	0.3–0.4
Sand, gravel	0.15–0.35
Silt	0.3–0.35
Rock	0.1–0.4 (depending on type of rock)
Ice	0.36
Concrete	0.15

For granular soils such as sand or gravel, though the stress-strain curves of disturbed and undisturbed samples are different, the final strengths are similar, as shown in Figure 8.32. This is because, when achieving the ultimate condition, the friction characteristics, which are not much influenced by disturbance, are the major factor influencing the strength. As a result, the strength parameters, c, ϕ_0, and $\Delta\phi$, of sand and gravel, can be obtained directly from the triaxial test. According to Wong and Broms (1989), the failure strain of sandy or gravelly soils is rather small and the failure ratio (R_f) is about 0.5–0.6.

According to Duncan *et al.* (1980), for most types of sandy or gravelly soils, the stiff modulus exponent n is between 0.4 and 0.6. To simplify analysis, we usually assume $n = 0.5$. Poisson's ratio can be assumed to be a commonly adopted value in geotechnical analysis, for example, as listed in Table 8.2. Duncan *et al.* (1980) also found that for hard soils (such as dense soils), $K_{ur} \approx 1.2K$ and for soft soils (such as loose soils) $K_{ur} \approx 3.0K$.To simplify analysis, we may assume $K_{ur} = K$. Thus, only K has to be determined among the parameters required in excavation analysis. K can be obtained from the back analysis of excavation case histories or be computed from the seismic survey or other in situ tests. (Wong and Broms, 1989; Ou and Lai, 1994; Ou and Tang, 1994; Ou *et al.*, 1996a).

The undrained analysis for saturated clay should adopt s_u and $\phi = 0$, which can substitute for c and ϕ_0 (note: $\Delta\phi = 0$). According to Wong and Broms (1989), the failure strain for soft clay is relatively large, generally larger than 20%. That is, the failure ratio (R_f) is larger than that of sandy soils, generally between 0.8 and 0.9. Saturated clay, under undrained conditions, has no volume change and Poisson's ratio can be assumed to be 0.49. The relation between K_{ur} and K is as discussed above. The stiffness of saturated clay under the undrained condition relates only to the effective stress without having to do with the total stress. Thus, according to Eq. 8.17, we should let $n = 0$ so as to make

$$E_i = KP_a\left(\frac{\sigma_3}{P_a}\right)^0 = KP_a \tag{8.54}$$

The above equation represents E_i under a certain effective pressure. The E_i value does not change with the total stress (e.g. σ_3). Concerning the normalized behaviors of saturated clay, as discussed in Section 2.8.2, Chapter 2, s_u/σ_v' and E_i/σ_v' are both constants. That is, E_i/s_u should also be a constant. The values of E_i/s_u can be obtained through back analyses of excavation histories or reference to previous studies (Simons, 1974; Tavenas *et al.*, 1974; Holtz and Holm, 1979; Chang and Abas, 1980).

8.9.3 Parameters for the linear elastic elastoplastic model

Figure 8.33 shows the stress-strain behavior of soil simulated on the basis of the linear elastic elastoplastic model. In drained and coupled analyses, stress should be expressed in terms of the effective stress. Therefore, the strength parameters c' and ϕ' for sandy or gravelly soils can be directly obtained from soil tests. The secant Young's modulus, that is, the slope of the linear elastic part in Figure 8.33, can be used as the value of Young's modulus in Eqs 8.29–8.32. Because of the disturbance caused by sampling, however, Young's modulus and Poisson's ratio obtained from tests may not be capable of being directly used for analysis. In actual analysis, Poisson's ratio can be determined by referring to Table 8.2 and the Young's modulus—Tables 8.3 and 8.4, or empirical values, or computed through back analysis. According to Table 8.1, Young's modulus and Poisson's ratio can be easily transformed to be shear modulus and bulk modulus, which are often used in the effective stress analysis.

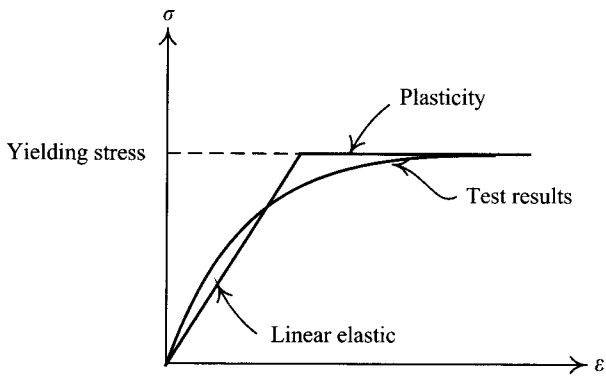

Figure 8.33 Stress-strain behavior of soil obtained from the laboratory test and that from the simulation based on Mohr-Coulomb linearly elastic elastoplastic model.

Table 8.3 Empirical equations for E_s (Bowles, 1988)

Soil type	*SPT-N* (kPa)	*CPT (same unit as q_c)*
Sand	$E_s = 500(N + 15)$	$E_s = (2 \sim 4)q_c$
(normally consolidated)	$E_s = (15,000 \sim 22,000) \ln N$	
	$E_s = (35,000 \sim 50,000) \log N$	$E_s = (1 + D_r^2)q_c$
Sand (saturated)	$E_s = 250(N + 15)$	
Sand (overconsolidated)	$E_s = 18,000 + 750N$	$E_s = (6 \sim 30)q_c$
Gravelly sand and gravel	$E_s = 1,200(N + 6)$	
	$E_s = 600(N + 15) \quad N \leq 15$	
	$E_s = 600(N + 15) + 2,000 \quad N > 15$	
Clayey sand	$E_s = 320(N + 15)$	$E_s = (3 \sim 6)q_c$
Silty sand	$E_s = 300(N + 6)$	$E_s = (1 \sim 2)q_c$
Soft clay		$E_s = (3 \sim 8)q_c$

Note
N—SPT-N value; q_c—point resistance in a CPT test; D_r—relative density; 1 kPa = 1 kN/m^2 = 0.1 t/m^2.

Table 8.4 Ranges of E_s for various soils (Bowles, 1988)

Soil type	E_s (MPa)
Very soft clay	2–15
Soft clay	5–25
Medium stiff clay	15–50
Stiff clay	50–100
Sandy clay	25–250
Silty sand	5–20
Loose sand	10–25
Dense sand	50–81
Loose gravel	50–150
Dense gravel	100–200
Shale	150–5000
Silt	2–20

Notes
1 The table only lists the possible range of E_s for soils. E_s of in situ soils is related to water content, density, stress history, etc.
2 1 MPa = 1×10^6 N/m^2 = 100 t/m^2.

As discussed in Section 8.8.3, the undrained analysis of clay can either adopt the total stress analysis or the effective stress analysis. With the effective stress analysis, the effective strength parameters, such as c' and ϕ', and effective stress deformation parameters, such as G' (or G) and B', should be used. Besides, the stiffness of porewater (B_w) should be input to account for the undrained behavior. With the total stress analysis, undrained strength parameters s_u and $\phi = 0$ should be used. Besides, Young's modulus (E) and Poisson's ratio (ν) are preferably used as input parameters instead of the shear modulus (G) and the bulk modulus (B). Poisson's ratio (ν) is usually assumed to be 0.49 to satisfy the condition that the volume change is 0. Concerning how to determine the undrained analysis parameters and other advanced discussion, please refer to the literature (Mana, 1978; Naylor and Pande, 1981; Britto and Gunn, 1990; Potts and Zdravkovic, 1999).

8.9.4 *Parameters for the Cam-clay model and other high order models*

As mentioned in Section 8.3.3, the Cam-clay model is capable of simulating the nonlinear and plastic behavior. The Cam-clay model requires the following parameters: E, ν, M, λ, and κ, where M and the friction angle of soil ϕ' have the following relation:

$$M = \frac{6 - \sin\phi'}{3 - \sin\phi'} \tag{8.55}$$

As shown in Figure 8.17, λ and κ are the slopes of the isotropic consolidation curve and unloading curve in terms of $\ln p'$, respectively. In conventional soil mechanics, C_c and C_s are the one-dimensional consolidation and unloading curves in terms of $\log p'$, respectively.

According to the chain rule, the above two have the following relations:

$$\lambda = \frac{C_c}{2.303} \tag{8.56}$$

$$\kappa = \frac{C_s}{2.303} \tag{8.57}$$

C_c and C_s can be derived from either the one-dimensional consolidation test or the index test (see Section 2.2). In general, the result of the consolidation test is little affected by the disturbance of sampling and the obtained C_c and C_s are therefore highly reliable.

The Cam-clay elastoplastic model and Mohr-Coulomb elastoplastic model use the same constitutive law (Eqs 8.29–8.32) but different yielding functions. In the Mohr-Coulomb elastoplastic model, the secant Young's modulus, that is, the slope of the linear elastic part in Figure 8.33, can serve as the value of Young's modulus in Eqs 8.29–8.32. Tables 8.3 and 8.4 list the secant Young's modulus commonly used in analyses. In the Cam-clay elastoplastic model, Young's modulus in Eqs 8.29–8.32 should be equal to the slope of the unloading/reloading line rather than the secant Young's modulus, as shown in Figure 8.34. As a result, Young's modulus may not necessarily be obtained from Tables 8.3 or 8.4 but Poisson's ratio can be chosen from Table 8.2. However, it is suggested that Young's modulus be obtained according to the following method:

Differentiate Eq. 8.38 at both sides, and we have

$$de = -\kappa \frac{dp'}{p'} \tag{8.58}$$

According to the definition of bulk modulus, we can derive the effective bulk modulus (under the drained condition) as:

$$B' = -\frac{dp'}{d\varepsilon_v} = -\frac{dp'}{de/(1+e)} = \frac{(1+e)p'}{\kappa} \tag{8.59}$$

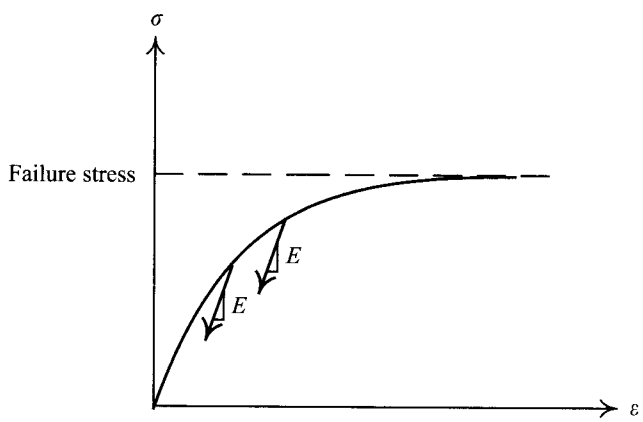

Figure 8.34 Stress-strain behavior of soil obtained from the simulation using Cam-Clay elastoplastic model.

The parameter κ can be obtained through the isotropic consolidation test or one can use C_s as derived from the one-dimensional consolidation test. With B' and ν' given, we can then convert them into E' or G'.

As discussed in the previous section, the type of stress used in the drained analysis or coupled analysis is the effective stress. The effective stress analysis of clay based on the Cam-clay model requires five deformation parameters, M, λ, k, B', and G.

Since the Cam-clay model is an effective stress based model, it can only be used in the effective stress analysis. As discussed in Section 8.9.3, the parameters B' and G are preferably used in the effective stress analysis. When adopting B' and G as the parameters, we can first obtain B' using Eq. 8.59, then find ν' by referring to Table 8.2. With B' and ν' known, we can then compute G'. Let G be equal to G'. Then by input of an appropriate value of the stiffness of water, we are able to perform effective stress undrained analysis. For more discussion of the determination of the parameters, with undrained analysis based on the Cam-clay model, please refer to the literature (Finno, 1983; Borja, 1990; Britto and Gunn, 1990; Finno and Harahap, 1991; Ou and Lai, 1994).

8.10 Determination of structural parameters

In analysis, the inertia of moment (I) and stiffness (EI) of a retaining wall such as sheetpiles, soldier piles, column piles, and diaphragm walls should be reduced rationally. The axial stiffness (AE/L) of a strut or floor slab should also be reduced. The reasons and how much should be reduced are the same as used with the beam on elastic foundation method. Readers can refer to Section 7.6. They will not be repeated here.

8.11 Discussion of accuracy of analysis results

The finite element method is capable of computing the displacement at every node of a mesh after excavation, thus obtaining the deformation of the retaining wall and ground settlement as well as the stresses in an element. The accuracy of the finite element method is closely related to the selected soil model and corresponding parameters. In theory, the better the soil model capable of simulating the deformation characteristics of soil, the higher the analysis accuracy. Such models are usually quite complicated and require parameters that are not necessarily obtainable through conventional soil tests. Nevertheless, Clough and Mana (1976) pointed out that as long as the parameters are selected appropriately, no matter which soil model is adopted, the computed deformation should come out rather close to the observation. What the appropriate parameters are, however, do not necessarily relate to the true soil properties. Neither do they have physical meanings.

The bending moment (or stress) of a retaining wall is the multiplication of EI and the second derivative of the deformation curve. Therefore, as long as the accurate deformation curve is obtained, the bending moment of the wall can also be obtained accurately.

Though the finite element method can accurately predict the deformation and bending moment of a retaining wall, it is not capable of accurately predicting the ground settlement using the general elastoplastic models, as shown in Figure 8.35. As a result, the finite element method is rarely adopted for the prediction of ground settlement.

According to Smith *et al.* (1992), inside the initial yielding surface of clayey soils should be two sub-yielding surfaces Y1 and Y2, which divide the stress space into four areas, as shown in Figure 8.36. Area 1, which is the innermost one of the four, is very small in

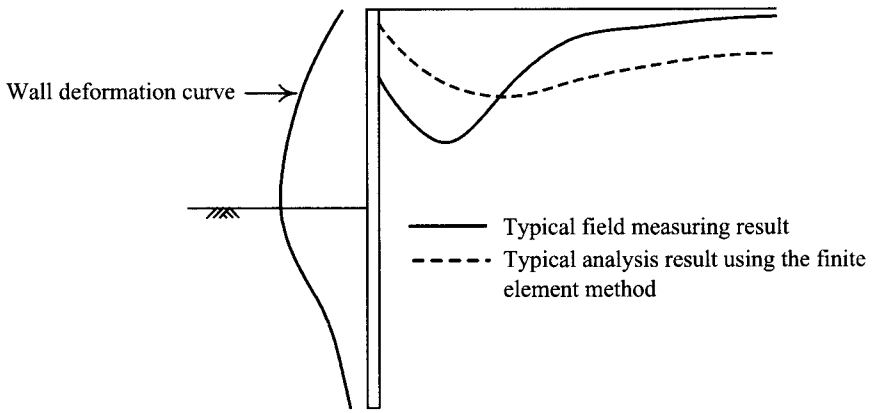

Figure 8.35 Comparison of excavation-induced settlement derived from a typical finite element analysis with field measurement.

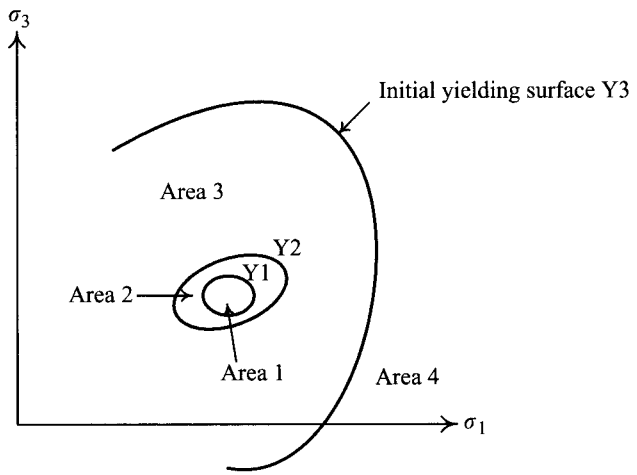

Figure 8.36 Yielding surface for clayey soils.

range. The soil behavior is linear elastic and the strain is completely recoverable. The strain is usually between 10^{-5}% and 10^{-3}%. When the stress path extends to Area 2, the soil behavior changes to nonlinear elastic and the stiffness of the soil decreases rapidly though the strain is still completely recoverable. In general, the strain is basically smaller than 10^{-2}%. When the stress path develops into Area 3, if the loading is removed (unloaded), the strain will no longer be recoverable and a permanent deformation is generated. Plastic strain is thus generated, that is, the soil behavior is inelastic. Compared with Area 4, the deformations occurring in Area 3 are relatively smaller. When exceeding the yielding surface Y3 and entering Area 4, the soil deformations and plastic strain are all largely increased and a large quantity of deformation is also generated. Smith's study also discovers that the soil stiffness in Area 1 (with small strain) is very high. Because of general elastoplastic models such as

the Cam-clay model, all assume the stress path within the (initial) yielding surface (i.e. Y3) is elastic in behavior and cannot take into consideration the high stiffness of soil in Area 1, and also because the soil within the influence range and outside of the excavation zone is not much influenced by excavation and thus has very small strain, that is, the soil is very possibly at the linear (or nonlinear) elastic stage, the finite element method is thereby incapable of predicting the ground settlement accurately. Figure 8.35 shows a prediction result using the Mohr-Coulomb elastoplastic model or the Cam-clay model to analyze the ground settlement.

The author adopted the three-surface kinematic hardening soil model (3-SKH model), which was developed by Atkinson and Stallebrass (1991) to simulate the behavior of clays at over-consolidated stress state and at small strain, to compute the movement in excavations. As Figure 8.37 displays, both the wall deformation and ground surface settlement can be accurately computed.

Moreover, this section also provides a simplified analysis method considering the small strain condition on the basis of many studies (Wang *et al.*, 1999). The method assigns about three times as large as the secant Young's modulus to the soil outside the primary influence zone, defined in Section 6.4. For more simplification, the influence zone may also be defined on the basis of excavation depth, that is, the range of small strain of soil is adjusted with the advance of excavation, as shown in Figure 8.38. The results of ground surface settlement obtained according to the above simplified analysis method are quite close to the *in situ* observations. Though the method is empirically oriented, it is still a useful method for the analysis of ground surface settlement.

8.12 Summary and general comments

This chapter first introduced the basic theories of the finite element method, then the commonly used soil models and structural models, and lastly the application of the method to

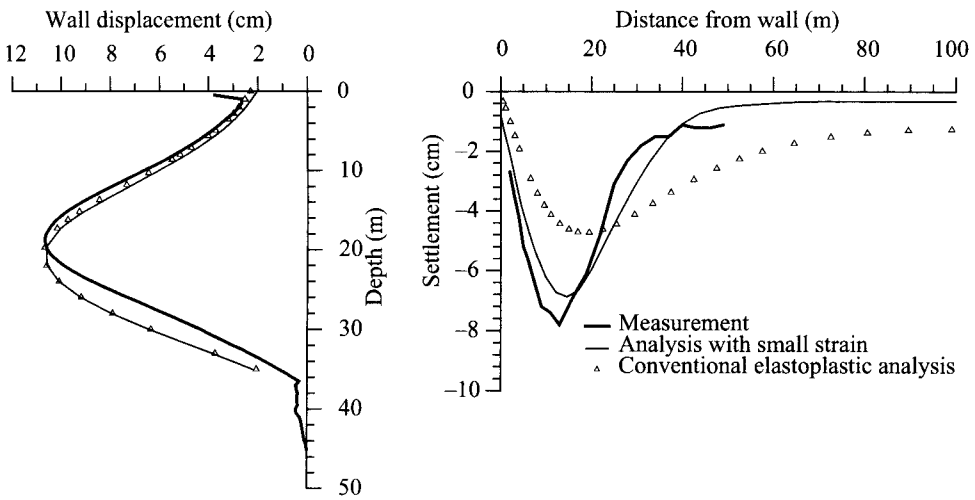

Figure 8.37 Comparison between the measured and analytic wall displacements and surface settlements at the final stage.

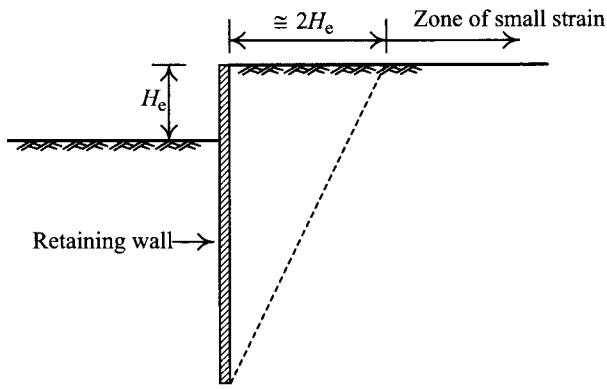

Figure 8.38 Zone of small strain in an excavation.

excavations. Though the finite difference method is different, in its deduction, from the finite element method, with the same soil models, structural models, excavation simulations, and analysis environment, the related subject-items of the finite element method introduced in this chapter can also be applied to the finite difference method. The main contents of this chapter are summarized as below:

1 The analysis method of the beam on elastic foundation method (Chapter 7) can be divided into undrained analysis, drained analysis, and partially drained analysis. The corresponding types of stress used in these analyses are the total stress, the effective stress, and the total stress respectively. The undrained behavior of clay can only be analyzed using the beam on elastic foundation method with total stress analysis. The finite element method can also be divided into undrained analysis, drained analysis, and partially drained analysis. It is also split into total stress analysis and effective stress analysis. What's more, it has the coupled method to take into account the interactive behaviors between the effective stress, the porewater pressure, and deformations. The undrained behavior of clay can be analyzed using the finite element method with the total stress analysis method, the effective analysis method, or the coupled analysis method.
2 The conventional plane strain analysis method can not analyze the deformation on the short side of the diaphragm wall due to the corner effect. It is neither capable of analyzing the partially improved soils in excavations or those done featuring property protection measures such as counterfort walls or cross walls. These deformation behaviors are three-dimensional and have to be analyzed using the three-dimensional analysis method.
3 Though without strict theoretical foundation, the hyperbolic model has the merits of simulating the nonlinear, inelastic behaviors and characteristics of the stress-strain relation dependent on the confining pressure and is thereby extensively applied to geotechnical engineering. With the effective or total stress given, the model can be used in terms of either the effective stress or the total stress.
4 The Mohr-Coulomb elastoplastic model assumes that the stress-strain relation before yielding can be expressed by a linear elastic curve whose slope is close to the secant Young modulus. After yielding, the yielding criterion follows the Mohr-Coulomb criterion.

This chapter provides some techniques to determine the parameters of the effective stress drained analysis, the effective stress undrained analysis, and the effective stress coupled analysis using the Mohr-Coulomb elastoplastic model.

5 The Cam-clay elastoplastic model is rigorously based on theoretical foundations. The required parameters can be obtained through conventional laboratory tests since they are hardly affected by the disturbance caused by sampling. As a result, the model is widely applied. This chapter provided detailed techniques for the determination of the parameters for the effective stress drained analysis, the effective stress undrained analysis, and the effective coupled analysis using the Cam-clay elastoplastic model. It is noted that the elastic Young's modulus for the Cam-clay model should be equal to the slope of the unloading/reloading line rather than the secant Young's modulus.

6 The finite element method can accurately predict the deformation and bending moment of a retaining wall but cannot do as well with the ground settlement. The reason is that the commonly used elastoplastic models cannot simulate the very stiff behaviors of soil at small strain. The author proposed a simplified analysis method of considering the small strain. The method gradually adjusts the range of the soil affected by small strain according to the different excavation depths. The stiffness of the soil inside the excavation zone and that outside, within the distance equal to one excavation depth from the wall (which represents the influence range), can be assumed to be the value as computed in Section 8.9. The stiffness of the soil outside the excavation zone beyond the distance equal to the excavation depth (from which it follows is outside the influence range) can be assumed to be at small strain and three times as large as the above value.

Problems

8.1 Explain why, when Poisson's ratio of soil is 0.5, the volume strain would be 0.

8.2 Explain why the perfectly plastic model can only produce plastic strain without elastic strain.

8.3 Explain why the drained shear modulus is the same as the undrained shear modulus.

8.4 Same as Example 6.1, the excavation of Building P. The excavation profile and geological conditions are as shown in Figure 6.41. The observations of deformations in all the excavation stages are as shown by Figure 6.42. If we analyze the deformation and stress of the retaining wall using the finite element method (or the finite difference method) and the hyperbolic model, estimate the required parameters for each soil layer.

8.5 Same as above. Use the finite element method (or the finite difference method) and the parameters determined in the previous problem to analyze the deformation of the retaining wall at each stage and compare the results with the observations.

8.6 Same as Problem 8.4. If we adopt the Mohr-Coulomb elastoplastic model to simulate the stress-strain behaviors of sand and clay, the latter of which is analyzed with the effective stress undrained analysis method, determine the required parameters for each soil layer.

8.7 Same as above. Use the finite element method (or the finite difference method) and the parameters obtained in the previous problem to analyze the deformation at each stage. Compare the results with the observations.

8.8 Same as Problem 8.6. If we use the Mohr-Coulomb elastoplastic model to analyze the excavation-induced deformation and stress of the retaining wall, except that the total stress undrained analysis method is to be adopted for the clayey layer, determine the required input parameters for each layer of soil.

8.9 Same as above. Use the finite element method (or the finite differential method) and the parameters obtained in the previous problem to analyze the deformation at each stage. Compare the results with the observations.

8.10 Same as Problem 8.4. If we adopt the Mohr-Coulomb elastoplastic model to simulate the stress-strain behavior of sandy soils and the Cam-Clay elastoplastic model for the stress-strain behaviors of clayey soils using the effective stress undrained analysis, determine the required parameters for each layer of soil.

8.11 Same as above. Use the finite element method (or the finite difference method) and the parameters obtained in the previous problem to analyze the deformation at each stage. Compare the results with the observations.

8.12 Same as Problem 6.11. The excavation profile and geological profile of Building S are as shown in Figure P6.11. The observations of deformations at all the stages are as shown in Figure P7.14. If we use the finite element method (or the finite difference method) and the hyperbolic model to analyze the excavation-induced wall deformation and stress, estimate the input parameters for each layer of soil.

8.13 Same as Problem 8.12. Use the finite element method (or the finite difference method) and the parameters obtained in the previous problem to analyze the deformation at each stage. Compare the results with the observations.

8.14 Same as Problem 8.12. If we use the finite element method (or the finite difference method) to analyze the excavation-induced deformation and stress of the retaining wall and adopt the Mohr-Coulomb elastoplastic model to simulate the stress-strain behaviors of sand and clay, to the latter of which the effective stress undrained analysis is applied, determine the input parameters required for each layer.

8.15 Same as above. Use the finite element method (or the finite difference method) and the obtained parameters from the previous problem to analyze the deformation at each stage. Compare the results with the observations.

8.16 Same as Problem 8.14. If we use the Mohr-Coulomb elastoplastic model to analyze the excavation-induced wall deformation and stress except that total stress undrained analysis is to be adopted this time for the clayey layers, determine the input parameters required for each layer.

8.17 Same as above. Use the finite element method (or the finite difference method) and the parameters obtained in the previous problem to analyze the deformation at each stage. Compare the results with the observations.

8.18 Same as Problem 8.12. If we adopt the Mohr-Coulomb elastoplastic model to simulate the stress-strain behaviors of sand and the Cam-clay elastoplastic model for the clay with effective stress undrained analysis, determine the input parameters required for each soil layer.

8.19 Same as above. Use the finite element method (or the finite difference method) and the parameters obtained in the previous problem to analyze the deformation at each stage. Compare the results with the observations.

8.20 Same as Problem 6.4. Figure P6.4 shows the excavation profile and geological profile of Building R in Taipei. The measured deformation of the retaining wall at each stage is as shown in Figure P7.17. If we use the finite element method (or the finite difference

method) along with the hyperbolic model to analyze the excavation-induced wall deformation and stress, estimate the input parameters required for each layer of soil.

8.21 Same as above. Use the finite element method (or the finite difference method) and the parameters obtained in the previous problem to analyze the deformation at each stage and compare the results with the observations.

8.22 Same as Problem 8.20. If we use the finite element method (or the finite difference method) to analyze the wall deformation and stress induced by excavation and adopt the Mohr-Coulomb elastoplastic model for the simulation of the stress-strain relation for both sand and clay, for the latter of which the effective stress undrained analysis is to be performed, determine the input parameters required for each soil layer.

8.23 Same as above. Use the finite element method (or the finite difference method) and the parameters obtained in the previous problem to analyze the deformation at each stage and compare the results with the observations.

8.24 Same as Problem 8.22. If we use the Mohr-Coulomb elastoplastic model to analyze the excavation-induced wall deformation and stress except that total stress undrained analysis is to be performed for clay, determine the input parameters required for each soil layer.

8.25 Same as above. Use the finite element method (or the finite difference method) and the parameters obtained in the previous problem to analyze the deformation at each stage and compare the results with the observations.

8.26 Same as Problem 8.20. If we adopt the Mohr-Coulomb elastoplastic model to simulate the stress-strain behavior of sand and the Cam-clay elastoplastic model for clay along with the effective stress analysis method, determine the input parameters required for each soil layer.

8.27 Same as above. Use the finite element method (or the finite difference method) and the parameters obtained above to analyze the deformation at each stage and compare the results with the observations.

Chapter 9

Dewatering of excavations

9.1 Introduction

According to investigations, most problems encountered in deep excavation have direct or indirect relations with groundwater. Therefore, whether groundwater has been properly dealt with is a crucial point for the success of an excavation. Groundwater-induced problems in an excavation may arise from insufficient investigation of groundwater or geological conditions that lead to inability to fully control the groundwater. It may also arise from misunderstanding of the influence of groundwater, so that a wrong excavation method is adopted. Thus, it is necessary to perform detailed investigations of groundwater and its influences on soils or structures during excavation.

The permeability of clay is lower than 10^{-6} cm/s (see Section 2.2), from which it follows that the flow velocity of groundwater in clay is rather slow. As a result, to lower the groundwater level or decrease the water content of clay below the groundwater level in a short time period requires large amounts of energy or chemical methods to force the movement of groundwater in clay. When the groundwater level is lowered or the water content is decreased, the properties of clay will change significantly. The shear strength will increase and the compressibility will decline. In geotechnical engineering, the methods are often categorized as soil improvement methods. However, soil improvement methods are not the subject of the present chapter. This chapter is confined to the introduction of dewatering methods, which are employed to lower groundwater levels. Besides, with the low permeability of clay, that is, the flow velocity of groundwater in clay is small, the possibility of groundwater leaking into the excavation zone, which will cause much inconvenience during construction, need not be considered. There is no occurrence of boiling in clay, either. Therefore, when clay is encountered in an excavation, the groundwater level can be ignored in practical engineering applications, except in cases of the strengthening of soil.

The permeability of sand or gravel is usually greater than 10^{-3} cm/s, which follows that the flow velocity of groundwater in sand or gravel is rather high and groundwater probably will leak into the excavation zone during excavation and cause much trouble. In the worst cases, it may bring about the loosening of soils, sand boiling, or upheaval failure. To avoid such conditions, it is necessary to design comprehensive dewatering schemes before or during excavation. On the other hand, with the higher flow velocity of sand or gravel, simple methods such as pumping are usually enough to lower the groundwater levels.

This chapter will explain the goals of dewatering in excavation and introduce some commonly used methods of dewatering, including their basic theories and design methods.

9.2 Goals of dewatering

As explained above, dewatering methods are the methods of lowering the groundwater level in sandy or gravelly grounds rather than in clayey grounds. Generally speaking, the goals of lowering the groundwater level are to keep the excavation bottom dry, to prevent leakage of water or sand, to avoid sand boiling or upheaval failure, and to forestall the occurrence of floating basements, as explicated in the following:

1 To keep the excavation bottom dry: With the higher flow velocity of groundwater in sand or gravel, groundwater may well flow into the excavation zone, which will cause inconvenience for construction. To keep the excavation bottom dry, the groundwater level is generally lowered to 0.5–1 m below the excavation surface, as shown in Figure 9.1. Groundwater flows so slowly in clayey soils that flowing of groundwater into the excavation zone will not occur. There is no need to lower the groundwater level in clay.

2 To prevent leakage of groundwater or soils: To excavate in sandy or gravelly soil, with a high groundwater level, using either soldier piles or sheetpiles, which are not satisfactorily watertight, or diaphragm walls or bored piles with joints that may have defects will risk the possibility of the leaking of groundwater into the excavation zone through the retaining wall. The leakage of groundwater and soils may lead to disastrous results and bring about collapses and failures of excavations in the worst cases, when the leaking is great enough to enlarge the holes in the retaining wall. For more detailed content, please see Section 11.7.1.

3 To avoid sand boiling: To keep the excavation bottom dry when excavating in sandy or gravelly soils requires lowering the groundwater level within the excavation zone to 0.5–1 m below the excavation bottom at least. While excavation proceeds, the difference between the groundwater levels within and outside the excavation zone grows larger. When the hydraulic gradient around the excavation bottom grows larger or equals the critical hydraulic gradient of soils, sand boiling will occur. Many methods are available to avoid sand boiling. One of them is to lower the groundwater level outside the excavation zone. However, the possibility of ground settlement outside the excavation zone has to be considered (see Figure 9.2).

4 To forestall the upheaval failure: As shown in Figure 9.3, there exists a permeable layer (such as sand or gravel) underlying the clayey layer. The water pressure from the permeable layer will generate an upheaving force against the clayey layer. When the

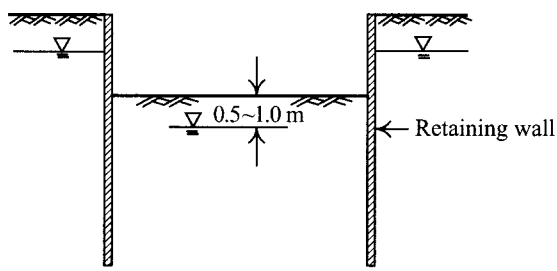

Figure 9.1 Keeping the excavation bottom dry by lowering the groundwater level beneath the excavation bottom.

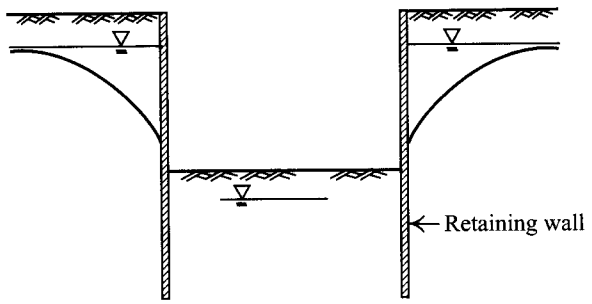

Figure 9.2 Lowering the groundwater level outside of the excavation zone to avoid sand boiling.

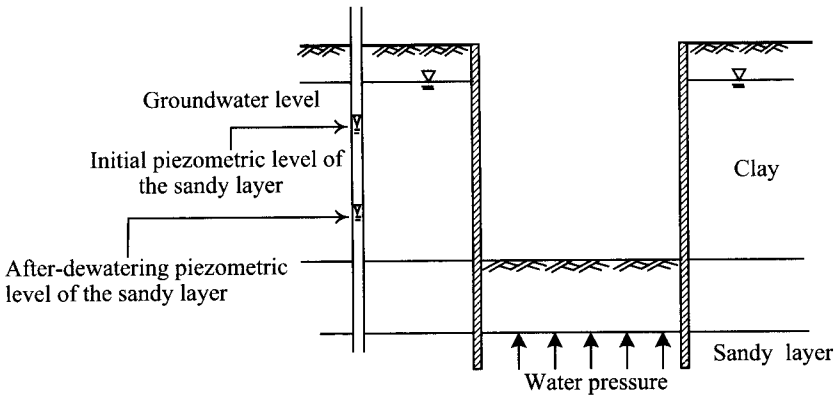

Figure 9.3 Lowering the piezometric level in sandy soils to avoid upheaval failures.

water pressure acting on the bottom of the clayey layer is larger than the total weights of the clayey layers, upheaval failure will occur. One of the methods to prevent the occurrence of upheaval failure is to lower the piezometric pressure of the permeable layer by pumping.

5 *To keep the basement from floating*: With the completion of excavation, one starts the construction of basements. In sandy soils, with the light weight of structures during the stage of basement construction (the weight of the basement only), the phenomenon of the floating of the basement is likely to happen if the weight of structures is smaller than the water pressure acting on the foundation base. Once the floating phenomenon has happened, with the differential heaves of the foundation, the floated basement will not necessarily sink back to the original elevation while building construction proceeds, which may lead to damage of the structures. In the worst condition, the basement may need to be demolished or reconstructed. Therefore, dewatering is usually required at the stage of basement construction to keep the upheaving force on foundation bottoms smaller than the weight of structures during construction. Dewatering is to be continued till the upheaving force is smaller than the weight of structures during construction.

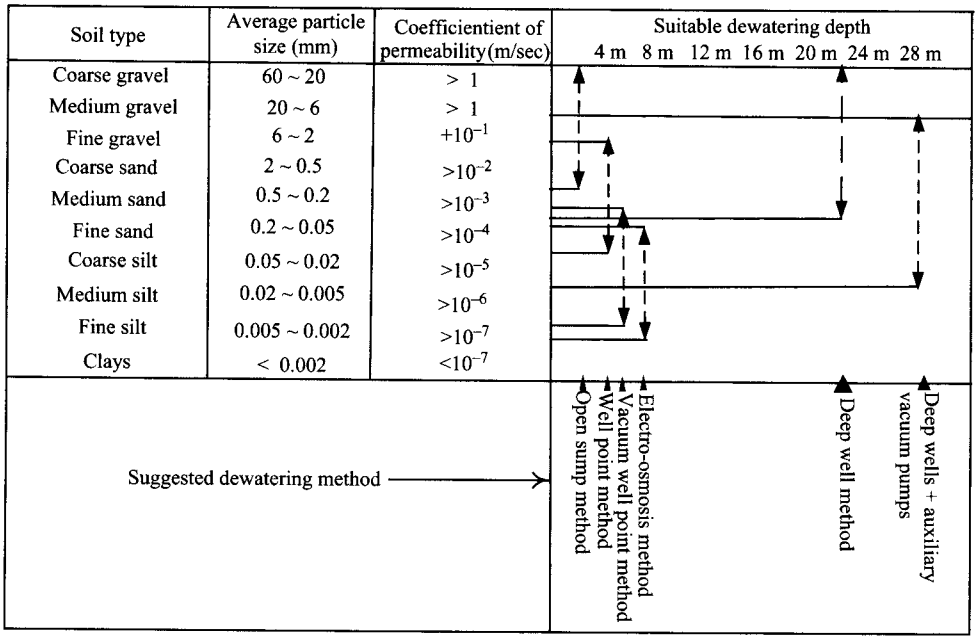

Figure 9.4 Application conditions for various dewatering methods (redraw from Quinion and Quinion (1987)).

9.3 Methods of dewatering

Some commonly used methods of dewatering in excavations include the open sump or ditch method, the deep well method, and the well point method. Figure 9.4 diagrams the application areas of these methods. The following will explain the basic principles and implementation of each method.

9.3.1 Open sumps or ditches

The open sump method is to collect the groundwater seeping onto the excavation bottom in an open sump, placed in the excavation bottom, by gravity or other natural means and pump the collected water out. If the excavation area is very large or the base is a long narrow shape, several sumps may be placed along the longer side or simply use a long narrow sump, which is called an open ditch. Both the open sump and the ditch are gravity draining methods. In practice, the former is more widely used than the latter.

As shown in Figure 9.5, open sumps are usually placed near the retaining wall at the lowest ground or excavation surface. The depth of an open sump is generally 0.6–1 m. The side walls of the open sump are sometimes protected to prevent them from collapse. Some common protective measures are slope side walls, wood planks, iron barrels, and concrete culverts. Figure 9.6 is a photo of protecting the open sump by concrete culverts.

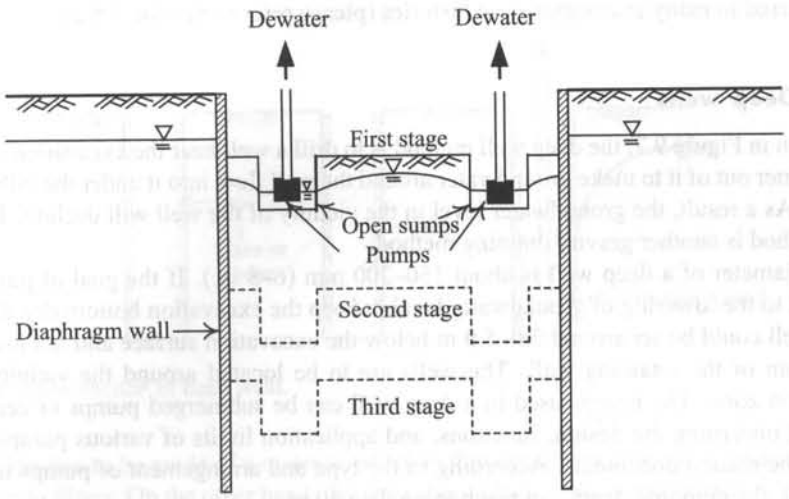

Figure 9.5 Dewatering method: the open sump method.

Figure 9.6 Photo of a concrete culvert protecting the side wall of a sump.

The open sump method is the most common and economical method of dewatering. However, its application is confined to permeable layers such as sandy and gravelly soils. Since the bottom of the open sump is lower than the excavation bottom, it will shorten the seepage path along which groundwater from outside seeps into the excavation zone and as a result the exit gradient on the sump bottom will be larger than that on the excavation surface. This fact

may bring about sand boiling on the sump bottom, which has to be prevented. Sand boiling has occurred in many excavation case histories (please refer to Section 5.8.2).

9.3.2 *Deep wells*

As shown in Figure 9.7, the deep well method is to drill a well near the excavation zone and pump water out of it to make groundwater around the well flow into it under the influence of gravity. As a result, the groundwater level in the vicinity of the well will decline. The deep well method is another gravity draining method.

The diameter of a deep well is about 150–200 mm (6–8 in.). If the goal of pumping is confined to the lowering of groundwater level to keep the excavation bottom dry, the depth of the well could be set around 2.0–5.0 m below the excavation surface and not lower than the bottom of the retaining wall. The wells are to be located around the vicinity of the excavation zone. The pumps used in a deep well can be submerged pumps or centrifugal pumps. Concerning the design, functions, and application limits of various pumps, please consult the related documents. According to the type and arrangement of pumps used in a deep well, the pumping depth can reach more than 30 m.

Figure 9.8 diagrams the construction of a deep well. As illustrated in the figure, drill the well to the designed depth, install a case (e.g. a PVC pipe) and a screen, and place filters between the well sides and the case. A well screen is also a filtering device that serves as the intake portion of the well. A screen permits groundwater to enter the well from the aquifer, and prevents sediment from entering the well. After filters are placed, the well has to be flushed to wash away the muddy soils generated during the drilling process, so as to avoid mud clogs in the filters, which will reduce the efficiency of the well.

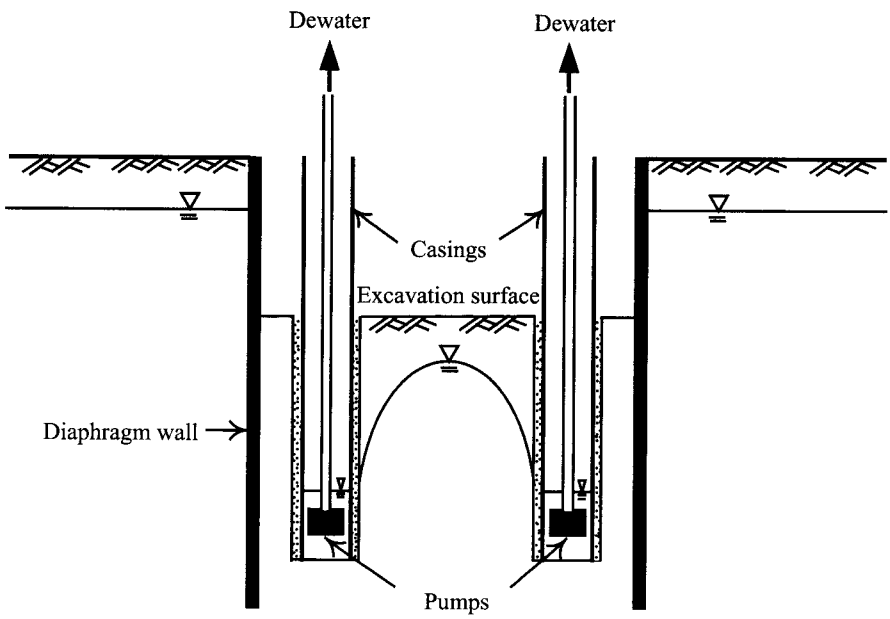

Figure 9.7 Dewatering method: the deep well method.

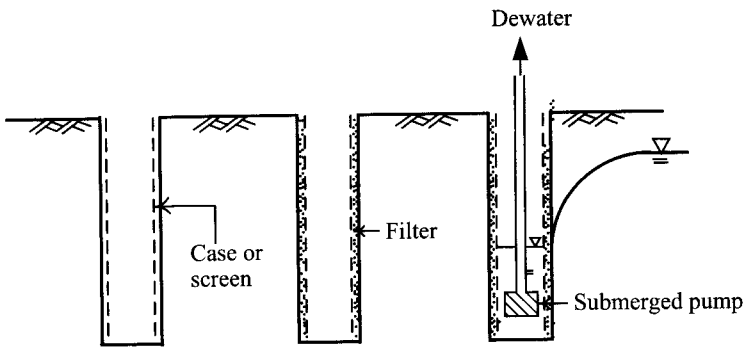

Figure 9.8 Construction of deep wells.

The filter has to be made of a material which is fine enough to prevent soil particles from flowing into filters. On the other hand, the filter should have voids large enough to keep good permeability and to avoid flowing into the well screen. Therefore, the JSA (1988) proposes the filter should meet the following criteria:

The criterion that the in situ soil particles do not flow into the filter

$$\frac{D_{15}(\text{filter})}{D_{85}(\text{ground})} < 5$$

The criterion that the filter material keeps good permeability

$$\frac{D_{15}(\text{filter})}{D_{15}(\text{ground})} > 5$$

The criterion that the filter material does not flow into the filtering screen of the well

$$\frac{D_{85}(\text{filter})}{D(\text{screen diameter})} > 2$$

9.3.3 Well points

The well point method is also called the vacuum well point method. The method is to place the collecting points connected to the pumping pipe inside a small-diameter well and have them arranged in a line or in a rectangle. The collecting points are usually separated by 0.8–2.0 m. The top of the pumping pipe is connected to the common collecting pipe, which is then pumped out under vacuum, drawing out pore water from the soil and lowering the groundwater level accordingly. Figure 9.9 is a schematic diagram illustrating dewatering by way of the well point method. The method is a type of the forced draining method.

The collecting pipes are usually arranged around the vicinity of an excavation site. Collecting points are the main structures of the well point method. A collecting point is usually 100 cm long, has an external diameter of 5–7 cm, and many small holes are bored along the side to collect groundwater. On the front end is usually installed a spurting device, which is used to help the collecting point penetrate into the ground using high pressure water. As

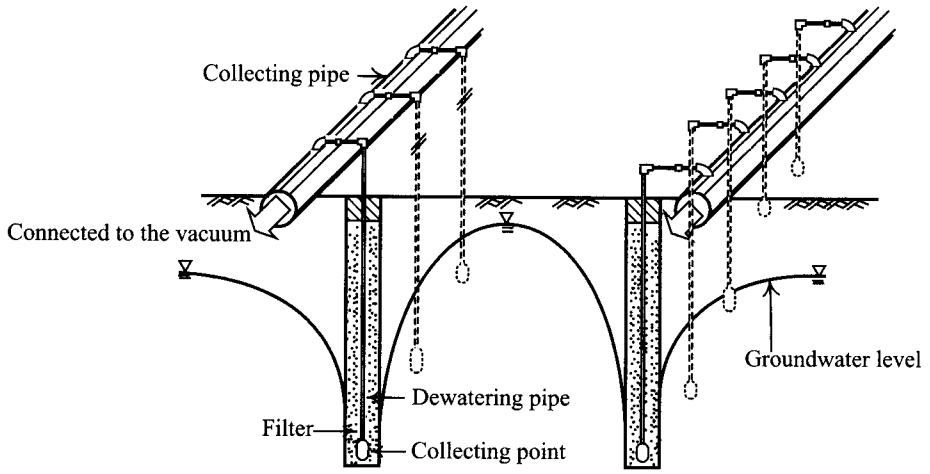

Figure 9.9 Dewatering method: the well point method.

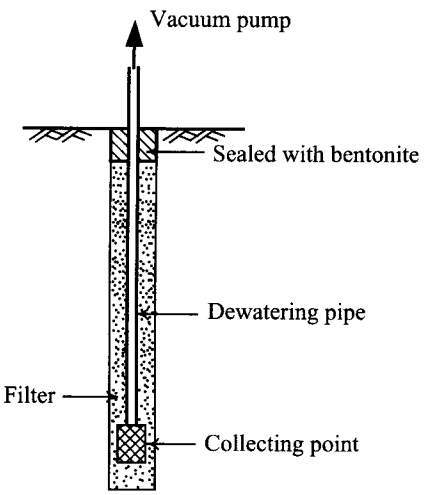

Figure 9.10 Configuration of a well point.

shown in Figure 9.10, the space between a collecting point and the well side are backfilled with filters to protect the collecting point from obstruction. The well can be enveloped by bentonite near the ground surface to increase the degree of vacuum and the efficiency of the well accordingly.

The principle of the well point method can be illustrated as the U-pipe shown in Figure 9.11. When both ends of a pipe are acted on by the same amount of atmospheric pressure, the water in the pipe is stable and still. Once a vacuum pump is used at the right end, the pressure is unbalanced at the two ends. The water table of the right end of the U-pipe will rise and a

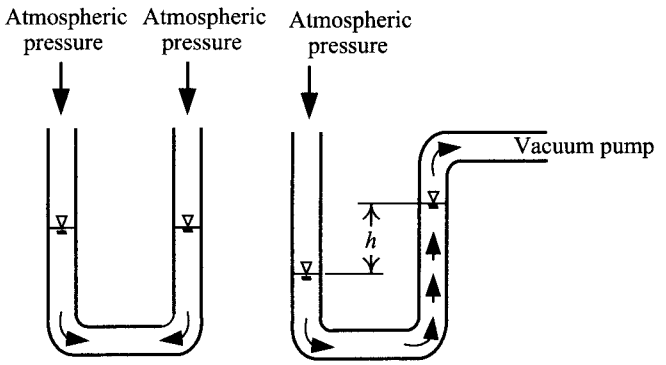

Figure 9.11 U-pipes acted on by vacuum pumps.

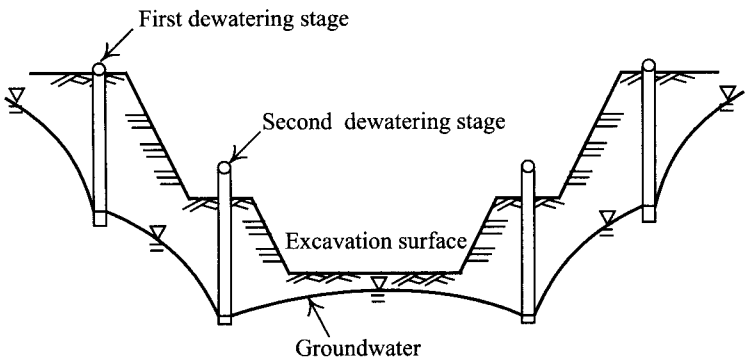

Figure 9.12 Two-stage well point dewatering.

height difference (h) is thus generated. When the right end of the U-pipe reaches the complete vacuum state, h will be 1 atmospheric pressure, or 1.033 kg/cm^2, which equals a 10.33 m high water column. Obviously, the height to which the water table rises relates to the degree of vacuum at the right end.

The principle of the well point method is similar to the just-mentioned principle of the U-pipe. Acted on by a vacuum pump, the pressure inside a collecting point is far lower than the pressure of groundwater which is exposed to atmospheric pressure, which leads to the groundwater being sucked into the collecting point. Since groundwater is sucked into the well out of vacuum and drained instead of flowing into it by gravity, the well point method is a type of forced drainage. The method is not only applicable to soils with high permeability but those whose permeability reaches as low as 10^{-4}–10^{-5} cm/s, such as silts.

Theoretically, the dewatering depth of the well point method can reach as deep as 10.33 m. It is, however, impossible to achieve the condition of total vacuum inside the well. Besides, head loss is unavoidable since there exists friction, which is generated by groundwater flowing through soils, filters, collecting points, pumping pipes, and collecting pipes. As a result, the dewatering depth can at best reach the depth of 5–6 m. In fine sands or silty sands, it can reach a depth of only 3–4 m (Quinion and Quinion, 1987).

When the dewatering depth goes beyond 6 m, it is recommended to carry out the well point method in phases, as shown in Figure 9.12. The deep well method can also supplement the well point method under such conditions.

9.4 Well theory

The well theory is aimed at the relationship between the discharge quantity and the drawdown. The relationship is affected by a number of factors: the numbers of wells, their structures, the geological conditions, and pumping time. The relationship between the discharge quantity and drawdown can be either solved by mathematical well formulas or numerical groundwater modeling. The former are inferred by assuming ideal conditions, whereas the latter is applicable to any geological or pumping condition and is therefore widely adopted. There are a great number of well formulas and it is impossible to introduce all of them here. Only the most widely used well formulas are to be discussed here for reference and application. As for the methods of numerical groundwater modeling, please refer to the referent books (e.g. Powers, 1992). Table 9.1 summarizes the well formulas for single well under various conditions. The theories will be explicated as follows.

9.4.1 Confined aquifers

Permeable layers are also designated as aquifers. When both above and below an aquifer, with the piezometric level higher than the top of the aquifer, impermeable layers are found the aquifer is called a confined aquifer.

When pumping an aquifer with a single well, the piezometric level will decline and a virtual drawdown cone will be formed, centered at the well, as shown in Figure 9.13. From the beginning of pumping, the area of the virtual drawdown cone will grow with the continuation of pumping. After a long period, the expansion rate of the area of the virtual drawdown cone will decline or stop expanding. This section is to introduce the pumping-induced drawdown according to the penetration depth of the well into an aquifer and the expansion conditions of the virtual drawdown cone.

9.4.1.1 Full penetration wells

A full penetration well is one that fully penetrates through the aquifer and its flow direction is thus horizontal (Figure 9.14a). Theis (1935) derived an equation of the drawdown curve with regard to time based on the following assumptions:

- The aquifer has a uniform thickness and is a homogeneous and isotropic confined aquifer.
- The well has to be one that fully penetrates through the aquifer.
- The well is 100% efficient. That is to say, no drop exists between the water table in the well and the drawdown curve.
- Meets the Dupuit-Thiem assumption. That is, the hydraulic gradient of any point on the drawdown curve is the slope at the point.
- No recharge water is within the influence range.
- The radius of the well is so small that the amount of retained water can be ignored.

Table 9.1 Summary of commonly used well formulas

	Confined aquifer		*Free aquifer*	
	Full penetration well	*Partial penetration well*	*Full penetration well*	*Partial penetration well*
Nonequilibrium equation	Theis's equation: $s = \frac{Q}{4\pi T}\left\{-0.5772 - \ln u - \sum(-1)^n \frac{u^n}{n \times n!}\right\}$ Jacob's modified equation: $s = \frac{Q}{4\pi T}(-0.5772 - \ln u)$ (Symbols are as shown in Figure 9.15)	—	If the drawdown induced by dewatering is far smaller than the thickness of the aquifer, Theis's and Jacob's equations can be used instead.	—
Equilibrium equation	Thiem's equation: $Q = \frac{2\pi kD(s_1 - s_2)}{\ln(r_2/r_1)}$ (Symbols are as shown in Figure 9.15)	Kozeny: $Q = \frac{2\pi T(H - h_w)}{\ln(R/r_w)}\mu$ $\mu = \frac{D_1}{D}\left(1 + 7\sqrt{\frac{r_w}{2D_1}}\cos\frac{\pi D_1}{2D}\right)$ (Symbols are as shown in Figure 9.19)	Dupuit-Thiem's equation: $Q = \frac{\pi k(h_2^2 - h_1^2)}{\ln(r_2/r_1)}$ (Symbols are as shown in Figure 9.20)	Hausman's suggestion: $Q = \frac{\pi k\left[H^2 - h_w^2\right]\alpha}{\ln(R/r_w)}$ $\alpha = \sqrt{\frac{H - D_1}{H}}\sqrt[4]{\frac{H + D_1}{H}}$ (Symbols are as shown in Figure 9.21)

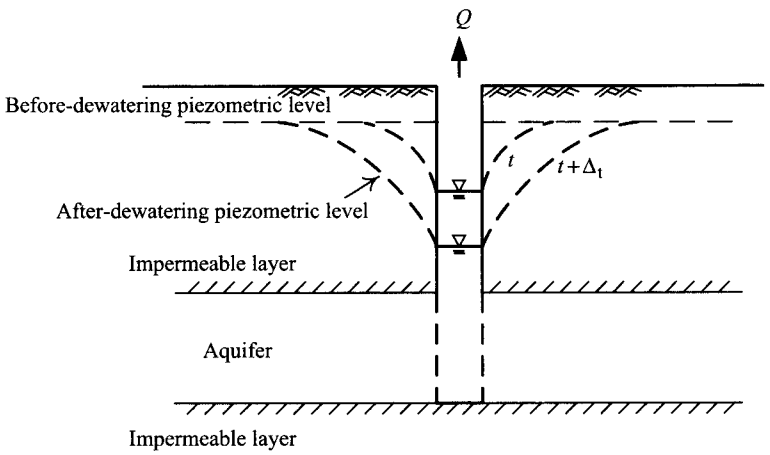

Figure 9.13 Dewatering in confined aquifers.

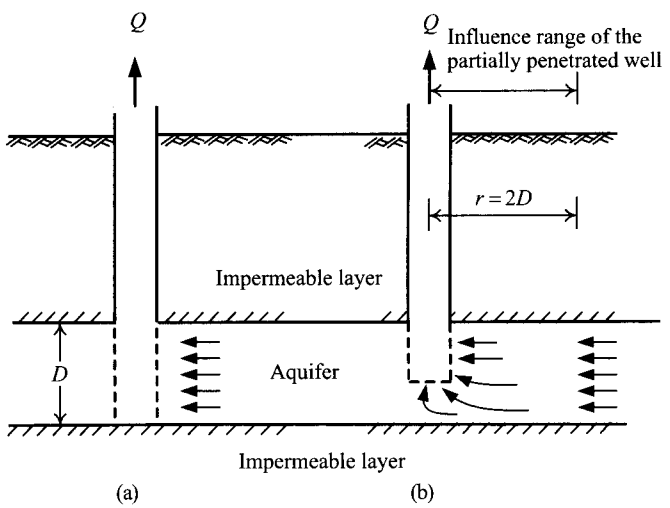

Figure 9.14 Flow directions around a well in confined aquifers: (a) full penetration well and (b) partial penetration well.

Theis's drawdown equation is written as follows (Figure 9.15):

$$s = \frac{Q}{4\pi kD} W(u) = \frac{Q}{4\pi T} W(u) \tag{9.1}$$

$$W(u) = \int_u^{\infty} \frac{e^{-u}}{u} \mathrm{d}u = -0.5772 - \ln u - \sum_{n=1}^{\infty} (-1)^n \frac{u^n}{n \times n!} \tag{9.2}$$

$$u = \frac{r^2 S}{4Tt} \tag{9.3}$$

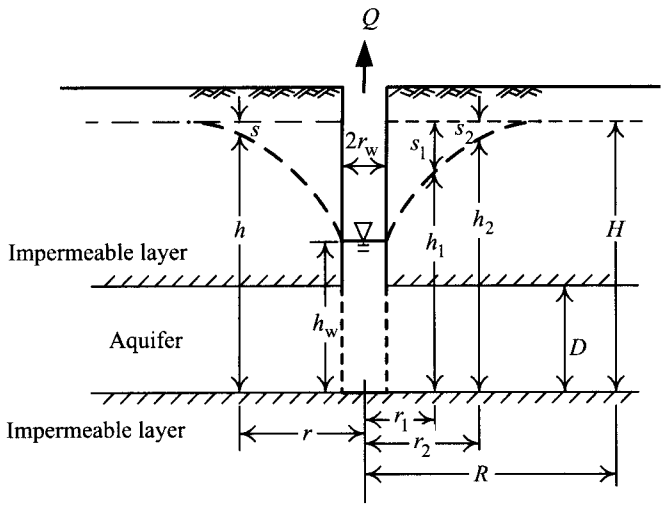

Figure 9.15 Symbol diagram of dewatering in confined aquifers.

where

s = drawdown
Q = discharge quantity
k = coefficient of permeability or permeability
D = thickness of the aquifer
$T = kD$ = coefficient of transmissivity
$W(u)$ = well function
u = parameter of the well function
r = distance to the center of the well
S = coefficient of storage or storativity
t = time since pumping started.

Equation 9.1 is Theis's nonequilibrium equation. Table 9.2 lists the values of well functions calculated from Eq. 9.2. Figure 9.16 is the $W(u) \sim 1/u$ relation curve, which is also called the standard curve.

Habitually, the coefficients of permeability, transmissivity, and storage are all called hydraulic parameters. The coefficient of permeability is an intrinsic parameter of a soil, which is defined and can be tested as introduced in Section 2.2.4 in this book. The coefficient of transmissivity is the coefficient of permeability multiplied by the thickness of the aquifer. Since the thickness of a confined aquifer is a constant, the coefficient of transmissivity of a confined aquifer is also a constant.

The coefficient of storage is defined as the drained volume of the pore water due to lowering a unit head per unit surface area of an aquifer (Figure 9.17). Since soil in a confined aquifer is always in the saturated state, the drainage of pore water during dewatering should be caused by the decrease of the thickness of the aquifer. Since the decrease of heads follows the increase of effective stress, the thickness of the aquifer will reduce as a result.

Table 9.2 Well function $W(u)$ (Ferris *et al.*, 1962)

N	$u = N \times 1$	$u = N \times 10^{-1}$	$u = N \times 10^{-2}$	$u < 10^{-2}$
1.0	0.2194	1.8229	4.0379	
1.1	0.1860	1.7371	3.9436	
1.2	0.1584	1.6595	3.8576	
1.3	0.1355	1.5889	3.7785	
1.4	0.1162	1.5241	3.7054	
1.5	0.1000	1.4645	3.6374	
1.6	0.08631	1.4092	3.5739	
1.7	0.07465	1.3578	3.5143	
1.8	0.06471	1.3098	3.4581	
1.9	0.05620	1.2649	3.4050	adopts $W(u) = -0.5772 - \ln u$
2.0	0.04890	1.2227	3.3547	
2.1	0.04261	1.1829	3.3069	
2.2	0.03719	1.1454	3.2614	
2.3	0.03250	1.1099	3.2179	
2.4	0.02844	1.0762	3.1763	
2.5	0.02491	1.0443	3.1365	
2.6	0.02185	1.0139	3.0983	
2.7	0.01918	0.9849	3.0615	
2.8	0.01686	0.9573	3.0261	
2.9	0.01482	0.9309	2.9920	
3.0	0.01305	0.9057	2.9591	
3.1	0.01149	0.8815	2.9273	
3.2	0.01013	0.8583	2.8965	
3.3	0.008939	0.8361	2.8668	
3.4	0.007891	0.8147	2.8379	
3.5	0.006970	0.7942	2.8099	
3.6	0.006160	0.7745	2.7827	
3.7	0.005448	0.7554	2.7563	
3.8	0.004820	0.7371	2.7306	
3.9	0.004267	0.7194	2.7056	
4.0	0.003779	0.7024	2.6813	
4.1	0.003349	0.6859	2.6576	
4.2	0.002969	0.6700	2.6344	
4.3	0.002633	0.6546	2.6119	
4.4	0.002336	0.6397	2.5899	
4.5	0.002073	0.6253	2.5684	
4.6	0.001841	0.6114	2.5474	
4.7	0.001635	0.5979	2.5268	
4.8	0.001453	0.5848	2.5068	
4.9	0.001291	0.5721	2.4871	
5.0	0.001148	0.5598	2.4679	
5.1	0.001021	0.5478	2.4491	
5.2	0.0009086	0.5362	2.4306	
5.3	0.0008086	0.5250	2.4126	
5.4	0.0007198	0.5140	2.3948	
5.5	0.0006409	0.5034	2.3775	
5.6	0.0005708	0.4930	2.3604	
5.7	0.0005085	0.4830	3.3437	
5.8	0.0004532	0.4732	2.3273	
5.9	0.0004039	0.4637	2.3111	
6.0	0.0003601	0.4544	2.2953	
6.1	0.0003211	0.4454	2.2797	

Table 9.2 Continued

N	$u = N \times 1$	$u = N \times 10^{-1}$	$u = N \times 10^{-2}$	$u < 10^{-2}$
6.2	0.0002864	0.4366	2.2645	
6.3	0.0002555	0.4280	2.2494	
6.4	0.0002279	0.4197	2.2346	
6.5	0.0002034	0.4115	2.2201	
6.6	0.0001816	0.4036	2.2058	
6.7	0.0001621	0.3959	2.1917	
6.8	0.0001448	0.3883	2.1779	
6.9	0.0001293	0.3810	2.1643	
7.0	0.0001155	0.3738	2.1508	
7.1	0.0001032	0.3668	2.1376	
7.2	0.00009219	0.3599	2.1246	
7.3	0.00008239	0.3532	2.1118	
7.4	0.00007364	0.3467	2.0991	
7.5	0.00006583	0.3403	2.0867	
7.6	0.00005886	0.3341	2.0744	
7.7	0.00005263	0.3280	2.0623	adopts $W(u) = -0.5772 - \ln u$
7.8	0.00004707	0.3221	2.0503	
7.9	0.00004210	0.3163	2.0386	
8.0	0.00003767	0.3106	2.0269	
8.1	0.00003370	0.3050	2.0155	
8.2	0.00003015	0.2996	2.0042	
8.3	0.00002699	0.2943	1.9930	
8.4	0.00002415	0.2891	1.9820	
8.5	0.00002162	0.2840	1.9711	
8.6	0.00001936	0.2790	1.9604	
8.7	0.00001733	0.2742	1.9488	
8.8	0.00001552	0.2694	1.9393	
8.9	0.00001390	0.2647	1.9290	
9.0	0.00001245	0.2602	1.9187	
9.1	0.00001115	0.2557	1.9087	
9.2	0.000009988	0.2513	1.8987	
9.3	0.000008948	0.2470	1.8888	
9.4	0.000008018	0.2429	1.8791	
9.5	0.000007185	0.2387	1.8695	
9.6	0.000006439	0.2347	1.8599	
9.7	0.000005771	0.2308	1.8505	
9.8	0.000005173	0.2269	1.8412	
9.9	0.000004637	0.2231	1.8320	

Following from the above elucidation, the coefficient of storage of a confined aquifer, which generally ranges between 0.0005–0.001, is similar to the compressibility of soils (Powers, 1992).

When pumping time (t) is rather long or the distance (r) is quite short, the parameter u will be very small, as listed in Table 9.2. Thus, when $u \leq 0.05$, the high order of the multinomial at the right side of the equation can be ignored. Equation 9.2 can then be rewritten as

$$s = \frac{Q}{4\pi T}(-0.5772 - \ln u) \tag{9.4}$$

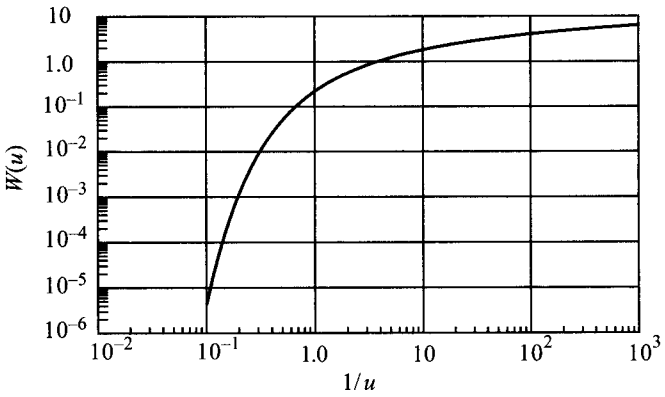

Figure 9.16 Standard curve of the well function.

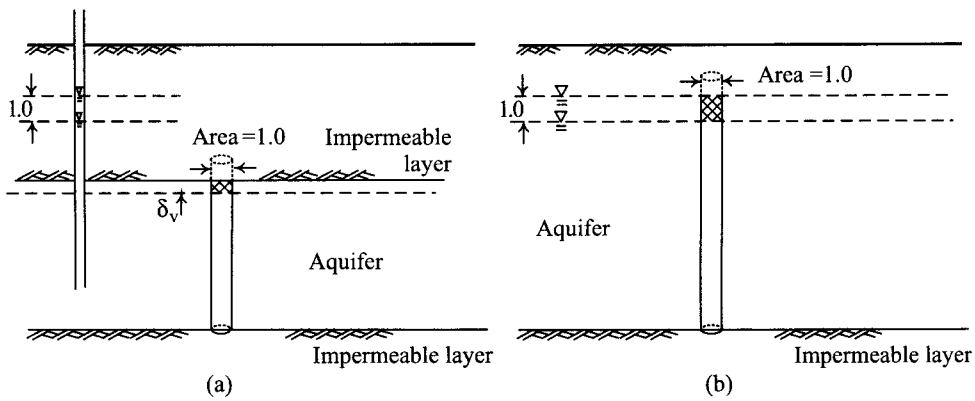

Figure 9.17 Definition of coefficient of storage: S = water drained from a volume of $\delta_v \times 1.0$: (a) confined aquifer and (b) free aquifer.

which can also be written as

$$s = \frac{0.183Q}{T} \log \frac{2.25Tt}{r^2S} \tag{9.5}$$

Equation 9.4 or 9.5 is called Jacob's modified nonequilibrium equation (Jacob, 1940), which is only applied when $u \leq 0.05$.

Assuming the influence range of pumping is defined as the distance where the drawdown just declines to 0, the influence range of pumping-induced drawdown (R) can be calculated from Eq. 9.5 as

$$R = \sqrt{\frac{2.25Tt}{S}} \tag{9.6}$$

In addition to the above equation, many people have proposed different influence ranges of pumping-induced drawdown. One of them is Kozeny's (Kozeny, 1953):

$$R = 1.5\frac{\sqrt{Hkt}}{n} \tag{9.7}$$

Where

n = porosity of the soil
H = groundwater level before pumping
t = pumping time
k = coefficient of permeability.

Sichart (1928):

$$R = 3000 s_w \sqrt{k} \tag{9.8}$$

Equation 9.8 is an empirical formula where R represents for the influence range measured by meter; s_w is the drawdown in the well, also measured by meter; k is the coefficient of permeability and its unit is m/sec.

Assume a hypothetical dewatering case: $Q = 1.0\,\mathrm{m}^3/\mathrm{min}$, $T = 1.0\,\mathrm{m}^2/\mathrm{min}$, $S = 0.0001$. Analyze the relationship between drawdown and pumping time in terms of the logarithm scale using separately Theis's and Jacob's equations, as shown in Figure 9.18a. As illustrated in the figure, when t is considerably large, causing $u \leq 0.05$, the relationship between the drawdown and pumping time in terms of the logarithm value becomes linear, which is also Jacob's modified nonequilibrium equation.

Similarly, the relationship between drawdown and distance on the logarithm scale, as shown in Figure 9.18b, can be computed following Theis's and Jacob's equations, respectively. We can see when r is rather small, it also leads to $u \leq 0.05$, which is to say drawdown

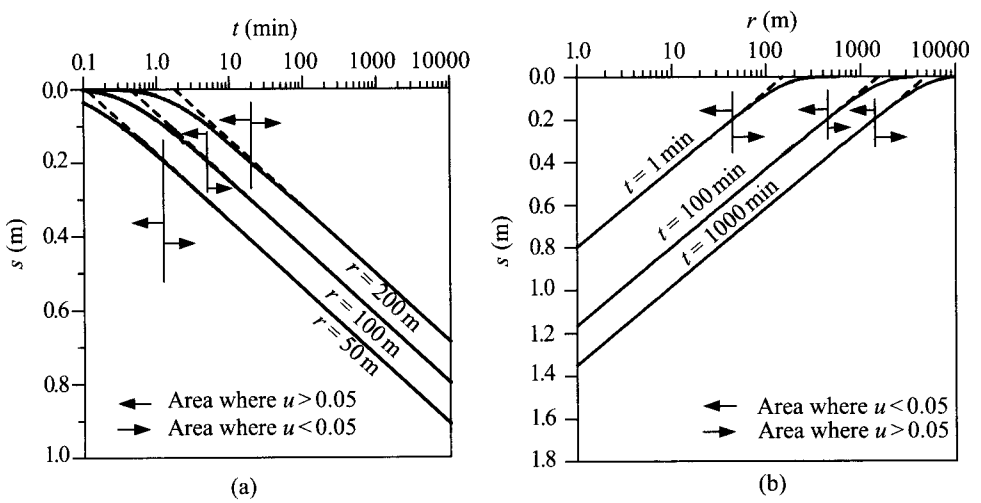

Figure 9.18 Variations of drawdowns in confined aquifers: (a) relation between drawdowns and time and (b) relation between drawdowns and distances.

and distance on the logarithm scale have a linear relationship. The influence range of pumping in Eq. 9.6 is expressed by the intersection point where the extension of the line meets the line $s = 0$.

Assume the drawdown curve achieves equilibrium after pumping, (which follows that the drawdown curve will not expand with regard to pumping time). Thiem's equilibrium equation (Thiem, 1906) can thus be derived from the differential equation of the drawdown curve (see Figure 9.15)

$$Q = \frac{2\pi kD(s_1 - s_2)}{\ln(r_2/r_1)} \tag{9.9}$$

where r_1 and r_2 are the distances of the first observation well and the second observation well to the well center, respectively, s_1 and s_2 are drawdowns in the first and the second observation well, respectively.

Equation 9.9 is the most common equation of pumping introduced in the soil mechanics textbooks. Let R be the influence range and substitute for r in the above equation. We can have drawdown (s) at any distance. Thus, Thiem's equilibrium equation can be rewritten as follows:

$$s = \frac{Q\ln(R/r)}{2\pi kD} \tag{9.10}$$

Let the drawdown in the well be $(H - h_w)$, the radius of the well be r_w, and substitute them into Eq. 9.9. We then have Thiem's equilibrium equation rewritten as:

$$Q = \frac{2\pi kD(H - h_w)}{\ln(R/r_w)} \tag{9.11}$$

where

H = piezometric level before pumping
h_w = groundwater level in the well after pumping
r_w = radius of the well.

Equation 9.9 is derived from the differential equation of the drawdown curve, assuming that drawdown after pumping is in equilibrium and that the drawdown curve does not expand with pumping time. Substitute the influence range (R) of Eq. 9.6 into Eq. 9.5, Jacob's modified nonequilibrium equation, we then have Eq. 9.9. Thus, Thiem's equilibrium equation is a special case of Jacob's modified nonequilibrium equation. That is to say, when the drawdown curve does not expand any more, the pumping time coming to t and the influence range extending to$R$, Jacob's modified nonequilibrium equation will be identical to Thiem's equilibrium equation.

After pumping for a period of time, turn off the pump and the drawdown curve will gradually return to the original water table. The relationship between the recovered drawdown curve and time can obtain the coefficient of transmissivity or permeability, as is designated as the recovery method. According to Theis (1935), the relationship between the residual drawdown and time can be expressed as follows:

$$s' = \frac{Q}{4\pi T}\ln\frac{t}{t'} = \frac{2.3Q}{4\pi T}\log\frac{t}{t'} \tag{9.12}$$

where

s' = residual drawdown, that is, the distance between the water level in the pumping well and the original groundwater level
Q = recovered quantity, equivalent to discharge quantity
T = coefficient of transmissivity
t = time since pump started.
t' = time since pump is stopped.

The recovery method can be used to examine the results of pumping tests. What's more, during a long period of pumping and dewatering, the activities of pumping may be suspended temporarily for certain reasons and the drawdown curve will recover gradually. The recovery method can be used under such conditions. The results can not only offer extra data but be compared with those of pumping tests.

9.4.1.2 *Partial penetration well*

In engineering practice, the partial penetration well is more widely used than the full penetration well. As shown in Figure 9.14b, within the range of $r \leq 2D$, the flow lines in the vicinity of the well are not necessarily horizontal. Instead, some are vertical. For most types of soils, the vertical coefficients of permeability are about one-tenth of the horizontal one. Thus, the well formulas concerning partial penetration wells need modifying.

There have been many nonequilibrium theories for partial penetration wells, and most of them are very complicated. This chapter will leave them aside. For interested readers, please see the related literature (Hantush, 1962; Kruseman and de Ridder, 1990).

There are also many equilibrium theories available. They are not, nevertheless, so complicated as nonequilibrium theories. This section will introduce a formula derived by Kozeny (1953).

As shown in Figure 9.19, when $r > 2D$, the effects of a partial penetration well can be ignored since its drawdown curve can be fully solved when seen as a full penetration well. When $r \leq 2D$, however, the amount of drawdown for a partial penetration well is larger than that for a full penetration well. According to Kozeny's derivation (1953), the quantity of water to be pumped to achieve the designed drawdown can be expressed as follows:

$$Q = \frac{2\pi T(H - h_w)}{\ln(R/r_w)}\mu \tag{9.13}$$

$$\mu = \frac{D_1}{D}\left(1 + 7\sqrt{\frac{r_w}{2D_1}}\cos\frac{\pi D_1}{2D}\right) \tag{9.14}$$

where μ = coefficient of modification; D_1 = penetration depth of the well; D = thickness of the aquifer. Other parameters mean the same as in the equation of the full penetration well.

9.4.2 *Free aquifers*

A free aquifer, also called an unconfined aquifer, refers to an aquifer which is exposed to the atmosphere and is underlain by an impermeable layer. The analyses of free aquifers

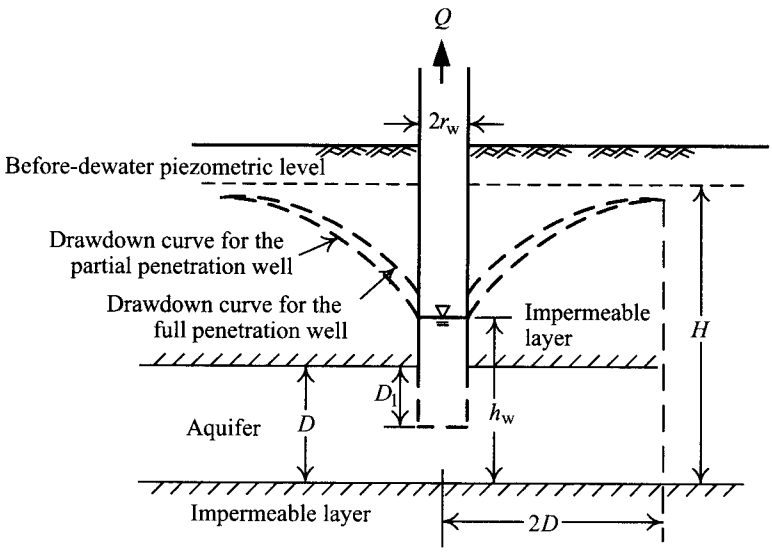

Figure 9.19 Drawdown curve for partial penetration wells in confined aquifers.

are also divided into full penetration wells and partial penetration wells as explicated in the following:

9.4.2.1 *Full penetration well*

The solution for nonequilibrium equations of pumping-induced drawdown in free aquifers is quite complicated. The reason is mainly that the coefficient of transmissivity is not a constant and varies with pumping time and distance. What's more, the vertical directions of flow near the well are so crucial that they cannot be ignored in the derivation. There can still be found some approximate solutions for nonequilibrium equations of pumping-induced drawdown. For interested readers, please refer to books dealing with groundwater (e.g. Marino and Luthin, 1982). This section will not go into the subject.

On the other hand, if the drawdown is much smaller than the thickness of aquifers, the thickness of aquifers can thus be assumed to be a constant during dewatering. Since the coefficient of transmissivity is the product of the coefficient of permeability and the thickness of the aquifer, the coefficient of transmissivity is also a constant. Theis's nonequilibrium equation or Jacob's modified nonequilibrium equation can also be applied to pumping in free aquifers accordingly. The required hydraulic parameters are also the coefficients of transmissivity (T) and storage (S).

As in Section 9.4.1, the coefficient of storage is given as the drained volume of the pore water due to lowering a unit head per unit surface area of an aquifer. The drainage per unit surface area of a free aquifer is caused by the decline of groundwater level (Figure 9.17b). Therefore, in a free aquifer, the coefficient of storage is the same as the ratio of free water in the soil to the soil volume (Powers, 1992). Its value is either smaller than or the same as the porosity of soil. For example, if the porosity of soil is 30% and two-thirds of pore water

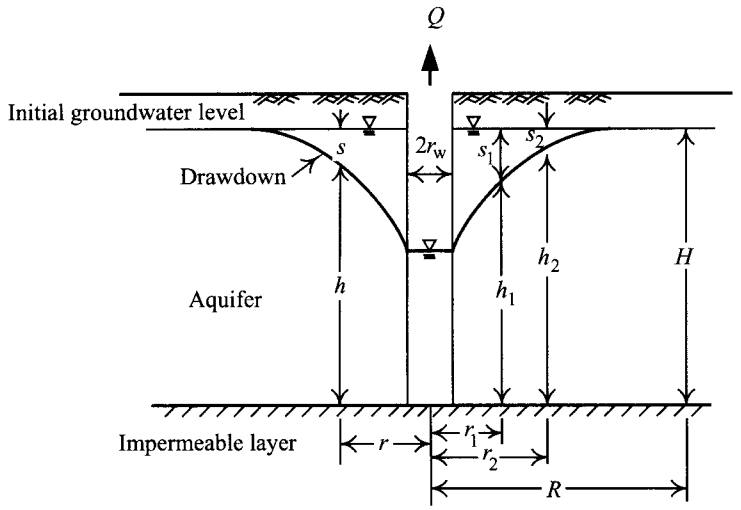

Figure 9.20 Drawdown in free aquifers for the full penetration well.

is drained as a result of the lowering of groundwater level by pumping, the coefficient of storage will then be 20% or 0.2. For most free aquifers, the coefficient of storage would be around 0.2–0.3.

As shown in Figure 9.20, under the Dupuit-Thiem assumption (Dupuit, 1863; Thiem, 1906), the equilibrium equation of drawdown of a full penetration well in a free aquifer is

$$Q = \frac{\pi k(h_2^2 - h_1^2)}{\ln(r_2/r_1)} = \frac{\pi k(h_2^2 - h_1^2)}{2.3\log(r_2/r_1)} \tag{9.15}$$

where h_1 and h_2 are the heights of the water levels at the distances of r_1 and r_2, respectively.

Equation 9.15 is the generally adopted equation in books on soil mechanics. Substitute the influence range (R) and the radius of the well (r_w) for r_2 and r_1, respectively, in the above equation; we then have

$$Q = \frac{\pi k(H^2 - h_w^2)}{\ln(R/r_w)} \tag{9.16}$$

Equation 9.15 can also be rewritten to obtain the groundwater level or drawdown at any distance (r) as follows:

$$H^2 - h^2 = \frac{Q\ln(R/r)}{\pi k} \tag{9.17}$$

or

$$h^2 - h_w^2 = \frac{Q\ln(r/r_w)}{\pi k} \tag{9.18}$$

where h is the groundwater level at the distance of r.

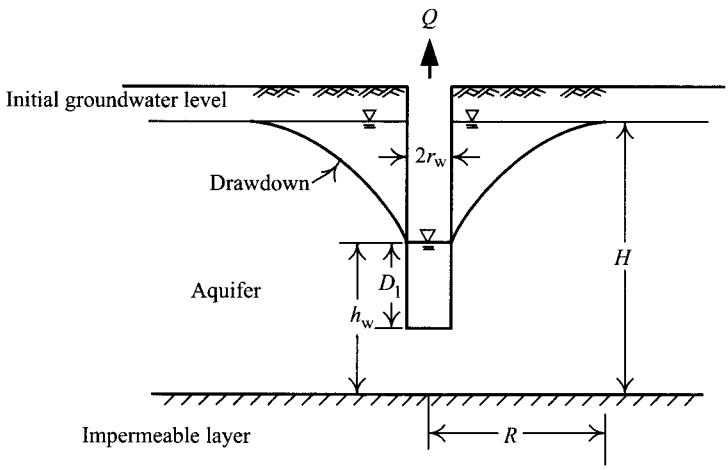

Figure 9.21 Drawdown in free aquifers for the partial penetration well.

9.4.2.2 *Partial penetration well*

The same as the full penetration well, the nonequilibrium equation of drawdown of a partial penetration well is rather complicated and is not to be discussed in this book. For interested readers, please refer to related literatures (e.g. Marino and Luthin, 1982). This section only introduces an equation proposed by Hausman (1990), which is

$$Q = \frac{\pi k(H^2 - h_w^2)\alpha}{\ln(R/r_w)} \tag{9.19}$$

$$\alpha = \sqrt{\frac{H - D_1}{H}}\sqrt[4]{\frac{H + D_1}{H}} \tag{9.20}$$

For the elucidation of the above signs, please see Figure 9.21.

9.4.3 Group wells

Pumping with multiple wells at the same time will encounter problems of intervention. Figure 9.22a diagrams the multiple wells in a free aquifer. Assuming only well #1 is used in pumping, in the equilibrium state, the required quantity of water to be pumped for well #1 can be computed according to Eq. 9.17:

$$Q_1 = \frac{\pi k(H^2 - h_1^2)}{\ln(R/r_1)} \tag{9.21}$$

where

R = influence range
r_1 = distance from well #1 to point P

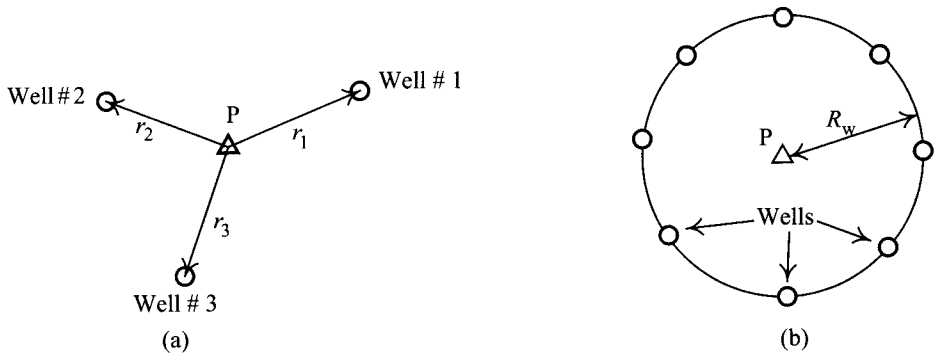

Figure 9.22 Group wells: (a) notations and (b) circular arrangement of wells.

H = groundwater level before pumping
h_1 = groundwater level at a distance of r_1 from the well.

Similarly, if well #2 is used exclusively, the required quantity of water to be pumped can also be computed using the same equation. Assuming there exist n wells, pumping simultaneously in a free aquifer, the total quantity of water to be pumped under equilibrium would be (Forchheimer, 1930)

$$Q_{\text{tot}} = \frac{\pi k(H^2 - h^2)}{\ln R - (1/n)\ln r_1 r_2 \cdots r_n} \tag{9.22}$$

where

Q_{tot} = total quantity of water to be pumped
n = number of wells
h = groundwater level at point P
$r_1, r_2 \ldots r_w$ = distances from well #1, #2... to point P.

When the well group is arranged in a circle (see Figure 9.22b), the above equation can be simplified. The total quantity of water to be pumped at the center P is

$$Q_{\text{tot}} = \frac{\pi k(H^2 - h^2)}{\ln(R/R_w)} \tag{9.23}$$

Equation 9.22 can also be used to calculate the groundwater level in a pumping well. Let r_1 be the radius of the pumping well#1 (i.e. $r_1 = r_w$) and $r_2 \ldots r_n$ be the distances from well#1 to well#2...#n, respectively, as shown in Figure 9.23. With the total quantity of water to be pumped Q_{tot}, the groundwater level in well#1 can be obtained by substituting those values in Eq. 9.22.

No simple and reliable equations to compute the total quantity of water to be pumped for the multiple wells in the nonequilibrium state or in confined aquifers are available so far. Generally speaking, the total quantity of water to be pumped for the multiple wells in the nonequilibrium state or in confined aquifers can be estimated through numerical simulations of groundwater. We can also adopt the method of linear superposition. The results, however, have to be confirmed by pumping tests.

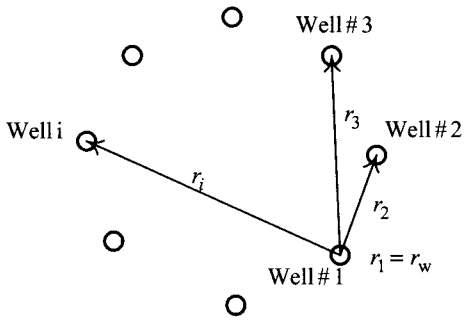

Figure 9.23 Computation of the water level in well #1 among the group wells.

Table 9.3 Result of a step drawdown pumping test

Pumping rate (m^3/hr)	*Drawdown in the pumping well* (m)
50	4.06
65	5.81
80	7.81
90	9.7
100	11.95

9.5 Pumping tests

Two types of pumping tests, that is, the step drawdown and constant rate tests, are usually carried out before dewatering. The major objective of a step drawdown test is to determine the capacity of a well while the main goal of a constant rate test is to obtain the hydraulic parameters, such as, the coefficients of permeability, transmissivity, and storage. Although there are full and partial penetration well theories, as introduced in Section 9.4, the test well for a pumping test should fully penetrate into the aquifer in order for its results to be analyzed using the well theories of the full penetration well, considering the equations for a partial penetration well are too complicated and some of them are empirical formulas.

9.5.1 Step drawdown tests

In a step drawdown test, the well is pumped at several successively higher pumping rates and the drawdown for each rate is recorded. The entire test is usually carried out within one day. Usually, 5 to 8 pumping rates are applied, each lasting 1–2 h. Details of the testing can be checked in Powers (1992) and Driscoll (1989).

Assume the result of a step drawdown test is as listed in Table 9.3. Figure 9.24 displays the relationships between pumping rates and drawdowns in terms of the logarithm scale. As shown in the figure, line $\overline{45}$ is of steeper slope than line $\overline{123}$. Obviously, when the pumping rate is equal to 90 m^3/h or 100 m^3/h, the drawdown in the well increases substantially and the well is in the condition of overpumping. The pumping rate at the intersection of line $\overline{123}$ and line $\overline{45}$ is thus the capacity of the well.

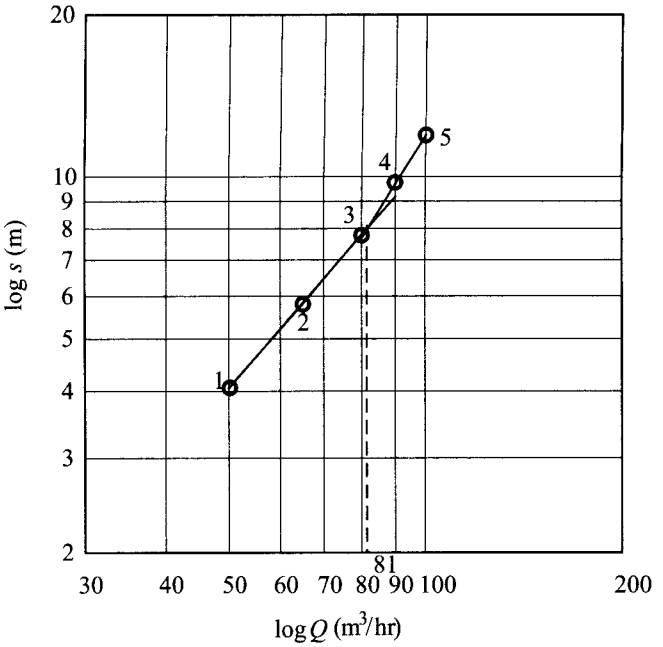

Figure 9.24 Relation between drawdowns and pumping rates for a step drawdown test.

9.5.2 Constant rate tests

Based on the result of a step drawdown test, we can select an appropriate pumping rate, slightly smaller than the capacity of the well, to pump the water for a long period of time and the drawdown for each observation well is recorded. This section will introduce the analytical methods for constant rate pumping tests in confined and free aquifers, respectively.

9.5.2.1 Confined aquifers

Given the results of pumping tests of a confined aquifer, the coefficients of transmissivity and storage of the aquifer can be obtained using the nonequilibrium and the equilibrium equations. Assuming the drawdown curve is under the nonequilibrium condition, according to Theis's nonequilibrium equation, we have

$$\log s - \log W(u) = \log(Q/4\pi T) = \text{constant} \tag{9.24}$$

$$\log(t/r^2) - \log(1/u) = \log(S/4T) = \text{constant} \tag{9.25}$$

The relational curve of $\log W(u) - \log(1/u)$ is called the standard curve, as shown in Figure 9.16. The relational curve of $\log s - \log(t/r^2)$ is called the data curve. From Eqs 9.24 and 9.25, we can see that the standard curve and the data curve are quite similar, given the same scale. If we superpose the two curves onto the same diagram of coordinates, the curves

of $\log s$ and $\log W(u)$ are identical except for a shift of constant $\log(Q/4\pi T)$. Similarly, the curves of $\log(t/r^2)$ and $\log(1/u)$ are also identical except for a shift of constant $\log(S/4T)$. Taking advantage of the characteristic between the standard curve and the data curve, the hydraulic parameters can be derived as follows:

1 Depict the standard curve $W(u) - (1/u)$ on the coordinate diagram on the logarithm scale.
2 Depict the data curve $s - t/r^2$ in the same scale as that of the standard curve on another coordinate diagram on the logarithm scale. If there exists only one observation well, the values of s and t obtained from the well can be directly adopted (i.e. r is a constant; t a variable). If there is more than one observation well, we can also adopt the values of $s - t/r^2$ at a specific time (i.e. t is a constant; r a variable).
3 Shift the coordinate sheets to make the data and standard curves meet. Be sure to keep the coordinates parallel to each other.
4 Pick a point, called the matching point, and read the values of $W(u)$, $1/u$, s and t/r^2 at the point. For convenience in computing, pick a whole number such as 0.1, 1, or 10 on the data or standard curve.
5 Substitute the values of $W(u)$, $1/u$, s and t/r^2 into Eqs 9.1 and 9.3, T and S can then be obtained.

As for the detailed computing process for Theis's nonequilibrium equation, please refer to Example 9.1. Besides, since the computing of Theis's nonequilibrium equation is too complicated, it is rarely adopted. To compute hydraulic parameters using a nonequilibrium equation, Jacob's nonequilibrium equation is most widely used.

When t is so great or r is small enough that $u \leq 0.05$, Jacob's nonequilibrium equation can be used to obtain hydraulic parameters. Similarly, we can depict the relations between s and $\log t/r^2$, whose values are obtained from a certain observation well (i.e. r is a constant; t a variable). If there is more than one well, the $s - t/r^2$ relation at a specific time (i.e. t is a constant; r a variable) can also be adopted. According to the $s - \log t/r^2$ curve and Eq. 9.5, we have

$$T = 0.183\frac{Q}{(\Delta s)_J} \tag{9.26}$$

where $(\Delta s)_J$ = slope of $s - \log t/r^2$ curve, the value of which equals the decreased amount of s when t/r^2 increases by a factor of ten.

The coefficient of transmissivity can thus be derived using the above equation. If we extend the line segment of $s - \log t/r^2$, the corresponding value of t/r^2 is $(t/r^2)_{s=0}$ where the extended line intersects with $s = 0$ at $(t/r^2)_{s=0}$ (see Figure 9.18). According to Eq. 9.5, we can compute the coefficient of storage by the following equation:

$$S = 2.25T\left(\frac{t}{r^2}\right)_{s=0} \tag{9.27}$$

where $(t/r^2)_{s=0}$ is the corresponding value of t/r^2 when $s = 0$.

The detailed procedures of computing Jacob's nonequilibrium equation are as illustrated in Example 9.1.

If the drawdown curve of a pumping test reaches equilibrium or changes little, Thiem's equilibrium equation can then be adopted for the calculation of hydraulic parameters. According to Eq. 9.9, the coefficient of permeability can be obtained as follows:

$$k = \frac{Q\ln(r_2/r_1)}{2\pi D(s_1 - s_2)} = \frac{0.366Q}{D(s_1 - s_2)}\log\frac{r_2}{r_1} \tag{9.28}$$

and the coefficient of transmissivity is

$$T = kD = \frac{Q\ln(r_2/r_1)}{2\pi(s_1 - s_2)} \tag{9.29}$$

If there are two or more observation wells, first establish the relations between the drawdown (s) and the distance on the logarithm scale ($\log r$) for each well, which will be similar to Figure 9.18b. Then the coefficient of transmissivity can be derived from Eq. 9.28 as

$$T = \frac{0.366Q}{(\Delta s)_T} \tag{9.30}$$

where $(\Delta s)_T$ is the slope of the $s - \log r$ curve and its value equals the decreased amount of s when r increases ten times.

Similarly, if we extend the line segment of the $s - \log r$ curve, the extended line will intersect with $s = 0$ at R (as shown in Figure 9.18b). The same as earlier discussions, R represents the influence range of the drawdown. According to the influence range in Eq. 9.6, the coefficient of storage can be derived as

$$S = \frac{2.25Tt}{R^2} \tag{9.31}$$

Similarly, the detailed computing procedures of Thiem are as illustrated in Example 9.1.

The coefficient of transmissivity can also be derived from the recovery method. Similarly, depict the $s' - \log(t/t')$ relation according to the observation of each well. Using Eq. 9.12, we can derive

$$T = \frac{0.183Q}{(\Delta s')_r} \tag{9.32}$$

where $(\Delta s')_r$ = the slope of the $s' - \log(t/t')$ curve and its value is the decreased amount of s' when t/t' increases ten times. As for the detailed computing procedure of the recovery method, please see Example 9.1.

9.5.2.2 *Free aquifers*

If the pumping-induced drawdown is much smaller than the thickness of the free aquifer, both Theis's nonequilibrium equation and Jacob's modified nonequilibrium equation for confined aquifers are applicable and the required hydraulic parameters are also the coefficients of transmissivity and storage. If the drawdown is not much smaller than the thickness of the aquifer, neither Theis's nonequilibrium equation nor Jacob's modified nonequilibrium equation for confined aquifers is applicable to the pumping in a free aquifer. More complicated

equations or numerical simulations of groundwater are to be utilized. Please refer to related books on groundwater for the subject.

If there are two observation wells, let the distances between the pumping well and the two observation wells be r_1 and r_2, respectively and the water levels in the two observation wells are separately h_1 and h_2. According to Eq. 9.15, the coefficient of permeability will be

$$k = \frac{2.3Q}{\pi(h_2^2 - h_1^2)} \log \frac{r_2}{r_1} \tag{9.33}$$

9.6 Dewatering plan for an excavation

A dewatering plan includes the selection of dewatering methods, the estimation of the hydraulic parameters or the pumping tests, the computation of the pumping rate for single well, determination of the number of wells, the computation of drawdown and the influence range, etc. This section will introduce these procedures step by step.

9.6.1 Selection of dewatering methods

As discussed in Section 9.3, the commonly used dewatering methods include the open sump or ditch method, the deep well method, and the well point method. The applicable soil types and dewatering depths of the above three methods can be found in Figure 9.4. With the advance of technology, pumps have been improved in their performance and the dewatering depths have also been greatly raised accordingly. In practical engineering, one or more methods can be adopted in a single phase or many phases, as shown in Figure 9.12.

9.6.2 Determination of hydraulic parameters

For equilibrium equations (e.g. Thiem's equilibrium equation), the coefficient of permeability (k) is the only required hydraulic parameter. The coefficient of permeability can be obtained from laboratory constant head tests, falling head tests, empirical formulas, or pumping tests.

Because of disturbance caused by sampling, the specimen cannot fully represent the in situ soils and the complicated soil stratum conditions. The results of laboratory constant head or falling head tests are thus not applicable to the analyses and design of dewatering in an excavation. In Section 2.2.4 are illustrated some related empirical formulas for the estimation of the coefficient of permeability. Tables 2.5 and 2.6 give typical values of coefficients of permeability for some major urban soils in the world. The most reliable method of obtaining the coefficient of permeability is the in situ pumping test. These have been elucidated in Section 9.5 with regard to the analytical methods for their results.

As discussed in Section 9.4, nonequilibrium equations (e.g. Theis's and Jacob's nonequilibrium equations) require the coefficients of transmissivity (T) and coefficient of storage (S). The coefficient of transmissivity of a confined aquifer equals the product of the coefficient of permeability and the thickness of the aquifer and is thereby a constant. If the pumping-induced drawdown of an unconfined aquifer is far less than the thickness of an aquifer, the thickness of the aquifer can be assumed to be constant and one can obtain the coefficient of transmissivity accordingly.

The coefficient of storage of a confined aquifer, which ranges from 0.0005 to 0.001, is about the same as the compressibility of the soil. The coefficient of storage of an unconfined aquifer is a little smaller than the porosity of a soil and ranges from 0.2 to 0.3.

9.6.3 Determination of the capacity of wells

The efficiency of a well cannot reach 100% since there exist friction losses. As a result, we have to estimate the pumping capacity of each well.

The quantity of groundwater that flows into a deep well (Q) can be expressed as follows:

$$Q = 2\pi r_w h_w k i_e \tag{9.34}$$

where i_e = the entry hydraulic gradient of groundwater flowing into a well, h_w = the groundwater level at which groundwater flows into the well (see Figure 9.25).

According to Sichart and Kyrieleis (1930), the entry hydraulic gradient cannot be larger than

$$i_{e,max} = \frac{1}{15\sqrt{k}} \tag{9.35}$$

where k is the coefficient of permeability.

If one substitutes $i_{e,max}$ for i_e in Eq. 9.34, the pumping capacity of a deep well (Q_w) will be

$$Q_w = 2\pi r_w h_w \frac{\sqrt{k}}{15} \tag{9.36}$$

The above equation is an empirical formula where the units of r_w and h_w are m, the unit of k is m/s, and the unit of Q_w is m^3/s.

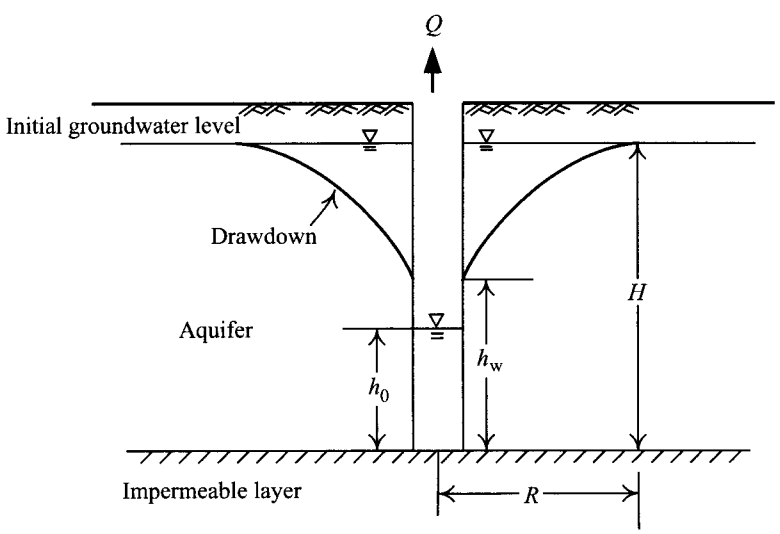

Figure 9.25 Efficiency of pumping.

Table 9.4 Relationship between coefficient of permeability and Q_w for well points (JSA, 1988)

k (cm/s)	$Q_w(\times 10^{-3}m^3/min)$
1.0×10^{-3}	1–5
5.0×10^{-3}	5–10
1.0×10^{-2}	10–20
5.0×10^{-2}	40–

Table 9.5 Relationship between soil type and Q_w for well points (JSA, 1988)

Soil type	$Q_w(\times 10^{-3}m^3/min)$
Gravel	50–70
Coarse gravel	30–50
Coarse sand	20–25
Sand	Around 15
Fine sand	8–10

Because the value of h_w is difficult to estimate, assume it to be about the groundwater level in the deep well at the preliminary estimation. That is, $h_w = h_0$. Then examine it using the results of the pumping test. When pumping is carried out, the capacity of each deep well in the multiple wells may be smaller than the above calculated Q_w for there exists intervention among wells. The influence among the wells in the multiple wells can be estimated by pumping test or numerical simulation of groundwater.

Since Q_w is critical to the design and the cost of executing a dewatering program, an appropriate factor of safety should be used. However, as elucidated in Section 9.5.1, the most reliable method of predicting Q_w is to conduct a step drawdown pumping test.

The well point method is also affected by friction loss and group effect, which relate to the type of soil or the coefficient of permeability. Tables 9.4 and 9.5 list some suggested values of the capacities of the well point method (JSA, 1988).

9.6.4 *Estimation of the number of wells*

There have to be enough pumping wells at an excavation site to lower the groundwater level to a depth below the excavation surface. Generally speaking, the groundwater level has to be at least 0.5–1 m below the excavation surface. The design of deep wells is elucidated as follows:

1 Compute the total quantity of water to be pumped in the excavation area
Assume the excavation site is an imaginary well, with a radius of R_w (see Figure 9.26) and compute the required total quantity (Q_{tot}) of water to be pumped in the imaginary well using either equilibrium or nonequilibrium equations. The computation of the pumped water is as discussed in Sections 9.4.1 and 9.4.2.

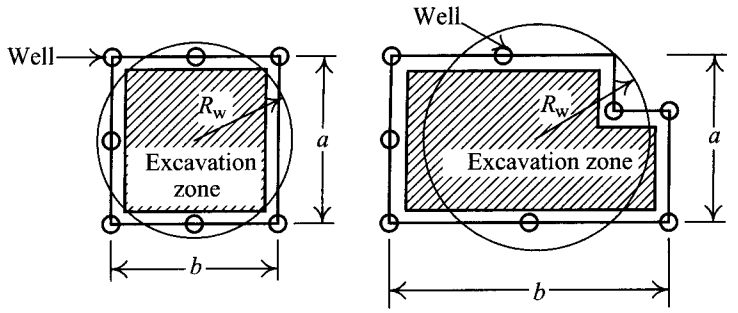

Figure 9.26 Radius of an imaginary well.

The radius of the imaginary well (R_w) can be computed by way of the equivalent area or perimeter, for example,

$$R_w = \sqrt{\frac{a \times b}{\pi}} \quad \text{or} \quad R_w = \frac{a+b}{\pi} \tag{9.37}$$

2 Compute the pumping capacity of each well
Determine the radius of each deep well and assume its water level to be h_w, which should be a little lower than the water level, usually 0.5–1 m below the excavation surface, at the excavation center (see Figure 9.7). Therefore, the capacity of each well (Q_w) can be estimated following the method introduced in Section 9.6.3.

3 Compute the number of deep wells
The number of the deep wells (n) is

$$n = \frac{Q_{tot}}{Q_w} \tag{9.38}$$

4 Examine the assumed water level in each well
The total quantity of water and the number of wells determined, the assumed water level (h_w) has to be examined. Under equilibrium and in a free aquifer, the water level in a well can be obtained following the methods introduced in Section 9.4.3. If the derived water level differs from the assumed h_w, repeat step 2 to 4 till the computed and assumed values match each other.

5 Examine the drawdown at the excavation center
Following the same method in step 4, compute the drawdown at the excavation center and corners and check if the computed values are smaller than the designed values.

As shown in Figure 9.27, there are four full penetration wells in an excavation site. To obtain the drawdown at the excavation center (point A) with the four wells pumping simultaneously, use Eq. 9.1 or 9.4 to compute the drawdown of each well at point A and add up the values to find the total drawdown at point A if pumping time is not long and the drawdown curve is under nonequilibrium condition.

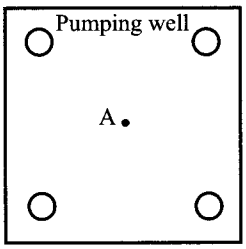

Figure 9.27 An excavation site with pumping wells.

The design procedures of the well point are explicated as follows:

1 Compute the total quantity of water to be pumped in the excavation area
The method of computing the total quantity of water to be pumped is identical to the deep well method introduced above.
2 Compute the number of well points
With the general span of 0.7–2 m between well points, assume the span as a and the number of well points can be obtained by

$$n = \frac{L}{a} \tag{9.39}$$

where L is the length of the collecting pipes, which are usually arranged around the excavation site.
3 Examine the pumping capacity
Check whether the pumping capacity of each well point is within the suggested range (Tables 9.4 and 9.5).
4 Examine the drawdown at the excavation center
The method of examination is identical of that with the deep well method.

9.6.5 Computation of the influence range of drawdown

In Section 9.4, the influence range of drawdown is defined as the distances from which the drawdown is none. The influence range can be either obtained by extending the line segment of the $s \sim \log r$ curve to intersect the line $s = 0$ or computed using Eqs 9.6–9.8. The influence range thus obtained, however, is too large to be meaningful in engineering practice. Therefore, the reasonable influence range should be computed on the basis of $s = s_a$ (s_a is the allowable drawdown). For example, if the objective of computing the influence range of drawdown is to estimate the influence on the supply of water or the amount of settlement, it is feasible to assume a value of s_a (e.g. $s_a = 0.5$ m) and compute the influence range. If the objective of computing the influence range is to back analyze hydraulic parameters, it may be still necessary to assume $s = 0$ or use Eq. 9.6–9.8 to compute the influence range. Note that drawdown does not necessarily cause settlement and the influence range of drawdown does not equal the influence range of settlement, either. As for the discussion of the influence range of settlement, please refer to Section 9.7.

Figure 9.28a shows a diaphragm wall penetrating through the impermeable layer. Since pumping is confined to the excavation area, it will not have influence outside the excavation zone and the influence range of drawdown is 0 accordingly. Figure 9.28b shows the pumping is carried out outside of an excavation zone and the influence range of drawdown extends by a distance outside the excavation zone as a result. Figure 9.28c shows the pumping is executed under an impermeable layer. While water is pumped in a confined aquifer,

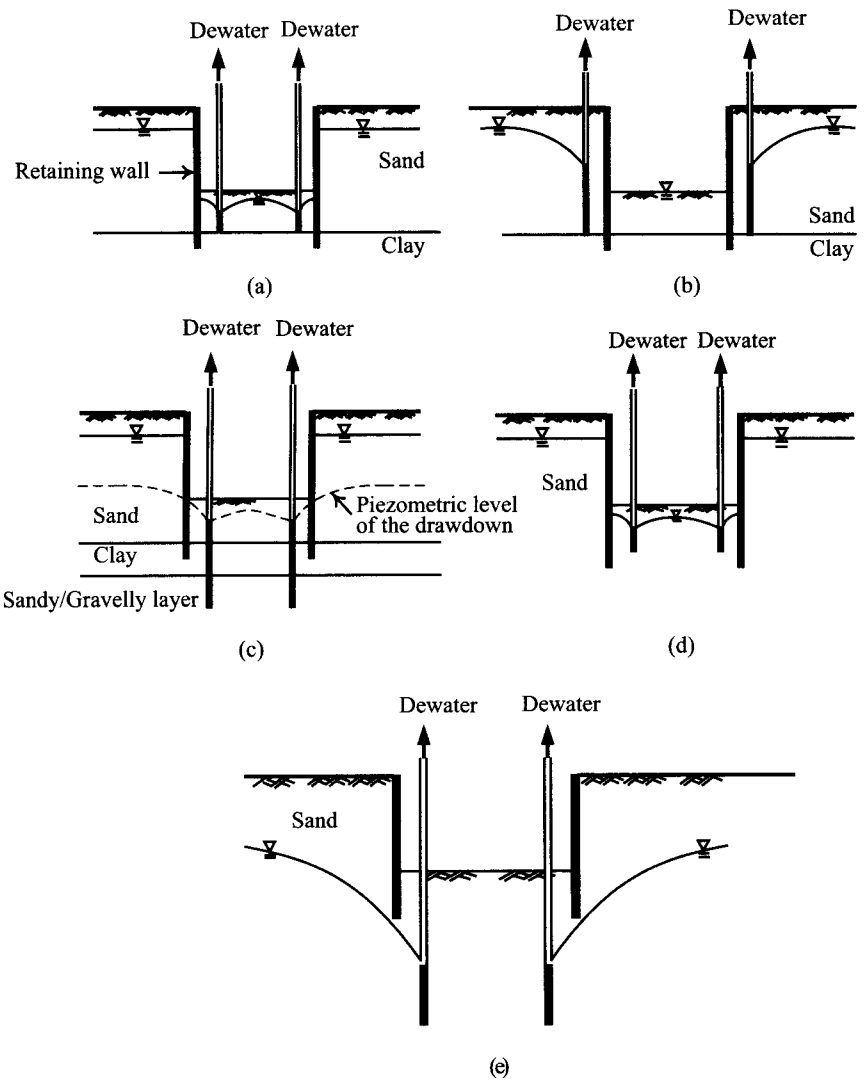

Figure 9.28 Influence of dewatering in excavations: (a) dewatering within the excavation zone and above an impermeable layer, (b) dewatering outside of the excavation zone and above an impermeable layer, (c) dewatering in a sandy/gravelly layer below the excavation zone, (d) dewatering in a sandy layer within the excavation zone, and (e) dewatering in a sandy layer below the wall bottom.

the decrease of piezometric level in the confined aquifer may cause settlement though the groundwater level above the impermeable layer does not necessarily come down. Figure 9.28d is a diaphragm wall located in a permeable layer and the well depth is less than the depth of the wall. As a result, pumping will not cause drawdown of groundwater level outside the excavation zone. Figure 9.28e is a case in which the well depth is larger than the depth of the wall and the influence range of drawdown may extend outside the excavation zone by a distance.

9.7 Dewatering and ground settlement

Dewatering will decrease the porewater pressure and increase the effective stress of soils accordingly. In sandy or gravelly soils, the increase of effective stress will produce elastic settlement. In clayey soils, not only elastic settlement but consolidation settlement will be induced. Generally speaking, the amount of elastic settlement is far less than that of consolidation settlement and usually can be neglected. As far as dewatering and pumping are concerned, the consolidation settlement should be considered.

The amount of consolidation settlement induced by pumping can be computed using Terzaghi's one-dimensional consolidation theory as follows:

For normally consolidated clay:

$$\delta_v = \frac{H}{1+e_0} C_c \log \frac{\sigma'_{vo} + \Delta\sigma}{\sigma'_{vo}} \tag{9.40}$$

For overconsolidated clay:

$$\delta_v = \frac{H}{1+e_0} C_s \log \frac{\sigma'_p}{\sigma'_{vo}} + \frac{H}{1+e_0} C_c \log \frac{\sigma'_{vo} + \Delta\sigma}{\sigma'_p} \tag{9.41}$$

where

δ_v = consolidaiton settlement
H = thickness of the clay
e_0 = initial void ratio
C_c = coefficient of compressibility, which can be derived from consolidation tests or by referring to the data illustrated in Section 2.3.
C_s = the coefficient of swelling, derived from consolidation tests or by referring to Section 2.3 for its value.
σ'_{v0} = vertical effective overburden pressure in the clay
σ'_p = preconsolidation pressure
$\Delta\sigma$ = the increment of vertical effective pressure caused by pumping.

Whether dewatering or pumping will cause settlement relates to the locations of wells, the depths and the drawdowns. Figure 9.28a shows a case where there is no drawdown outside the excavation zone. Thus, the effective stress outside the excavation zone stays unchanged and no elastic settlement or consolidation settlement occurs as a result. Figure 9.28b shows a case where pumping causes drawdown outside the excavation zone. The effective stress of clay increases under such a condition and consolidation settlement will occur. Figure 9.28c shows

the result of pumping in the permeable layer underlying a clay layer below the diaphragm wall. Though pumping does not cause the groundwater level in the impermeable layer to decline, it causes the decline of the piezometric level in the confined aquifer and the increase of effective stress in the clayey layer. Consolidation settlement occurs as a result. Figure 9.28d is a case where no drawdown outside the excavation zone is generated and no consolidation settlement is to occur, either. Figure 9.28e shows the condition where pumping is carried out at a certain depth below the wall bottom and induces drawdown of groundwater outside the excavation zone. With sandy soils, however, only elastic settlement is to occur whereas consolidation settlement will not.

We can see from the above elucidation that pumping outside an excavation containing clay layers will generate settlement; if it is a purely sandy ground, pumping outside of an excavation will basically not cause settlement (consolidation settlement). It does not follow, however, that pumping outside an excavation to lower the groundwater level is always feasible. The reason is that the in situ geological conditions are usually too complicated to make sure no clayey soils are mingled in. Considering the above possibility, pumping outside an excavation zone is recommended to be carried out, along with the recovery method, to avoid the drawdown of the groundwater level as shown in Figure 9.29.

Theoretically, the influence range of dewatering-induced settlement is the distance from which settlement declines to 0. However, the definition has little meaning in engineering practice. As explicated, drawdown is the major cause of settlement. If we apply Theis's nonequilibrium theory to compute the influence range of drawdown, the range will work out as extremely far. The result of Jacob's modified nonequilibrium equation is similar. Does it follow that the influence range of settlement is actually extremely far? Certainly not. Thus, the reasonable settlement influence range should be determined on condition that $\delta = \delta_a$ (δ_a is the allowable settlement) or when the angular distortion is small. As for the determination of the allowable settlement and the angular distortion, please refer to Section 11.2.

EXAMPLE 9.1

Figure 9.30 shows the allocation of the pumping wells and observation wells. The thickness of the permeable layer is 10 m, the distances between the pumping well center and the observation wells K-1, K-2, and K-3 are 10, 20, and 30 m, respectively. The radius of the

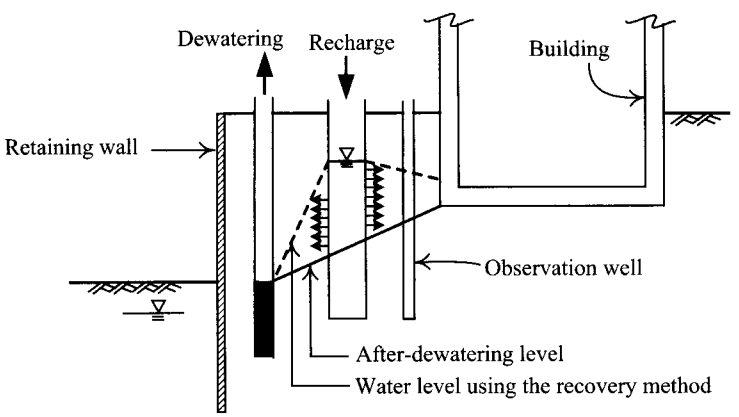

Figure 9.29 Recovery method.

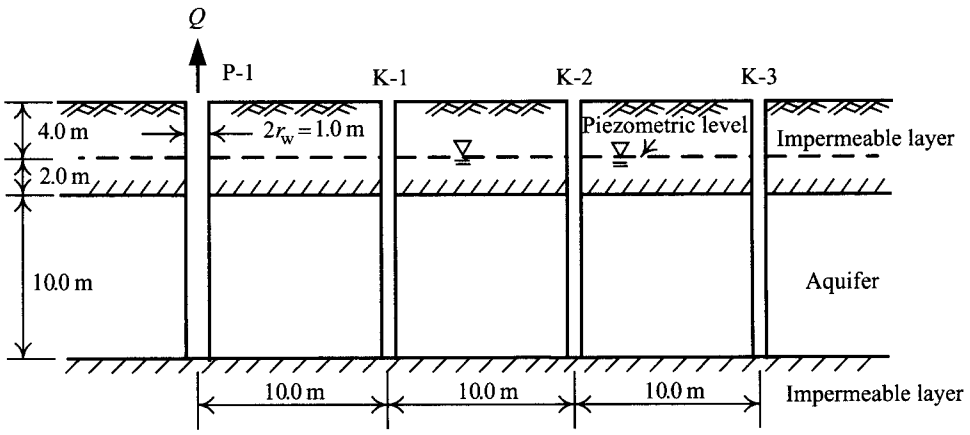

Figure 9.30 Pumping test and the soil condition.

Table 9.6 Results of the pumping test

Time t (s)	*Drawdown s (cm)*			
	Pumping well	*Observation well K-1*	*Observation well K-2*	*Observation well K-3*
0	0	0	0	0
30	10.0	0.3	0	0
60	12.5	0.6	0.1	0
120	15.5	1.1	0.3	0.1
240	18.1	2.1	0.7	0.3
480	20.2	3.5	1.2	0.6
900	22.4	5.0	2.0	1.0
1,800	24.8	6.6	3.4	1.8
3,600	27.5	8.4	4.9	3.1
5,400	29.2	9.4	6.0	4.1
7,200	30.9	10.2	6.7	4.7
10,800	32.0	11.3	7.7	5.6

well $r_w = 0.5$ m; the pumping rate $Q = 2{,}000$ cm^2/sec; Table 9.6 lists the drawdowns observed in the pumping well and the three observation wells. Table 9.7 lists the recovered water levels after pumping is stopped. Compute the coefficients of transmissivity and storage using the methods of Theis, Jacob, and Thiem, and the recovery method, respectively.

SOLUTION

1 Theis's nonequilibrium equation:
Choose one of the four wells (including the pumping well) and take its observation data for analysis. We can use either r (the location of the well) as a variable at a specific time t, or t as a variable at a specific location. Let K-2 be the object of analysis and t the variable. Compute the $s-t/r^2$ relation as shown in Table 9.8. According to the procedures suggested in Section 9.5.2, depict the standard and data curves and superimpose one onto

Table 9.7 Recovered water levels in the pumping well

Time t (sec)	*Time after pumping is stopped t′* (sec)	*t/t′*	*Residual drawdown s′* (cm)
10,800	0	—	32.0
10,830	30	361	15.2
10,860	60	181	12.6
10,920	120	91	9.8
11,040	240	46	7.5
11,280	480	23.5	4.9
11,700	900	13	3.3
12,600	1,800	7	2.3
14,400	3,600	4	1.6
18,000	7,200	2.5	1.1

Table 9.8 Computation based on time as variable (observation well K-2, $r = 20$ m)

t (sec)	t/r^2 (sec/cm^2)	s (cm)
30	7.5×10^{-6}	0
60	1.50×10^{-5}	0.1
120	3.0×10^{-5}	0.3
240	6.0×10^{-5}	0.7
480	1.20×10^{-4}	1.2
900	2.25×10^{-4}	2.0
1,800	4.5×10^{-4}	3.4
3,600	9.00×10^{-4}	4.9
5,400	1.35×10^{-3}	6.0
7,200	1.8×10^{-3}	6.7
10,800	2.7×10^{-3}	7.7

the other. As shown in Figure 9.31, we have the coordinates of the match point as:

$$s = 2.4 \text{ cm}, t/r^2 = 0.00065 \text{ sec/cm}^2, W(u) = 1, 1/u = 10$$

$$T = \frac{QW(u)}{4\pi s} = \frac{2000 \times 1}{4 \times \pi \times 2.4} = 66.3 \text{ cm}^2/\text{sec}$$

$$k = \frac{T}{D} = \frac{66.3}{1000} = 6.63 \times 10^{-2} \text{ cm/sec}$$

$$S = 4Tu\left(\frac{t}{r^2}\right) = 4 \times 66.3 \times \frac{1}{10} \times 0.00065 = 1.72 \times 10^{-2}$$

We can also carry out analysis using r as a variable at a specific time t. Table 9.9 lists the $s - t/r^2$ relations for wells P-1, K-1, K-2, and K-3 at $t = 7200$ sec. From

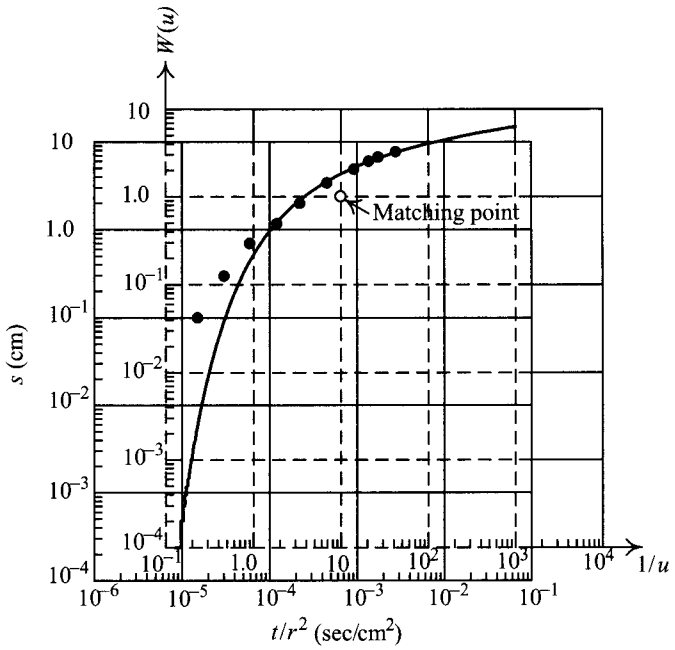

Figure 9.31 Theis's method (*r* is constant while *t* is a variable).

Table 9.9 Computation based on distance as variable (t = 7200 sec)

Variant	*Pumping well P-1*	*Observation well K-1*	*Observation well K-2*	*Observation well K-3*
r (cm)	50	1,000	2,000	3,000
t/r^2 (sec/cm^2)	2.88	7.2×10^{-3}	1.8×10^{-3}	8.0×10^{-4}
s (cm)	30.9	10.2	6.7	4.7

Figure 9.32, we can have the coordinates of the match point as

$$s = 2.9 \text{ cm}, t/r^2 = 0.01 \text{ sec/cm}^2, W(u) = 1, 1/u = 100$$

$$T = \frac{QW(u)}{4\pi s} = \frac{2000 \times 1}{4 \times \pi \times 2.9} = 54.8 \text{ cm}^2/\text{sec}$$

$$k = \frac{T}{D} = \frac{54.8}{1000} = 5.48 \times 10^{-2} \text{ cm/sec}$$

$$S = 4Tu\left(\frac{t}{r^2}\right) = 4 \times 54.8 \times \frac{1}{100} \times 0.01 = 2.19 \times 10^{-2}$$

2 Jacob's modified nonequilibrium equation:
Jacob's modified nonequilibrium equation also has two ways to analyze: use either *t* or *r* as the variable. First, using *t* as the variable, the computation is as follows:
According to the data of well K-2 listed in Table 9.8, plot the $s-\log t/r^2$ relation as shown in Figure 9.33 where we have $(\Delta s)_J = 5.61$ cm and $(t/r^2)_{s=0} = 0.00012$ sec/cm^2.

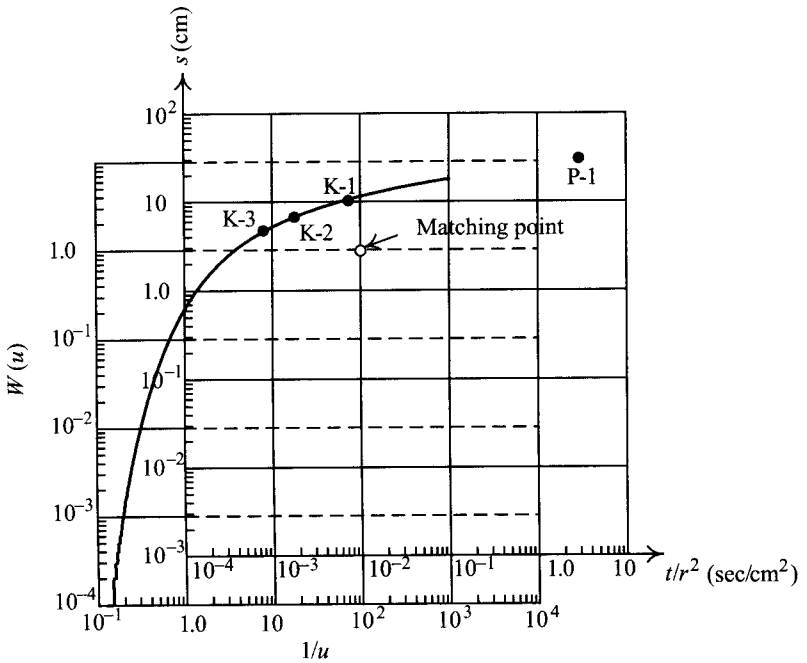

Figure 9.32 Theis's method (*t* is constant while *r* is a variable).

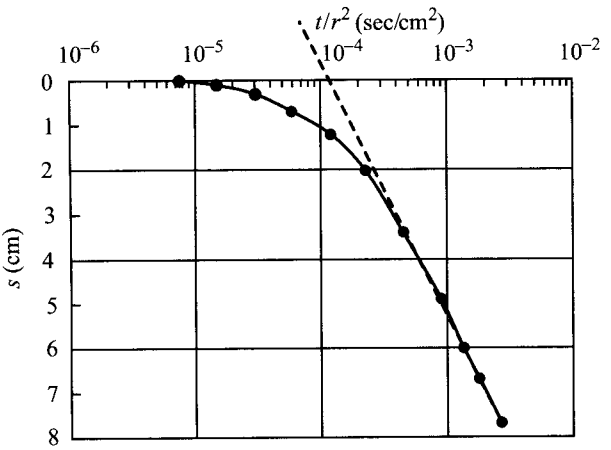

Figure 9.33 Jacob's method (*r* is constant while *t* is a variable).

Using Eq. 9.26, we have

$$T = 0.183\frac{Q}{(\Delta s)_J} = 0.183\frac{2000}{5.61} = 65.2 \text{ cm}^2/\text{sec}$$

$$k = \frac{T}{D} = \frac{65.2}{1000} = 6.52 \times 10^{-2} \text{ cm/sec}$$

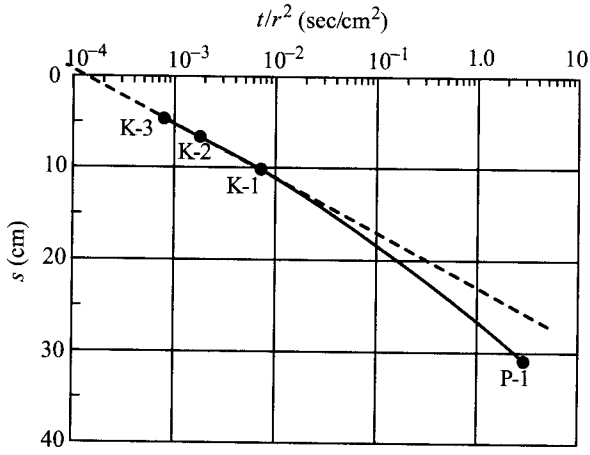

Figure 9.34 Jacob's method (t is constant while r is a variable).

Using Eq. 9.27, we have

$$S = 2.25T\left(\frac{t}{r^2}\right)_{s=0} = 2.25 \times 65.2 \times 0.00012 = 1.76 \times 10^{-2}$$

On the other hand, it is also feasible to carry out analysis using r as the variable. According to the data in Table 9.9, depict the $s - \log t/r^2$ curve as shown in Figure 9.34. The relations between K-3, K-2, K-1, and P-1 are nonlinear. Considering the lower accuracy of the data of P-1, only adopt the data of K-3, K-2, and K-1 for regression analyses as shown in the figure where we have $(\Delta s)_J = 6.1$ cm and $(t/r^2)_{s=0} = 0.00012$ sec/cm^2. Using Eq. 9.26, we then have

$$T = 0.183\frac{Q}{(\Delta s)_J} = 0.183\frac{2000}{6.1} = 60 \text{ cm}^2/\text{sec}$$

$$k = \frac{T}{D} = \frac{60}{1000} = 6.0 \times 10^{-2} \text{ cm/sec}$$

Using Eq. 9.27, we have

$$S = 2.25T\left(\frac{t}{r^2}\right)_{s=0} = 2.25 \times 61 \times 0.00012 = 1.65 \times 10^{-2}.$$

3 Thiem's equilibrium equation:
Assume wells K-1, K-2, and K-3 reach equilibrium when $t = 10,800$ sec. From Table 9.6, depict the $s \sim \log r$ curve as shown in Figure 9.35 where we have $(\Delta s)_T$, the decreased amount of s when r increases ten times, equal to 12.1 cm. That is to say, when $\log r_2/r_1 = 1.0$, $s_1 - s_2 = 12.1$ cm. Using Eq. 9.28, we have

$$k = \frac{0.366Q}{D(s_1 - s_2)}\log\frac{r_2}{r_1} = \frac{0.366 \times 2000}{1000 \times 12.1} = 6.05 \times 10^{-2} \text{ cm/sec}$$

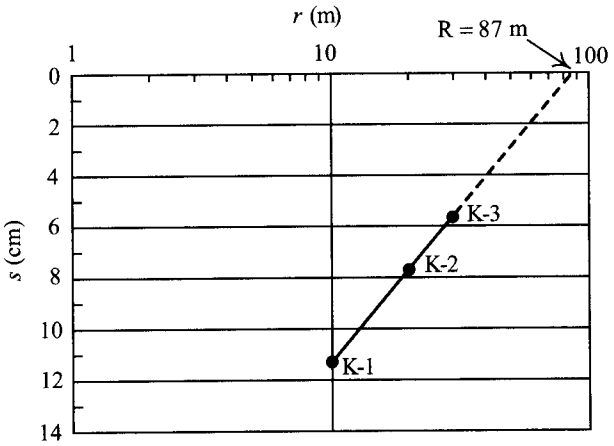

Figure 9.35 Thiem's method.

The coefficient of transmissivity can be derived from $T = kD$, or find R on the figure $R = 87$ m and use Eq. 9.30 to obtain

$$T = \frac{0.366Q}{(\Delta s)_T} = \frac{0.366 \times 2000}{12.1} = 60.5 \text{ cm}^2/\text{sec}$$

Using Eq. 9.31, we obtain

$$S = \frac{2.25Tt}{R^2} = \frac{2.25 \times 60.5 \times 10800}{(8700)^2} = 1.94 \times 10^{-2}$$

4 The recovery method:
According to the data in Table 9.6, plot the $s' - \log(t/t^2)$ curve as shown in Figure 9.36, where we can find $(\Delta s')_r = 8.5$ cm. Using Eq. 9.32, we then obtain

$$T = \frac{0.183Q}{(\Delta s')_r} = \frac{0.183 \times 2000}{8.5} = 43.1 \text{ cm}^2/\text{sec}$$

and the coefficient of permeability

$$k = \frac{T}{D} = \frac{43.1}{1000} = 4.31 \times 10^{-2} \text{ cm/sec}$$

Table 9.10 lists the results of the methods of Theis, Jacob, and Thiem, and the recovery method. As shown in the table, Thiem's method cannot obtain the coefficient of storage. The coefficients of permeability derived from Theis's and Jacob's methods are very close.

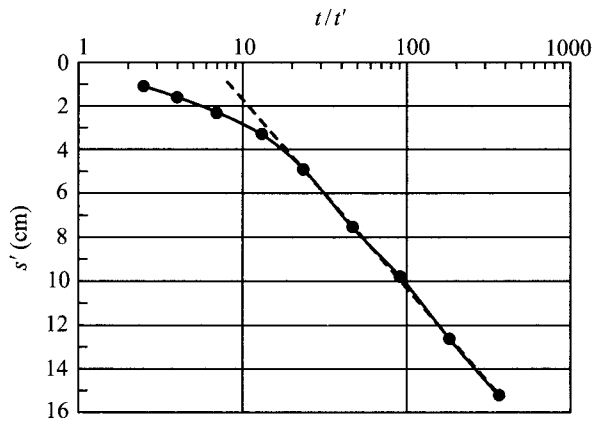

Figure 9.36 Recovering method.

Table 9.10 Hydraulic parameters from various methods

Method	*k* (cm/sec)	*T* (cm^2/sec)	*S*
Theis's method (*t* as variable)	6.63×10^{-2}	66.3	1.72×10^{-2}
Theis's method (*r* as variable)	5.48×10^{-2}	54.8	2.19×10^{-2}
Jacob's method (*t* as variable)	6.52×10^{-2}	65.2	1.76×10^{-2}
Jacob's method (*r* as variable)	6.00×10^{-2}	60.0	1.62×10^{-2}
Thiem's method	6.05×10^{-2}	60.5	1.94×10^{-2}
Recovering method	4.31×10^{-2}	43.1	—

EXAMPLE 9.2

According to the analysis results of Theis's method listed in Table 9.10 (distance as a constant; time as a variable), estimate the required total quantity of water to be pumped in Figure 9.37.

SOLUTION

According to Example 9.1, we know

$$k = 6.63 \times 10^{-2} \text{ cm/sec} = 3.98 \times 10^{-2} \text{ m/min}$$

$$S = 1.72 \times 10^{-2}$$

Using the method of equivalent area, compute the radius of the imaginary well as follows:

$$R_w = \sqrt{\frac{a \times b}{\pi}} = \sqrt{\frac{45 \times 45}{\pi}} = 25.4 \text{ m}$$

The excavation depth is 9 m. The groundwater level is to be lowered to 1 m below the excavation surface. As a result, the drawdown $s = 7$ m. Assume the pumping time

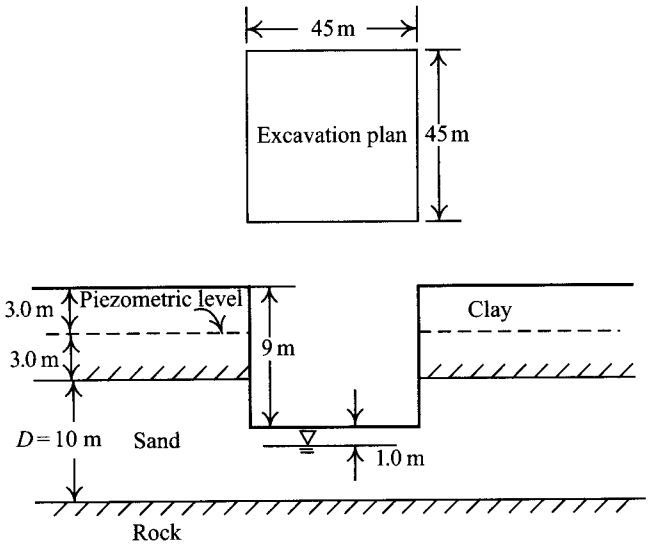

Figure 9.37 Plan and profile of an excavation.

$t = 15$ days $= 21{,}600$ min. Then, the well parameter is

$$u = \frac{R_w^2 S}{4kDt} = \frac{(25.4)^2 \times 1.72 \times 10^{-2}}{4 \times 3.98 \times 10^{-2} \times 10 \times 21{,}600} = 3.23 \times 10^{-3}$$

With $u < 0.01$, we can use Jacob's nonequilibrium equation. From Table 9.2, we have

$$W(u) = -0.5772 - \ln u = 7.46$$

and the required total quantity of water to be pumped is

$$Q_{\text{tot}} = \frac{4\pi kDs}{W(u)} = \frac{4 \times \pi \times 3.98 \times 10^{-2} \times 10 \times 7.0}{7.46} = 4.69 \text{ m}^3/\text{min}.$$

EXAMPLE 9.3

The thickness of a sandy soil layer is about 40 m, below which is an impermeable rocky stratum. The groundwater level is at the ground surface. The coefficient of permeability of the sandy layer is 2.0×10^{-3} cm/sec; the coefficient of storage is 0.2. Here is an excavation site of 100 m × 50 m; the excavation depth is 8.5 m. For the convenience of excavation and restricted time of construction, the well point method is to be adopted to lower the groundwater level to 1.0 m below the excavation surface within 15 days. Design the numbers of the well points.

SOLUTION

To lower the groundwater level by 9 m within 15 days may leave the drawdown in the nonequilibrium condition. Thus, a nonequilibrium equation is to be adopted for analyses. With the drawdown within the excavation zone to be 9.5 m, which is far less than the

thickness of the aquifer, we can choose either Theis's or Jacob's nonequilibrium equation. The circumference of 100 m × 50 m can be converted to an equivalent radius of

$$R_w = \frac{a+b}{\pi} = \frac{100+50}{\pi} \approx 47.7 \text{ m}$$

The coefficient of permeability $k = 2.0 \times 10^{-3}$ cm/sec $= 1.2 \times 10^{-3}$ m/min
The coefficient of transmissivity $T = kD = 1.2 \times 10^{-3} \times 40 = 0.048$ m^2/min
The pumping time $t = 15$ days $= 21{,}600$ min
The well parameter

$$u = \frac{R_w^2 S}{4Tt} = \frac{47.7^2 \times 0.2}{4 \times 0.048 \times 21{,}600} = 0.11$$

Refer to values in Table 9.2, we have the value $W(u) \approx 1.737$. With the pumping height limited to about 5 m for well points and the required amount of dewatering about 9 m, dewatering has to be carried out in two phases:

Assume the discharge quantity of each well point $Q_w = 0.01$ m^3/min (see Tables 9.4 and 9.5). The dewatering height of the first phase $s = 5$ m (the groundwater level lowered from GL0.0 to GL-5.0 m). A possible drawdown curve is as shown in Figure 9.12. The required quantity of water to be pumped will be

$$Q_1 = \frac{4\pi Ts}{W(u)} = \frac{4 \times \pi \times 0.048 \times 5}{1.737} = 1.74 \text{ m}^3/\text{min}$$

and the required number of well points will be

$$n_1 = \frac{Q_1}{Q_w} = \frac{1.74}{0.01} = 174$$

Assume the collecting pipes are arranged along the two longer sides of the excavation site, which is 200 m long in total. The distance between two well points will be

$$a = \frac{200}{174} = 1.15 \text{ m} \rightarrow \text{adopt } 1 \text{ m}$$

The dewatering height of the second phase $s = 4.5$ m (the groundwater level lowered from GL-5 to GL-9 m). A possible drawdown curve is also as shown in Figure 9.12. The quantity of water to be pumped will be

$$Q_2 = \frac{4\pi Ts}{W(u)} = \frac{4 \times \pi \times 0.048 \times 4.5}{1.737} = 1.56 \text{ m}^3/\text{min}$$

$$n_2 = \frac{Q_2}{Q_w} = \frac{1.56}{0.01} = 156$$

Assume the collecting pipes are also arranged along the two longer sides of the excavation site. The distance between two well points will be

$$a = \frac{200}{156} = 1.28 \text{ m} \rightarrow \text{adopt } 1.2 \text{ m}$$

9.8 Summary and general comments

This chapter first explains the goals, the importance, and applicability of excavation-related dewatering, and then introduces the dewatering methods. Last, we introduce the procedure of designing a dewatering system. The contents of this chapter are summarized as follows:

1 The dewatering methods introduced in this chapter are methods for lowering the groundwater level in sandy or gravelly soil rather than in clayey soil. The goal of dewatering is to keep the excavation bottom dry, prevent leakage of sand or water, avoid sand boiling or upheaval failures, and forestall the floating of the basement, etc. The commonly used dewatering methods are the open sump or ditch method, the deep well method, the well point method, etc.
2 Well equations are distinguished into those applied to confined aquifers and to free aquifers. They also vary with the degree of penetration of a well into the aquifer and whether the drawdown curve has reached equilibrium.
3 As far as confined aquifers are concerned, this chapter introduced the full penetration well equations, including Theis's nonequilibrium equation, Jacob's modified nonequilibrium equation, and Thiem's equilibrium equation. Concerning partial penetration wells, only equilibrium equations are introduced, considering the complexity of nonequilibrium equations.
4 The nonequilibrium equations for free aquifers are too complicated, so this chapter left them aside and introduced only Dupuit-Thiem's equilibrium equations for full and partial penetration wells. If the pumping-induced drawdown, nevertheless, is much less than the thickness of the aquifer, Theis's nonequilibrium equation and Jacob's modified nonequilibrium equation are also applicable to free aquifers.
5 Hydraulic parameters include the coefficient of permeability, the coefficient of transmissivity, and the coefficient of storage. The coefficient of transmissivity is the coefficient of permeability multiplied by the thickness of aquifers. For the coefficient of permeability of typical soils, please refer to Section 2.2.4. The coefficient of storage for confined aquifers, ranging between 0.0005 and 0.001, is about the same as the compressibility of the soil. The coefficient of storage for free aquifers, ranging between 0.2 and 0.3, is about the same as the porosity of the soil. To obtain accurate coefficients of transmissivity and storage one has to resort to in situ pumping tests.
6 A dewatering plan in an excavation includes the selection of a dewatering method, the determination of hydraulic parameters, the analysis of the results of pumping tests, the estimation of required total quantity of water to be pumped in the excavation zone, the computation of numbers of pumping wells, and the computation of the influence zones of drawdown and settlement.

Problems

9.1 What are the objectives of dewatering in excavations?
9.2 Explicate the different dewatering methods and their separate application ranges.
9.3 Explain the meanings of the coefficients of permeability, transmissivity, and storage for confined aquifers and free aquifers, respectively.
9.4 Explicate the dewatering plan for excavations in sandy soils.

9.5 Suppose there exists a confined aquifer. Its thickness is 40 m; $k = 0.005$ cm/sec; $S = 0.004$. Above the aquifer is a 9 m thick clayey layer. The piezometric level is 3 m below the ground surface. Assume a 20-cm-diameter well that fully penetrates into the confined aquifer. When the pumping rate $Q = 0.6$ m^3/min, what will be the drawdown in the observation well 10 m from the pumping well after one hour of dewatering using Theis's and Jacob's methods, respectively?

9.6 Same as the previous problem. Assume the change rate in the water level in the observation well is small 10 hours later. Use Thiem's method to compute the drawdown in the observation well.

9.7 Redo Problem 9.5 and assume $k = 0.001$ cm/sec; $S = 0.001$ this time.

9.8 Same as the previous problem. Assume the change rate in the water level in the observation well is small after a 15 hours long dewatering. Use Thiem's method to compute the drawdown in the observation well.

9.9 Suppose soil conditions are the same as in Problem 9.5. Assume there exists an excavation, 30 m × 30 m in dimension and 10 m in excavation depth. To keep the stability of excavation, a dewatering plan is made to lower the piezometric level of the confined aquifer to 0.5 m below the excavation surface within five days. Estimate the quantity of water required to be pumped and the number of wells.

9.10 Suppose soil conditions are the same as in Problem 9.7. Assume a 100 m × 100 m excavation. The excavation depth is 12 m. To keep the stability of excavation, a dewatering plan is made to lower the piezometric level of the confined aquifer to 0.5 m below the excavation surface before starting the excavation. Estimate the quantity of water required to be pumped and the number of wells.

9.11 Suppose a rock layer 40 m below the ground surface underlying a highly permeable sandy layer. The groundwater level is 1 m below the ground surface. The coefficient of permeability of sand $k = 0.05$ cm/sec and the coefficient of storage $S = 0.3$. Assume a 20-cm-diameter full penetration well going through the sand layer and reaching the rocky layer. When the pumping rate $Q = 0.7$ m^3/min, compute the drawdown in the observation well 4 m away from the deep well after 2 hours of dewatering.

9.12 Same as the previous problem. When the water level in the pumping well is 2 m below the ground surface (i.e. the drawdown is 1 m). Assume a small change rate of the water level in the observation well is recorded after a certain period of pumping. Compute the drawdown in the observation well using the Dupuit-Thiem method.

9.13 Redo Problem 9.11 but assume the coefficient of permeability of sand $k = 0.01$ cm/sec and the coefficient of storage $S = 0.01$ this time.

9.14 Same as the previous problem. When the water level in the pumping well is 4 m below the ground surface (i.e. the drawdown is 3 m). Assume after pumping for a certain period the water level in the observation well changes little, compute the drawdown in the observation well using Dupuit-Thiem's method.

9.15 Suppose soil conditions are the same as Problem 9.11. Assume a 40 m × 40 m excavation base. The excavation depth is 8 m. To keep the stability of excavation, a dewatering plan is made to lower the groundwater level in the sandy soil to 0.5 m below the excavation surface within five days. Estimate the total quantity of water to be pumped and the number of wells.

9.16 Same as above. Assume the dewatering adopts the well point method. Compute the required number of wells.

9.17 Same as Problem 9.13. Assume there exists an 80 m × 40 m excavation and the excavation depth is 6 m. To keep the stability of excavation, a dewatering plan is made to lower the groundwater level to 1 m below the excavation surface within 10 days. Estimate the total quantity of water to be pumped and the number of deep wells.

9.18 Same as the previous problem. Assume the dewatering adopts the well point method. Design the number of well points.

9.19 We carry out a pumping test in a confined aquifer. Given the pumping rate $Q = 788\ m^3/day$ and the observation results in an observation well 20 m away from the center of the pumping well as listed in Table P9.19, use Jacob's method to compute the coefficients of transmissivity and storage.

Table P9.19 Results of a pumping test for an excavation

t (min)	s (m)	t (min)	s (m)
0	0	18	0.680
0.10	0.04	27	0.742
0.25	0.08	33	0.753
0.50	0.13	41	0.779
0.70	0.18	48	0.793
1.00	0.23	59	0.819
1.40	0.28	80	0.855
1.90	0.33	95	0.873
2.33	0.36	139	0.915
2.80	0.39	181	0.935
3.36	0.42	245	0.966
4.00	0.45	300	0.990
5.35	0.50	360	1.007
6.80	0.54	480	1.050
8.30	0.57	600	1.053
8.70	0.58	728	1.072
10.0	0.60	830	1.088
13.1	0.64		

9.20 Same as the previous problem but use Theis's method this time.

Chapter 10

Design of retaining structural components

10.1 Introduction

With the stability analyses of an excavation (Chapter 5), the penetration depth of the retaining wall can be determined. With the stress and deformation analyses, the bending moment and shear of the retaining wall and the strut (or anchor) load can be obtained. Once these values are known, the detailed design of the retaining wall and struts can be carried out.

This chapter will introduce the analysis and design of the structural components used in braced excavations and anchored excavations. The involved knowledge includes soil mechanics, foundation engineering, reinforced concrete design, and steel structure design. As a result, engineers of various disciplines are involved in the design, including civil engineers, structural engineers, geotechnical engineers, etc. Any engineer engaged in excavation design and construction should familiarize himself with the design of retaining structural components.

The contents of this chapter are confined to the design of the structural components used in braced excavations or anchored excavations. As described in Chapter 3, there are many methods of excavation. Though the design methods that will be introduced in this chapter can not cover all excavation methods, the basic principles of the analyses and designs for these methods are similar and the methods here can be applied to other excavation methods with some modifications.

10.2 Design methods and factors of safety

The working stress method and the strength design method are the design methods for reinforced concrete. The allowable stress method (abbreviated as the ASD method) and the ultimate strength design method are the design methods for steel structures. The working stress method for reinforced concrete is similar to the allowable stress method for steel structures in design concepts, both making the stress of the structural member under the working load smaller than the allowable stress. The allowable stress is the ultimate strength of the structural member divided by a factor of safety, which is mostly derived from experience without rigorous theoretical foundation, and the uncertainty of loads and material strengths is implicitly included in the factor of safety.

The strength design method for reinforced concrete and the ultimate strength design method for steel structures are to transform the uncertainty or variation of external loads into load factors and the uncertainty of the strengths of materials or structural members into reduction factors following the methods of probabilities. The method is sometimes called the load

resistance factor design (LRFD) method. Since the uncertainty of the loads on structures does not relate to the structural materials themselves, the load factors for reinforced concrete and steel structure should be identical if the LRFD method is adopted (including both the strength design method and ultimate strength design method). Their reduction factors, on the other hand, should be different since the uncertainty of the material strength relates to the properties of the materials. This book adopts the load factors and the strength reduction factors for the LRFD method according to the codes recently announced (AISC, 2001; ACI, 2005).

Reinforced concrete and steel are frequently used in an excavation as structural components. Wood is sometimes used too. These materials are combined for use in most cases. To design reasonably, it is necessary to adopt the LRFD method, adopting the same load factors and different strength reduction factors according to the material of the structural member. However, in most countries, the LRFD method as well as the ASD method is used for the design of high rise steel structures. Few adopt the LRFD method for the design of steel struts in excavations. This chapter is going to follow the general application in practice, different design methods for different structural components.

The structural components in excavations are basically temporary structures. Some structures, the diaphragm walls for example, are temporary structures, which also serve as permanent structures after the construction is finished. Some country building codes suggest the allowable stress for temporary structural material should be magnified. Therefore, for diaphragm walls during construction, the allowable stress would be magnified by a factor λ without the earthquake force considered. After the construction is finished, on the other hand, with the diaphragm wall serving as the outer wall of the basement, the allowable stress would not be magnified with the earthquake force taken into consideration.

Some country building codes suggest that the load for temporary structural member is assumed to be $\lambda = 1.25$.

10.3 Retaining walls

The penetration depth of a retaining wall directly affects the stability of the excavation. Concerning the design of the penetration depth of a retaining wall, please refer to the contents of Chapter 5. This section focuses on designs for sections and dimensions of different types of retaining walls. Table 3.2 lists the comparative values of nominal stiffness for different retaining walls for the references in preliminary design.

To design the sections and dimensions of a retaining wall, the first thing is to carry out the stress analysis. Three methods can be adopted for the stress analysis of a retaining wall: the assumed support method, the beam on elastic foundation method, and the finite element method, which have been introduced in Chapters 6–8 separately. The actual construction procedures should be simulated in a stress analysis. Because the maximum bending stress occurring at each construction stage does not take place at the same depth, the design of the wall sections should adopt the envelope of the maximum bending stresses of all the construction stages. Figure 10.1 illustrates the typical diagrams of bending moment and shear at each stage for the stress analysis of a retaining wall.

According to the mechanics of materials, the bending moment and shear of a retaining wall are the products of EI and the quadratic and cubic differential values of the deformation curve, respectively. If any two computed wall deformation curves are close, their computed bending moment and shear should be close too. To analyze the stresses of a retaining wall

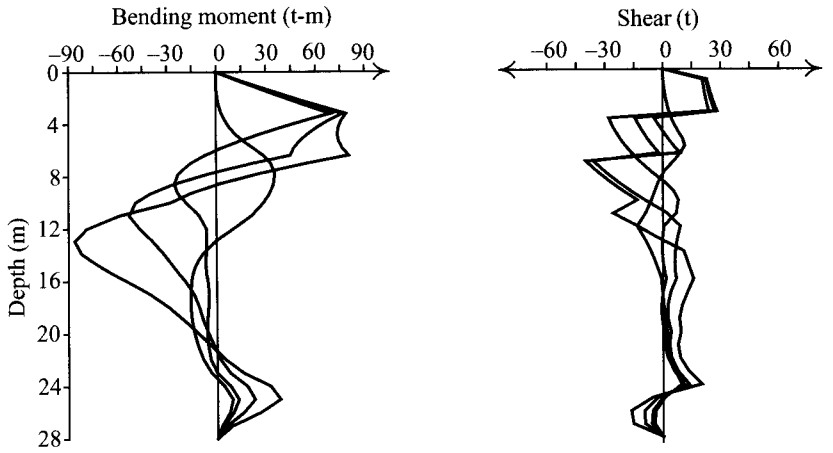

Figure 10.1 Typical bending moment and shear diagrams of a retaining wall by stress analysis.

using the beam on elastic foundation method or the finite element method, it is necessary to ensure the analytical pattern of the wall deformation be close to the observed or empirical values.

Basically, the deformation curves computed with the finite element method and the beam on elastic foundation method also relate to the selected parameters. The correct choosing of the parameters is a question of experience and is still to be studied. As a result, to discuss the differences of the results with the beam on elastic foundation method and the finite element method, respectively, is meaningless.

The assumed support method and its determination of the assumed support are too rough. Besides, the method cannot simulate the construction process completely. Thus, the analytic result using the assumed support method and those using the finite element method or beam on elastic foundation method may be different. The results of the assumed support method may be only applicable to small scaled excavations.

10.3.1 Soldier piles

The commonly used types of soldier piles in excavations are the H steel, I steel, and rail piles. Concerning the dimensions and properties, the books on steel structures or the AISC Specification can be referred to. Types of rail pile are usually classified in terms of weight per length (kg/m). The rail pile, having a smaller section and therefore easier to drive into soils, is mostly used in hard soils or cobble-gravelly soils. Appendix C also displays the shapes of those steel sections and the dimensions, having been mentioned in this book, with their properties. Concerning the properties, strengths and shortcomings, and construction of soldier piles, please refer to Section 3.3.1.

The dimensions of soldier piles and the distance between them are determined based on the results of stress analysis. Then take the maximum bending moment (M_{max}) from the typical bending moment envelope (Figure 10.1). According to the ASD method, we can obtain the

Table 10.1 Dimensions and spans for some commonly used soldier piles

Soldier pile type	*Span* (cm)
H300 × 300 × 10 × 15	150
H250 × 250 × 9 × 14	120
H200 × 200 × 8 × 12	100
50 kg/m steel rail	100

section modulus of the soldier pile as

$$S = \frac{M_{\max}}{\lambda \sigma_a} \tag{10.1}$$

where

σ_a = allowable stress of the steel
λ = short-term magnified factor of the allowable stress, which can be found from the country building codes.

The dimensions and spans of rail piles can thus be selected according to the computed section modulus. Basically, under a certain stress, the longer the span, the larger the required dimension of the soldier pile and the thicker the lagging. On the contrary, the shorter the distance, the smaller the required dimension of the soldier pile and the thinner the lagging. The numbers of soldier piles are then increased. Table 10.1 lists the commonly adopted spans between soldier piles for reference in preliminary design.

To compute the thickness of the laggings, we usually assume the lagging to be the simply supported beam on the soldier piles. The computed thickness of the lagging often comes out larger than the commonly used laggings in general excavations, which are around 3–4 cm thick. Considering the lateral earth pressure on the back of the wall is not necessarily uniformly acting on the laggings, sometimes it is centering on soldier piles, which are of higher rigidity, sometimes the pressure is less than expected due to the effect of soil arching, the 3–4 cm thick lagging is often adopted if the excavation is shallow.

10.3.2 Sheet piles

The sections of sheet piles are various. U-shaped, Z-shaped, and line-shaped sheet piles are frequently used in some countries, as shown in Figure 3.19 (also see Appendix C). Concerning the characteristics, strengths and shortcomings, and construction of sheet piles, please refer to Section 3.3.2.

The dimensions of a sheet pile are determined on the basis of the results of the stress analysis. According to the envelope of bending moments (Figure 10.1), take the maximum bending moment $M_{\max}$ and compute the section modulus using Eq. 10.1, which is then used to find the dimension of the sheet pile by consulting the related steel manual.

10.3.3 Column piles

Column piles used in excavations include the PIP pile, reinforced concrete pile, and the mixed pile. The reinforced concrete pile can be further divided into the reversed pile and the all casing pile. Basically, the stiffness of the reinforced concrete pile is the highest, the PIP pile the second best, and the mixing pile the smallest. Concerning the characteristics, strengths and shortcomings, and construction of column piles, see Section 3.3.3.

Column piles bear the axial load and flexural load simultaneously. Therefore, their behavior is similar to that of the reinforced concrete columns. No matter which type of column pile is used, it is necessary to transform the flexural rigidity per pile into that per unit width in a plane strain analysis. The thus obtained bending moment and shear envelopes are then used for the design of reinforced concrete columns. Since the design of the columns is extremely complicated, to save space, this book is not going to go into the subject. If the reader is interested, please refer to the design chart of reinforced concrete columns or the American Concrete Institute (ACI) code.

10.3.4 Diaphragm walls

The design of a diaphragm wall includes specifying the wall thickness and the reinforcements. The thickness is usually determined according to the results of the stress analysis, the deformation analysis, and the feasibility of detailing of concrete reinforcements. According to the experience of excavations in Taipei, the thickness of a diaphragm wall can be assumed to be $5\%H_e$ (H_e is the excavation depth) in the preliminary design.

The design of reinforcements usually follows the widely used strength design method (the LRFD method). The major items of design include the vertical main reinforcement, the horizontal main reinforcement, the shear reinforcement, and the lap splice length and development length of the reinforcement. Figure 10.2 illustrates the three-dimensional view, the plan, and the side view of the reinforced cage of a diaphragm wall. The design of reinforcements of a diaphragm wall is based on the bending moment and shear envelope obtained from the stress analysis. Concerning the detailed design process, please refer to the ACI code. This section excerpts from the ACI code for reinforcements of a diaphragm wall.

The deformation of the retaining wall in the central section of the site is usually assumed to be in the plane strain condition during analysis. Therefore, the unit width ($b = 1$ m) of the diaphragm wall is usually used for flexural stress analysis. To be consistent with common usage in reinforced concrete design, the signs used in this section are identical to those commonly used in the design. The definitions of the designed and nominal bending moments and shears are as follows:

$$M_u = \frac{L_F M}{\lambda} \tag{10.2}$$

$$M_n = \frac{M_u}{\phi} \tag{10.3}$$

$$V_u = \frac{L_F V}{\lambda} \tag{10.4}$$

$$V_n = \frac{V_u}{\phi} \tag{10.5}$$

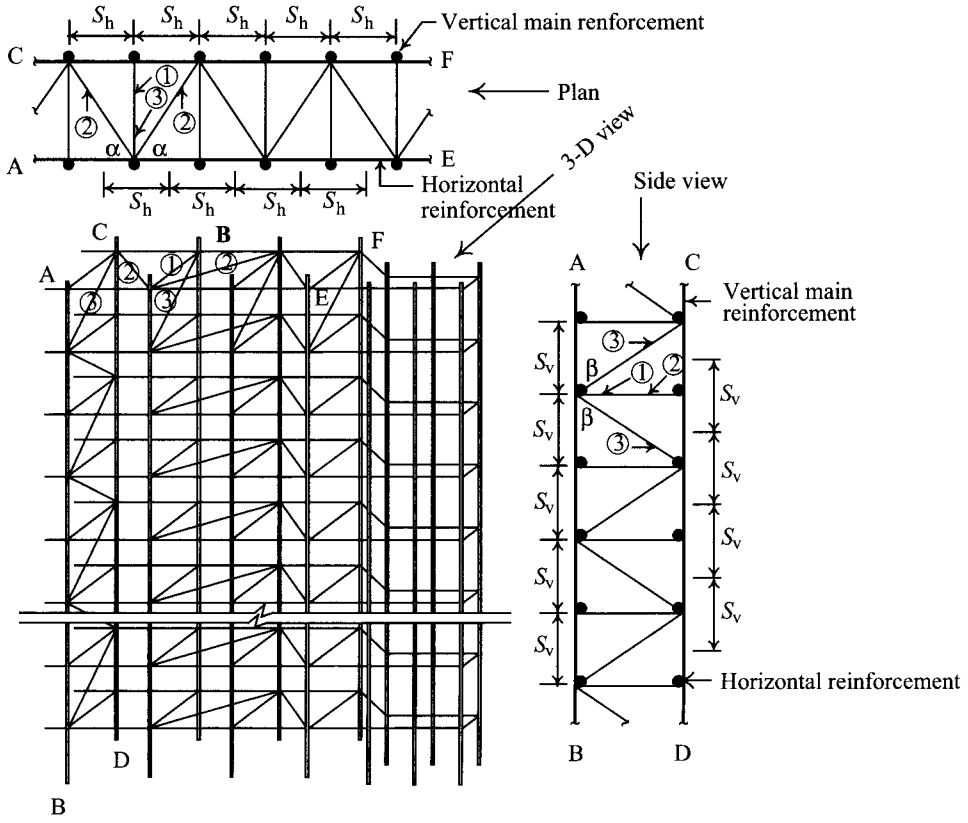

Figure 10.2 Plan, 3-D view, side view of a steel cage of diaphragm wall (1, 2, and 3 represent shear reinforcements).

where

M_u = bending moment for design
M_n = nominal bending moment, also called the capacity of bending moment
V_u = shear for design
V_n = nominal shear, also called the capacity of shear
M = bending moment obtained from stress analysis
V = shear obtained from stress analysis
L_F = Load resistance factor; according to ACI (2005), L_F is equal to 1.6; according to ACI (2002), L_F is equal to 1.7
ϕ = strength reduction factor; according to ACI (2005), for bending moment $\phi = 0.9$, for shear $\phi = 0.75$; according to ACI (2002), for bending moment $\phi = 0.9$, for shear $\phi = 0.85$
λ = short-term magnified factor of allowable stress, which can be found in country building codes.

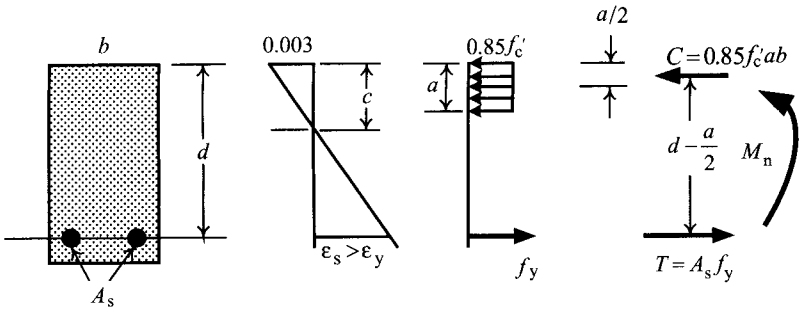

Figure 10.3 Stress in the ultimate state on a section of the reinforced concrete beam (reinforcements are smaller than those in the balanced state).

10.3.4.1 Vertical main reinforcement

As shown in Figure 10.3, suppose the thickness (t) of a reinforced concrete beam is given. The nominal resistant bending moment of concrete of the width of b is

$$M_R = \frac{1}{\phi}\left[\rho_{max} f_y \left(1 - 0.59\frac{\rho_{max} f_y}{f_c'}\right)\right] bd^2 \tag{10.6}$$

where

d = distance from extreme compression fiber to centroid of tension reinforcement
ρ_{max} = maximum reinforcement ratio that does not contain compression reinforcement, $\rho_{max} = 0.75\rho_b$
f_c' = compressive strength of concrete
f_y = yielding strength of reinforcements
ρ_b = reinforcement ratio producing balanced strain conditions.

The balanced reinforcement ratio can be computed as follows

$$\rho_b = \frac{0.85f_c'}{f_y}\beta_1\left(\frac{6120}{6120 + f_y}\right) \tag{10.7}$$

where the measurement unit of f_c' and f_y is kg/m^2; β_1 relates to the strength of concrete, which is generally under 280 kg/cm^2. High performance concrete has been used to construct diaphragm walls recently. Thus, β_1 can also be computed by the following equation:

$$\beta_1 = \begin{cases} 0.85 & f_c' \le 280 \text{ kg/cm}^2 \\ 0.85 - 0.05\left(\dfrac{f_c' - 280}{70}\right) \ge 0.65 & f_c' > 280 \text{ kg/cm}^2 \end{cases} \tag{10.8}$$

where the measurement unit of f_c' is kg/cm^2.

When $M_u \leq \phi M_R$, the only item to be designed is tension reinforcements, which can be computed as follows:

Let the strength ratio of the material be $m = \dfrac{f_y}{0.85f'_c}$.

Since $\dfrac{M_u}{\phi} = M_n = \rho f_y \left(1 - \dfrac{0.59\rho f_y}{f'_c}\right) bd^2$

We then have the reinforcement ratio, deriving from the above equation:

$$\rho = \frac{1}{m}\left(1 - \sqrt{1 - \frac{2mM_n}{f_y bd^2}}\right) \tag{10.9}$$

The required area of tension reinforcements is

$$A_s = \rho bd. \tag{10.10}$$

If $M_u > \phi M_R$, it follows that the maximum resistance of concrete (under the condition that the tension reinforcement has achieved its yielding strength) is still smaller than the designed bending moment. That is to say, the diaphragm wall is to be thickened or compression reinforcements have to be designed. The design of compression reinforcements can follow the method of the *doubly reinforced beam*, which is as follows:

let the ratio of the tension reinforcement be $\rho_1 = 0.75\rho_b$, then

$$A_{s1} = \rho_1 bd \tag{10.11}$$

$$T_1 = A_{s1} f_y \tag{10.12}$$

$$C_c = T_1 = 0.85f'_c ba \tag{10.13}$$

Deriving from the above equation,

$$a = \frac{T_1}{0.85f'_c b} \tag{10.14}$$

The bending moment provided by the tension reinforcement is

$$M_1 = T_1\left(d - \frac{a}{2}\right) \tag{10.15}$$

$$M_2 = M_n - M_1 \tag{10.16}$$

Thus, the area of tension reinforcements corresponding to M_2 is

$$A_{s2} = \frac{M_2}{f_y(d - d')} \tag{10.17}$$

where d' = distance from extreme compression fiber of the wall to the centroid of compression reinforcements.

The required area of tension reinforcements is

$$A_s = A_{s1} + A_{s2}. \tag{10.18}$$

The required area of compressive reinforcements is

$$A'_s = A_{s2}\frac{f_y}{f'_s} \tag{10.19}$$

$$f'_s = E_s\varepsilon'_s \leq f_y \tag{10.20}$$

where E_s = Young's modulus of reinforcements and ε'_s = strain of the compression reinforcements, which can be computed as follows:

$$\varepsilon'_s = \left(\frac{c - d'}{c}\right) \times 0.003 \tag{10.21}$$

where $c = a/\beta_1$ (see Figure 10.3).

10.3.4.2 Horizontal main reinforcement

The retaining wall with one dimensional deformation does not need to be reinforced horizontally. If shrinkage and temperature are to be considered, horizontal reinforcements will be needed. According to the ACI code, the reinforcement with shrinkage and temperature effects is

$$A_s = \begin{cases} 0.002A_g(f_y < 4200\ \text{kg/cm}^2) \\ 0.0018A_g(f_y = 4200\ \text{kg/cm}^2) \\ 0.0018(4200/f_y)A_g \geq 0.0014A_g(f_y > 4200\ \text{kg/cm}^2) \end{cases} \tag{10.22}$$

where A_g = thickness of the retaining wall × unit width; the reinforcement for shrinkage and temperature effects (A_s) has to be placed evenly on both sides of the wall.

10.3.4.3 Shear reinforcement

According to the ACI code, the nominal shear of concrete is

$$V_c = 0.53\sqrt{f'_c}bd \tag{10.23}$$

where V_c is the nominal shear of concrete (also called the capacity of shear, the maximum shear resistance of concrete) and is measured by kg. The unit of f'_c is kg/cm^2. The unit width b is usually taken to be 100 cm.

When the designed shear (V_u) is smaller than ϕV_c, it is theoretically unnecessary to design reinforcement. In practice, the shear reinforcement still has to be designed in order to be able to hang the steel cage into the trench.

As illustrated in Figure 10.2, three types of shear reinforcements are used in the steel cage of a retaining wall, main shear reinforcement—type 1, and two small slant reinforcements—types 2, and 3. As a result, the nominal shear (capacity of shear) of the retaining wall per unit width is

$$V_n = V_c + V_s \tag{10.24}$$

where V_s is nominal shear of shear reinforcements.

Since the horizontal distance between any two shear reinforcements is identical, the sectional area of the shear reinforcement per unit width ($b = 100$ cm) is

$$A_v = \frac{100A_b}{S_h} \tag{10.25}$$

where

A_v = total sectional area of all shear reinforcements on the horizontal section per unit width (cm)
A_b = sectional area of a single shear reinforcement (cm)
S_h = horizontal distance between shear reinforcements (cm).

The nominal shear of the type 1 (i.e. main shear reinforcement) is

$$V_{s1} = \frac{A_v f_y d}{S_v} \tag{10.26}$$

where S_v = vertical distance between the main shear reinforcements.

The nominal shear of the type 2 (i.e. small slant reinforcement) is

$$V_{s2} = \frac{A_v f_y d}{S_v} \sin\alpha \tag{10.27}$$

where α = angle between the small slant reinforcement and the horizontal reinforcement.

The nominal shear of the type 3 (i.e. small slant reinforcement) is

$$V_{s3} = \frac{A_v f_y d}{s_v} \sin\beta \tag{10.28}$$

where β = angle between the small slant reinforcement and the vertical reinforcement.

The nominal shear offered by all shear reinforcements per unit width is

$$V_s = V_{s1} + V_{s2} + V_{s3}. \tag{10.29}$$

What's noteworthy, for the convenience of hanging the steel cage into the trench, the shear reinforcement is usually welded to the vertical main reinforcement. Actually, the method does not conform to the ACI code, welding being unable to make the shear reinforcement develop its full strength as expected. Figures 10.4a and 10.4b show the numbers of the shear reinforcements (#3 or D10 reinforcement, distance = 20 cm) within the range of a 45° shear crack line for the 100 and 50 cm thick retaining walls, respectively. As shown in the figure, in a 100 cm thick retaining wall containing five #3 D10 reinforcements, the first and fifth reinforcements do not extend fully and only 3/5 (60%) of the reinforcements can develop their strength to the expected level. The actual strength of shear reinforcements is 60% of the nominal shear (V_s) computed using Eq. 10.29. Similarly, only 1/3 (33%) of the reinforcements in the 50 cm thick retaining wall can develop full strength as expected.

Another method is to fix the type 1 (i.e. main shear reinforcements) onto the vertical main reinforcement with the help of a 90° hook (conforming to the ACI code) while the type 2 and type 3 (i.e. two small slant shear reinforcements) are still to be welded onto it.

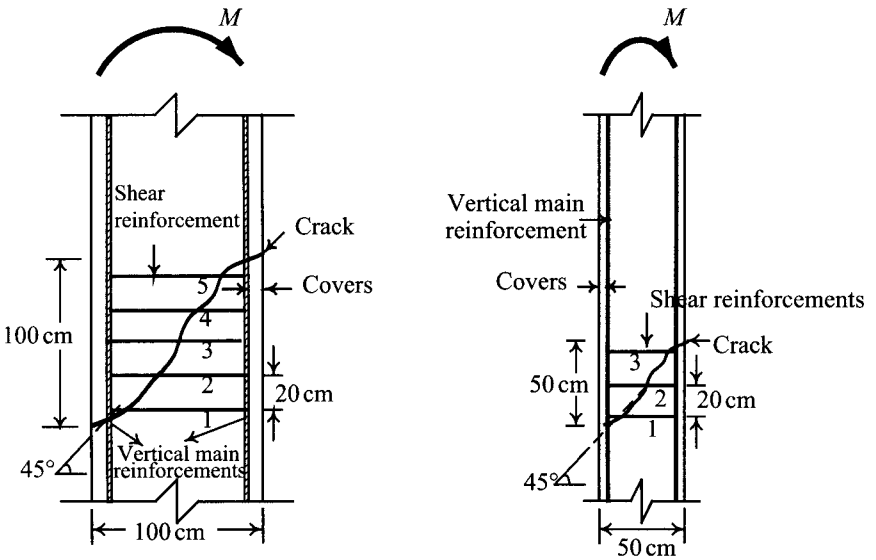

The first and fifth shear reinforcements cannot develop fully and therefore do not have the expected strength

(a)

The first and third shear reinforcements cannot develop fully and therefore do not have the expected strength

(b)

Figure 10.4 Effective capacity of shear reinforcements welded to a steel cage: (a) thickness of the diaphragm wall = 100 cm and (b) thickness of the diaphragm wall = 50 cm.

10.3.4.4 Lap splice length and development length

The minimum lap splice length and development length of reinforcements of a diaphragm wall can be designed according to the ACI code, or they can be determined using Eqs 10.30 and 10.31. The coefficient 1.25 is to magnify the lap splice length and development length, considering the effects of concrete casting in bentonite fluid, which leads to a smaller bond stress.

$$\text{Development length} \quad L_d = 1.25(c\ell_d) = \frac{0.075cA_b f_y}{\sqrt{f'_c}} \tag{10.30}$$

$$\text{Lay splice length} \quad L_d = 1.25(c\ell_d) = \frac{0.091cA_b f_y}{\sqrt{f'_c}} \tag{10.31}$$

where A_b = the sectional area of a single reinforcement; if applied to a vertical reinforcement and $c = 1$ and to horizontal reinforcement, $c = 1.4$.

We can then proceed to the reinforcement design on the basis of the above method. Figure 10.5 is a typical reinforcement design in a diaphragm wall. The three dimensional picture of a steel cage in a diaphragm wall is shown in Figure 10.2.

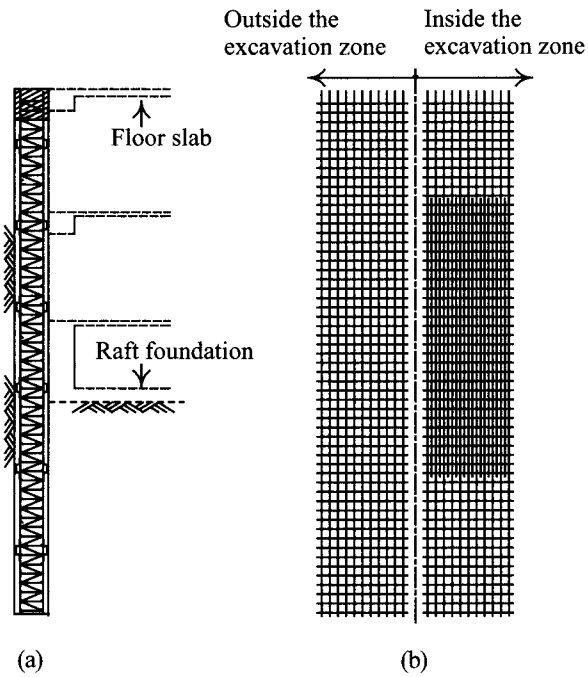

Figure 10.5 Design of reinforcements in a steel cage of the diaphragm wall: (a) profile and (b) side view.

10.4 Structural components in braced excavations

Figure 10.6 shows the commonly used structural components of the retaining wall in a braced excavation. In addition to the retaining wall, the main components of the strutting system include horizontal struts, wales, rakers, end braces, corner braces, and center posts. Figure 10.7 shows the plan of a typical braced excavation. Figures 10.8a–10.8c are the three-dimensional picture, the plane view, and the photo of the joint of the struts with a center post. If the earth pressure on the back of the retaining wall grows too large or the strutting distance is to be widened, the strut system can be designed as double struts, as shown in Figure 10.9. Figures 10.10a–10.10c are the three-dimensional picture, the plane view, and the photo of the joining of the double struts with a center post.

The strut system begins to bear the earth pressure on the back of the retaining wall once excavation is started. The success of the strut system is a pivotal factor in the safety of excavations. Its design and construction has to be carefully carried out. The load on struts can be computed using the apparent earth pressure method (Chapter 6), the beam on elastic foundation method (Chapter 7), or the finite element method (Chapter 8). Readers interested in the subject can find detailed elucidation in these chapters.

In this section are introduced the commonly used designing methods for a strut system. As for the special considerations in designing a strut system, please refer to related literature (e.g. Tsai *et al.*, 1996).

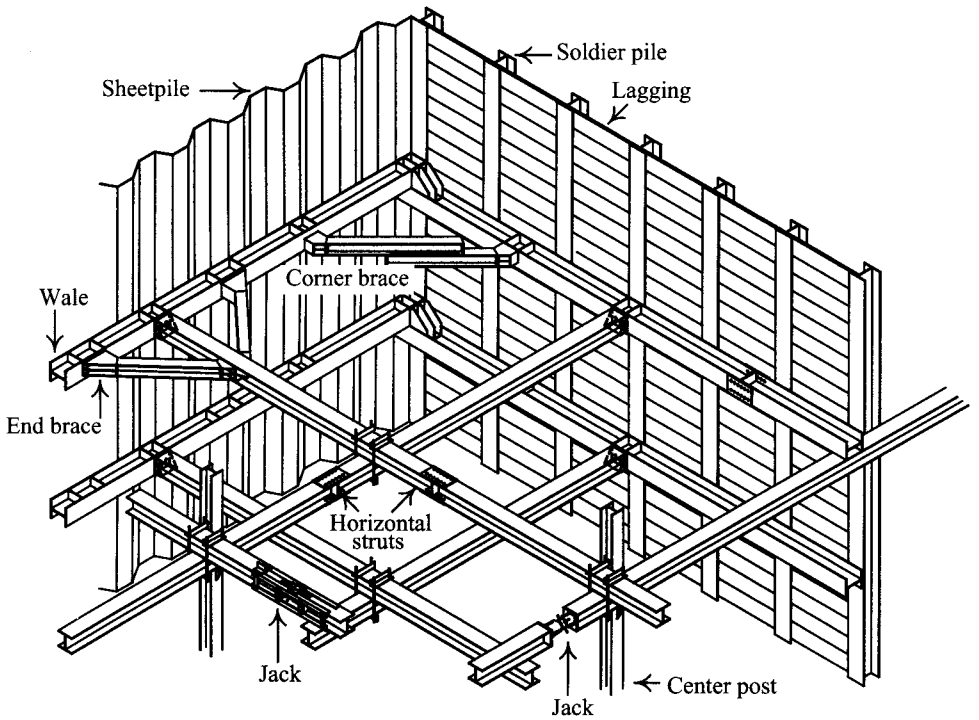

Figure 10.6 Components of a strutting retaining system.

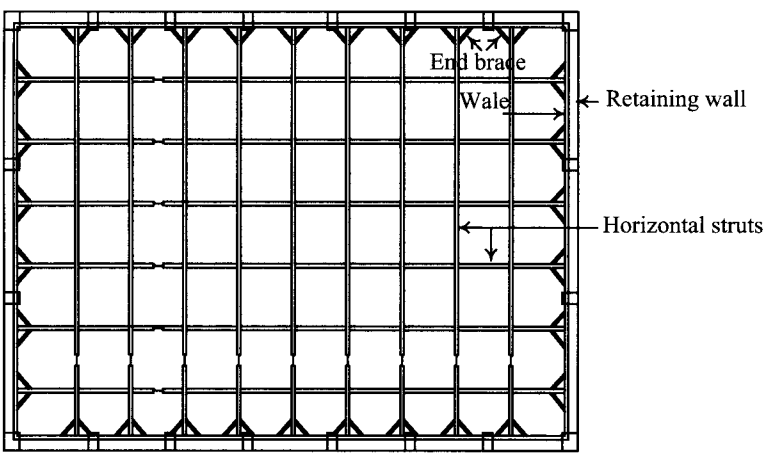

Figure 10.7 Single strutting system.

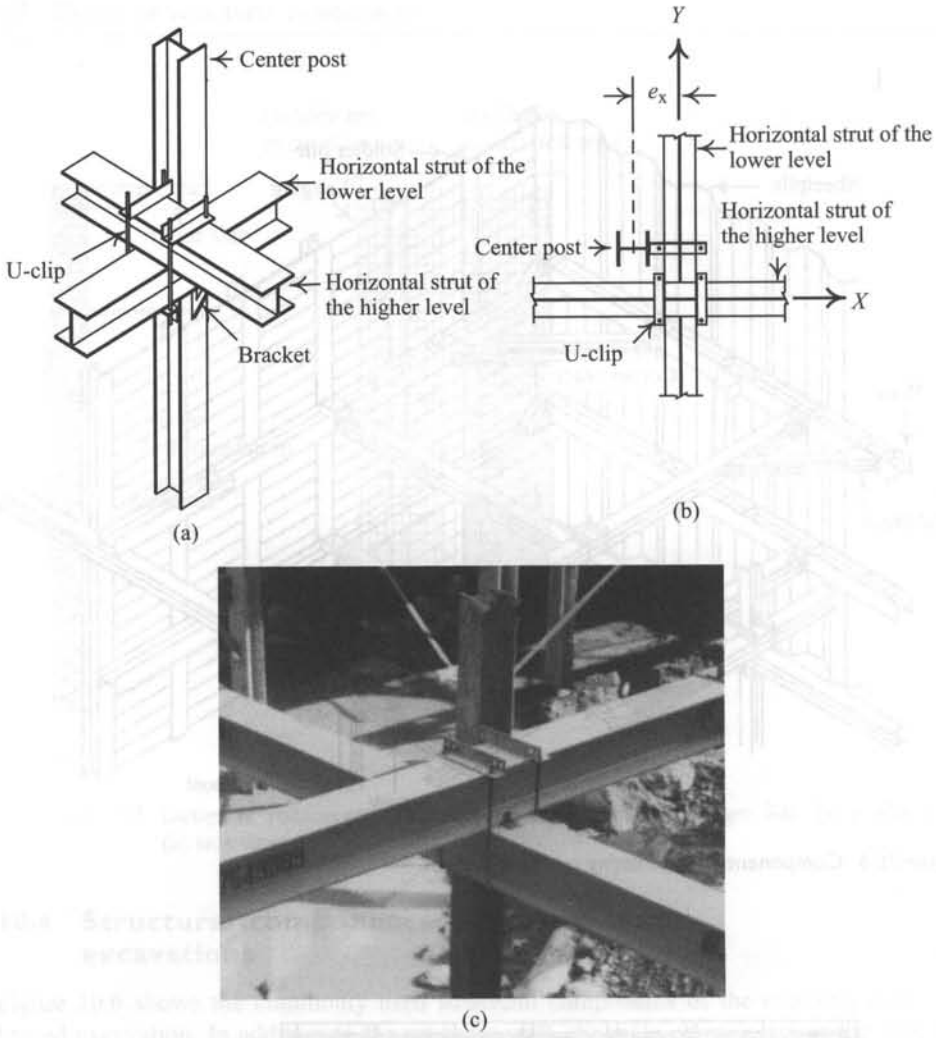

Figure 10.8 Joint of a single strut and a center post: (a) 3-D view, (b) plan view, and (c) photo.

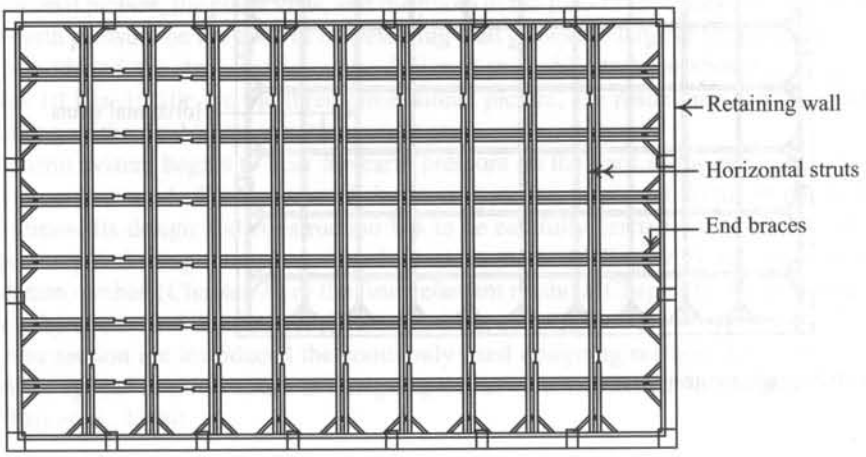

Figure 10.9 Double strutting system.

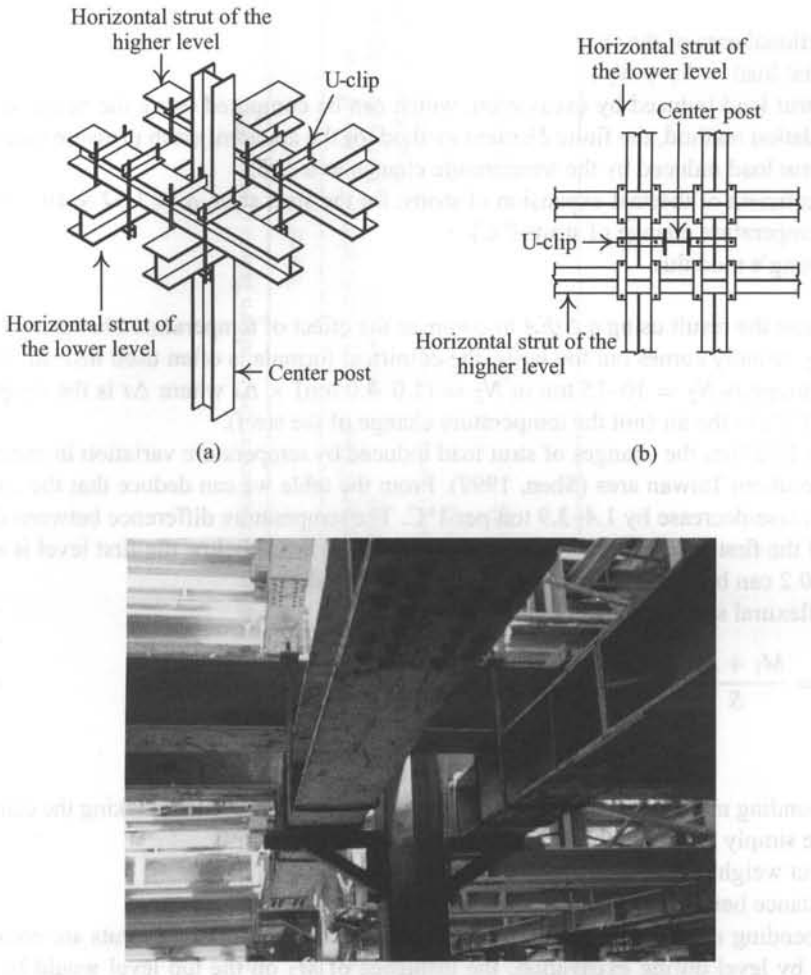

Figure 10.10 Joint of a double strut and a center post: (a) 3-D view, (b) plan view, and (c) photo.

10.5 Strut systems

10.5.1 Horizontal struts

10.5.1.1 Stress computation

A strut is usually subjected to the axial compressive load as well as the flexural load. The axial compressive stress can be computed as follows:

$$f_a = \frac{N}{A} \tag{10.32}$$

where

A = sectional area of the strut
N = axial load = $N_1 + N_2$
N_1 = strut load induced by excavation, which can be computed using the beam on elastic foundation method, the finite element method, or the apparent earth pressure method
N_2 = strut load induced by the temperature change = $\alpha \Delta t E A$
α = coefficient of thermal expansion of struts; for the steel strut, $\alpha = 1.32 \times 10^{-5}/°C$
Δt = temperature change of struts (°C)
E = Young's modulus.

Because the result using $\alpha \Delta t E A$ to compute the effect of temperature change on the strut load, N_2, usually comes out too large, the empirical formula is often used instead. The JSA (1988) suggests N_2 = 10–15 ton or N_2 = (1.0–4.0 ton) × Δt where Δt is the temperature change (°C) in the air (not the temperature change of the steel).

Table 10.2 lists the changes of strut load induced by temperature variation in excavations in the southern Taiwan area (Shen, 1999). From the table we can deduce that the strut load will increase/decrease by 1.4–3.9 ton per 1°C. The temperature difference between day and night of the first level of struts is large and that of the levels below the first level is smaller. Table 10.2 can be used as a reference for preliminary design.

The flexural stress can be computed as follows:

$$f_b = \frac{M_1 + M_2}{S} \tag{10.33}$$

where

M_1 = bending moment produced by the strut weight and the live load; taking the center post as the simply supported hinge, then $M_1 = wL^2/8$.
w = strut weight + live load $\cong$ 0.5 ton/m
L = distance between two adjacent center posts
M_2 = bending moment caused by the uplift of the center post; since struts are constructed level by level during excavation, the influence of M_2 on the top level would be largest while that on the lowest level would be the smallest
S = section modulus.

10.5.1.2 Allowable stress

Struts bear both the axial compressive force and the moment simultaneously during excavation. Thus, the allowable compressive stress has to be computed based on the beam-column theory. The allowable axial compressive stress of a strut can be selected from the tables and figures offered by the AISC Specification or computed using the following equation:

$$\frac{KL}{r_y} < C_c \quad F_a = \frac{\left[1 - \frac{1}{2}((KL/r_y)/C_c)\right] F_y}{\frac{5}{3} + \frac{3}{8}[(KL/r_y)/C_c] - \frac{1}{8}[(KL/r_y)/C_c]^3} \cdot \lambda \tag{10.34}$$

$$\frac{KL}{r_y} > C_c \quad F_a = \frac{12}{23} \frac{\pi^2 E}{(KL/r_y)^2} \cdot \lambda \tag{10.35}$$

Table 10.2 Relations between the temperature difference and the change of strut load of excavations in the southern Taiwan (Shen, 1999)

	Summer			*Winter*		
	Change of strut load (t)	*Average temperature change (°C)*	*Change of strut load per unit degree of temperature change (t/°C)*	*Change of strut load (t)*	*Average temperature change (°C)*	*Change of strut load per unit degree of temperature change (t/°C)*
The first level of struts	35–40	11.3	3.1–3.5	15–25	11.1	1.4–2.3
The second level of struts (including struts below)	10–25	6.7	1.5–3.7	10–25	6.4	1.6–3.9

where

KL/r_y = effective slenderness ratio of the strut on the flexural plane where K can be taken as 1.0
L = unsupported length of the strut, usually distance between the two adjacent center posts
r_y = radius of gyration of the cross section of the strut in the direction of the weak axis
C_c = critical slenderness ratio = $\sqrt{2\pi^2 E/F_y}$
E = Young's modulus of struts
F_y = yielding stress of struts
λ = short-term magnified factor of the allowable stress, which can be found in country building codes.

The allowable flexural stress (F_b) of a strut can be derived from the tables and figures offered by the AISC Specification. However, the flexural stress (f_b) of a strut, during normal excavation (i.e. the uplift of the center post is not much), is not large. To simplify the design, we can assume $F_b = 0.6F_y \cdot \lambda$.

10.5.1.3 Examination of combined stresses

According to the AISC Specification, the stress on each section of a strut should satisfy the following equation:

$$\frac{f_a}{F_a} \leq 15\% \quad \frac{f_a}{F_a} + \frac{f_b}{F_b} \leq 1.0 \tag{10.36}$$

$$\frac{f_a}{F_a} > 15\% \quad \frac{f_a}{F_a} + \frac{C_m f_b}{(1 - f_a'/F_e')F_b} \leq 1.0 \tag{10.37}$$

where

C_m = coefficient of modification = 0.85
$1/(1 - f_a/F_e')$ = amplification factor
F_e' = allowable Euler stress = $\lambda \cdot 12\pi^2 E/[23(KL/r_x)^2]$
KL/r_x = effective slenderness ratio on the flexural plane
r_x = radius of gyration of the strut in the direction of the strong axis
E = Young's modulus of struts
λ = short-term magnified factor of the allowable stress, which can be found in country building codes.

10.5.2 End braces and corner braces

For construction convenience or other reasons, the distances between two adjacent struts in some positions come to be a little over the allowable distance in the arrangement of horizontal strutting. If we add one more strut, the distance becomes too narrow. Under such a condition, an end brace or corner brace may be used to adjust the condition. The function of an end brace or corner brace is then to shorten the span of the wale (see the next section on the design of the wale) without adding more struts, as shown in Figure 10.11. End braces are usually symmetrically installed at 45° angles against the wale.

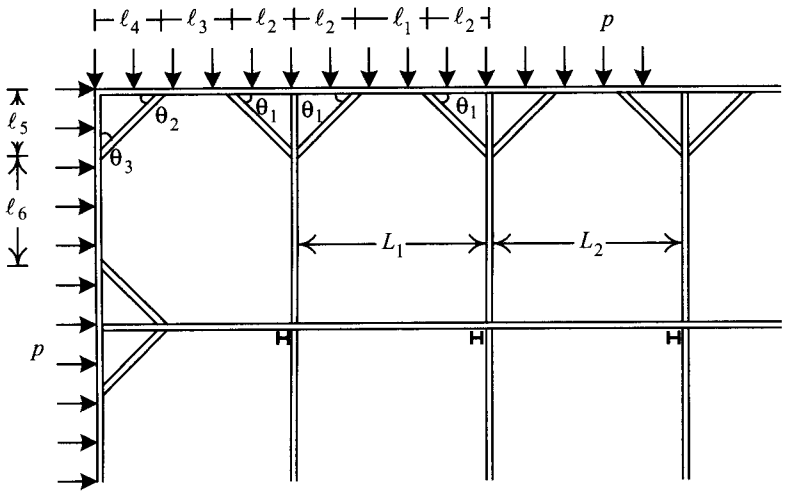

Figure 10.11 Distance and angle between struts and end braces or corner braces.

As shown in Figure 10.11, the axial force on the end brace is

$$N = p\left(\frac{\ell_1 + \ell_2}{2}\right)\frac{1}{\sin\theta_1} \tag{10.38}$$

where

p = apparent earth pressure or the strut load per unit width
ℓ_1, ℓ_2 = spans (see Figure 10.11)
ϕ_1 = angle between the end brace and the wale (usually 45°).

Similarly, the axial force on a corner brace, as shown in Figure 10.11, is

$$N_1 = p\frac{\ell_3 + \ell_4}{2}\frac{1}{\sin\theta_2} \tag{10.39}$$

$$N_2 = p\frac{\ell_5 + \ell_6}{2}\frac{1}{\sin\theta_3} \tag{10.40}$$

where ℓ_3, ℓ_4, ℓ_5, ℓ_6 = the spans (see Figure 10.11), ϕ_2, ϕ_3 = angles between the corner brace and the wale, 45° in most cases.

To be conservative, the designed load can be assumed to be the maximum value between N_1 and N_2. The design of the end and corner braces is identical to that of the horizontal struts and will not be mentioned again.

10.5.3 Wales

The function of wales is to transfer the earth pressure on the retaining wall to the struts. For analysis, the earth pressure can therefore be assumed to act on the wale directly. The earth

pressure can be obtained from the apparent earth pressure method or by transforming the strut load, computed using the finite element method or beam on elastic foundation method. As a matter of fact, the wale is usually acted on by the earth pressure as well as the axial force from the end brace or corner brace. That is to say, the wale bears simultaneously the moment and the axial force and its design falls in the domain of the beam-column system. With ample lateral support, the analyses of secondary moment and buckling for wales can be saved.

To compute the maximum bending moment and shear of wales, the wales can be viewed as simply supported beams with struts as supporting hinges, or viewed as fixed end beams, as shown in Figure 10.12.

If a wale is viewed as a simply supported beam, then:

$$M_{\max} = \frac{1}{8}pL^2 \tag{10.41}$$

$$Q_{\max} = \frac{1}{2}pL. \tag{10.41a}$$

If viewed as a fixed end beam, we have

$$M_{\max} = \frac{1}{12}pL^2 \tag{10.42}$$

$$Q_{\max} = \frac{1}{2}pL \tag{10.42a}$$

where

$M_{\max}$ = maximum bending moment of the wale
$Q_{\max}$ = maximum shear of the wale

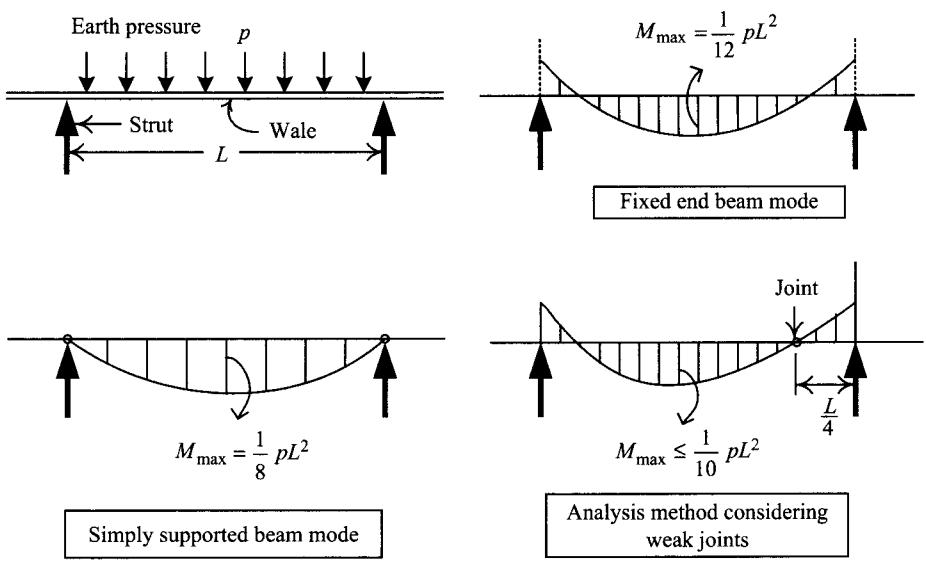

Figure 10.12 Computation of the bending moment of a wale.

L = distance between struts
P = earth pressure.

Because the length of a wale is limited, the wales have to be joined in the field. The strength of the joint is not fully rigid and the joint could easily become the weakest part of the structure. Thus, the joints had better be located at the places where the stress is smaller. According to the bending moment distribution diagram of a continuous or a simply supported beam, if the joint is located at the places one-fourth of the span from the support, the maximum bending moment of the wale would be

$$M_{\max} \leq \frac{1}{10} pL^2. \tag{10.43}$$

As a result, in design practice, if the wale is assumed to be a simply supported beam, it may not work out as economical. If it is designed to be a fixed end beam, it may tend to be insecure. The more reliable method is to locate the joint at the place one-fourth of the span from the support and compute the maximum bending moment and shear as follows

$$M_{\max} = \frac{1}{10} pL^2 \tag{10.44}$$

$$Q_{\max} = \frac{1}{2} pL. \tag{10.44a}$$

When there are no end braces, L is the horizontal distance between struts. When there are end braces, the distance between struts can be reduced properly. Generally speaking, when $\theta \leq 60°$, $L = \ell_1 + \ell_2$ (see Figure 10.11). When $\theta > 60°$, less conservative design can be made: $L = \ell_1$.

Viewed from the viewpoint of mechanics, the wale is also subjected to the axial stress. If sheet piles or soldier piles with end braces are used, the axial force on the wale can be designed by choosing the larger one between the following two computing results:

$$N = p\left(\ell_5 + \frac{\ell_6}{2}\right) \tag{10.45}$$

or

$$N = p\left(\frac{\ell_1 + \ell_2}{2}\right)\frac{1}{\tan\theta_1}. \tag{10.46}$$

Since the corners of a diaphragm wall have an arching effect, to determine the axial load of a wale around a corner of an excavation with diaphragm walls, it is necessary to use Eq. 10.46. If sheet piles or soldier piles are used, take the maximum value among the computed results of Eqs 10.45 and 10.46.

10.5.4 Center posts

In a braced excavation, center posts are usually set to bear the weight of struts, the materials on the struts, and other extra loading out of the movement of the retaining system. Center posts, usually H steels, are often installed by striking the piles into soils directly. Considering that the noise and vibration caused by striking may influence adjacent properties (especially

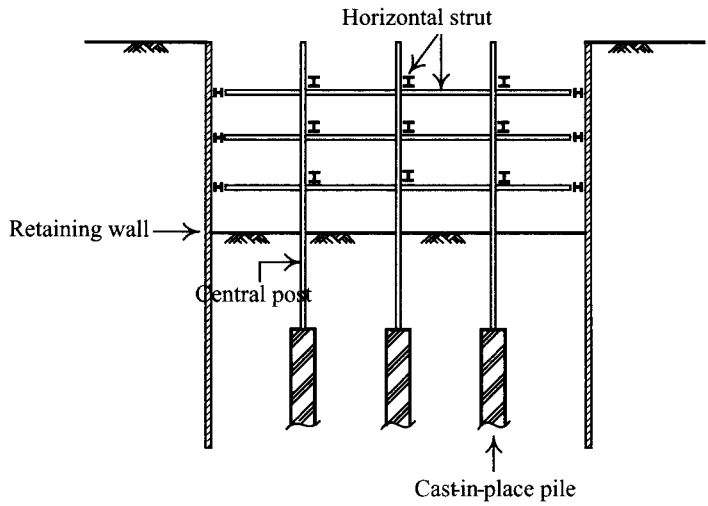

Figure 10.13 Installation of center posts onto cast in situ piles.

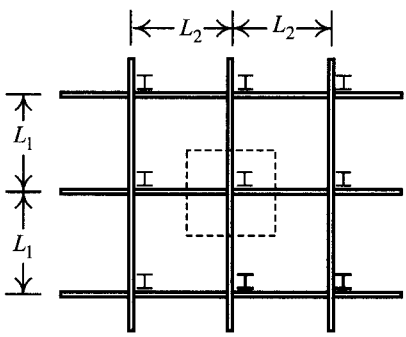

Figure 10.14 Distribution of strut weight on a center post.

when the installation is carried out in hard soils), when the embedment depths are designed deeper, or the pile driver is not powerful enough, the H steel is sometimes embedded into soils by way of pre-boring or inserted into a cast-in-place pile, as shown in Figure 10.13.

The design of a center post includes the design of the section and the embedment depth. Before designing the section, the load on the center post has to be determined first (Figure 10.14). The possible axial loads on each center post are:

1 Weight of the horizontal strut and the live load, P_1

$$P_1 = \sum_{i=1}^{n} w_i(L_1 + L_2) \tag{10.47}$$

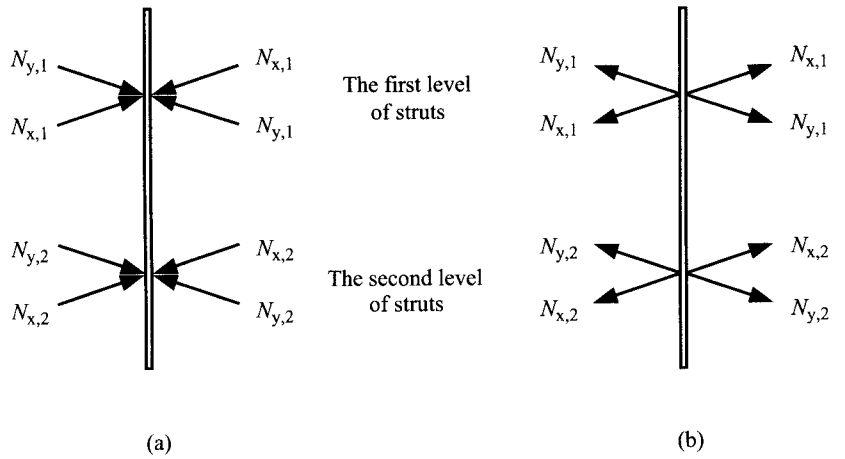

Figure 10.15 Action of the axial force of struts on a center post: (a) when the center post settles and (b) when the center post heaves.

where

w_i = strut weight of each level and its live load
L_1, L_2 = distance between struts
n = number of the levels.

2 Weight of the center post above the excavation surface, P_2.
3 Slant compressive force on the horizontal strut, P_3.

If the construction of a center post is defective or there occurs a differential settlement between the center post and the retaining wall, these conditions may cause the center post to move downward or upward by the axial force of the strut. Suppose the tilt angle of a horizontal strut is θ, as shown in Figure 10.15, the downward or upward force on the center post would be

$$P_3 = \sum_{i=1}^{n} 2(N_{x,i} + N_{y,i}) \sin\theta \tag{10.48}$$

where

$N_{x,i}$ = load on the struts of each level in the x direction
$N_{y,i}$ = load on the struts of each level in the y direction
θ = tilt angle of the horizontal strut.

In analysis, the tilt angle of the horizontal strut is difficult to estimate. According to the data of field observations of excavations (Shen, 1999), the tilt angle θ can be reasonably assumed to be $\sin\theta \cong 1/50$.

To be conservative in analysis, the center post can be assumed to be subject to the axial force of the strut and generate a downward force. Thus, the total load on the center post would be

$$P = P_1 + P_2 + P_3. \tag{10.49}$$

In the double strutting system, the moments generated by the weight (the live load included) of two struts, which eccentrically act on the center post, can be assumed to be mutually offset (see Figure 10.10). In the single strutting system, the moment caused by the strut weight (the live load included) eccentrically acting on the center post can be computed by the following equation (see Figure 10.8a and 10.8b)

$$M = (P_2 + P_3)e_x \tag{10.50}$$

where e_x = eccentricity distance.

As shown in Figure 10.8, as far as the single strutting system is concerned, the center post, using only one bracket to support the weight of horizontal struts in both the x and y directions, generates a unidirectional eccentric moment, as computed by Eq. 10.50.

The buckling length of a center post should take the maximum unsupported length during the process of excavation, floor construction, and strut dismantling. As shown in Figure 10.16, the buckling length of the center post L is

$$L = \max(L_1, L_2, L_3, L_4, L_5). \tag{10.51}$$

Because the center post bears, simultaneously, the axial force and bending moment, it is the beam-column system that is to be adopted in analysis. Choose a proper section and then use Eqs. 10.47–10.51 to examine it.

As discussed earlier, the center post may bear vertical loads and uplift forces caused by the tilt of the horizontal strut. As a result, to design the embedment depth of the center post, one has to take both vertical loads and uplift forces into consideration. The analysis method is identical with that for piles though a pile is of circular section.

Center posts are usually H steel. The sectional area of the H steel used to compute the point load resistance (Q_p) is the sum of the cross sectional area of the H steel and its soil plug. To compute the skin friction, the surface area of the H steel is the total surface area of the H steel enclosed region, as shown in Figure 10.17. This section will summarize the commonly used equations for the design of center posts. For detailed theories, please refer to the related books, such as local building codes or books on pile foundations.

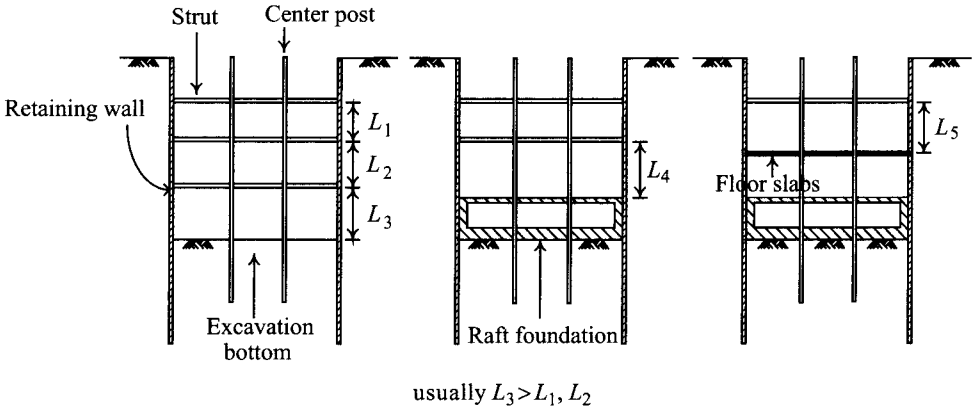

Figure 10.16 Unsupported length of center posts.

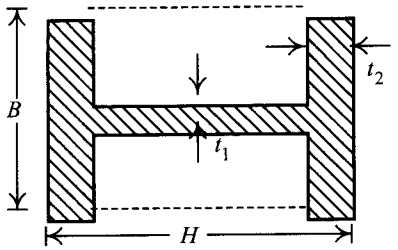

$A_p = B \times H$

$A_s = 2(B+H) \times$ embedded depth of the column

Figure 10.17 Area to be adopted for the computation of the vertical bearing capacity of center posts of the H pile.

10.5.4.1 Vertical bearing capacity

The ultimate vertical bearing capacity can be expressed as follows:

$$Q_u = Q_p + Q_s = f_s A_s + q_p A_p \tag{10.52}$$

where

Q_u = ultimate vertical bearing capacity of the center post
Q_p = point load resistance of the center post
Q_s = skin frictional resistance of the center post
f_s = unit frictional resistance of the center post
A_s = surface area of the center post
q_p = the unit point resistance per unit area of the center post
A_p = sectional area of the center post.

The allowable vertical bearing capacity of the center post is

$$Q_a = \frac{Q_u}{FS} = \frac{Q_s + Q_p}{FS} \tag{10.53}$$

where Q_a is the allowable vertical bearing capacity and FS is the factor of safety.

Under general conditions (low possibility of earthquake, general excavation, good geological conditions), the above factor of safety can be taken to be FS = 2. If considering the possibility of earthquake or the excavation is of high risk (e.g. in soft soils), the above factor of safety can be taken to be FS = 3.

In sandy soils, the point resistance of the center post can be computed as

$$\text{Driven pile: } q_p = 40N(\text{t/m}^2) \tag{10.54}$$

$$\text{Drilling pile: } q_p = 15N(\text{t/m}^2) \tag{10.55}$$

where N is the average standard penetration number within the influence range of the bottom end of the center post.

Generally speaking, N value can be taken as the average value within the range four times of the center post diameter above the bottom end of the center post and one center post diameter below it. The frictional resistance of the center post for both the driven and drilling piles is

$$f_s = 0.2N(\text{t/m}^2) \tag{10.56}$$

where N is the average standard penetration number within the depth of the center post embedded in the sandy soils (from the ground surface to the bottom end of the center post).

In clayey soils, to be conservative, the f_p value of the center post is usually assumed to be 0 and the f_s can be computed as follows:

$$f_s = c_w = \alpha s_u \tag{10.57}$$

where

c_w = adhesion between the surface of the center post and the surrounding soils
s_u = undrained shear strength of clay
α = reduction value of undrained shear strength. It relates to the undrained shear strength of the clay, the installation method of the center post, and its embedment depth. It can be found from Figure 4.12. Besides, the cast-in situ piles (center posts) embedded in clayey soils have lower α-values because they do not compress the soil during the construction and are usually installed in boreholes filled with bentonite fluid. Skempton (1959) suggests the α-value be between 0.3 and 0.6—0.45 in most cases.

10.5.4.2 Pullout resistance

The allowable pulling out resistance of a center post is

$$R_a = W_p + \frac{1}{FS} f_s A_s \tag{10.58}$$

where

W_p = weight of the center post, the influence of groundwater considered
f_s = frictional resistance per unit area of the center post, which can be estimated using Eq. 10.57 or 10.58
A_s = surface area of the center post
FS = factor of safety. As far as the short-term behavior of a structure (such as a center post) is concerned, FS can be assumed to be 3.

10.6 Structural components in anchored excavations

Figure 10.18 illustrates an excavation with anchored support system. As shown in the figure, in addition to the retaining wall, the main structural component is the anchor system, which consists of an anchor and a wale. The following will introduce the analysis and design of anchored excavations.

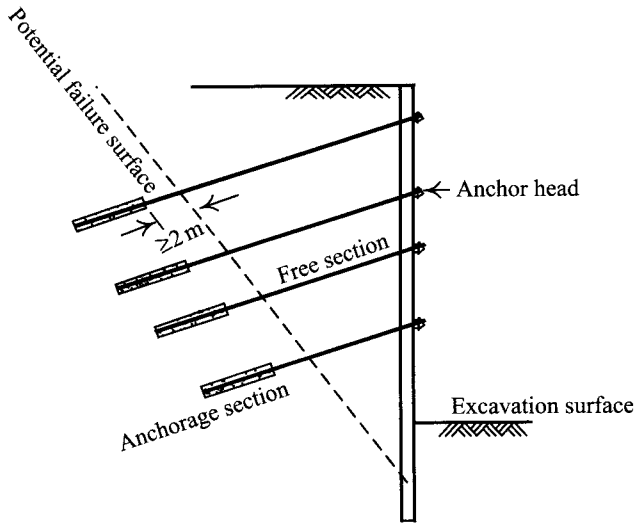

Figure 10.18 Anchored excavation.

10.7 Anchor systems

Anchors are categorized into permanent anchors and temporary ones. They are applied extensively. The design of an anchor involves the soil properties, the materials of the anchor, grouting, and the construction details. The last is especially crucial in determining the quality of the anchor. Concerning the general rules of the design and construction of an anchor, please refer to related literature and specifications referred to in this section.

Anchors in excavations belong to the category of temporary anchors. This section will only introduce the design of the anchor system of the retaining wall in excavations.

10.7.1 Components of anchors

An anchor is basically composed of the anchor head, the free section, and the fixed section, as shown in Figure 10.19. The anchor head is used to transmit the force or preload generated by the displacement of the retaining wall to the free section, which in turn transmits the force or preload to the fixed section and offers the elastic strain necessary for preloading. The function of the fixed section is to transmit the force from the free section to soil layers.

As shown in Figure 10.19, to make the axial center of the anchor head match that of the anchor, a bearing plate is usually designed under the anchor head. To make sure the tendon of the free section can deform freely when preloaded, the free section is usually covered by a plastic pipe to isolate the tendon from grouts (or soils). The anchor head is made of a locking device and a bearing plate. Figure 10.20 illustrates the general types of anchor heads.

Anchors can be categorized into the frictional resistance type, the bearing resistance type, and the composite type according to the characteristics of the bearing force provided by the fixed section (Figure 10.21). The anchoring force of the frictional resistance type of anchors comes from the friction or adhesion between the fixed section and surrounding soils. The

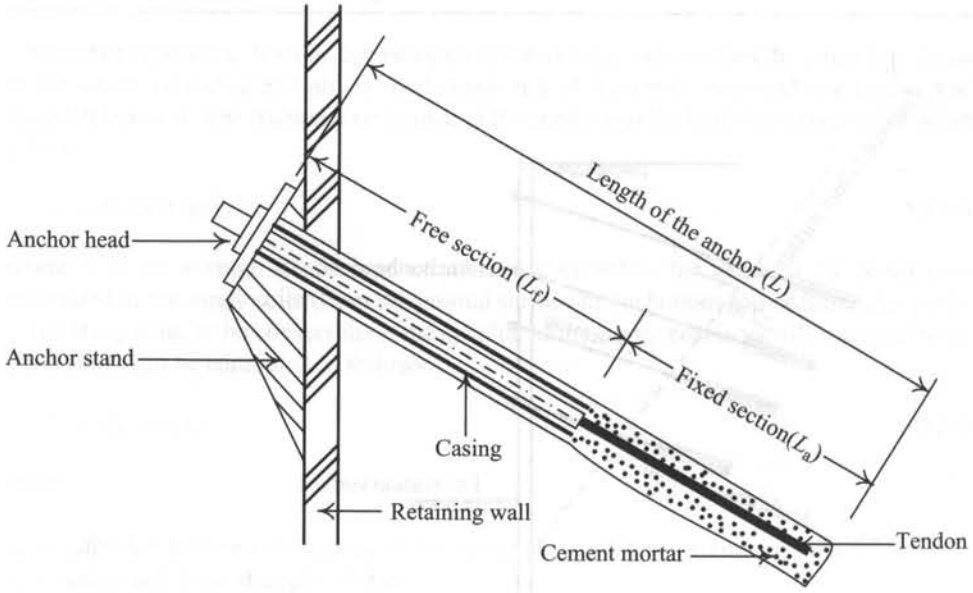

Figure 10.19 Configuration of an anchor.

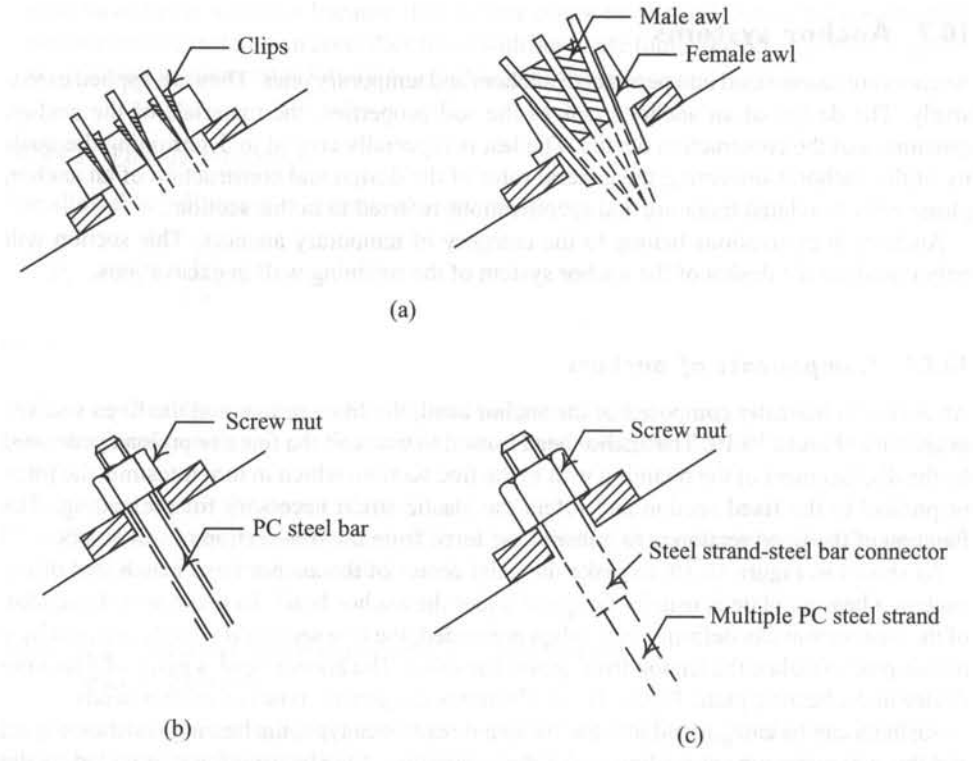

Figure 10.20 Types of anchor heads: (a) locked by wedges, (b) locked by screw nuts, and (c) composite lock (CICHE, 1998).

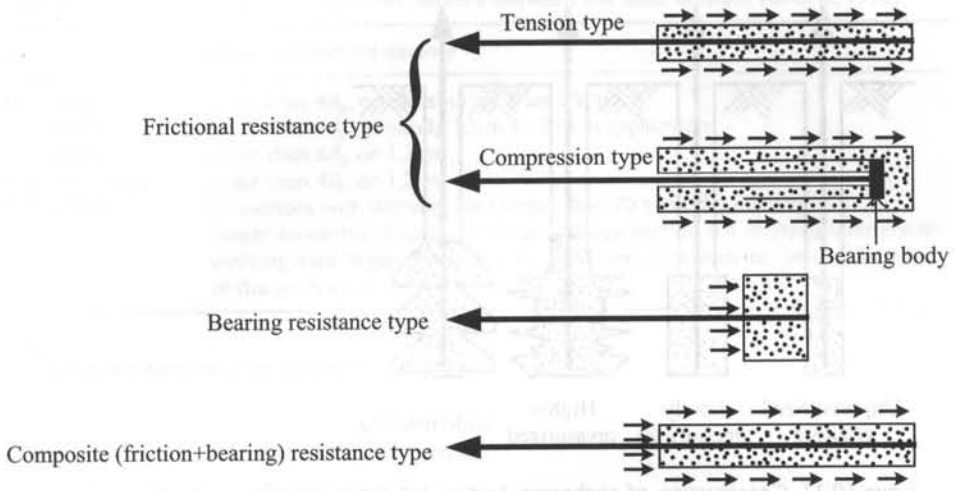

Figure 10.21 Types of anchorage body: (a) frictional resistance type, (b) bearing resistance type, and (c) composite resistance type (redrawn after CICHE, 1998).

anchoring force of the bearing resistance type lies in the bearing capacity of soils surrounding the fixed section, which is usually underreamed. This type is called the underreamed anchor. The composite type is a mixed form possessing the characteristics of both the frictional resistance and bearing resistance types. According to the bearing type of the tendon in the fixed section, the frictional resistance type can be further categorized into the tension type and compression type.

Anchorage bodies can be formed through direct grouting without pressure, low grouting pressure (the grouting pressure lower than 10 kg/cm^2), high grouting pressure (the grouting pressure greater than 20 kg/cm^2) and underreaming, as shown in Figure 10.22.

10.7.2 Analysis of anchor load

The horizontal component of the anchor load can be computed using the half method or underneath pressure method of the apparent earth pressure method, or be analyzed using the beam on elastic foundation method or the finite element method. The related analytical method is identical to that for the braced excavation except that the horizontal component computed from analysis has to be transformed into the anchor load because the axial center of the anchor is not perpendicular to the retaining wall. As shown in Figure 10.23, the anchor load is

$$T_w = \frac{P}{\cos\theta} \tag{10.59}$$

where

T_w = designed load of the anchor
P = horizontal component obtained from analysis
θ = angle between the axis of the anchor and the horizontal plane.

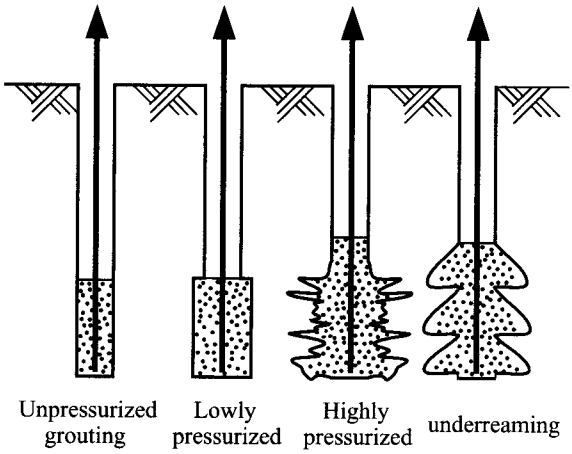

Figure 10.22 Construction of anchorage bodies: (a) direct grouting (without grouting pressure), (b) low grouting pressure, (c) high grouting pressure, and (d) underreaming (redrawn after CICHE, 1998).

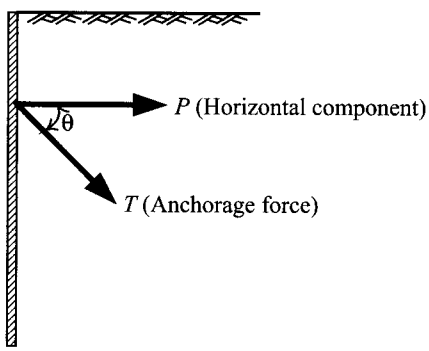

Figure 10.23 Anchorage force and its horizontal component.

10.7.3 Arrangement of anchors

In related literature and specifications on anchors, group anchor effects are seldom discussed. The design of anchors is usually based on a single anchor pattern. Under such conditions, the minimum distance between anchors has to be limited so that the group anchor effect will not be produced or the installation of an anchor may cast a bad influence on the adjacent anchors. Table 10.3 lists the related specifications on the minimum distance between anchors. Generally speaking, the minimum horizontal distance between anchors in an excavation can be set to be 1.5 m. The commonly adopted distances between anchors are basically not longer than 4.5 m (considering the design of wales, please refer to Section 10.7.4). Besides, both FIP (1982) and BSI (1989) require the horizontal distance between the fixed section and underground structure to be longer than 3 m.

Table 10.3 Specifications for the minimum distance between the fixed sections (CICHE, 1998)

Rule	*Suggested minimum distance*
FIP (1982)	Larger than $4d_b$, or not shorter than 1.5 m
BSI (1989)	Larger than $4d_b$, generally 1.5 m to 2 m in application
PTI (1989)	Larger than $6d_b$ or 1.2 m
AASHTO (1992)	Larger than $4d_b$ or 1.2 m
DIN (1988)	For anchors with working load larger than 70 tons, the minimum center-to-center distance of the anchorage section is 1 m; For anchors with working load larger than 130 tons, the minimum center-to-center distance of the anchorage section is 1.5 m

Note
d_b refers to the diameter of the anchorage section.

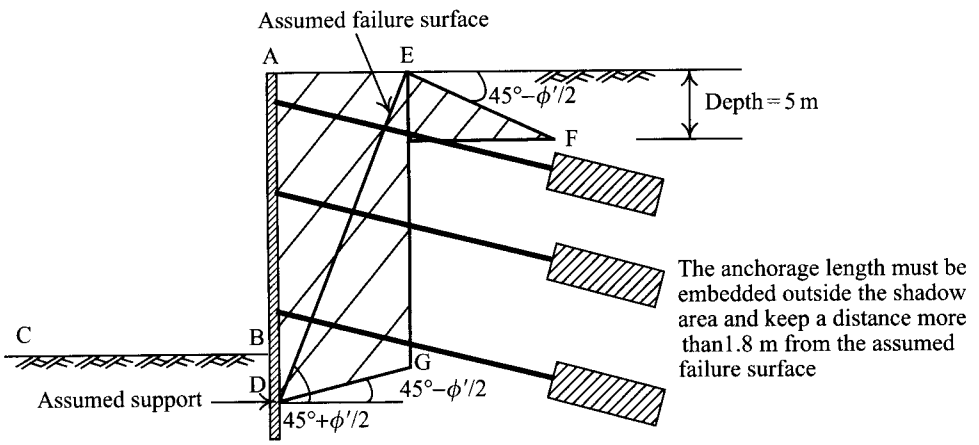

Figure 10.24 Locations of the anchorage sections in soil (redrawn after BSI, 1989).

The determination of the vertical distance between anchors depends on the analytical results of the anchor load. The vertical distance between anchors is about 2.5–4.5 m and at least 1–1.5 m above the floor slabs. Besides, both FIP (1982) and BSI (1989) require the vertical distance between the fixed section and underground structure be longer than 3 m. The fixed section has to be 5 m away from the ground surface (see Figure 10.24).

To maintain the overall stability of the anchor and the retaining wall, the fixed section of the anchor should be placed outside the potential failure surface at least 2 m away from it, as shown in Figure 10.25. The determination of the potential failure surface is still under study and no final conclusion has been drawn yet. Some commonly adopted potential failure surfaces are the active failure zone starting from the excavation bottom, that starting from the bottom of the retaining wall, and that starting from the assumed support, as shown as planes **ab**, **ef**, and **cd** in Figure 10.26. The design on the basis of the active failure zone starting from the excavation bottom is not conservative, while the one using the basis of the active failure zone starting from the bottom of the retaining wall is more conservative. The active failure zone starting from the assumed support is in between and seems more

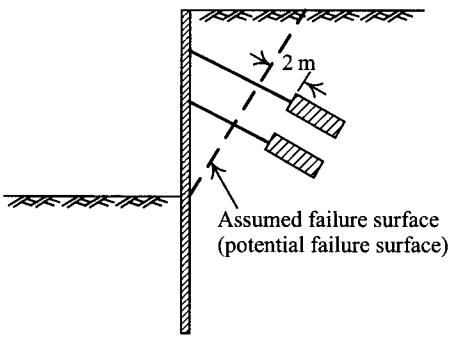

Figure 10.25 Distance between an anchorage section and the potential failure surface.

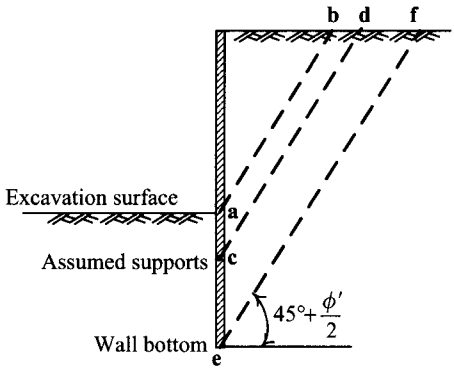

Figure 10.26 Potential failure surfaces in excavations.

reasonable. To determine the location of the assumed support in Figure 10.26, please refer to Section 6.10.3. The location of the fixed section can also be chosen with reference to the BSI code (1989), as shown in Figure 10.24. The line segments DG and EF are the possible passive failures, considering the preload of the anchor.

Theoretically, if an anchor is installed with the same direction of loading, it is able to develop the maximum capacity. Considering the installation quality, to clear the dregs in the drilling bore of the anchor, the installation angle should not be smaller than 10°. The fixed section should be placed in a bearing layer (such as a sandy layer, gravelly layer, or rocks) or soils with high strength. Generally speaking, the deeper the soils, the higher the strength. It is more suitable to place the fixed section in deeper soil. As a result, an anchor is usually installed with a certain slope. The steeper the slope, however, the larger the dragging down force on the retaining wall. When the installation angle exceeds 45°, it becomes dangerous. That is to say, without going beyond 45°, the installation angle should fall within the range $10° \leq \theta \leq 45°$.

10.7.4 Design of anchor heads, anchor stands, and wales

As discussed earlier, an anchor head consists of a locking device and a bearing plate. The locking device should be tested before using and its locking capacity should be large enough to make the tendon bear 80% of the ultimate loading without being damaged. If the locking device is used with a wedge clip, the locked tendon should not slide too much. The bearing strength of the bearing plate should be large enough to resist the maximum pulling force during the process of preloading and excavation.

The function of an anchor stand is to transfer the load on the wale or the retaining wall to the anchored soil layer. Anchor stands can be categorized into reinforced concrete anchor stands and steel anchor stands. The detailing of reinforcements of the concrete anchor stand should be carefully designed to meet safety requirements. Under the working load, the allowable compressive stress of the concrete anchor stand should be smaller than 30% of the 28th-day strength of concrete. Figure 10.27 illustrates the common types of anchor stands.

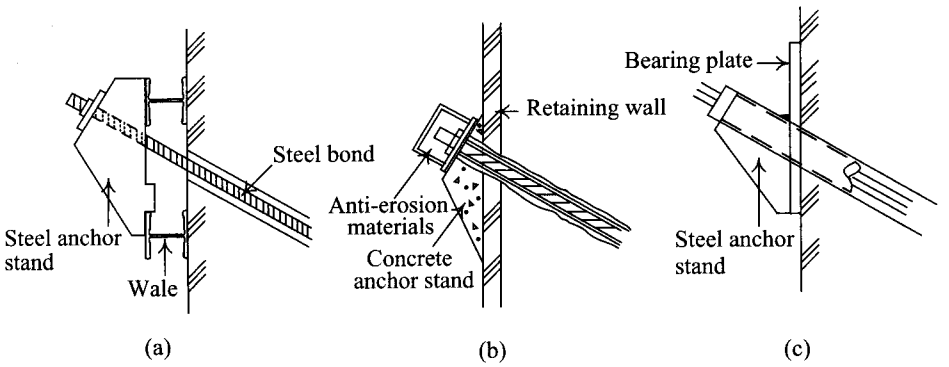

Figure 10.27 Commonly used anchor stands.

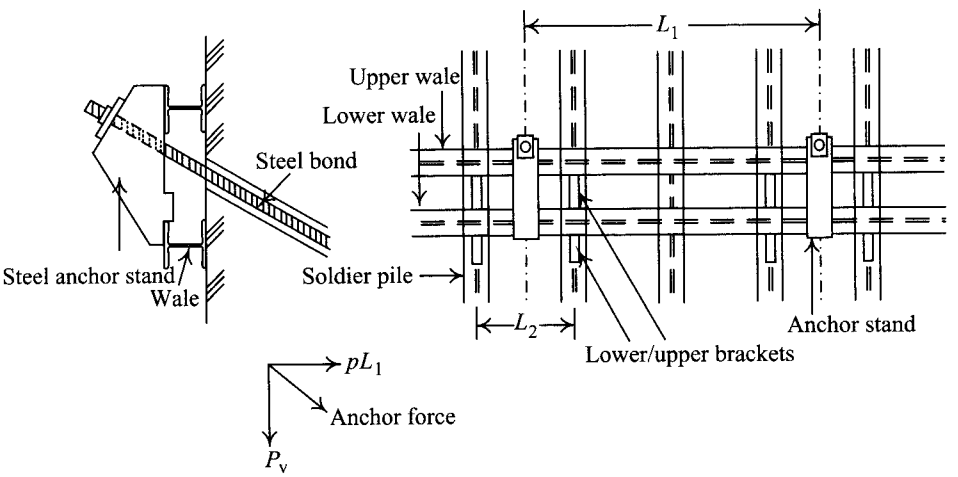

Figure 10.28 Configuration of wales in anchored system.

Generally two parallel H-steels or I-steels serve as wales (Figure 10.27a). Bearing only the horizontal force, wales are beam structures. The design of wales should consider the stresses in both the weak and strong axes. Referring to Figure 10.28, the stress of a wale can be examined as follows:

1 Stress computation in the direction of strong axis: Viewing the wale between two anchors as a simply supported beam structure, the maximum bending moment and shear are

$$M_{\max} = \frac{1}{8} p L_1^2 \tag{10.60}$$

$$Q_{\max} = \frac{1}{2} p L_1 \tag{10.61}$$

where

M_{max} = maximum bending moment in the direction of strong axis
Q_{max} = maximum shear in the direction of strong axis
p = lateral earth pressure on the wale
L_1 = horizontal distance between anchors.

As in the design of a wale in the braced excavation introduced in Section 10.5.3, if the joint is placed at the distance of one-fourth of the span from the support, the maximum bending moment can be computed by the following equation:

$$M_{max} = \frac{1}{10} pL^2. \tag{10.62}$$

The bending stress and shear stress of the wale in the direction of the strong axis should satisfy the following criteria:

$$\sigma = \frac{M_{max}/2}{S_x} \leq \sigma_a \tag{10.63}$$

$$\tau = \frac{Q_{max}/2}{A_w} \leq \tau_a \tag{10.64}$$

where

S_x = section modulus of the member in the direction of the strong axis
A_w = area of the web of the member
σ_a = allowable bending stress of the member = $(0.6 \sim 0.66)F_y \cdot \lambda$
τ_a = allowable shear stress of the member= $0.4F_y \cdot \lambda$
F_y = yielding stress of the member
λ = short-term magnified factor of the allowable stress, which can be found in country building codes.

2 *Stress computation in the direction of the weak axis*: As shown in Figure 10.28, viewing the wale between the brackets supporting the anchor as a beam, the maximum bending moment and shear of the wale are

$$P_v = pL_1 \tan\theta \tag{10.65}$$

$$M_{max} = \frac{1}{4} P_v L_2 = \frac{1}{4} pL_1 L_2 \tan\theta \tag{10.66}$$

$$Q_{max} = \frac{1}{2} P_v = \frac{1}{2} pL_1 \tan\theta \tag{10.67}$$

where

M_{max} = maximum bending moment in the direction of weak axis
Q_{max} = maximum shear in the direction of weak axis
P_v = vertical component of the anchorage force at the support
L_2 = distance between the brackets supporting the anchor.

The bending stress and shear stress of the wale in the direction of the weak axis should satisfy the following conditions

$$\sigma = \frac{M_{max}/2}{S_y} \leq \sigma_a \tag{10.68}$$

$$\tau = \frac{Q_{max}/2}{A_f} \leq \tau_a \tag{10.69}$$

where

S_y = section modulus of the member in the direction of weak axis
A_f = area of a single flange of the member
σ_a = allowable bending stress of the member = $0.75F_y \cdot \lambda$
τ_a = allowable shear stress of the member = $0.4F_y \cdot \lambda$
F_y = yielding stress of the member
λ = short-term magnified factor of the allowable stress, which can be found in country building codes.

Diaphragm walls have high stiffness and do not necessarily need wales. Only the reinforcement of the diaphragm wall at anchor supports has to be examined. The wale can be regarded as inside the diaphragm in design as shown in Figure 10.29.

10.7.5 Design of the free section

The free section is composed of a tendon and a plastic casing. Three types of tendons are available: steel bars, steel wires, and strands. The seven-wire strand is common in many countries, usually available in sizes of 13 mm (0.5 in), 15 mm (0.6 in), and 18 mm (0.7 in). The ultimate tensile strength varies from 1570 to 1765 N/mm^2. The allowable tensile force can be computed as follows:

$$P_w = P_u/F_t \tag{10.70}$$

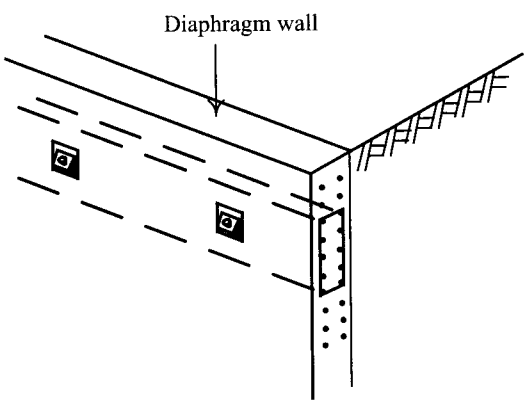

Figure 10.29 Wales located inside the diaphragm wall.

Table 10.4 Factor of safety for single anchor (CICHE, 1998)

Classification	*Tensile force of tendons (F_t)*	*Anchoring force (F_a)*	*Bond force of tendons (F_b)*
Temporary anchors whose working period is not longer than 6 months and which do not affect public safety when failing[1]	1.4	2.0	2.0
Temporary anchors whose working period is not longer than 2 years and which do not affect public safety, though having certain influence, when failing without alert	1.6	2.5[2]	2.5[2]
Permanent or temporary anchors which are highly risky in rusting or which affect public safety seriously due to failure[1]	2.0	3.0[3]	3.0[2]

Source: The table is from CICHE (1998), incorporating specifications made by BSI (1989) and FIP (1982).

Notes
1 The temporary anchors in this table refer to those whose working periods are not longer than 2 years. Otherwise, they are classified as permanent anchors.
2 With complete proving test results, the minimum factor of safety can be 2.
3 If creep of soil is to be encountered, the factor of safety can be increased to 4.

where F_t = designed safety factor for the tendon. Table 10.4 lists the commonly used factors of safety, P_u = ultimate tensile force.

The number of tendons is

$$n = \frac{T_w}{P_w}. \tag{10.71}$$

As discussed above, T_w is computed using Eq. 10.59, transforming the horizontal component, as analyzed using the apparent earth pressure method, the beam on elastic foundation method, or the finite element method.

As Figures 10.24 and 10.25 illustrate, the free section has to extend beyond the potential failure zone by at least 2 m. If the free section is too short, the stresses in soils caused by the fixed section will easily affect the retaining wall. In addition, the anchor behavior will tend to be fragile, any small displacement possibly bringing about large stress, and threatening the security of the anchor. Therefore, the free section has to be at least 4 m long.

10.7.6 Design of the fixed section

The fixed section of an anchor should be placed 2 m away from the potential failure zone. The design of a fixed section includes the bond forces between tendons and grouts and the anchorage force between the fixed section and soils.

The bond forces between tendons and grout have to be large enough so that the designed strength of the anchor can fully develop. Table 10.4 suggests the safety factors between tendons and grout. As for the allowable bond forces between tendons and cement grout, we can use the values as suggested by JSF (1990), as shown in Table 10.5.

The anchorage force between the fixed section and soils is introduced, as follows, in terms of the friction type of anchor and the underreamed anchor.

Table 10.5 Allowable bond force of tendons in cement mortar (JSF, 1990)

Types of tendons	*Designed compressive strength of cement mortar* (kg/cm^2)				
	150	*180*	*240*	*300*	*>400*
Temporary anchors					
Steel wire	8	10	12	13.5	15
Round steel bar	8	10	12	13.5	15
Steel strand	8	10	12	13.5	15
Multiple steel strand	8	10	12	13.5	15
Permanent anchors					
Steel wire	—	—	8	9	10
Round steel bar	—	—	8	9	10
Steel strand	—	—	8	9	10
Multiple steel strand	—	—	8	9	10

10.7.6.1 Friction type of anchor

The ultimate anchorage force, T_u, for a friction type of anchor can be computed by the following equation:

$$T_u = \pi d_b L_a \tau_{ult} \tag{10.72}$$

where

T_u = ultimate anchorage force
d_b = diameter of the fixed section
L_a = length of the fixed section
τ_{ult} = average ultimate shear resistance strength per unit area (also called the frictional strength) between the fixed section and soils.

The designed load on the anchor is

$$T_w = \frac{T_u}{F_a} \tag{10.73}$$

where F_a = safety factor of the designed anchorage force; the commonly used factors of safety are listed in Table 10.4.

The strength between the fixed section and the surrounding soil, τ_{ult}, changes with the types of soils where the fixed section is placed, the failure mode of the fixed section, the grouting pressure, and the installation method. Many investigators have proposed some empirical formulas to estimate τ_{ult}. Given the complexity of the computing of τ_{ult}, this section lists the commonly used methods for readers' reference, incorporating the related specifications and some investigators' research results.

1 Anchorage in rocks: Null pressurized anchors are often used for rocks (see Figure 10.22). Littlejohn's suggestion (1970) is usually taken for the ultimate shear resistance strength between the fixed section and rocks. That is, let τ_{ult} be $0.1q_u$ (for block rocks) or $0.25q_u$ (for

Table 10.6 Ultimate frictional strength of an anchorage body (JSF, 1990)

Type of soil	τ_{ult} (kg/cm^2)
Rock	
Hard rock	15–25
Soft rock	10–15
Weathered rock	6–10
Mudstone	6–12
Gravel	
$N = 10$	1.0–2.0
$N = 20$	1.7–2.5
$N = 30$	2.5–3.5
$N = 40$	3.5–4.5
$N = 50$	4.5–7.0
Sand	
$N = 10$	1.0–1.4
$N = 20$	1.8–2.2
$N = 30$	2.3–2.7
$N = 40$	2.9–3.5
$N = 50$	3.0–4.0
Clay	1.0c

Note
N is standard penetration test number, c is cohesion, and τ_{ult} is ultimate frictional strength after pressure grouting.

weathered rocks) where q_u is the axial compressive strength of rock. Another choice is to adopt the suggestions by JSF (1990), as shown in Table 10.6.

2 *Anchorage in sandy soils*: The τ_{ult}-value of an anchor in sandy soils can be computed as follows:

$$\tau_{ult} = \sigma_v' \tan \delta \tag{10.74}$$

where σ_v' is the average effective overburden pressure above the fixed section and δ is the angle of friction between the fixed section and soils.

Because anchors in sandy soils are usually the low pressure type (see Figure 10.22), the average ultimate shear strength of sand is usually determined on the basis of experience or field tests. Therefore, JSF (1990) suggests that the ultimate shear strength of a fixed section in sand (see Table 10.6).

The ultimate shear resistance strength of the fixed section of a high pressure type of anchor in sandy soils is difficult to estimate. Therefore, it is often estimated by way of empirical formulas and then examined through field tests (Section 10.8).

3 *Anchorage in clayey soils*: Anchors in clays are usually installed following the null pressurized grouting method (see Figure 10.22). The ultimate shear resistance strength of the fixed section in clayey soils can be expressed as follows:

$$\tau_{ult} = \alpha s_u \tag{10.75}$$

Table 10.7 Specifications for the length of the fixed section (CICHE, 1998)

Specifications	*Minimum suggested distance*
FIP (1982) and BSI (1989)	No shorter than 3 m, except if the proving test result is satisfactory in fulfilling the design, and not longer than 10 m, under normal condition
PTI (1980)	No shorter than 3 m
JSF (1990)	Between 3 and 10 m
GCO (1989)	No shorter than 3 m
AASHTO (1992)	In soil, no shorter than 4.6 m; in rock, 3 m

where s_u = undrained shear strength of clay, α = reduction factor for undrained shear strength the value of the reduction factor relates to the undrained shear strength and can be obtained from Figure 4.12. Theoretically, the anchorage force in clayey soils can be computed using the above equation. With the low strength of normally consolidated or lightly overconsolidated clay, placing a fixed section should be avoided in such soils for lack of friction under normal conditions. If such a placement is necessary, underreamed anchors are recommended.

As Eq. 10.72 shows, the longer the fixed section, the larger the anchorage force. However, many investigators have found that when the length of the fixed section exceeds some critical value, more lengthening of the fixed section can hardly increase its anchorage force. Thus, the length of the fixed section has to be limited. In principle, the length of the fixed section is best when between 3 and 10 m. If out of this range, it is better to carry out field tests to examine the ultimate anchorage force. Table 10.7 lists specifications on the minimum and maximum lengths of the fixed section.

10.7.6.2 Underreamed anchors

Theoretically, the anchorage force of an underreamed anchor can also be inferred according to the theory of bearing capacity of soil. However, because of the complexity of the installation of an underreamed anchor, the actual anchorage force is usually far from the inferred result. As such, the anchorage force of an underreamed anchor is usually obtained from field tests, which will be introduced in Section 10.8.

10.7.7 Preloading

The anchor installed, it usually needs to be preloaded and locked, which is called locked preloading or the locked load. The locked load is usually a little larger than the designed load of the anchor because the slipping of the wedge clips during the process of locking will cause some loss of the anchor preload. After locking, the remaining force is called the effective load. Both the tendons and fixed section are loaded after preloading the anchor. The displacement of the fixed section is not large at the initial stage of preloading (sometimes even after preloading) and thus the preload mainly acts on the tendons, which deform accordingly and in a heavily stressed state.

10.7.8 Design of retaining walls

The stress analysis of an anchored wall can use the assumed support method, the beam on elastic foundation method, or the finite element method, which are all identical for analysis of braced excavation. Because of the installation angle of the anchor, however, a downward dragging force will be produced on the retaining wall. Thus, we have to examine whether the vertical bearing capacity of the wall is larger than the total downward dragging force of each of the levels of anchors. The vertical bearing capacity of the wall equals the sum of point bearing capacity of the wall bottom and the frictional resistance of the wall surface. The computing is similar to that of foundation piles. We can also use Eqs 10.52–10.57 directly.

10.8 Tests of anchors

Influenced by the process of fabrication, grouting, and geological conditions, the actual ultimate load of an anchor has to be examined through field tests. The tests are classified into many methods in terms of their different aims, though their common goal is to understand the deformation behaviors and load capacities of the anchor.

In engineering circles, anchor tests can be distinguished into the proving test, the suitability test, and the acceptance test. The major international specifications (FIP, 1982; DIN, 1988; BSI, 1989; CICHE, 1998) for the three types of tests are not identical, but are all based on similar principles. This section will not discuss the differences among them but explicate the objectives and procedures according to the specification of FIP.

10.8.1 Proving test

The proving test is also called the precontract test. The aim of the test is to understand the feasibility of installing anchors in the soils in a certain area. The objectives of proving tests usually include the understanding of the soil properties, the anchorage properties, and the installation characteristics. Especially when it is conducted in areas where no anchors have been used or to test the length of special types of fixed sections or types of anchors, the proving test is especially important. The items in a proving test include examinations of the anchor stand, the anchor head, the jack, the anti-erosion measures, the manufacture of the fixed section, the grouting procedure, the anchor installation, the length of the anchorage, the anchoring capacity, and the creep properties, etc. As listed above, a proving test should include, as much detail as possible, every condition that may be encountered in the field, so that the engineer is able to judge the reliability of the anchor system and its installation.

The procedure of a proving test suggested by FIP (1982) is as follows:

1 As shown in Figure 10.30, add an initial load of 0.1–$0.2P_p$, P_p representing the maximum test load, onto the anchor to eliminate the bad contact at the initial stage of the test. The value of P_p is controlled at below 90% of the yielding strength of the tendon or 80% of its ultimate tensile force.
2 Add the load increment (ΔP), which equals 1/6 to 1/10 of ($P_p - P_i$). After loading for certain durations Δt and $n\Delta t$, record the deformations in relation to loads. n can be 1 or 10. The relations between Δt and loads are suggested as listed in Table 10.8.
3 Unload the anchor to P_i, measure its elastic deformation ΔL_{el} and permanent deformation ΔL_{pl}.

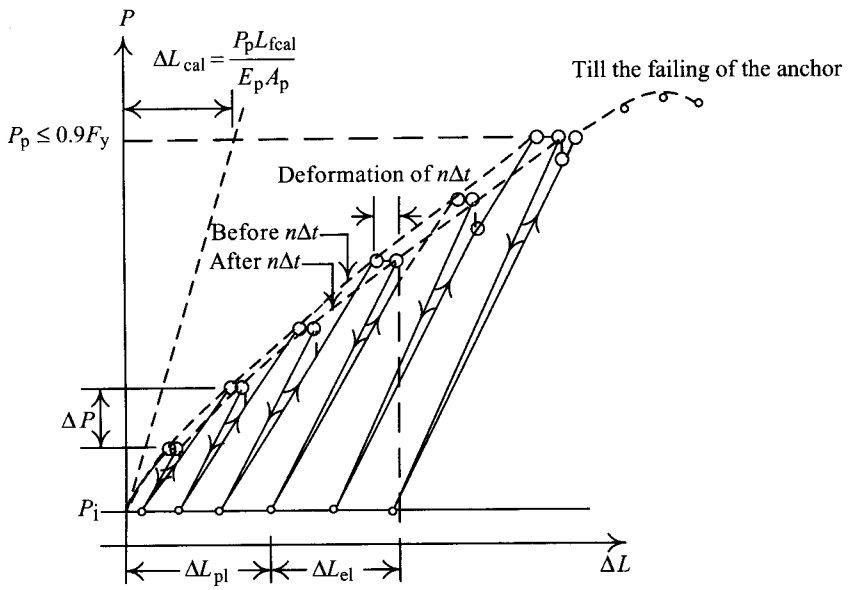

Figure 10.30 Procedure of an anchor proving test.

Table 10.8 Pressure keeping time at the loading stage (FIP, 1982)

Pressure keeping time at each stage	Δt (min.)
Rocks and cohesionless soils	>5
Lightly clayey soils and overconsolidated soils	>15
Normally consolidated soils and clayey silts	>180

4 Keep adding the load increments ΔP and repeat steps (2) and (3).
5 After achieving the maximum test load, keep loading the anchor at a certain rate till the anchor system totally fails. Take out the whole anchor and inspect the shape of the anchorage body, the length of the free section, the failing conditions of the fixed section, and especially the grouting and anti-erosion device surrounding the tendon.

The testing finished, plot the load-deformation relationship for Δt and $n\Delta t$, respectively, as shown in Figure 10.31. The intersection point of the two tangent lines in the figure is then the limit of load P_{lim}. Since the P_{lim} value derived from the $10\Delta t$ curve is smaller than that from the Δt curve, the smaller P_{lim} is usually used in design. The designed load of an anchor cannot be larger than either the result of Eq. 10.73 or $0.9P_{lim}$.

The installation or grouting of an anchor finished, the free section of the anchor has to maintain the designed length lest too much grout may obstruct the free section and cause insufficient length of the free section. The result of a proving test can be used to infer the effective length of the free section $L_{f,eff}$ and the permanent deformation ΔL_{pl}. According to

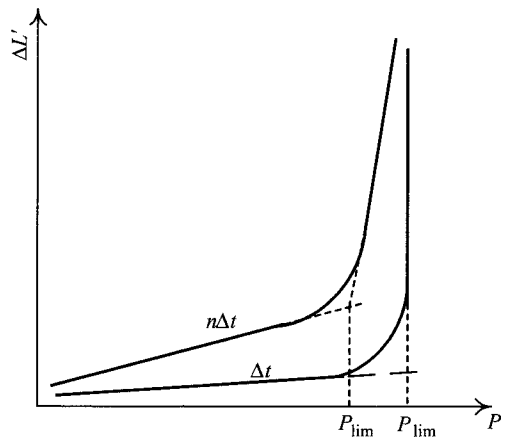

Figure 10.31 Relation between load and deformation with respect to Δt and $n\Delta t$.

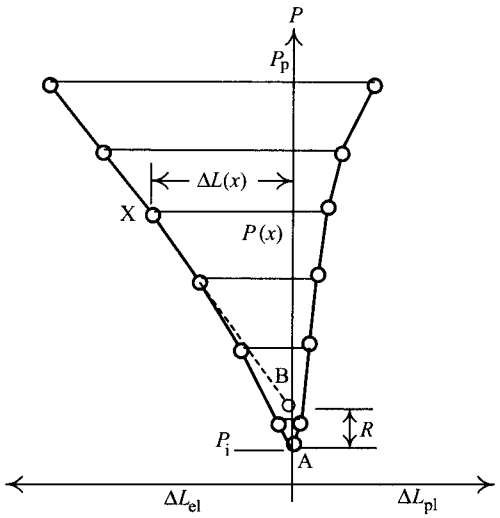

Figure 10.32 Elastic and permanent deformations (redrawn after Ou, 1986).

FIP's suggestion (1982) (see Figure 10.32), $L_{f,eff}$ can be computed by the following equation:

$$L_{f,eff} = \frac{\Delta L_{el}(x) A_p E_p}{P(x) - P_i - R} \tag{10.76}$$

where

ΔL_{el} = elastic deformation under the load of $P(x)$
A_p = total sectional area of tendons
E_p = Young's modulus of tendons (usually assumed to be 2100 t/cm^2)
P_i = initial load
R = resistance caused by friction, as shown by line segment AB in Figure 10.32.

In Eq. 10.76, $\Delta L_{el}(x)/[P(x) - P_i - R]$ represents the slope of line segment BX. Within P_{lim}, $L_{f,eff}$ should fall within the following range:

$$0.9L_{f,cal} \leq L_{f,eff} \leq L_{f,cal} + k \cdot L_{a,cal} \tag{10.77}$$

where

$L_{f,cal}$ = designed length of the free section
$L_{a,cal}$ = designed length of the fixed section
k = the reduction factor for the fixed section. $k = 0.5$, the tendon is fixed in cement grout by bond force (tension type of anchor); $k = 1$, it is fixed at the bottom of the cement grout by a mechanical method (compression type of anchor). The schematic diagrams of both the tension types of anchors and compression types of anchors are shown in Figure 10.21.

The lower limit of Eq. 10.77 is for preventing grout from leaking into the free section during the process of grouting the fixed section, which may reduce the length of the free section. The setting of the upper limit is to consider the conditions of the lengthening of the free section, for example, when grouting is slightly insufficient but the pulling force is large enough, or when cement separates from the tendon, causing the increase of effective free section (Liao and Ou, 1988).

10.8.2 Suitability test

The design of anchorage force is based on theoretical analysis and thereby all anchored excavations need suitability tests. The conditions in a suitability test have to be consistent with those of future use. The aim of the test is to examine the designed load of the anchor, that is, to make sure that the anchor is capable of offering sufficient loading capacity. The results of the test are the basis of the criteria for the acceptance test during the construction of anchors. The method of conducting a suitability test is basically identical to that of a proving test except for the maximum testing load. Generally speaking, in a suitability test, the maximum testing load of a permanent anchor is taken to be 1.5 times the designed load and that of a temporary anchor 1.2 times. Neither should exceed 80% of the ultimate tensile force or 90% of the yielding strength of tendons.

10.8.3 Acceptance test

The aim of an acceptance test is to examine the quality of the anchors while working. All anchors should be examined with acceptance tests. The acceptance test not only tests the anchorage capacity of an anchor but requires the deformation and the length of the free section to be close to the results of the suitability test. To shorten the testing time, the repeated loading and unloading process of a suitability test is skipped. The procedure for an acceptance test is as follows:

1 Add an initial load, whose value is about 1/10 of the maximum testing load, that is, $P_i = 0.1P_p$ and measure the deformation of the anchor. P_p is the maximum testing load, which is the same as in the suitability test.

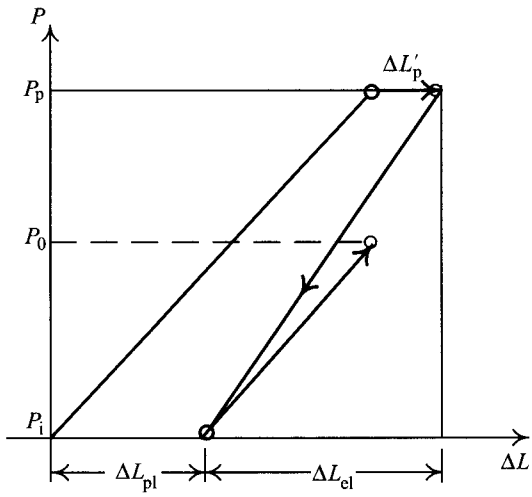

Figure 10.33 Procedure of an anchor acceptance test (redrawn after FIP, 1982).

2 Increase the anchor load to P_p and record the increment of deformation, ΔL, with respect to the change from P_i to P_p. Keep P_p within the time duration, $n\Delta t$, and record its increment of deformation, ΔL_{pl}, again.
3 Unload the anchor to P_i and record ΔL_{pl}.
4 Increase the load to the locked load, P_0, and then lock the anchor right away. The locked load is usually a little larger than the designed load because the slipping of the wedge clips during the process of locking will cause some loss of the anchor preload, as shown in Figure 10.33.

10.9 Summary and general comments

This chapter introduces the analyses and designs of structural components to be used in braced excavations and anchored excavations. The structural components introduced in this chapter include retaining walls, struts, end braces, corner braces, center posts, wales, and parts of anchor systems. The disciplines involved in these analyses and designs include soil mechanics, foundation engineering, reinforced concrete design, and steel structure design. The strength design method (or the LRFD method) and the working stress method (or the allowable stress method) are the two common design methods for the related structures. Viewed from the perspective of design reasonability, the strength design method or the LRFD method is usually a better choice. Considering the design habits of engineers in some countries, however, this chapter introduces the strength design method for the design of column piles and diaphragm walls but uses the allowable stress method for the design of soldier piles, sheet piles, and strutting systems. In fact, many practicing engineers have confirmed that the design results of the strength design method for column piles and diaphragm walls are simultaneously economical and secure, and those of the allowable stress method for soldier piles, sheet piles, and strutting system are able to provide excavation safety.

Though there are many excavation methods, the principles of design and analysis are similar. The methods introduced in this chapter, though not all encompassing, can be applied to other excavation methods with some modifications.

The contents of this chapter can be summarized as follows:

1 Soldier piles and sheet piles must be designed based on the maximum bending moment and shear. For detailing of reinforcements, column piles and diaphragm walls have to be designed based on the envelopes of bending moment and shear diagrams of each excavation stage obtained from analysis using the assumed support method, the beam on elastic foundation method, or the finite element method. The design of diaphragm walls is identical to that of general reinforced concrete and can refer to the ACI code or other related codes. Due to the convenience of hanging reinforcement cages into trenches, shear reinforcements are usually welded to the vertical main reinforcement. Not conforming to the ACI Code, welding will prevent the shear reinforcement from developing its full strength as predicted. This chapter offers feasible suggestions to consider this question reasonably in the design of shear reinforcements.
2 A strutting system includes struts, end braces, corner braces, wales, and center posts. The analysis of the load on struts is introduced in Chapters 6–8. This chapter introduces their stress analysis and design details. The basic design methods all conform to the AISC Specification.
3 The design of an anchor system includes the design of a free section and a fixed section, the arrangement of anchors, the design of wales, the design of the anchor stand, etc. The load analysis of anchors is the same as that of struts except that the derived horizontal load has to be transformed into the anchor load since the latter is installed into soils with an angle. Considering the installation quality, the location of the fixed section, and the bearing capacity of the retaining wall, the installation angle of an anchor is usually set between 10° and 45°. This chapter also offers the basic designing methods for the free section and the fixed section and the methods to infer the ultimate anchorage force. In fact, the anchorage force relates closely to the installation method, the geological conditions, and the configuration of the fixed section. The determination of the anchorage force still remains to be studied.
4 Affected by the field assemblage of components, the grouting process, and variations in soils, the actual ultimate load of an anchor provided by soils is not necessarily the same as that inferred from theoretical or empirical estimation. Therefore, the estimated result has to be examined through in situ tests. Anchor tests are basically classified into the proving test, the suitability test, and the acceptance test. The major specifications for these three types of tests are basically the same in principle, except for some details. Many investigators have discussed their similarities and differences. When designing and building in practice, it is recommended to consult related literature and case histories.

Problems

10.1 Figure P10.1 illustrates a 3.2 m deep excavation. The retaining wall is cantilever H piles arranged with a span of 1.5 m. The dimensions of the H piles are H300 × 300 × 10 × 15 (properties, see Appendix C) and the embedment depth is 5 m. The laggings are 4.2 m thick. Examine the safety of the retaining wall and laggings

(Note: the stress of a cantilevered retaining wall can be computed using a computer program or the methods introduced in Chapter 6).

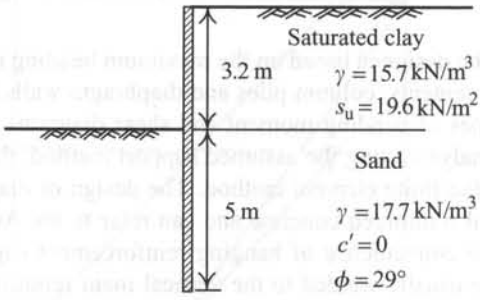

Figure P10.1

10.2 Here is an excavation site which is 30 m wide and 50 m long. The braced excavation method is adopted. The final excavation depth is 9.5 m. Figure P10.2 illustrates the depths for the excavation stages and the locations of the struts and floor slabs. The groundwater level is rather deep. The properties of soils at the site are $c' = 0$,

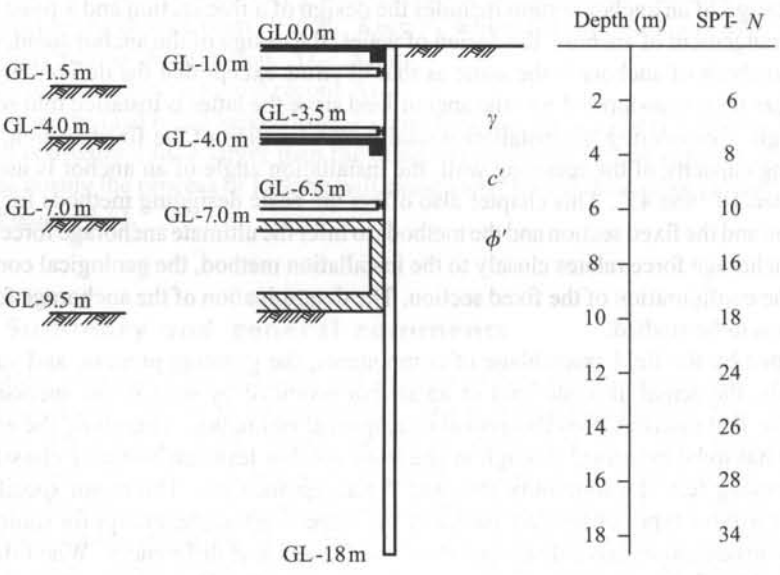

Figure P10.2

$\phi' = 28°$, and $\gamma = 21.6\,kN/m^3$. If soldier piles (H piles) are adopted as the retaining wall, determine suitable dimensions and distances of the soldier piles, based on the bending moment and shear diagrams obtained from the results of the finite element method or the beam on elastic foundation method, which simulate each excavation stage as well as basement construction stages, including strut dismantling and floor slab construction stages. (The dimensions of the piles and struts and distances

between the piles have to be first assumed to compute the stiffness of the retaining wall and the struts, which are then used for analysis. After analysis, suitable dimensions of the retaining wall and struts can be selected. If necessary, analyze again.)

10.3 Same as Problem 10.2, except sheet piles are adopted this time as the retaining wall. Select suitable sheet piles.

10.4 Same as Problem 10.2, except PIP piles are adopted this time as the retaining wall. Select suitable dimensions of the PIP piles and design the reinforcements.

10.5 Same as Problem 10.2, except the all casing pile is adopted this time as the retaining wall. Select suitable dimensions of the cased piles and design the reinforcements.

10.6 Same as Problem 10.2, except a 50 cm thick diaphragm wall is adopted this time as the retaining wall. Design the reinforcements according to the bending moment and shear diagrams of the wall generated by excavation.

10.7 Same as above, suppose the retaining wall is to be the outer wall of the basement, that is, the permanent earth pressure and earthquake force on the basement are to be considered. Design the reinforcements (the reinforcement design during the excavation process included).

10.8 Same as Problem 10.2. Design the horizontal struts and center posts (the apparent earth pressure method or the beam on elastic foundation method can be used to compute the strut load).

10.9 Same as Problem 10.2. If the strutting system is an anchor system, the location of the anchor stand is the same as that of the horizontal strut in Problem10.2 and the installation angle of the anchor being 30°, compute the working load of the anchor per unit width.

10.10 Same as Problem 10.9. Suppose the tendons of the free section are made of steel strands and the fixed section is of the friction resistance type. Design the number of steel strands and the lengths of the free and fixed section.

10.11 Same as above. Design the wales and examine the diaphragm wall safety generated by the downward dragging force from the anchor.

10.12 Elucidate the proving test, suitability test, and the acceptance test.

10.13 As in Example 7.2 and Figure 7.22, suppose there exists an excavation which is 40 m wide and 50 m long. The retaining strutting system is the diaphragm wall and steel struts. Analyze the strut load using the apparent earth pressure method or beam on elastic foundation method and design the struts.

10.14 Same as above, according to the analysis results, select the suitable thickness of the diaphragm wall and design the reinforcements.

10.15 As in Problem 10.13, if the strutting system is the anchor instead, whose anchor stands are located at the same depths as the horizontal strut in Figure 7.22 and whose installation angle is 30°, compute the strut load using the apparent earth pressure method or the beam on elastic foundation method.

10.16 As above, suppose the tendon of the free section is steel strands and the fixed section is the friction resistance type. Design the number of steel strands and the lengths of the free section and the fixed section.

10.17 Same as above, design the wales and examine the diaphragm wall safety generated by the downward dragging force from the anchor.

Chapter 11

Excavation and protection of adjacent buildings

11.1 Introduction

In the past, with shallower excavations, the influence of excavation on the surrounding environment was not great. Recently, with the increase of excavation depth and scale in urban areas, the magnitude and extent of ground settlement increases, which frequently damages the adjacent buildings.

Generally speaking, the protection of adjacent buildings during excavation can be divided into the following three procedures: (a) before-excavation plan (b) monitoring and prevention during the construction, and (c) compensation after damages have been done. The most important job in a before-excavation plan is a comprehensive geological investigation, on the basis of which is carried out the analysis and design. Although a thorough geological investigation and advanced analytical techniques may incur some extra costs, compared with the total construction cost, they do not amount to a significant increment. Helping engineers have better control of excavation conditions, they actually save costs as a whole.

Second, to have a good relationship with the owners of the adjacent buildings is also necessary in case damages do occur. Before excavation, the buildings within the influence range of excavation have to be properly evaluated. For example, if there exist cracks before excavation, they have to be measured and recorded or photoed to forestall dispute. As for the determination of the settlement influence range, please refer to the empirical formulas introduced in Section 6.4.2 in this book or solve it by way of finite element analysis. For predictable but unavoidable damages, cracks in brick or old houses induced by the construction of retaining walls or by excavation for example, risk management and construction damage insurance are important. Lastly, construction safety should be strictly maintained and the concepts of environmental protection should be fully apprehended.

Monitoring systems should be implemented in the vicinity of excavations. The monitoring items have to be carefully chosen and the monitoring results should be reasonably explained. The phenomenon of bottom heaving should be monitored in excavations in clayey soils. The other items to be monitored are the deformation of the retaining wall and the ground surface. If excavation is carried out in sandy soils, leakage through the retaining wall should be carefully watched. Emergency measures should be prepared in advance against any possible disaster or damage.

Once damage has occurred, in addition to adopting proper measures to prevent it from expanding, the contractor, in sincerity, should try to solve the problem. The causes of damage are not necessarily construction flaws. Damage may arise from design mistakes. Thus, a just and professional third party should be invited to determine the responsibility and compensation.

This chapter is confined to the protection of adjacent buildings by means of design and during construction. As for non-technical topics such as compensation and failure evaluation, please refer to related documents.

11.2 Allowable settlement of buildings

11.2.1 Allowable settlement under the building weight

Settlement will occur under the weight of a building. Too much settlement will cause the components of a building, such as beams, columns, walls, and foundations, to crack or be damaged. The amount of settlement relates to the type, area, and materials of the building, the soil properties, and the type of the foundation. The mechanism of settlement-induced damage is rather complicated and related studies are still insufficient. The following is a synthesis of results from previous studies (Polshin and Tokar, 1957; Skempton and McDonald, 1957; Bjerrum, 1963; Burland and Wroth, 1974; Grant *et al.*, 1974; Burland *et al.*, 1977; Wahls, 1981; JSA, 1988; AIROC, 1989; Boscardin and Cording, 1989).

Figure 11.1 gives the definitions of various deformation parameters. Figure 11.1a is the condition of settlement of a building without rigid body rotation. Figure 11.1b is the condition of settlement of a building with rigid body rotation. Points A, B, C, and D are the points

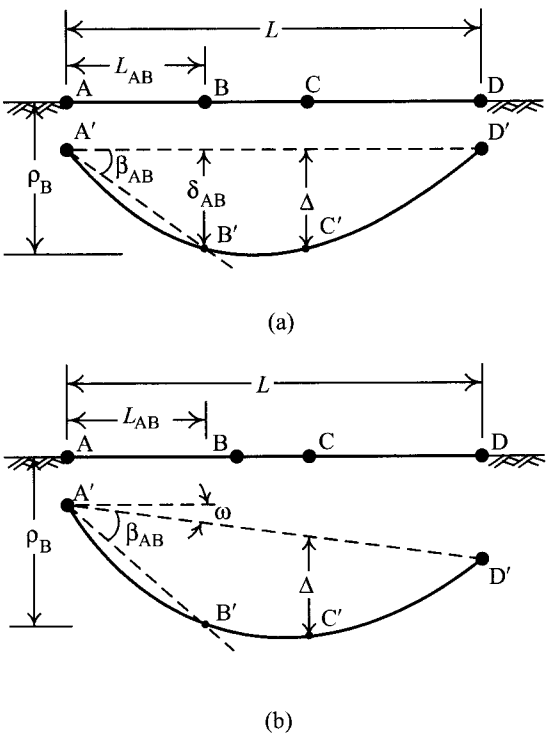

Figure 11.1 Parameters of settlements of buildings: (a) settlement without rigid rotation and (b) settlement with rigid rotation.

before settlement whereas A′, B′, C′, and D′ are those after settlement. The definitions of deformation parameters are given as follows (Wahls, 1981):

ρ_i = total settlement at point i
δ_{ij} = differential settlement between points i and j
ω = rigid body rotation
Δ = relative deflection
Δ/L = deflection ratio
$\beta_{ij} = \delta_{ij}/L_{ij} - \omega$ = angular distortion between point i and j
L_{ij} = distance between referent points i and j.

The tiltmeter (see Section 12.4.2 in Chapter 12) is a widely used instrument to measure the degree of tilt in engineering practice. The measured value is called the tilt angle, which is basically the sum of the angular distortion and the rigid body rotation. If the building is subject solely to rigid body rotation, its members will not distort or get deformed. Thus, the beams, columns, walls, and foundations will not crack either. However, it may cause some functional obstruction or visual anxiety. Since the influence of rigid body rotation has been excluded from the definitions of the angular distortion and the deflection ratio, the directly relevant parameters concerning member deformation or cracking are the differential settlement, the angular distortion, and the relative deflection (the deflection ratio).

Bjerrum (1963) proposed relations between the angular distortion and the damages of buildings as shown in Table 11.1, according to his observations and Skempton and McDonald's study (1957). Many investigators (Burland and Wroth, 1974; Grant *et al.*, 1974; Burland *et al.*, 1977; Boscardin and Cording, 1989) after him also carried out various studies on the allowable settlement of a building. Their study results are basically similar to Bjerrum's proposed values. Table 11.2 summarizes allowable angular distortion for RC frames and reinforced brick structures suggested by those researchers.

Since the degree of damage of a structural member relates to the degree of distortion of the member, that is, the bending moment or angular distortion of the member, Table 11.1 or 11.2 can apply to any RC framed buildings and reinforced brick structures on all kinds of soils as well as to those with individual footing or mat foundations.

The failure mode of a non-reinforced bearing wall (such as a brick wall), as shown in Figure 11.2, is different from that of an RC frame or a reinforced brick structure. Thus, its

Table 11.1 Limiting values of angular distortion (Bjerrum, 1963)

Angular distortion	*Type of damage*
1/750	Dangerous to machinery sensitive to settlement
1/600	Dangerous to frames with diagonals
1/500	Safe limit to assure no cracking of buildings (factor of safety included)
1/300	First cracking of panel walls (factor of safety not included)
1/300	Difficulties with overhead cranes
1/250	Tilting with high rigid buildings become visible
1/150	Considerable cracking of panel and brick walls
1/150	Danger of structural damage to general buildings
1/150	Safe limit for flexible brick walls (factor of safety not included)

Table 11.2 Allowable angular distortion for RC framed or reinforced brick structures

Angular distortion	*Behaviors of buildings*
1/500	Nonstructural damage (factor of safety included)
1/300	Nonstructural damage, such as cracks, occur on panel walls
1/150	Structural damage

Table 11.3 Allowable deflection ratio for non-strengthened non-reinforced brick structures (Burland and Wroth, 1974)

Type of deformation	*Allowable deflection ratio* (Δ/L)
Sagging	1/2,500 for $L/H = 1$ 1/1,250 for $L/H = 5$
Hogging	1/5,000 for $L/H = 1$ 1/2,500 for $L/H = 5$

Note
L and H represent the length and height of a building, respectively.

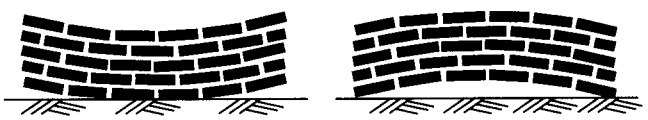

(a) (b)

Figure 11.2 Failure patterns of unreinforced load bearing walls: (a) sagging and (b) hogging.

allowable settlement is represented by the maximum deflection ratio. Table 11.3 lists the proposed values of allowable deflection ratios of non-reinforced brick structures by Burland and Wroth (1974). Similarly, the values are also applicable to all kinds of soils.

In addition to representing the allowable settlement with angular distortion, differential settlement and total settlement are often used to explore the allowable settlement of a building. Figure 11.3 shows the framed structure with individual footings in sandy soils. Assume the differential settlement between the two columns is δ_{ij} under the effect of building weight. If nonstructural damage is not generated, according to Table 11.1 or 11.2, the building would have to meet the following criterion

$$\frac{\delta_{ij}}{L_{ij}} \leq \frac{1}{300} \tag{11.1}$$

where L_{ij} is the distance between the two columns. δ_{ij} is the differential settlement between the two columns. In Europe and America, in most cases, the typical distance between two

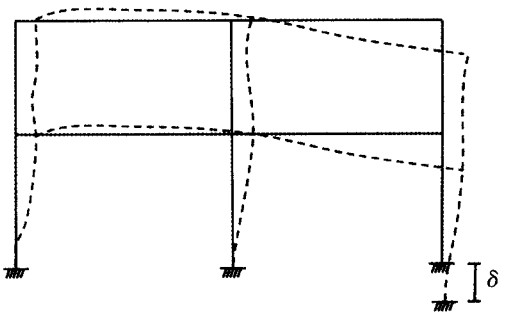

Figure 11.3 Differential settlement of a structure with individual footings.

columns is about 20 feet (6 m). Thus, the above equation can be rewritten as

$$\delta_{ij} \leq \left(\frac{1}{300}\right) \times 20 \text{ ft} \approx \frac{3}{4}\text{in} \approx 2.0 \text{ cm} \tag{11.2}$$

Since differential settlement is not easily measured, by experience, the differential settlement in sandy soils is about three-fourths of the total settlement (including the required safety factor). Then,

$$\rho_i \approx \frac{4}{3}\delta_{ij} \approx 1.0 \text{ in} = 2.5 \text{ cm} \tag{11.3}$$

This is how the allowable settlement of the individual foundations in sandy soils is assumed to be 2.5 cm is derived.

Settlement of buildings on clayey soils is usually more uniform. Thus, Eq. 11.3 is not applicable, though Eqs 11.1 and 11.2 are still valid. Therefore, it is necessary to derive the allowable settlement of buildings on clayey soils under the effect of building weight in terms of the total settlement.

Table 11.4 summarized the values of the allowable total settlement and the differential settlement proposed by some investigators and national professional societies (Skempton and McDonald, 1957; Terzaghi and Peck, 1967; Grant *et al.*, 1974; JSA, 1988; AIROC, 1989). The values listed in Table 11.4 are basically exclusively applicable to buildings with column distance of 6 m. For those with column distance longer or shorter than 6 m, Table 11.4 is not applicable for estimating their allowable settlements.

11.2.2 Excavation-induced allowable settlement

Settlement of buildings will occur as a result of excavation. However, buildings may have settled due to their own weight before excavation. How large the allowable settlement of a building should be, with the start of excavation, becomes a complicated problem. Nevertheless, studies on this subject are scant.

Theoretically, the allowable settlement of a building is constant. With the existing settlement caused by the weight of the building itself, the allowable settlement after excavation is started will not be large. The amounts should be smaller than those listed in Tables 11.1–11.4.

Table 11.4 Allowable settlement for RC structures (Yen and Chang, 1991)

Type of foundation	*Soil*	*Total settlement* (cm)	*Differential settlement* (cm)	*Note*
Individual footings	Sand	2.5	2.0	TP
		5.0	3.0	SM
		3.0	—	J
Individual footings	Clay	7.5	—	SM
		10.0	—	J,A
Mat foundation	Sand	5.0	2.0	TP
		5.0–7.5	3.0	SM
		6.0–8.0	—	J
		—	3.0	G
Mat foundation	Clay	7.5–12.5	4.5	SM
		20.0–30.0	—	J,A
		—	5.6	G

Notes
TP: Terzaghi and Peck (1967).
SM: Skempton and MacDonald (1957), corresponding to the angular distortion of 1/300.
J: JSA (1988).
A: AIROC (1989).
G: Grant *et al.* (1974), corresponding to the angular distortion of 1/300.

Nevertheless, some investigators believe that although the inherent weight of buildings has induced some settlement, the members of buildings will gradually conform to the settlement and adjust their loading capability over a long period of time. As a result, their allowable settlement will not be too small and should not be far from the proposed values listed in Tables 11.1–11.4.

What's more, according to Boscardin and Cording's study (1989), if lateral movement of a building has been produced, the allowable vertical settlement of the building will decrease. They also proposed the relationship between the degree of damage of a building and vertical settlement and lateral strain. Nevertheless, since extra parameters (the lateral strain), which are not easily obtained, are required when applying their study results to engineering practice, Boscardin and Carding's study results are not readily applicable.

Whether a member of a building will crack should relate to the bending moment on it, that is, angular distortion or relative deflection. The allowable values listed in Tables 11.1–11.3 are expressed in angular distortion or relative deflection. Therefore, although the mechanism of damage caused by excavation-induced settlement is different from that of damage caused by building weight-induced settlement, the values in Tables 11.1–11.3 are still applicable and useful for the evaluation of excavation influence on adjacent buildings.

According to the above elucidation and the analyses of actual measured settlement of 42 buildings located next to excavation sites in Taipei (Yen and Chang, 1991), the author suggests that for RC framed buildings with individual footings on all kinds of soils, the allowable total settlement and the allowable differential settlement should be in the range of 2.5–5 cm and 2–3 cm, respectively. As for the mat foundation, the angular distortion is recommended for use instead of total or differential settlement.

Please note that buildings with mat foundations are mostly high-rise and most mat foundations are quite thick. With the same thickness of mat foundation, the smaller the mat area,

Table 11.5 Allowable settlement of buildings recommended by TRTS

Type of foundation	*Maximum settlement* (mm)	*Tilt angle*	*Angular distortion*	*Deflection ratio*	
				Hogging	*Sagging*
RC raft foundation	45	1/500	1/500	0.0008	0.0012
RC individual footings	40	1/500	1/500	0.0006	0.0008
Brick individual footings	25	1/500	1/2500	0.0002	0.0004
Temporary buildings	40	1/500	1/500	0.0008	0.0012

Note
Tilt angles are the measurement value on the tiltmeter, whose principle and application are discussed in Section 12.4.2, Chapter 12.

the higher the stiffness. Under such a condition, the value measured by a tiltmeter is mostly rigid body rotation. Thus, with no significantly observable distortion of building frames or cracks on panel walls, a building can still be observed to be slanting (refer to Section 11.4.4). The higher the building, the more obvious the slant. Such slant is not only unacceptable for the residents, a slanted building is dubious in its earthquake resistance. In other words, the allowable tilt of a high rise building is to be evaluated from the relative degree of slant.

Table 11.5 lists the allowable settlement induced by excavation proposed by the Taipei Rapid Transit System (TRTS), according to its construction experience and many investigators' studies. Table 11.5 is valuable for reference since it sums up many years' experience of design and construction.

11.3 Introduction to soil improvement methods

The chemical grouting method, the deep mixing method, and the jet grouting method are the three main methods of soil improvement in excavations. Although they use different principles, all these methods are similar in their purpose, that is, the improvement of the soil shear strength or the decrease of the permeability of soil.

11.3.1 Chemical grouting method

The chemical grouting method is to inject the grouting material into soil strata by low pressure. With the condensation of the grouting material, the soils will be strengthened and the permeability and settlement be decreased. The grouting pressure for the chemical grouting method is usually lower than 20 kg/cm^2 and the method is, therefore, also called the low pressure grouting method. Figure 11.4 diagrams the implementation of the chemical grouting method (the single packer method in the example).

Various materials are used for grouting, depending on the purpose of grouting and the properties of rock and soil. Grouting materials are usually categorized into four major types on the basis of the flowing properties and major contents of the materials:

1 *Suspension type*: including cement, clay (or bentonite), or clay (or bentonite) mixed with cement.

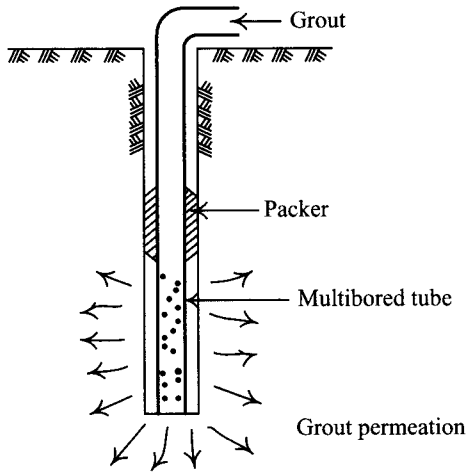

Figure 11.4 Schematic diagram of chemical grouting (Single packer method).

Table 11.6 Classification of waterglass solutions as grouting materials

Alkaline type	*Non-alkaline or neutral grouting materials*
Waterglass + acidic reagent (of which there are many to be chosen) Waterglass + metallic salt reagent (such as calcium chloride) Waterglass + alkaline reagent (sodium aluminate)	Waterglass + acidic reagent

2 *Waterglass solution type*: waterglass is a solution of sodium silicate. Adding some chemicals in waterglass brings about different grouting effects. Table 11.6 lists the general categories of the grouting materials for waterglass solution.
3 *Suspension and waterglass solution type*: mixtures of waterglass solution and other suspension materials, such as waterglass mixed with cement or waterglass mixed with fly ash and cement. The characteristics are a blend of the suspension type and the solution type.
4 *Polymer solution type*: polymer materials include the urea type, the acrylic type, the urethane type, and the lignin type. Generally, polymer materials have good effects. Nevertheless, most of them are highly poisonous and are forbidden for use.

If chemical grouting is used in pure sandy soils with a pressure lower than 10 kg/cm^2, the grout will permeate into the voids of the sand and achieve a good effect of soil improvement without destroying the soil structure. The method is then sometimes called permeation grouting. The solution type of grouting material is often adopted for this method.

For clayey soils, the permeation method is not applicable. A higher pressure (about 20 kg/cm^2) is usually needed to inject the grout into soils, which will produce many cracks. The phenomenon is called hydraulic fracturing. The grouting-induced hydraulic fracturing

Table 11.7 Grouting materials for different soils

Soil type	*Grouting material*
Clayey soils, including silt, clay and loam	• Cement suspension type • Waterglass suspension type • Non-alkaline waterglass suspension type
Sandy soils, including sand, silty sand, etc.	• Permeable solution type
Sand-gravel	• Suspension type (large voids) • Permeable solution type (small voids)
Seam	• Cement type • Suspension type

will form an arborescent structure, which acts like reinforced soil and is certainly useful to improve the strength of soils. The method, sometimes also called fracturing grouting, usually adopts the suspension type of grouting materials.

Table 11.7 lists the grouting materials for various soils, and serves as a reference for a preliminary plan of chemical grouting.

11.3.2 Jet grouting method

The jet grouting method implants a grouting pipe, with a jet, into the soil to a certain depth with the help of a boring machine and emits high pressure grout or water (about 20 MPa), pounding and cutting soils at the same time. When the pulsing current, at high pressure and speed, exceeds the strength of soils, the soil particles will be separated from the soil body. Some fine soil particles will flow with water or grout out of the ground while other soil particles will mix with the grout, under the influence of pounding, centrifugal force and gravity. The mixed soil particles will be rearranged into a grout-soil mixture. When the grout is congealed, it forms a solid body. Figure 11.5 shows a diagram of the sequence of jet grouting.

Some commonly used methods of jet grouting are the single tube method, the double tube method, and the triple tube method, as shown in Figure 11.6. The single tube method is to implant the boring rod with a special jet fixed on the side of the rod bottom with the help of the boring machine and emit pressurized grout (about 20 MPa) into soil to cut and destroy soil bodies. With the rotation and lift of the rod, the grout and the cut soils will be churned and mixed. After a certain period, the whole of the grout and soil will congeal and form a column. The method is often called the CCP (chemical churning pile) method.

As shown in Figure 11.6b, the configuration of the double tube is a coaxial double jet. The inner jet emits grouting materials at 20 MPa while the outer one pumps compressed air at 0.7 MPa. Under the double effect of jetting grout and the surrounding air pressure, the capability to destroy and cut soil is highly enhanced. With the rotational jetting and lift of the double jet, grouting materials and cut soils are churned and mixed and form a column-like solid body together. The diameter of the column formed with the double tube method is larger than that formed with the single tube method. The method is often called JSG (Jumbo Special Grouting) method, or JSP (Jumbo Special Pile) method.

The triple tube is a jet which emits water, air, and grouting materials simultaneously. As shown in Figure 11.6c, on the side of the bottom of the grouting pipe is attached a coaxial

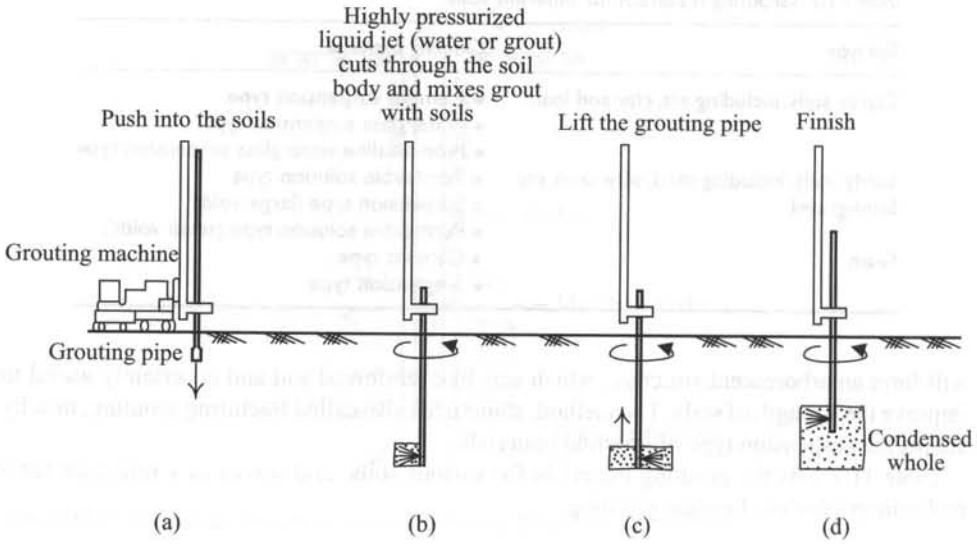

Figure 11.5 Procedure of the jet grouting method.

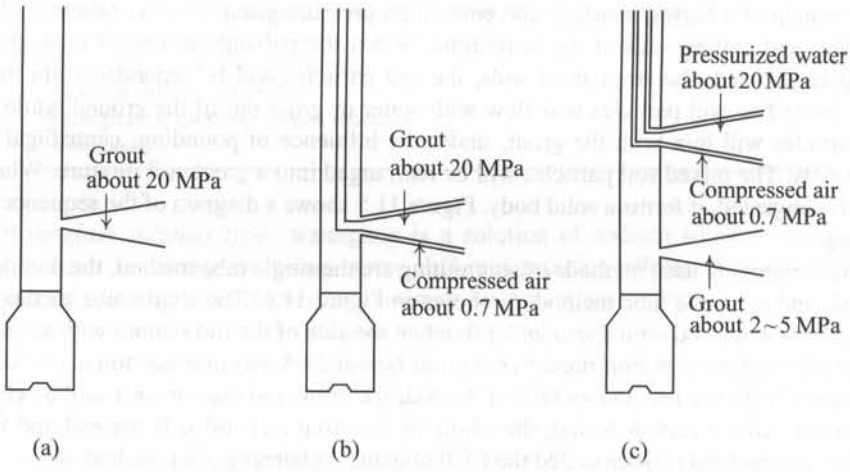

Figure 11.6 Types of the jet grouting method: (a) single tube method, (b) double tube method, and (c) triple tube method.

double jet, the inner one of which emits water at about 20 MPa while the outer one emits compressed air at about 0.7 MPa. Under the double contribution of high pressurized water and the surrounding air, the power of cutting and destroying soil bodies is greatly enhanced. Grouting materials of 2–5 MPa are emitted from another jet right below the double jet. With the rotation and lift of the jet, the grouting materials and the cut soils will be churned and mixed and form a column-like solid body. The diameter of the column formed with the triple

tube method is larger than that formed with the double tube method. The method is often called the CJG (Column Jet Grout) method.

The commonly used grouting materials for jet grouting are lime (calcium oxide or calcium hydroxide) and cement. Sometimes fine aggregate or fly ash is added. Besides, depending on the functions of the machine and the soil properties, fluid materials (such as cement mortar or cement grout) or dry materials (such as cement or lime powders) are employed.

11.3.3 Deep mixing method

The deep mixing method (DMM), installs mixing vanes connected to a hollow rod with the help of wash boring, which destroys soil bodies with the vanes and jets out grouting materials with certain pressure. The destroyed soil body and the grouting materials will be mixed up completely and form a solid column. Figure 11.7 diagrams the sequence of the implementation of the DMM.

Similar to the jet grouting method, the DMM adopts lime and cement for grouting materials. Besides, whether fluid materials such as cement mortar or cement grout, or dry materials such as cement or lime powders are to be adopted depends on the functions of the grouting machine and the soil properties.

11.3.4 Compaction grouting method

The compaction grouting method has been applied in property protection for more than 50 years. The method has the benefit of low cost and has been successful in many cases.

The compaction grouting method injects pressurized cement mortar with high consistency, low slump, and low plasticity into soils. The cement mortar does not easily flow into the voids of soils and will therefore form a grouting bulb, which will in turn make an interface with the soils around. Squeezing the cement mortar into soils continuously, the grouting bulb will expand and press the soils around to compact them. Besides, the grouting bulb expands in radiation though faster in lateral direction (because the lateral stress of soils is smaller

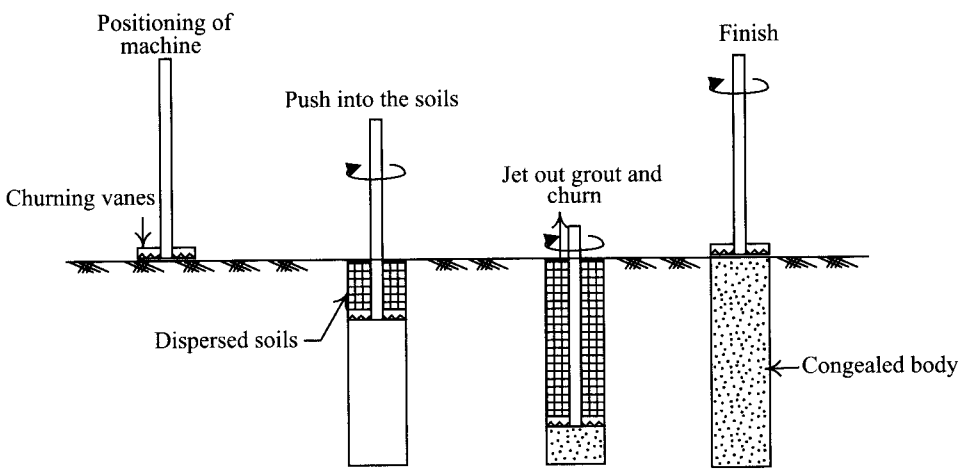

Figure 11.7 Procedure of the deep mixing method.

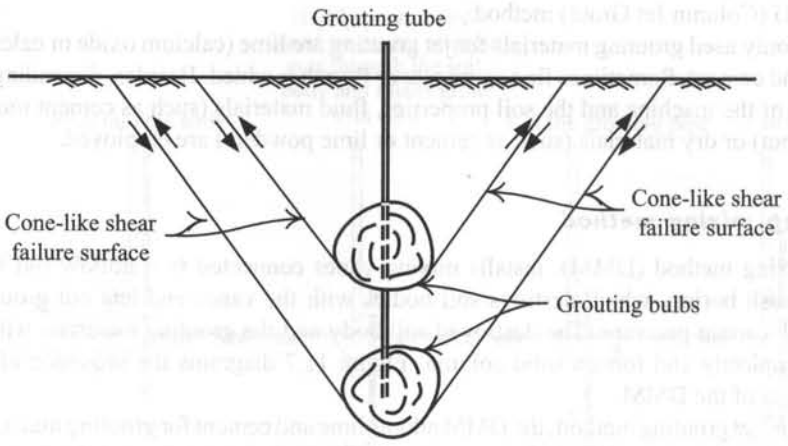

Figure 11.8 Compaction grouting method.

than the vertical stress). When the soils are compacted to a certain degree, nevertheless, the expansion in the lateral direction will stop. Instead, the grouting bulbs begin to expand upward and generate an upheaving force, which will make a cone-shaped shear zone above. When the upheaving force exceeds the weight of overburden or the building, the phenomenon of ground surface heave or building upheaval will occur as shown in Figure 11.8.

The materials used in the compaction grouting method have to be designed to achieve high consistency, low slump, and low plasticity. Otherwise, they may flow into the voids of soils. On the other hand, they have to have a certain fluidity to be well transported. Sand mortar and cement mortar are two widely used grouting materials. Fly ash and bentonite are widely adopted additives.

Drawing from the above elucidation, compaction grouting can make soils in the vicinity of injection points compact and improve them as a result. It can also uplift a building to restore it from over-settlement.

11.4 Building protection using the characteristics of excavation-induced deformation

11.4.1 Reduce the unsupported length of the retaining wall

Figures 11.9a and 11.9b are identical in the final excavation depth, the number of excavation stages, the number of strut levels, and the location of struts. The only difference between them is the distance between the location of strut and the excavation surface. In Figure 11.9a, each level of struts is installed 0.5 m above the excavation surface. When the first stage of excavation is completed, the unsupported length of the wall is 2 m. When the first level of struts is installed at the depth of GL-1.5 m and excavation proceeds to GL-5.5 m, the unsupported length of the wall is 4 m. When the second level of struts is installed and excavation proceeds to the third stage, the unsupported length of the wall is also 4 m. With the completion of the third level of struts, the unsupported length is 4.5 m.

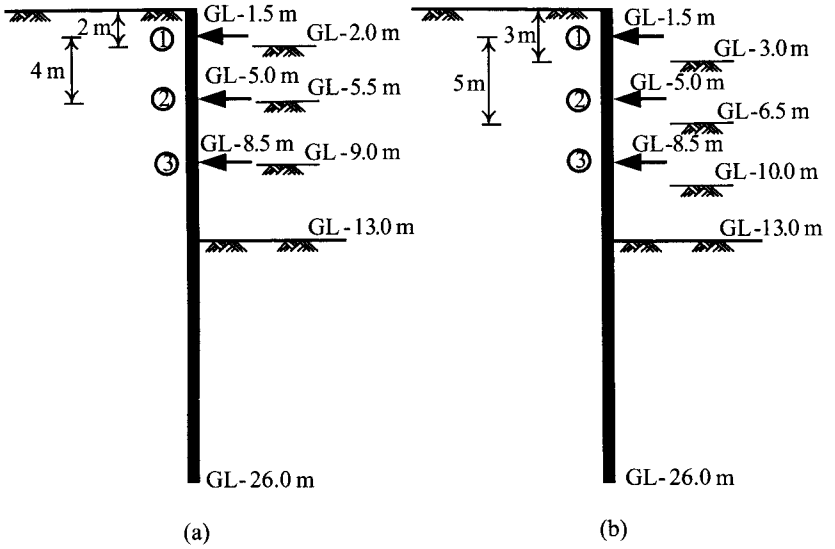

Figure 11.9 Influence of the distance between the strut and the excavation surface on the unsupported length: distance between the strut and the excavation surface is (a) 0.5 m and (b) 1.5 m.

In Figure 11.9b, each level of struts is installed 1.5 m above the excavation surface. As a result, during the first stage of excavation, the unsupported length of the wall is 3 m. Evaluated similarly, the unsupported lengths of the wall at the second and the third stages are both 5 m. The unsupported length after completion of the final stage of excavation is 4.5 m.

As elucidated above, except for the last stage of excavation where the unsupported lengths in the two cases are identical, the unsupported lengths illustrated in Figure 11.9a are smaller than those in Figure 11.9b at other stages of excavation, with the same earth pressure on the back of the retaining wall. Actually, the total deformation of the retaining wall or ground settlement is the accumulated deformation at every stage of excavation. Thus, the deformation in Figure 11.9a should be smaller than that in Figure 11.9b. That is to say, the location of struts should be as close to the excavation surface as possible. Generally, considering the convenience of strut installation, the distance between struts and the excavation surface is about 0.5 m.

11.4.2 Decrease the influence of creep

The definition of creep is given as the condition where deformation increases with time, provided the stress remains constant. Creep usually occurs in clayey soils. The softer the soils, the more obvious the characteristics of creep. Creep relates to time and stress. It increases with the increase of the stress level and time and covers a long period of time. Since soils near the retaining wall and on the excavation surface may be on the verge of the ultimate condition, the stress level must be high. As a result, soils with prominent characteristics of creep are susceptible to over settlement. As for the influence of creep of soils on excavation, please refer to Section 6.6.

To prevent creep from occurring, especially when excavating in soft clayey soils, struts have to be installed as soon as each stage of excavation is completed. Strut installation usually takes a few days in braced excavations. If the top-down construction is adopted, it takes a few weeks to construct floor slabs. During the process of strut installation or floor slab construction, creep may continue worsening. The expedient way to handle this is to lay a layer of pure cement, usually at least 10 cm thick, on the excavation surface as soon as the excavation stage is completed (which is also necessary in practice to facilitate the construction machines operating on the excavation surface). It is not easy to examine the effect of such a measure in the prevention of creep though it is considered to be useful to a certain extent from both theoretical and empirical points of views.

11.4.3 Take advantage of corner effect

As elucidated in Section 6.9, with the lateral stiffness and the resulting arch effect around corners, deformation of diaphragm walls and ground settlement around corners are both smaller than those in the central section. The corners for soldier piles, sheet piles, and bored piles, which are not continuous in the horizontal direction and have no lateral stiffness, accordingly, do not have much difference in deformation or ground settlement from the central section. Thus, if the building is located at a corner or on the shorter side (see Figure 11.10), diaphragm walls can be utilized to take advantage of corner effects for the protection of buildings.

11.4.4 Take advantage of the characteristics of ground settlement

If ground settlement can be accurately predicted or observed, the characteristics of ground settlement can also be utilized for property protection. The TNEC (Taipei National Enterprise Center) case history will be used for illustration. For the geological conditions, excavation process and monitoring results of TNEC, please refer to the index in Appendix B in this book.

Figure 3.33a diagrams the positions of the excavation site and Building A, which is a twelve floor building with one level of basement. The building is about 40 m high with a basement of 6 m depth. It adopts mat foundations, which covers an area of about

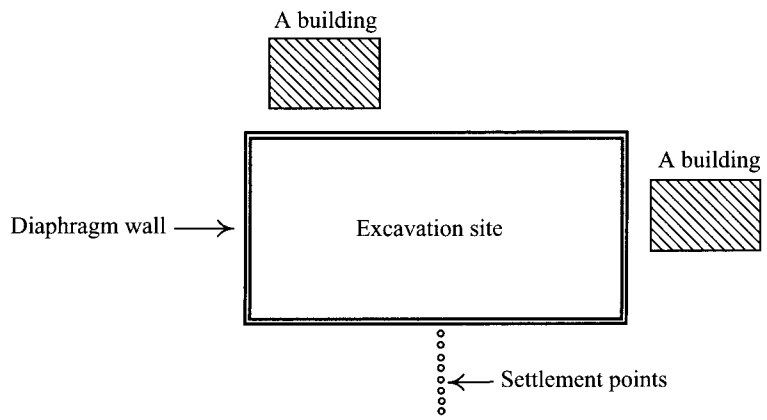

Figure 11.10 Buildings located at corners or along the shorter side of an excavation.

16 m × 17 m. As shown in the figure, the building is right next to the west side of the excavation site, separated from the retaining wall by only 1.5 m. During trench excavation and diaphragm wall construction, there appeared several cracks on the ground surface in the vicinity of the building. Therefore, the contractor installed two tiltmeters, B-1 and B-2, on the building.

When the construction of the diaphragm wall was finished, the measurements on B-1 and B-2 showed that Building A had tilted east by 1/838. To reduce settlement, the contractor improved the soils below the mat foundation with jet grouting of 35 cm diameter in the hope of reducing movement. Figures 11.11a and 11.11b illustrate the plan and profile of the soil improvement, respectively. The improvement started from corner **a** on the north-east side of the building and was implemented at every other pile. The depths ranged from GL-6 to GL-20 m. Tiltmeters were strictly monitored during the process of improvement.

Unfortunately, the plan of improvement failed since the tilt of the building worsened. According to the measurements from B-1 and B-2, the building continued to slant toward the excavation site (eastward) during the process of improvement, as shown in Figure 11.12. One of the results of B-1 showed the maximum angle of tilt achieved 1/491 toward the excavation zone while Building A did not show any sign of cracking on the panel walls.

Though the angle of tilt 1/491 for Building A was not a large amount, nor did the panel walls in the building begin cracking, it could be observed to slant visually. This is because Building A covered a relatively small area compared to its height and was very close-up next to Building B, which was little affected by excavation and therefore could be seen as a vertical standard.

The reason for the slant of the building was either insufficient control of the implementation of jet grouting or the grouting-induced disturbance, which made the soil strength weaken, according to preliminary judgment. Right during the process of grouting when the grout materials (cement grouts) had not congealed, the tilt of the building continued worsening with the execution of the soil improvement. Though the building could be observed to slant visually, the interior was kept intact. The reason might be that the mat foundations, which covered a relatively small area, had great rigidity. As a result, the tilt was basically rigid body rotation.

With the continuation of excavation, the angle of tilt of Building A, however, began declining. When the excavation was finished, the readings on B-1 and B-2 were separately 1/1,375 and 1/2,864. The phenomenon of the declining angle of tilt of Building A can be explained by the shape of the settlement profile. As shown in Figure 11.11, though no settlement is observed on a section perpendicular to line segment $\overline{ab}$, it can be assumed to be similar to the settlement profile of the main observation section (note: main observation section can refer to Figure 3.33a). Plot the settlement profile of the main observation section (Figure 6.8) and the relative positions of Buildings A and B on Figure 11.12. As shown in the figure, the settlements at corners **a** and **b** of the building were smaller than those at corners **c** and **d** during excavation. As a result, with the excavation proceeding and the increase of excavation depth, the building slant kept being drawn back and the angle of tilt declining.

From the above discussion on TNEC, it follows that an accurate prediction of settlement during the process of excavation will help property protection. The characteristics of ground surface settlement can be predicted by way of the simplified method (Section 6.8) or the finite element method. They can also be derived from measurements. Though the location of the building is sometimes difficult for the installation of settlement points, they could still be set on another side to obtain the representative settlement profile. Thus, the predicted settlement profile could be modified according to field observation.

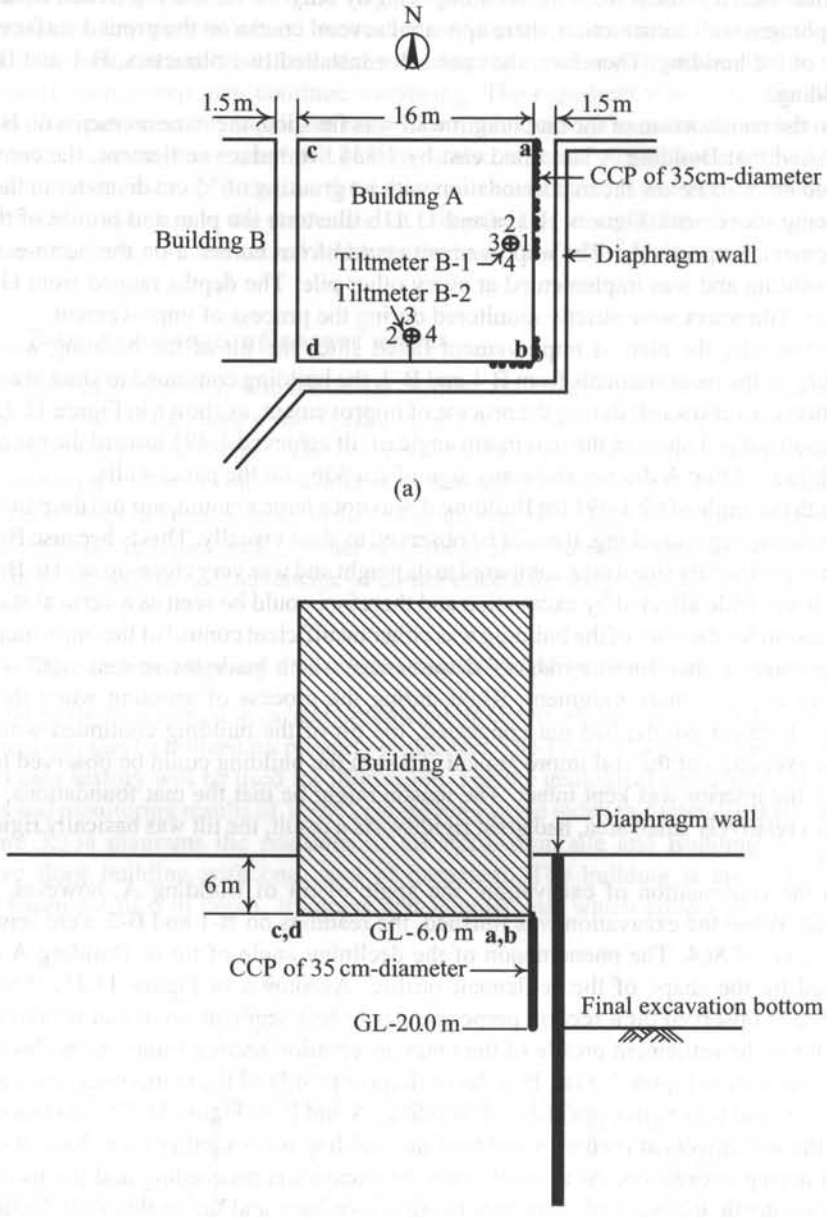

Figure 11.11 Arrangement of grouting at the building in the vicinity of the TNEC excavation: (a) plan and (b) profile.

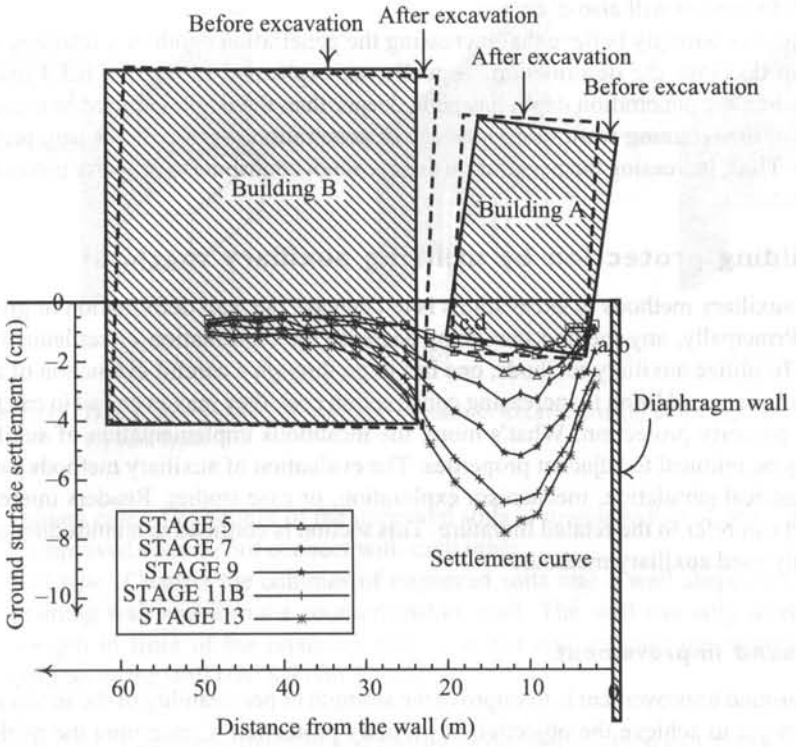

Figure 11.12 Slanting conditions of the buildings after excavation for the TNEC excavation.

11.5 Building protection by increasing stiffness of the retaining-strut system

Theoretically, the increase of the stiffness of a retaining wall can reduce the wall deformation and the ground settlement. The methods of increasing the system stiffness of the retaining-strut system include increasing the stiffness or thickness of the retaining wall, decreasing the horizontal span of struts, increasing the stiffness of each strut, and decreasing the vertical span of struts, etc. As explained in Section 6.3.5, the increase of thickness of a retaining wall does not help much in decreasing deformation.

When the axial stiffness of the strut is not large enough, increasing the stiffness of struts (such as by cutting the horizontal span or increasing the stiffness of each strut) can effectively reduce the deformation of a retaining wall. However, when the axial stiffness of struts is already rather large, more increase of stiffness will not reduce the deformation accordingly, the reason for which is as shown in Section 6.3.6.

Decreasing the vertical distance of struts is an effective way of reducing the deformation of a retaining wall. The reason is that cutting the vertical distance implies the increase of number of strut levels. That is to say, the rigidity of the retaining system is increased. Deformation will decrease as a result. From another perspective, since the deformation of a retaining wall is the accumulated result of the excavation stages, the cutting of the vertical distance will decrease

the unsupported length of the retaining wall at each excavation stage (see Section 11.4.1). Therefore, deformation will also decrease.

Some engineers wrongly believe that increasing the penetration depth of a retaining wall can also help decrease the deformation. Actually, as explicated in Section 6.3.4 and by Figure 6.5, when the penetration depth has gone deeper than the depth required to maintain the stability of the retaining wall, more increase of penetration depth will not help prevent deformation. Thus, increasing the penetration depth cannot contribute to property protection.

11.6 Building protection by utilizing auxiliary methods

The goal of auxiliary methods in excavations is to decrease the wall deformation or ground settlement. Principally, any method that helps decrease the deformation or settlement can be adopted. To utilize auxiliary methods, one has to go through a careful evaluation of their effects. Otherwise, in addition to increasing construction cost, they may even fail in catching the time for property protection. What's more, the incautious implementation of auxiliary methods may be inimical to adjacent properties. The evaluation of auxiliary methods can be done by numerical simulation, mechanism exploration, or case studies. Readers interested in the subject can refer to the related literature. This section is confined to an introduction to the commonly used auxiliary methods.

11.6.1 Ground improvement

The goal of ground improvement is to improve the strength or permeability of the in situ soils and their strength to achieve the objective of property protection. Concerning the methods of ground improvement applied in excavations, please refer to Section 11.3.

The first step of ground improvement is to determine the location of improvement. Ground improvement outside an excavation zone will decrease the active earth pressure acting on the retaining wall and within the excavation zone will increase the passive resistance of soils against the retaining wall. The ideal measure is to improve the soils both inside and outside the excavation zone. Nevertheless, the cost may be too high.

According to Ou and Wu's (1990) parametric study using the finite element method, the effects within the excavation zone are better than those outside, given the same conditions. Judged from mechanisms, once excavation is started, the retaining wall will move toward the excavation zone and the active earth pressure is thus produced no matter whether the soils outside the excavation have been improved or not. Therefore, the earth pressure acting on the retaining wall will not be decreased too much. On the other hand, the ground improvement inside the excavation zone will always directly restrain the movement of the retaining wall. Obviously, the effects of ground improvement inside the excavation zone are better than improvement outside.

The location determined, it follows to determine the arrangement of improvement. To resist the forward movement of the retaining wall, some commonly used arrangements include the block type, the column type, and the wall type, as shown in Figure 11.13. The arrangements of these types are elucidated as follows.

1 *Block type*: Within a specific area, improve the soils fully. Replace the soil bodies within the area completely or have them completely combined with chemicals into treated soils.

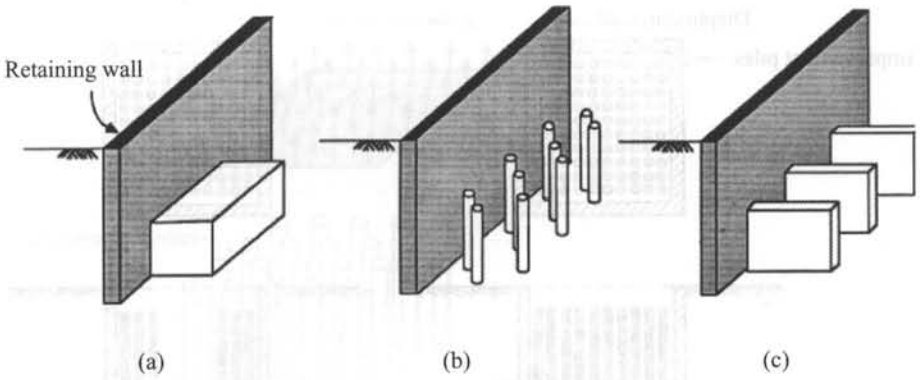

Figure 11.13 Typical arrangement of soil improvement in excavations: (a) block type, (b) column type, (c) wall type.

2 *Column type*: The pattern of the improved soils is similar to that of piles. The columns of improved soils do not connect with each other.
3 *Wall type*: Connect the columns of improved soils into a wall shape, which joins the retaining wall and forms a counterfort-like wall. The wall can only increase the soil strength in front of the retaining wall. It is not able to raise the moment-resistance stiffness of the wall (see Section 11.6.2).

Figure 11.14a diagrams the plan and profile of the column type of ground improvement. Under such a condition, the passive resistance can be computed on the basis of the properties of the treated soils (composite soils). Figure 11.14b is a partial improvement within the excavation zone. Under such a condition, the passive resistance of soils against the retaining wall will be smaller than that obtained on the basis of the properties of fully treated soils (composite soils).

To ensure ground improvement capable of property protection, improvement should be analyzed in terms of the strength of the treated soil, its diameter, span, depth, location, and range. The soils within the area can be viewed as a composite material in analysis. When the composite soil body bears vertical load (see Figure 11.15), according to the principle of force equilibrium, the strength of the composite soil can be written as

$$\tau_{eq} = \tau_t I_r + \tau_s (1 - I_r) \tag{11.4}$$

where

τ_t = shear strength of the treated soil
τ_s = shear strength of the untreated soil
I_r = improvement ratio, that is, the area of the treated soil divided by the total area.

The above equation is applicable to an area with loading condition similar to Figure 11.15, such as the area outside the excavation zone. The compressive strengths of the treated and untreated soils are used for such a condition. However, the area inside the excavation zone

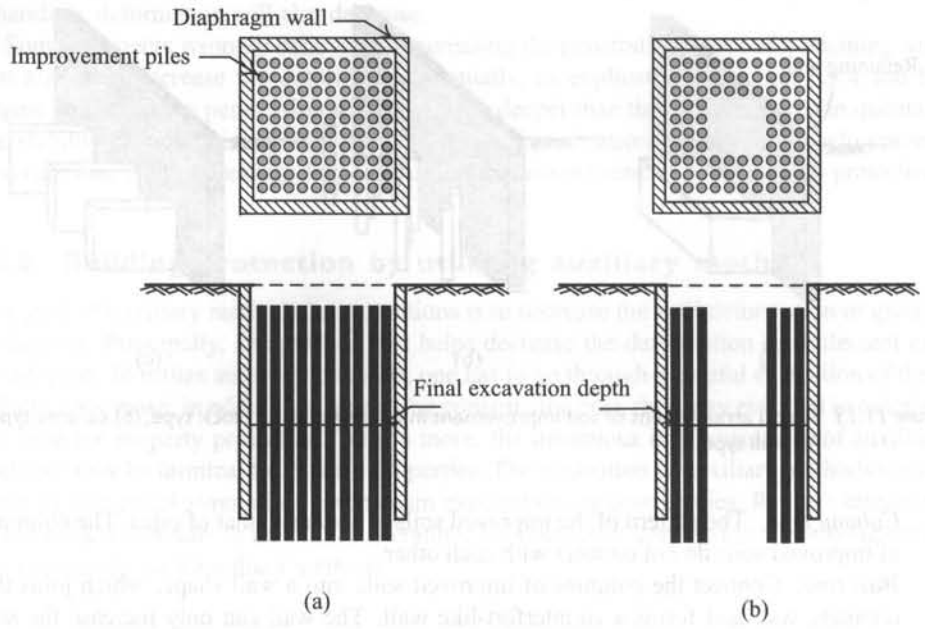

Figure 11.14 Soil improvement within excavation zone: (a) improvement over the whole zone and (b) partial improvement.

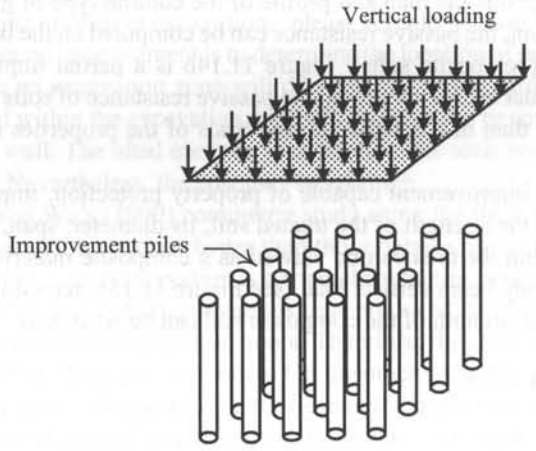

Figure 11.15 Composite soil bodies subjected to vertical loading.

is mainly subjected to the vertical unloading, that is, axial extension (see Figure 11.16). The tensile shear strength of the treated and untreated soils should be used instead of compressive strength.

In engineering practice, compressive strength tests are often carried out rather than extension tests. Therefore, some engineers prefer to adopt the following formula to estimate

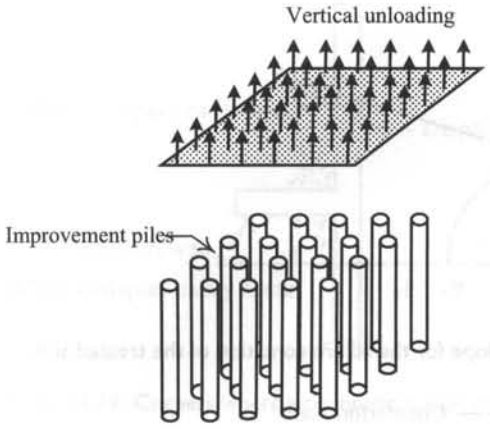

Figure 11.16 Composite soil bodies subjected to vertical unloading.

the strength of the composite material for the area inside the excavation.

$$\tau_{eq} = \alpha \tau_t I_r + \tau_s (1 - I_r) \tag{11.5}$$

where

τ_t = shear strength of the treated soil (compressive)
τ_s = shear strength of the untreated soil (compressive)
I_r = improvement ratio
α = modification factor, around 0.3, which is about equal to the ratio of tensile strength to compressive strength of the treated material.

When the untreated soils are clayey soils, the undrained shear strength (s_u) should be adopted for the value of τ_s in Eq. 11.4 or 11.5, which would be about 1/2–1/6 of the unconfined compression strength (depending on the quality of the treated soils). Thus, the analysis of the composite soils should adopt τ_{eq} and $\phi = 0$ (similar to the undrained shear strength).

Besides, according to Clough and Tan's (1980) study, if the untreated soils are granular soils (such as sand, gravel), the friction angle of the treated soil will be close to that of the untreated soil. Assuming the friction angle for the treated soil is ϕ, according to the Mohr's circle representing the failure of the treated soil in Figure 11.17, we have

$$\frac{\sigma_1 - \sigma_3}{2} = \left(c \cot \phi + \frac{\sigma_1 + \sigma_3}{2} \right) \sin \phi \tag{11.6}$$

Substitute $\sigma_3 = 0$ and $\sigma_1 = q_u$ into the equation and simplify it, and we have

$$c = \frac{q_u}{2} \frac{1 - \sin \phi}{\cos \phi} \tag{11.7}$$

where q_u is the unconfined compression strength.

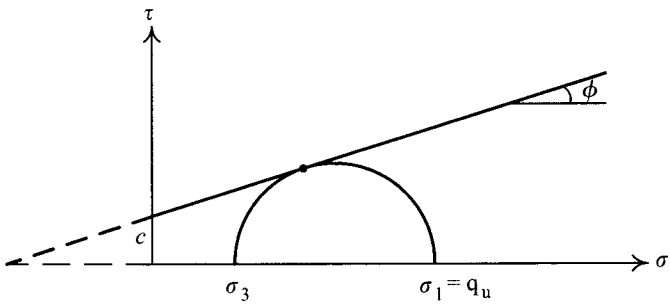

Figure 11.17 Mohr's circle and the envelope for the failure condition of the treated soil.

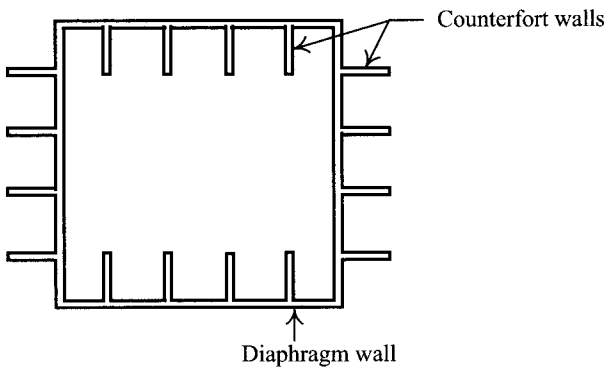

Figure 11.18 Locations of counterfort walls.

The value of τ_{eq} can be computed from τ_t (given the values of c and ϕ of treated soils) and τ_s (untreated soils). It is also feasible to compute c_{eq} using Eq. 11.4 or 11.5, and then τ_{eq} can be computed based on c_{eq} and ϕ.

11.6.2 Counterfort walls

Figure 11.13c diagrams the wall type of ground improvement, which usually contacts the retaining wall without forming a whole structure with it. Thus, when the retaining wall is bent and deformed, there will be produced a relative displacement between the wall-type soil body and the retaining wall. That is to say, the wall-type soil body does not increase the moment-resistance of the retaining wall though it increases the strength of soils in front of the retaining wall. If the wall in Figure 11.13c is constructed as a counterfort (also called buttress), that is, constructed by way of the diaphragm wall method (either reinforced or not) and forms a whole structure with the diaphragm wall (retaining wall), like a T-beam in reinforced concrete structures, the counterfort will greatly enhance the capability of moment-resistance.

The location of the counterfort can be arranged either at the inner or the outer side of the retaining wall as shown in Figure 11.18. When arranged at the inner side, it would be mostly subjected to tensile force. Theoretically, the counterfort should be reinforced under such a condition. The actual cases using counterforts, nevertheless, show that unreinforced counterforts are useful as well in increasing the moment-resistance stiffness. The counterfort

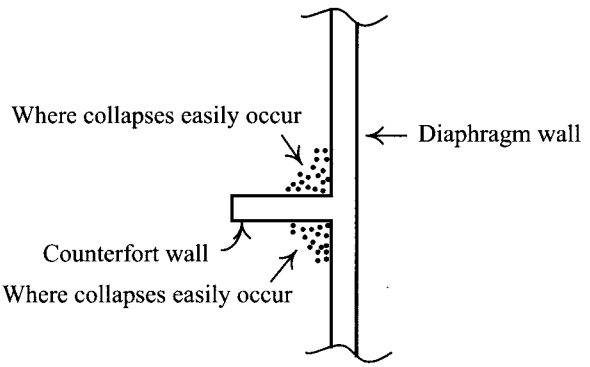

Figure 11.19 Corners where a counterfort wall, connecting to diaphragm walls, easily collapses.

constructed at the inner side of the retaining wall should be dismantled with the increase of the excavation depth.

If no property rights are involved, the counterfort can be constructed on the outer side of the wall. The reason is that the counterfort will be subjected to compression force when it is bent or deformed. There is no need to place reinforcements in the counterfort. Besides, it also saves the trouble of dismantling it during the excavation process. If the counterfort need not be dismantled as the excavation is proceeding, it can offer stiffness throughout the whole course of excavation and the construction of the basement.

Theoretically, the counterfort can be cast into a whole structure with the retaining wall. However, there exists the problem of collapse near the concave corners of trenches, as shown in Figure 11.19. Jet grouting in this area is one of the measures to avoid the collapse of trenches. Figure 11.20 display two commonly used counterforts using diaphragm wall construction methods.

Figure 11.21 is the plan for the construction of a counterfort wall of an excavation. The excavation was about 44 m long, 42 m wide, and 8.6 m deep. The diaphragm wall was 0.6 m thick with a penetration depth of 21 m. Excavation was carried out at four stages. From the ground surface to GL-20 was soft clay. From GL-20 to GL-26 m, there was silty sand. Below GL-26 m, there was gravelly soil. To protect buildings in the vicinity of the excavation site, the T-shaped counterforts, as shown in Figure 11.20a, were constructed along the 42 m side.

Figure 11.22 illustrates the measured deformations of the retaining wall with (as shown as SI4 in Figure 11.21) and without (as shown as SI6 in Figure 11.21) counterforts in the central section at the last excavation stage. The deformation of the retaining wall at SI4 was much smaller than that at SI6. Use of counterforts was certainly effective in reducing wall deformation in this case.

Ou and Wang (1997) carried out parametric studies to investigate the behaviors of counterfort retaining/diaphragm walls using the three-dimensional finite element method and drew the following conclusions:

1 The deformation behaviors of the counterfort diaphragm wall can be successfully analyzed or predicted using the three dimensional finite element method.
2 The deformation behavior of the counterfort diaphragm wall has much to do with whether it penetrates into the hard soil stratum (sandy or gravelly soils) or not. In other words, it

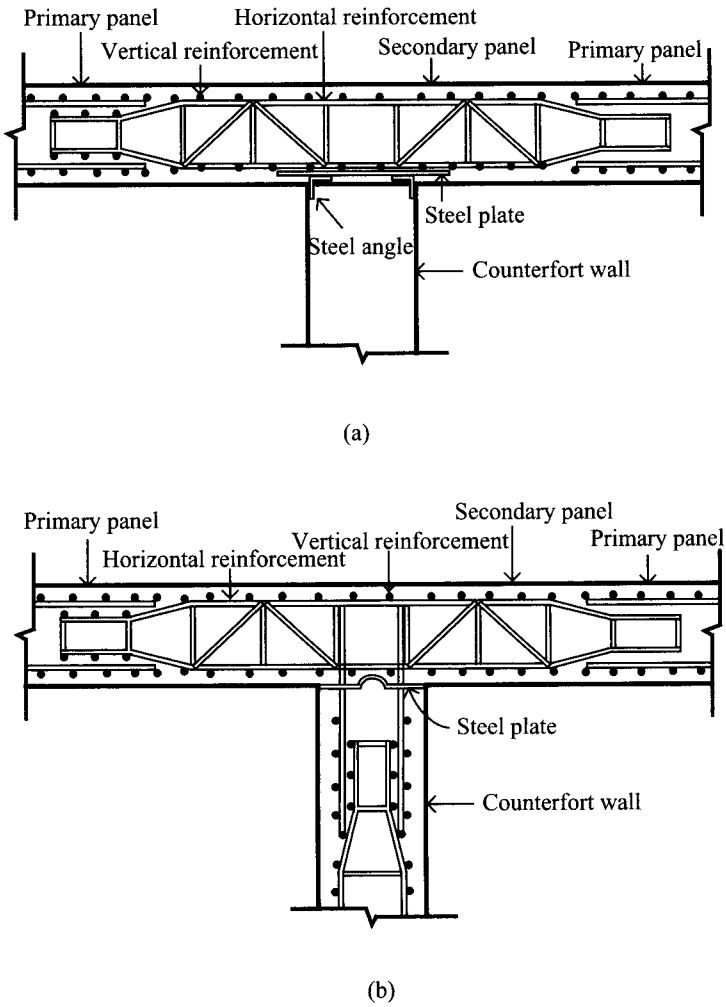

Figure 11.20 Types of counterforts: (a) unreinforced and (b) reinforced.

relates to whether the wall bottom is effectively restrained or not. If the wall bottom is restrained, with the extra moment-resistant stiffness offered by the counterfort diaphragm wall, the deformation of the diaphragm wall can be reduced effectively. Otherwise, if the bottom of the counterfort diaphragm wall is not well restrained, the whole wall, from top to bottom, will be pushed linearly because of the high rigidity of the counterfort diaphragm wall. Under such a circumstance, the wall behaves like a rigid body and thus, a significant amount of displacement at the wall bottom may occur. Though the maximum wall deformation may be reduced, the area covered by the displacement curve of the diaphragm wall may not decrease much. That is, the settlement will not be reduced effectively. Figure 11.23 shows the plan of a hypothetical excavation and the shapes, locations, and arrangement of the counterforts. The soils at the excavation site are thick

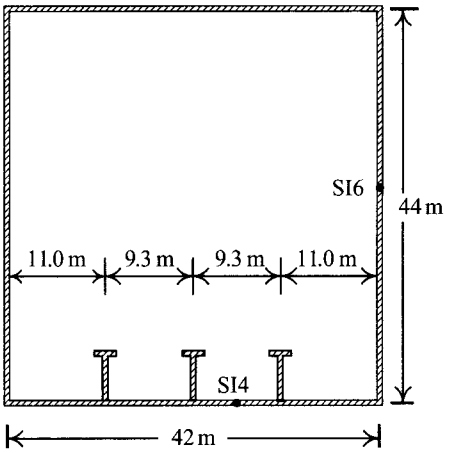

Figure 11.21 Plan of an excavation with T-counterfort walls.

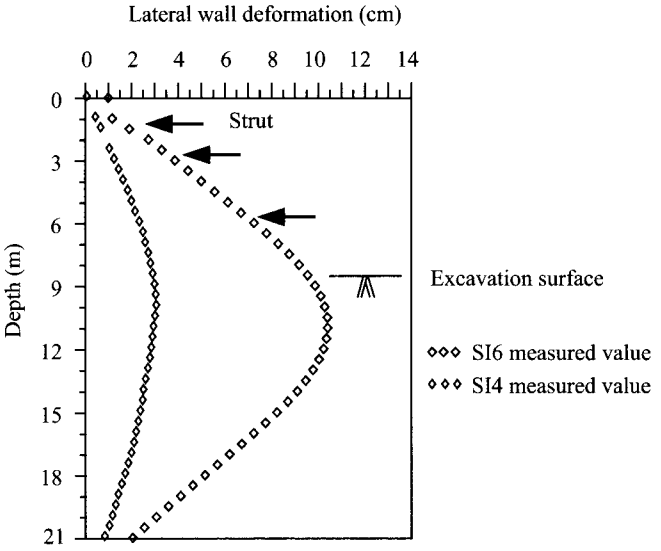

Figure 11.22 Measurements of lateral deformation of the wall at SI4 and SI6.

soft clays and the hard soil stratum is located so deep that the counterfort diaphragm wall does not penetrate it. Figure 11.24 illustrates the relations between the lateral deformation of the counterfort diaphragm wall in the central section and the numbers of counterforts. As shown in the figure, we can see that although the lateral deformation of the diaphragm wall decreases with the numbers of counterforts, the displacement of the bottom of the diaphragm wall is slightly increased. The diaphragm wall shows high rigidity, but the area covered by the displacement curve of the diaphragm wall does not decrease much.

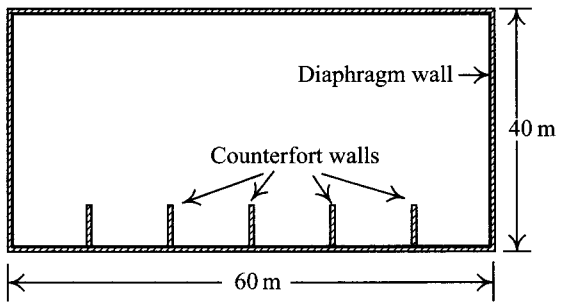

Figure 11.23 Arrangement of counterfort walls in a hypothetical excavation.

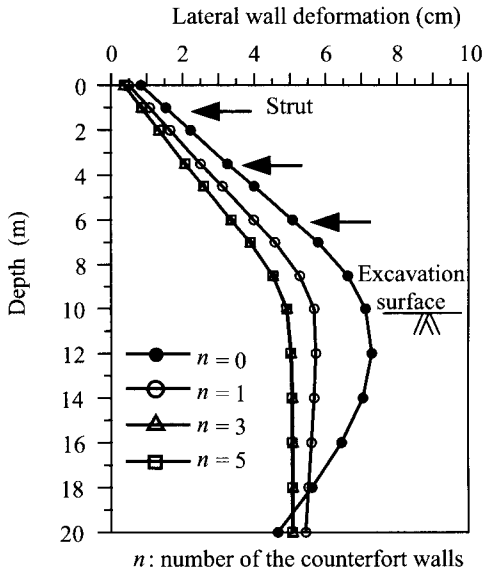

Figure 11.24 Relations between the deformation of a diaphragm wall and the number of counterfort walls (note: counterfort walls not penetrated into hard soils).

3 The counterfort can only restrain the wall deformation at the part where it is placed. If the deformation of the whole diaphragm wall, that is, along the excavation border, is to be reduced, several counterforts have to be placed evenly along the excavation border. Figure 11.25 illustrates the relations between the maximum wall deformation and the distance from the corner using the three-dimensional finite element analysis. In practical design, the span of the counterforts can be determined referring to successful case histories or may be obtained from the three-dimensional finite element analysis.

11.6.3 Cross walls

The arrangement of cross walls is schematically shown in Figure 11.26. One constructs a wall connecting the opposing two retaining walls before excavation is started. It can be

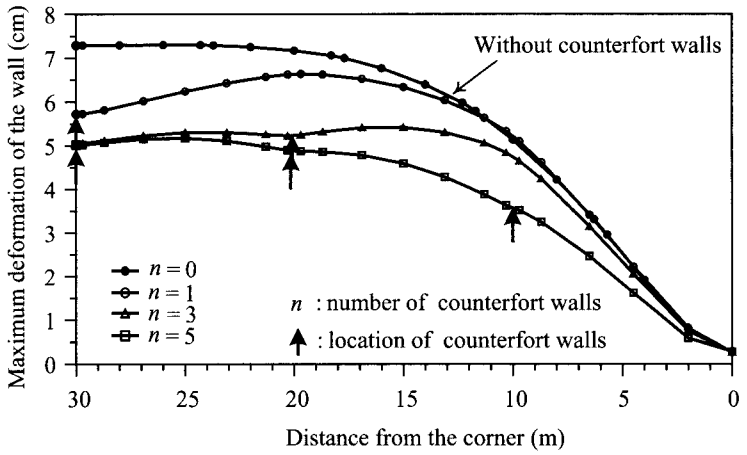

Figure 11.25 Influence of the number of counterfort walls on the maximum wall deformation in different positions.

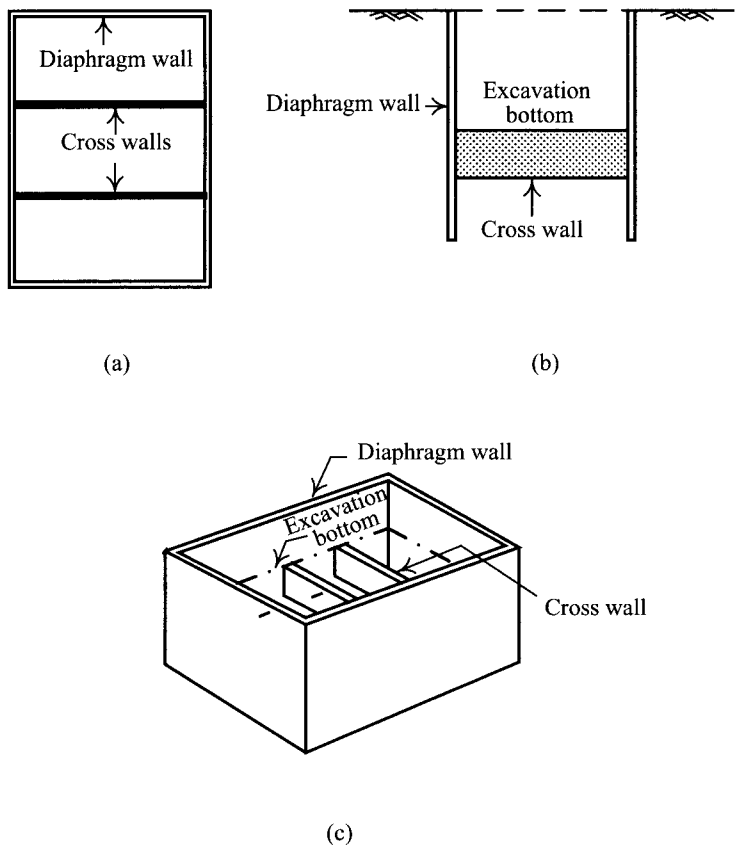

Figure 11.26 Configuration of cross walls: (a) plan, (b) profile, and (c) three-dimensional view.

constructed using ground improvement techniques (such as jet grouting or deep mixing). To obtain a better construction quality or compressive strength, the cross wall can also be constructed by unreinforced diaphragm walls (the unconfined compression strengths of treated soils are usually between 10 and 20 kg/cm^2 whereas that of concrete diaphragm wall can achieve 280 kg/cm^2 with a minimum of 100 kg/cm^2).

The mechanism of the cross wall for reducing wall deformation is quite different from that of ground improvement. The designing principle of ground improvement is to enhance the strength of soils in front of the wall, considering them too soft to have enough passive resistance. The cross wall should be viewed as a strut, which exists before excavation and owns a great deal of compression strength (especially for unreinforced diaphragm walls). Theoretically, the locations where cross walls have been placed are less susceptible to deformation because they are restrained from moving. The effects of the cross wall on reducing lateral deformation of a retaining wall are quite obvious.

To ensure that cross walls can effectively reduce deformation of the retaining wall, the design of cross walls has to consider compression strength, depth, and span of two cross walls. Since the behaviors of the diaphragm wall with cross walls are three dimensional, neither the traditional two-dimensional plane strain analysis nor the beam on elastic foundation method can simulate behaviors of cross walls. Thus, to design cross walls, one has to resort to the three-dimensional finite element method or successful case histories.

Figure 11.27a is the plan of an excavation case located in Taipei. The excavation was about 76 m long, 25 m wide, and 13.5 m deep. The retaining wall was a 70 cm thick, 30 m deep diaphragm wall. To protect buildings in the vicinity, two cross walls were constructed. They were constructed the same way as the diaphragm wall except not reinforced. The thickness of the cross walls was the same as the diaphragm wall. It was constructed from GL-13.5 to GL-20 m. Soils were backfilled above the cross walls (GL0.0–GL-13.5 m), as shown in Figure11.27b.

Figure 11.28 compares the measured values with the computed values using the three-dimensional finite element method for the wall deformation in the central section of the longer side of the excavation site (SIDI in Figure 11.27a) at the last excavation stage. To

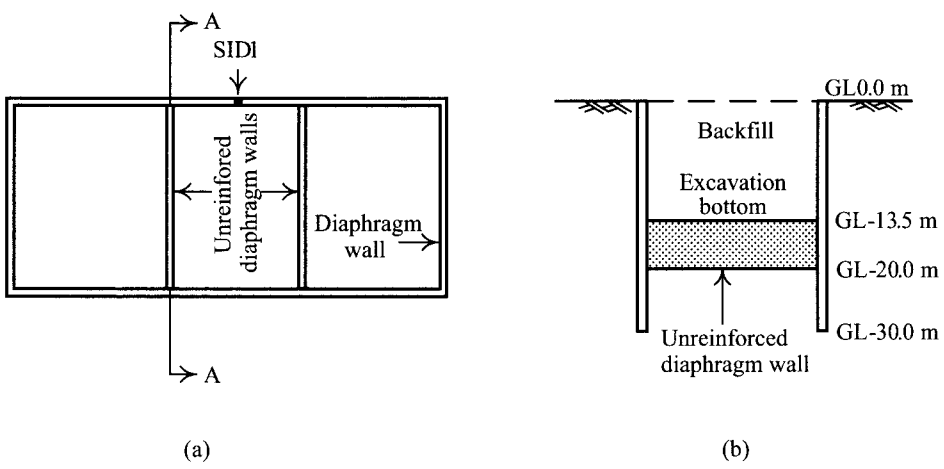

Figure 11.27 Cross walls in excavations: (a) plan and (b) profile.

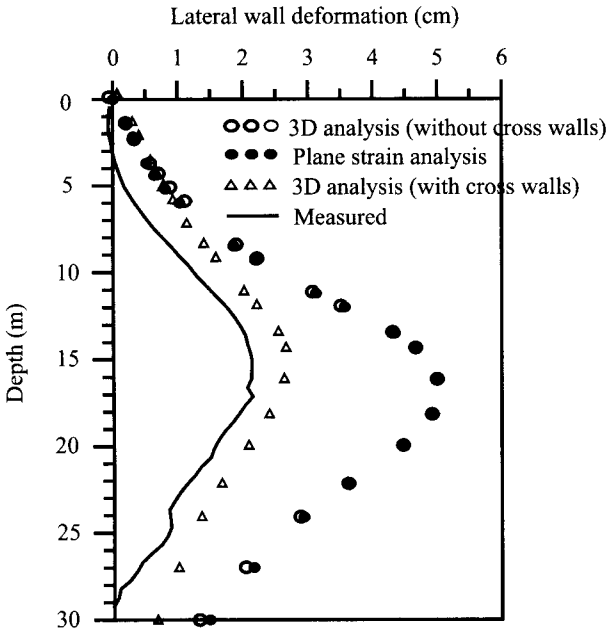

Figure 11.28 Measured and computed lateral deformations of the diaphragm wall with cross walls.

understand the effects of the cross walls on reducing the deformation of the diaphragm wall, the conditions without cross walls were also analyzed using the three-dimensional and the plane strain finite element methods. The analysis results indicated that the plane strain analysis yields almost identical results with the three-dimensional analysis for the condition without cross walls. The results from three-dimensional analyses were very close to those from field measurements. The cross walls were effective in reducing the deformation of the diaphragm wall. The three-dimensional finite element method is useful in simulating wall deformation with cross walls, too.

Ou and Lin (1999) conducted a series of parametric studies on the basis of 14.5 m deep excavations and 31 m deep diaphragm walls to explore the behaviors of cross walls. The results are as follows:

1 In the cases where the cross walls were constructed with the same depth as the diaphragm wall (GL-0–GL-31 m), the deformations of the diaphragm wall were the smallest. The cases where the cross walls were constructed above the excavation surface (GL-0–GL-14.5 m) had the least effect on reducing wall deformation, though they still worked. In the cases where the cross walls were constructed between the excavation surface and 6.5 m below it (GL-14.5–GL-21 m), they had fairly good effects, only inducing a slightly larger deformation than those of cross walls with the same depth as the diaphragm wall. The deformation for cross walls constructed from the excavation surface to the bottom of the diaphragm wall (GL-14.5–GL-31 m) were similar to those constructed from the excavation surface to 6.5 m below it (GL-14.5–GL-21.0 m).

2 For convenience of construction, the trenches above cross walls have to be backfilled with soils, which are usually replaced with low strength concrete. Thus, to save the cost, cross walls are best constructed between the excavation surface and 5 or 6 m below it.
3 For a single excavation, it may be necessary to design one or several cross walls. The deformation of a retaining wall is the smallest at the location where cross walls are constructed. The relations between deformation, the number of cross walls, and the distances of cross walls from corners, respectively, are similar to Figure 11.25.

11.6.4 Micro piles

Micro piles are also called soil nails. Since they were first applied in Europe to strengthen or underpin existing buildings, they have been used for more than 40 years. They have also been applied to property protection in many countries. Some successful case histories have been documented in the literature (Woo, 1992) and many more unsuccessful cases were not recorded.

Because the mechanisms of micro piles for property protection are indirect and systematic studies are also lacking, though successfully applied in some excavations, most of them are designed on an empirical basis and without theoretical support.

In practice, the diameter of a micro pile varies from 10 to 30 cm. The reinforcements can be steel bars, steel rails, H steels, or even steel cages. The construction process of micro piles is as follows. First, bore to the designed depth with casings or by other drilling measures and then place reinforcements into the bores. Inject cement mortar into bores under a certain pressure. Pull out the casing little by little and add more mortar. The micro piles are usually arranged in a single row or multiple rows. The distance between piles is three to five times the pile diameter, depending on the soil strength. No matter if the arrangement is the single row or the multiple row type, they should be intermingled by 5–30 degrees as shown in Figure 11.29.

There are two design principles for use of micro piles. The first is they have to pass the potential failure surface so that the shear strength of micro piles and the pull-out resistance can restrain the failure of soils and reduce the possibility of ground settlement accordingly, as shown in Figure 11.29. The potential failure surface, however, is usually rather large and the micro piles passing it are limited in number. The shear strength and pull-out resistance of the micro piles are not too large. Thus, whether the design is useful remains to be evaluated.

The other principle is to design many small-diameter micro piles enveloping the retaining wall to reinforce the soils through the process of steel placing and grouting. Especially in sandy soils, grouts may permeate into soils extensively and reinforce a larger area of soils. They may even form a quasi-gravity retaining wall. Figure 11.30a diagrams the micro piles in two rows, which perform as gravity retaining wall-like structure, as shown in Figure 11.30b. The method may be capable of stabilizing the retaining wall and reducing the active earth pressure on the retaining wall or increasing the resistance to the failure surface. Thus, ground settlement would be reduced.

Nevertheless, neither of the principles has been proved useful through systematic studies. Theoretically, micro piles can be applied to sandy and clayey soils alike. Actually, with the larger strength of sand and the extensive permeation of grouts into voids, grouting would be effective to certain extent in sandy soils. In clayey soils, on the contrary, the low soil strength and small voids in soils, which would prevent the grout from permeation, render the effects of micro piles, like many toothpicks in a soybean curd, dubious.

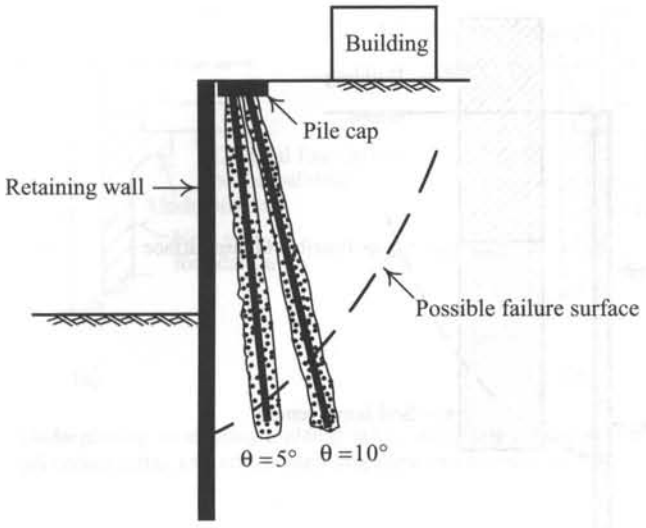

Figure 11.29 Mechanism of micro piles to protect buildings.

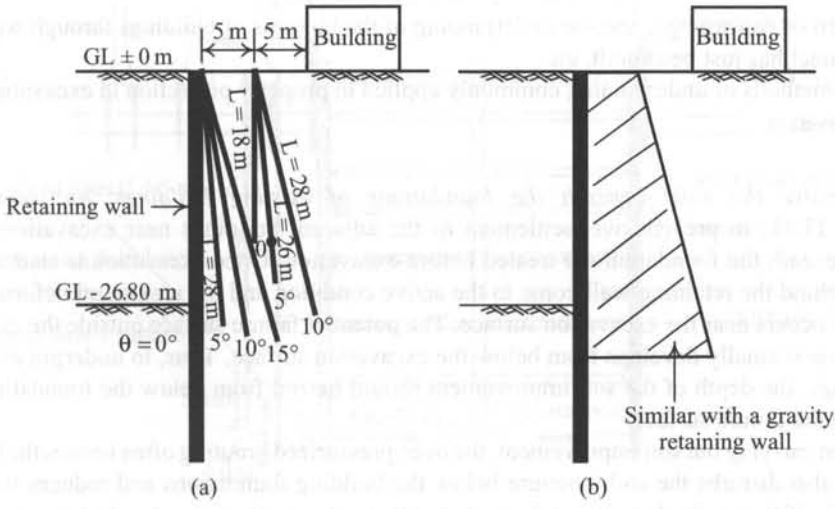

Figure 11.30 Mechanism of micro piles to protect buildings: (a) arrangement of micro piles and (b) serving as a gravity retaining wall.

11.6.5 Underpinning

Underpinning is to strengthen the existing foundations of a building, to improve the soils, or, to replace the original foundations. The applications of underpinning are quite extensive, including property protection in excavations, the prevention of natural settlement of heavy buildings, the strengthening of the foundations of buildings which have been unsuitably

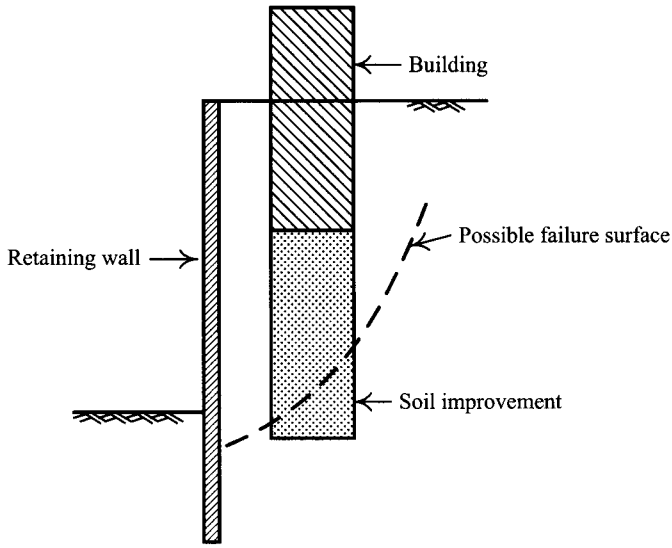

Figure 11.31 Underpinning an existing building by soil improvement.

designed or constructed, and the underpinning of the bottoms of buildings through which a new tunnel has just been built, etc.

The methods of underpinning commonly applied in property protection in excavation are as follows:

1 Improve the soils beneath the foundations of existing buildings: As shown in Figure 11.31, to prevent over-settlement of the adjacent buildings near excavations, the soils beneath the foundation are treated before excavation. Once excavation is started, the soils behind the retaining wall come to the active condition and the maximum deformation usually occurs near the excavation surface. The potential failure surface outside the excavation zone normally develops from below the excavation surface. Thus, to underpin existing buildings, the depth of the soil improvement should extend from below the foundations to outside the failure surface.

When carrying out soil improvement, the over-pressurized grouting often heaves the building. It also disturbs the soil structure below the building foundations and reduces the soil strength. If the method is not implemented with prudence, it may not only turn out to be a failure in strengthening the foundation soils but may also worsen slanting conditions and damage buildings. Thus, a detailed plan referring to successful case histories is required before implementation.

2 Add an extra foundation to existing buildings: For fear of the insufficient bearing capacity of the foundations of existing buildings, an extra foundation could be constructed near the original foundation before excavation. Such an underpinning measure is usually implemented before excavation. The implementation, without weakening the original foundations, does not need to be accompanied by the measure of load transfer, which will be introduced in the next.

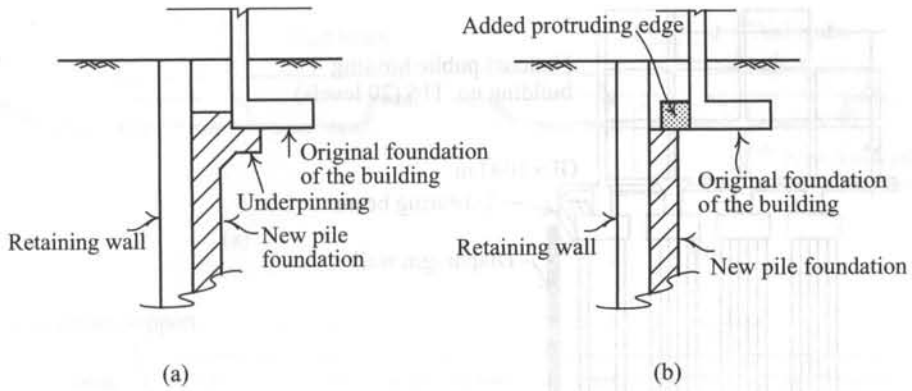

Figure 11.32 Underpinning an existing building: (a) constructing a bracket and foundation piles and (b) constructing an extra protruding edge and foundation piles.

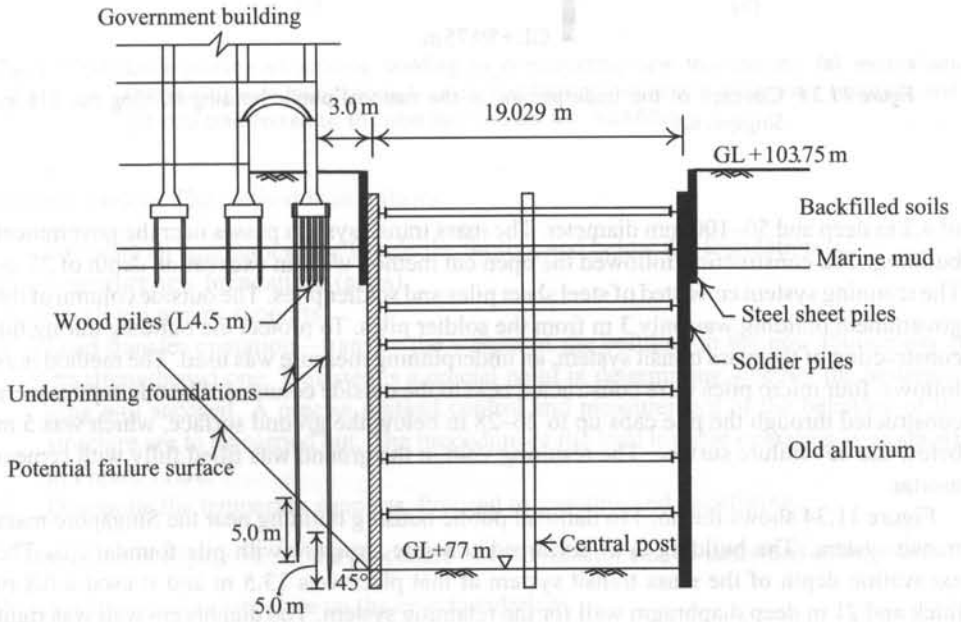

Figure 11.33 Underpinning foundations of a government building near an excavation of Singapore's mass transit system.

Figures 11.32–11.34 are some possible underpinning methods. Figure 11.32a shows a method of constructing new piles beside the retaining wall to support the foundations of existing buildings. Figure 11.32b shows a method of constructing a protruding part to the side of the foundations of existing buildings to join the newly constructed piles. Figures 11.33 and 11.34 use the underpinning methods adopted in the construction of the Singapore mass transit system (Huang, 1992). In Figure 11.33, the government building is a brick building with wood piles

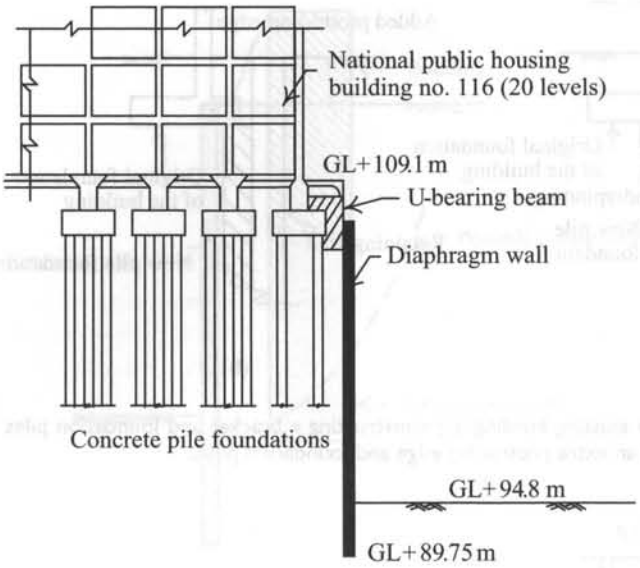

Figure 11.34 Concept of the underpinning in the national public housing building no. 116 in Singapore.

of 4.5 m deep and 50–100 mm diameter. The mass transit system passes near the government building. The construction followed the open cut method with an excavation depth of 27 m. The retaining system consisted of steel sheet piles and soldier piles. The outside column of the government building was only 3 m from the soldier piles. To protect the building during the construction of the mass transit system, an underpinning measure was used. The method is as follows: four micro piles were constructed next to the outside columns. The micro piles were constructed through the pile caps up to 26–28 m below the ground surface, which was 5 m below the 45° failure surface. The resulting void in the ground was filled fully with cement mortar.

Figure 11.34 shows the no. 116 national public housing building near the Singapore mass transit system. The building is a reinforced concrete structure with pile foundations. The excavation depth of the mass transit system at that place was 13.5 m and it used a 0.8 m thick and 21 m deep diaphragm wall for the retaining system. The diaphragm wall was right next to the edge of the building. To protect the building from damage during the construction process, some underpinning measures were taken to protect the pile caps at the border. The idea of the underpinning was to construct a U-shaped bearing beam, supported by newly constructed piles, to clip the existing pile cap.

The two cases, as illustrated in Figures 11.33 and 11.34, still exhibited significant settlements after excavation. Whether the underpinning methods worked to reduce settlement in these cases is still dubious. Interested readers can refer to the original documents.

3 *Construct new foundations under existing buildings*: Figure 11.35 diagrams the underpinning method in which an additional foundation is constructed beneath the building's original one. With the new foundation constructed, the original one may weaken or even

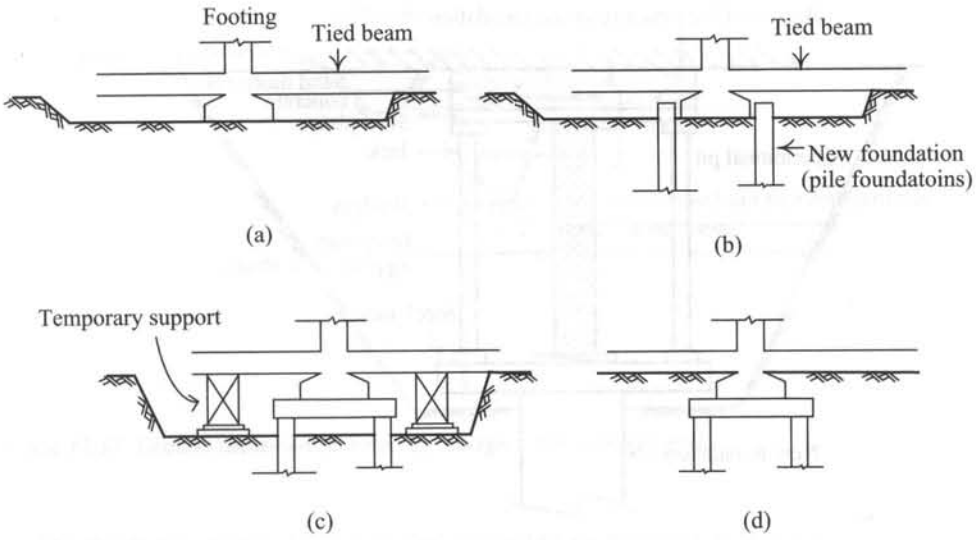

Figure 11.35 Underpinning an existing building by constructing new foundations: (a) excavation, (b) building new foundations, (c) installing bearing beams and temporary supports, and (d) load transferred to the new foundations and backfilling.

become useless. The method is as follows:

1 Excavate an operation space beside the footing and below the foundation.
2 Construct new foundations (piles).
3 Install temporary supports.
4 Load transfer operation—transfer the weight of the building to the new foundation or the strengthened one. This step is a crucial point in determining whether the underpinning will succeed. A precise preload control and measurement of the behavior of the structure are to be carried out. The procedure of the load transfer operation is as shown in Figure 11.36.
5 Dismantle the temporary supports. Proceed to grouting and backfilling.

As shown in Figure 11.36, the procedure of load transfer can be described as follows:

1 Set jacks and a steel plate on the new foundation.
2 Lay sand mortar or concrete between the building bottom and another steel plate, which is set on the top of the jack.
3 Preload the steel plate or the foundation using jacks. Preloading usually takes the building as the reaction frame. The direct adding of the weight of the building onto the new foundation usually produces settlement. The aim of preloading is to have the new foundation acted on by a preload in advance to accelerate settlement.
4 Place temporary supports between the two steel plates.
5 Hammer wedges into the voids of the temporary supports.
6 Dismantle the jacks and fill the operation space with concrete. The underpinning is thus completed.

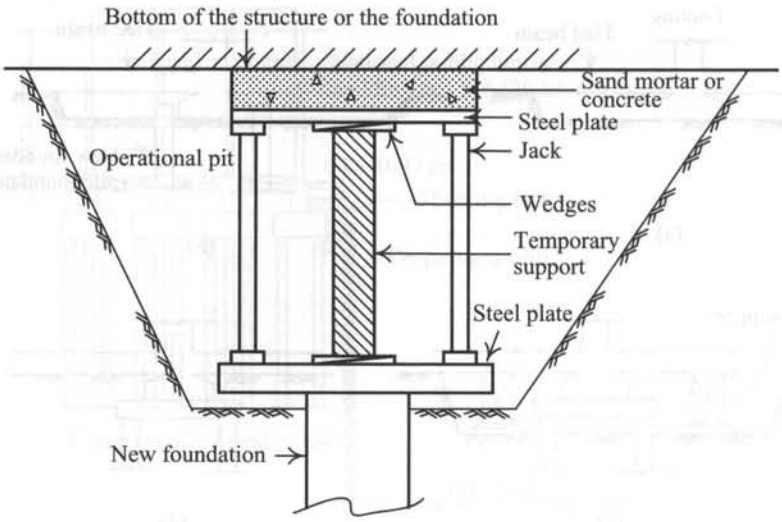

Figure 11.36 Schematic diagram of load transfer operation.

11.7 Construction defects and remedial measures

If possible construction defects in excavations are known in advance, the remedial measures for such defects can be prepared and the adjacent buildings can thus be protected accordingly. Some commonly found construction defects are as follows:

11.7.1 Leakage through the retaining wall

In excavations in sandy soils with high groundwater levels, if the retaining wall is broken or not satisfactorily watertight, one will encounter the problems of water or sand leaking through the wall, which can be extremely dangerous. If the leaking amount becomes large enough, it will enlarge the holes in the wall rapidly and the excavation site will collapse as a result.

Even when leaking is not serious, it is still dangerous to a certain extent. The reason is that water is often intermingled with fine soils (such as silt). Though the fine soils flowing to the excavation zone are not much at first, they will be accumulated day by day without causing any alarm (e.g. they may be swept away once they leak into the excavation zone). As a result, the soils outside the excavation zone will badly lack fine soils and the soil structure will grow quite unstable. Once the ground is acted on by any extra load or vibration, the ground surface will collapse, as shown in Figure 11.37. Because the flowing directions of groundwater are complicatedly intertwined, the area from where the fine soils have been taken away can hardly be known. As a result, the settlement may occur near or far and may be local or overall. The outcome is possibly disastrous.

Settlement and the losing of fine soils caused by leakages in the retaining wall will only occur in soils with high permeability (such as sandy soils). Clayey soils have low permeability and there exists cohesion between particles. Therefore, even when the retaining wall leaks, no possibility of settlement or losing fine soils has to be considered.

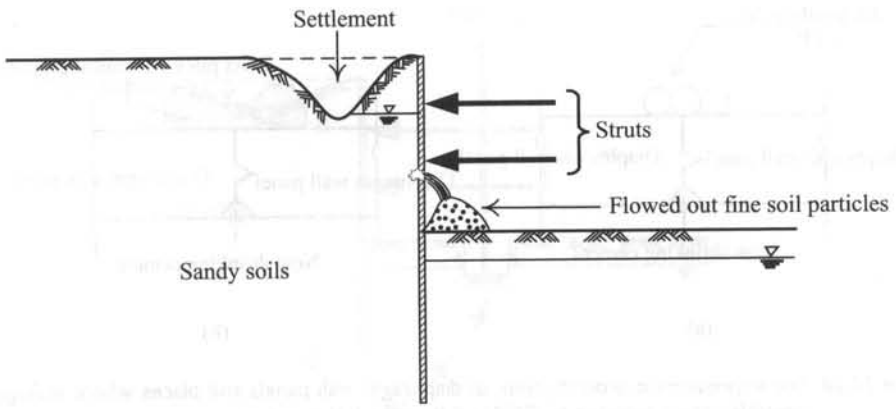

Figure 11.37 Ground settlement induced by leakage in the retaining wall.

The causes and remedial measures due to leakage are generally as follows:

1 The soldier piles or laggings are not satisfactorily watertight. Excavation below the groundwater level is susceptible to water leaking even though grouting is implemented in advance as a rule. That is because the quality of grouting is not easily guaranteed. Though sheet piles are much more watertight, if they are used too many times or are unsuitably placed, they may still leak at the joints. Soldier piles and sheetpiles are to be avoided when excavating in sandy soils with high groundwater tables.
2 If the quality of the concrete used in a diaphragm wall is not well controlled, water leakage is likely to happen, especially at the joints between panels. Besides, during the process of casting, if the process of lifting Tremie pipes is flawed, for example, the position of the flaw on the plan and its elevation should be recorded immediately so that grouting can be implemented at the place where the concrete casting is flawed before excavation. The joints between the panels of the diaphragm wall may be similarly treated sometimes in case leaking from the panel joints is suspected.
3 When two retaining walls with different rigidities are joined, different deformations will be produced as a result of earth pressure. The condition is especially susceptible to cracking and has to be remedied by grouting at joints.
4 If there exist pipes under the retaining wall, the construction will be confined by insufficient space. As a result, the construction quality of the bottom of the wall is not easily controlled, which may produce flaws that lead to leakage. These places should be treated by grouting before excavation.
5 When installing a ground anchor in granular soils with high groundwater levels, cutting the diaphragm from inside the wall with a drilling machine would easily bring about leakage through the drilled place. Leakage may occur directly through the diaphragm wall, through the gap between the bore and the casing of the anchor, or from the void of the cable bundle. Special techniques of implementation have to be adopted to prevent leaking, such as grouting at the place where the anchor is installed.

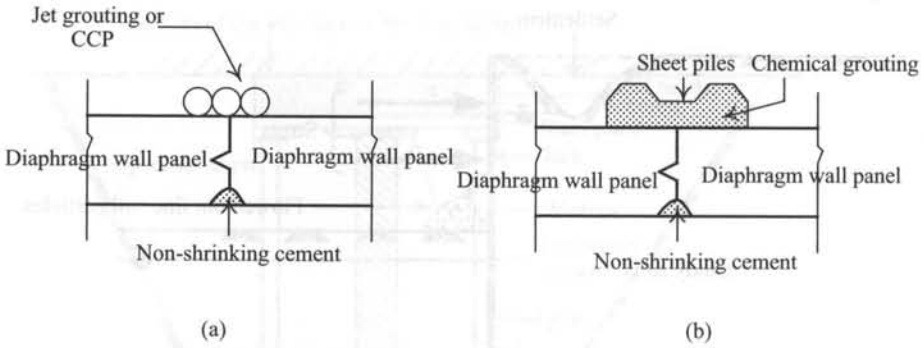

Figure 11.38 Soil improvement around joints of diaphragm wall panels and places where leakage is possible: (a) jet grouting or CCP and (b) chemical grouting.

As discussed above, if engineers judge a place would possibly leak, sealing and grouting have to be carried out in advance before excavation. Sealing and grouting can resort to jet grouting (e.g. CCP piles), tightly lined and connecting to the outer wall to make a sealing cofferdam. Sealing and grouting can also resort to chemical grouting. To prevent the grouts from irregular flowing, we can set several sheetpiles outside the joints and limit grouting to between the sheetpiles and the diaphragm wall, as shown in Figure 11.38.

If a small, slow leak occurs during excavation, we can use a coagulation agent mixed with cement to seal the leakage, then clear the fragile impurities and fill the crevices with a filling agent, such as nonshrinking cement, at last. If leaking is serious and safety is threatened, the first thing is to do is to stop the spurting. Generally, the method is to stuff the spurting hole with straws or other textiles that are water straining and then block it with sand bags to reduce the flow and lower the rate of leaking. Simultaneously, sealing and grouting is implemented on the outer side of the retaining wall. Fast setting grout must be used to seal the hole and stop the leak. When grouting and sealing are implemented on the outer side of the retaining wall, if not well carried out, the retaining strut system may be influenced, for example, there may be strut twist or wall crack. Thus, the grouting and sealing operation has to be carefully performed. The best way is to install suitable equipment to monitor the process closely. The mingled impure concrete has to be cleared out of the temporarily treated spurting hole and then filled with nonshrinking cement.

Due to the high pressure of jetting, jet grouting tends to disturb the soils and bring about the failure of soil structures, which renders the method unsuitable for the treatment of water leaking. Instead, chemical grouting is recommended. The choice of grout should be limited to those with high strength and the capability of controlling setting time. However, those that can set within 2–3 seconds are not sufficiently reliable in gluing strength and easily yield when pressed by increasing water pressure. The best choice for now is cement mixed with no.3 waterglass (which sets within 15–20 seconds at best), controlled by way of the 1.5 shot method to enhance its setting.

11.7.2 Dewatering during excavation

Dewatering is usually necessary to keep the excavation surface dry for excavations in sandy or gravel soils. It is basically not required for excavations in clayey soils except for lowering

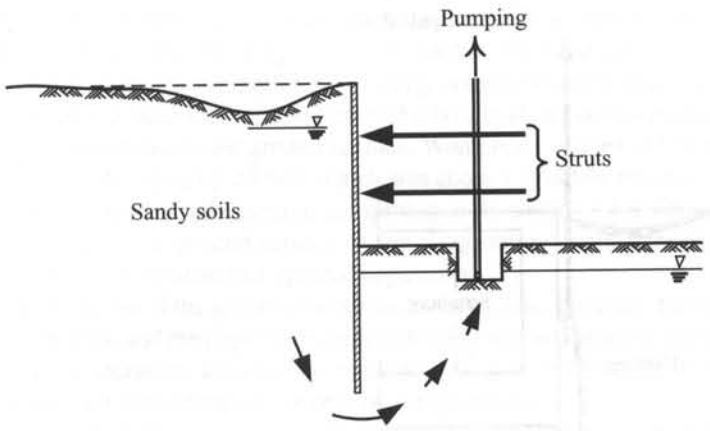

Figure 11.39 Ground settlement induced by pumping.

the groundwater pressure of the permeable soil below the clayey soil to prevent upheaving failure. Pumping outside the excavation zone is likely to lower the groundwater level around the excavation site. If the site consists of clayey soils, it may raise the effective stress of the clay and bring about consolidation settlement of soils outside the excavation zone. The settlement may be uniform or nonuniform, depending on the geological conditions. Pumping, if not carried out carefully, could carry fine soils out of the grounds, which will cause settlement, too, as shown in Figure 11.39.

11.7.3 Construction of the retaining wall

Constructing a diaphragm wall, under normal conditions, will produce settlement inevitably because of the unloading caused by the excavation of trenches. For settlement caused by the construction of diaphragm walls, please refer to Section 6.2 in this book. On the other hand, if the level or unit weight of bentonite fluid in the trench is insufficient, it is very likely to bring about movement or even collapse of the trench, which further induces ground settlement, during the construction of a diaphragm wall.

When the PIP pile (see Section 3.3.3) is adopted as the retaining wall, the loosening of soils caused by boring or the defective backfill of sandy grouts, which both produce voids in soils, will cause movement of the surrounding soils and ground settlement accordingly.

Driving a sheetpile into sandy soils with high groundwater levels by vibration usually causes settlement because of the effects of compaction. If excavation is carried out in clayey soils, pile driving will cause heaves of the nearby soils. What's more, the ground settlement will occur due to the consolidation effect.

11.7.4 Pulling out the used piles

If sheetpiles or soldier piles are used as the retaining walls in an excavation, after the construction of the basement is finished, to save cost, the sheet piles or soldier piles are often pulled out for repeated use. Pulling out the piles, however, will take out soils around the piles and generate voids in the soil, as shown in Figure 11.40. The generated voids are not easily

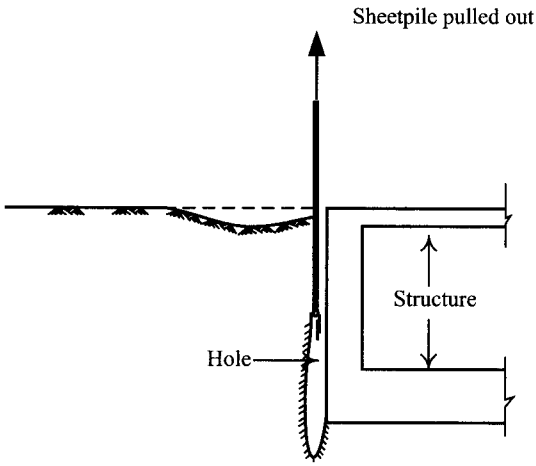

Figure 11.40 Ground settlement induced by pulling out of the used piles.

filled by way of grouting or with sand. As a result, settlement is produced. To prevent this, leave the piles close to buildings in place.

11.7.5 Over-excavation

To determine the excavation depth for each excavation stage, it is necessary to carry out stress and deformation analyses before excavation. Nevertheless, some contractors do not follow the designed depth of excavation and over-excavate for their own benefit or convenience. If the supervising unit is ignorant of the situation or incapable of monitoring the contractors, over-excavation may happen. Over-excavation is really dangerous. It will produce unpredicted large amounts of deformation of the retaining wall or ground settlement under good conditions. Under worse conditions, it may cause the collapse of the excavation.

11.8 Building rectification methods

The principle of building rectification is similar to that of underpinning. The latter, however, refers to the strengthening of the original foundations or addition of a new foundation before excavation to prevent excavation-induced settlement and the resulting property damages. The building rectification method is used to uplift over-settled or leaning buildings, caused by excavation, construction defects, or the liquefaction of soils below the foundations after earthquakes, to their proper location.

Some commonly used building rectification methods are compaction grouting, chemical grouting, and underpinning, etc. This section will explicate these methods in the following.

11.8.1 Compaction grouting

Although the compaction grouting method is widely applied in geotechnical engineering, in most cases, it is used to uplift the settled buildings.

Theoretically, the compaction grouting method is limited in its application to buildings under a certain weight. No related studies in the literature indicate the maximum building weight the compaction grouting method is capable of uplifting. Graf (1992) once lifted up a 4.5 m × 4.5 m square footing by 5 cm using compaction grouting. The footing was 1.2 m deep and bore a dead load of 500 tons and a live load of six driveways. The grouting bulb was 5.75 m deep below the ground surface. Wong *et al.* (1996) uplifted one of the footings of a four floor building by 24 mm, which was about 1 m below the ground surface. Grouting was implemented from the bottom up, starting at the depth of 8 m below the ground surface up to 3 m below the ground surface. When the grouting depth grew higher than 4.5 m, the foundation could be observed uplifted apparently.

A detailed plan of the grouting pressure, grouting rate, grouting depth, arrangement of the grouting points, and the implementation method is required before proceeding to the building rectification operation. Besides, the building should be equipped with complete monitoring instruments for immediate adjustment of the operation.

To uplift a building, the ways of grouting are two: either bore through the floor of the building and grout vertically or grout slantingly from the building side, as shown in Figure 11.41. The former has better effects since it is more direct. Nevertheless, it will affect the use of the building. The latter is less effective but has the benefit of not disturbing the use of the building.

Basically, the arrangement of the grouting points should be aimed at the place where settlement is the largest. The major grouting point should be arranged at a larger depth. The places where settlements are smaller can be arranged as the minor grouting points where the depths are slightly shallower than the major one, as shown in Figure 11.42 (Nonveiller, 1989). The sequence of grouting should follow the degrees of settlement, beginning with the place where settlement is largest and then proceeding to the minor points next to it. The operation is to be repeated till the desired amount of lifting is achieved. If the lifting amount is too large, the operation can be carried out in stages.

Here is a case of a four-floor building with 16 columns in Taipei, each of which is supported by an individual footing embedded 1 m below the ground surface. Influenced by the construction of CP263 of the Taipei rapid transit system, the footings of the buildings settled

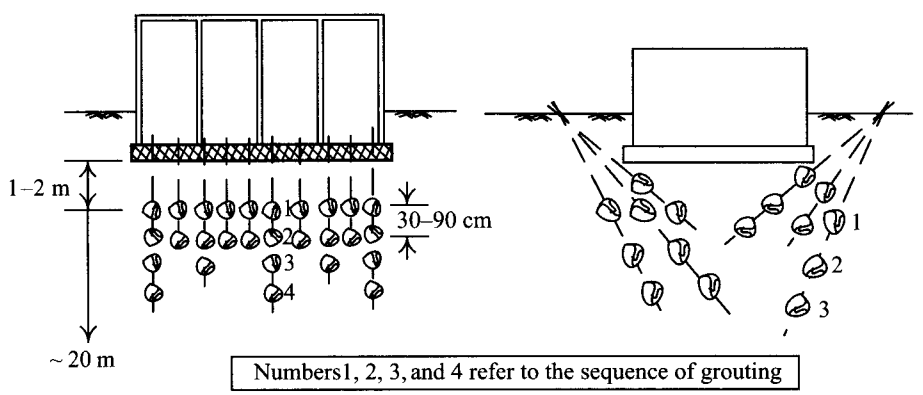

Figure 11.41 Procedure and grouting positions of the compaction grouting method (redraw from Nonveiller, 1989).

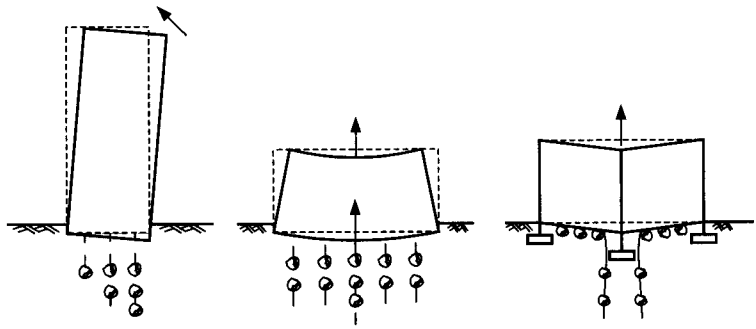

Figure 11.42 Arrangement of the injection points with the compaction grouting method for the rectification of buildings (redraw from Nonveiller, 1989).

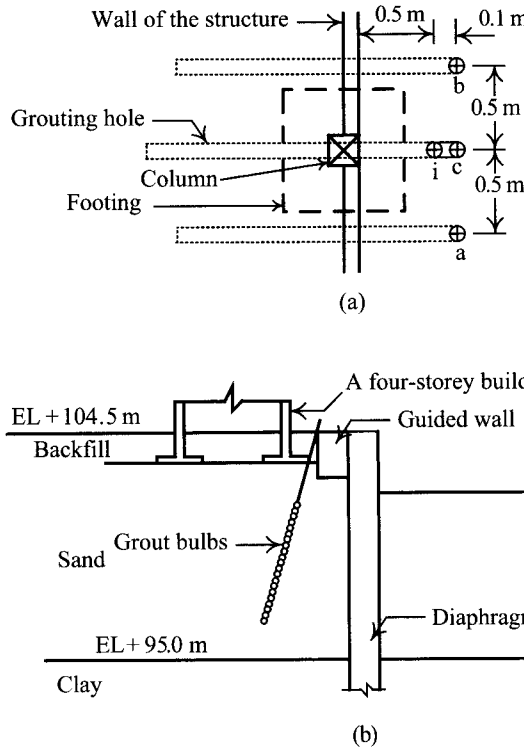

Figure 11.43 Case history of building rectification by the compaction grouting method: (a) plan and (b) profile (Wong *et al.*, 1996).

by 2–4.4 cm, variously. To rectify the building, compaction grouting was implemented at all of the footings. Figure 11.43 diagrams the arrangement of the grouting points and the operation sequence of compaction grouting at one of the footings. The other 15 footings were similarly grouted and uplifted as illustrated in Figure 11.43. As shown in the figure,

point *i* was the major grouting hole whose slant angle was 12°. The minor grouting holes were *a* and *b*, slanted by 15°. The next minor grouting hole *c* was, also slanted by 15°. The grouting sequence was *i*, *a*, *b*, and then *c*. The grouting depth was between 3 and 8 m, from the bottom up. The grouts consisted of 320 kg gravels, 1040 kg silty sand, 160 kg cement, and water of about 425–526 kg per cubic meter. Grouting was carried out at the rate of 0.00708 m^3/min. The pre-designed grouting pressure at *i* was 40 kg/cm^2 whereas that at *a*, *b*, and *c* was 35 kg/cm^2. The outcome of grouting was satisfactory, correcting the building as planned.

11.8.2 Chemical grouting

The development of grout in chemical grouting is not easily controlled and any small incaution might lead to the unpredictable flowing of grouts, which would cause damage to structures and pipes and reduce the effects of grouting. A detailed plan of the grouting pressure, the arrangement of injecting points, the amount of injection, and the measures for preventing fugacious flowing of grouts should be made before implementing chemical grouting to rectify a building. Generally speaking, the grouting pressure, the arrangement of injection points, and the amount of injection are all determined on the basis of empirical experience and adjusted according to the monitoring of the heave of the building. No quantitative methods are available so far. Besides, referring to past case histories is recommended. For the prevention of grout flows going where they are not wanted, there are two methods: installing sealing piles (such as sheetpiles) within the grouting range or reducing setting time of grouts.

The cost of chemical grouting to correct a slanting building is relatively low. Nevertheless, the operation of carrying out a chemical grouting for building rectification is highly technical and ingenious, any incaution easily leading to damage to structures and pipes.

We will take a case history from the construction of the Taipei rapid transit system for illustration. The slanting building had 12 floors of superstructure and one floor of basement with a mat foundation located 4.9 m below the ground surface (Wong *et al.*, 1996). The building was influenced by the construction of the Taipei rapid transit system so that it settled 100 mm at the southeastern corner. The building tilted about 1/100 eastward and 1/200 southward. Figure 11.44a diagrams the plan of the building and the arrangement of the grouting holes for the building rectification operation. The grouting holes on row A and B were set at angles of 22.5° and 31.5° with respect to the vertical line below the building, as shown in Figure 11.44b. The geological conditions are as shown in Figure 11.44b. To prevent the grouts from fleeing, the contractor installed a row of continuous jet grouting piles for sealing (called the JSG method) and limited the setting time to 60 seconds.

The grouts consisted of cement of 250 kg, no.3 sodium silicate solution of 0.25 m^3, and water of 0.671 m^3 per cubic meter. The congealing time was between 34 and 60 seconds.

To set the grouting pressure uniformly on the base of the foundation, three to four grouting machines were used simultaneously, each set to pump between 0.02 and 0.04 m^3/min of grouting. First row A was grouted and then row B after row A was totally grouted. The grouting depth of each row was between GL-13–GL-9 m, starting from the bottom and lifting the drilling rod gradually up. With the clayey soil below the depth of GL-13.8 m (see Figure 11.44b) and the sandy soil above, the grouting operation took the sandy soil below the depth of GL-13 m as the bearing stratum where a larger amount of pressurized grouts was injected to constitute a solid ground in preparation for uplifting the building. With the lifting of the drilling rod, the grouting rate and pressure were lowered gradually. According

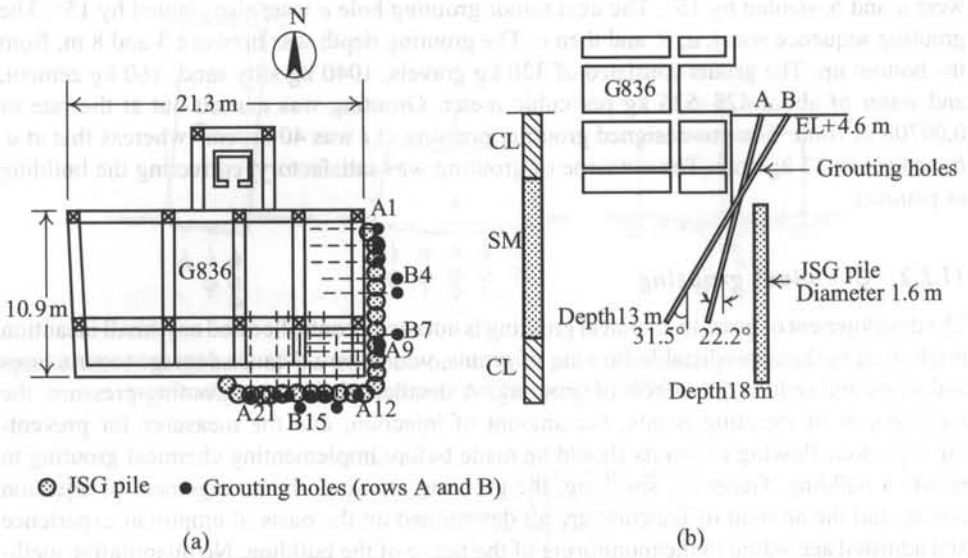

Figure 11.44 Case of building rectification by the chemical grouting method: (a) plan and (b) excavation and geological profile (note: A9 stands for the ninth grouting point in row A and B7 the seventh grouting point in row B, etc) (Chu and Chou, 1998).

to the above principles and experience, the control values of the grouting pressure and flow were determined.

After 11 days' building rectification, the building was uplifted. The contour map of lifting heights is shown in Figure 11.45. As it shows, the building was satisfactorily corrected and the lifted height was distributed lineally, which shows that the influence of the rectification operation on the structure of the building was slight.

11.8.3 Underpinning

The principle of the underpinning for rectifying buildings is similar to that of the underpinning method introduced in Section 11.6.5. The only difference is that the latter aims at prevention before excavation, transferring the load of the building to a new foundation which is not to be influenced by excavation. Therefore, jacks are not necessarily required to uplift the building. The former is to solve an existing problem, correcting a building problem due to excavation. Since the building has already settled, jacks are required to uplift the building. The procedure of the underpinning method is as shown in Figure 11.46. First excavate a sufficient working space, where underpinning piles are to be constructed, around the mat foundation or the individual footing under the column, then set a jack between the pile cap and the mat slab to uplift the building, and last proceed to the load transfer operation.

The underpinning rectification method can be applied to mat foundations and individual footings. Its strength is that the target or range of rectification is specific, without the problem of grout fleeing, which frequently occurs in grouting methods, or worrying about wrongly

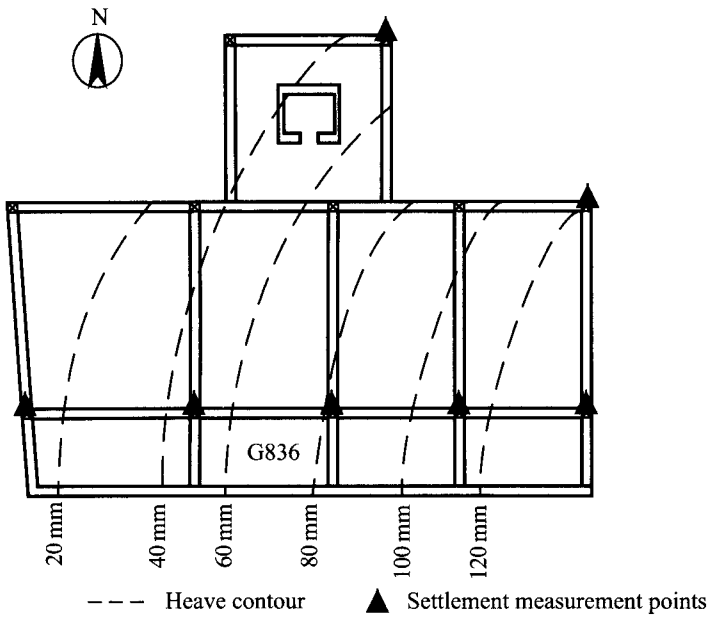

Figure 11.45 Distribution of the heave of the buildings (Chu and Chou, 1998).

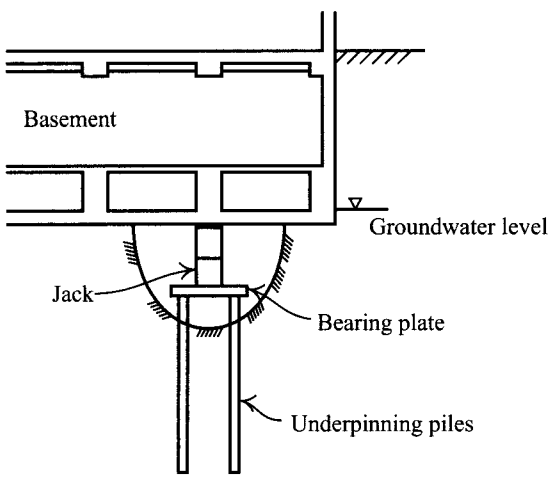

Figure 11.46 Rectification of buildings by the underpinning method.

uplifting a column. The shortcoming is that it costs much more and requires advanced techniques. If not designed well, the building might settle instead due to the settlement of the bearing pile induced by underpinning. A mat foundation that has been underpinned might become a partial pile foundation and change its designed stress distribution.

11.9 Summary and general comments

This chapter has introduced allowable settlements of buildings, relative deflection, and angular distortion and the methods of property protection. Some of them can be analyzed quantitatively whereas the others are only based on empirical experience and rely on monitoring systems. The content of this chapter can be summarized as follows:

1 Increasing the thickness of the retaining wall, enhancing the stiffness of struts, and reducing the horizontal or vertical span of struts are all helpful to reduce the deformation of the retaining wall and the ground settlement induced by excavation. However, these measures are limited in their effects. If the wall deformation or settlement is still too large, auxiliary methods such as ground improvement, the construction of counterforts or cross walls will be needed to further reduce wall deformation or settlement.
2 Struts should be installed as close to the excavation surface as possible to reduce the unsupported length so that the wall deformation or ground settlement can be reduced. If excavating in clayey soils, it is necessary to shorten the waiting time or to install the struts as soon as possible so that the influence of creep can be reduced to the least.
3 Corner effects or the characteristics of settlement can be taken advantage of to help protect buildings.
4 Chemical grouting, the deep mixing method, and jet grouting are the most widely used methods to improve soils in deep excavations. Generally, ground improvement within the excavation zone is better than that outside the excavation zone. The arrangements of ground improvement include the block type, column type, and wall type. Numerical analyses are required before proceeding to ground improvement to determine the strength of the soil body, its diameter, depth, location, and the range of improvement.
5 The counterfort has to be cast into a whole body with the diaphragm wall in order to serve as a reinforced concrete section of a T-beam, enhancing the moment resistance of the diaphragm wall. If the counterfort only contacts the diaphragm wall, without being cast into a whole body, once the diaphragm wall deforms, a relative displacement will be generated between the diaphragm wall and the counterfort. That is to say, the counterfort is useless in increasing the moment resistance of the diaphragm wall. Besides, the counterfort wall has to penetrate into the hard soils (such as sandy or gravelly soils) so that the bottom of the counterfort wall can be restrained effectively and help reduce ground settlement.
6 The designing principle of cross walls is to view the cross walls as struts which exist before excavation and are capable of bearing high compressive force. Thus, theoretically, the place where a cross wall is constructed in advance is less likely to move when excavation because it is restrained by the cross wall. The effect of the cross wall on reducing the lateral deformation of the retaining wall is obvious. From the economical perspective, when the cross wall is placed between the excavation surface and 5–6 m below, it is the most efficient in reducing the wall deformation and ground settlement.
7 Micro piles have been applied to property protection in excavation projects for many years. Some successful case histories have been documented though other unsuccessful ones have not. Because the mechanism of micro piles in property protection is not direct, there has not been a systematic study of their mechanism yet. As a result, though there have been successful case histories, most of them were designed on the basis of empirical experience and lack theoretical foundations.

8 Some underpinning methods require load transfer operations whereas others do not. Underpinning methods require more advanced techniques and are also expensive, though whether they are effective in reducing the wall deformation and ground settlement is still debatable.
9 Construction defects in excavations will certainly increase extra wall deformation and ground settlement. It can hardly be predicted by way of theoretical analysis or eliminated accordingly. The only way is to prevent it from happening and be prepared with the emergency measures.
10 No matter whether buildings settle too much due to excavation, defective construction, or soil liquefaction caused by earthquakes, they may be remedied by way of building rectification. Some commonly used building leveling methods include compaction grouting, chemical grouting, and underpinning.

Problems

11.1 Here is a factory with the column span, 15 m. Estimate the allowable angular distortion, the allowable differential settlement, and the allowable total settlement.
11.2 Choose a building and estimate its allowable angular distortion, allowable differential settlement, and allowable total settlement according to its materials, structures, foundation type and importance of the building.
11.3 Explain the reason why struts should be installed as close to the excavation surface as possible.
11.4 Figure 11.9 illustrates two identical excavations in both geological and excavation conditions except for the excavation depths of stages. Assume the soil at the site is the normally consolidated clay and the groundwater level is at the ground surface. The basic properties of the clay are as follows: $\gamma_{sat} = 18.6\,kN/m^3$, $c' = 0$, $\phi' = 30°$, and $s_u/\sigma'_v = 0.3$. The thickness of the diaphragm wall is 60 cm. The stiffness of the struts is 30,000 kN/m/m (unit width). The preload is 45.0 kN/m (unit width). Analyze the excavations as shown in Figures 11.9a and 11.9b through the computer program and compare the deformation characteristics of the two cases to find out which one is to produce more deformation of the retaining wall.
11.5 Rework Problem 11.4. Assume the soils at the excavation site are sandy soils and the groundwater level is at the ground surface. The basic properties of the soils are as follows: $\gamma_{sat} = 20.6\,kN/m^3$, $c' = 0$, and $\phi' = 33°$. The SPT-N values of the soils are as illustrated:

Depth (m)	*SPT-N*
0–5	6–9
5–8	8–16
8–13	14–20
13–18	18–23

11.6 Explain why the deformation of the retaining wall or ground settlement with the top down method is larger than that with the bottom up method.

11.7 The increase of the strut stiffness can reduce the wall deformation or ground settlement caused by excavation. Explain why, however, the increase of the strut stiffness can not help reduce the wall deformation or ground settlement once the strut stiffness has reached a certain level.

11.8 Assume the strut stiffness is constant. Explain why the increase of the levels of struts (i.e. the reducing of the vertical span of struts) can help reduce the wall deformation caused by excavation from the perspective of the deformation characteristics at each excavation stage.

11.9 Here is an excavation in soft clay whose undrained shear strength is $s_u = 98.1\ kN/m^2$. A soil improvement is to be carried out on the soil. The improvement pile has an uniaxial compressive strength (q_u) of $1{,}472\ kN/m^2$. The diameter of the improvement pile is 60 cm. The piles are arranged as shown in Figure P11.9. Estimate the shear strength of the composite material.

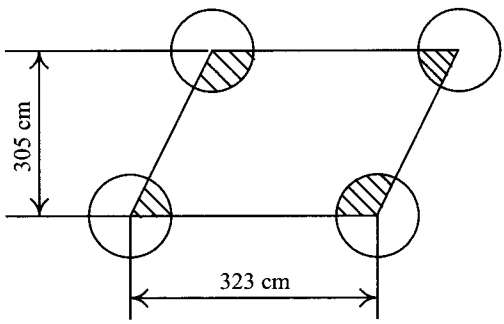

Figure P11.13

11.10 Same as in Problem 11.9 but change the soils to be sandy soils. Before the improvement, the effective cohesion and friction angle are $c' = 0$, and $\phi' = 30°$. The uniaxial compressive strength after improvement grows to be $5{,}000\ kN/m^2$.

11.11 Assume the uniaxial compression strength of an improvement pile to be $1{,}472\ kN/m^2$ and the diameter of the pile is 80 cm. The piles are arranged as shown in Figure P11.11. Rework Problem 11.9.

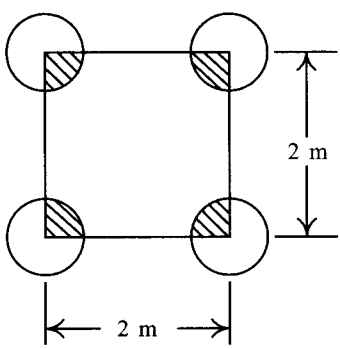

Figure P11.11

11.12 Assume the uniaxial compressive strength of an improvement pile to be 5,000 kN/m^2 and the diameter of the pile is 80 cm. The piles are arranged as shown in Figure P11.11. Rework Problem 11.10.

11.13 Find a case history of ground improvement in an excavation from related journals or conference papers and elucidate the effects of the improvement. The contents of the elucidation should include the geometric conditions (such as the thickness and depth of the retaining wall), the geological profile, the ground improvement method, the improvement range, and the effects.

11.14 Figure 11.23 diagrams the plan of an excavation in clayey soils. The groundwater level is at the ground surface. The final excavation depth is 10 m. The retaining wall is a diaphragm wall, which is 50 cm thick and 20 m deep. The basic properties of the soils: $s_u = 68.7$ kN/m^2 and $\gamma_{sat} = 17.7$ kN/m^3. Estimate the maximum lateral resistance of soils per unit width (i.e. the passive pressure) on the front of the wall below the excavation surface without any auxiliary methods. To avoid too much wall deformation caused by excavation, many counterforts are to be constructed perpendicular to the retaining wall at the inner side of the wall. The counterforts are 50 cm and 2 m long. The depth of a counterfort is from the excavation surface to the wall bottom (GL-10–GL-20 m) and the distance between any two counterforts is 10 m. The counterforts only contact the diaphragm wall without forming a whole body with it. When the diaphragm wall moves toward the excavation zone, estimate the maximum lateral resistance of the wall per unit width. How much is the lateral resistance of the wall increased after the counterforts are constructed?

11.15 Rework Problem 11.14 and assume the soils at the site are sandy soils this time. The groundwater level is also at the ground surface. The basic properties of the sand: $\gamma_{sat} = 20.6$ kN/m^3, $c' = 0$, and $\phi' = 33°$.

11.16 Find a case history of constructing counterfort walls in an excavation from related journals or conference papers or one which is under construction and elucidate the effects of the counterfort walls. The contents of the elucidation should include the geometric conditions (such as the thickness of the retaining wall and the wall depth), the geological profile, the sizes of the counterforts, and the effects.

11.17 Figure 11.23 diagrams the plan of an excavation in clayey soils. The final depth of the excavation is 10 m and adopts a 50 cm thick, 20 m deep diaphragm wall as the retaining wall. Assume two cross walls are constructed by unreinforced concrete walls. The cross walls are 50 cm thick and separated by a distance of 20 m from each other. The depth of the cross walls is from the excavation surface to 6 m below it (GL-10–GL-16 m). They connect with the retaining wall without forming a whole body with the retaining wall. Elucidate how an analysis of the deformation behavior of the retaining wall using the plane strain method should be conducted. What is the shortcoming of the plane strain method in the analysis of an excavation with installation of cross walls?

11.18 Find a case history of constructing cross walls in an excavation from related journals or conference papers or one which is under construction and elucidate the effects of the cross walls. The content of the elucidation should include the geometric conditions (such as the thickness of the retaining wall and the wall depth), the geological profile, the sizes of the cross walls, and the effects.

11.19 Figure 11.23 diagrams the plan of an excavation, whose final excavation depth is 10 m and which adopts a 50 cm thick, 20 m deep diaphragm wall as the retaining

wall. Condition A: construct five 50 cm thick and 5 m long counterforts to form a whole body with the retaining wall. The counterforts are constructed by unreinforced concrete walls, from the excavation surface to the bottom of the diaphragm wall (GL-10–GL-20 m) and are separated by 10 m. Condition B: construct five cross walls. The thickness and depth of the cross walls and distance between them are all identical to the above counterforts. Which condition will yield less wall deformation?

11.20 When applying micro piles to property protection in excavations, assuming the design principle as shown in Figure 11.29, what is the mechanism of the micro piles in property protection? Elucidate it.

11.21 When applying micro piles to property protection in excavations, assuming the design principle as shown in Figure 11.30, what is the mechanism of the micro piles in property protection? Elucidate it.

11.22 Find a case history of applying micro piles to property protection in excavations from related journals or conference papers or one which is under construction and elucidate the effects of the micro piles. The contents of the elucidation should include the geometric conditions (such as the thickness of the retaining wall and the wall depth), the geological profile, and the construction and arrangement of micro piles.

11.23 What types of underpinning methods are there? Which one is most likely to induce extra settlement of the building and why?

11.24 Explain why the load transfer operation in underpinning methods requires the procedure of preloading?

11.25 Find a case history of applying underpinning methods to property protection in excavations from related journals or conference papers or one which is under construction and elucidate the effects of underpinning. The contents of the elucidation should include the geometric conditions (such as the thickness of the retaining wall and the wall depth), the geological profile, the construction of underpinning, and the effects.

11.26 When excavating in sandy soils, what types of defective construction will often happen and cause property damage in the vicinity of the excavation?

11.27 When excavating in soft clay, what types of defective construction will often happen and cause property damage in the vicinity of the excavation?

11.28 Find a case history of property damage caused by defective construction in excavation from related journals or conference papers or one which is under construction and elucidate the causes of damage. Elucidate the geometric conditions (such as the thickness of the retaining wall and the wall depth), the geological profile, and investigate the causes of property damage.

11.29 What types of building rectification methods are there? Elucidate the strengths and shortcomings of the methods separately.

11.30 Find a case history of building rectification from related journals or conference papers or one which is under construction and elucidate the effects of the method. Include the causes of building settlement, the process, and effects of rectification, etc.

Chapter 12

Monitoring systems

12.1 Introduction

Though in the past theories of excavation analysis and design were not advanced, with conservative design and shallower excavation depths, few construction calamities occurred. In recent years, with the high development of construction activity, excavation depths grow deeper and deeper. What's more, these excavations are usually located in densely populated areas and more and more problems of property damage are encountered. Though the technologies of analysis, design, and construction have improved significantly, they are not necessarily capable of coping with changes during excavation. Thus, a well-arranged monitoring system will be helpful not only to monitor the excavation conditions but to ensure the safety of excavation.

Generally, the objects of an excavation monitoring program can be summarized as the following:

1 *To ensure the safety of excavation*: To ensure the safety of excavation is the first thing for an excavation monitoring program. Before a calamity happens, there will be some signs, such as an extraordinary increase of the wall or soil deformation or stress. A monitoring system can issue an immediate warning to help engineers adopt effective measures to forestall a calamity when these signs appear.
2 *To ensure the safety of the surroundings*: Excavations are usually located in busy commercial areas or densely populated residential areas. It is almost impossible to avoid influencing the surrounding buildings, underground pipes, public utilities, and pedestrians. The designer has to consider all these factors and establish a monitoring system to ensure the safety of people and property during excavation.
3 *To confirm the design conditions*: Since the existing analysis theories are not satisfactorily mature and the geological investigations can not fully represent the in situ conditions and the complicated construction environment, the analysis results do not necessarily meet the actual conditions. Back analyses based on monitoring results can help modify and correct the original design, reduce the cost, shorten the excavation period, and change the basis of design. Further, they can serve as a reference for similar designs in the future and help enhance the excavation techniques.
4 *To follow long-term behavior*: An important construction project finished, the monitoring system can be retained for long-term follow up, studying whether the long-term behavior of the case conforms to the original hypotheses.

5 *To supply factual materials for legal judgment*: Information obtained from monitoring systems, along with the construction records, can serve as evidential data when a calamity or property damage occurs. Understanding the true causes of the events can avoid unnecessary disputes and help the restoration and compensation work. The excavation can be least delayed.

Principally, the generally adopted geotechnical instruments for monitoring programs can also be applied to excavation projects. Considering the particularities of excavations, such as the monitoring time period, the rapid change of stress and strain of structures and soils, serious impact on environment, and the economic factors, some special instruments and their installation methods have been developed or have proved suitable for excavation. The purpose of this chapter is to introduce the basic measurement items and principles of an excavation monitoring program. For more detailed instrument types or principles, please refer to the literature (Hanna, 1985; Dunnicliff, 1988; ICE, 1989).

12.2 Elements of a monitoring system

Monitoring field performance is basically the measurement of the physical quantities of some objects, such as deflection, stress and strain, etc. The common monitoring items in excavations are (1) movement of the structure or soil (2) stress or strain of the structure or soil (3) water pressure and level. The monitoring objects of movement include the lateral deformation of the retaining structure and soils, the tilt of the building, the settlement of the ground surface and the building, the heave of the excavation bottom and the uplift of the central post, etc. The measurements of stress and strain include those of the strut load, the stress of the retaining structure, and the earth pressure on the wall. The measurement of water pressure refers to the water pressures within the excavation zone, outside the excavation zone, and on the retaining wall.

In principle, the types of monitoring instruments in an excavation are not special. As long as they meet the budget and the criterion of accuracy, any instruments or methods are feasible. Most of the instruments can be divided into electronic and nonelectronic types. The electronic type is more sensitive and easy to read. They can also be composed into an automatic or semi-automatic monitoring system. Nevertheless, the precision is easily influenced by the installation process and the surroundings. The durability of electronic instruments needs examination because an excavation usually needs to be monitored over a long period. Thus, when installing an electronic instrument in the field for long-term monitoring, durability needs special attention.

Generally speaking, the instruments for plane surveying, such as tapes, levels, and theodolites can be used for the measurement of movement. The measurement of the tilt angle can also resort to those for plane surveying (same as above) or electronic instruments. Electronic instrument sensors include strain gauges and force balance accelerometers, etc. The most common instruments to measure stress or strain are the strain gauge or the electronic transducer that takes the strain gauge as the measurement unit. Since the strain gauge is widely used directly or indirectly in monitoring systems, Section 12.3 will introduce the commonly used types and basic principles of strain gauges. This chapter will omit general instruments for plane surveying. Please refer to related books on plane surveying if interested in the subject.

The types of monitoring systems can be categorized into manual, automatic, and semi-automatic systems. A manual monitoring system is one that requires human reading of the measured values, no matter if it is electronic or mechanical. An automatic system is one that is equipped with electronic sensors, which are connected to a central computer system by cable or wireless connection for every monitoring instrument on the excavation site. When excavating, these values are transferred to the computer center periodically and then computed and shown on computer monitors. Thus, continuous values of measurement can be obtained. The method is expensive, though effective, and saving the trouble of human reading of measured values. It is usually only applied to excavation projects that are especially sensitive environmentally.

An automatic monitoring system can supply continuous measured values but is usually too expensive. Manual monitoring systems do not cost much but are incapable of supplying continuous measured values. As a result, some excavations adopt a semi-automatic monitoring system instead. The so-called semi-automatic system refers to one that employs electronic sensors for crucial parts, but counts on human reading for the others. The values from the electronic sensors are collected periodically by cable or wireless to a data logger near the excavation site. The engineers then collect the data from the data logger. The method can save cost and obtain continuous values as well.

Since the manual monitoring system is still most widely used in excavations, the monitoring instruments and methods that will be introduced in this chapter are basically those that count on human reading.

12.3 Principles of strain gauges

The strain gauge is often used as a measurement unit in many monitoring systems. This section will introduce the commonly used strain gauges for reference in the choice of monitoring instruments.

There are many ways to measure strains. They can be obtained directly by a strain gauge or computed from other physical quantities. The types of strain gauges are many, though the more commonly used in excavations are the resistance strain gauge and the vibrating wire strain gauge. This section will introduce the principles of the two types of strain gauges.

12.3.1 Wire resistant type of strain gauges

Figure 12.1 diagrams the basic configurations of three commonly used resistance strain gauges. Figure 12.1a is a bonded wire resistance strain gauge, which consists of a base (insulating plate) and a fine resistance wire (with a diameter between 0.02 and 0.025 mm) attached to it. The resistance wire, 2–60 mm long, is usually made of copper and nickel alloy or nickel and chromium alloy with its resistance set at 120 ohm. Since the strain gauge adopts a metal wire for the resistor, it is called the bonded wire resistance strain gauge. If the resistor is a thin piece of foil (made of the same material as the bonded wire strain gauge), which is directly attached to the base and photo-etched to set the resistance value (also 120 ohm in most cases), the strain gauge is called the foil resistance strain gauge, as shown in Figure 12.1b. Another type adopts a fine metal wire circling two sets of insulating rods, which are fixed onto the object of measurement. This type of strain gauge is called the unbounded wire resistance strain gauge, as shown in Figure 12.1c.

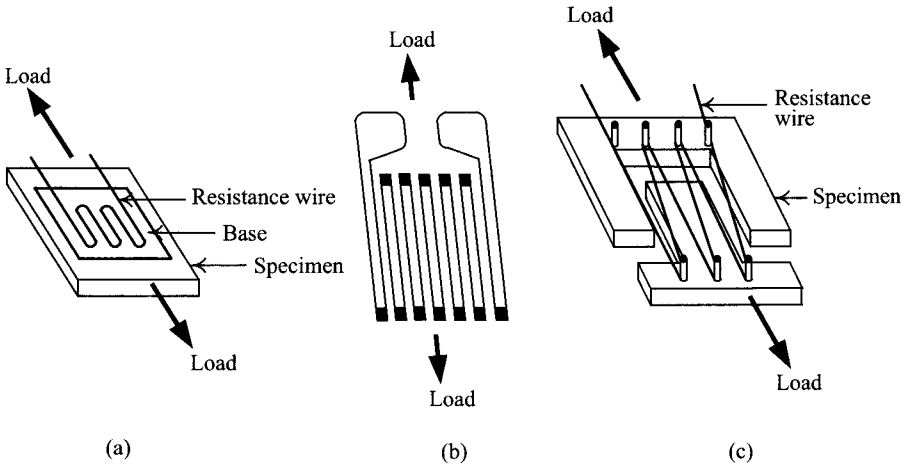

Figure 12.1 Commonly used resistance strain gauges: (a) bonded wire resistance strain gauge, (b) foil resistance strain gauge, and (c) unbonded wire resistance strain gauge.

Though different in constitution, the principles are similar. The resistor will produce resistance when electrified, the values of which vary with the materials of resistance wire. When the wire grows finer and longer, resistance will be increased. Otherwise, it will be decreased. When the object is lengthened due to loading, the wire becomes finer and longer, and resistance will be increased. When the object is compressed by a load, the resistance reduces.

Assume the length, section area, diameter, and resistance of the metal wire (the resistance wire) before it is strained are ℓ, A, d, and R. The resistance, R, can be expressed as follows:

$$R = \rho \frac{\ell}{A} \tag{12.1}$$

where ρ is the coefficient of resistance of the metal wire.

Differentiate the above equation on both sides, we have

$$\frac{\Delta R}{R} = \frac{\Delta \rho}{\rho} + \frac{\Delta \ell}{\ell} - \frac{\Delta A}{A} = \frac{\Delta \rho}{\rho} + \frac{\Delta \ell}{\ell} + 2\nu \frac{\Delta \ell}{\ell} \tag{12.2}$$

where ν is Poisson's ratio of the metal wire.

Let the strain of the wire be ε. Then $\varepsilon = \Delta \ell / \ell$. The above equation can be simplified as

$$\frac{\Delta R/R}{\varepsilon} = (1 + 2\nu) + \frac{\Delta \rho / \rho}{\varepsilon} \tag{12.3}$$

Assume the change rate of the coefficient of resistance of the wire has a direct proportion to that of its volume. Then

$$\frac{\Delta \rho}{\rho} = m \frac{\Delta V}{V} \tag{12.4}$$

where m is a constant, which can be obtained from tests on the metal material.

On the other hand,

$$\frac{\Delta V}{V} = (1 - 2\nu)\frac{\Delta \ell}{\ell} \tag{12.5}$$

Substitute the above two equations into Eq. 12.3, we have

$$\frac{\Delta R/R}{\varepsilon} = (1 + 2\nu) + m(1 - 2\nu) = (1 + m) + 2\nu(1 - m) \tag{12.6}$$

Let $K = (1 + m) + 2\nu(1 - m)$. Then the above equation can be simplified as

$$\frac{\Delta R/R}{\varepsilon} = K \tag{12.7}$$

where K can be viewed as the constant of the instrument, which can be obtained from the tests on the material properties of the wire. As illustrated above, the change rate of the resistance of the wire has a proportional relation with the strain. If the change in amount of resistance is measured, the strain can be derived.

The strain-induced change of resistance is too small to be measured directly, nevertheless. Generally a Wheatstone bridge is used to transform the change in amount of resistance to voltage and amplify the change in resistance. Figure 12.2 diagrams the basic circuit of a Wheatstone bridge. There are four bridge arms, where on each a resistor is installed. R_1, R_2, and R_3 are the resistance of the bridge that are constant, not influenced by strain. R_g is the resistance of the strain gauge, which is the only resistance that can be changed in the bridge. V_{in} is the input voltage of the bridge and V_{out} the output voltage.

Assume the electric current passing through R_1 and R_2 is I_1 while that through R_g and R_3 is I_2. According to Ohm's law, we can derive I_1 and I_2 as follows:

$$I_1 = \frac{V_{in}}{R_1 + R_2} \tag{12.8}$$

$$I_2 = \frac{V_{in}}{R_g + R_3} \tag{12.9}$$

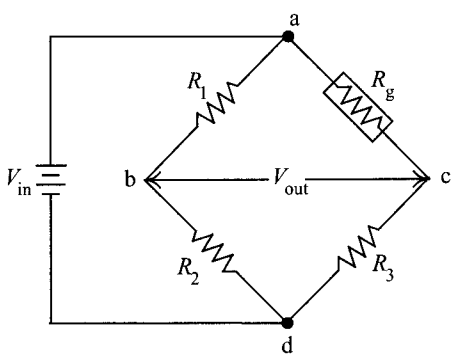

Figure 12.2 Wheatstone bridge.

Thus, the voltages between points a and b and points a and c are separately

$$V_{ab} = R_1 I_1 \tag{12.10}$$

$$V_{ac} = R_g I_2 \tag{12.11}$$

And the output voltage, V_{out} (the voltage between points b and c) is

$$V_{out} = \frac{R_1 V_{in}}{R_1 + R_2} - \frac{R_g V_{in}}{R_3 + R_g} = \frac{V_{in}(R_1 R_3 - R_2 R_g)}{(R_1 + R_2)(R_3 + R_g)} \tag{12.12}$$

As illustrated above, when $R_1 R_3 = R_2 R_g$ or $R_1/R_2 = R_g/R_3$, then $V_{out} = 0$. In application, before strain of the object is produced, we can adjust the resistance of one of the bridges (e.g. R_2) to make $V_{out} = 0$ (i.e. to satisfy the relation $R_1 R_3 = R_2 R_g$) and obtain the resistance of the strain gauge (R_g). When strain is produced, readjusting R_2 to make $V_{out} = 0$, we can have the change in resistance, ΔR_g. From $\Delta R_g/R_g$ and Eq. 12.7, we have the strain of the strain gauge, that is, the strain of the object. This is the principle of the equilibrium bridge under which the strain of an object has a linear relationship with the change of the rate of the resistance.

Rewrite Eq. 12.12 into the following form:

$$\frac{V_{out}}{V_{in}} = \frac{R_1}{R_1 + R_2} - \frac{R_g}{R_3 + R_g} \tag{12.13}$$

The above equation is valid both before and after strain. Let the resistance be $R_g + \Delta R_g$ after straining and let ΔV represent the difference between the V_{out}/V_{in} values before and after straining. Then

$$\Delta V = \left(\frac{V_{out}}{V_{in}}\right)_{strained} - \left(\frac{V_{out}}{V_{in}}\right)_{unstrained} \tag{12.14}$$

If we substitute Eq. 12.7 into the above equation, we can derive the relationship between the change rate of resistance ($\Delta R_g/R_g$) and ΔV, which is usually nonlinear. This is the so-called nonequilibrium bridge.

As discussed above, though in the equilibrium bridge the relation between the strain and the change rate of resistance is linear, it has to be adjusted manually to set the output voltage equal to 0. Though in the nonequilibrium bridge the relation between the strain and the change rate of resistance is nonlinear, the strain can be precisely computed through computer programming. Even when the input voltage is unstable, the instantaneous input and output voltages can still be measured and used for computing strain.

To measure the strain gauge, one can resort to the quarter bridge method, the half bridge method, or the full bridge method. The quarter bridge method is to place a single strain gauge on one of the four bridges whereas high precision resistors are placed on the other three bridges. Figure 12.3a diagrams the typical quarter bridge method, which is usually applied to measuring the strain of members in a structure or building. The quarter bridge method can not cope with the problems of thermo-compensation.

The half bridge method is to place strain gauges on two bridges while the other two are set with high precision resistors. Figure 12.3b diagrams the half bridge method, which can generate output twice as large as that generated by the quarter bridge method and can be used

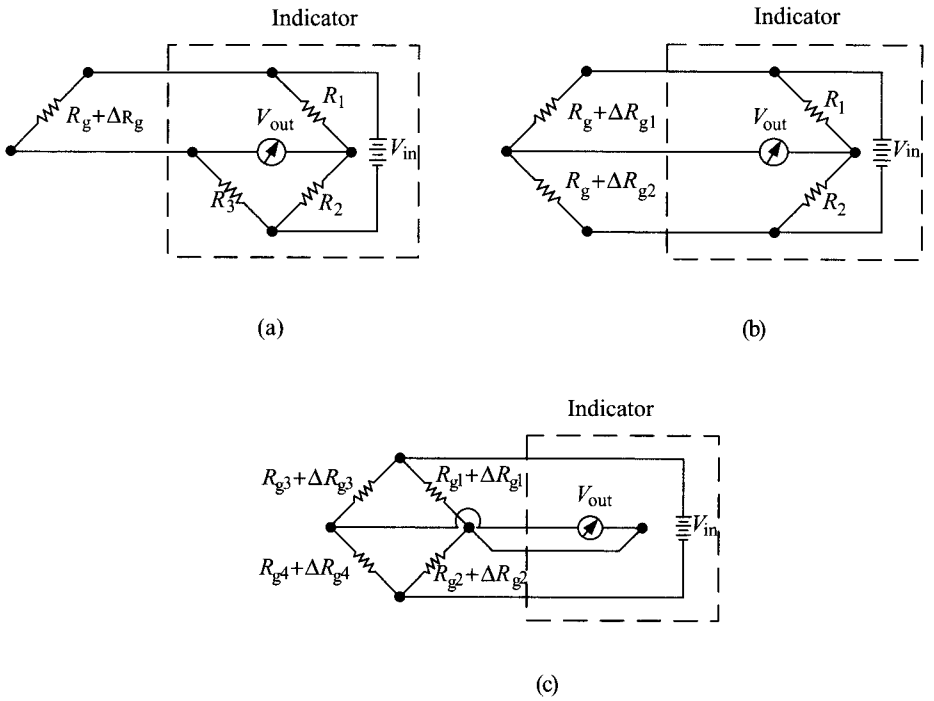

Figure 12.3 Measuring methods of a strain gauge: (a) quarter bridge method, (b) half bridge method, and (c) full bridge method.

with thermo-compensation sets. The full bridge method is to install strain gauges on four bridges. Figure 12.3c also displays the schematic diagram of the full bridge method. For the procedures of computing strains using quarter bridge, half bridge, and full bridge methods and their detailed elucidation, please refer to related documents (e.g. Dunnicliff, 1988).

Since the resistance type of strain gauge takes advantage of the change in resistance to measure the strain, any pollution such as dust, the change of temperature or humidity, or the length of the wire will all influence the measurement of strain. If water invades the interior of the strain gauge, the measured value of strain will become invalid because water is an electric conductor. Thus, under general conditions, the resistance type of strain gauges is better used indoors. However, if the strain gauge is well waterproofed, it can also be used outdoors. The strength of the resistance type is that it is sensitive and can be miniaturized to serve as a small instrument measuring unit.

12.3.2 Vibrating type of strain gauges

The basic configuration of the vibrating type of strain gauge is as illustrated in Figure 12.4. The vibrating wire is fixed to an object. The length of the wire changes with the deformation of the object influenced by external factors (such as temperature or force), which causes the change of the natural frequency of the wire. The strain of the object is thus obtained through measurement of the natural frequency of the wire.

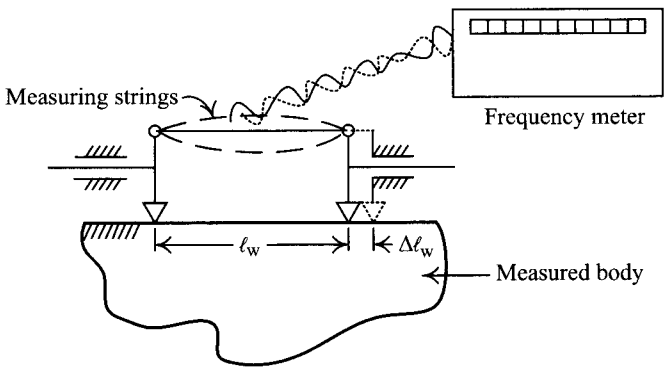

Figure 12.4 Configuration of a vibrating strain gauge.

Assume the mass of the wire per unit length is m, the wire length is ℓ_w and the tensile or compressive force acting on the wire is F. We can compute the natural frequency of the wire as follows:

$$f = \frac{1}{2\ell_w}\sqrt{\frac{F}{m}} \tag{12.15}$$

According to mechanics of material, the tensile or compressive force can be expressed as follows:

$$F = \sigma_w a = \varepsilon_w E_w a \tag{12.16}$$

where

σ_w = tensile stress or compressive stress of the wire
a = section area of the wire
E_w = Young's modulus of the wire
ε_w = strain of the wire.

If we substitute Eq. 12.16 into Eq. 12.15, we have

$$f = \frac{1}{2\ell_w}\sqrt{\frac{\varepsilon_w E_w a}{m}} \tag{12.17}$$

From the above equation, we can further derive the relation between the strain of the wire and its frequency as follows:

$$\varepsilon_w = \frac{f^2}{K} \tag{12.18}$$

where $K = E_w a/(4\ell_w^2 m)$ = constant of the instrument, which can be directly determined according to the material properties of the wire.

If the object and the strain gauge are well welded, the deformation of the object and that of the wire will be identical. That is to say,

$$\varepsilon_w \ell_w = \varepsilon_s L_s \tag{12.19}$$

where ε_s is the strain of the object and L_s is the length of the strain gauge.

As a result,

$$\varepsilon_s = \frac{\varepsilon_w \ell_w}{L_s} \tag{12.20}$$

As elucidated above, as long as the natural vibrating frequency of the wire can be measured, the stress and strain of the wire and the object can also be derived.

To measure the strain, connect the strain gauge with the sensor where the direct currents produce a magnetic field that will vibrate the wire. The natural frequency of the strain gauge is measured by the sensor simultaneously. After conversion by the constant of the instrument, the stress and strain of the wire and the object can be derived.

Since the vibrating type of strain gauge takes advantage of the vibrating frequency of the wire to obtain the strain of an object, the frequency is not influenced by resistance, and the cable (the signal cable) can be extended as long as needed for field measurement. The vibrating type of strain gauge, however, is not as sensitive as the resistance type. If applied for long-term monitoring, humidity or water may invade the gauge and erode the wire. The problem of creep is also to be considered for long-term use. These factors will change the frequency of the strain gauge and influence the measured values. Applying the vibrating type to such conditions, one has to take these problems into consideration.

12.4 Measurement of movement and tilt

Excavation will cause the structures and soils within the influence range to move. The directions of movement may be horizontal, or vertical, or both. According to the characteristics of the object to be monitored, the monitored items of movement, such as horizontal movement, vertical movement or both, or tilt of the object, is thus able to be determined. Generally, the lateral deformation of the retaining structure, the lateral deformation of soils, the tilt of the structure, the ground settlement, and the settlement of the building are the basic items of measurement for an excavation. This section will introduce the principles and the details of measurement.

12.4.1 Lateral deformation of retaining walls and soils

The lateral deformation of a retaining wall (such as soldier piles, diaphragm wall, etc.) is one of the important monitoring items of excavation. The lateral deformation of a retaining wall relates closely to the ground settlement (or the settlement of the buildings). The magnitude and shape of lateral deformation of the retaining wall can be used for the judgment of the safety of the retaining wall or the buildings in the vicinity.

To explore the characteristics of an excavation or for some special objectives, it is sometimes required to measure the lateral deformation of soils. The strain at a specific point in the soil can be computed if extensometers, used to measure vertical movement at a point in the soil, are installed near an inclinometer casing (Ou *et al.*, 2000a). The results can

be used to understand the tendency to movement of soil. This data is important for excavation studies though difficult to apply to the judgment of excavation safety.

The inclinometer casing and the inclinometer are commonly used devices for the measurement of the lateral deformation of retaining walls or soils. The common dimensions of an inclinometer casing include 1.9″OD × 1.50″ID, 2.75″OD × 2.32″ID, and 3.34″OD × 2.87″ID (OD represents the outer diameter and ID the inner diameter). An inclinometer casing has four tracks, which constitute the two perpendicular axes, along each of which two sets of wheels of the inclinometer are embedded. The two ends of an inclinometer casing are the male and female unit joints, respectively, by which several inclinometers can be connected (or couplers can be used) to measure greater depth. The spiral of an inclinometer casing should be as small as possible. Otherwise, the tracks may not be on a vertical plane. This is a factor influencing the precision of measurement. Figure 12.5a is a photo of some inclinometer casings and the types of sections.

Some commonly used materials for inclinometer casings are ABS pipes, aluminum pipes, and PVC pipes. They are elucidated as follows:

1 *ABS pipes*: ABS (acrylonitrile/butadiene/styrene) is a macromolecule material. Four tracks are made inside the pipe using lathes. As a result, the tracks are hollowed in the pipe (see Figure 12.5b). The strengths of an ABS pipe are the high flexibility, multiple dimensions, and the high tightness between joints, which enables them to be installed without crevices which let in grouts to influence the measurement result. It is also less likely to produce a high spiral in its manufacture or installation. Its shortcomings are as follows: it costs a lot and if the lathe is not well controlled, the tracks are easily made too deep and the pipe too thin as a result, which may, in turn, lead to the breaking of the pipe when acted on by porewater pressure.

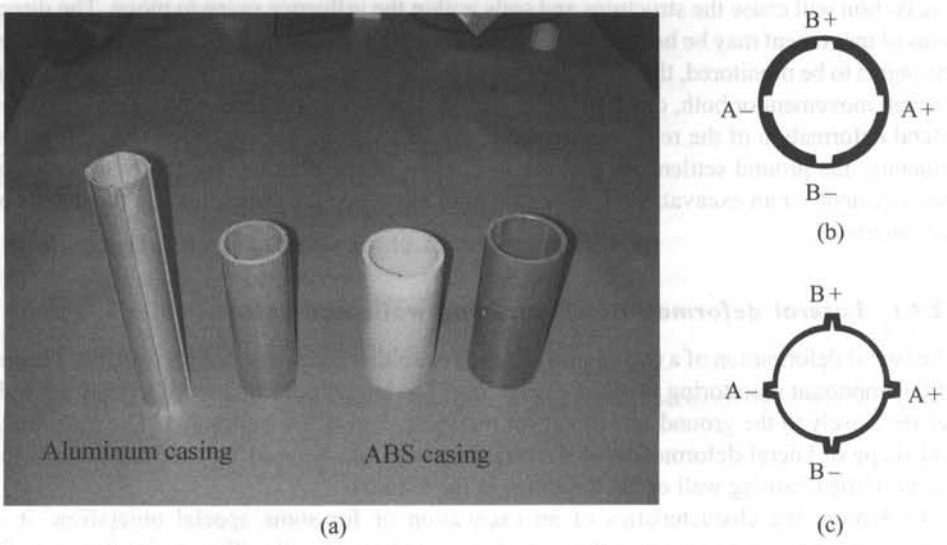

Figure 12.5 Inclinometer casings: (a) photo, (b) tracks made inside the casing, and (c) external tracks protruding from the casing.

2 *Aluminum pipes*: These are usually formed through injection molding. The measuring tracks are external to the pipe (Figure 12.5c). The size usually comes as 1.9″OD. Their strengths are the light weight, ease of transportation, and lower cost. Their shortcomings are: they are easily eroded and are not suitable for long-term measurement in salty areas; the width of tracks, influenced by the manufacturing process, may be too large and the wheels of the inclinometer may not be tightly embedded in the tracks. The spiral is also larger than the ABS or PVC pipes.
3 *PVC pipes*: These are usually formed through injection molding, too. The strengths of PVC pipes are: they can be made in multiple sizes; they are heavier than ABS pipes, therefore, the phenomenon of spiraling induced by the uplift of groundwater is less likely to happen during installation. The shortcomings are that they are easily deformed as a result of sun exposure. PVC pipes are also more fragile and easily break. The spiral is a little larger than ABS pipes.

Figure 12.6 illustrates the photo and the basic configuration of an inclinometer. As shown in the figure, the inclinometer is a four foot (two pair of wheels) instrument containing a tilt measuring sensor (also called an electronic pendulum). The top of the inclinometer is connected to a cable, which is, in turn, connected to a readout on the ground surface. According to the type of measuring unit of the sensor, the inclinometer can be divided into resistance type, vibrating type, and force balance accelerometer type. The basic principle of the resistance and vibrating types are as elucidated in Section 12.3. The force balance accelerometer type places a pendulum amid the magnetic field of coils of a location detector.

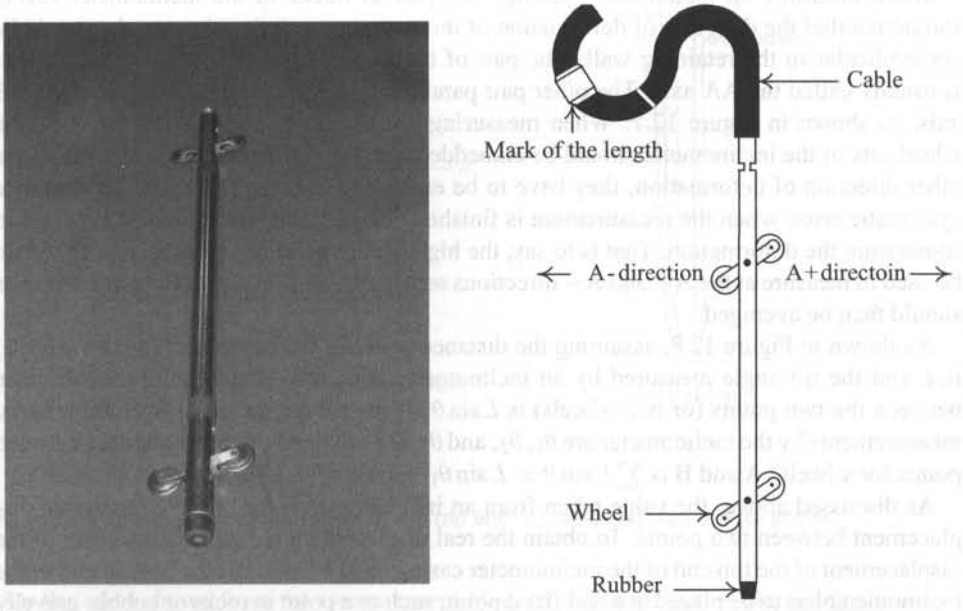

Figure 12.6 An inclinometer.

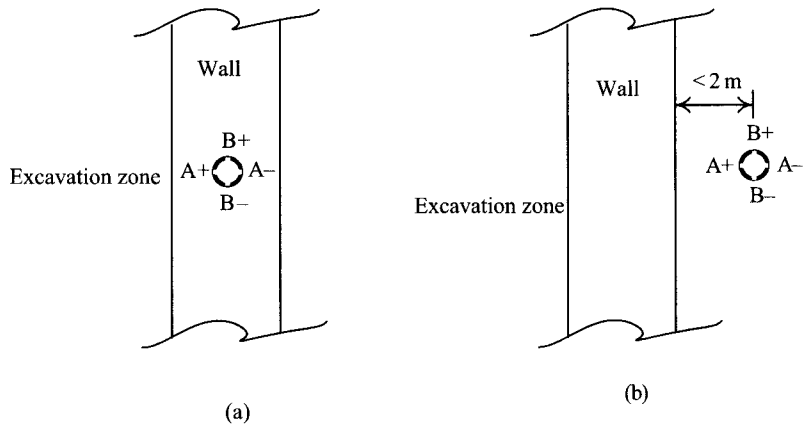

Figure 12.7 Installation of inclinometer casings with diaphragm walls: (a) installed in the diaphragm wall and (b) installed outside of the diaphragm wall.

When a tilt is produced, the coil magnetic field of the location detector can then detect the displacement of the pendulum with respect to the vertical line. The signal is then converted into a voltage by the detector. The voltage going through the coil will generate a force to have the pendulum recover its original place. Have the measured voltage converted and we can then get the tilt angle.

When installing an inclinometer casing, one pair of tracks of the inclinometer casing should parallel the direction of deformation of the retaining wall, in other words, should be perpendicular to the retaining wall. The pair of tracks perpendicular to the retaining wall is usually called the AA axis. The other pair paralleling the retaining wall is called the BB axis, as shown in Figure 12.7. When measuring the lateral deformation of the wall, the wheel sets of the inclinometer should be embedded into the AA track. When measuring the other direction of deformation, they have to be embedded into the BB track. To eliminate systematic error, when the measurement is finished, the inclinometer should be reversed to re-measure the deformation. That is to say, the high foot (wheel) of the inclinometer should be used to measure at the A+ and A− directions separately. The results of the measurements should then be averaged.

As shown in Figure 12.8, assuming the distance between the two points (or two wheels) is L and the tilt angle measured by an inclinometer is θ, the relative horizontal distance between the two points (or two wheels) is $L \sin\theta$. If the tilt angles taken from three serial measurements by the inclinometer are θ_1, θ_2, and θ_3, the relative horizontal distance between points (or wheels) A and B is $\sum L \sin\theta = L \sin\theta_1 + L \sin\theta_2 + L \sin\theta_3$.

As discussed above, the value taken from an inclinometer is the relative horizontal displacement between two points. To obtain the real displacement curve, an adjustment of the displacement of the top end of the inclinometer casing must be made or the bottom end of the inclinometer has to be placed at a real fixed point, such as a point in rocks or cobble-gravelly soils.

The displacement at the top of the casing can be measured using a tape, level, or theodolite against a datum line drawn before excavation, as shown as d_1 in Figure 12.9a. The reason is

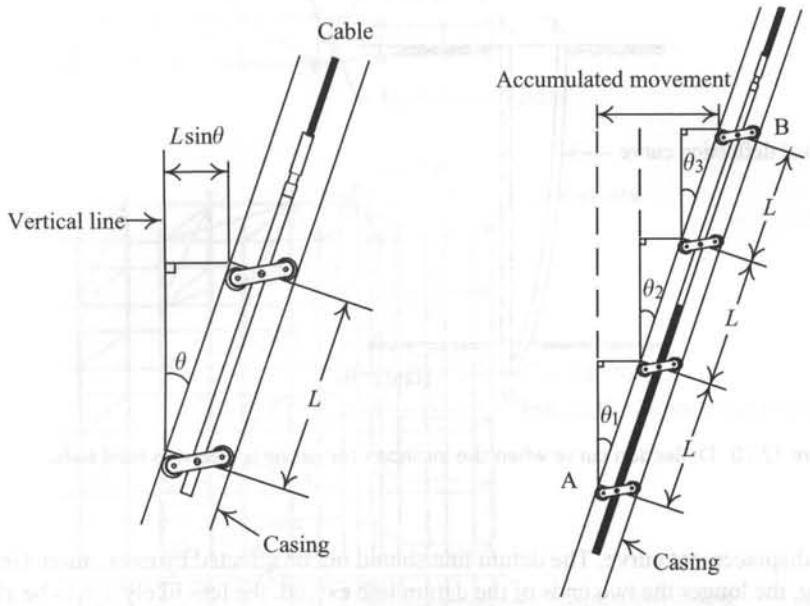

Figure 12.8 Principle of the measuring of lateral movement by an inclinometer.

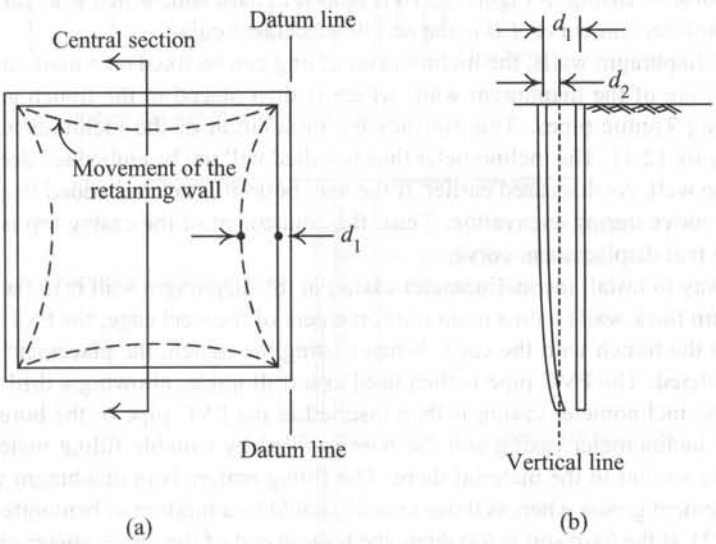

Figure 12.9 Modification of movement of the top end of casings: (a) plan and (b) profile.

that the curve drawn from the measurement of an inclinometer is the relative displacement with respect to the bottom end of the inclinometer casing. Suppose the displacement of the casing top measured using an inclinometer is d_2. The amount of d_2 is the displacement of the casing top relative to the bottom. If we move the curve laterally by $(d_1 - d_2)$, we can obtain

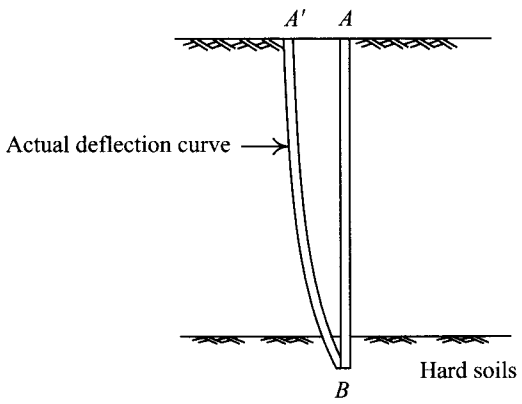

Figure 12.10 Deflection curve when the inclinometer casing is placed in hard soils.

the real displacement curve. The datum line should not be affected by excavation. Generally speaking, the longer the two ends of the datum line extend, the less likely it is to be affected. Nevertheless, if the base environment is not suitable, the end of the datum line can be set at a corner. The reason is that the displacement at the corner is relatively small. The bottom of the inclinometer casing in Figure 12.10 is placed in hard soil, which is a real fixed point. Thus, the displacement curve $A'B$ is the real displacement curve.

In case of diaphragm walls, the inclinometer casing can be fixed on a main reinforcement of the steel cage of the diaphragm wall, which is then placed in the trench and cast with concrete using Tremie pipes. This finishes the installation of the inclinometer casing, as shown in Figure 12.11. The inclinometer thus installed will not be embedded deeper than the bottom of the wall. As discussed earlier, if the wall bottom is not embedded in hard soil, the bottom may move during excavation. Thus, the adjustment of the casing top is to be made to obtain the real displacement curve.

Another way to install the inclinometer casing in the diaphragm wall is to fix a PVC pipe with 5–10 mm thick walls onto a main reinforcement of the steel cage; the PVC pipe is then lowered into the trench with the cage. When casting the trench, the placement of the PVC pipe is completed. The PVC pipe is then used as a drill guide, allowing a drill to reach the hard soil. The inclinometer casing is then inserted in the PVC pipe or the bore. The space between the inclinometer casing and the bore is filled by suitable filling materials whose properties are similar to the material there. The filling materials in diaphragm wall or hard soil can be cement grouts whereas those in soils should be a mixture of bentonite and cement (Figure 12.12). If the hard soil is too deep, the bottom end of the inclinometer casing should at least extend beyond the bottom of the diaphragm wall by more than the excavation width, that is, the total depth of the casing should be larger than $H_e + B$, where H_e = excavation depth, B = excavation width.

Since the movement of the soils near the retaining wall is quite close to that of the wall, the inclinometer casing can also be placed in the soils within 2 m of the outer side of the wall to measure the lateral displacement of the wall (Ou *et al.*, 1998; 2000a), as shown in Figure 12.7b. Figure 12.13 diagrams the embedment of the inclinometer casing outside

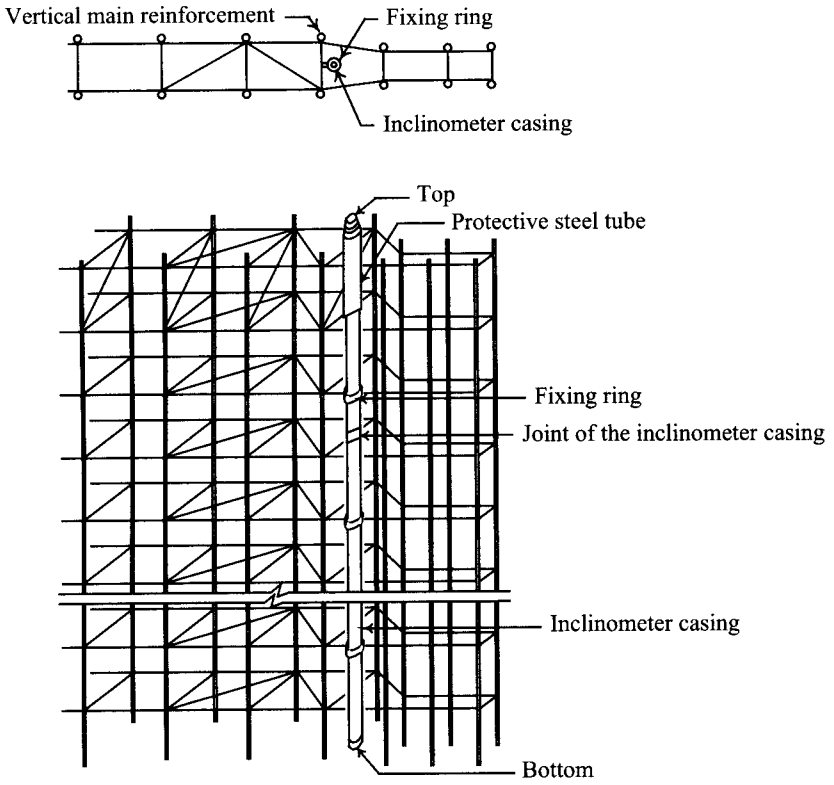

Figure 12.11 Inclinometer casings in a diaphragm wall.

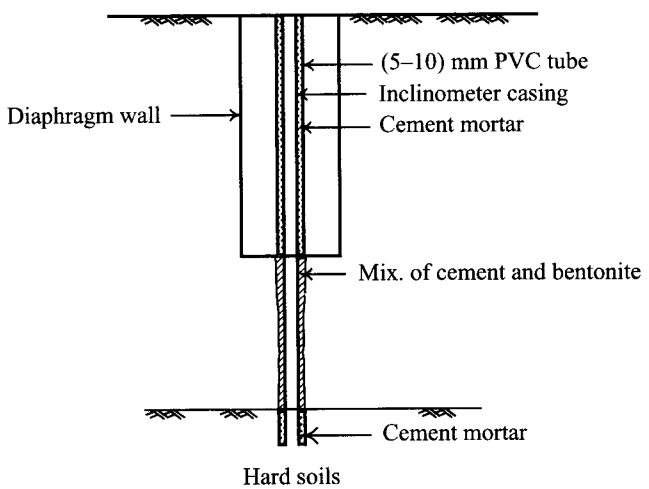

Figure 12.12 Schematic diagram of the installation of the inclinometer casing in a diaphragm wall.

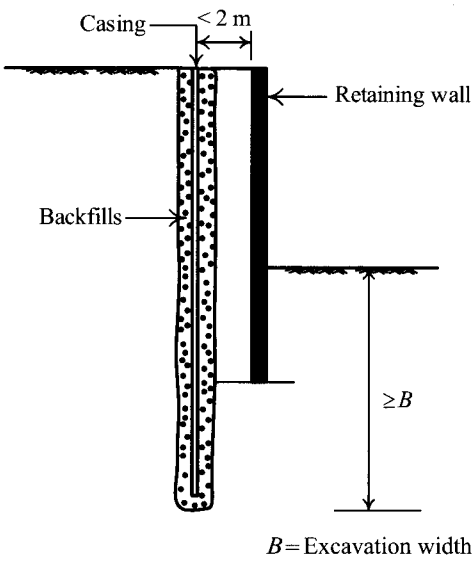

Figure 12.13 An inclinometer casing outside of the diaphragm wall.

the diaphragm wall. The installation is especially effective for sheetpiles and soldier piles because the inclinometer casing is not easily fixed directly on sheetpiles or soldier piles.

The inclinometer casing should be installed on the section with the largest lateral displacement. The largest displacement usually occurs in the central section of the excavation site (Figure 12.9a). Thus, the inclinometer casing should be installed in the central section of the retaining wall or in soils near it. After the inclinometer casing is embedded, the initial value should be taken first as a baseline to compare after excavation values to obtain the deformation of the retaining wall at the stage.

12.4.2 Tilt of buildings

Buildings will slant because of ground settlement and thereby be damaged. The tilting of buildings should be monitored during excavation. The tilt of a building can be estimated by the relative settlement between two reference points, using measuring devices for plane surveying such as the level, or theodolite, divided by the horizontal distance between these two reference points. If the two reference points are located on the two adjacent columns or foundation footings, the measured value is the angular distortion (see Section 11.2). Besides, the tilt of a building can also be monitored using a tiltmeter, the value produced by which is called the tilt angle.

A commonly used device to measure the tilt of a building is one consisting of a datum plate, a tiltmeter, and an indicator. The datum plate is usually made of ceramics which are not affected by temperature change. The plate is fixed to the object that is going to be measured. The tiltmeter is mainly to measure the degree of tilt of the datum plate, which represents the tilt of the structure the plate is fixed to. The tiltmeter is similar to the inclinometer (see Section 12.4.1) in measurement principle. The same as the inclinometer, the tiltmeter contains

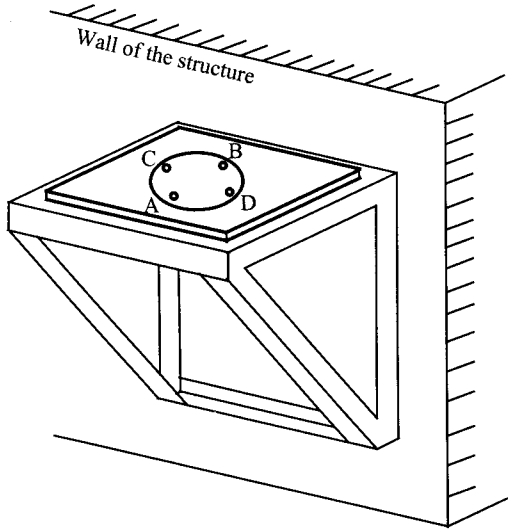

Figure 12.14 Horizontal type of datum plate fixed to the wall of a structure.

a sensor, which can be categorized into resistance type, vibrating type, and force balance accelerometer type, etc.

According to the type of tiltmeter, the datum plate can be divided into horizontal and vertical types. Figure 12.14 diagrams the basic design of a horizontal type datum plate. Figure 12.15 is a photo of a tiltmeter with a vertical datum plate. As shown in the figure, on the plate are four protruding objects that form two axes perpendicular to each other. One of the axes is perpendicular to the wall of the building whereas the other is parallel to it, the AB and CD axes in Figure 12.14, respectively.

The tilt angle in the AB direction is taken first. Then turn the sensor by 180 degrees and measure the tilt angle in the AB direction again. Average the two measured values to eliminate the instrumental systematic error. The averaged value is thus the tilt angle in the AB direction. Use the same method to measure the tilt angle in the direction parallel to the wall (CD axis).

As discussed in Section 11.2, the tilt of a building contains the rigid body rotation and the angular distortion. The value taken by a tiltmeter is the tilt of the structure at the place where the datum plate is fixed. To make the measured value represent the safety of the building, the most suitable location of the datum plate has to be determined according to the structural behavior of the building and the convenience of measurement. The roof and walls are the most commonly selected locations.

Generally speaking, the buildings within the influence range of excavation should be equipped with tiltmeters. For the determination of the influence range of excavation, refer to Section 6.4.

With the datum plate placed, take the initial measurement to obtain the initial value to be deducted from the value taken after excavation is started. The difference is the tilt angle of the building at the excavation stage.

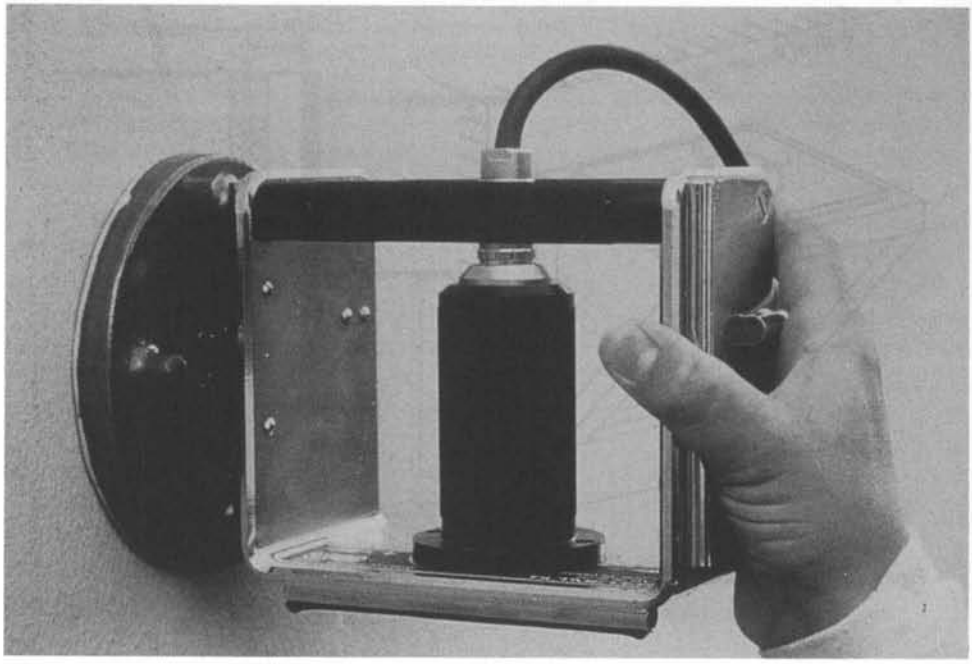

Figure 12.15 Photo of a vertical type of datum plate with an inclinometer.

12.4.3 Ground settlement and building settlement

The simplest method to measure ground settlement is marking the ground surface with steel nails (called settlement nails), to make a foresight to a fixed point and backsight to the nails using a level to obtain the ground settlement at the points where the nails are driven in. The fixed point is the datum point outside the influence range of excavation. A certain position of a building with the pile foundation can be assumed to be a fixed point. If there are not any buildings with pile foundations nearby, a marking object in the distance or outside the influence range of settlement has to be adopted (for the determination of the influence range of settlement, see Section 6.4). If necessary, a permanent benchmark has to be set to serve as a fixed point.

The surrounding ground of an excavation may be soil, asphalt pavement, or concrete pavement. The asphalt pavement and concrete pavement have relatively high rigidities. That is, even though the soil below them has settled, the pavements do not necessarily show signs of settlement. Thus, the settlement nails have to be driven through the pavements so that the settlement of the nails can represent the real settlement of the soil. Figure 12.16 illustrates a possible way of setting the settlement nails.

In addition to the vicinity of the buildings, settlement nails should also be set in the central area of the excavation zone and along a direction perpendicular to the retaining wall (Figure 12.17) to obtain the representative settlement profile (e.g. Figure 6.8). That is because the behaviors of the retaining wall and the soil near the central section are close to plane strain

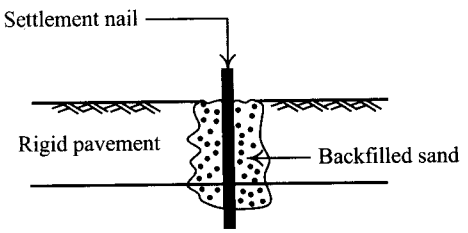

Figure 12.16 Schematic diagram of the installation of a settlement nail.

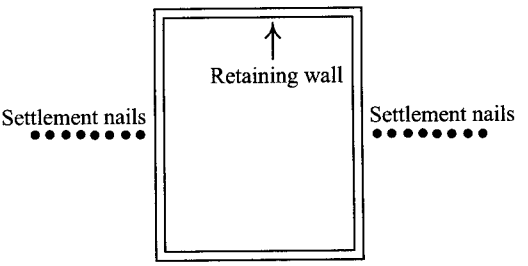

Figure 12.17 Layout of settlement marks in order to obtain the representative settlement profile.

and the ground settlement and lateral deformation of the wall there are larger than those in any other sections. If the initial settlement profile of the central area of the excavation is known, it will be easier to predict the ground settlements at the last excavation stage and in other sections (see Section 6.8).

The measurement of the settlement of buildings is the same as that of ground settlement except that the settlement nails are to be set on the buildings themselves, on the wall or on the columns, for example.

12.4.4 Heave of excavation bottoms

Excavation will cause the excavation bottom to heave. Too much heaving is usually dangerous for the strutting system and causes settlement of the soils in the vicinity. Under worse conditions, it may lead to the failure of the excavation. Thus, the magnitude of the heave of the soils at the excavation bottom should be monitored constantly.

The heave of an excavation bottom is usually measured with heave gauges, which consist of a cross shaped iron plate, an aluminum rod, and a galvanized iron casing, as shown in Figure 12.18. The cross shaped iron plate is placed below the excavation bottom. It is shaped in a cross to enlarge the contact area with the surrounding soils, so that when the soils below the excavation bottom heave, they will cause the heave gauges to move upward accordingly. The top of the cross shaped iron plate is connected to a 2.54 cm diameter aluminum rod extending to the ground surface for the measurement of the heave of the gauge. The aluminum rod is protected by a galvanized iron pipe to seclude the aluminum rod from the soils.

The installation of the heave gauge is as follows:

1 Connect the cross iron plate with the aluminum rod.
2 Drive the galvanized iron casing into the soil 50 cm below the excavation surface using a wash boring machine and hammer it deeper by another 50 cm. It should be 100 cm below the excavation surface in total.
3 Keep boring to a depth of about 150 cm below the excavation surface. Pour 100 cm thick bentonite into the bore.

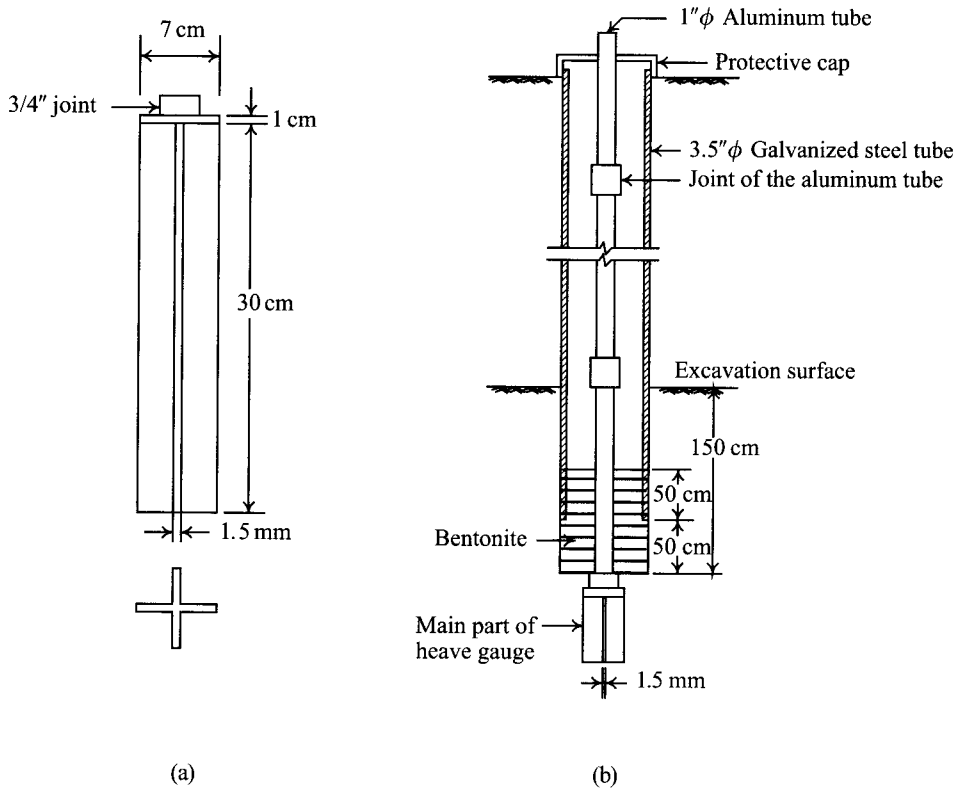

Figure 12.18 Schematic diagram of the installation of a heave gauge: (a) main part of the heave gauge and (b) heave gauge installed.

4 Put the heave gauge that is already connected to the aluminum rod into the casing and then push into the soil.
5 Take some protective measures with the top of the heave gauge (i.e. the top of the aluminum rod) to finish the installation of the heave gauge.

The measurement of heave is to measure the elevation differences of the aluminum rod before and after excavation (of a certain stage) using a level against a fixed point or permanent benchmark. Thus, we obtain the movement of the excavation bottom during a certain stage of excavation.

The heave gauge has to be installed at the position where heave is the largest, which is usually found around the center of the excavation zone. For detailed elucidations, please refer to Section 5.5.

The magnitude of heave or the rate of heaving of the excavation bottom can be measured using a heave gauge for reference for the judgment of the excavation safety. The heave gauge, however, is often damaged during excavation. Besides, the critical value of heave or the heaving rate is not easily determined. As a result, the uplift of the central post often

replaces the heave gauge for the measurement of the heave of the excavation bottom in recent practice.

The uplift of the central post will bend the struts and produce secondary bending moment on them. When the bending moment is too large and exceeds the allowable value, it will bring about the failure of the strutting system (see Section 10.5). Besides, if the changing rate of the uplift of the central post is too large, it means the excavation bottom is unstable.

The measurement of the central post is identical to that of a heave gauge. That is, measure the initial elevation of the central post using a level against a fixed point or permanent benchmark before excavation and then measure the elevation of the central post, repeating the same procedure, after excavation is started. Deduct the former from the latter, and we obtain the uplift of the central post at the excavation stage. Usually there are many central posts in an excavation zone. The one with the largest uplift or the two adjacent ones with the largest differences of uplift can be selected for measurement.

12.5 Measurement of stress and force

12.5.1 Strut load

The loading of the struts has to be monitored constantly during excavation lest it may exceed the allowable value and endanger the safety of the excavation. Some commonly used devices to measure the strut load are the strain gauge, the load cell, and the hydraulic jack gauge.

The strain gauge is a widely used device to measure the strut load. Placed outdoors and exposed to sun, rain, and dust, the vibrating type is more suitable and favored. If the exterior of the resistance type is well waterproofed, it can also be used to measure the strut load. Though the resistance type is more accurate, the installation cost is higher. Concerning the resistance and vibrating types of strain gauges, please refer to Section 12.3.

To install a strain gauge, weld the strain gauge onto the web of a strut using a point welding instrument and have the track of the sensor fitted with the strain gauge; fix the sensor onto the strut with two iron plates and protect the sensor from water with water repellent glue around it, as shown in Figure 12.19. Figure 12.20 is a photo of the strain gauge fixed onto a strut. Since the loading on a strut is not necessarily even, to measure the strut load correctly, on both sides of the web of a strut are fixed strain gauges and the averaged value of the two gauges is taken for the result.

The load cell can be divided into the mechanical type, the hydraulic type, and the electronic type. Mechanical load cells contain either a torsion level system or an elastic cup spring that is deformed during loading. Deformation is sensed by a dial indicator and calibrated to force. Mechanical load cells are seldom used to measure the strut load. A hydraulic load cell consists of a liquid-filled chamber connected to a pressure measurement unit. By recording the change in pressure of the fluid on the pressure pad, load can be determined.

The electronic type can be further divided into the resistance load cell and the vibrating one. Figure 12.21 diagrams the basic configuration of an electric load cell. Figure 12.22 is a photo of a load cell. As shown in the figure, the main part of the load cell is a circular box made of steel or aluminum alloy where about four strain gauges are fixed inside or attached to the exterior. The accuracy of the electric load cell is the same as the strain gauge but it costs more. The load cell is usually applied when the strain gauge is not easily installed, on a wood or steel pipe of struts for example.

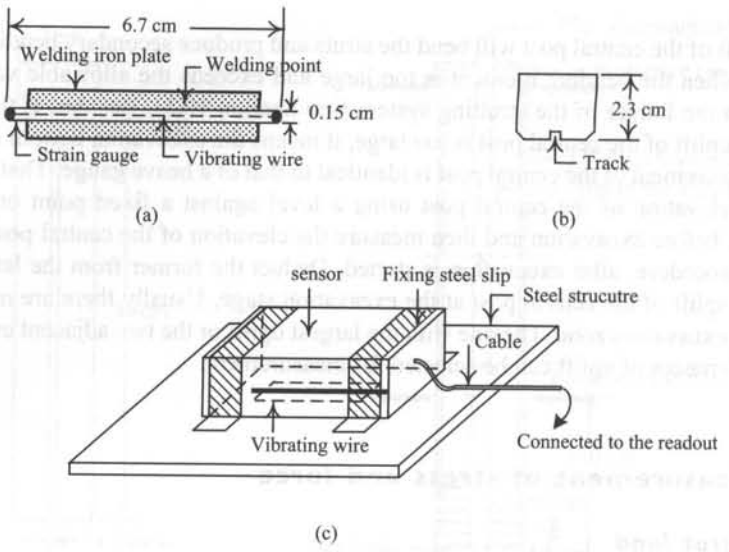

Figure 12.19 Schematic diagram of the installation of a vibrating wire strain gauge: (a) a vibrating wire strain gauge, (b) section of the sensor, and (c) fixed sensor.

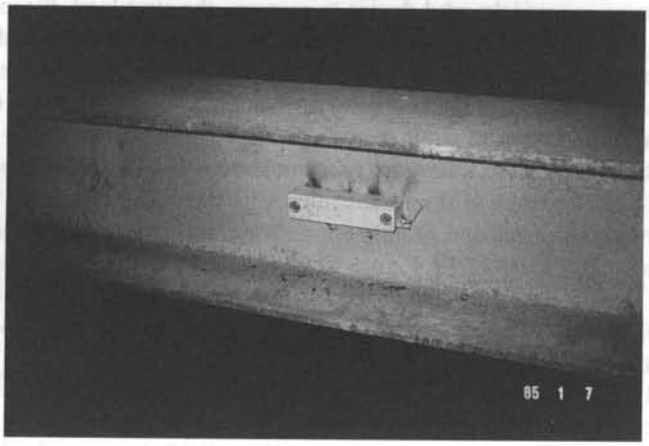

Figure 12.20 Photo of a strain gauge fixed on a strut.

After struts have been installed in an excavation, hydraulic jacks are often necessary to preload the struts so that they can be tightly connected with the wales and the lateral deformation of the retaining wall can be decreased. After preloading, the pressure gauge of the hydraulic jack can also be used for the measurement of the strut load. Figure 12.23 is a photo showing how a jack is set between struts. Nevertheless, misalignment of struts, off-center strut loading, non-parallel bearing plates, and transverse relative movement of bearing plates all cause friction between the valve and cell cylinder and render the measurement of

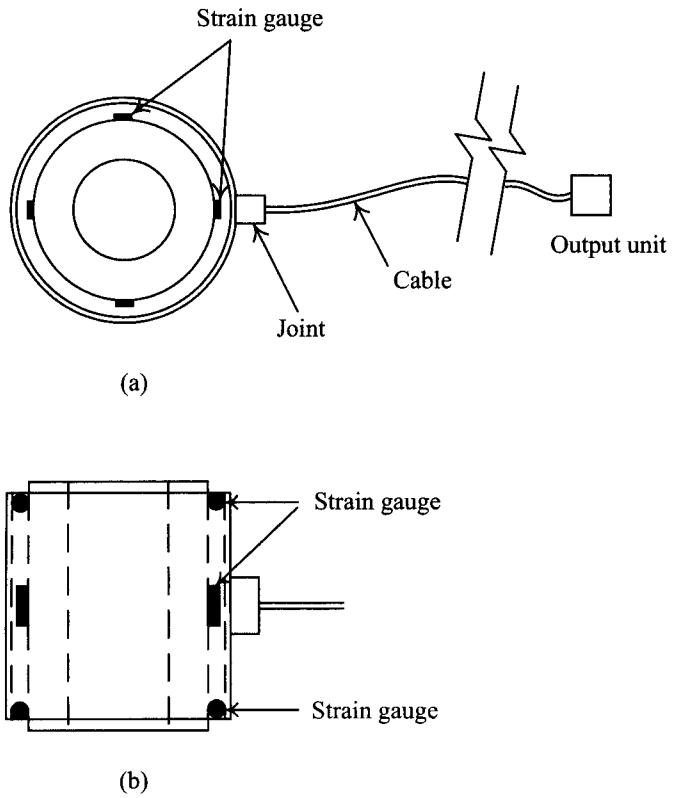

Figure 12.21 Schematic configuration of a load cell: (a) plan view and (b) side view.

the strut load inaccurate. Temperature changes and pressure gauge inaccuracy may cause additional error. Using pressure gauges of hydraulic jacks to measure the strut load is not reliable as a result.

The strain gauge or load cell should be installed at the position where the strut load is about the largest. The same as for conditions in the measurement of the lateral deformation of a retaining wall, the central area of an excavation site is usually the place where the largest strut load occurs. Thus, the central area of an excavation site should be equipped with the strain gauges or load cells (see Figure 12.9a).

12.5.2 Stress of the retaining wall

The stress of the retaining wall sometimes has to be measured constantly during the process of excavation lest the stress may exceed the allowable value and endanger the excavation safety.

The stresses of soldier or sheetpiles can be measured by fixing commonly used strain gauges on them. As for column piles or diaphragm walls, the rebar stress meter has to be

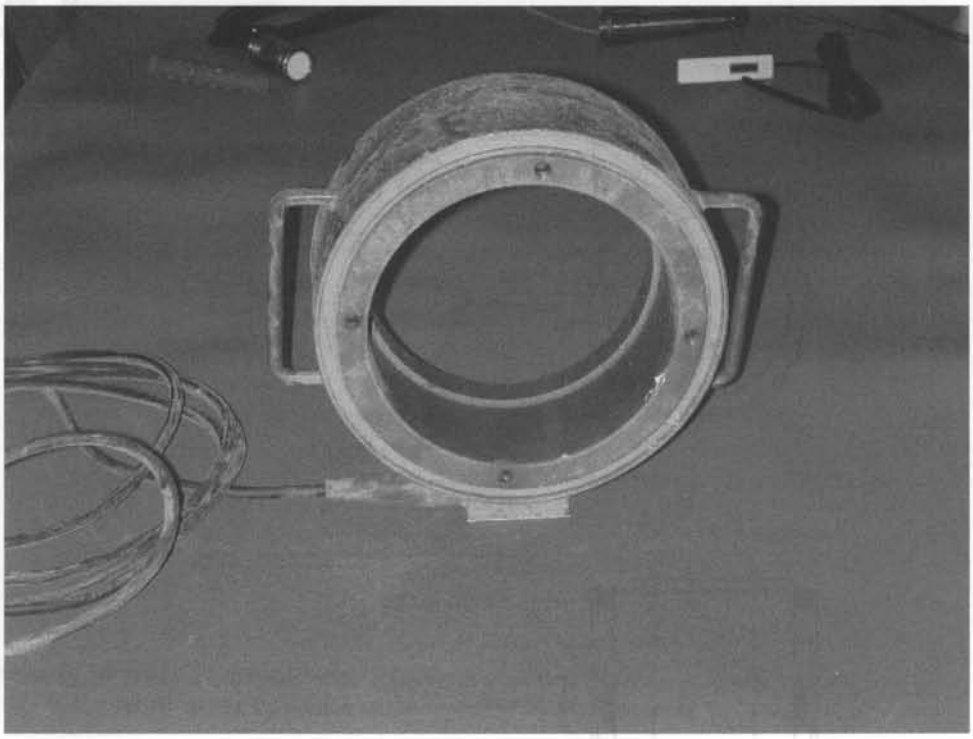

Figure 12.22 Photo of a load cell.

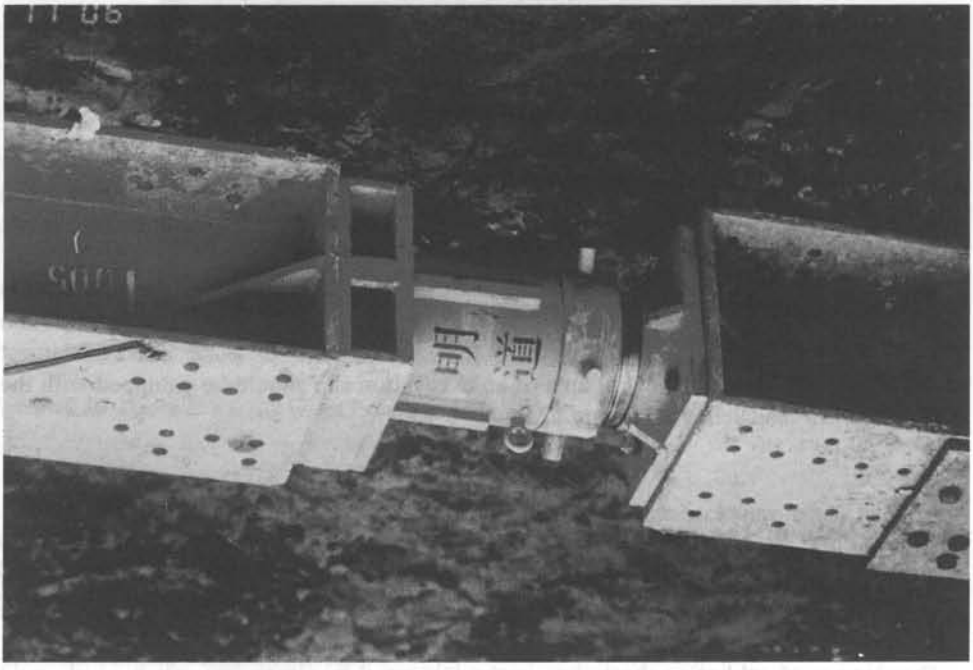

Figure 12.23 Photo of a jack between struts.

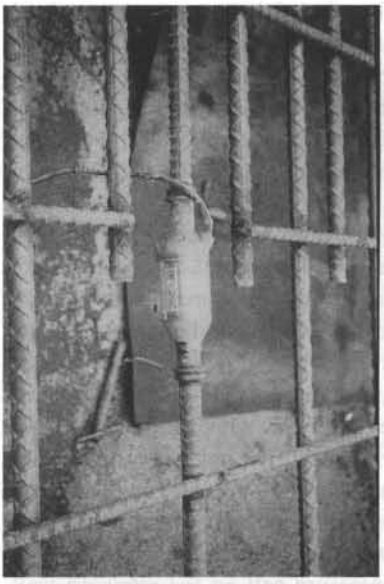

Figure 12.24 Rebar stress meter on a steel cage.

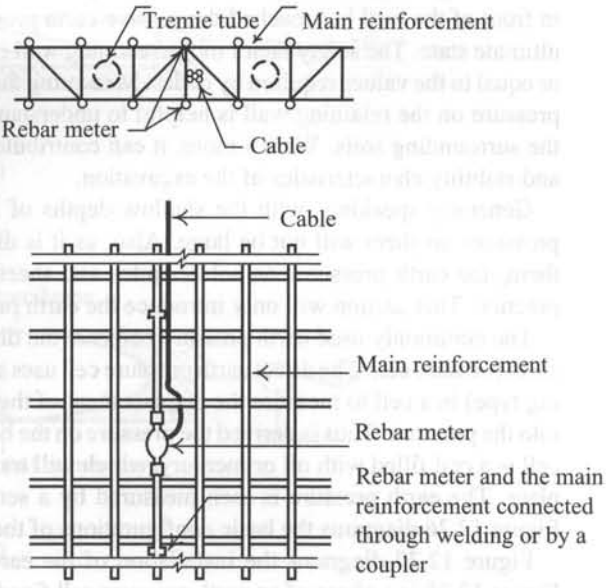

Figure 12.25 Installation of a rebar stress meter.

installed onto the steel inside the retaining wall to measure the load. The rebar stress meter contains a strain gauge, which is usually the resistance type. The exterior of the strain gauge has to be enveloped in many layers of water repellent membranes, because, when the steel or the retaining wall is acted on by a force and bends, repellent membranes may break, causing the strain gauge to contact water. Since water is also an electric conductor, water will change the resistance of the strain gauge and influence the measurement. Figure 12.24 is a photo where a rebar stress meter is fixed on the steel cage.

Figure 12.25 diagrams the installation of a rebar stress meter. As shown in the figure, cut a main reinforcement at the designed depth and connect a rebar stress meter onto the main reinforcement by way of welding or a coupler. Last, pull the wire out of the steel cage to finish the installation of the rebar stress meter.

The rebar stress meter should be installed at the place where the stress of the wall is the largest. As shown in Figure 12.9a, the retaining wall and soils at the center of an excavation site have the largest lateral deformation. The load on the retaining wall here should also be larger than other sections. The largest lateral deformation of the retaining wall, in the same section, is usually found near the excavation bottom (see Section 6.3). Thus, the largest stress of the reinforcement in the section should occur within several meters above or below the excavation bottom, which is also the place for the installation of the rebar stress meter.

12.5.3 Earth pressure on the retaining wall

Before excavation, the earth pressure on the retaining wall is the at-rest earth pressure. After excavation, with the retaining wall moving toward the excavation zone, the earth pressure acting on the back of the wall (outside the excavation zone) decreases. The limiting value of the earth pressure on the back of the wall is called the active earth pressure. On the other

hand, the earth pressure on the front of the wall (inside the excavation zone) increases and the limiting value is called the passive earth pressure. When the earth pressure at every depth in front of the wall has reached the passive earth pressure, the retaining wall is called in the ultimate state. The safety factor of the retaining wall in the ultimate state has to be larger than or equal to the values required by codes. Measuring the total earth pressure and effective earth pressure on the retaining wall is helpful to understand the bearing behavior of the wall and the surrounding soils. What's more, it can contribute to the exploration of the deformation and stability characteristics of the excavation.

Generally speaking, with the shallow depths of soldier piles and sheetpiles, the earth pressures on them will not be large. Also, as it is difficult to install measuring devices on them, the earth pressures on soldier piles and sheetpiles are not measured in engineering practice. This section will only introduce the earth pressure cell used on diaphragm walls.

The commonly used earth pressure cells are the direct earth pressure cell and the indirect earth pressure cell. The direct earth pressure cell uses strain gauges (of the resistance or vibrating type) in a cell to measure the displacement of the bearing plate, which is then converted into the pressure. Thus is derived the pressure on the bearing plate. The indirect earth pressure cell is a cell filled with oil or mercury, which will transmit the earth pressure on the bearing plate. The earth pressure is then measured by a sensor on the exterior of the instrument. Figure 12.26 diagrams the basic configurations of the two types of earth pressure cells.

Figure 12.27 diagrams the installation of the earth pressure cell on the retaining wall. Figure 12.28 is a photo of an earth pressure cell fixed on a steel cage. The installation of the earth pressure cell is elucidated as follows:

1 Assemble a steel cage and set it on a platform.
2 Weld reaction plates onto the cage and bolt a hydraulic jack to the reaction plates.
3 Add a bearing plate containing an earth pressure cell to one end of the hydraulic jack or two plates on each end. Extend the cable and hydraulic pipe along with the main reinforcement to the top of the cage and fix them.
4 Examine whether there exists the phenomenon of soil collapsing from the trench wall at the positions where the earth pressure cells are to be installed. If not, place the cage with the earth pressure cells into the trench and measure the value of the earth pressure in bentonite fluid.
5 Connect the hydraulic pipe of the jack with a manpowered pump and add pressure slowly to make the earth pressure cells move toward the faces of the trench walls. When the readings on the cells change, it follows that the earth pressure cells and the trench walls are contacting each other slightly. Keep pumping with the hydraulic pump and repeat preloading and unloading to improve the contacting condition. Lastly, add a light preload (of about 105% of the bentonite fluid pressure or the equivalent at-rest lateral earth pressure) and fix it (Figure 12.27b).
6 When casting the concrete of the diaphragm wall using Tremie pipes, because the unit weight of concrete is heavier than that of bentonite, the trench walls may be pushed outward. In this situation, the readings of the earth pressure cells should be constantly taken. If the readings reveal signs of decreasing, more pumping is required to bring the earth pressure cells and the trench walls to full contact.
7 Dismantle the hydraulic pump. The installation is then finished.

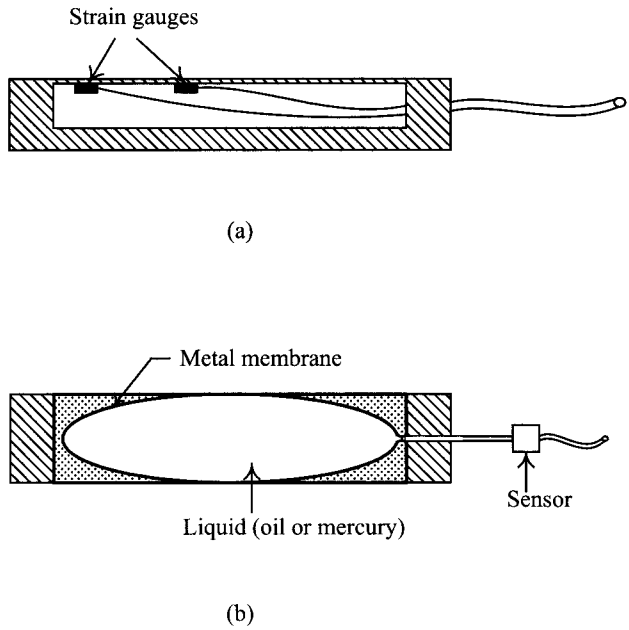

Figure 12.26 Configurations of the earth pressure cell: (a) direct type and (b) indirect type.

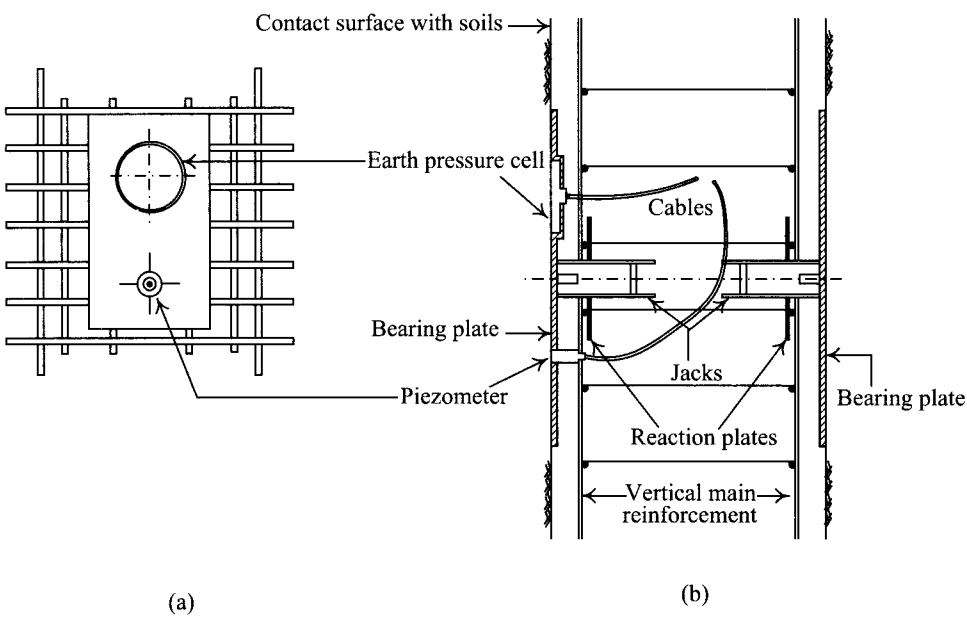

Figure 12.27 Installation of the earth pressure cell/piezometer: (a) earth pressure cell/piezometer on a steel cage and (b) earth pressure cell/piezometer in a trench.

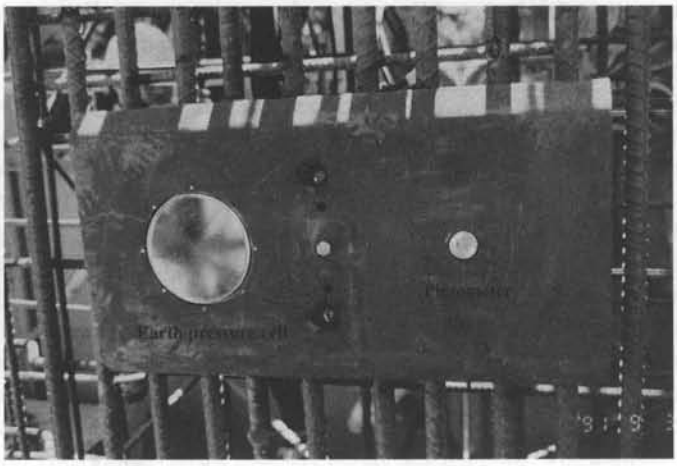

Figure 12.28 Photo of an earth pressure cell/piezometer on a steel cage.

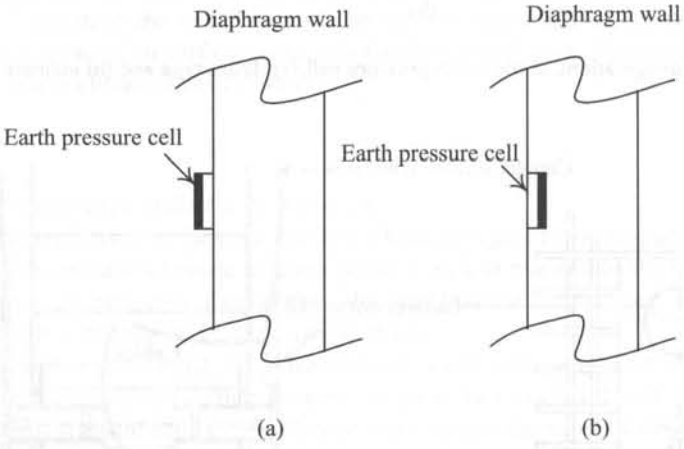

Figure 12.29 Failures of the installation of an earth pressure cell: (a) stress concentration caused by the protruding of the earth pressure cell and (b) earth pressure cell enveloped by concrete.

The contact between the earth pressure cells and the trench walls is a crucial point to the success of the installation. If preloading is too much, stress concentration, which will influence the accuracy of readings, will occur. If preloading is insufficient, the earth pressure cells may be enveloped by concrete during the Tremie casting, as shown in Figure 12.29. To ensure success, the installation of the earth pressure cells has to be carried out under the direction of experienced engineers.

The earth pressure measured by an earth pressure cell is the total earth pressure. To obtain the effective earth pressure, an electronic piezometer has to be added on the bearing plate next to the earth pressure cell, as shown in Figure 12.27a.

According to the reason for its use, the earth pressure cell can be set on the active side, the passive side, or both. The same as with the inclinometer, rebar stress meter, strain gauge, and settlement points on the ground surface, the central section of the excavation site is the one where the earth pressure cell should be installed, considering the largest earth pressure on the section.

The maximum value of the earth pressure on the front of the retaining wall is the passive earth pressure, whereas the minimum on the back of the wall is the active earth pressure. Earth pressures on the wall usually fall between the two limiting values. An excavation design usually has taken these values into consideration. Thus, though measuring the earth pressures on the retaining wall is helpful to understand the bearing behavior of the wall and the surrounding soils, the results are not easily applied to the judgment of the excavation safety.

12.6 Measurement of water pressure and groundwater level

12.6.1 Water pressure

Some commonly used piezometers in excavations are the open standpipe piezometer, the pneumatic piezometer, and the electronic piezometer. The piezometer can be installed in the soils within the excavation site, soils outside the excavation site, or on the diaphragm wall. Those installed on a diaphragm wall are usually electronic piezometers. The installation of piezometers in the diaphragm wall is as explicated in Section 12.5.3. In the present section, only piezometers installed in soils are to be introduced.

The basic configuration of an open standpipe piezometer, also called the Casagrande piezometer, is as diagramed in Figure 12.30. As shown in the figure, the main part of the open standpipe piezometer is a permeating pipe made of porous stone. The bottom end of the permeating pipe is a lid and the top end is connected to a vertical pipe (usually a PVC pipe). When groundwater enters into the permeating pipe, it will go up along the vertical pipe. When it goes up to the height which balances the water pressure at the level where the permeating pipe is placed, the height in the vertical pipe is then the water pressure at the center of the permeating pipe.

The height in the vertical pipe can be measured using a water level indicator, which is a coaxial cable of negative and positive poles in which the groundwater can be seen as the electrolyte. Put the indicator into the vertical pipe, contacting the water, a low-current circuit would then be formed and a signal be generated to reveal the height of water in the vertical pipe. The open standpipe piezometer is simple in its principle and reliable in its result, with easy installation. It is required, however, to wait till the groundwater has fully flowed into the vertical pipe before the height is measured. As a result, measuring the water pressure in clayey soils usually takes a long time in waiting.

The pneumatic piezometer, also called the closed piezometer, is as diagramed in Figure 12.31, illustrating its basic configuration. When the air pressure in the air pipe is smaller than the water pressure, p, as shown in the figure, the air keeps flowing into the pipe, and the air pressure will grow. When the air pressure in the pipe is equal to or exceeds the water pressure, p, the membrane moves outward and the air current is facilitated, air will flow out of it and the air pressure will thus be decreased. The largest reading of the air pressures in the pipe is then the water pressure. Nitrogen and CO_2 are the most widely used

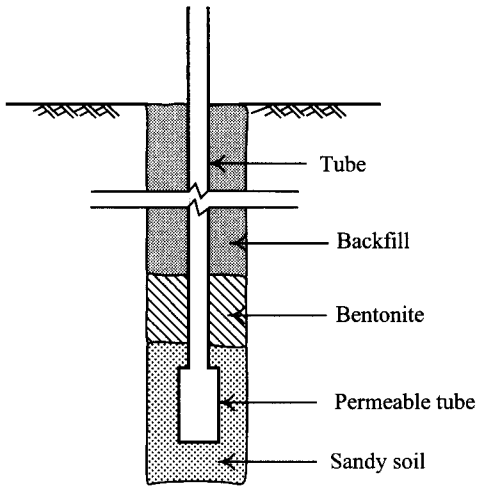

Figure 12.30 Schematic configuration of an open standpipe piezometer.

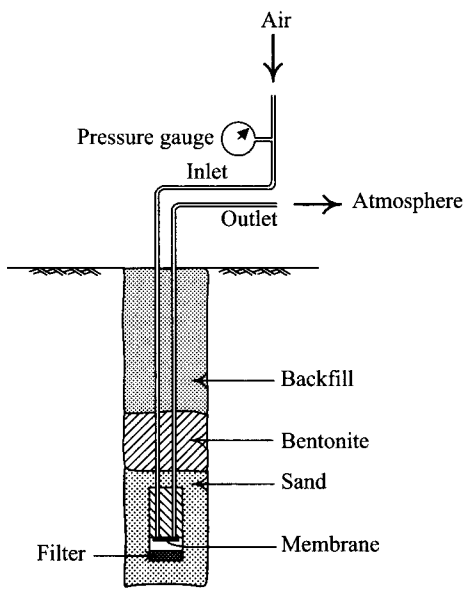

Figure 12.31 Schematic configuration of a pneumatic piezometer.

gases. Using a pneumatic piezometer to measure the water pressure does not require water in great quantity to flow into the main part of the piezometer and thus does not take a long time to wait. It is suitable to be used in clayey as well as sandy soils. Many details of the installation, however, are to be taken care of and the measuring devices and procedures are more troublesome than the open standpipe piezometer.

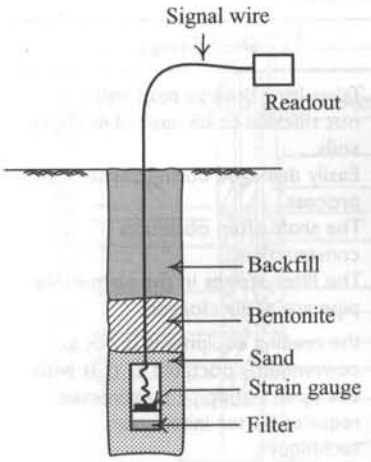

Figure 12.32 Schematic configuration of an electronic piezometer.

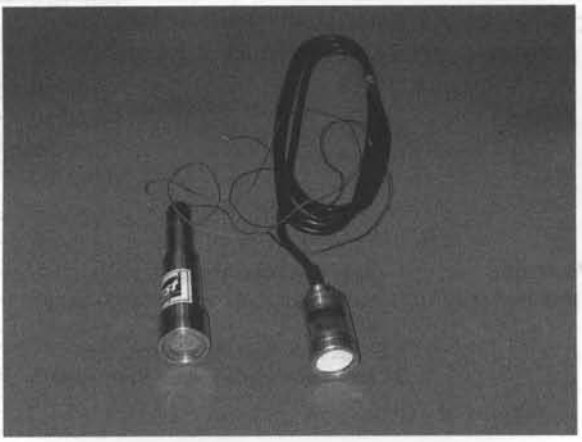

Figure 12.33 Photo of an electronic piezometer.

The electronic piezometer is similar in its basic design to the earth pressure cell (see Figure 12.26) except it isolates the bearing plate from the influence of earth pressure. Therefore, a permeable stone is placed in front of the bearing plate which is acted on by groundwater flowing through the permeable stone. Thus, the water pressure is measured. The electronic piezometer can be divided into the resistance and vibrating types. Figure 12.32 diagrams the basic configuration and the installation of the electronic piezometer. Figure 12.33 is a photo of electronic piezometers. The strengths and shortcomings of the open standpipe piezometer, the pneumatic piezometer, and the electronic piezometer are listed in Table 12.1.

The installation of a piezometer in soils is elucidated as follows:

1 Bore a hole using a drill machine to 50 cm below the designed depth.
2 Place the main part of the piezometer (no matter whether it is the open standpipe type, the pneumatic type, or the electronic type) in the bored hole and have the center of the piezometer located at the designed depth. Fill the bored hole with sandy soil. The sandy soil is used to help groundwater permeate into the main part of the piezometer and be measured.
3 Seal the top (or both ends) of the sandy soil with bentonite to avoid groundwater from other elevations reaching the permeable pipe and influencing the measurement results. Above the bentonite is again filled with sandy soils to provide sufficient overburden weight to stabilize bentonite and sealing.

In the same hole can be placed more than one piezometer, all of them requiring sealing to avoid water pressure from other elevations, as shown in Figure 12.34. Depending on the monitoring aim, the piezometer can be embedded in clayey or sandy soils. Using one in clayey soils can derive the effective stress by way of measuring excess pore water pressure induced by soil deformation during excavation. Neither the excess pore water

Table 12.1 Strengths and shortcomings of various types of piezometers

Type	*Strengths*	*Shortcomings*
Open standpipe piezometer	1 Reliable 2 Can measure the permeability of soils 3 Can take groundwater sample 4 Applicable to sandy layers 5 Durable	1 Takes long time to read and is not suitable to be applied in clayey soils. 2 Easily damaged during construction process. 3 The shaft often obstructs construction. 4 The filter stones in the permeable pipe are easily clogged.
Pneumatic piezometer	1 Does not take long time to read; applicable to sandy and clayey soils 2 Does not obstruct construction 3 Not easily damaged or destroyed	1 the reading equipment is not as conveniently portable as that with the open standpipe piezometer. 2 requires better installation techniques. 3 The membrane is susceptible to erosion in the long term and thereby the durability is affected.
Electronic piezometer	1 Does not take long time to read; applicable to sandy and clayey soils 2 Easy to read 3 Does not obstruct construction 4 Not easily damaged or destroyed 5 Though usually not durable, some specially designed types of electronic piezometers are also good in durability 6 Fits automatic systems	1 For long-term usage, durability and accuracy of readings have to be considered. 2 Is more expensive

pressure nor the effective stress directly relates to excavation safety. They are, nevertheless, helpful to understand the deformation behaviors and stability characteristics. The piezometer aimed as above elucidated should be embedded in the central section of the excavation site.

The piezometer embedded in sandy or permeable soils can monitor the variation of water pressure, which is helpful for the diagnosis of the excavation safety. If the water pressure changes abruptly while the stress on the reinforcement of the retaining wall is abnormal, it must get extraordinary attention and an effective remedial measure should be adopted to safeguard the excavation safety. Piezometers aimed as above should be embedded around the excavation site. They can also be placed within the excavation zone to help judge the safety factor regarding sand boiling or upheaving (see Sections 5.7 and 5.8).

12.6.2 Groundwater level

The instrument for groundwater level is the observation well where a vertical pipe with many holes, enveloped with two layers of nylon net, is placed. The installation procedure of the

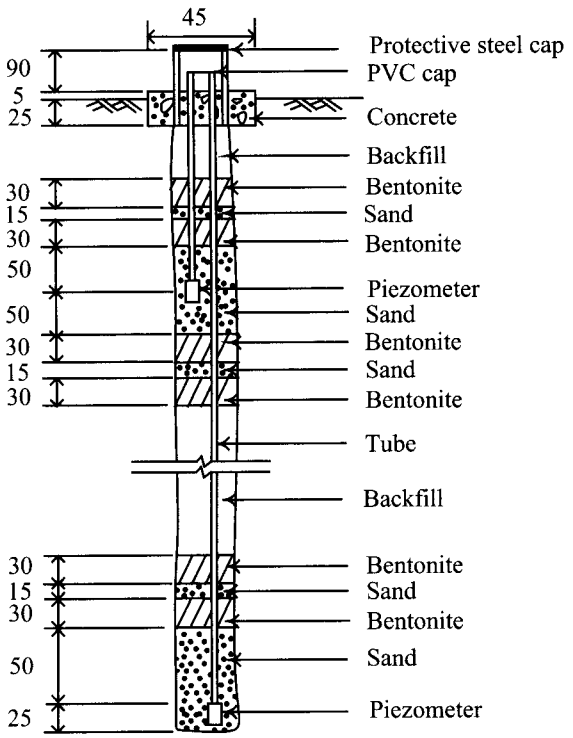

Figure 12.34 Two piezometers installed in the same bore (the unit for numbers in the figure is cm).

vertical pipe is as elucidated in the following (see Figure 12.35):

1 Bore to the designed depth using a drill machine.
2 Fill the bottom of the bored hole with sand.
3 Place the water observation pipe into the hole and fill the space with sand.
4 Take some protective measures on the top of the vertical pipe. Thus is finished the installation of the observation pipe.

After groundwater flows into the pipe and the water level inside reaches the stable state, the water level in the pipe is then the groundwater level. As with the open standpipe piezometer, the water level in the pipe can be measured using a water level indicator.

The aim of the observation well is to monitor the change of the groundwater before or during excavation and to supply information for the determination of the excavation method, the design of water pumping, and the management of construction period.

12.7 Other measurement objects

The monitoring instruments or devices introduced above are the commonly used ones for excavations. In addition to them, to observe other characteristics of an excavation or for

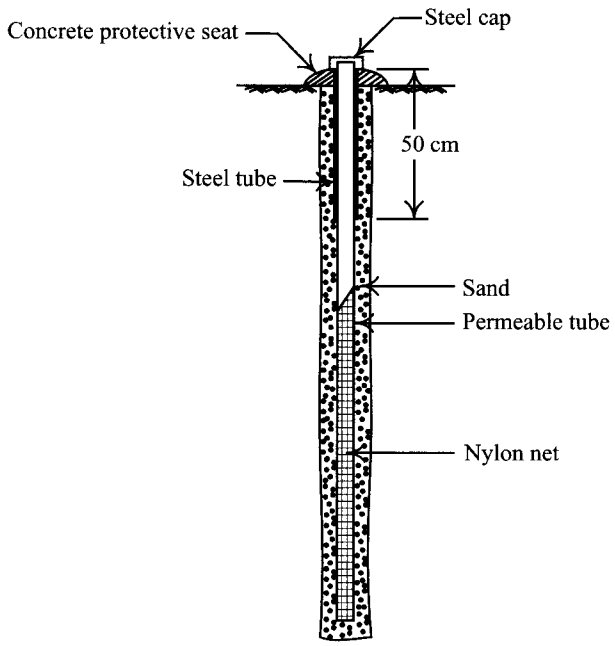

Figure 12.35 Installation of an observation well.

other special objectives, some other types of monitoring instruments can also be employed in excavations. For example, the extensometer is used for the measurement of settlement of the soils below the ground surface. The crackmeter can be used for the measurement of the cracks on the walls or columns of the buildings. The concrete stressmeter can be used to measure the stress of concrete. Because these instruments or devices are not frequently used in general excavations, the book is not going to introduce them at length. Interested readers can refer to related literature for details.

12.8 Plan of monitoring systems

A complete plan of a monitoring system should include the following items: (1) determination of the monitoring parameters, (2) determination of the locations of the monitoring instruments or devices, (3) analyses of the prediction values of the parameters, (4) choice of the specifications of the monitoring instruments, (5) determination of the installation specifications of the instruments, (6) setting of the alert and action levels, and (7) determination of the measurement frequency. According to the sequence of execution, they are elucidated as follows:

1 Determination of the monitoring parameters: Excavation-related materials are soils, retaining walls, and struts. Excavation will produce physical quantities such as stress and strain on, and displacement of these materials, which can be measured using instruments. Considering the cost, it is impossible to measure every physical quantity within the excavation

influence range. Thus, suitable parameters have to be determined according to the excavation scale, geological conditions, and the situations of adjacent properties.

2 *Determination of locations of the monitoring instruments*: The measurement parameters determined, what follows is the selection of the locations and embedment depth of the instruments. The proper locations and embedment depths of the instruments should be able to unveil the excavation behaviors and the physical quantities representing the critical conditions of excavation.

3 *Analyses of the prediction values of the parameters*: According to the soil properties, the type of the retaining wall, and the excavation conditions, predict the monitoring parameters for each of the excavation stages. The methods of prediction, including the simplified method, the beam on elastic foundation method, and the finite element method, are as elucidated in Chapters 6–8 in this book. The prediction results are not only helpful to the determination of the specifications of instruments but also useful to the setting of the alert and action levels.

4 *Choice of the specifications of the monitoring instruments*: With the monitoring parameters for excavation stages, the specifications of the instruments can be then determined.

5 *Determination of the installation specifications of the instruments*: Whether the monitoring parameters are accurate affects the judgment of the excavation safety. Though the precisions of the instruments are important, whether they have been correctly installed also influences the measurement results. As a result, appropriate installation specifications have to be mapped out according to the characteristics of the instrument and the geological conditions.

6 *Setting of the alert and action levels*: The alert level is an important index for the judgment whether the excavation is under normal conditions. The action level is the value indicating the immediate necessity of measures to be taken. Before excavation, the alert and action levels for each excavation stage should be determined in advance. For the meanings and determination methods, refer to Section 12.9.

7 *Determination of the measurement frequency*: The measurement frequency refers to the times of the measurement taken within a certain period. Basically, the measurement frequency has to be increased during the process of excavation. During the waiting time, in which no excavation activities are in progress, it may be reduced properly. Table 12.2 reflects the measurement frequencies of the CH218 of the Taipei Rapid Transit System (TRTS). Generally speaking, the measurement items and frequencies of TRTS are quite rigorous because they are excavations of large scale and any property damage may cause serious loss. For general excavations, Table 12.2 can be used as a reference with some proper modification on the basis of the excavation scale.

12.9 Application of monitoring systems

From Sections 12.4–12.7 are introduced the commonly used monitoring instruments and items in excavations. Among them, the groundwater level, earth pressure, and the water pressure outside the excavation zone are indexes for the diagnosis of the abnormal behavior in excavations. The results from those monitoring items are not directly used for the judgment of the excavation safety.

The lateral deformations of the retaining structure and soils, the tilt and settlement of the building, the ground settlement, and the heave of the excavation bottom, the uplift of the central post, the strut load, the stress of the retaining structure, and the water pressure

Table 12.2 Measuring frequency of the monitoring system in the CH218 of Taipei Mass Transit System (Chang, 1991)

Instrument	*Minimum monitoring frequency*
1 Bench mark	Check the permanent bench mark every three months
2 Settlement point	
a on the building near the excavation	Once a week
b on the buildings next to excavations of tunnels	Once a month before a shield passes; during grouting operation, monitor constantly, then once a week till settlement comes to stability
c on the pavement	Once every two weeks
d on the pipes of public facilities	Once every two weeks
3 Inclinometers in soils and diaphragm walls	Once a week. Take extra readings before preloading, installing and dismantling of struts.
4 Settlement gauges in soil	Once a month before a shield passes.
5 Strain gauges	Once a day after installing and preloading struts for ten days; after that, once a week. Constantly monitor during casting of diaphragm walls.
6 Observation wells/ piezometers	Once a week; once a day during dewatering
7 Earth pressure cells/electronic piezometers on diaphragm walls	Once a week
8 Rebar stress meters	Once a week; take extra readings around the preloading of struts and after their dismantling
9 Vibrating wire strain gauges	Constantly monitor during the grouting operation

within the excavation zone are directly related to the safety of both excavations and adjacent properties. Each monitoring item can be set with the alert and action levels separately. These measured values and alert and action levels all contribute to the understanding of the existing conditions of the excavation and serve as the basis to judge whether and when emergency measures are to be taken.

An alert level is an important indicator that tells whether the excavation is under abnormal conditions. An action level is the limit indicating the necessity for emergency measures. Under normal conditions, measured values will vary with the excavation depth. Generally speaking, when the measured value exceeds the alert level, it follows that the excavation is under a certain abnormality and engineers have to make a judgment of the cause of abnormality, in addition to being cautious, though the excavation can continue. When the measured value exceeds the action level, it indicates the excavation is under dangerous conditions and has to be suspended right away to take necessary measures to restore the stability.

In fact, there are many objects of measurement related to the safety of an excavation. That some of the measured values grow beyond the action levels does not necessarily lead to the conclusion that the excavation is really under unsafe conditions. To our certainty, however, the more measured values grow beyond the action levels the closer the excavation is to failure.

Engineers have to make their own judgment of the present conditions of safety on the basis of the relations between the measured values and the alert/action levels and the characteristics of the excavation.

The setting of alert and action levels is based on empirical experiences so far and no generally accepted standard formula is available. In engineering practice, the allowable value is usually taken as the action level and 80% of the allowable value the alert level. The allowable value is a generally accepted physical quantity, taking the factor of safety into consideration. For example, if the allowable settlement of a building with the individual foundation is 2.5 cm (see Section 11.2), the action level for the building settlement is then 2.5 cm and the alert level 2 cm. Table 12.3 illustrates the alert and action levels of CH218 of the Taipei Rapid Transit System and the corresponding emergency measures.

The above discussed alert and action level do not vary with the excavation depth. As a result, some illogical conditions may occur. For example, for a 20 m deep excavation, when excavation reaches the depth of 12 m, the settlement of the adjacent building is equal to 2.6 cm, which is beyond the action level already. According to the criterion, the excavation has to be suspended immediately and emergency measures have to be taken. The building settlement, however, will increase with the increase of the excavation depth no matter which emergency measures are taken or auxiliary methods are employed, though the increased rate of settlement may be reduced with the implementation of the emergency measures or auxiliary methods. The total settlement of the building at the final stage may exceed the allowable settlement and serious damage may be engendered accordingly. On the other hand, however, if the excavation is approaching the last stage, the emergency measure or auxiliary method may be economically inefficient and have little effect.

Though this method is sometimes illogical, it is still applicable to most excavations. The main reason is that the action level has had the safety factor considered and there remains some room for the increase of deformation or stress when the measured value is over the action level. Whether it is enough to last through the excavation process, however, is another question.

Considering that this method has its shortcoming, the author proposes to take advantage of feedback analysis for the safety evaluation of excavations and adjacent properties. Figure 12.36 diagrams the flow chart of feedback analysis in the evaluation of the property safety. As shown in the figure, make sure whether the buildings are within the influence range of excavations before excavation; if not, the safety of the buildings is not to be considered and excavation can continue. If they are, depending on the types of the buildings and their foundations, the allowable settlement of the buildings, δ_a, can be determined (see Section 11.2). Then predict the ground settlement for each excavation stage δ_i as well as that for the last stage δ_f. If δ_f derived from the analysis is larger than δ_a, it implies that the buildings will come out damaged when the excavation is finished. The excavation plan has to be re-evaluated. If necessary, auxiliary methods can be used. Repeat the process till δ_f is smaller than δ_a, which means the safety of the buildings can be secured and the excavation can be re-started.

After the excavation is started, if the measured value (δ_m) of ground settlement for the ith stage equals the predicted value, δ_i, it means that the prediction is accurate and the excavation can continue.

If δ_m is larger than δ_i, it means the prediction is inaccurate and the excavation may come out unsafe. A feedback analysis is now required. That is to say, the excavation sequence and

Table 12.3 Control values for the monitoring system of the CH218 of Taipei Mass Transit system (Chang, 1991)

Area	*Instrument*	*Alert value*	*Action value*
Excavations	1 Inclinometers (inside the wall)	60 mm	85 mm or 1/350
	2 Inclinometers (in soil)	30 mm	40 mm
	3 Observation wells/ piezometers (outside of the wall)	−2 m	−3 m
	4 Observation wells/ piezometers (within the excavation zone)	Within 1m below excavation surface and F.S. against sand boiling lower than 1.25	Dewatering fails
	5 Strain gauges	90% of the designed load	125% of the designed load
	6 Rebar stress meter	250 MPa	350 MPa
Adjacent buildings	1 Settlement points (on buildings)	22 mm	25 mm
	2 Differential settlements of buildings	1/600	1/500
	3 Tiltmeters (buildings)	1/800	1/500
	4 Vibrating wire strain gauges	Any strain monitored during grouting	1.0 mini-strain

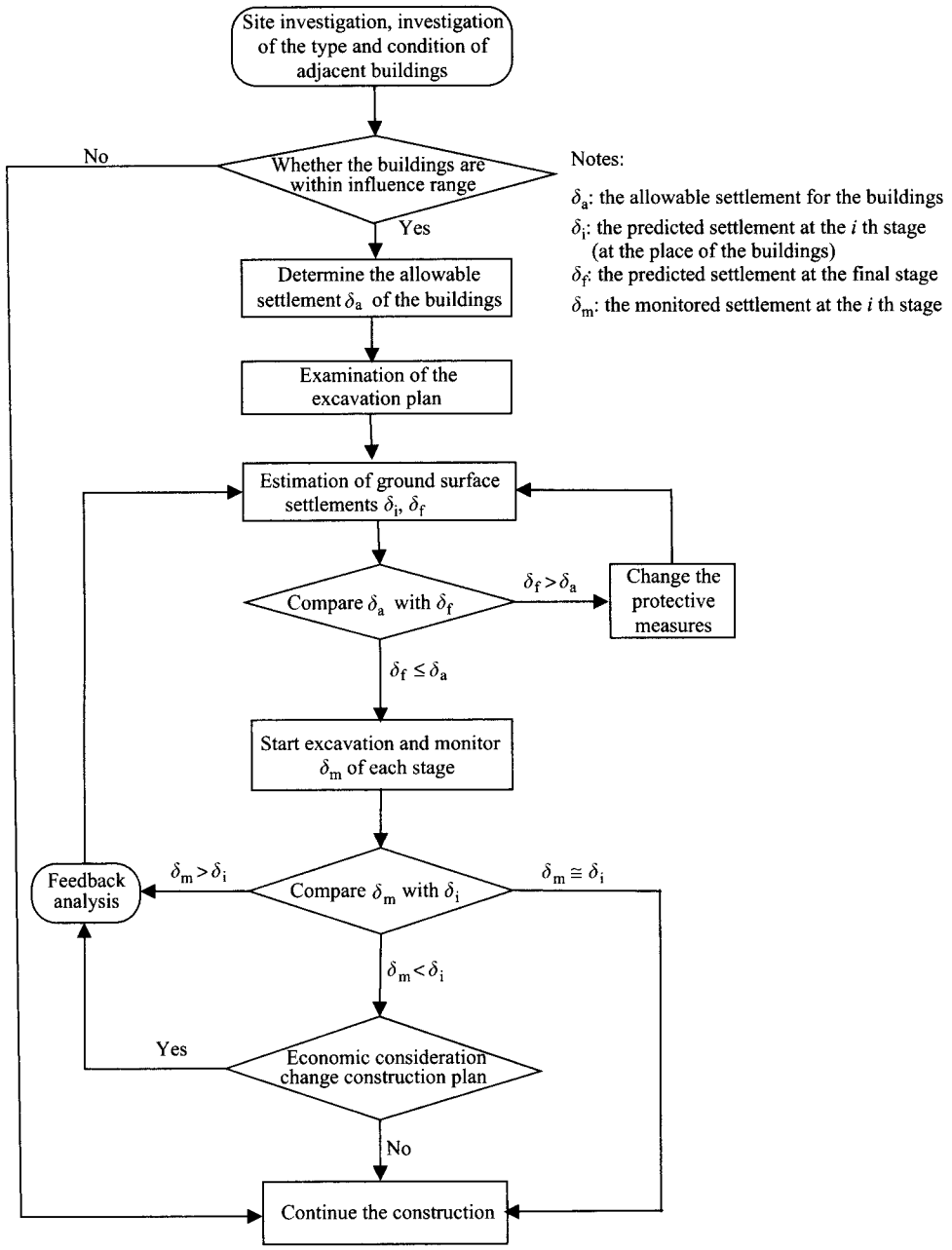

Figure 12.36 Feedback analysis using settlements as parameter.

soil parameters used in the analysis have to be adjusted till δ_i is about equal to δ_m. Under such a condition, if δ_f is larger than δ_a, it means the buildings will come out damaged when excavation is finished. The excavation plan thus has to be re-evaluated and auxiliary methods have to be added to it. If δ_f is still smaller than δ_a, it means the excavation is within the safety range and can be continued.

If δ_m is smaller than δ_i, it means that, though the prediction is not accurate, with the measured value smaller than the predicted one, the prediction is conservative and the excavation-induced ground settlement will not cause damage to the buildings. The excavation can be continued or a re-examination of the excavation plan can be made to reduce the cost (e.g. decrease the numbers of the strut levels).

Though Figure 12.36 takes ground settlement for example, it is the same principle for the lateral deformation of the retaining wall, strut load, and the heave of the excavation bottom.

12.10 Summary and general comments

The aim of this chapter is to introduce the instruments for excavation monitoring programs and related principles. The monitoring plan and its application to the evaluation of the excavation safety are also discussed. The contents of this chapter are summarized as follows:

1 The commonly used monitoring instruments for excavation can be divided into three categories: those for displacement or deformation, for stress or force, and for water pressure and water level. The monitoring items for displacement or deformation include the lateral movement of the retaining wall and soils, the tilt of buildings, the settlement of ground surface or buildings, and the heave of the excavation bottom, etc. The measurements of stress or force include strut loads, the stress of the retaining structure, and the earth pressure on the wall. Generally speaking, the monitoring of the groundwater level, earth pressure, and the water pressure outside the excavation zone are used for the evaluation of the abnormal behaviors in an excavation whereas the lateral deformation of the retaining structure and soils, the tilt and settlement of buildings, the ground settlement, the heave of the excavation bottom, the uplift of central posts, the strut load, the stress of retaining structures, and the water pressure within the excavation zone are for the judgment of the safety of excavations and adjacent properties.

2 There are no specific types of instruments or special rules for excavation monitoring programs. If it accords with economic principles and is accurate enough, any instruments or methods can be used. Most of the instruments or devices can be basically divided into the electronic and nonelectronic types. The electronic type is sensitive in response and easier to use. Their accuracy, however, is often influenced by the installation process and the surroundings. When applied in the long term, their durability has to be watched.

3 There are three main categories of monitoring systems: the manual monitoring system, the semi-automatic monitoring system, and the automatic monitoring system. The manual monitoring system is cheaper but is incapable of obtaining continuous readings. It is the most widely adopted monitoring system. The automatic monitoring system costs much more but is capable of obtaining continuous measured values. It is usually applied only to the excavations which are sensitive to environmental impacts. The semi-automatic system is in between, having the strengths and shortcomings of both the above systems. A complete monitoring system plan should include the determination of the monitoring parameters, the selection of the locations of the instruments or devices,

the prediction of the excavation parameters, the specifications of the instruments, the setting of the installation specifications, the setting of the alert and action levels, and the determination of the measurement frequencies, etc.

4 The following factors all contribute to the evaluation of the safety of excavation and adjacent properties: the lateral deformations of the retaining structure and soils, the tilt and settlement of the buildings, the ground settlement, the heave of the excavation bottom, the uplift of the central post, the strut load, the stress of the retaining structure, and the water pressure within the excavation zone. The more of they show the sign of approaching failures, the closer the excavation is to failure.

5 To evaluate the safety of an excavation, the alert and action levels can be set against the monitoring object. When the measured value goes beyond the alert level, it implies the excavation is under a certain abnormality and the cause of such abnormality has to be found, as well as, more caution must be used, though the excavation can continue. When the measured value keeps increasing and is over the action level, it indicates the excavation may be under dangerous conditions and the excavation has to be suspended right away to take emergency measures. Though there are some illogical points, this is basically applicable to most excavations.

6 The evaluation of the excavation safety can also resort to the feedback analysis. The method has the benefit of early prediction of the safety of excavation and the properties in the initial stages of excavation. It also helps to select the proper auxiliary methods as early as possible in the initial excavation stages or even to adopt a more economical method. The method is troublesome and also requires better analytical techniques. It is, however, more reasonable in its result than others.

Problems

12.1 What is the object of setting up the monitoring system in an excavation?

12.2 Explain the basic principle of the resistance type of strain gauges.

12.3 Elucidate the basic principle of the vibrating type of strain gauges.

12.4 Compare the strengths and shortcomings of the resistance type and vibrating type of strain gauges.

12.5 If the depth of the bottom of the inclinometer casing within the diaphragm wall is the same as that of the diaphragm wall, the displacement of the bottom of the diaphragm wall cannot be obtained and the true displacement curve is not to be obtained accordingly. How can we obtain the true displacement curve of the diaphragm wall? Please propose two to three methods.

12.6 Suppose an inclinometer casing is installed within a 21 m deep diaphragm wall to the same depth. To measure the tilt first, place the inclinometer at the bottom of the casing and take the reading, which is the sine function of θ, the tilt of the inclinometer. Then the reading is taken again, lifting the inclinometer by 50 cm. Repeat the process until the top of the casing is reached. The setting of the indicator is $\sin 30° = 12,500$. Before excavation, the initial value from the inclinometer is as illustrated in Table P12.6. When excavation reaches the depth of 5 m, the displacement of the casing top is 1.5 cm and the measured values from the inclinometer in the A^+ and A^- directions are also listed in the same table. Compute the displacements of the diaphragm wall at each depth and plot the diagram of displacement versus depth.

Table P12.6

Depth (m)	Initial value		Measured value after 5 m excavation	
	Direction of +A	Direction of −A	Direction of +A	Direction of −A
0.00				
0.50	377	−389	266	−302
1.00	342	−356	299	−321
1.50	384	−400	343	−364
2.00	684	−700	650	−654
2.50	750	−766	710	−736
3.00	481	−498	439	−473
3.50	387	−404	346	−366
4.00	265	−276	222	−248
4.50	83	−101	51	−64
5.00	3	−19	−33	17
5.50	23	−39	−12	−5
6.00	150	−162	115	−123
6.50	109	−124	88	−106
7.00	118	−134	103	−120
7.50	25	−40	18	−41
8.00	−4	−8	−12	−5
8.50	179	−198	182	−203
9.00	64	−76	71	−91
9.50	118	−133	135	−145
10.00	−32	12	−31	−14
10.50	−494	483	−454	436
11.00	−461	443	−450	438
11.50	230	−253	261	−306
12.00	416	−428	443	−467
12.50	168	−186	216	−229
13.00	2	−20	41	−58
13.50	29	−46	67	−85
14.00	35	−50	74	−90
14.50	64	−79	105	−122
15.00	67	−79	108	−126
15.50	53	−68	94	−115
16.00	−256	236	−215	187
16.50	−230	215	−181	174
17.00	−161	147	−119	101
17.50	−149	135	−107	90
18.00	−94	78	−64	42
18.50	28	−43	71	−89
19.00	−287	272	−249	213
19.50	−533	520	−491	474
20.00	−510	494	−463	445
20.50	−197	173	−168	141
21.00				

12.7 Elucidate why the measured value on the tiltmeter on the wall of a building does not necessarily represent the angular distortion.

12.8 To monitor the ground settlement induced by excavation, what is the benefit of the settlement profile measured from the settlement marks which are perpendicular to the

retaining wall and set in the central section of the excavation site, as far as excavation safety and property protection are concerned?

12.9 What are the objects of monitoring the heave of an excavation bottom and the uplift of central posts?

12.10 Elucidate the installation process of a rebar stress meter.

12.11 Describe the most suitable location and depth of a rebar stress meter on the retaining wall.

12.12 To measure the strut load, the commonly used methods are the hydraulic jack pressure, the load cell, and the strain gauge. Elucidate their strengths and shortcomings.

12.13 Describe the object of monitoring the strut load.

12.14 Elucidate the installation process of an earth pressure cell.

12.15 Explain the object of monitoring the lateral earth pressure on the retaining wall.

12.16 The commonly used devices to measure water pressures are the open standpipe piezometer, the pneumatic piezometer, and the electronic piezometer. Explicate their strengths and shortcomings separately.

12.17 What is the object of installing piezometers within an excavation zone?

12.18 What is the object of installing piezometers outside the excavation zone?

12.19 Explicate the similarities and dissimilarities between an observation well and a piezometer in installation.

12.20 Judging on the basis of the installation process of an observation well, can it be used to monitor the water pressure?

12.21 Explicate the planning of a complete monitoring system in excavations.

12.22 How can we achieve the goal of excavation safety and property protection with the help of a monitoring system?

Appendix A

Conversion factors

Meter (symbol: m), gram (symbol: g), and Newton (symbol: N) are the basic units of length, mass, and force for the SI system, respectively. Prefixes, as listed in Table A.1, are used to form multiples of SI units. For example, km = 10^3 m, MN = 10^6 N.

Table A.1

Factor	*Prefix*	*Symbol*	*Factor*	*Prefix*	*Symbol*
10^{18}	exa	E	10^{-1}	deci	d
10^{15}	peta	P	10^{-2}	centi	c
10^{12}	tera	T	10^{-3}	milli	m
10^{9}	giga	G	10^{-6}	micro	μ
10^{6}	mega	M	10^{-9}	nano	n
10^{3}	kilo	k	10^{-12}	pico	p
10^{2}	hecto	h	10^{-15}	femto	f
10^{1}	deka	da	10^{-18}	atto	a

A.1 Length

Table A.2

SI units to British units	*British units to SI units*
1 km = 0.6214 mile (US)	1 mile (US) = 1.609 km
1 m = 1.094 yd	1 yd = 0.9144 m
1 m = 3.281 ft	1 ft = 0.3048 m
1 cm = 0.3937 in	1 in = 2.54 cm
1 mm = 0.03937 in	1 in = 25.4 mm

Note
1 mile (US) = 1,760 yd = 5,280 ft, 1 ft = 12 in.

A.2 Area

Table A.3

SI units to British units	*British units to SI units*
$1\ km^2 = 0.3861\ mile^2$	$1\ mile^2 = 2.59\ km^2$
$1\ m^2 = 1.196\ yd^2$	$1\ yd^2 = 0.8361\ m^2$
$1\ m^2 = 10.764\ ft^2$	$1\ ft^2 = 0.09290\ m^2$
$1\ cm^2 = 0.155\ in^2$	$1\ in^2 = 6.452\ cm^2$
$1\ mm^2 = 1.55 \times 10^{-3}\ in^2$	$1\ in^2 = 645.2\ mm^2$

A.3 Volume or section modulus

Table A.4

SI units to British units	*British units to SI units*
$1\ m^3 = 1.308\ yd^3$	$1 yd^3 = 0.765\ m^3$
$1\ m^3 = 35.32\ ft^3$	$1\ ft^3 = 0.0283\ m^3$
$1\ m^3 = 61,023\ in^3$	$1\ in^3 = 16.387 \times 10^{-6}\ m^3$
$1\ cm^3 = 0.061024\ in^3$	$1\ in^3 = 16.387\ cm^3$
$1\ mm^3 = 0.061024 \times 10^{-3}\ in^3$	$1\ in^3 = 16.387 \times 10^3\ mm^3$
$1\ L = 0.03532\ ft^3$	$1\ ft^3 = 28.32\ L$
$1\ L = 0.220$ gal (BS)	1 gal (BS) = 4.546 L
$1\ L = 0.2642$ gal (US)	1 gal (US) = 3.785 L

Note
$1\ m^3 = 1,000$ L (liter).

A.4 Moment of inertia

Table A.5

SI units to British units	*British units to SI units*
$1\ mm^4 = 2.403 \times 10^{-6}\ in^4$	$1\ in^4 = 0.4162 \times 10^6\ mm^4$
$1\ cm^4 = 0.02403\ in^4$	$1\ in^4 = 41.62\ cm^4$

A.5 Mass

Table A.6

SI units to British units	*British units to SI units*
1 Mg = 0.9842 long ton	1 long ton = 1.016 Mg
1 Mg = 1.102 short ton	1 short ton = 0.9072 Mg
1 kg = 2.205 lb	1 lb = 0.4536 kg
1 kg = 0.06852 slug [lb − force/(ft.s^2)]	1 slug = 14.59 kg

Note
1 Mg = 1 ton, 1 long ton (US) = 2,240 lb, 1 short ton (BS) = 2,000 lb.

A.6 Density

Table A.7

SI units to British units	*British units to SI units*
1 Mg/m^3 = 62.43 lb/ft^3	1 lb/ft^3 = 0.01602 Mg/m^3
1 kg/m^3 = 0.06243 lb/ft^3	1 lb/ft^3 = 16.02 kg/m^3
1 g/cm^3 = 62.43 lb/ft^3	1 lb/ ft^3 = 0.01602 g/cm^3

Note
1 Mg/m^3 = 1 ton/m^3 = 1 g/cm^3 = 10^{-3} kg/cm^3.

A.7 Force or weight

Table A.8

SI units to other units	*Other units to SI units*
1 N = 0.10197 kg-force	1 kg-force = 9.807 N
1 kN = 0.10197 ton-force	1 ton-force = 9.807 kN
1 N = 0.2248 lb-force	1 lb-force = 4.448 N
1 kN= 0.2248 kip-force	1 kip-force = 4.448 kN
1 kN = 0.1004 long ton-force	1 long ton-force = 9.964 kN
1 kN = 0.1124 short ton-force	1 short ton-force = 8.896 kN

Note
N = kg · m/s^2.

A.8 Stress or pressure

Table A.9

SI units to other units	*Other units to SI units*
1 MPa = 10.197 kg-force/cm^2	1 kg-force/cm^2 = 0.09807 MPa
1 MPa = 101.97 ton-force/m^2	1 ton-force/m^2 = 9.807 × 10^{-3} MPa
1 kPa = 0.010197 kg-force/cm^2	1 kg-force/cm^2 = 98.07 kPa
1 kPa = 0.10197 ton-force/m^2	1 ton-force/m^2 = 9.807 kPa
1 MPa = 0.06475 long ton-force/m^2	1 long ton-force/m^2 = 15.44 MPa
1 MPa = 0.145 kip-force/in^2	1 kip-force/in^2 = 6.895 MPa
1 MPa = 145 lb-force/in^2	1 lb-force/in^2 = 6.895 × 10^{-3} MPa

Note
1 Pa = 1 N/m^2, 1 bar = 100 kPa, 1 kg-force/cm^2 = 10 ton-force/m^2, Atmospheric pressure: 1 P_a = 1.033 kg-force/cm^2 = 10.33 ton-force/m^2 = 101.34 kN/m^2.

A.9 Unit weight

Table A.10

SI units to other units	*Other units to SI units*
1 MN/m^3 = 101.97 ton-force/m^3	1 ton-force/m^3 = 9.807 × 10^{-3} MN/m^3
1 kN/m^3 = 0.10197 ton-force/m^3	1 ton-force/m^3 = 9.807 kN/m^3
1 kN/m^3 = 6.366 lb-force/ft^3	1 lb-force/ft^3 = 0.1571 kN/m^3

Note
1 kg-force/cm^3 = 1,000 ton-force/m^3.
Unit weight of water γ_w = 1 ton-force/m^3 = 62.429 lb-force/ft^3.

Appendix B

Indices of the case histories

TNEC and buildings P, Q, R, and S

This book refers to the case histories of the excavations of the Taipei National Enterprise Center (TNEC) and the buildings P, Q, R, and S for elucidation of the characteristics of excavations and for exercises. The case histories have clear excavation process and sufficient geological data. They are useful not only for the exploration of the excavation behaviors but for the examination of the results of theoretical analyses.

B.1 TNEC

The TNEC excavation is described in Section 3.6. The plane view of the site and the observation system are as shown in Figure 3.33. The construction sequence of the foundation excavation is as shown in Figure 3.34 and Table 3.3.

The geological condition of the excavation site is elucidated in Section 2.11. The basic properties of soils and the results of strength tests are shown in Figure 2.37.

The lateral deformation of the diaphragm wall and the ground surface settlement at each excavation stage are shown in Figure 6.8. Relationships between time and lateral deformation and ground surface settlement, respectively, are as shown in Figures 6.20–6.22. The soil displacements outside the excavation zone are shown in Figure 6.15. The heaves and heaving rate of the excavation bottom are shown in Figure 6.19.

The variation of bending moment of the diaphragm wall is as shown in Figures 7.13 and 7.14.

There were six buildings in the vicinity of the excavation site of TNEC. During the process of excavation, the variations of tilts of the buildings are described in Section 11.4.4 and shown in Figures 11.11 and 11.12.

Besides, the referent documents and other study results of TNEC are provided in the references.

B.2 Building P

The foundation excavation of Building P is described in Example 6.1. The excavation and geological profiles are shown in Figure 6.41. The lateral deformation of the retaining wall at each stage is shown in Figure 6.42.

B.3 Building Q

The foundation excavation of Building Q is described in Example 6.2. The excavation and geological profiles are shown in Figure 6.43.

B.4 Building R

The foundation excavation of Building R is described in Problem 6.4 in Chapter 6. The excavation and geological profiles are shown in Figure P6.4. The lateral deformation of the retaining wall at each stage is shown in Figure P7.17.

B.5 Building S

The foundation excavation of Building S is described in Problem 6.11. The excavation and geological profiles are shown in Figure P6.11. The lateral deformation of the retaining wall at each stage is shown in Figure P7.14.

Commonly used steel sections or piles

Types of steel sections vary with different regions or countries. This section displays some commonly used types of steel sections in some Asian countries. The sections that have been mentioned in this book are provided with their properties in this appendix.

C.1 H-steel (or W-section)

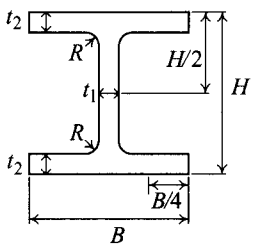

Moment of inertia	$I = Ar^2$
Radius of gyration	$r = \sqrt{I/A}$
Section modulus	$S = I/e$
Area	A

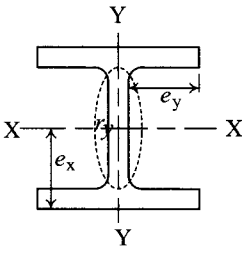

Table C.1

Section	Dimension (mm)				Area (cm^2)	Weight (kg/m)	I (cm^4)		r (cm)		S (cm^3)	
	$H \times B$	t_1	t_2	R			I_x	I_y	r_x	r_y	S_x	S_y
200 × 200	200 × 200	8	12	13	63.53	49.9	4,716	1,601	8.62	5.02	472	160
250 × 250	250 × 250	9	14	16	92.18	72.4	10,833	3,648	10.84	6.29	867	292
300 × 300	300 × 300	10	15	18	119.78	94.0	20,410	6,753	13.05	7.51	1,361	450
350 × 350	350 × 350	12	19	20	173.87	136.5	40,295	13,583	15.22	8.84	2,303	776
400 × 400	400 × 400	13	21	22	218.69	171.7	66,621	22,409	17.45	10.12	3,331	1,120

C.2 I-section

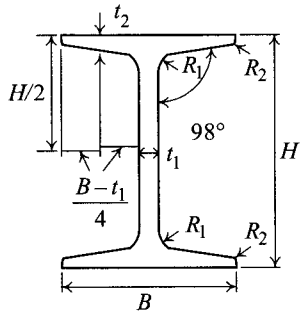

Moment of inertia	$I = Ar^2$
Radius of gyration	$r = \sqrt{I/A}$
Section modulus	$S = I/e$
Section area	A

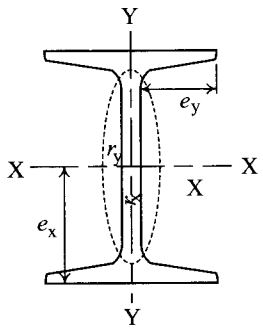

C.3 U-section sheet piles

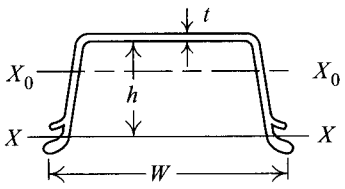

YSP sheet pile

Table C.2

Type	*Dimension*			*Area* (cm^2)	*Weight* (kg/m) *(per unit length)*		*I* (cm^4)		*S* (cm^3)	
	W (mm)	*h* (mm)	*t* (mm)		*A single pile*	*Per 1.0 meter width*	*A single pile*	*Per 1.0 meter width*	*A single pile*	*Per 1.0 meter width*
YSP-I	400	75	8.0	46.49	36.5	92.2	429	3820	66.4	509
YSP-II	400	100	10.5	61.18	48.0	120	984	8690	121	869
YSP-III	400	125	13.0	76.42	60.0	150	1,920	16,400	196	1,310
YSP-IV	400	155	15.5	96.99	76.1	190	3,690	31,900	311	2,060
YSP-V	420	175	22.0	134.0	105	250	5,950	55,200	433	3,150

C.4 Z-section sheet piles

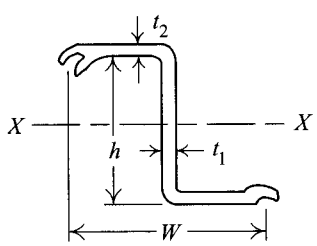

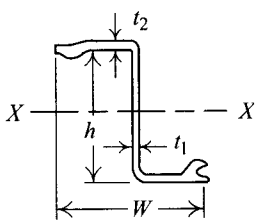

C.5 Line-section sheet piles

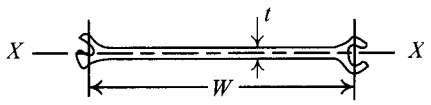

C.6 Rail piles

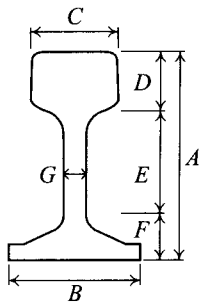

Table C.3

Types (kg)	*Dimension* (mm)							*Area* (cm^2)	*Weight* (kg/m)	*I* (cm^4)	*r* (cm)	*S* (cm^3)
	A	*B*	*C*	*D*	*E*	*F*	*G*					
37[1]	122.24	122.24	62.71	36.12	64.69	21.43	13.49	47.30	37.20	952	4.49	149
50[1]	153.00	127.00	65.00	49.00	74.00	30.00	15.00	64.20	50.40	1,960	5.53	242
60[1]	174.00	145.00	65.00	49.00	94.90	30.10	16.50	77.50	60.80	3,090	6.31	321

Note
1 Types of the rail pile are expressed in weight per unit length (per 1 m).

Appendix D

Definition of plane strain

Figure D.1 illustrates an infinitely long diaphragm wall. Acted on by earth pressure from outside, the wall moves inward toward the excavation zone. The lateral displacement of the wall and the surrounding soils (in x direction) changes with the variation of the depth (in y direction). There also exists some amount of vertical displacement of the wall and the surrounding soils. At the same depth, the lateral displacements of the wall and soils in different positions (along z direction) are the same. That is, the displacement along z direction is zero. Since displacement only occurs in two directions, the displacement behavior is called a two-dimensional behavior.

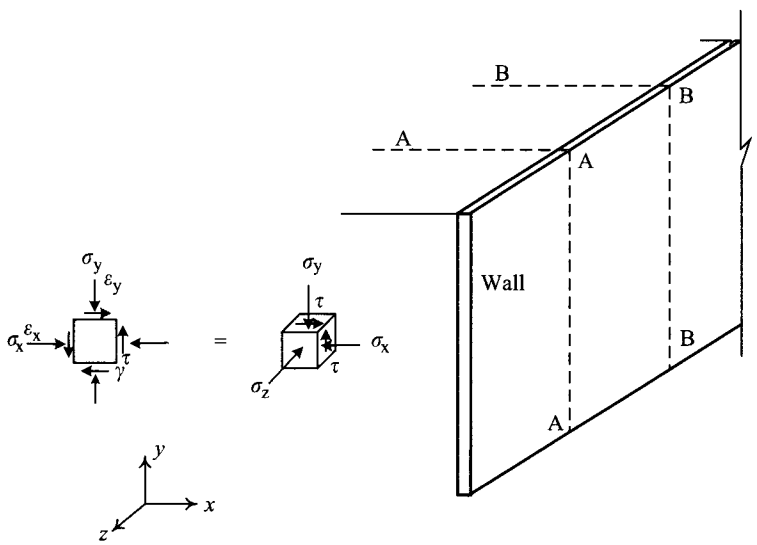

Figure D.1

Because the displacement of the wall and soils only occurs in the x and y directions, the normal strains and shear strains in the z direction are all none, so, it follows that the strains are only found on the xy plane (i.e. the $z = 0$ plane). The behavior is called the plane strain or two-dimensional plane strain behavior.

Since the strain in the z direction is zero, the σ_z-value of each section (e.g. Sections A-A and B-B) is the same. That is to say, the stress condition on each section of the soil is the same. When performing an analysis, we can take any section to be a representative.

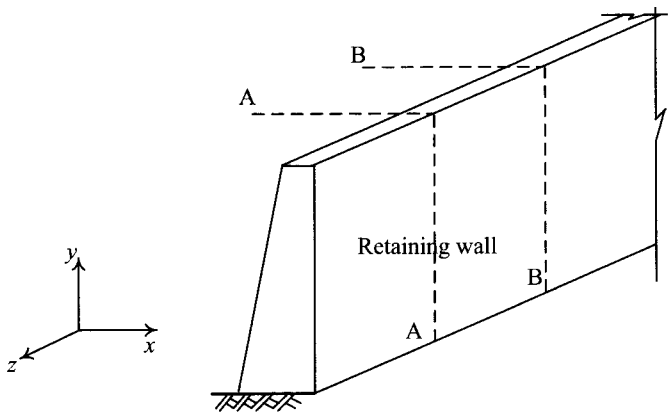

Figure D.2

Analysis of structures subject to plane strain behavior is much simpler than those with three-dimensional behavior. Therefore, in most books on geological engineering or foundation engineering, three-dimensional problems are often simplified into plane strain problems, as well as possible. For example, the flow net, seepage, the bearing capacity of continuous or strip foundations, the safety factor for slope stability, the lateral deformation of a retaining wall, and the stability analysis of excavations, etc, are all analyzed on the basis of plane strain condition.

Answers to selected problems

Chapter 2

2.1 At GL-21 m, $\sigma_v = 359.9\ kN/m^2$, $u_w = 186.4\ kN/m^2$, $\sigma'_v = 173.5\ kN/m^2$

2.3 (1) Short-term condition
At GL-27.5 m, $\sigma_v = 529.5\ kN/m^2$, $u_w = 220.7\ kN/m^2$, $\sigma'_v = 308.8\ kN/m^2$
(2) Long term condition
At GL-27.5 m, $\sigma_v = 529.5\ kN/m^2$, $u_w = 196.2\ kN/m^2$, $\sigma'_v = 333.3\ kN/m^2$

2.5 The undrained shear strength (i.e. shear stress on the failure surface) $= 32.0\ kN/m^2$

2.9 NC clay, $c' = 0$ (1) $196.2\ kN/m^2$ (2) $45 + \phi'/2 = 60$ degree

2.11 After sampling, $\sigma'_c = 66.89$, $w_f = 26.5\%$, $p'_f = 55\ kN/m^2$, $q_f = 20\ kN/m^2$
(1) $\sigma_1 = 75\ kN/m^2$, $\sigma_3 = 35\ kN/m^2$ (2) $u_f = 63.1\ kN/m^2$

2.13 $s_{u,avg} = 40\ kN/m^2$, $q_u = cN_c = 40 \times 5.7 = 228\ kN/m^2$

Chapter 4

4.1 K_0 condition, total lateral force $= 513.1$ kN/m, $z = 2.87$ m (from foundation bottom)

4.3 (a) $K_a = 0.283$, $P_a = 1721.2$ kN/m, $z = 8.67$ m (from the wall bottom) (b) $K_a = 0.26$, $P_{a,h} = 1306.4$ kN/m, $z = 8.67$ m (c) $K_a = 0.275$, $P_{a,h} = 1387.1$ kN/m, $z = 8.67$ m

4.5 (a) Rankine $K_{p,h} = K_p = 3.54$ $P_{p,h} = 5,385$ kN/m
(b) Coulomb $K_{p,h} = K_p \cos\delta = 19 \cos 34 = 15.75$ $P_{p,h} = 23,895$ kN/m
(c) Caquot-Kerisel $K_{p,h} = K_p \cos\delta = 9.4 \cos 34 = 7.79$ $P_{p,h} = 11,853$ kN/m
$z = 4.33$ m (from the wall bottom)

4.7 Depth of tension crack $= 4.0$ m, consider the porewater pressure in the tension crack, when $z = 0$ m, $s_u = 100\ kN/m^2$; $z = 4$ m(−), $s_u = 100\ kN/m^2$, $z = 4$ m(+), $s_u = 0.3\sigma'_v = 9.83\ kN/m^2$; $z = 40$ m, $s_u = 0.3\sigma'_v = 98.28\ kN/m^2$
(a) $z = 0$ m, $\sigma_a = -200\ kN/m^2$, $\sigma_w = 0$; $z = 4$ m(−), $\sigma_a = -128\ kN/m^2$, $\sigma_w = 39.24\ kN/m^2$; $z = 4$ m(+), $\sigma_a = 52.34\ kN/m^2$; $z = 40$ m, $\sigma_a = 523.44\ kN/m^2$; $P_a = 10,443$ kN/m, $z = 13.3$ m (from the wall bottom) (b) $z = 0$ m, $\sigma_a = -245\ kN/m^2$, $\sigma_w = 0$; $z = 4$ m(−); $\sigma_a = -173\ kN/m^2$, $\sigma_w = 39.24\ kN/m^2$; $z = 4$ m(+), $\sigma_a = 47.92\ kN/m^2$; $z = 40$ m, $\sigma_a = 479.21\ kN/m^2$; $P_a = 9,567$ kN/m, $z = 12.3$ m

4.9 (a) $P_p = 6480$ kN/m, $z = 7.8$ m (from the wall bottom) (b) $P_p = 7114$ kN/m, $z = 7.8$ m

4.11 Assume the porewater pressure is linearly distributed between GL-4 m and GL-19.0 m
(a) $P_a = 2,389$ kN/m, $z = 5.3$ m (from the wall bottom) (b) $P_p = 1,167$ kN/m. $z = 3.7$ m

4.13 Lateral force due to line load = 293.6 kN/m; Active pressure resultant = 2852 kN/m (water pressure in the tension crack is considered)

4.15 Lateral force due to line load = 566 kN/m, location of line of action = 6 m (from the wall bottom); Active pressure resultant = 7845 kN/m (water pressure in the tension crack is considered), location of line of action = 9.4 m

4.17 $K_a = 0.27, K_p = 9.7$ (a) water pressure at the wall bottom = 264.87 kN/m^2, $P_a = 4,618$ kN/m, $z = 9.25$ m (from the wall bottom), $P_p = 10,316$ kN, $z = 4.99$ m
(b) water pressure at the wall bottom = 185.09 kN/m^2, $P_a = 4,832.8$ kN/m, $z = 9.3$ m , $P_p = 8,134.7$ kN, $z = 5.1$ m
(c) water pressure at the wall bottom = 198.6 kN/m^2, $P_a = 3,920.8$ kN/m, $z = 9.3$ m (from the wall bottom) , $P_p = 6470.3$ kN, $z = 5.1$ m

Chapter 5

5.1 $K_a = K_{a,h} = 0.33, K_p = K_{p,h} = 3.0, H_{p,cal} = 2.72$ m, $H_{p,d} = 2.72 * 1.5 = 4.08$ m

5.3 $\tan\phi'_m = \tan\phi'/FS_s\phi'_m = 21.2°$ $K_a = K_{a,h} = 0.47$ $K_p = K_{p,h} = 2.2$, $H_{p,d} = 5.1$ m

5.5 Push-in analysis, $H_p = 3.5$ m; basal heave analysis, $H_p = 2.5$ m; for design, $H_p = 3.5$ m

5.7 Assume the soil above the lowest level of strut is clay
The slip circle method:
When $H_p = 15$ m, $F_b = 2.06$; when $H_p = 20$ m, $F_b = 2.08$
Terzaghi's method:
When $H_p = 15$ m, $F_b = 2.13$; when $H_p = 20$ m, $F_b = 2.13$

5.9 Active side, $s_{u(GL\text{-}16m)} = 51.35$ kN/m^2, $s_{u(GL\text{-}19m+H_p)} = 59.21+2.62H_p$ kN/m^2
Passive side, $s_{u(GL\text{-}16m)} = 59.21$ kN/m^2, $s_{u(GL\text{-}19m+H_p)} = 59.21+2.62H_p$ kN/m^2
Push-in analysis, $H_p = 26.7$ m; basal heave analysis, $H_p = 10$ m; for design, $H_p = 26.7$ m

5.11 (1) $H_p = 15$ m
$s_{u(GL\text{-}19.86m)} = 61.46$ kN/m^2, $s_{u(GL\text{-}34m)} = 98.51$ kN/m^2
$s_{u1} = (0 + 62.46)/2 = 31.23$ kN/m^2, $s_{u2} = (62.46 + 98.51)/2 = 31.23$ kN/m^2
$$F_b = \frac{s_{u2}N_cB/\sqrt{2}}{W - s_{u1}H_e} = 1.54$$
(2) $H_p = 20$ m
$s_{u(GL\text{-}24.86\ m)} = 74.56$ kN/m^2, $s_{u(GL\text{-}39\ m)} = 111.61$ kN/m^2
$s_{u1} = (0 + 74.56)/2 = 37.28$ kN/m^2, $s_{u2} = (74.56 + 111.61)/2 = 93.09$ kN/m^2
$F_b = \frac{s_{u2}N_cB/\sqrt{2}}{W - s_{u1}H_e} = 1.92$

5.13 1 The slip circle method: $F_b = 2.06$
2 Terzaghi method: $F_b = 2.45$
3 Bjerrum and Eide method:
$N_{c,s} = 5.53, f_d = 1.09, f_s = 1 + 0.2\frac{B}{L} = 1.1, F_b = 2.30$

5.15 Terzaghi method: $s_{u1,avg} = 27$ kN/m^2, $s_{u2,avg} = 75$ kN/m^2, $F_b = 1.37$
Bjerrum and Eide method:
$s_{u1,avg} = (0 + 113.9)/2 = 57$ kN/m^2; $s_{u2,avg} = 50$ kN/m^2

$N_{c,s} = 5.4; f_s = 1.1; f_d = 1.12$
$F_b = 1.16$

5.17 $K_a = 0.25$, $K_p = 8$; $K_{a,h} = K_a \cos\delta = 0.23$, $K_{p,h} = K_p \cos\delta = 7.35$
From $F_p = M_r/M_d = 1.5$, $d_0 = 4.57$ m, $H_p = 1.2d_0 = 5.48$ m
$S = 713.15$ kN/m, $R = 626.87$ kN/m; $S > R$
The required penetration depth $H_p = 5.48$ m

5.19 $K_{a,h} = 0.211$, $K_{p,h} = 7.346$, $H_p = 3.79$ m, $H_{p,d} = 1.5 \times 3.79 = 5.69$ m

5.21 $K_a = 0.283$, $K_p = 0.354$, $H_p = 0.99$ m, $H_{p,d} = 1.5 \times 0.99 = 1.5$ m

5.23 $H_p = 9.4$ m, $H_{p,d} = (1.5)(9.4) = 14.1$ m

Chapter 6

6.5 Excavation in soft clay and high strut stiffness, concave settlement profile. Assume $\delta_{hm} = 0.5\%H_e$, $\delta_{vm} = 0.75\delta_{hm}$, the maximum lateral movement, maximum settlement and primary settlement influence zone are:
When GL-5.0 m, $\delta_{hm} = 2.5$ cm, $\delta_{vm} = 1.88$ cm, PIZ = 32 m
When GL-8.55 m, $\delta_{hm} = 3.4$ cm, $\delta_{vm} = 2.40$ cm, PIZ = 32 m
When GL-12.4 m, $\delta_{hm} = 5$ cm, $\delta_{vm} = 3.5$ cm, PIZ = 32 m
When GL-15.4 m, $\delta_{hm} = 7.7$ cm, $\delta_{vm} = 5.8$ cm, PIZ = 32 m
When GL-16.9 m, $\delta_{hm} = 8.5$ cm, $\delta_{vm} = 6.4$ cm, PIZ = 32 m
When GL-20.0 m, $\delta_{hm} = 10$ cm, $\delta_{vm} = 7.5$ cm, PIZ = 32 m

6.7 Ou and Hsieh's method is more reasonable.

6.9 Ou and Hsieh's method: about 1/333
Clough and O'Rourke's method: 0
Bowles's method: 1/830

6.21 $s_{u,avg} = 21.5$ kN/m^2, $\gamma H_e/s_{u,avg} = 11.47 > 4$
$s_{u,b} = 82.6$ kN/m^2, $N_b = \gamma H_e/s_{u,b} = 2.99 < 4$, take $m = 1$
$P_a = \gamma H_e - 4s_u = 160.6$ kN/m^2; $P_a = 0.3\gamma H_e = 74$ kN/m^2; $P_a = 160.6$ kN/m^2
Strut load at the 1st level of struts = 125 kN/m
Strut load at the 2nd level of struts = 405 kN/m
Strut load at the 3rd level of struts = 578 kN/m
Strut load at the 4th level of struts = 578 kN/m

6.29 $K_{a,h} = 0.24$, $K_{p,h} = 7.3$, Assume $F_p = 1.0$; $F_p = M_r/M_d$, $d_0 = 3.5$ m
The bending moment and shear of the wall at various depths is

Depth (m)	*Shear* (kN/m)	*Bending moment* (kN-m/m)
0	0	0
1	−6.2	2
2	−25	17
3	−56	56
4	−87	130
5	−43	202
6	−88	187
7	305	0

Chapter 9

9.5 Theis's method: $s = 1.48$ m; Jacob's method: $s = 1.47$ m

9.7 Theis's method: $s = 6.99$ m; Jacob's method: $s = 6.96$ m

9.9 Total $Q = 1.524$ m^3/min. Assume $r_w = 0.1$ m, $Q_w = 0.64$ m^3/min, $Q_{max} = 2\pi r_w D\frac{\sqrt{k}}{15} = 2 \times \pi \times 0.1 \times 40 \times \frac{\sqrt{0.00005}}{15} = 0.71$ m^3/min
Number of wells $= 1.524/0.64 = 2.4$, take 3 wells
Drawdown induced by each well $= 2.38$ m. Drawdown induced by 4 wells $= 2.38*3 = 7.14$ m < 7.5 m (NG), take four wells

9.11 Assume drawdown is much less than thickness of the aquifer, then Theis's or Jacob's formula can be used. $s = 0.20$ m

9.13 $s = \frac{Q}{4\pi T}(-0.5772 - \ln u) = 1.42$ m $< D = 39$ m (OK)

9.15 $r_w = 0.1$ m, $Q_w = 1.77$ m^3/min, 14 wells

9.17 $R_w = (a + b)/\pi = 38.2$ m, the required total $Q_{tot} = 3.291$ m^3/min
$r_w = 0.1$ m, $Q_w = 1.14$ m^3/min, $n = Q_{tot}/Q_w = 3.291/1.14 = 2.9$, take 3 wells

9.19 $S = 3.47 \times 10^{-4}$

References

ACI (2002), *Building Code Requirements for Structural Concrete (ACI 318-02) and Commentary (ACI 318R-02)*, American Concrete Institute, Farmington Hills, Michigan.

ACI (2005), *Building Code Requirements for Structural Concrete (ACI 318-05) and Commentary (ACI 318R-05)*, American Concrete Institute, Farmington Hills, Michigan.

AIROC (1989), *Specification for the Design of Building Foundation*, Architecture Institute of the Republic of China.

AISC (2001), *Load and Resistance Factor Design Specification for Structural Steel Buildings*, Illinois.

Alpan, I. (1967), The empirical evaluation of the coefficient K_0 and K_{0R}, *Soils and Foundations*, Vol. VII, No. 1, pp. 31–40.

American Association of State Highway and Transportation Officials (AASHTO) (1992), *Ground Anchors*, AASHTO.

American Petroleum Institute (1993), *Foundation design, 6th Section, Recommended Practice for planning, Design and Constructing Fixed Offshore Platform*, 20th Edition, American Petroleum Institute, pp. 57–72.

ASTM (1978), *Standard Test Method for Field Vane Shear Test in Cohesive Soil*, Designation: D2573-72, American Society for Testing and Materials, pp. 346–348.

Atkinson, J. H. and Stallebrass, S. E. (1991), A model for recent stress history and non-linearity in the stress-strain behavior of over-consolidated soil, *Proceeding of the 7th International Conference on Computer Methods and Advances in Geomechanics*, Cairns 1, pp. 555–560.

Bergado, D. T., Asakami, H., Alfaro, M. C., and Balasubramaniam, A. S. (1991), Smear effects of vertical drains on soft Bankok clay, *Journal of Geotechnical Engineering*, Vol. 117, No. 10, pp. 1509–1530.

Bjerrum, I. (1963), Allowable settlement of structures, *Proceedings of European Conference on Soil Mechanics and Foundation Engineering*, Weisbaden, Germany, Vol. 2, pp. 35–137.

Bjerrum, L. (1971), Recent Research on the Consolidation and Shear Behavior of Normally Consolidated Clays, NGI Internal Report 50302, Imperial College, London, England.

Bjerrum, L. (1972), Embankments on soft ground, *Proceeding of Specialty Conference on Performance of Earth and Earth Supported Structures*, Vol. 2, pp. 1–54.

Bjerrum, L. (1973), Problems of soil mechanics and construction on soft clay, State-of-the-Art Report, Session 4, *Proceedings of Eighth International Conference on Soil Mechanics and Foundation Engineering*, Moscow, USSR, Vol. 3.

Bjerrum, L. and Eide, O. (1956), Stability of strutted excavation in clay, *Geotechnique*, Vol. 6, pp. 32–47.

Bonaparte, R. and Mitchell, J. K. (1979), The Properties of San Francisco Bay Mud at Hamilton Air Force Base, California, Geotechnical Engineering Research Report, Department of Civil Engineering, University of California, Berkeley, CA.

Borja, R. I. (1990), Analysis of incremental excavation based on critical state theory, *Journal of Geotechnical Engineering*, ASCE, Vol. 116, No. 6, June, pp. 964–985.

Boscardin, M. D. and Cording, E. J. (1989), Building response to excavation induced settlement, *Journal of Geotechnical Engineering*, ASCE, Vol. 115, No. 1, pp. 1–15.

Bowles, J. E. (1988), *Foundation Analysis and Design*, 4th Ed., McGraw-Hill Book Company, New York, USA.

British Standard Institute (BSI DD81) (1989), *British Standard Code of Practice for Ground Anchorages*, BSI.

Britto, A. M. and Gunn, M. J. (1990), *Critical State Soil Mechanics via Finite Elements*, Ellis Horwood Limited, Chichester.

Brown, P. T. and Booker, J. R. (1985), Finite element analysis of excavation, *Computers and Geotechnics*, Vol. 1, pp. 207–220.

Burland, J. B. and Potts, D. M. (1981), The overall stability of free and propped embedded cantilever retaining walls, *Ground Engineering*, July, pp. 28–38.

Burland, J. B. and Wroth, C. P. (1974), Settlement of buildings and associated damage, *Proceedings of Conference on Settlement of Structures*, Pentech Press, London, England, pp. 611–654.

Burland, J. B., Broms, B. B., and de Mello, V. F. B. (1977), Behavior of foundations and structures, *Proceedings of 9th International Conference on Soil Mechanics and Foundation Engineering*, Vol. 2, Tokyo, Japan, pp. 495–546.

Caquot, A. and Kerisel, J. (1948), *Tables for the Calculation of Passive Pressure, Active Pressure, and Bearing Capacity of Foundations*, Gauthier-Villars, Paris.

Caspe, M. S. (1966), Surface settlement adjacent to braced open cuts, *Journal of the Soil Mechanics and Foundations Division*, ASCE, Vol. 92, SM4, pp. 51–59.

Chang, C. S. and Abas, M. H. B. (1980), Deformation analysis for braced excavation in clay, *Application of Plasticity and Generalized Stress-Strain in Geotechnical Engineering*, Edited by Young and Selig, ASCE, pp. 205–215.

Chang, R. F. (1991), An introduction to geotechnical observational system of the mass rapid transit system, MRT Technology, Bureau of TRTS.

Chen, W. F. and Saleeb, A. F. (1982), *Constitutive Equations for Engineering Materials, Vol. 1 Elasticity and Modeling*, John Wiley & Sons, New York.

Chou, H. L. and Ou, C. Y. (1999), Boiling failure and resumption of deep excavation, *Journal of Performance of Constructed Facilities*, ASCE, Vol. 13, No. 3, pp. 114–120.

Chu, H. and Chou, L. M. (1989), Building correction near the construction of Taipei Rapid Transit System, *Sino-Geotechnics*, No. 66, pp. 75–84.

Chu, J., Bo, M. W., Chang, M. F., and Choa, V. (2002), Consolidation and permeability properties of Singapore marine clay, *Journal of Geotechnical and Geoenvironmental Engineering*, Vol. 128, No. 9, pp. 724–732.

CICHE (1998), *Criteria and Descriptions for Design and Construction of Anchors*, Chinese Institute of Civil and Hydraulic Engineering, Taipei.

Clough, G. W. (1969), Finite Element Analysis of the Soil-Structure Interaction in U-Frame Locks, PhD Dissertation, University of California, Berkeley, CA.

Clough, G. W. and Mana, A. I. (1976), Lessons learned in finite element analysis of temporary excavation in soft clay, *Proceedings of the 2nd International Conference on Numerical Method in Geomechanics*, Edited by C. S. Desai, Blacksburg VA, ASCE, Vol. 1, pp. 496–510.

Clough, G. W. and O'Rourke, T. D. (1990), Construction-induced movements of in situ walls, Design and Performance of Earth Retaining Structures, ASCE Special Publication, No. 25, pp. 439–470.

Clough, G. W. and Tan, D. Y. (1980), Ground control for shallow tunnels by soil grouting, *Journal of Geotechnical Engineering Division*, ASCE, Vol. 106, No. 9, pp. 1037–1057.

Coulomb, C. A. (1776), Essai sur une application des regles de maximis et minimis a quelques problemes de statique, relatifs a l'architecture, *Mem. Roy. des Sciences*, Paris, Vol. 3, pp. 38.

Cowland, J. W. and Thorley, C. B. B. (1985), Ground and building settlement associated with adjacent slurry trench excavation, Ground Movements and Structures, Pentech Press, London, UK, pp. 723–738.

Culmann, C. (1875), *Die graphische statik*, Meyer and Zeller, Zurich.
Darcy, H. (1856), *Les Fontaines Publiques de la Ville de Dijon*, Dalmont, Paris.
Das, B. M. (1995), *Principles of Foundation Engineering*, PWS Publishing Company, MA, p. 448.
Dawson, M. P., Douglas, A. R., Linney, L. F., Friedman, M., and Abraham, R., (1996) Jubilee Line Extension, Bermondsey Station Box: Design Modifications, Instrumentation and Monitoring, Geotechnical Aspect of Underground Construction in Soft Ground, London, pp. 99–104.
Desai, C. S. and Nagaraj, B. K. (1988), Modeling of cyclic normal and shear behavior of interfaces, *Journal of the Engineering Mechanics Division*, Vol. 114, No. 7, pp. 1198–1216.
Desai, C. S. and Siriwardane, H. J. (1984), *Constitutive Law for Engineering Materials*, Prentice-Hall, Englewood Cliffs, NJ.
Deutsche Industrie Norm (DIN) (1988), Verpressanker fur Vorubergehende Zwecke im Lockergestein, Bemessung, Ausfuhrung und Prufung.
Diaz-Rodriguez, J. A., Leroueil, S., and Aleman, J. D. (1992), Yielding of Mexico City and other natural clays, *Journal of Geotechnical Engineering*, Vol. 118, No. 7, pp. 981–995.
Driscoll, F. G. (1989), *Groundwater and Wells*, Johnson Filtration Inc., St Paul, MN.
Duncan, J. M. and Chang, C. Y. (1970), Nonlinear analysis of stress and strain in soils, *Journal of the Soil Mechanics and Foundations Division*, ASCE, Vol. 96, No. 5, pp. 637–659.
Duncan, J. M. and Seed, H. B. (1966), Strength variation along failure surfaces in clay, *Journal of the Soil Mechanics and Foundation Division*, Vol. 92, SM5, pp. 81–104.
Duncan, J. M., Byrne, P., Wong, K. S., and Mabry, P. (1980), Strength, Stress-strain and Bulk Modulus Parameters for Finite Element Analysis of Stresses and Movements in Soil Masses, "Report No.UCB/GT/80-01, College of Engineering Office of Research Services, University of California, Berkeley, CA.
Dunnicliff, J. (1988), *Geotechnical Instrumentation for Monitoring Field Performance*, John Wiley & Sons, New York.
Dupuit, J. (1863), Etudes Théoretiques et Pratiques sur le Mouvement des eaux.
Federation Internationale de la Precontrainte (FIP) (1982), Recommendation for the Design and Construction of Prestressed Concrete Ground Anchors. FIP.
Ferris, J. G., Knowles, D. B., Brown, R. H., and Stallman, R. W. (1962), Theory of aquifer tests, USGS, Water-Supply Paper 1536-E, 174 pp.
Finno, R. J. (1983), Response of Cohesive Soil to Advanced Shield Tunneling, PhD Dissertation, Sanford University, Stanford, CA.
Finno, R. J. and Harahap, I. S. (1991), Finite element analyses of HDR-4 excavation, *Journal of Geotechnical Engineering*, ASCE, Vol. 117, No. 10, pp. 1590–1609.
Finno, R. J., Bryson, S., and Calvello, M. (2002a), Performance of a stiff support system in soft clay, *Journal of Geotechnical and Geoenvironmental Engineering*, Vol. 128, No. 8, pp. 660–671.
Finno, R. J., Calvello, M., and Bryson, S. (2002b), Analysis and Performance of the Excavation for the Chicago-State Subway Renovation Project and its Effects on Adjacent Structures – Final Report, Department of Civil Engineering, Northwestern University.
Forchheimer, P. (1930), Hydraulik, Teubner.
Fredlund, D. G. (1997), An introduction to unsaturated soil mechanics, *Unsaturated Soil Engineering Practice*, ASCE, pp. 1–37.
Geotechnical Control Office (GCO) (1989), Model Specification for Prestressed Ground Anchors.
Gerber, E. (1929), Untersuchungen uber die Druckverteilung im Orlich belasteten Sand, Technische Hochschule, Zurich.
Goodman, R. E., Taylor, R. L., and Brekke, T. L. (1968), A model for mechanics of jointed rock, *Journal of the Soil Mechanics and Foundation Division*, Vol. 94, No. 3, pp. 637–658.
Graf, E. D. (1992), Compaction grouting, 1992, Grouting/Soil Improvement and Geosynthetics, ASCE Special Publication No. 30, pp. 275–287.
Grant, R., Christian, J. T., and Vanmarcke, E. H. (1974), Differential settlement of buildings, *Journal of the Geotechnical Division*, ASCE, Vol. 100, No. 9, pp. 973–991.

Hanna, T. (1985), Field Instrumentation in Geotechnical Engineering, Trans. Tech Publication, Germany.

Hantush, M. S. (1962), Aquifer tests on partially penetrating wells, *Transactions, ASCE*, Vol. 127, Part 1, 284–308.

Harr, M. E. (1962), *Groundwater and Seepage*, McGraw-Hill Book Company, New York, p. 26, 125.

Harza, L. F. (1935), Uplift and seepage under dams in sand, *Transaction*, ASCE.

Hausman, M. R. (1990), *Engineering Principles of Ground Modification*, McGraw-Hill Publishing Company, New York.

Hazen, A. (1892), *Physical Properties of Sands and Gravels with Reference to Their Use in Filtration*, Report Mass. State of Health.

Higgin, K. G., Mair, R. J., and Potts, D. M. (1996), *Numerical modeling of the influence of the Westminster Station excavation and tunneling on the Big Ben clock tower*, Geotechnical Aspect of Underground Construction in Soft Ground, London, pp. 525–530.

Holtz, R. D. and Holm, B. B. (1979), Long-term loading tests at Ska-Edeby Sweden, *Proceedings of the ASCE Specialty Conference on Performance of Earth and Earth-Supported Structures*, Purdue University, Vol. 1, Part 1, pp. 435–464.

Holtz, R. D. and Kovacs, W. D. (1981), *An Introduction to Geotechnical Engineering*, Prentice-Hall, Inc., Englewood Cliffs, NJ, pp. 256.

Hsieh, P. G. (1999), Prediction of Ground Movements Caused by Deep Excavation in Clay, PhD Dissertation, Department of Construction Engineering, National Taiwan University of Science and Technology, Taipei, Taiwan, R.O.C.

Hsieh, P. G. and Ou, C. Y. (1997), Use of modified hyperbolic model in excavation analysis under undrained condition, *Geotechnical Engineering*, SEAGS, Vol. 28, No. 2, pp. 123–150.

Hsieh, P. G. and Ou, C. Y. (1998), Shape of ground surface settlement profiles caused by excavation, *Canadian Geotechnical Journal*, Vol. 35, No. 6, pp. 1004–1017.

Hsu, J. H. (1997), *Design of Deep Excavation*, TWCE, Taipei.

Huang (1992), Case histories of underpinning during the construction of the Singapore mass transit system, *Sino-Geotechnics*, No. 40, pp. 77–90.

ICE (1989), *Geotechnical Instrumentation in Practice, Purpose, Performance and Interpretation, Proceedings of the Conference on Geotechnical Instrumentation in Civil Engineering Projects*, Organized by the Institution of Civil Engineers, London.

Jacob, C. E. (1940), On the flow of water in an elastic artesian aquifer, *Transaction, American Geophysical Union*, pp. 574–586.

Jaky, J. (1944), The coefficient of earth pressure at rest, *Journal of the Society of Hungarian Architects and Engineers* (in Hungarian), Vol. 8, No. 22, pp. 355–358.

James, R. G. and Bransby, P. L. (1970), Experimental and theoretical investigation of a passive earth pressure problem, *Geotechnique*, Vol. 20, No. 1, pp. 17–37.

Janbu, N. (1963), Soil compressibility as determined by oedometer and triaxial tests, European Conference on Soil Mechanics and Foundation Engineering, Wissbaden, Germany, Vol. 1, pp. 19–25.

JSA (1988), *Guidelines of Design and Construction of Deep Excavations*, Japanese Society of Architecture.

JSF (1990), *Design and Construction Criteria of Ground Anchors*, Japanese Soil and Foundation Society.

Kashef, A. I. (1987), *Groundwater Engineering*, McGraw-Hill Book Company, New York, p. 165.

Konder, R. L. (1963), Hyperbolic stress-strain response: cohesive soils, *Journal of the Soil Mechanics and Foundation Division*, ASCE, Vol. 89, No. 1, pp. 115.

Kozeny, J. (1953), *Hydraulik*, Springer, Verlag.

Kruseman, G. P. and de Ridder, N. A. (1990), Analysis and Evaluation of Pumping Test Data, Wageningen, Netherlands : International Institute for Land Reclamation and Improvement.

Ladd, C. C. and Foote, R. (1974), New design procedure for stability of soft clay, *Journal of Geotechnical Engineering Division*, ASCE, Vol. 100, GT7, pp. 763–786.

Ladd, C. C. and Lambe, T.W. (1963), The strength of undisturbed clay determined from undrained tests, Laboratory Shear Testing of Soils, ASTM Special Technical Publication No. 361, pp. 342–371.

Ladd, C. C., Bovee, R. B., Edgers, L., and Rixner, J. J. (1971), Consolidated-Undrained Plane Strain Shear Tests on Boston Blue Clay, Research Report R72-82, No. 284, Department of Civil Engineering, Mass. Inst. of Technology, Cambridge, 354p.

Ladd, C. C., Foote, R., Ishihara, K., Schlosser, F., and Poulous, H. G. (1977), Stress-Deformation and Strength Characteristics, State-of-the-Art Report, *Proceedings of the Ninth International Conference on Soil Mechanics and Foundation Engineering*, Tokyo, Vol. 2, pp. 421–494.

Lade, P. V. and Duncan, J. M. (1973), Cubical triaxial tests on cohesionless soil, *Journal of the Soil Mechanics and Foundation Division*, ASCE, Vol. 99, No. 10, pp. 793–812.

Lambe, T. W. and Whitman, R. V. (1969), *Soil Mechanics*, John Wiley & Sons, New York.

Lee, K. H. (1983), Treatment of panel joint of diaphragm wall construction, *Sino-Geotechnics*, No. 4, pp. 3–10.

Lee, K. H. (1988), Types of panel joint of diaphragm wall, *Sino-Geotechnics*, No. 21, pp. 34–42.

Lee, F. H., Yong, K. Y., Quan, K. C. N., and Chee, K. T. (1998), Effect of corners in strutted excavations: field monitoring and case histories, *Journal of Geotechnical and Geoenvironmental Engineering*, Vol. 124, No. 4, pp. 339–349.

Liao, H. J. and Ou, C. D. (1988), Anchored behavior and field testing of prestressed anchors, *Sino-Geotechnics*, No. 24, pp. 81–91.

Lin, H. D. and Lin, C. B. (1999), A preliminary study for the frictional resistance and loading factor of the cast-in-site pile, *Journal of the Chinese Institute of Civil and Hydraulic Engineering*, Vol. 11, No. 1, pp. 13–21.

Littlejohn, G. S. (1970), Soil Anchors, *Proceedings of Conference on Ground Engineering*, Institute of Civil Engineering, London.

Liu, C. C., Hsieh, H. S., and Huang, C. S. (1997), A study of the stability analysis for deep excavations in clay, The Seventh Geotechnical Conference, Taipei, pp. 629–638.

Lo, K. Y. (1962), Shear strength properties of a sample of volcanic material of the valley of Mexico, *Geotechnique*, Vol. 12, No. 4, pp. 303–318.

Mackey, R. D. and Kirk, D. P. (1967), At rest, active and passive earth pressures, *Proceedings of Southeast Asia Regional Conference on Soil Engineering, Bangkok*, pp. 187–199.

Mana, A. I. (1978), Finite Element Analysis of Deep Excavation Behavior in Soft Clay, PhD Dissertation, Stanford University.

Mana, A. I. and Clough, G. W. (1981), Prediction of movements for braced cut in clay, *Journal of Geotechnical Engineering Division*, ASCE, Vol. 107, No. 6, pp. 759–777.

Marino, M. A. and Luthin, J. A. (1982), *Seepage and Groundwater*, Elsevier Scientific Publishing Company, New York.

Marsland, A. (1953), Model experiments to study the influence of seepage on the stability of a sheeted excavation in sand, *Geotechnique*, Vol. 3, No. 6, pp. 223–241.

Mesri, G., Rokhsar, A., and Bohor, B. F. (1975), Composition and compressibility of typical samples of Mexico city clay, *Geotechnique*, Vol. 25, No. 3, pp. 527–554.

Milligan, G. W. E. (1983), Soil deformation near anchored sheet-pile walla, *Geotechnique*, Vol. 33, No. 1, pp. 41–55.

Miyoshi, M. (1977), Mechanical behavior of temporary braced wall, *Proceedings of the 9th International Conference on Soil Mechanics and Foundation Engineering*, Tokyo, Vol. 2, No. 2/60, pp. 655–658.

Moh, Z. C., Nelson, J. D., and Brand, E. W. (1969), Strength and deformation behavior of Bangkok clay, *Proceedings of the 7th International Conference on Soil Mechanics and Foundation Engineering*, Mexico city, pp. 287–295.

Moh, Z. C., Chin, C. T., Liu, C. J., and Woo, S. M. (1989), Engineering correlations for soil deposits in Taipei, *Journal of the Chinese Institute of Engineers*, Vol. 12, No. 3, pp. 273–283.

Mohr, O. (1900), Welche Umstande bedingen die Elastizitatsgrenze und den Bruch eines Materiales *Zeitschrift des Vereines Deutscher Ingenieure*, Vol. 44, pp. 1524–1530; 1572–1577.

Mononobe, N. (1929), Earthquake-proof construction of masonary dams, *Proceedings of the World Engineering Conference 9*, pp. 274–280.

NAVFAC DM7.2 (1982), Foundations and Earth Structures, Design Manual 7.2, Department of the Navy, USA.

Naylor, D. J. and Pande, G. N. (1981), *Finite Elements in Geotechnical Engineering*, Pineridge Press, Swansea, UK.

Ng, C. W. W. (1992), An Evaluation of Soil-Structure Interaction Associated with a Multi-Propped Excavation, PhD Thesis, University of Bristol, UK.

Nicholson, D. P. (1987), The design and performance of the retaining wall at Newton station, *Proceeding of Singapore Mass Rapid Transit Conference*, Singapore, pp. 147–154.

Nonveiller, E. (1989), *Grouting Theory and Practice*, Elsevier, Amersterdam, pp. 225–227.

Okabe, S. (1926), General theory of earth pressure, *Journal of the Japanese Society of Civil Engineers*, Vol. 12, No. 1.

Ou, C. D. (1986), Basic design theory and tests of ground anchors, *Sino-Geotechnics*, No. 14, pp. 4–15.

Ou, C. Y. (2001), Personal files.

Ou, C. Y. and Hsiao, J, L. (1999), Stability Analysis of Deep Excavations in Sand, Geotechnical Research Report No. GT99005, Department of Construction Engineering, National Taiwan University of Science and Technology, Taipei, Taiwan, R.O.C.

Ou, C. Y. and Hsieh, P. G. (2000), Prediction of Ground Surface Settlement Induced by Deep Excavation, Geotechnical Research Report No. GT200008, Department of Construction Engineering, National Taiwan University of Science and Technology.

Ou, C. Y. and Hu, M. Y. (1998), Stability Analysis of Excavations in Clay, Geotechnical Research Report No. GT99007, Department of Construction Engineering, National Taiwan University of Science and Technology, Taipei, Taiwan, R.O.C.

Ou, C. Y. and Lai, C. H. (1994), Finite element analysis of deep excavation in layered sandy and clayey soil deposits, *Canadian Geotechnical Journal*, Vol. 31, pp. 204–214.

Ou, C. Y. and Lin, Y. W. (1999), Application of Cross Wall to Deep Excavations, Geotechnical Research Report No. GT99006, Department of Construction Engineering, National Taiwan University of Science and Technology, Taipei, Taiwan, R.O.C.

Ou, C. Y. and Shiau, B. Y. (1998), Analysis of the corner effect on the excavation behavior, *Canadian Geotechnical Journal*, Vol. 35, No. 3, pp. 532–540.

Ou, C. Y. and Shiau, W. D. (1993), Characteristics of consolidation and strength of Taipei silty clay, *Journal of the Chinese Institute of Civil and Hydraulic Engineering*, Vol. 5, No. 4, pp. 337–346.

Ou, C. Y. and Tang, Y. G. (1994), Soil parameter determination for deep excavation analysis by optimization, *Journal of the Chinese Institute of Engineers*, Vol. 17, No. 5, pp. 671–688.

Ou, C. Y. and Wang, I. W. (1997), Measures for Reducing Wall Deformation in Deep Excavations, Geotechnical Research Report No. GT97006, Department of Construction Engineering, National Taiwan University of Science and Technology, Taipei, Taiwan, R.O.C.

Ou, C. Y. and Wu, C. H. (1990), Deformation behavior of excavations in sandy soils due to grouting, *Journal of the Civil and Hydraulic Engineering*, Vol. 2, No. 2, pp. 169–182.

Ou, C. Y. and Yang, L. L. (2000), Ground Movement Induced by the Construction of Diaphragm Wall, Geotechnical Research Report No. GT200005, Department of Construction Engineering, National Taiwan University of Science and Technology, Taipei, Taiwan, R.O.C.

Ou, C. Y., Hsieh, P. G., and Chiou, D. C. (1993), Characteristics of ground surface settlement during excavation, *Canadian Geotechnical Journal*, Vol. 30, pp. 758–767.

Ou, C. Y., Wu, T. S., and Tseng, J. R. (1995), Prediction of stress-strain behavior of soils based on Cam-clay plasticity model, *Journal of the Chinese Institute of Civil and Hydraulic Engineering*, Vol. 7, No. 1, pp. 95–100.

Ou, C. Y., Chiou, D. C., and Wu, T. S. (1996a), Three-dimensional finite element analysis of deep excavations, *Journal of Geotechnical Engineering*, ASCE, Vol. 122, No. 5, pp. 337–345.

Ou, C. Y., Wu, T. S., and Hsieh, H. S. (1996b), Analysis of deep excavation with column type of ground improvement in soft clay, *Journal of Geotechnical Engineering*, ASCE, Vol. 122, No. 9, pp. 709–716.

Ou, C. Y., Liao, J. T., and Lin, H. D. (1998), Performance of diaphragm wall constructed using Top-Down Method, *Journal of Geotechnical and Geoenvironmental Engineering*, ASCE, Vol. 124, No. 9, pp. 798–808.

Ou, C. Y., Liao, J. T., and Cheng, W. L. (2000a), Building response and ground movements induced by a deep excavation, *Geotechnique*, Vol. 50, No. 3, pp. 209–220.

Ou, C. Y., Shiau, B. Y., and Wang, I. W. (2000b), Three-dimensional deformation behavior of the TNEC excavation case history, *Canadian Geotechnical Journal*, Vol. 37, No. 2, pp.438–448.

Ou, C. Y., Hsieh, P. G., and Duan, S. M. (2005), A Simplified Method to Estimate the Ground Surface Settlement Induced by Deep Excavation, Geotechnical Research Report No. GT200502, Department of Construction Engineering, National Taiwan University of Science and Technology.

Padfield, C. J. and Mair, R. J. (1984), Design of Retaining Walls Embedded in Stiff Clay, CIRIA Report No. 104, England, pp. 83–84.

Pande, G. N. and Sharma, K. G. (1979), On the joint/interface elements and associated problems of numerical III-conditioning, *International Journal for Numerical and Analytical Methods in Geomechanics*, Vol. 3, pp. 301–312.

Peck, R. B. (1943), Earth pressure measurements in open cuts Chicago (III) subway, *Transactions*, ASCE, Vol. 108, p. 223.

Peck, R. B. (1969a), Advantages and limitations of the observational method in applied soil mechanics, *Geotechnique*, Vol. 19, No. 2, pp. 171–187.

Peck, R. B. (1969b), Deep excavation and tunneling in soft ground, *Proceedings of the 7th International Conference on soil Mechanics and Foundation Engineering*, Mexico City, State-of-the-Art Volume, pp. 225–290.

Peck, R. B. and Ireland, H. O. (1961), Full-scale lateral load test of a retaining wall foundation, *Proceedings of 5th International Conference on Soil Mechanics and Foundation Engineering*, Vol. 2, pp. 453–458.

Peck, R. B., Hanson, W. E., and Thornburn, T. H. (1977), *Foundation Engineering*, John Wiley & Sons, New York.

Pestana, J. (2001), Private communication.

Poh, T. Y. and Wong, I. H. (1998), Effects of construction of diaphragm wall panels on adjacent ground: field trial, *Journal of Geotechnical and Environmental Engineering*, ASCE, Vol. 124, No.8, pp.745–756.

Polshin, D. E. and Tokar, R. A. (1957), Maximum allowable non-uniform settlement of structures, *Proceedings of the 4th International Conference on Soil Mechanics and Foundation Engineering*, Vol. I, London, pp. 402–406.

Post-Tensioning Institute (PTI) (1980), Recommendations for Prestressed Rock and Soil Anchors, PTI.

Potts, D. M. and Zdravkovic, L. (1999), *Finite Element Analysis in Geotechnical Engineering*, Thomas Telford, London.

Potyondy, J. G. (1961), Skin friction between various soils and construction materials, *Geotechnique*, Vol. 11, pp. 339–353.

Powers, J. P. (1992), *Construction Dewatering*, John Wiley & Sons, New York.

Quinion, D. W. and Quinion, G. R. (1987), *Control of Groundwater*, Thomas Telford, London.

Rankine, W. M. J. (1857), On stability on loose earth, Philosophic Transactions of Royal Society, London, Part I, pp. 9–27.

Reddy, A. S. and Srinivasan, R. J. (1967), Bearing capacity of footing on layered clay, *Journal of the Soil Mechanics and Foundations Division*, ASCE, Vol. 93, No. 2, pp. 83–99.

Rehnman, S. E. and Broms, B. B. (1972), Lateral pressures on basement wall: results from full-scale tests, *Proceedings of 5th European Conference on Soil Mechanics and Foundation Engineering*, Vol. 1, pp. 189–197.

Rendon-Herrero, O. (1980), Universal compression index equation, *Journal of the Geotechnical Division*, Vol. 106, No. 11, pp. 1179–1200.

Robertson, P. K. and Campanella, R. G. (1989), *Guidelines for Geotechnical Design Using the Cone Penetrometer Test and CPT with Pore Pressure Measurement*, Hogentogler Co., Inc.

Roscoe, K. H. and Burland, J. B. (1968), On the generalized stress-strain behavior of 'wet' clay, Engineering Plasticity, In *Engineering Plasticity*, edited by Heyman and Leckie, Cambridge University Press, Cambridge, pp. 535–609.

Rowe, P. W. and Peaker, K. (1965), Passive earth pressure measurements, *Geotechnique*, Vol. 15, No. 1, pp. 57–78.

Sachdeva, T. D. and Ramakrishnan, C. V. (1981), A finite element solution for the two-dimensional elastic contact problems with friction, *International Journal for Numerical and Analytical Methods in Engineering*, Vol. 17, pp. 1257–1271.

Schmidt, B. (1967), Lateral stresses in unaxial strains, Bulletin, No. 23, Danish Geotechnical Institute, pp. 5–12.

Seed, H. B., Noorany, I., and Smith, I. M. (1964), Effects of Sampling and Disturbance on the Strength of Soft clay, Report TE-1, University of California, Berkeley, CA.

Sharma, K. G. and Desai, C. S. (1992), Analysis and implementation of thin-layer element for interfaces and joints, *Journal of Engineering Mechanics*, Vol. 118, No. 12, pp. 2444–2461.

Shen, M. S. (1999), *Hazard Mitigation Technology of Construction*, Wen-Sen Publisher, Taipei.

Sichart, W. (1928), *Das Fassungsvermogen von Rohrbrunnen*, Julius Springer, Berlin.

Sichart, W. and Kyrieleis, W. (1930), Grundwasser Absekungen bei Fundierungsarbeiten, Berlin.

Simons, N. E. (1974), Normally consolidated and highly overconsolidated cohesive materials, General Report, *Proceedings of the Conference on Settlement of Structures*, Cambridge University, British Geotechnical Society, pp. 500–530.

Simpson, B. (1992), Retaining structures: displacement and design, *Geotechnique*, Vol. 42, No. 4, pp. 541–576.

Skempton, A. W. (1944), Notes on the compressibility of clays, *Quarterly Journal of the Geological Society of London*, Vol. 100, pp. 119–135.

Skempton, A. W. (1951), The bearing capacity of clays, *Proceeding of Building Research Congress*, Vol. 1, pp. 180–189.

Skempton, A. W. (1954), The pore-pressure coefficients A and B, *Geotechnique*, Vol. 4, pp. 143–147.

Skempton, A. W. (1959), Cast in-situ bored piles in London clay, *Geotechnique*, Vol. 9, No. 4, pp. 153–173.

Skempton, A. W. (1960), Correspondence, *Geotechnique*, Vol. 10, No. 4, p.186.

Skempton, A. W. and McDonald, D. H. (1957), Allowable settlement of buildings, *Proceedings, Institute of Civil Engineers*, Part III, Vol. 5, pp.727–768.

Smith, P. R., Jardine. R. J., and Hight, D. W. (1992), The yielding of Bothkennar clay, *Geotechnique*, Vol. 42, No. 2, pp. 257–274.

Spangler, M. G. (1938), Horizontal pressures on retaining walls due to concentrated surface loads, Iowa State University Experimental Station, Bulletin, No. 140.

Tan, T. S., Lee, F. H., Chong, P. T., and Tanaka, H. (2002), Effect of sampling disturbance on properties of Singapore clay, *Journal of Geotechnical and Geoenvironmental Engineering*, Vol. 128, No. 11, pp. 898–906.

Tavenas, F. A., Blanchette, G., Leroueil, S., Roy, M., and LaRochelle, P. (1974), Immediate settlement of three test embankments on Champlain clay, *Canadian Geotechnical Journal*, Vol. 11, No. 1, pp. 109–141.

Terzaghi, K. (1922), Der Grundbrunch on Stauwerken und Seine Verhutung, Die Wasserkraft, Vol. 17, pp. 445–449, Reprinted in *From Theory to Practice in Soil Mechanics*, John Wiley & Sons, New York, pp.146–148, 1961.

Terzaghi, K. (1925), *Erdbaumechanik auf Bodenphysikalischer Grundlage*, Dueticke, Vienna.

Terzaghi, K. (1936), Relation between soil mechanics and foundation engineering: Presidential Address, *Proceedings of First International Conference on Soil Mechanics and Foundation Engineering*, Boston, Vol. 3, pp. 13–18.

Terzaghi, K. (1943), *Theoretical Soil Mechanics*, John Wiley & Sons, Inc., New York, N.Y.

Terzaghi, K. (1955), Evaluation of coefficient of subgrade reaction, *Geotechnique*, Vol. 5, No. 4, pp. 297–326.

Terzaghi, K. and Peck, R. B. (1967), *Soil Mechanics in Engineering Practice*, John Wiley & Sons, New York.

TGS (2001), Design Specifications for the Foundation of the Building, Taiwanese Geotechnical Society.

Theis, C. V. (1935), The relation between the lowering of the piezometric surface and the rate and discharge of a well using ground water storage, *Transactions of the American Geophysical Union 16th Annual Meeting*.

Thiem, G. (1906), *Hydrologische Methoden*, JM Gephardt, Leipzig.

Tsai, J. S., Jou, L. D., and Wang, W. C. (1996), Support constraint of strut bracing system in deep excavation, *Journal of the Chinese Institute of Civil and Hydraulic Engineering*, Vol. 8, No. 3, pp. 471–476.

Vaid, Y. P. and Campanella, R. G. (1974), Triaxial and plane strain behavior of natural clay, *Journal of the Geotechnical Engineering Division*, ASCE, Vol. 100, GT3, pp. 207–224.

Vesic, A. B. (1961), Bending of beams on isotropic elastic solid, *Journal of the Engineering Mechanics Division*, ASCE, Vol. 87, No. 2, pp. 35–53.

Wahls, H. E. (1981), Tolerable settlement of building, *Journal of the Geotechnical Division*, ASCE, Vol. 107, No. 11, pp.1489–1504.

Wang, J. D., Lin, H. D., and Wu, M. F. (1999), Ground surface settlement induced by deep excavation in clay, *Sino-Geotechnics*, No. 76, pp. 51–62.

Whittle, A. J., Hashash, Y. M., and Whitman, R. V. (1993), Analysis of deep excavation in Boston, *Journal of Geotechnical Engineering*, ASCE, Vol. 119, No. 1, pp. 69–90.

Winkler, E. (1867), Die Lehre Von Elasticitaet Und Festigkeit, Pray (H. Dominicus), pp.182–184.

Wong, K. S. and Broms, B. B. (1989), Lateral deflection of braced excavation in clays, *Journal of Geotechnical Engineering*, ASCE, Vol. 115, No. 6, June, pp. 853–870.

Wong, L. W., Shau, M. C., and Chen, H. T. (1996), Compaction grouting for correcting building settlement, *Grouting and Deep Mixing*, Edited by Yonekura, Terashi and Shibazaki, A. A. Balkema, Rotterdam, The Netherlands.

Woo, S. M. (1992), Method, design and construction for building protection during deep excavation, *Sino-Geotechnics*, No. 40, pp. 51–61.

Woo, S. M. and Moh, Z. C. (1990), Geotechnical characteristics of soils in the Taipei Basin, *Proceedings of the Tenth Southeast Asian Geotechnical Conference*, Vol. 3, Taipei, pp. 51–65.

Wu, W. T. (1987), Engineering characteristics of subzones of Taipei Basin, *Sino-Geotechnics*, No. 22, pp. 5–27.

Xanthakos, P. (1994), *Slurry Walls as Structural System*, 2nd Edition, McGraw-Hill, Inc., New York.

Yen, D. L. and Chang, G. S. (1991), A study of allowable settlement of buildings, *Sino-Geotechnics*, No. 22, pp. 5–27.

Index

Excavation is an important segment in foundational engineering (for example, in the construction of the foundations or basements of high rise buildings, underground oil tanks, a subway or a mass transit system). Most books on general foundation engineering introduce the basic analysis and design of excavation, but are not usually capable of dealing with the analysis and design in practice. With economic development and urbanization, excavations go deeper and become larger in scale, sometimes even carried out in difficult soils. These conditions require advanced analysis and design methods and construction technologies. This book is aimed at both theoretical explication and practical applications. From basic to advanced, the book tries to attain theoretical rigorousness and consistency. Each chapter is followed by problems and solutions so that the book can be readily taught at senior undergraduate and graduate levels. On the other hand, the book also deals with design practice. The analysis methods introduced in the book can be used for analysis and design in actual excavations as they are the correct methods currently used in the engineering circle. Based on interaction between research results, analysis experience and teaching experience, the book is aimed at both teachers and engineers in advanced analysis and design.

Chang-Yu Ou is professor at the Department of Construction Engineering, National Taiwan University of Science and Technology, Taipei.

Taylor & Francis
Taylor & Francis Group

www.tandf.co.uk/engineering
Printed in Great Britain

ISBN 0-415-40330-8

an informa business